A NOVEL APPROACH,

USING REGIONAL CLIMATE MODEL,

TO DERIVE PRESENT AND FUTURE

INTENSITY-DURATION-FREQUENCY CURVES

LIEW SAN CHUIN

NATIONAL UNIVERSITY OF SINGAPORE

2012

A NOVEL APPROACH,

USING REGIONAL CLIMATE MODEL,

TO DERIVE PRESENT AND FUTURE

INTENSITY-DURATION-FREQUENCY CURVES

LIEW SAN CHUIN
(B.Eng.(Hons), USM)

A THESIS SUBMITTED

FOR THE DEGREE OF
DOCTOR OF PHILOSOPHY

DEPARTMENT OF CIVIL AND ENVIRONMENTAL ENGINEERING

NATIONAL UNIVERSITY OF SINGAPORE

2012

DECLARATION

I hereby declare that the thesis is my original work and it has been written by me in its entirety. I have duly acknowledged all the sources of information which have been used in the thesis.

This thesis has also not been submitted for any degree in any university previously.

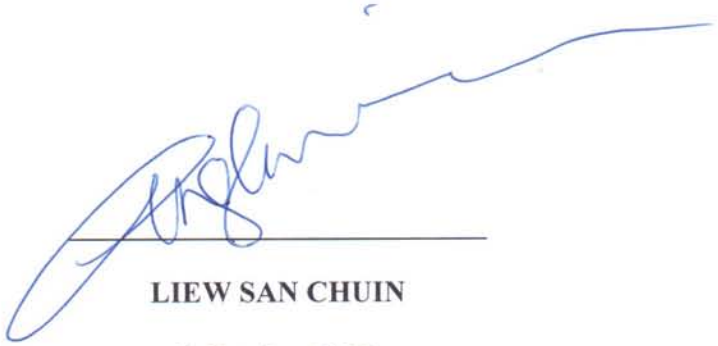

LIEW SAN CHUIN

7 October 2012

This page is intentionally left blank.

DEDICATION

To my dearest parents and sister

This page is intentionally left blank.

ACKNOWLEDGEMENTS

I would like to extend my heartfelt gratitude and thanks to an outstanding and wonderful mentor, my supervisor, Assoc. Prof. Liong Shie-Yui, who, throughout my 4 years research period, gave me constructive comments and unstinted support which have motivated me to undertake this study. I greatly appreciate his willingness to share his vast experience and guidance; his logical way of thinking has been a great value for me. The encouragement he gives me and the patience and unwavering faith he has in me. Thank you for being there for me and supporting me throughout.

I also wish to express my sincere gratitude and thanks to Dr. V. Srivatsan, a young and capable climatologist, who has been a source of endless ideas and inspiration. I would like to thank him for his guidance and constant students and research engineers group discussion.

My deepest gratitude to my colleagues at the TMSI namely Dr. Doan Chi Dung, Dr. Nguyen Ngoc Son, Dr. He Shan, Mr. Vu Minh Tue, Mr. Dao Anh Tuan whom I have consulted during the course of the research and not forgetting Mr. Ethan Nguyen for his IT support.

A special acknowledgement is dedicated to Tropical Marine Science Institute (TMSI) and Building and Construction Authority (BCA) for providing me resources and facilities to carry out this research. In addition, this research was carried out at the National Supercomputer Centre in Tianjin where the

simulations and calculations were performed on TianHe-1 (A). The excellent technical assistance and overall support from the centre are gratefully acknowledged. I would also like to thank Center for Hazards Research (CHR) and Center for Environmental Sensing and Modeling (CENSAM), Singapore-MIT Alliance for Research and Technology (SMART). Both centers have provided me great hands-on and practical experiences through collaborative research projects. The facilities have provided me the resources needed to produce my works and dissertation. All the experience gathered resulted in various papers; one paper co-authored with Assoc. Prof. Liong and Dr. Srivatsan, has won the 'Best Paper Award'* at the 18th Congress of the Asia and Pacific Division of the International Association for Hydro-Environment Engineering and Research 2012 (IAHR-APD 2012, 19-23 August 2012, Jeju, Korea). The award is given out biennial to recognize high quality contribution in hydraulic and water resources research.

I also wish to credit the support of the following professionals, associates and friends for sharing their experiences and knowledge namely Prof. Ismail Abustan, Er. Dr. Ong Chee Wee, Dr. Tan Czhia Yheaw and Ms. Nandar Kyaw.

I would like to extend my gratitude to my parents, my sister for their never-ending love, support, tolerance and sacrifice in encouraging me to complete this research.

To the remaining people whom I am unable to list down, I owe them my sincere appreciation and thanks for the feedback, assistance, tolerance and

help rendered. Last but not least, deepest appreciation and thanks to National University of Singapore for the award of this research scholarship throughout the four years period.

* Best Paper Award - “A Novel Approach, Using Regional Climate Model, to Derive Present and Future IDF Curves for Data Scarce Sites”

Liew San Chuin, Angelia
August 30, 2012

This page is intentionally left blank.

TABLE OF CONTENTS

This page is intentionally left blank.

SUMMARY

Lack of sufficiently long rainfall records is common in most Southeast Asia countries. This leads to improper designs of urban drainages and stormwater infrastructure systems. Optimal designs of stormwater systems rely very much on the rainfall Intensity-Duration-Frequency (IDF) curves. As climate has shown significant changes in rainfall characteristics in many regions, the adequacy of the existing IDF curves is called for particularly when the rainfall are much more intense. For site with short or no rainfall record, developing IDF curves for the future climate is even challenging. The current practice for such regions is, for example, to 'borrow' or 'interpolate' data from regions of climatologically similar characteristics.

This study presented a novel approach to develop present and future climate IDF curves using high resolution climate outputs using Regional Climate Model (30 × 30 km over the study domain) driven by Reanalysis data (ERA-40) for ungauged sites, e.g. Jakarta, Indonesia. In this study, a well validated (3-step) Downscaling-Comparison-Derivation (DCD) approach was applied to develop present day IDF curves at stations with short or no rainfall record. Extremes from projected rainfall (6-hourly results; ERA-40) are first used to derive IDF curves for 3 sites (meteorological stations) where IDF curves exist; biases observed resulting from these sites are captured and serve as very useful information in the derivation of present day IDF curves for ungauged sites.

The proof-of-concept analyses showed that the IDF curves derived from WRF/ERA40 fairly consistently underestimate each IDF curves ranging from +38% (lower bound) to +45% (upper bound); thus, present day climate derived IDF curves fall within a specific range, +38% to +45%. This range allows designers to decide on a value within the lower and upper bounds, normally subjected to engineering, economic and environmental concerns. The range of bias correction showed reasonable results when applied to and compared with site assumed to be ungauged (validation site; Darmaga Station).

For the anticipated changes in rainfall intensities due to climate change, this study continues to propose the development of future climate IDF curves. Two sites (Jakarta Meteorological Station and Darmaga Station) were selected; one with long rainfall record while the other is from an ungauged basin. The derivation of future IDF curves was done by applying the 'simple delta' (Δ_i) method (simulated future minus present day rainfall intensities) on the high resolution outputs. Two Global Climate Models (GCMs; CCSM3.0 and ECHAM5) and three emission scenarios (A1FI, A2 and A1B) were considered.

The proposed approach can be extended to other emission scenarios and using different GCMs so that a bandwidth of uncertainties can be assessed to create appropriate and effective adaptation strategies to address climate change and its impacts. Same approach can also be applied for other cities, where in this study a "by-product" of the research work presented the changes in and comparisons between extreme rainfalls of the 3 mega cities, Singapore, Kuala Lumpur and Jakarta. The study has shown that the intensity of extreme

rainfall is projected to increase significantly in particular towards the end of the 21st Century.

Keywords: IDF curves, ungauged sites, reanalysis data, Regional Climate Model, Climate Change, emission scenarios

This page is intentionally left blank.

LIST OF PUBLICATIONS

Following are the publications arising from the research:-

Best Paper Award:

1) Liew, S.C., Liong, S-Y. and V. Raghavan, S. 2012. A novel approach, using regional climate model, to derive present and future IDF curves for data scarce sites. 18th Congress of International Association of Hydraulics Engineering and Research – Asia Pacific Division, 2012

Journal Article:

1) Liew, S.C., Liong, S-Y. and V. Raghavan, S. 2012. A novel approach, using regional climate model, to derive present and future IDF curves for data scarce sites. Journal of Hydro-Environmental Research *(Accepted)*

2) Liew, S.C., Liong, S-Y. and V. Raghavan, S. 2012. How to construct future IDF curves, under changing climate, for sites with scarce rainfall records? Hydrological Processes *(Under Review)*

Public Talk and Invited Lecture:

1) Liong, S-Y., V. Raghavan, S. and Liew, S.C. 2012. Flood Risks at Rainfall Record Scarce Sites: Climate Model derived IDF curves. APEC Typhoon Symposium, Taipei, Taiwan, 4^{th} – 7^{th} June 2012 *(Invited Speaker)*

2) Liong, S-Y., V. Raghavan, S., Vu, M.T. and Liew, S.C. 2012. Regional Climate Modelling and Impact Studies. HydroAsia, Incheon, South Korea, 20^{th} – 25^{th} August 2012 *(Invited Lecture)*

Book Authored:

1) Liew, S.C., Liong, S-Y. and Vu, M.T. 2011. A Study of Urban Stormwater Modeling Approach on Singapore Catchment. Hydrological Science (HS) Volume of Advances in Geosciences (*Published*)

2) Vu, M.T., Liong, S-Y, Liew, S.C. and V. Raghavan, S. 2011. A novel methodology for developing inundation maps under climate change scenarios using one-dimensional model. Hydrological Science (HS) Volume of Advances in Geosciences *(Published)*

International/Regional Conference:

1) Liew, S.C., V. Raghavan, S., Liong, S-Y. and Sanders, R. 2012. Development of Intensity-Duration-Frequency Curves: Incorporating Climate Change Projection. 10th International Conference on Hydro-Informatics 2012, Hamburg, Germany.
(Full Paper and Oral Presentation)

2) Liew, S. C., V. Raghavan, S. and Liong, S-Y. 2010. Climate Change Modeling to Predict Future Rainfall Event in Jakarta, Indonesia. 9th International Conference on Hydro-informatics 2010, Tianjin, China.
(Full Paper and Oral Presentation)

3) Liew, S.C., Liong, S-Y. and Vu, M.T. 2010. A Study of Stormwater Modeling Approach Using SOBEK on Urban Catchment. 9th International Conference on Hydro-informatics 2010, Tianjin, China.
(Full Paper and Oral Presentation)

4) Liew, S.C., V. Raghavan, S. and Liong, S-Y. 2011. Economic Implications of Climate Change for Southeast Asia Regions. 8th Asia Oceania Geosciences Society (AOGS) Conference, Taipei, Taiwan.
(Abstract and Oral Presentation)

5) Vu, M.T., V. Raghavan, S. Nguyen, N.S., Liew, S.C. and Liong, S-Y. 2012. Uncertainties in Climate Projections Over Southeast Asia. AOGS – AGU (WPGM) Joint Assembly, Singapore.
(Abstract and Oral Presentation)

6) Vu, M.T., Liong, S-Y, Liew, S.C. and V. Raghavan, S. 2009. Floodmap Development for Urban Watersheds with Respect to Climate Change. 6th Asia Oceania Geosciences Society (AOGS) Conference, Singapore.
(Abstract and Oral Presentation)

LIST OF TABLES

LIST OF FIGURES

This page is intentionally left blank.

ACRONYMS AND ABBREVIATION

ADB	Asian Development Bank
AGCM	Atmospheric General Circulation Model
AMS	Annual Maximum Rainfall Series
AOGCM	Atmospheric Ocean General Circulation Model
APHRODITE	Asian Precipitation Highly Resolved Observational Data Integration Towards the Evaluation of Water Resources
AR4	Fourth Assessment Report
CCC	Canadian Climate Centre
CCCMA	Canadian Climate Centre for Modelling and Analysis
CCSM	Community Climate System Model
CCSR/NIES	Center for Climate System Research/National Institute for Environmental Studies
CDC	Connecting Delta Cities
CGCM	Canadian Global Circulation Model
CLM	Community Land Model
CO_2	Carbon dioxide
CPC	Climate Prediction Center
CRCM	Canadian Regional Climate Model
CRU	Climate Research Unit
CTL	Hindcast run
DCD	Dynamical Downscaling, Comparison and Derivation
DD	Dynamical Downscaling
DDF	Depth-Duration Frequency

DWD	Deutscher Wetterdienst
ECHAM	European Centre Hamburg Model
ECMWF	European Centre for Medium-Range Weather Forecasts
EDS	Expanded downscaling technique
EEPSEA	Economy and Environmental Program for Southeast Asia
ERA40	ECMWF 40 years Re-Analysis
EV1/EV(1)	Gumbel or Extreme Value 1 distribution
EV2	Frechet distribution
GCM	General Circulation Model
GEV	Generalized Extreme Value
GFDL	Geophysical Fluid Dynamics Laboratory
GHG	Greenhouse gas
GISS	Goddard Institute for Space Studies
GMSD	Ghanaian Meteorological Service Department
GNO	Generalized NOrmal
GPA	Generalized PAreto
GPCC	Global Preciptiation Climatology Centre
HadCM3	Hadley Centre Coupled Model, version 3
ICID	International Commission on Irrigation & Drainage
ICR	Indonesia Country Report
IDF	Intensity-Duration-Frequency
IPCC	Intergovernmental Panel on Climate Change
JJA	June, July, August
K-NN	K-Neareast Neighbour
LP3/LP(3)	Log-Pearson type 3 distribution

MAE	maximum absolute error
MIROC	Model for Interdisciplinary Research On Climate
MIT	Massachusetts Institute of Technology
MM5	Pennsylvania State University / National Center for Atmospheric Research mesoscale model
MPIM	Max Planck Institute for Meteorology
MRI/JMA	Japan and the Meteorological Research Institute of Japan Meteorological Agency
NASA	National Aeronautics and Space Administration
NCAR	National Center for Atmospheric Research
NCDC	National Climatic Data Center
NCEP	National Centers for Environmental Prediction
NCM	Non-central moments
NDJF	November, December, January, February
NOAA	National Center for Atmospheric Research (NCAR), the National Oceanic and Atmospheric Administration
P(3)/PE3	Pearson Type III
P90p	90^{th} percentile of daily rainfall
PGW	pseudo global-warming run
PPCC	probability plot correlation coefficient
PRECIS	Providing REgional Climates for Impacts Studies
PRUDENCE	Prediction of Regional scenarios and Uncertainties for Defining European Climate change risks and Effects
RCM	Regional Climate Model
REMO	Regional Climate Model developed by Max Planck Institute in Hamburg
RIHN	Research Institute for Humanity and Nature
RMSA	Root Mean Squared Anomaly

RMSE	Root Mean Squared Error
RRMSE	Relative Root Mean Square Error
SD	Statistical Downscaling
SDII	mean intensity per wet day
SEA	Southeast Asia
SO_2	Sulfur Dioxide
SRES	Special Report on Emission Scenarios
STARDEX	STAtistical and Regional dynamical Downscaling Extremes for European regions
TMSI	Tropical Marine Science Institute
TRMM	Tropical Rainfall Measuring Mission
UCAR	University Corporation for Atmospheric Research
UNFCCC	United Nations Framework Convention on Climate Change
VASClimO	Variability Analysis of Surface Climate Observations
WMO	World Meteorological Organization
WRF	Weather Research and Forecasting
WWF	World Wildlife Fund

LIST OF SYMBOLS

M_1, M_2 and M_3	Non-central moments
N_R	Mean number of rainy hours during a one-day period with rain
σ_O	Domain averaged mean of the observations
σ_M	Domain averaged mean of the modelled estimates.
$\bar{x}$	Mean
x_i	Each data value
N	Number of observations
S_N	Root Mean Squared Anomaly
$X_{Sim,i,j}$	Simulated values
$X_{Obs,i,j}$	Observed values
I_{max}	The expected extreme value for rainfall intensities
T	Return periods
k	Shape
μ	Location
σ	Scale parameters
Δ_i	Climate change factor (climate responses, 'simulated future rainfall intensities minus present day rainfall intensities'

This page is intentionally left blank.

CHAPTER 1 INTRODUCTION

1.1 BACKGROUND

The world is now facing the greatest environmental threat humanity has ever faced - “Climate Change” and the next few years is our last best chance to keep the extent of climate change and the global vulnerability within manageable limits. Climates are changing because our earth is warming, as stated, among others, in the research findings of the National Center for Atmospheric Research (hereafter, NCAR), USA (NCAR, 2003). According to the World Meteorological Organization (WMO), the annual average temperature for the globe between 1961 and 1990 was around 57.2°F (14.0°C) and in 2011, the WMO estimated that the global temperature was about 0.74°F (0.41°C) above long-term. The global mean surface temperature has increased by 0.76°C since pre-industrial times and the temperature rise is accelerating, as reported by the Intergovernmental Panel on Climate Change (hereafter, IPCC) (IPCC, 2007). It has been reported that we are likely to exceed a 1.6°C increase in global average temperature above pre-industrial levels; if we allow the increase to reach 2°C, we are likely to face irreversible effects with decreasingly effective and increasingly expensive adaptation options (Case et al., 2007; Cruz et al., 2007).

1.1.1 Global Climate Change

A deeper understanding and quantification of climate processes and their incorporation in climate models have progressed rapidly especially since the inception of the IPCC in 1988. There has always been uncertainty in understanding a system as complex as climate and climate change; but there is now stronger evidence that significant global warming is occurring. The amount of heat the earth absorbs is simply greater than it can bounce back into space, due to greenhouse gases (hereafter, GHG) already accumulated in the atmosphere, and increasingly, by the secondary impacts of climate change such as the melting of ice sheets.

The evidence of climate change comes from direct measurements of rising surface air temperatures, sub-surface ocean temperatures, and from phenomena such as increases in average global sea levels, retreating glaciers and changes to many other physical and biological systems. The existence of GHG in the atmosphere is indeed vital to life on earth as without their presence average temperatures would have been about 30°C lower than they are today. However, human activities are now causing the greenhouse gases in the atmosphere to increase well above pre-industrial level of about 275 ppmv (parts per million by volume). By July 2012, we are nearing 400 ppmv, according to the measurements taken at the Mauna Loa observatory in Hawaii, USA. Levels of GHG such as carbon dioxide (hereafter, CO_2), methane and nitrous oxide gases are rising, and CO_2 is being pumped into the atmosphere at a rate more than double of present levels. Increases in temperature and rising

of the sea level are expected well beyond the year 2100 even if the concentrations of GHG in the atmosphere were to stabilize now (Figure 1.1).

Under different IPCC GHG emissions scenarios, namely A1, A2, A1B, A1FI, A1FI, B1 and B2, (their detailed description can be found in Appendix A) which represent different possible socio-economic future worlds, it has been noted that, warmer global temperatures in the atmosphere and oceans lead to climate changes that affects rainfall patterns, worsens the severity of storms and droughts, alters growing seasons, expedites melting of ice sheets and influences changes in humidity and sea levels with major impacts on low-lying regions throughout the world. Simulations for each of the six IPCC GHG emission scenarios, A1B, A1FI, A1T, A2, B1 and B2, showed that by the end of this century, the global mean temperature increase—from the 1980–2000 levels—could reach nearly 4°C, with a range from 1°C to 6°C, with the other scenarios considered (

Figure 1.2) (IPCC, 2007a).

Figure 1.3 shows the different plausible CO_2 emission, CO_2 concentrations, sulphur dioxide (hereafter, SO_2) emission levels, temperature change and sea level rise under these scenarios. Although a warming trend is global, different areas around the world will experience different specific changes in their climates, which will have unique impacts on their local eco-systems and mankind. Figure 1.4 shows the equilibrium global mean surface temperatures (otherwise, climate sensitivity) from the different General Circulation Models (hereafter, GCM) for future climates under various scenarios of increasing GHG concentrations. For the next two decades a

warming of about 0.2°C per decade is projected for a range of Special Report on Emissions Scenarios (hereafter, SRES) emissions scenarios. Even if the concentrations of all GHGs and aerosols had been kept constant at year 2000 levels, a further warming of about 0.1°C per decade would be expected.

Increasing global temperatures, resulting from increased anthropogenic emissions of CO_2, will change the hydrologic cycle, which is likely to bring shifts in timing and magnitude of climate and hydrological variables' extremes (e.g. temperature, precipitation and stream flow). Changes in the frequency of hydrologic extremes are expected at many locations, possibly resulting in a combination of increased risk of spring time flooding and/or reductions in summer stream flow. Such projected changes in hydrologic extremes will have serious implications for planning, operation and design, for example, of water resources systems. Changing regional climate could also alter forests, crop yields; affect, for examples, landslides, coastal erosion, human health and bio-diversity.

Climate models show that the projected temperature increase ranges between 1.5°C and 4°C. At Massachusetts Institute of Technology (MIT), Emanuel (2011) mentioned that even though these projections contain uncertainty, this does not mean we should do nothing. Recent estimates by National Aeronautics and Space Administration (NASA)'s Goddard Institute for Space Studies (GISS) and the National Climatic Data Center (NCDC) show that 2005 and 2010 tied in place for the planet's warmest year since reliable, widespread instrumental measurements became available in the late

19th century, exceeding that of 1998 by a few hundredths of a degree (Cole and McCarthy, 2011; Hansen et al., 2006; NCDC, 2011). Another estimate by the Climatic Research Unit (hereafter, CRU) at the University of East Anglia, United Kingdom, shows 2005 as the second warmest year, behind 1998 with 2003 and 2010 in tie for third warmest year (Jones, 2011).

Climate change is a global problem and requires immediate attention to act. In the recent years, addressing climate change has been high on the international policy agenda. There is now a consensus that, to prevent global warming from reaching dangerous levels, action is needed to control GHG emissions and stabilize their atmospheric concentration within a range of 450 to 550 ppmv (IPCC, 2007a). Without such global actions, climate change impacts are likely to intensify in the decades to come. Increasing global mean temperature influences the hydrologic cycle where, with hydrologic change, more heavy precipitation events will occur at some places. In recent decades severe flooding events have been witnessed, in developing countries in particular, more frequently both in urban and less urban cities causing significant impacts on the economic, environments, infrastructures and human losses. The IPCC mentioned that there will be a significant increase in the number of heavy precipitation events and an increase in the number of tropical cyclones. This in turn will lead to sea level rise, massive flooding, landslides, and changes in ecosystems (IPCC, 2007b). Since these projected climate changes will impact water resources, agriculture, bio-diversity, energy, and health, one of the key challenges of climate research is the application of climate models to quantify future climate change and its impacts on both the

physical environment and the society through the employment of impact models (Hewitson and Crane, 1996).

In view of this, the challenge is to develop appropriate and effective adaptation strategies to mitigate climate change. While climate change will compound environmental and socio-economic problems, it is critical that all sustainable development policies and initiatives include climate change adaptation and resilience building. It has therefore become very evident that climate change is happening at an alarming rate and the society has the responsibility to act now (Case et al., 2007). Climate change and its impacts are and will probably continue to be one of the most important problems the world needs to deal with throughout this century.

Studying the impacts of climate change on hydrological regimes has become a priority area in both research and in water and catchment management strategies. Detailed regional climate scenarios that are used as input to hydrological impacts study may primarily be obtained from the coarse-scale output of GCMs. GCMs are the primary tools for the prediction of global climate. GCMs are true representation of the global circulation in the atmosphere, ocean, cryosphere and land surface. However, the raw outputs from GCMs are inadequate basis for assessing the effects of climate change on land-surface processes at regional scales. This is because the spatial resolutions of GCMs are too coarse to resolve important sub-grid scale processes (most notably, the hydrological cycle) and also for the same reason, the GCM output is often unreliable at individual and sub-grid box scales

(Wilby et al., 1999). Most hydrological impacts study needs to simulate sub-grid scale phenomenon and therefore require input data (e.g. precipitation) at similar sub-grid scale (normally much higher resolution). Therefore, GCMs are not well suited for studying regional-scale hydrological variability.

Giorgi (1990) mentioned that although GCMs represent the main features of the global atmospheric circulation reasonably well, their performance in reproducing regional climatic details, precipitation in particular, is rather poor, because of their coarse spatial resolution. Thus, due to their coarse spatial resolutions and their inability to include mesoscale atmospheric features in their large scale circulation, the GCMs do not simulate the precipitation fields with adequate fine scale details to be utilized for hydrological impact studies. This is particularly significant because simulating precipitation is a challenge, as it is one climate variable highly variable over space and time.

Hence, there is a great need for "downscaling" the GCM climate information to desired scales – regional or local. Of particular importance for the management of water resources systems are those procedures dealing with the linkage of the large-scale climate variability to the historical observations of the climate variable of interest (e.g., precipitation and temperature). If this linkage could be established, then the projected change of climate conditions given by a GCM could be used to predict the resulting change of the selected climate variables for hydrological impact studies. The required linkage can be developed using a different downscaling methods, of which the dynamical

downscaling is one which has gained much importance amongst the climate research community. Dynamical downscaling (hereafter, DD) methods using Regional Climate Models (hereafter, RCMs) have consequently been developed to bridge the gap between the coarse resolution of the climate model outputs and the need for climate variables at finer spatial resolution.

1.1.2 Obtaining High Resolution Climate Outputs through Dynamical Downscaling

The concept of downscaling implies that the regional climate is only conditioned but not completely determined by the state of a larger scale; there is an 'added value' expected when downscaling such large scale information to a regional or a local scale (IPCC, 2001). Some of the areas where this technique can enhance large scale information are: simulation of the spatial structure of temperature and precipitation in complex topography, land-use distribution, regional and local atmospheric circulations that include mesoscale connective systems, sea and land breeze effects and tropical storms (Giorgi, 1990). Some processes at high temporal frequencies include precipitation frequencies, surface wind variability, monsoon front onset and withdrawal and occurrences of extreme weather events (IPCC, 2001).

The need for regional scale information is also emphasized by the fact that climate projections with GCMs do not allow regional examinations such as water balances or trends of extreme precipitation due to their low spatial resolution. Downscaling of the global simulations to the regional scale

becomes necessary when local scale information is needed by impact models (IPCC, 2007a). This clearly applies to impact studies, say, in the case of studying the extreme events over a municipal water infrastructure, as most of the river basins and municipalities are smaller than the typical resolutions (~300 km) of the GCM; such sub-grid scale precipitation are not resolved by large scale models and need to be driven by high resolution data for better assessments of regional scale impacts.

There are two fundamental approaches for downscaling of large scale information to regional or local scales. The first is a statistical/empirical method which establishes relationships between large scale climate variables and local climates and the other is a dynamical method where a higher resolution climate model, widely known as a RCM, is driven using the GCMs' initial and lateral boundary conditions. The former technique is called 'Statistical Downscaling' (hereafter, SD) and the latter, 'Dynamical Downscaling'. The downscaling approach executed in this thesis is based only on DD. In this thesis, the focus is placed on areas with very short or no station data record (ungauged sites); DD's strength will, of course, first be demonstrated on its projection of current climate and compared with their counterparts at sites with long and reliable observation data records. Assessment of future climate and its applications then follow.

Note that: (1) DD method involves the extraction of regional scale information from large-scale GCM data and is based on the modeling of regional climate dynamical processes (described in detail in Chapter 3); and

(2) SD method, on the other hand, requires observational data at the location of interest to calibrate the statistical downscaling model. Thus, the SD method cannot be considered for sites with short or no station data record.

DD technique uses comprehensive physical models of the climate system and allows direct modeling of the dynamics of the physical systems that characterize the climate of a region. This technique employs RCMs which are climate models run at high spatial resolutions over a limited area of the globe. The minimum horizontal spatial resolution that is generally used for a RCM is around 25 km though slightly lower and higher resolutions RCMs are now used for climate modeling experiments (IPCC, 2007a). The present study deals specifically on the dynamical downscaling approach. The DD is performed on the Southeast Asian region with a particular focus over Jakarta region, using the RCM Weather Research and Forecast, commonly known as WRF. RCM WRF was run at 30 km to simulate the climate and physical processes in greater detail for a limited area of the globe, whilst drawing information about initial conditions, time-dependent lateral and surface boundary conditions from the global reanalyses data and GCMs. An overview of the RCM WRF is given in Chapter 3.

One of the main advantages of the dynamical downscaling techniques is that they provide high resolution information of climate variables derived from mesoscale atmospheric processes not resolved by GCMs. These RCMs provide as output multiple variables in a self-consistent manner and do not assume a fixed relationship between the variable of interest and the large scale

circulation. While the RCMs provide consistency with the large scales of their driving GCMs, the main disadvantages of RCMs are that they are computationally very time demanding and expensive and also inherit the large scale errors from the driving GCMs. The application of this DD technique for climate research has come to be known as Regional Climate Modeling, which is discussed in detail in Chapter 2.

The regional climate model simulated climate variables (e.g. precipitation and near surface air temperature) from the downscaled GCMs can subsequently be used as input for hydrological impacts studies. However, RCMs are inevitably subject to uncertainties which propagate through the hydrological scheme and eventually influence the study results. Uncertainties in regional climate simulations are potentially caused by a multitude of factors; the most important of which are missing or inadequate parameterisation of important sub-grid scale processes (e.g. convection), shortcomings of numerical methods used, choice of horizontal and vertical resolutions, uncertainties in boundary forcing, treatment of boundary forcing, choice of regional model domain (size and position) and internal model variability (Kotlarski et al., 2005). Therefore, it is strongly recommended to account for uncertainties in climatological input parameters e.g. by adopting an ensemble approach, i.e. carrying out multiple simulations using different or perturbed initial and lateral boundary conditions.

Ideally, several observational data sources should be utilised and biases should be calculated with respect to each single reference data source. Hence,

this would mean that an assessment of climate model uncertainties have to be made and its suitability in driving impact models be addressed. This would be one of the prime factors that need to be considered for developing climate change scenarios, especially for those regions which suffer from paucity of observed records.

1.2 CLIMATE CHANGE -- VULNERABILITY OF SOUTHEAST ASIA REGION

While climate change is a dominant global issue, it is also one of the most significant challenges confronting the Southeast Asian (SEA) region in the 21st century (Asian Development Bank, ADB, 2009) (hereafter, ADB). Climate change is already affecting the region. SEA, as a tropical region, has endured climate extremes that include the monsoon, tropical cyclones, El Nino and La Nina events, extreme variability in rainfall and very high temperatures. According to the report published by Asian Development Bank (ADB, 2009), further climate change is likely to make these conditions more acute and challenging with regard to the physical impact on people, their livelihoods and the environment as a whole. Several countries in Southeast Asia are very vulnerable to climate changes and have the least capacity to adapt themselves to the changing climate (Francisco, 2008). Also, Southeast Asian region has fewer resources to adapt socially, technologically and financially, wanting international assistance to support adaptation measures in the context of national planning for sustainable development, more capacity building and

transfer of technology and funds (United Nations Framework Convention on Climate Change, UNFCCC, 2007).

Apart from the social conditions, the economic conditions of many countries are such that it will be very hard for them to invest on the necessary mitigation measures. Over the last 50 years, the average temperature in Southeast Asia has increased at a rate of 0.1°C to 0.3°C per decade and the sea level has risen by 1 mm to 3 mm each year (ADB, 2009). According to the latest Assessment Report from the IPCC (IPCC, 2007a), for Southeast Asia, the increase in temperature is likely to be similar to the global trend showing an increase in the mean surface temperatures. The frequency and intensity of extreme weather events have also increased in recent decades. This includes more heat waves (such as increases in the number of hot days and warm nights and decreases in the number of cold days and cold nights); a significant increase in the number of heavy precipitations events; and an increase in the number of tropical cyclones (Meehl et al., 2007). It has also been projected that precipitation in boreal winter is very likely to increase in the southern parts of Southeast Asia while precipitation in summer is likely to increase in most of Southeast Asia. Furthermore, extreme rainfall and winds associated with tropical cyclones are also projected to increase in Southeast Asia (Figure 1.5). These climatic changes have led to massive flooding, landslides, and droughts in many parts of the region, causing extensive damage to property, assets and human life. Climate change is also exacerbating water shortages in many areas, constraining agricultural production and threatening food security, causing forest fires and degradation, damaging coastal and marine resources,

and increasing the risk of outbreaks of infectious diseases (ADB, 2009). Figure 1.6 shows annual flood frequency for SEA regions. The figure shows that Jakarta, Bangkok and southern Vietnam have high annual flood frequency. If climate change is not adequately addressed, it could seriously hinder the region's sustainable development and their preparedness to face the impacts.

Southeast Asia region is also likely to share the general tendency for daily extreme precipitation to become more intense under enhanced greenhouse conditions, particularly where the mean precipitation is projected to increase. The northern part of the Southeast Asian region is likely to be affected by any change in tropical cyclone characteristics and there is evidence in general of likely increases in tropical cyclone intensity, but less consistency about how occurrence will change (Walsh, 2004; IPCC, 2007a).

A study conducted in 2009 by Economy and Environmental Program for Southeast Asia (hereafter, EEPSEA) (Yusuf and Francisco, 2009) has identified regions in Southeast Asia which are most vulnerable to climate change (Figure 1.7). The scale used is 0-1 indicating the lowest vulnerability level (0) to the highest vulnerability level (1). The Indonesia, Philippine, Thailand and Vietnam are likely to suffer more from climate change than other regions, in terms of increased frequency and intensity of extreme weather events, declining crop yields, loss of rich forests, damage to coastal resources, increased outbreaks of diseases, and associated economic losses and human suffering. The Southeast Asian regions especially have a high stake in taking action against climate change (ADB, 2009). In the overall assessment,

however, Jakarta (Indonesia) comes out as the top most vulnerable regions in SEA. This is because Jakarta is at the intersection of all the climate-related hazards, except tropical cyclones. It is frequently exposed to regular flooding but most importantly, it is highly sensitive because it is among the most densely-populated regions in SEA (Yusuf and Francisco, 2009).

The focal city of this study is Jakarta, the capital of Indonesia. The study is quite challenging as Jakarta's hydrological data record is quite poor, in both quantity and quality. According to Manton et al. (2001), for Indonesia, appropriate rainfall data do not exist from before 1960 and homogenous temperature data were not available for the study. "Good data = good science" and hence the lacking of data in Jakarta is a big challenge in any study because model results cannot be verified. Furthermore, this data sparse metropolitan city has been experiencing frequent flooding annually. The worst event in the recorded history of Jakarta was in February 2007 where 70% of the city was seriously inundated with some areas up to 7 m.

1.2.1 Study Site – Jakarta, Indonesia

As indicated in the earlier section, in the context of understanding climate vulnerabilities in Southeast Asia, this thesis focuses on one of the highly vulnerable locations in Southeast Asia - Jakarta, Indonesia.

Indonesia is an archipelago located between two oceans, the Pacific and Indian, and two continents, Asia and Australia. The whole territory

consists of 13,677 islands of which about 6000 are uninhabited. About 70% of its 190 million populations live on Java, its fifth largest island. Indonesia lies between 95^{o} and 141^{o} East and between 6^{o} North and 11^{o} South. Yearly rainfall varies widely between 700 mm on central parts of Timor to 7,000 mm on western parts of Java, while yearly evapotranspiration is between 1,200 mm and 1,400 mm (Framji et al., 1982).

The study site, Jakarta, is the capital and the largest city of Indonesia. Jakarta is centered at the coordinates of about 6° 15'S and 106° 50'E, covering an area of 662 km^2. Over the last half century, the city population rose rapidly from 2.7 million in 1960 to 9 million in 2007 (Badan Pusat Statistik (hereafter BPS) Jakarta, 2007). At present, Jakarta has a registered population size of about 10 million people. Figure 1.8 shows the location of Jakarta, and its catchment area, located on the northwest coast of Java at the mouth of the Ciliwung River, the largest among 12 rivers crossing the city. Its official metropolitan area, called Jabodetabekjur (area of about 1,500 km^2), is the sixth-largest in the world with over 28 million population (BPS Jakarta, 2010).

Jakarta's tropical climate is characterized by year-round high temperatures of 24°C to 33°C. Long-term mean annual rainfall in Jakarta area is between 1,500 mm and 2,500 mm (Tambunan, 2007). The monsoonal climate brings very intense rainfall each rainy season (typically between the months of October and April). The highest observed precipitation total for a single month in Jakarta is more than 800mm (Connecting Delta Cities (hereafter, CDC), 2009).

The topography of Jakarta varies, with the northern part just meters above current sea level and lying on a flood plain; some parts are lower than sea level due to heavy groundwater pumping over decades (for water consumption) which is rampant in Jakarta. The southern part of the city is hilly. In addition to the Ciliwung River, there are about 12 other rivers that drain the hilly southern part of the city into the sea. The Ciliwung River is the most significant river and divides the city west to east. River floods occur mainly during the rainy season, as extreme rainfalls in the city and/or in the mountainous upstream regions (Bogor in particular) lead to the overflowing of drainage systems, causing large-scale inundations in many parts of the city, including public facilities and roads (CDC, 2009).

Besides these hydrological reasons, the flood problem is worsened by population pressure and socio-culture problems. In this metropolitan city, there are many communities which are unplanned and are occupied by squatters and illegal settlements with no infrastructure for waste disposal. Wastes are washed into drainage ways and hypothesized to cause increased flooding due to clogging of drainage. The site is therefore "naturally" highly prone to both coastal and riverine flooding such as that experienced in 1996, 2002 and 2007 (Texier, 2008). The flood of February 2007 was the worst in the history of Jakarta; almost 70% of the urban area was affected (Pakeh et al., 2007). Recent floods, such as the flood of 2007, can partly be explained by the inadequate drainage design capacity of the sewage system. Thus, the assessment of extreme precipitation is an important problem in hydrologic risk analysis and design. This is also why the evaluation of rainfall extremes, as

embodied in the Intensity-Duration Frequency (hereafter, IDF) relationship, has been a major focus particularly in stormwater infrastructures design.

An another study done by World Wildlife Fund (hereafter, WWF) on climate change effects impacting 11 major coastal cities in Asia showed that Jakarta ranked second as most vulnerable to climate change impacts, largely because of the low lying areas, densely populated, significant flooding and landslides and relatively low adaptive capacity (Figure 1.9). Climate change has and will continue to have impacts on Indonesia. The wet season in Jakarta has become wetter and therefore the city experiences more severe flooding; this is compounded by clogged sewage pipes and waterways, many non-functional gates and pumping systems, and the fact that much of the city is near, at, and/or below sea level (WWF, 2009).

As stated in the Indonesia Country Report (hereafter, ICR) (ICR, 2007), extreme weather and climate events cause serious floods, drought and wild fires in Indonesia. These events have caused serious impact on Indonesian economy and human living. Wild fire occurred in El-Nino 1997 has caused huge economic loss and damaged people's livelihoods – increasing poverty rates by one-third or more. Drought occurred in 1972 has also impacted millions of people. Flood occurred in early February 2007 which lasted for about 22 days also affected thousands of people and destroyed about 1,500 houses. Flood hazards have become common in many part of Indonesia regions. In the period 2001 to 2004, about 530 floods were reported, occurring in almost all provinces. The scale of damage has also been increasing. This

country report is one of important references that provide information on impact of climate variability and climate change on a number of major sectors in Indonesia.

According to Soehodho (2011), Jakarta's Deputy Governor, Jakarta is grappling with the impacts of climate change on lower-income populations. The city's poor are often disproportionately affected by catastrophic weather events like floods. Furthermore, Jakarta generally lacks in proper rainfall and runoff records. This leads to inadequate design of the water resource infrastructure systems. Under changing climate, potential shifts in extreme rainfall at the local level demand revisions of the existing water infrastructure management regulations as well as changes in drainage design practices.

Jakarta, as a metropolitan city, is probably the best example of how challenging it is to attempt to lower the risk of flood catastrophy. With changing climate it is of paramount importance to study whether Jakarta will experience more intense rainfall. Increase in projected rainfall intensities require the derivation of future rainfall IDF curves and incorporated in the code of practice for future drainage design.

1.2.2 Data Scarcity Problems in Study Region

The use of simulation modeling approaches to evaluate how the systems respond to historical climates and how the systems will respond to change in management practices has been widely applied. This approach requires long

records of historical daily climatic data as well as reliable information on impacts of past and present variable climates (ICR, 2007). However, in most developing countries, historical records of daily climate data are not well maintained (Boer and Faqih, 2004).

The availability of geographical and climatological data, with emphasis on rainfall information, is often more critical than the choice of complexity of the hydrological model used for the success of a model application (Gan et al., 1997). Accurate estimation of rainfall is the primary requirement for hydrological modeling. Predictions from rainfall–runoff models are often unsatisfactory because spatial variability in rainfall is poorly represented in regions where data are scarce; furthermore the catch of conventional raingauges is representative of only a small radius around the instrument. Current raingauge networks are often too sparse to measure rainfall with adequate spatial and temporal scales, especially for heavy convective storms. Furthermore, floods are more destructive over tropical river basins that lack adequate surface stations necessary for real-time rainfall monitoring, i.e., the ungauged river basins (Hossain and Katiyar, 2006). Nevertheless, flood prediction is becoming ever more challenging in these medium-to-large river basins due to the systematic decline of in situ rainfall networks world-wide. The gradual erosion of these conventional rainfall data sources has lately been recognized as a major concern for advancing hydrologic monitoring, especially in basins that are ungauged or already sparsely instrumented (Shikhlomanov et al., 2002; Stokstad, 1999). For more

detailed monitoring of extense areas, a dense raingauge network is needed (Collischonn et al., 2008).

Flood estimation at a catchment scale is important for many hydrological applications. A key factor for accurate flood estimates is accurate rainfall intensities of various frequencies and durations for input in hydrologic design and risk analysis. The relation between these three components, storm intensity, storm duration and storm return interval, is represented by a family of curves called the IDF curves. In engineering practice, IDF curves are used to determine rainfall intensity a storm sewer must be able to handle. This is also why the evaluation of rainfall extremes, as embodied in the IDF relationship, has been a major focus particularly in stormwater infrastructures design.

The IDF curves are commonly used in the design of urban infrastructure such as culverts and stormwater drainage systems. It provides information on the frequencies of rainfall extremes of various intensities and durations

Thus, the objective of this thesis is to propose an approach to derive the present and future IDF curves for sites with very short or no station data record. This thesis will demonstrate how both the present and future IDF curves are derived through data resulting from DD. The resulting IDF curves are immensely important to policy makers in the climate change related adaptation measures.

1.2.3 Impacts of Climate Change on Hydrology

The tremendous importance of water in both society and nature draw attention to the necessity of understanding how a change in global climate could affect the availability and variability of regional water resources. From global and regional climate simulations summarised in the actual climate changes assessment report (IPCC, 2007), it can be expected that climate change will affect the hydrological cycle in many regions of the world. The hydrological changes, mainly driven by changes in patterns of precipitation and temperature, will affect surface as well as groundwater and other components of the hydrological cycle such as soil moisture and evapotranspiration. There have been many studies of climate change effects on hydrology and water resources which usually consists of three steps: (1) the development and use of general circulation models (GCMs) to provide future global climate scenarios under the effect of increasing GHG (2) the development and use of downscaling techniques (both RCMs and statistical methods) for "downscaling" the GCM output to the scales compatible with hydrological models and hydrological impacts study, and (3) the development and use of hydrological applications to simulate the effects of climate change on hydrological regimes at various scales (Xu et al., 2005).

In this context of changing climate, one major common impact that is likely to affect several regions in Southeast Asia is the water resources. With water scarcity problems on one hand and flooding threats on the other, it becomes a high priority to understand and address the issues to these

hydrological impacts. Extreme events like La Nina and tropical cyclones have brought heavy and intense rainfall in Southeast Asia, resulting in excessive runoff on already fragile ecosystems (due to poor land-use planning, law enforcement, unsustainable use) that cause massive flooding, landslides, severe erosion of river banks, and sedimentation. The effects of future climate change on hydrological cycle and hydrological system such as changing rainfall pattern and intensity is less understood and requires detailed modeling.

Climate change is also likely to result in a significant increase in the intensity and frequency of extreme precipitation events in many regions. Rainfall intensities of various frequencies and durations are the basic inputs in hydrologic design and risk analysis. The IDF curves provide information on the frequencies of rainfall extremes of various intensities and durations. The IDF curves are used in the design of urban infrastructure such as culverts and stormwater drainage systems. The estimation and use of the IDF curves are based on the rainfall stationarity hypothesis, i.e., extreme rainfall intensities and frequencies remain unchanged over time (Mailhot et al., 2007). However, climate change signals have shown significant increase in rainfall intensities and frequencies in many regions. As a result, a revisit of the existing IDF is called for to re-examine the adequacy of the current drainage system and capacity to meet the projected future rainfall extremes.

For data sparse sites, developing IDF is a challenge for both present and future climate. Jakarta, for example, though it has a sizable number of raingauges, the quality of the data is very much in question in addition to their

short and/or not continuous data record. The present day's IDF curves often cannot be developed from such data record. A novel approach is presented in this thesis to develop the present and future IDF curves using output from DD of a high spatial resolution RCM. Optimal mitigation measures can only then be taken when projected future rainfall is derived from high resolution RCM.

1.3 INTENSITY – DURATION – FREQUENCY CURVES UNDER CHANGING CLIMATE

The aims of the study are twofold. Firstly, this study proposes an approach to develop, both present and future, IDF curves for sites where short or no station data record is available; thus, no IDF curves exist. Obviously the approach will first be tested on site(s) where IDF curves for current climate exist. The IDF curves are derived from a simulation of a RCM which downscales a global reanalysis data. It is widely known that precipitation is the most difficult variable of all the climate variables to simulate. Secondly, the development of future IDF curves is presented from a RCM which downscales a GCM under the IPCC emissions scenarios.

The study then proceeds to demonstrate the proposed approach in developing IDF curves for sites such as Jakarta where there is short or no rainfall record (ungauged sites). The development of present and future (21st century) IDF curves is done by incorporating projections of climate change derived from dynamical downscaling. Details of the approach are presented later in Chapter 5.

Through dynamical downscaling method using RCM, extremes can be analyzed and thus future IDF curves (2011-2040, 2041-2070 and 2071-2100) can also be derived. IDF curves under different future climate scenarios (e.g. A1FI, A2 and A1B) are developed in the study. These will provide policy makers and practitioners in Jakarta immensely relevant information in their mitigation planning and measures.

1.4 OBJECTIVE AND SCOPE OF STUDY

The main aims of the present study are to perform dynamical downscaling and to develop the present and future IDF curves (under different emission scenarios) for Darmaga Station (in Jakarta) where rainfall data records are short and/or not continuous. More specifically, the objectives of this research are:

a. To downscale regional climates at high spatial resolution (30 km), for Southeast Asia, using a state-of-the-art Regional Climate Model WRF.

b. To determine the climate responses (temperature, winds and precipitation) over the study region, Jakarta inclusive, simulated by RCM driven by different GCMs and emission scenarios (A1B, A2 and A1FI) for the 21st century.

c. To present a novel approach in deriving present IDF curves for sites with very short or no rainfall records (ungauged sites), e.g. for Jakarta,

using downscaled output from RCM. To lend the concept its credibility, the approach will first be applied to three sites (Singapore, Kuala Lumpur and Jakarta Meteorological Stations) which have their existing IDF curves.

d. To develop future IDF curves (periods: 2011-2040, 2041-2070 and 2071-2100), for Jakarta, using different GCMs under A1B, A2 and A1FI emission scenarios. The future IDF curves are essential for policy-makers to create appropriate and effective adaptation strategies/measures to address climate change and its impacts.

1.5 STRUCTURE OF THESIS

This thesis consists of six chapters and the contents of subsequent chapters are briefly described below:

a. Chapter 2 presents reviews of the literature on climate modeling and climate hazards, particularly flooding, for the study region. The review includes research studies related to different GCMs, downscaling methodologies, the derivation of IDF curves for ungauged sites, the applications of downscaled outputs for derivation of IDF curves and finally the review of future IDF curves under different emission scenarios for climate change adaptation and impacts studies.

b. Chapter 3 introduces the overall research methodologies, data sets, climate models considered in this study.

c. Chapter 4 discusses the dynamical downscaling of RCM WRF driven by re-analysis data and different GCMs; analysis of projected trends of key climate variables (e.g. temperatures, winds and precipitation). Also presented in the chapter are future climate responses over study region.

d. Chapter 5 presents the novel approach to develop both the present and future IDF curves for data sparse sites such as the Darmaga Station (in Jakarta). Proof-of-concept of the proposed approach is first applied on sites with IDF curves (Singapore, Kuala Lumpur and Jakarta Meteorological Stations), to assess the quantities of the required bias correction; with which IDF curves at the ungauged basin is then derived. Chapter 5 also presents how projected changes in rainfall are reflected in the development of future IDF curves. The results of the present and future IDF curves for Darmaga Station are then presented.

e. Chapter 6 summarizes the main findings of work conducted in this thesis and proposes future work.

This page is intentionally left blank.

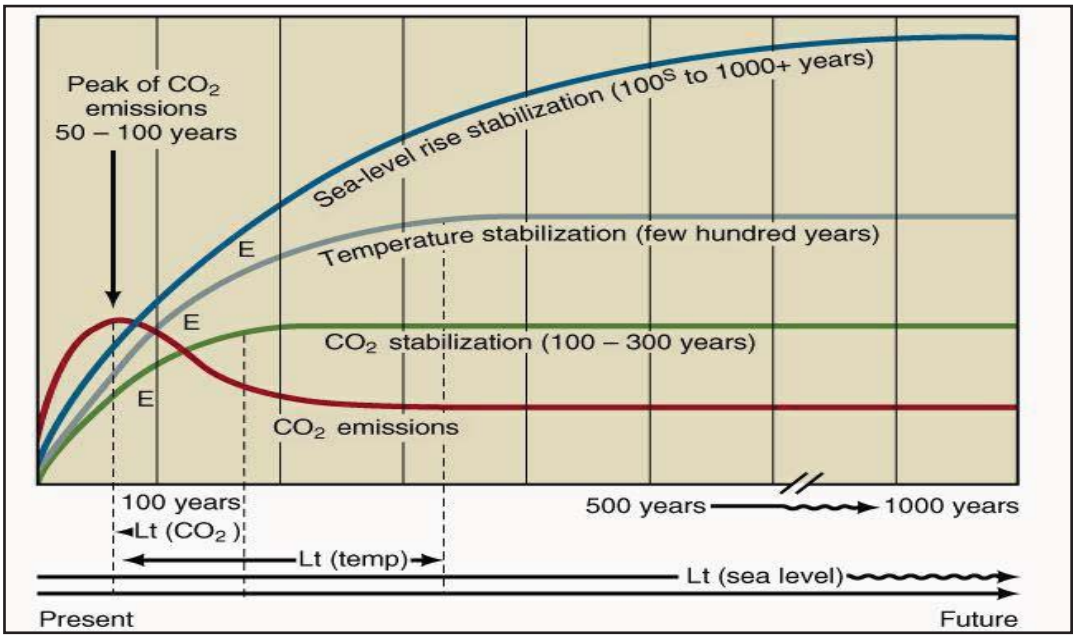

Figure 1.1: CO_2 concentrations, temperature and sea level continue to rise long after emissions are reduced
[Adapted from IPCC, 2007a]

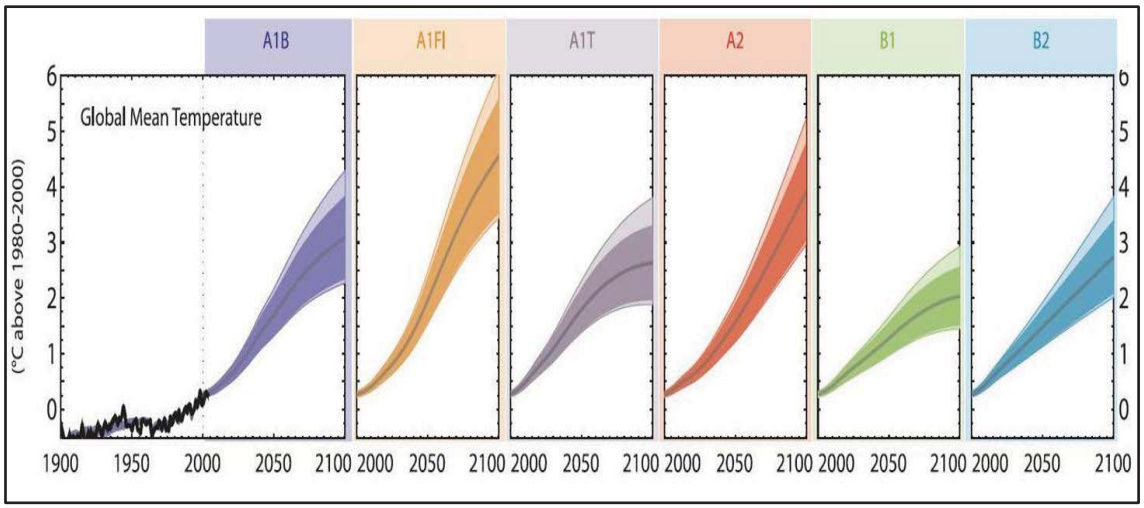

Figure 1.2: Multi-model means of surface warming as predicted by different GCMs for the IPCC emission scenarios A1B, A1FI, A1T, A2, B1 and B2. The values beyond 2100 are for the stabilization scenarios
[Adapted from IPCC, 2007a]

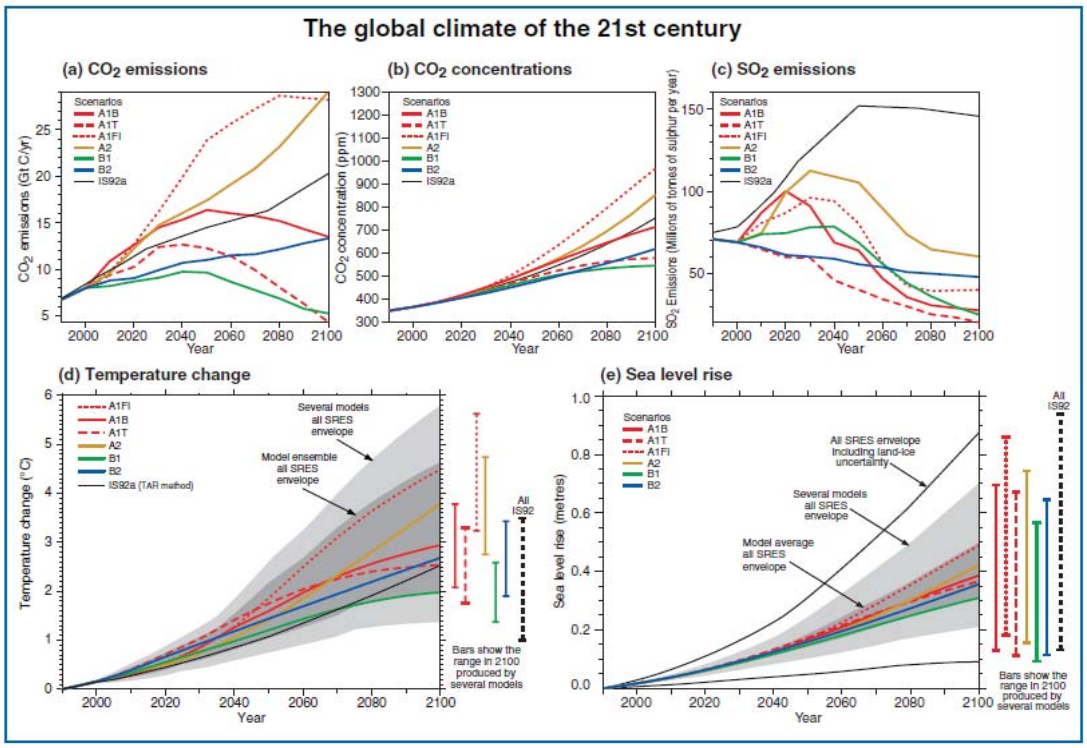

Figure 1.3: The global climate of the 21st century will depends on natural changes and the response of the climate system to human activities
[Adapted from IPCC Third Assessment Report of Working Group 1, 2001]

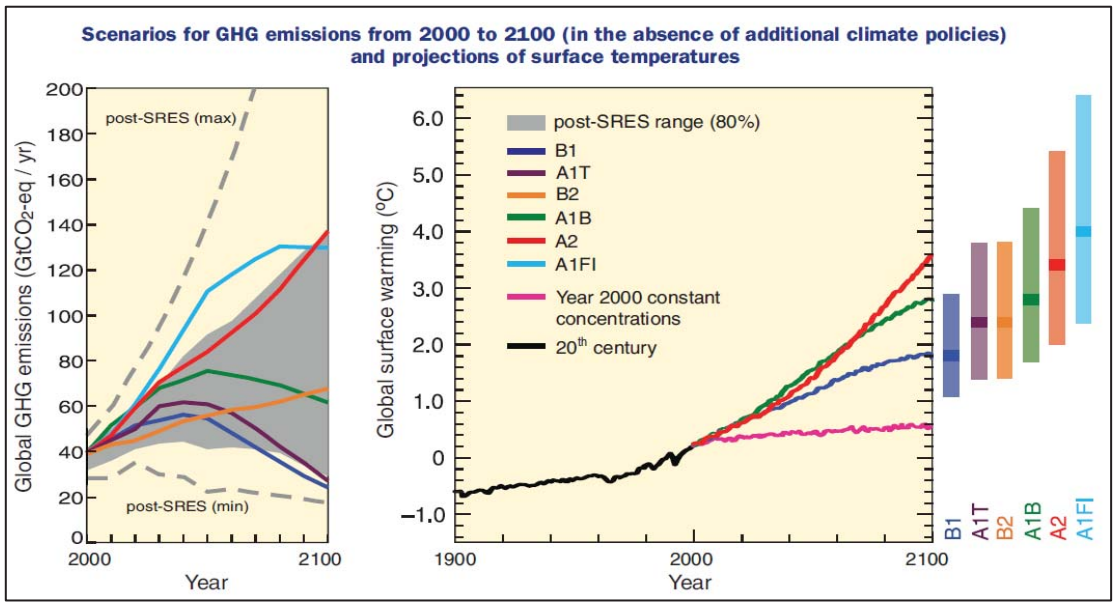

Figure 1.4: Continued GHG emissions at or above current rates would cause further warming and induce many changes in the global climate system during the 21st century that would very likely be larger than those observed during the 20th century
[Adapted from IPCC Climate Change 2007: Synthesis Report, 2007]

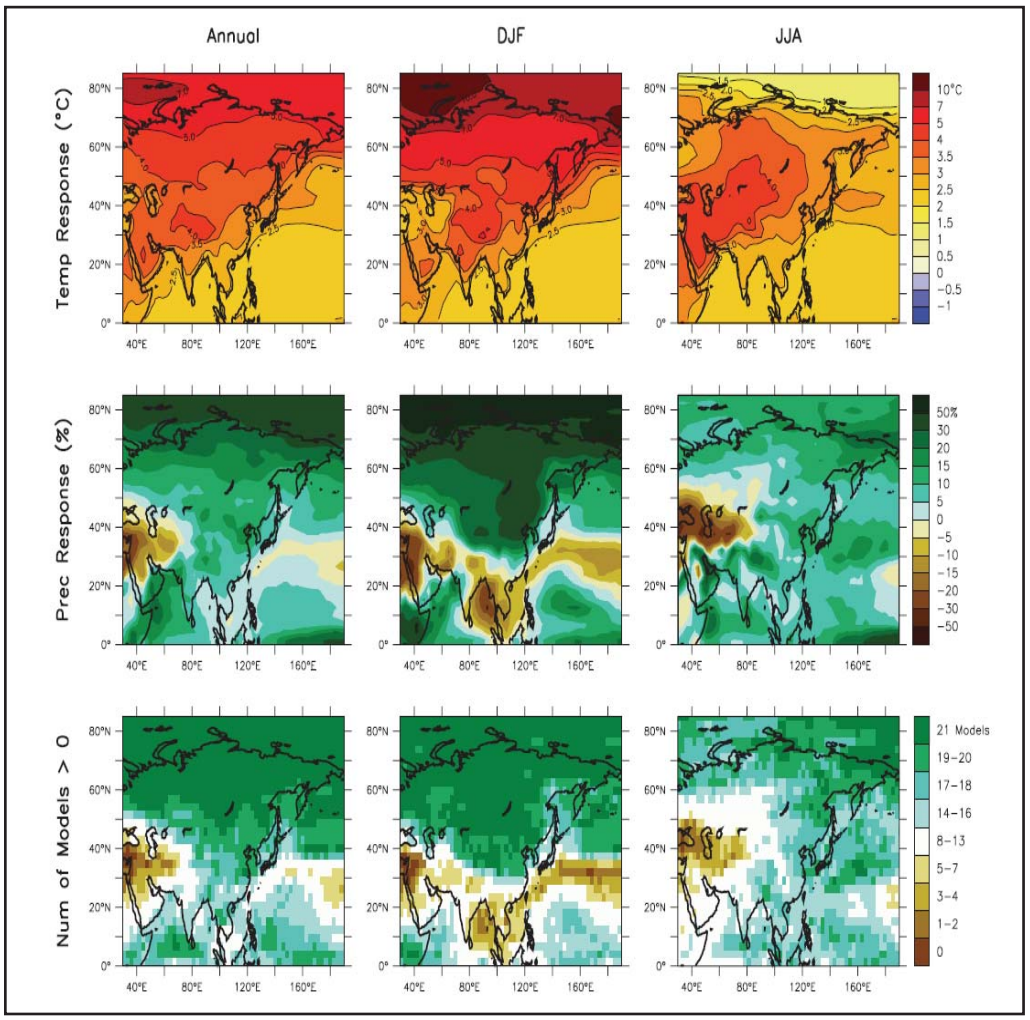

Figure 1.5: Temperature and precipitation changes over Asia from Multi Model Dataset (MMD)-A1B simulations
Top row: Annual mean, DJF and JJA temperature changes between 1960 to 1999 and 2080 to 2099, averaged over 21 models.
Middle row: same as top, but for fractional change in precipitation.
Bottom row: number of models out of 21 that project increases in precipitation
[Adapted from IPCC, 2007a]

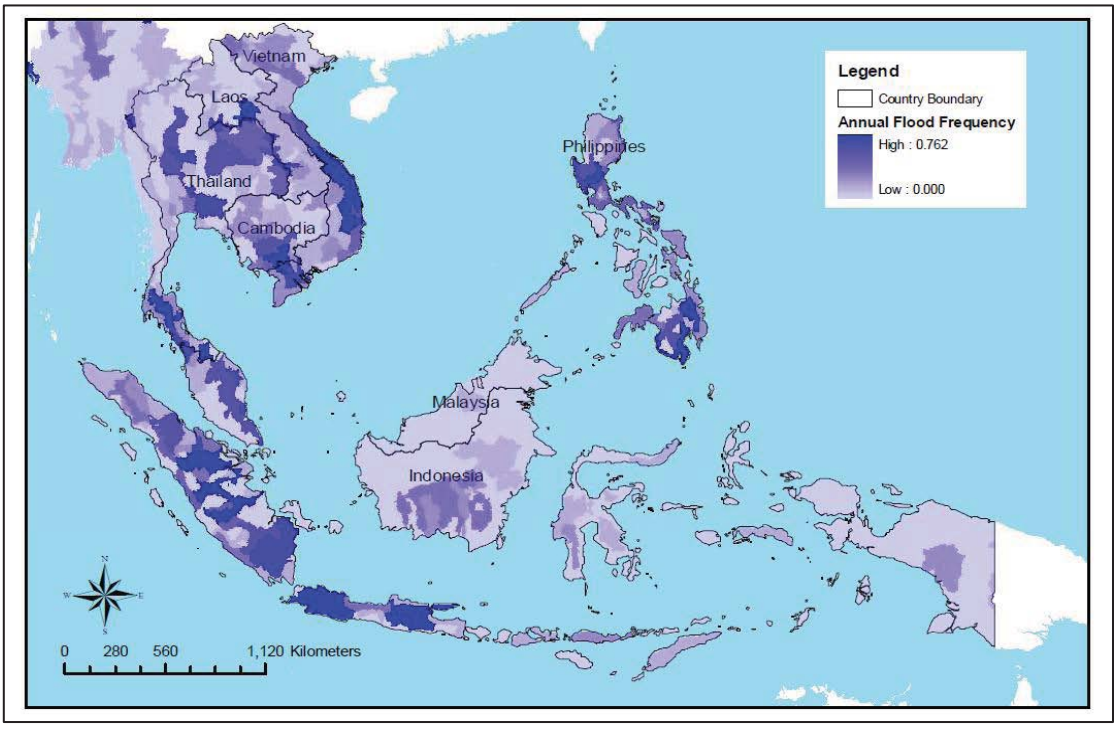

Figure 1.6: Annual flood frequency (event per year from 1980-2001)
[Adapted from Economy and Environmental Program for Southeast Asia (EEPSEA), Yusuf and Francisco, 2009]

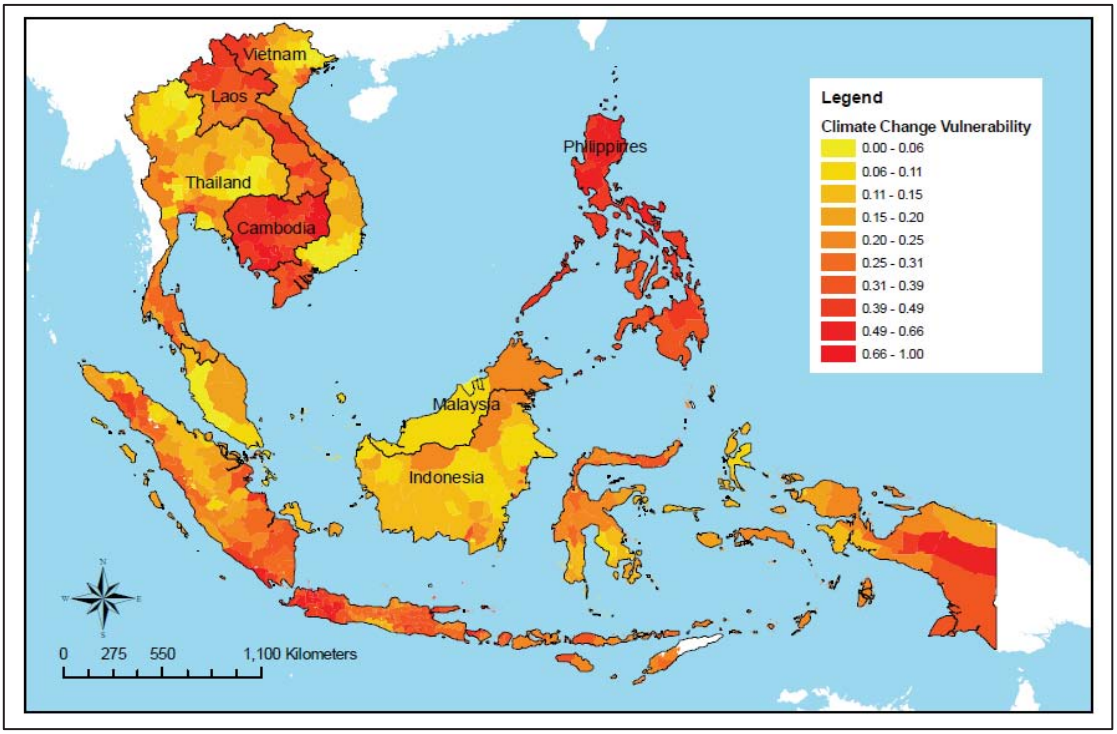

Figure 1.7: Climate change vulnerability map of Southeast Asia
[Adapted from Economy and Environmental Program for Southeast Asia (EEPSEA), Yusuf and Francisco, 2009]
Note: For the legend, the scale used is 0-1 indicating the lowest vulnerability level (0) to the highest vulnerability level (1).

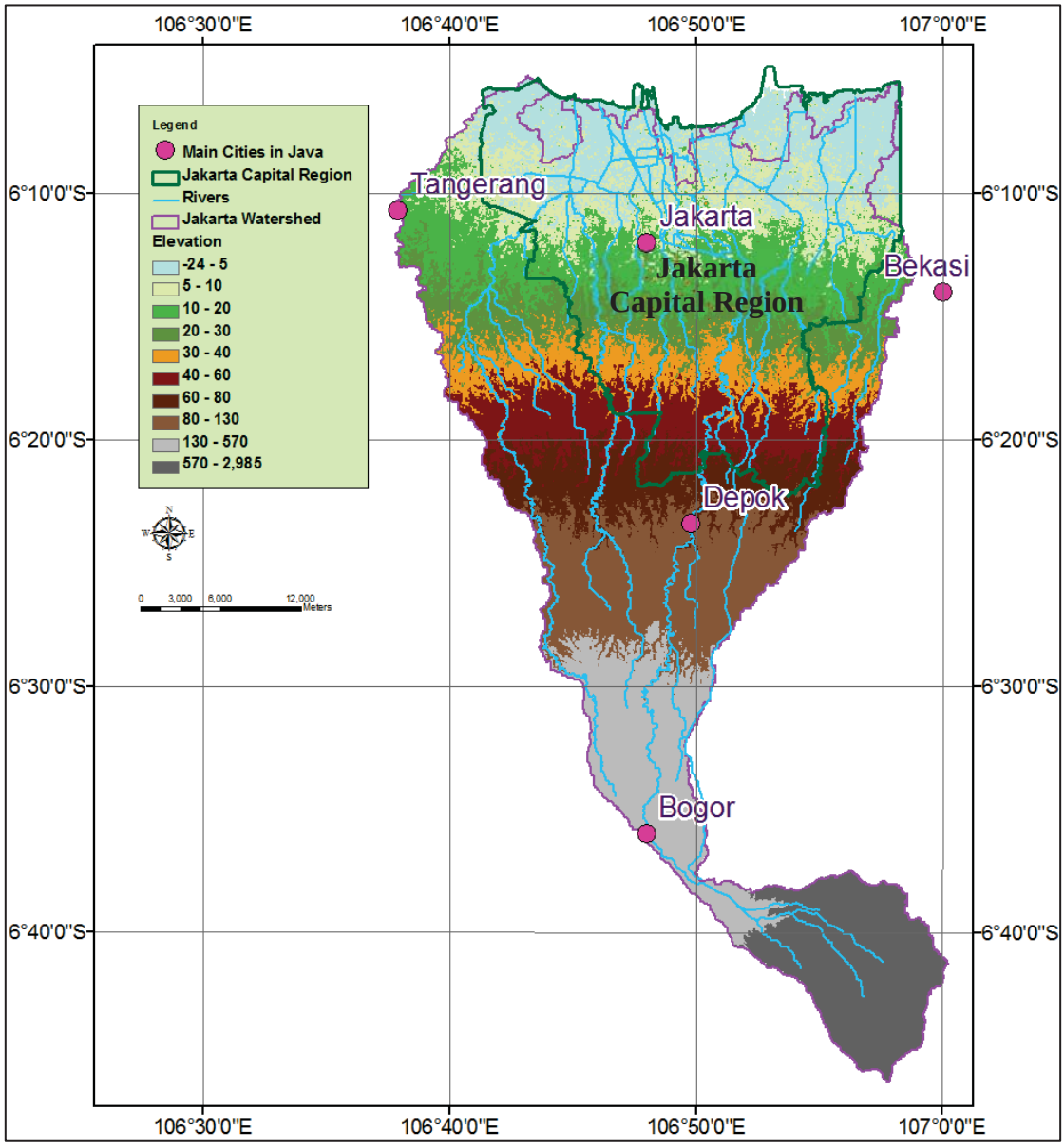

Figure 1.8: Map of watershed and the rivers crossing through Jakarta region

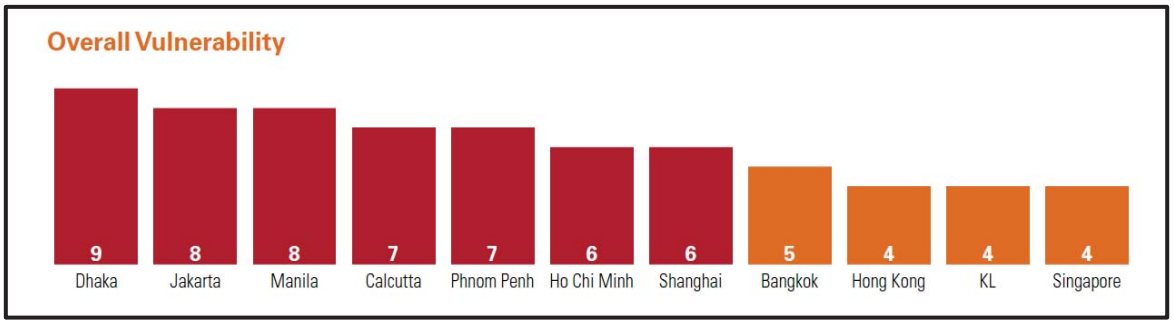

Figure 1.9: Overall climate vulnerability ranking among some Asian cities [Adapted from WWF, 2009]

This page is intentionally left blank.

CHAPTER 2 LITERATURE REVIEW

2.1 INTRODUCTION

In the IPCC's Fourth Assessment Report (AR4), projections of future climate are based on a broader range of global climate models, whose findings have confirmed that substantial warming is expected during the 21st century. Over the next two decades, the earth is projected to warm at about 0.2°C per decade. It has already been mentioned earlier than an assessment done by the Economy and Environmental Program for South East Asia (EEPSEA), an institute based in Singapore, stated that Indonesia, Philippines, Cambodia and Vietnam are likely to suffer more from climate change than other regions (Chapter 1, Figure 1.3). According to the IPCC (2007) projections, the mean surface air temperature in Southeast Asia is likely to increase between 0.75°C to 0.87°C by 2039, 1.32°C to 2.01°C by 2069 and 1.96°C to 3.77°C by 2100, depending on which emission scenario is likely to happen (Table 2-1). Climate change and associated impacts on human society have drawn considerable concerns from academic circles, public and governments (Zhang et al., 2010). Labat et al. (2004) indicated that the global warming has led to alterations to the global hydrological cycle and increased amplitude in the global and continental runoff has occurred. Higher air temperatures result in higher evaporation rates, higher atmospheric water vapour content and consequently, an accelerated hydrological cycle (Zhang et al. 2008a, b; Xu et al. 2006; Menzel and Burger 2002). Among the most significant potential

consequences of regional climate change are alterations in regional hydrological cycles and subsequent changes in river regimes.

With the introduction to the science of climate change and the concept of downscaling in Chapter 1, this chapter extends discussions on hydrological responses to global climate change, earlier studies that have been carried out for downscaling techniques, impact studies of climate change, introduces the proposed study site and also the development of rainfall Intensity-Duration-Frequency (IDF) curves for ungauged sites in this research work.

2.2 USE OF GLOBAL CLIMATE MODELS IN REGIONAL CLIMATE STUDIES

General Circulation Models, also known as Global Climate Models are the primary tools for the prediction of global climate. GCMs are mathematical representations of the global circulation in the atmosphere, ocean, cryosphere and land surface. Few studies (Sailor et al.; 2000; Charles et al., 1999; Giorgi, 1990) have mentioned that although GCMs represent the main features of the global atmospheric circulation reasonably well, their performance in reproducing regional climatic details is rather poor due to their coarse spatial resolution. GCMs provide reasonable simulation accuracy of present-day climate in a global, hemispheric or a continental scale but at a regional scale representation, the simulation accuracies are poor. The fact that the multimodel climate sensitivities have a large range is due to the uncertainties

associated with different GCMs in terms of their model physics, dynamics and internal model errors (Giorgi, 1990).

The application of GCM output in regional studies has the advantage that the simulated climate is internally and physically consistent (according to the physics represented in the model). In particular, simulated climate of a given region is consistent with that simulated for all other regions – a desirable property in general, but also valuable when regional climate is to be analyzed and compared across a number of regions. This consistency is not always preserved when downscaling techniques are applied. However, according to Whetton (2001) there are disadvantages in using GCM data in regional studies. GCMs show some simulation biases at continental and broader scales and more significant biases at regional (sub-continental) and finer scales. Climate features of a spatial scale of less than 200-300 km cannot be represented at all. GCMs are not well suited for answering the question for primary interest to hydrologists concerning regional-scale hydrologic variability. Due to their coarse spatial resolutions and their inability to include mesoscale atmospheric features in their large scale circulation, the GCMs do not simulate the precipitation fields with adequate fine scale details to be applied to impact models such as hydrological models. It should be emphasized again that some of the catchments are smaller than a GCM grid box. According to Xu (1999), GCMs operate on large spatial scale, and, furthermore, as the GCM-simulated temporal resolution corresponds to monthly averages at best, the direct usefulness of GCM output in impact studies and other applications is limited (Xu, 1999). In addition, the occurrences of extreme rainfall events and some

extreme weather systems such as tropical cyclones cannot be adequately represented at the spatial resolution of a GCM. Detailed climate studies at regional and sub-regional scales demand realistic simulated climate information at very fine spatial scales.

The deficiency of GCMs in providing detailed regional hydrological scenarios has been discussed in many studies including IPCC (2001), Xu (1999) and Schulze (1997). The major problem is the too coarse scale of the GCM estimates precipitation with large errors. GCMs, typically, are run at relatively coarse spatial resolutions of about 200 km to 450 km. The direct result of the poor spatial resolution of GCMs is a serious mismatch in the spatial scales between the available climate forecasts and the scale of interest to most climate forecast users. Some applications also require climate information at higher temporal resolution (Sun and Ward, 2006).

Study carried out by Andersson et al. (2006) in the Okavango River has laid the foundation for the use of scenario modeling as a tool for integrated water resource management in the Okavango River Basin. Four GCMs, namely Hadley Centre Coupled Model, version 3 (HadCM3), Center for Climate System Research/National Institute for Environmental Studies (CCSR/NIES), Canadian Climate Centre for Modelling and Analysis (CCCMA) and Geophysical Fluid Dynamics Laboratory (GFDL) with present day climate conditions and future climates under the A2 IPCC emission scenario were applied in this study. Results showed that there was considerable uncertainty about the magnitude and direction of future discharge

response associated with both the GCM and the IPCC emission scenarios. Figure 2.1 clearly demonstrates that different GCMs predicted future conditions in the Okavango Basin ranging from drier than present to wetter than present and there are differences in both degree of change and direction of change between the Okavango river catchment area and the Okavango Delta. In a related hydrological modeling study of the Okavango Delta, Murray-Hudson et al. (2006) applied a mathematical model to assess the impacts of changing hydrological inputs on the flooding in the delta. The assessment of effects of possible future changes (2020-2050) on the hydrological characteristics of the Okavango Delta was done by running a hydrological model of the Okavango Delta with discharge inputs from the Pitman model of the river basin. Three different GCMs namely HadCM3, GFDL and Canadian Climate Centre with the future A2 IPCC emission scenario were used to drive the hydrological model. The GCMs produced a wide spectrum of possible future conditions in the Okavango Delta as shown in Figure 2.2. The authors concluded that there was a large uncertainty about future climatic conditions and the modeled effects of climatic variation on the hydrology of the Delta.

A similar study of the future climate change impact on water resources was performed by Arnell (2004), who applied GCM outputs for estimating river flows under both present and future climates. The study recognized the uncertainties that exist amongst the climate projections of various GCMs; the results of this study are shown in Figure 2.3, which provides an indication of the effects of future climate change on long-term average annual river runoff

by the 2050s across the world, under the IPCC A2 emissions scenario estimated by different climate models. Figure 2.3 shows large uncertainties exist in some regions as simulated by different GCMs. Jones et al. (2004) pointed out that, current GCMs, which contain different representations of the climate system, project different patterns and magnitudes of climate change for the same period in the future when using the same concentration scenarios (Figure 2.4).

Giorgi et al. (2001) reported that GCMs cannot resolve the spatial structure of climate at the sub-basin scale used in the hydrological model. Despite recent advances in the representation of land-surface processes in GCMs, large uncertainties still exist in GCM simulated land-surface processes, which require further quantification through model intercomparisons and new model simulations. With uncertainties in such climate projections, impacts studies are challenging.

GCM projections are currently subject to substantial uncertainties in the modeling process that climate projections are not easy to incorporate into hydrological impact studies (Allen and Ingram, 2002; Forest et al., 2002; Mearns et al., 2001). It has been noticed that such uncertainties have produced biases in the simulation of river flows when using direct GCM outputs for hydrological impact studies. Some studies have found that uncertainties in climate change impacts on water resources are primarily due to the uncertainty in precipitation inputs and less due to the uncertainties in GHG emissions, in climate sensitivities or in hydrological models themselves (IPCC, 2007b). In

general, most of the studies that have been reviewed mentioned that there was considerable uncertainty about the magnitude and direction of any future discharge response associated with both the GCM and the IPCC GHG emission scenarios. The different ways of creating scenarios from the same source as a GCM can lead to substantial differences in the estimated effect of climate change, but that the hydrological model uncertainty may be smaller than errors in the modelling procedure or differences in climate scenarios (IPCC, 2007b).

Hence, before the GCM output information of key variables can be used to drive the impact models at a regional or a local scale, there is an intermediate step which requires the 'downscaling' of this large scale GCM information to regional scale information. Downscaling techniques (both regional climate models, hereafter RCMs, and statistical methods) for "downscaling" the GCM output to the scales compatible with hydrological model are carried out to limit such uncertainties that arise from GCMs.

2.3 DOWNSCALING APPROACHES

Downscaling methods have consequently been developed to bridge the gap between the coarse resolution of the climate model outputs and the need for surface weather variables at finer spatial resolution. Depending on the underlying principle and the degree of complexity attributed to them, downscaling methods range from less demanding statistical downscaling (SD) methods, which are established on the basis of a statistical relationship

between large-scale climate state and observed local weather variables (Beckmann and Buishand, 2002; Zorita and von Storch, 1999; Wilby et al., 1998; von Storch et al., 1993; Bardossy and Plate, 1992) to more complex and demanding dynamic downscaling (DD) methods, which implement a meso-scale physically based regional climate model nested within a GCM (Murphy, 1999; Christensen et al., 1998; Mearns et al., 1995).

The two fundamental approaches for downscaling of large scale information to regional or local scales were discussed in Chapter 1. There, discussed also the advantages of dynamical downscaling and why the statistical downscaling cannot be considered for site with short or no rainfall record, i.e. ungauged basins. This section further discusses some of the common shortcoming of statistical approach reported by different researchers.

The primary shortcoming of the statistical approach is the assumption that the relationship between the predictors and predictands is stationary, which cannot be proven in advance. However, because statistical downscaling methods are based on observed relationships, they have the potential to incorporate local or regional environmental factors that are not resolved by even the finest RCMs (Schoof et. al., 2009). Many other review papers have dealt with statistical downscaling concepts, their prospects and their limitations (Murphy 1999; Gyalistras et al., 1998; Wilby and Wigley, 1997; Zorita and von Storch, 1999; Hewitson and Crane, 1996; von Storch, 1995). It can be concluded that the advantages of using statistical downscaling are that this downscaling technique can easily be applied to analyze the output data

from different GCM experiments and are computationally inexpensive (IPCC, 2001) and in this respect, empirical downscaling is particularly advantageous in terms of computational efficiency. However, while the empirical techniques give a first-order response to the regional climate change that is physically consistent with the circulation, they are not capable of incorporating local-scale feedbacks. Moreover, data with which to develop relationships are not readily available in remote regions or regions with complex topography. Besides, these empirically-based techniques do not account for possible systematic changes in regional forcing conditions or feedback processes.

It has been reported that though the possibility of tuning the statistical model to the required regional or local information is a key advantage, a systematic assessment of the uncertainty of this type of technique, as well as a comparison with other techniques, is difficult and may need to be studied carefully (IPCC, 2001). The DD approach using RCMs, on the other hand, are able to accommodate such feedbacks, but it is arguable whether this provides any greater confidence in the downscaled solution, given the significant sensitivity of the RCM to choice of parameterization schemes and physics packages (Hewitson and Crane, 2006). In brief, SD method requires observational data at the location of interest to calibrate the statistical downscaling model. Thus, SD method cannot be considered for sites with short or no station data record.

2.3.1 Application of Dynamical Downscaling in Climate Research

As mentioned in Chapter 1, dynamical downscaling method involves the extraction of regional scale information from large-scale GCM data and is based on the modeling of regional climate dynamical processes. Regional climate modeling technique consists of using initial conditions, time-dependent lateral meteorological conditions derived from GCMs (or analyses of observations) and surface boundary conditions to drive high-resolution RCMs (e.g., von Storch et al., 2000; Cocke and LaRow, 2000; Dickinson et al., 1989). RCMs have been extensively tested for climate downscaling over many regions of the world (Seth and Rojas 2003; Nobre et al. 2001; Roads 2000; Fennessy and Shukla 2000; Sun et al. 1999a, b; Takle et al. 1999; Hong et al. 1999; Kanamitsu and Juang 1994; Giorgi and Marinucci 1991). This technique is discussed in detail in Chapter 3.

Soares et al. (2012) proposed a dynamically downscaled climatology of Portugal, produced by a high resolution, 9 km WRF simulation, forced by 20 years of ERA Interim reanalysis (1989–2008), nested in an intermediate domain with 27 km of resolution. Model results were compared with all available stations, 32 stations for temperature and 308 stations for precipitation, through the computation of mean climatologies, standard statistical errors on daily to seasonally timescales, and distributions of extreme events. Results show that WRF at 9 km outperforms ERA-Interim in all analyzed variables, with good results in the representation of the annual cycles in each region. The authors also concluded that, considering the PRUDENCE

and ENSEMBLES model evaluations, WRF at 9 km appears well placed in their error ranges, suggesting that WRF is a good candidate for regional climate modeling. Improved description of temperature spatial and temporal variability by WRF is due to a better representation of regional processes, related with orographic and coastal forcing. Many related downscaling studies have been performed in different part of the world.

Mastrangelo et al. (2011) investigated a long-lasting heavy precipitation event that occurred on 12th and 13th November 2004 in southeastern Italy. The analysis, based on observations and numerical outputs, focus on the synoptic and mesoscale features leading to convection and on the mechanisms controlling the convective systems responsible for the two observed rainfall maxima. A reference simulation obtained with the RCM WRF model has been compared to the available observations, showing that the precipitation pattern and amounts are realistically simulated, whereas the precipitation timing and the location of the maxima are reproduced less successfully. The simulation was overall satisfactory and was exploited to investigate the main mesoscale features of the event.

Heikkila et al. (2011) presented the first application of the WRF model to climatological simulations in Europe. Generally the WRF model performed very well in reproducing the observed climate in Norway. The results of 12 different regional climate model simulations from the ENSEMBLES project are also presented as a reference. Analyses were done on surface variables on complex terrain: precipitation, 2 m temperature and 10 m wind speed and

compare the model results with a large number of observations within Norway. The WRF simulations perform comparably well and the value added by the refinement of the resolution to 10 km is obvious (Figure 2.5). The ENSEMBLES mean has low biases and only a few of the models are performing better. In case of temperature, the WRF simulations have clearly lower biases than the individual ENSEMBLES models or the ENSEMBLES mean. The 10 km simulation reduces the bias compared with the 30 km simulation. The authors concluded that, higher resolution simulations are advantageous for producing regional future climate projections.

Salathe et al. (2010) performed two 100-year regional climate simulations using the WRF. One simulation is forced by the CCSM3 and the second is forced by a simulation of the ECHAM5. In overall details, both simulations presented in the study are quite consistent with the global forcing models used. Furthermore, due to the unique characteristics of the forcing models, the fine scale features simulated are substantially different, accentuating differences in the forcing scenarios and underscoring the need for extended simulations using a large ensemble of forcing models and regional models. There are important areas of agreement between the two simulations, suggesting that some local responses to global climate change are robust. Both simulations yield an increase in the measures of extreme precipitation even though the WRF CCSM3 simulation produced mostly reductions in total precipitation during winter and spring. There is substantial uncertainty in projections of extreme events in regional models, both from simulations with a single model and from multiple models. Quantitative estimates of this

uncertainty are required to assess the risk of future extreme events. Future work in regional climate modeling will therefore focus on large ensemble simulations with multiple models to better represent the probability of projected changes. Nevertheless, Salathe et al. (2010) reckoned that regional climate models provide important insight into how the regional climate may respond to global climate change.

A study done by Caldwell et al., (2009) using a 40 year Weather Research and Forecasting (hereafter, WRF) developed at the National Center of Atmospheric Research (NCAR) based dynamical downscaling experiment performed at 12 km horizontal grid spacing, centered on the state of California, and forced by a 1°× 1.25° Community Climate System Model ver. 3 (CCSM3.0) simulation also confirmed that dynamical downscaling adds value for regional climate prediction when compared to GCM results. Caldwell et al. (2009) concluded that the downscaled simulation to improve the spatial distribution of precipitation and surface temperature and to better capture extreme precipitation almost everywhere in the domain. Significant improvements have been achieved in the area of nested RCMs (Barstad et al., 2008; Varis et al., 2004; Christensen et al., 2001).

Seasonal forecasting study using REMO-RCM carried out by Sieck (2008) demonstrated that using the nesting technique in climate model has the advantage that mesoscale phenomena, which are not present in the driving fields due to the coarse horizontal resolution and which are for example initiated through a more detailed land surface representation in the regional

model, can develop within the simulation domain and without strong constraints from outside (see Figure 2.6). According to the authors, the study aimed to investigate the 'added value' to seasonal forecasting by dynamical downscaling and this finding is especially useful for precipitation which is essential in run-off forecasts one can expect benefits from the better resolved model and enhanced skill in spatial patterns and amount compared to the output from the coarse resolved global model.

An interdisciplinary project entitled Prediction of Regional scenarios and Uncertainties for Defining European Climate change risks and Effects (hereafter, PRUDENCE) was undertaken during the period November 2001 – October 2004 by a team of 21 European research groups based in nine countries with funding from the European Commission. Its primary objective was to provide high resolution climate change scenarios for Europe at the end of the twenty-first century using dynamical downscaling methods with climate models. PRUDENCE succeeded in designing, executing, analyzing, and synthesizing European high-resolution climate change simulations involving four high-resolution Atmospheric General Circulation Models (AGCMs) and eight RCMs. Figure 2.7 shows how well a RCM with a spatial resolution of 50 km is able to resolve topographic details compared to a GCM having a spatial resolution of about 300 km. Impact studies in PRUDENCE have compared various methods of scenario development and application. They provide convincing new examples that demonstrate how the application of RCM based scenarios can confer significant advantages over Atmospheric Ocean General Circulation Models (AOGCM) based scenarios in many impact

studies. On the other hand, they also indicate that RCMs do not yet provide a universal panacea, and some of the impact studies highlight potential limitations of relying solely on RCM based information. Overall, PRUDENCE represents the first comprehensive, continental scale intercomparison and evaluation of high resolution climate models and their applications. The results obtained and new insights gained are testimony to the vigorous and multifaceted nature of climate change research in Europe (Christensen et. al., 2007).

Study performed out by Jones et al. (2004) showed that RCMs can simulate current climate more realistically. Where terrain is flat for thousands of kilometres and away from coasts, the coarse resolution of a GCM may not matter. However, most land areas have mountains, coastlines, etc., on scales of 100 km or less, and RCMs can take account of the effects of much smaller scale terrain than GCMs. Since the terrain at this higher resolution was resolved well in an RCM, it was reported that the RCM was able to simulate precipitation to a reasonable accuracy. Figure 2.8 illustrates the simulated and observed winter precipitation over Great Britain by RCM PRECIS (Providing REgional Climates for Impacts Studies). The observations clearly show enhanced rainfall over the mountains of the western part of the country, particularly the north-west. This is missing from the GCM simulation, which shows only a broad north–south difference.

Another study carried out by Jones et al. (2004) has also concluded that RCMs represent smaller islands and are able to project climate change

with greater details. According to the authors, the coarse resolution of a GCM means that many islands are just not represented and, hence, their climate is projected to change in exactly the same way as surrounding oceans. However, land surface has a much lower thermal inertia than the oceans and will warm faster. If the land surface has any significant hills or mountains, these will have a substantial influence on rainfall patterns. In an RCM, many more islands are resolved, and the changes projected can be very different to those over the nearby ocean. Figure 2.9a shows Hadley Centre GCM projection of summer temperature change in and around the Mediterranean. Large islands such as Corsica, Sardinia and Sicily are not seen by the GCM, and hence they appear to warm at the same rate as the sea. In contrast, in the corresponding RCM PRECIS simulation, these islands are resolved and are seen to warm faster than the surrounding ocean, as might be expected. Therefore, impacts based on the GCM will create uncertainties. As shown in Figure 2.9b, when warming from increased GHG changes the patterns of wind flow over a region then the way mountains and other local features interact with this wind flow pattern will also change. This will affect the amount of rainfall and the location of windward rainy areas and downwind rain-shadow areas. Such changes will not be seen in the GCM, but the finer resolution of the RCM will resolve them. RCM PRECIS predicts that winter precipitation over the Pyrenees and Alps, two mountain ranges in Europe, will decrease substantially between now and the 2080s. The GCM for the same period shows there to be little change, or even an increase in rainfall over these areas (Figure 2.9b).

Though the applications of RCMs in climate research have many been shown to be advantageous, there are some issues related to RCMs and regional climate modeling that are sources of limitations and uncertainties in the model simulations that need to be considered while setting up the regional model experiments. What should also be placed as a caution are not only the advantages of RCMs in 'adding value', but also their limitations. The main theoretical limitations of this technique that remain to be improved are (1) the inheritance of systematic errors in the driving fields provided by global models (Varis et al., 2004; Hay et al., 2002). For example, boundary conditions from a GCM might themselves be so biased that they impact on the quality of the regional simulation, complicating the evaluation of the regional model itself (e.g., Hay et al., 2002). (2) Lack of two-way interactions between regional and global climate, and (3) the algorithmic limitations of the lateral boundary interface. Rojas and Seth (2003) and Mo et al. (2000) have reported that the results of RCM simulations are better when forced by reanalysis data than when embedded in a GCM. However, substantial differences exist among several reanalysis datasets, in particular, in the lower-atmospheric circulation and water vapour flux (Wang et al., 2004). Hence it becomes imperative to evaluate the skill of an RCM using realistic large-scale boundary conditions before it is nested into a GCM. Some research studies (Christensen and Christensen, 2008; Wang et al., 2004; Christensen and Christensen, 2003; Leung et al., 2003) have considered the strengths, limitations and challenges in the RCMs. However, it is not within the scope of this thesis to focus on what the advantages and limitations of RCMs are. Rather, the usefulness of RCMs as dynamical downscaling tool is recognized from numerous studies done by

the climate modelling community around the world and from the vast amount of literature available that bolsters this cause. It is also to be noted that improvement in the development of RCMs to yield more realistic simulations are continuing processes of model development. In addition to the knowledge gained from literature, it is also noted here that this research work has been done at the Tropical Marine Science Institute (TMSI), NUS, where one of the main research foci is climate modelling and dynamical downscaling. Therefore, the research experience gained during this PhD candidacy working on several climate change projects at TMSI also adds to the confidence in undertaking this research study.

2.4 ASSESSMENT OF CLIMATE CHANGE IMPACTS ON HYDROLOGICAL EXTREMES

The impacts of climate change on hydrology and water resources were discussed in Chapter 1. There, mentioned also how climate change impacts several regions in Southeast Asia especially data scarcity regions. Studying the impacts of climate change on hydrological regimes has become a priority area, both for process research and for water and catchment management strategies.

Based on the rationalities deduced by the IPCC, changes in the hydrological systems are expected due to climate change resulting from enhanced greenhouse effect (Basher et al., 2010; Bormann, 2009). Increased concentration of GHG is expected to alter the radiative balance of atmosphere,

causing increases in temperature and changes in precipitation patterns and other climatic variables (Houghton et al., 1990). As discussed in Chapter 1, climate change impacts would have significant implications on future water resources design and management.

2.4.1 RCM Simulations as Input for Hydrological Impacts Study

Due to the difficulties involved in the modeling of hydrological response to the global climate change, various approaches have been carried out by researchers working at different institutions (Xu et al., 2005). The issue of climate change and the future development of runoff and flood conditions are of importance within water resources research and a number of related studies deal with regional impact analysis and related uncertainties (Fowler et al., 2007; Kilsby et al., 2007; Thodsen, 2007; Wilk et al., 2006; Prudhomme et al., 2003; Menzel and Burger, 2002; Bergstrom et al., 2001).

Murshed et al. (2011) carried out a study to assess the present trend of high intensity rainfall, and then compared with the predicted future trend using PRECIS regional climate model to gather information on the effect of climate change on rainfall pattern and intensity. The study was demonstrated on the mean daily predicted rainfall over Asia most vulnerable city, Dhaka (WWF, 2009) using RCM PRECIS from 1951 to 2100 and observed by the station from 1953 to 2009. The RCM dynamically downscaled the data of the GCM, HadCM3Q with a resolution of 50 km from 250 km from 1951 to 2100 over the study area. The results (Figure 2.10) showed that the extreme rainfall

events over the Dhaka city have increased over the last decade. Both RCM and observed data showed increasing trends of rainfall. Hence, the climate change will impact the extreme rainfall events of the city.

Ma et al. (2010) studied the hydrological response to future climate change over Agano River Basin in Japan using the regional climate model WRF output. The authors conducted two numerical experiments, one was the hindcast run (CTL) used to reproduce past hydrological events of the 1980s and 1990s. The other was a pseudo global-warming run (PGW) used to project the hydrological response in the 2070s. NCEP/NCAR 6-hourly reanalysis data (Kalnay et al., 1996) was used as the lateral boundary condition for the CTL, whereas for the PGW, the lateral boundary condition was adopted, following the method of Hara et al. (2008). A global warming component was added to the NCEP/NCAR reanalysis data for the 1990s. Global warming components were estimated as the monthly average difference between the 10-year average of the 21st century projection, based on scenario A2 of the Special Report on Emissions Scenarios (SRES A2) (Nozawa et al., 2007), from 2071-2080, and the 20th century simulation from 1991-2000, from version 3.2 of the Model for Interdisciplinary Research on Climate (MIROC), an atmosphere-ocean coupled general circulation model. The PGW method allows for the comparison of climate in the present year and that in a PGW year that is similar to the control year in terms of interannual variation while including future climatology. Therefore, by the PGW method, the authors could evaluate the river discharge under a future climate. After the performance of the hydrological model was checked using a 20-year hind cast

for the period between 1980 and 1999, the authors conclude that the model was found suitable for future climate change studies.

Graham et al. (2007) carried out a research focuses on interpreting the hydrological response to projected changes in climate using dynamical downscaling technique. The work focused on drainage areas to the Baltic Basin, the Bothnian Bay Basin and the Rhine Basin. A total of 20 anthropogenic climate change scenario simulations from 11 different RCMs were used. Climate change inputs from different RCMs produced from the PRUDENCE experiment (Christensen and Christensen, 2007) were used in this study. Two hydrological models were used in this study; the conceptual rainfall-runoff HBV Model (Lindstrom et al. 1997) for the Baltic Basin and the physically based distributed WASIM (Water Balance Simulation) Model (Schulla, 1997) for the Rhine Basin. The details of the hydrological models and its application have been provided by Graham et al. (2007). The authors mentioned that using multiple RCMs helps identify how much the hydrological change signal can vary due to using different dynamical models to go from global to regional scale and by using different hydrological approaches, it helps to identify how much the signal can vary due to hydrological modelling. The RCM simulations were also tested by inputting precipitation and temperature results directly into a hydrological model. Results from this test are a further indication of the overestimation of precipitation from all models. This shows by example why hydrological change studies require an interface between climate models and hydrological models. The primary goal of hydrological change studies is to obtain a

plausible estimate of projected future climate impacts on hydrology and water resources. None of the methods investigated here are completely satisfactory in their approach. However, taken as a whole this work provides new insights. Graham et al. (2007) concluded that the use of the delta approach to transfer climate change to hydrological models offers a robust method to compare average outcome from different climate models, but not hydrological extremes.

Another application of RCM output was mentioned in a study by Fowler and Kilsby (2007) for simulating river flows in northwest England. Daily rainfall and temperature data were extracted from the multi-ensemble HadRM3H regional climate model (RCM) integrations for control (1960–1990) and future (2070–2100) time-slices. The output data from RCM HadRM3H were bias-corrected on observed mean statistics and used as input to hydrological models calibrated for eight catchments which are critical water resources in northwest England. If flows derived from the RCM data satisfactorily match those simulated using the observed dataset then there can be some confidence in the use of RCM results to predict future changes in flows. A comparison is made of flows generated using bias-corrected RCM data for the control scenario (1960–1990) and flows generated using the observed dataset (1961–1990) (Figure 2.11). The authors reported that the simulated daily flow distributions were reasonable and hence could be used with some confidence to examine future changes in flow regimes.

Research carried out by Menzel et al. (2006) in the German Rhine catchment aimed to study the impact analysis of global climate change on regional hydrology with special emphasis on discharge conditions and floods. The investigations are focussed on the major part of the German Rhine catchment with a drainage area of approximately 110,000 km^2. This area is subdivided into 23 sub-catchments. The simulated, large scale atmospheric fields, provided by two different GCMs, ECHAM4/OPYC3 model of the Max Planck Institute for Meteorology (Roeckner et al., 2006) and from the HadCM3 model of the Hadley Centre for Climate Prediction and Research (Gordon et al., 2000) was used and driven by the emission scenario IS95a (‘‘business as usual’’) are used as input to the method of expanded downscaling (EDS). The hydrological model HBV-D serves to simulate runoff conditions under present climate for the individual sub-basins. The details EDS method have been provided by Menzel et al. (2006). The investigations are focussed on the assessment of possible future runoff conditions under the impact of climate change. The study indicates a potential increase in precipitation (Figure 2.12), mean runoff (Figure 2.13) and flood discharge (Figure 2.14) for small return intervals. Menzel et al. (2006) pointed out that the errors of the hydrological model were shown to be relatively small. However, the uncertainty range that originates from the application of the whole model chain and two different GCMs is high. This leads to high cumulative uncertainties, which do not allow conclusions to be drawn on the development of future extreme floods. Menzel et al. (2006) also mentioned that due to the many uncertainties, projections given by the simulations should not be mistaken for predictions. The scenarios are only

helpful for the evaluation of possible developments and for raising preparedness against adverse conditions, such as the increasing threat of floods or droughts. In addition, Menzel and Schwandt (2004) also pointed out that the errors of the hydrological model were shown to be relatively small.

Kotlarski et al. (2005) analysed the regional simulations over Central Europe with respect to 2 m temperature and total precipitation using four regional climate models, REMO 5.0, REMO 5.1, MM5 and CLM 2.0. In the study, only 2 m temperature and total precipitation were considered as these two parameters are the most important atmospheric quantities in hydrological applications. The global ERA15 Reanalysis (1979–1993) (Gibson et al., 1997) has been downscaled over Central Europe using the four regional climate models and the simulation results were validated against three reference data sets (ERA15, CRU, DWD) and uncertainty ranges were derived (Figure 2.15). According to Kotlarski et al. (2005), differences between RCM results may be caused by different parameterisations of certain processes, different numerical techniques, different vertical resolutions and different regional model domains.

Menzel and Burger (2002) investigated the impacts of a climate change scenario on regional climate conditions and runoff characteristics for Mulde catchment, a meso-scale sub-basin of the Elbe in Germany. A hydrological model HBV-D has been applied to simulate discharge for present climate conditions. The expanded downscaling technique (EDS) was used to derive local climatic parameters for input in the hydrological model. The coupled atmosphere-ocean model ECHAM4/OPYC3, driven by the emission scenario

IS95a (‘‘business as usual’’), provided simulated global circulation patterns for application with EDS. The results as shown in Figure 2.16 indicate that an obvious increase in temperature is accompanied by a clear tendency to reduced precipitation over the investigated area for the next 100 years. These conditions lead to a decrease in simulated mean discharges of the Mulde. The authors advised to use a selection of a different GCM or even the application of another climate change scenario. Menzel and Schwandt (2004) also mentioned that due to the many uncertainties, projections given by the simulations should not be mistaken for predictions. The scenarios are only helpful for the evaluation of possible developments and for raising preparedness against adverse conditions, such as the increasing threat of floods or droughts.

Climate change is likely to result in a significant increase in the intensity and frequency of extreme precipitation events in many regions. Consequently, the existing IDF is called for to re-examine the adequacy of the current drainage system and capacity to meet future rainfall extremes. The objective of the study is to present an approach to derive present day and future climate IDF curves for regions with short or no rainfall record, using the high resolution outputs from RCM. This section assesses the application of RCM simulations as input for hydrological impacts study. The reviews of the development of present day and future climate IDF curves for regions with short or no rainfall records are presented in the following sections.

2.5 DEVELOPMENT OF RAINFALL INTENSITY – DURATION - FREQUENCY (IDF) CURVES

Rainfall intensities of various frequencies and durations are the primary inputs in hydrologic risk analysis and design. These inputs are commonly used in the design of urban infrastructure such as culverts and stormwater drainage systems. Optimal designs of these systems rely very much on the rainfall Intensity-Duration-Frequency (IDF) curves (Leteckova et al., 2011; Solaiman and Simonovic, 2011; Huang et al., 2010; Bara et al., 2009; Endreny and Imbeah, 2009; Prodanovic and Simonovic, 2007; Singh and Zhang, 2007; Nhat et al., 2006; Dupont and Allen, 2000; Koutsoyiannis et a.,1998; Maidment, 1993; Chow, 1964). The establishment of IDF relationship begin in the 1930s (Sherman, 1931; Bernard, 1932) and ever since different forms of IDF relationships have been constructed and published.

2.5.1 Statistical Distributions

The study of the statistics of extreme events is the first step for most of the hydrological studies (e.g. constructing IDF curves). In many situations, historical records containing observations from the past are the only reliable source of information. For flooding problem, the analysis of extreme events was introduced at the beginning of the 20th century (e.g., Fuller, 1914) to replace the earlier design flood procedures, such as envelope curves and empirical formulas, by more objective estimation methods. When longer flood records became available by the middle of the 20th century and with further

theoretical developments such as extreme value theory of Gumbel (1958), the method rapidly became what Klemes (1993) termed 'the standard approach to frequency analyses'.

Stedinger et al. (1993) indicated that 'frequency analysis' needs sufficient datasets to correctly determine a frequency distribution for a site. In poorly instrumented areas, rainfall records are often absent or short, compounding the statistical challenge of estimating extreme rainfall characteristics and designing flood control structures (Endreny and Imbeah, 2009). This forces hydrologists to use practical knowledge of the processes involved, and efficient and robust statistical techniques, to develop the best estimates of risk. These techniques are generally restricted, with 10 to 100 sample observations, to estimate events exceeded with a chance of at least 1 in 100, corresponding to exceedance probabilities of 1% or more.

In the literature, there are several different techniques, for constructing IDF curves that vary significantly. From the historical samples used for the construction of IDF curves, the more commonly used is annual maximum rainfall series (hereafter, AMS) of rainfall intensity, that is, the annual maximum values of every timescale. Methodologies for constructing IDF curves do not only vary in the samples used, but also may be based on different approaches. A review carried out by Grimaldi et al., (2011) on statistical hydrology showed that, the classical empirical forms to construct IDF curves were presented in Chow et al. (1988); a more general approach applied in United States was proposed by Chen (1983); general forms

consistent with the probability theory were suggested by Koutsoyiannis et al. (1998); forms in relation with L-moments were suggested by Hosking and Wallis (2005); approaches in relation with multifractals were demonstrated by Bendjoudi et al. (1997) and Veneziano et al. (2007); and forms in relation with copula functions were shown by Singh and Zhang (2007).

Selecting a suitable probability distribution function to fit extreme rainfall intensity data set is significant. There are many choices of distribution functions (e.g. GEV, Gumbel) and fitting methods (e.g., the method of moments, the maximum likelihood or the least-squares error methods); these may significantly affect the estimated parameters (details on parameter estimation are described in Chapter 3) of the IDF curves. However, the more popular probability distribution functions are the Extreme Value Type 1 (hereafter, EV1) and the Generalised Extreme Value (hereafter, GEV) distributions.

The EV1 or Gumbel distribution has been the prevailing model for rainfall extremes despite the fact that it results in the highest possible risk for engineering structures, i.e., it yields the smallest possible design rainfall values (Koutsoyiannis, 2004; Gellens, 2002). Koutsoyiannis et al., (1998) showed that the maximum intensity results in mostly from the extreme value distribution of the first or second type (EV1 or EV2). The EV1 (Gumbel distribution) and EV2 (Frechet distribution) models are special cases of the GEV distribution.

A recent study on development of probability based IDF curves under climate change (Solaiman and Simonovic, 2011) showed that due to changes in future precipitation extremes; the future rainfall may not follow the conventionally used Gumbel's distribution. The authors proposed to consider a generalized extreme value (GEV) distribution. However, the inherent uncertainties in the responses of GCM outputs do not guarantee GEV as the best fit for all GCMs.

Millington et al. (2011) further emphasized the suitability of the GEV distribution for data of the Upper Thames watershed (Canada). They reported that the Environment Canada's recommended distribution is the Gumbel (EV1) distribution, while in the United States the recommended distribution is the Log-Pearson type 3 (LP3). In their study, Millington et al. (2011) also investigated a third distribution, the Generalized Extreme Value (GEV) distribution on the Upper Thames watershed. Goodness-of-fit tests such as Anderson-Darling (AD), Kolmogorov-Smirnov (KS), and the Chi-Squared tests were performed by Millington et al. (2011) to decide the most appropriate distribution. L-Moment, often used in hydrology studies, was applied in this report for the parameter estimation of GEV, LP3 and EV1 parameters. L-Moment Ratio diagrams were also constructed to help establish the most suitable distribution. Figure 2.17 displays the 12-hour L-Moment ratio diagram where the average of the scenarios considered in this study is shown (red square), as well as the base distributions for comparison of GEV, EV1 and LP3. The EV1 distribution is shown as a single point (green triangle). Figure 2.17 shows that the data for the 12-hour storm follows the

GEV distribution very well. Results for other durations (1, 2, 6 and 24-hour) also showed that GEV distribution fits well to the Upper Thames River Watershed data. The authors reported the need for more studies to be carried out on the GEV distribution to ensure the most appropriate methods for predicting the extreme precipitation events.

The GEV distribution was adopted in many related studies mainly due to its high goodness of fit tests; also partially because the GEV distribution has gained popularity since the last decade (Hlavcova et al., 2005). Koutsoyiannis (2007) also reported that the Gumbel distribution may significantly underestimate the largest extreme rainfall amounts albeit its predictions for small return periods of 5 to 10 years are satisfactory. Several recent studies have also supported a three-parameter GEV over Gumbel distribution for flood frequency analysis (Millington et al., 2011; Solaiman and Simonovic, 2011; Koutsoyiannis, 2007; Rao and Kao, 2006; Mohd Daud et al., 2002).

The quantile function for GEV distribution is obtained as (1-1/T) and the maximum rainfall intensity is given as:

$$\boldsymbol{I_{max} = \mu + \frac{\alpha}{k}\left\{\left[-ln\left(1-\frac{1}{T}\right)\right]^{-k} - 1\right\}} \qquad \textbf{(2-1)}$$

where k, μ and α are shape, location and scale parameters, respectively.

Rao and Kao (2006) performed an IDF analysis for the state of Indiana in the United States. Hourly precipitation data from 144 rainfall stations are

collected from National Climate Data Center (NCDC) and five probability distributions, Gumbel (EV(1)), GEV, Pearson Type III (P(3)), Log-Pearson Type III (LP(3)) and Pareto distribution were tested. The adequacy of the fitted distributions was tested using two goodness-of-fit measures, Chi-Square and Kolmogorov-Smirnov tests. The results of the goodness-of-fit tests are shown in Table 2-2. Table 2-2 shows that EV(1), GEV, P(3), and LP(3) distributions provide good fits for most of the stations. For Chi-Square Test, EV(1) passes most tests, followed by LP(3) and GEV, while the fit of P(3) distribution is not as good. EV(1) has the best result, however, GEV and P(3) can fit better for higher extreme values. The authors were surprised that LP(3), which was traditionally considered as the best model in hydrological frequency analysis, did not perform as the best distribution. Besides, LP(3) also did not provide a good fit for extremely high values. Pareto distribution was shown not suitable for the Indiana rainfall data. From the KS test, except for the modified Pareto method, all the other distributions passed the test. The few cases which did not pass the KS test were affected by their extremely high values. The authors also observed that GEV and P(3) are better in predicting high values. By considering all the factors, Rao and Kao (2006) concluded that, GEV is better in predicting high value and is found suitable for the entire state of Indiana.

Huntingford et al. (2003) presented RCM predictions of extreme rainfall for a changing climate at three areas in the United Kingdom (Lewes, Shrewsbury and York). In the study, the annual maximum series are calculated over five durations of m=1, 7, 15, 30 and 60 days. A feature of the

autumn-2000 floods was the accumulated rainfall over a long period, creating the need to understand extremes in rainfall over durations longer than one day. GEV distributions were fitted to each annual maximum series and it provided a smooth linkage between rainfall maximum and return period. The annual maximum values and fitted GEV frequency distributions for both the RCM simulations and the observational data for the three regions of interest and the five selected (m) durations are shown in Figure 2.18. The authors also concurred that, GEV distributions are three-parameter curves that have traditionally been found to replicate the relation between annual maximum and return period.

A statistical analysis of at-site extreme rainfall processes was conducted in Peninsular Malaysia by Mohd Daud et al. (2002). Eight probability distributions were investigated to describe the annual external rainfall data of Peninsular Malaysia. There were two-parameter Gumbel and Gamma, the three-parameter GEV, Generalized NOrmal (GNO), Generalized PAreto (GPA), PEarson type 3 (PE3) and Log PEarson type 3 (LP3) and the five-parameter Wakeby. Parameter estimation was based on the L-moment method (Hosking, 1990). Quantitative goodness-of-fit tests such as the probability plot correlation coefficient (PPCC) (Filiben, 1975), root mean square error (RMSE), relative root mean square error (RRMSE) and the maximum absolute error (MAE) were employed to determine the probability distribution most appropriate for describing annual maximum rainfall series in Peninsular Malaysia. The results of the analysis were plotted onto a map of Peninsular Malaysia (Figure 2.19). 94% of the sites chose GEV for at least

one of the four criteria in the goodness-of-fit analysis. The authors then further constructed the IDF curves (2, 5, 10, 25, 50 and 100-year return periods) for each of the site based on the selected distribution. The curves were then compared to the curves produced from Gumbel distribution (default distribution used in Malaysia). Results in Figure 2.20 show that the curves coincide almost perfectly for the 2 and 5-year return periods; nevertheless, the differences became quite obvious for longer return periods. Detailed examination showed that GEV is sensitive towards the skewness of the datasets involved. GEV produced higher estimates than Gumbel when (highly skewed, skewness > 1), but when skewness <0 and 1, both distribution gave equivalent estimates. These results are shown in Figure 2.21 (a) and (b). Mohd Daud et al. (2002) concluded that GEV produces more conservative estimates, therefore reducing the possibility of over or under designing hydrological structures. Based on the quantitative goodness-of-fit tests, the authors concluded that GEV is the most suitable distribution for annual maximum rainfall in Peninsular Malaysia. In addition, GEV distribution is suitable to construct IDF curves for optimal design of stormwater infrastructures.

2.5.2 Development of Rainfall IDF Curves for Regions with Short or No Rainfall Record

A continuing problem in hydrology is the estimation of peak discharges for design purposes on catchments with only limited or no data available (Blazkova and Beven, 1997). Selecting proper rainfall time series as input to

simulations remains one of the main problems of practical concern in hydrological modeling. Currently, it is an established practice to use high-resolution historical rain series as input to hydrological model packages for detailed simulation of urban drainage systems. However, sufficiently long rain series are rarely available from the exact catchment in question and simulations are hence often based on available rain series from other locations (Mikkelsen et al., 2005).

A recent study using isopluvial and parameter contour maps method was carried out by El-Sayed (2011) to development of rainfall IDF curves for ungauged sites. The author first obtained the Annual Maximum Series (AMS) at each station for different durations, and then fitted with Log-Normal and Log-Pearson Type III. The results of the AMS rainfall depth (e.g. El Rawafaa station) for considered durations at different return periods were extracted from the best fit distribution and listed in Table 2-3. Using ARCGIS, the depth-duration frequency (DDF) values at different stations were interpolated by the Triangulation with Smoothing method. These values (Table 2-3) were used to develop isopluvial maps for a given duration over the whole region. Examples of typical isopluvial maps for 30-minute duration at 5 and 50 years return periods are shown in Figure 2.22. The authors obtained the rainfall depth for other stations (e.g. Ghandal, El Timed and El Godirat stations) from the isopluvial maps to construct IDF curves using the Kimijima Empirical Function (Equation 2.2) (Chow et al., 1988; Nhat et al., 2006). The Kimijima parameters for Ghandal, El Timed and El Godirat stations were determined and presented in Table 2-4. The Kimijima parameters (a, υ and b) were used

to get the parameter contour maps. The parameter values at the station points were interpolated by the Triangulation with Smoothing method. Figure 2.23 shows the parameters contour map with 10-year return period. From these parameter contour maps, it is possible to estimate the parameters set at any point in the region. Thus, the ungauged site of interest has its own 3-parameters Kimijima function and accordingly the rainfall IDF curves can be constructed by using these parameters.

$$\boldsymbol{i = \frac{a}{d^{v}+b}} \qquad \textbf{(2-2)}$$

Endreny and Imbeah (2009) conducted a study to generate rainfall IDF estimates for poorly instrumented areas in Ghana using short-record satellite data from Tropical Rainfall Measuring Mission (hereafter, TRMM) (Figure 2.24). The annual maximum rainfall data were ground gauge data from the Ghanaian Meteorological Service Department (hereafter, GMSD) and from TRMM satellite precipitation. In this research, GEV type II (GEV-II) probability distributions were fitted using two robust parameterization approaches, one called regional for combining regional and local data, the other called global for combining a global parameter and local data. There were four approaches to sampling from Ghanaian datasets. (1) Global method with GMSD parameters, (2) Global method with mixed GMSD and TRMM parameters (3) Global method with TRMM parameters and (4) Regional method with TRMM parameters. The best goodness-of-fit and least error were obtained with the mixed ground and satellite data parameterization approach, which used GMSD data to derive time-based parameters and

TRMM to derive distribution parameters. The representative IDF curves from Accra and Ho are shown in Figure 2.25. The results in Figure 2.25 reveal that the regional method could not incorporate GMSD data, and used only TRMM data, which led to substantial overestimation of rainfall intensity for short durations. The regional method was also limited to the 3 h to 24 h durations of original TRMM observations. The short TRMM record sets with duplicate observed depths at increasing durations caused the regional method to generate internal consistency errors in the IDF plots, suggesting the global method with regional application is best for Ghana. This leaves the global method with GMSD and global method with mixed GMSD and TRMM data as the most complete and representative curves for IDF generation in Ghana. Endreny and Imbeah (2009) concluded that the global method with mixed GMSD and TRMM data is preferable due to its IDF curves having sub-hourly durations.

Another study related to the development of isopluvial map was carried out by Raiford et al. (2007) over South Carolina, North Carolina, and Georgia. The aim of the study is to update the existing IDF curves in the regions and obtain these curves at ungauged sites throughout the region using the newly developed rainfall frequency analysis techniques. Raiford et al. (2007) first carried out an investigation on the L-moment method with X-10 test (Lu and Stedinger, 1992) to search for homogeneous regions within the study area regions. Three procedures were attempted to obtain homogeneous regions, (1) Jackknife method (Quenouille, 1956, 1949; Tukey, 1958), where all the sites were tested as a region. If the test failed, the site with the largest

chi-squared value was removed and the remaining sites were tested; (2) a graphical approach where all the data at a station for a particular duration was fitted to a GEV distribution using L-moments and sites that had curves with similar shapes were grouped into a region, and (3) To ensure that the homogeneous regions identified were geographically contiguous, regions were declared and then tested for homogeneity. If a region failed homogeneity test, a site was removed using the Jackknife method until a homogeneous region was obtained. In most cases more than half the sites had to be removed before a regional solution could be found. Raiford et al. (2007) found that the method was either unable to identify homogeneous regions that were geographically contiguous or too many stations had to be eliminated before a region could be considered homogenous. The authors then conducted at-site statistics to develop frequency relationships. Normal, Lognormal, GEV, Pearson type III, and Log Pearson type III probability distribution functions were used to fit the maximum annual precipitation (MAP) data at each gauging site for each duration. The chi-squared goodness-of-fit test was used to determine the best fit probability distribution. The distribution selected was then used to find depth-duration-frequency (DDF) values at 2, 10, 25, 50 and 100-year. Using a 0.5-degree latitude by 0.5-degree longitude grid, these DDF values were spatially interpolated to obtain isopluvial maps for all durations and return periods over the whole region. DDF values at the grid points were interpolated by the Kriging method. An example of such a map is shown in Figure 2.26. Using the DDF values at the site, the IDF curves were generated. Comparison of IDF values determined from the rainfall data at a specific station to the spatially interpolated values at the same location revealed no

significant difference. The authors deduced that the IDF curves can be obtained from the isopluvial maps at ungauged sites.

Similar to the development of isopluvial map, Nhat et al. (2006) carried out a study on the establishment of IDF curves for ungauged station in Red River Delta, Vietnam. In this study, the authors have generated the regional IDF formula parameters for ungauged areas using parameter contour maps to estimate rainfall intensity for various duration and return period. The study was carried out using data from seven gauged stations (Hanoi, Bacgiang, Haiduong, Namdinh, Ninhbinh, Thaibinh and Vanly) in Red River Delta. Frequency analysis techniques are used to develop the relationship between rainfall intensity, storm duration and return periods from the rainfall data obtain from the gauged station. Analysis of distribution for rainfall frequency is based on the Pearson Type III distribution, which is commonly used in Vietnam for this kind of analysis. The IDF curves for the seven stations were constructed using four empirical equations; Talbot, Bernard, Kimijima and Sherman, and the parameter for the four empirical equations were determined. Table 2-5 shows the constant parameters for the four empirical equations at the Hanoi station with 100 years return period. Similar procedures were applied for the other six stations to determine parameters a, b and e, for the same return period. From the results, the authors concluded that Kimijima and Sherman equations are acceptable fit to the IDF relationship in Vietnam. Nhat et al. (2006) then interpolated the parameter contour maps for a, b and e using Arc view/GIS. Figure 2.27 shows the contour map of parameters of Kimijima equation with 100 year return periods. The contour maps can then be used to

determine the rainfall IDF at Hungyen Station (ungauged station). Figure 2.28 demonstrated the 100 year return period IDF curves for Hungyen Station established from the contour maps as shown in Figure 2.27.

For the past twenty years, the development in analyzing rainfall data for ungauged sites focuses on the identification of homogenous regions. Several researchers have developed methods for determining homogenous regions described by the same statistical distribution. The probability distribution at all sites is expected to have the same coefficient of variation and skew. The best fit distribution for the whole region is determined using moment diagrams, growth curves, or bias testing (Raiford, 2007).

Mikkelsen et al. (2005), for example, selected the regional historical rainfall time series as input to urban drainage simulations at ungauged locations. In the study, a systematic regional analysis (regional model) was conducted based on newly developed statistical regionalization procedures, including L-moment analysis (Hosking and Wallis, 1997) and generalised least squares regression (Madsen and Rosbjerg, 1997; Stedinger and Tasker, 1985) with heteroscedastic sampling uncertainty and inter-site correlation due to spatial coverage and movement of individual rain storms (Madsen et al., 2002, 1998; Mikkelsen et al., 1996). Historical rain series from a total of 41 gauging stations from Danish Water Pollution Committee (DWPC) each with more than 10 years of observations were included in the investigation. Each rain series was filtered to extract a set of rainfall variables covering maximum average intensities per event (for durations between 1 min and 48 h) as well as

other volume based rainfall variables (rainfall depth per event and per day) and transformed rainfall variables (overflow volumes and necessary detention volume for simplified standard catchments). These rainfall characteristics were chosen since they reflect the most important features of rainfall with respect to urban drainage. The developed regional model allows estimation of extreme rainfall characteristics and associated estimation uncertainty at an arbitrary site in the country. The effect of varying maximum annual rainfall (MAR) on the IDF curves for the region 'Outside Copenhagen' is illustrated in Figure 2.29. The prediction uncertainty of regional rain data for region 'Outside Copenhagen' was caused by a combination of (1) sampling uncertainty due to a limited observation period; (2) sampling uncertainty due to a limited number of gauging stations; and (3) residual model uncertainty due to regional variations, which cannot be explained fully by the regional model (e.g., microclimatic variations and measurement errors). However, the uncertainty is still low when compared with historical rainfall time series used as direct input to simulation models; the uncertainty will be higher and the actual rain series may not fit very well to the regional model. The authors concluded that extreme rainfall is often very different even for minor physiographic differences and the uncertainty related to the use of point rainfall data at ungauged locations is generally underestimated.

Nguyen et al. (2002) proposed regional frequency analysis method for sites where rainfall records are limited or unavailable. In the study, a homogeneous region was defined as the region in which all annual maximum rainfall series at different sites must have similar properties of rainfall

occurrence within a given concurrent time period. If the occurrence of rainfalls at different rain gauges within a given concurrent period is similar (e.g. high correlation of the numbers of rainy hours within a given one-day interval), these gauges are thus considered as members of a homogeneous group. Principal component analysis (PCA) is performed using the series number of rainy hours observed at each rain gauge in order to assess the similarity of rainfall occurrences between these gauges. A case study is carried out using annual maximum rainfall series (AMS) from a network of 10 rain gauges in Quebec (Canada). To assess the scaling behaviour of these AMS, the log-log plots of the first three rainfall non-central moments (hereafter, NCMs) against duration are prepared for all 10 stations (e.g. Figure 2.30 shows plot for McGill station).

In this study, for homogeity criterion, Nguyen et al. (2002) suggested four stations Brebeuf, Dorval, McGill, and St-Hubert among the 10 gauges considered to be groupped into one homogeneous group. Further, to simulate the ungauged condition the Jacknife procedure is used in the present study. That is, one gauge was removed from a homogeneous group, and then regional relationships between the first three non-central moments (NCMs) (M_1, M_2 and M_3) and the mean number of rainy hours (N_R) in a one-day period were developed using the data from the remaining stations in the group. For example, if the site at McGill station was assumed to be ungauged, the regional relationships (Equations 2.3, 2.4 and 2.5) were obtained based on the available rainfall data at Brebeuf, Dorval, and St-Hubert.

$$M_1 = 0.619.N_R \quad \textbf{(2-3)}$$

$$M_1 = 0.2087.e^{0.025M_2} \quad \textbf{(2-4)}$$

$$M_3 = 200.38.e^{0.013M_2} \quad \textbf{(2-5)}$$

$\mathbf{N_R}$ is the mean number of rainy hours during a one-day period with rain

Hence, on the basis of Equations 2.3, 2.4 and 2.5 the first three NCMs and the distribution of maximum daily rainfalls for McGill can be computed if the mean number of rainy hours N_R for this ungauged site is known. Figure 2.31 shows comparison between empirical (observed) and estimated distributions of 1-day rainfall extremes at Brebeuf, Dorval, St-Hubert, and McGill stations for the case where rainfall data are missing (McGill regional curve) as well as for the case where rainfall data are available (McGill at-site curve). The good agreement between the estimated regional and empirical distributions for 1-day rainfall extremes as shown in this case study indicated the feasibility of the proposed regional estimation method. In addition, the authors also mentioned that the regional estimate of daily rainfall extreme distribution is as accurate as the at-site estimate in the case considered. This study demonstrated that regional frequency analysis, which uses data from many sites, has been shown to be able to reduce the uncertainties in the estimation of extreme events. However, one of the main difficulties in the use of this technique is related to the definition of "homogeneous" regions.

Various methods have been proposed for determining the homogeneous regions, but there is no generally accepted procedure in engineering practice.

Similar regionalization study for ungauged site was conducted in Peninsular Malaysia by Mohd Daud et al. (2002). The number of rainy hours experienced at each site corresponding to each annual maximum date of every site was the input data for the homogeneity study using principal component analysis (PCA). Indirectly, these data were able to incorporate the effect of monsoon seasons due to the temporal and spatial patterns of rain from the different mechanisms producing it. The estimation of quantiles for ungauged sites was done using two methods: (i) station-year and (ii) index-flood methods. The Jackknife procedure was employed in determining the accuracy of estimates obtained compared to the actual at-site estimates. For the station-year method some modification was done in the procedure whereby all the data within each homogeneous region (except for the assumed ungauged site) were pooled to produce the estimate (this method is referred hereby as the pooled station-year method). From the results of the principal component analysis (PCA), 13 of the stations were divided into homogeneous groups with distinct climatic and geographic characteristics. The clustering of homogeneous stations is shown on Figure 2.19 and named as Regions 1, 2, 3 and 4. A comparison of the two quantile estimation methods employed showed the pooled station-year method to be more favourable. The estimation study was done for Regions 1, 2 and 4. The pooled station-year method gave estimates that were closer to the at-site estimates for a larger number of sites compared to the index-flood method (an example is shown in Figure 2.32).

The relative root mean squared error (RRMSE) of the two methods is given in Table 2-6. Even though the differences in RRMSE values between the two methods are small, the authors concluded that the modified pooled station-year method used showed potential in giving accurate estimates of quantiles for ungauged sites within a homogeneous region.

An earlier study by Oyebande (1982) to overcome the two-fold problem of inadequate record length and coverage in Nigeria was carried out using regional analysis in which data for individual stations were lumped together or compounded according to rainfall zones to yield larger regional data samples (Figure 2.33 and Table 2-7). The study (Oyebande, 1982) presented two objectives, the first is to define detailed regions, or rather zones according to certain criteria, and the other is to use the longer records generated for the zones to obtain IDF relationships and estimates which can be applied to the respective zones with greater confidence. In the study, the zones were designated according to the climatic and topographic characteristics. The topographical characteristic was expressed by the altitude of the station above the mean sea level whereas the average rainfall pattern at the station was characterized by mean annual rainfall and mean number of rainy days per year. Gumbel distribution was applied to the annual extreme rainfall data sets generated by the 11 rainfall zones to estimate the parameters and hence the IDF curves. The 2-parameters (α and β) of Gumbel distribution were obtained by the method of moments. Table 2-7 and 2-8 present the estimates of parameters of the equation $x= \beta + (1/ \alpha) y$ for zones and for individual stations respectively. A close comparison of Table 2-8 and 2-9

reveals the station to station variation with the same zone; nevertheless, the author believes that the results obtained serve to meet the need for rainfall IDF relationships and estimates in various parts of Nigeria, both for short and longer recurrence intervals. The need has been particularly great because many large basins remain inadequately gauged while some are hardly gauged at all. The use of the results of this study to provide design floods could be done with greater confidence and somewhat calculable risk for each zone. Oyebande (1982) also suggested that the results could then be used to construct isarithmic or isopleth maps which not only provide the magnitude of extreme rainfalls of known duration and frequency at points required but also provide a total view of the statistical surface of the extreme rainfall in the country for each duration and frequency.

In practice, most of the research indicates the uncertainty related to homogeneity of the gauged and ungauged regions. However, the studies have helped to improve the current knowledge of the derivation of IDF curves for ungauged sites. In addition, no general assumption was made about the stationary or non-stationary character of the whole region or sub regions within the area of study (Leclerc and Quarda, 2007). The application of the proposed model within an area where a true regional non-stationary signal is observed could lead to better results than those obtained in the previous studies. Future work directed towards the identification of climatological variables and drainage basin characteristics related to non-stationarity in annual peak flow series are strongly recommended.

Studies carried out by Mikkelsen et al. (1998); Shaefer (1990) also showed that certain statistical rainfall characteristics vary systematically with the mean annual rainfall and, hence, this parameter seems to be of crucial importance when identifying representative rainfall input. According to Shaefer (1990), climatologically homogenous sub regions within the superregion were defined in terms of mean annual rainfall rather than geographic location. The sub regional values of the coefficients of variation, Cv and skew, γ were found to vary systematically with mean annual rainfall across the superregion

2.5.3 Derivation of Future IDF Curves under Changing Climate - Application of High Resolution Downscaled Climate Data

The estimation and use of the IDF curves are based on the rainfall stationarity hypothesis, i.e., extreme rainfall intensities and frequencies remain unchanged over time (Simonovic and Peck, 2009; Mailhot et al., 2007). However, this assumption is not valid under changing climatic conditions. Climate change signals have shown significant increase in rainfall intensities and frequencies in many regions (Simonovic and Peck, 2009). One of the expected hydro climatic impacts of climate change is the increase in the magnitude and frequency of extreme rainfalls which may serious impact the design, operation and maintenance of existing water infrastructure. These anticipated impacts will cause significant economic and human losses. Potential shifts in extreme rainfall at the local level demand revisions of the existing water infrastructure management regulations as well as changes in design practices. As a result,

the existing IDF curves require a significant overhaul; thus, a revisit of the existing drainage system is of paramount importance to minimize flood casualties.

Changes in future rainfall intensities are usually projected using GCM. However, these models cannot be used directly to project changes in extreme point rainfall because the temporal and spatial resolution is too coarse (Onof and Arnbjeg-Nielsen, 2009; Nguyen et al., 2007; Coulibaly and Shi, 2005; Huntingford et al., 2003). Optimal mitigation measures can be taken only when projected rainfall is derived from high resolution RCMs. From the RCM output, extremes can be analyzed and thus, IDF curves for future time slices can be derived which are extremely essential in drainage design.

Solaiman and Simonovic (2011) presented a methodology for updating the rainfall IDF curves for the City of London incorporating various uncertainties associated with the assessment of climate change impacts on a local scale. A total of 29 future climate scenarios developed from 11 Atmosphere Ocean Global Climate Models (hereafter AOGCMs) were used. The annual maximum series of rainfall were fitted to Gumbel distribution to develop IDF curves for 1, 2, 6, 12 and 24-hour durations for 2, 5, 10, 25, 50 and 100-year of return periods. Future IDF curves for 2080s were presented using statistical downscaling technique, stochastic weather generators. The model results show variable results, with wide range of increase in extreme rainfall. ECHAM5AOM A1B appears to be the wettest while MIROC3.2MEDRES A2 being the driest of all (Figure 2.34). However, due

to the uncertainties in the models, these data sets do not provide an accurate estimate of the future extreme events; rather they display that the future precipitation events will not be similar to the historical data. The authors suggested the use of a probability based IDF curve in order to apply the updated IDF information with higher level of confidence. In addition, the multi-model approach is also recommended for future studies (Solaiman and Simonovic, 2011).

Onof and Arnbjeg-Nielsen (2009) used an hourly weather generator approach to derive IDF values from hourly rainfall data. Future hourly data was obtained from RCM A2 scenario with a 10 km x 10 km resolution. The methodology presented by Onof and Arnbjeg-Nielsen (2009) is one approach to downscale the outputs from RCMs to scales that are relevant to urban drainage applications. However, the limitation of the study includes the stationarity assumption that the ratio of areal to the point estimates will remain unchanged with any changes in the climate.

Mailhot et al. (2007) performed an analysis of the Canadian Regional Climate Model (hereafter, CRCM), 45km x 45km resolution simulations under control (1961–1990) and future (2041–2070) climates. The CRCM simulations were driven by the Canadian Coupled Global Climate Model (CGCM2) following the SRES-A2 greenhouse gas emission scenario. Rainfall for 2, 6, 12 and 24-hour durations were extracted and analyzed using regional frequency analysis for grid boxes covering the Southern Quebec region. Results from the regional frequency analysis in control and future

climate were compared and is shown in Figure 2.35. As observed in Figure 2.35, estimates in future climate is predominantly higher than their corresponding values in control climate. It is therefore expected that the region of interest will experience increasing May-to-October Annual Maximum (MOAM) rainfall intensity in future climate for all durations at the grid box scale (similar results are obtained for 2 and 12-hour events). The amplitude of this shift between control and future periods will be estimated through a regional frequency analysis as shown in Figure 2.36. The plot displays the 90% confidence intervals of the ratio between estimates in control and future climates (vertical lines) for the different return periods and durations. Two main conclusions can be drawn from this graph. The first one is that differences between control and future estimates are significant (at the 90% confidence level) for 2-hour event up to 25-year return period and for 6-hour event up to 10-year return period while for 12 and 24-hour events significant differences are observed only for the 2 and 5-year return periods. The second conclusion is that, although 90% confidence intervals often cross the unit value, all ratio mean values are lower than one. Mailhot et al. (2007) concluded that since the spatial correlations between grid boxes are rather large and future values are systematically higher than their corresponding values in control climate, this provides a strong indication towards more intense heavy rainfalls in a future climate over Southern Quebec. The authors also proposed multi-model ensemble systems (different GCMs with different RCMs) as well as multi-member ensembles (investigation of possible sensitivity to initial conditions) to investigate the impact of model structures on future change in extreme rainfalls.

Prodanovic and Simonovic (2007) developed IDF curves for current and future climate for City of London using a K-Neareast Neighbour (K-NN) based weather generator (WG) algorithm. The authors considered three different scenarios (historic, wet and dry) used to evaluate changes in rainfall characteristics for the City of London. The scenario CCSRNIES B21 (wet) is selected as the upper bound of possible future rainfall generated by the GCMs. Similarly, the scenario CSIROM2kb B11 (dry) is regarded as the lower bound of possible future rainfall magnitude. The two scenarios are therefore selected to show the broad range of climate change impacts on rainfall magnitude. Results are shown in Figure 2.37. Outputs of the study indicate that, (1) rainfall magnitude (as well as intensity) will be different in the future; (2) The wet climate scenario (recommended for use in storm water management design standards) reveals significant increase in rainfall magnitude (and intensity) for a range of durations and return periods; (3) The increase in rainfall intensity and magnitude has major implications on ways in which current (and future) municipal water management infrastructure is designed, operated, and maintained. The authors also proposed that the design standards and guidelines currently employed by the City of London should be reviewed and/or revised in the lights of the results of this research to reflect the impacts of climatic change.

A more recent study by Simonovic and Peck (2009) was carried out using the similar K-NN weather generator algorithm to study the update of rainfall IDF curves for the City of London, Ontario under the conditions of changed climate.

Two climate change scenarios are used in this work: (i) Historic Climate Change Scenario and (ii) the GCM B21 (named Wet Climate Change Scenario, as it represents future climate conditions that are warmer and wetter than present). The simulation results indicate that rainfall magnitude will increase under climate change for all durations and return periods. The outputs of the study indicated that the rainfall magnitude will be different in the future and this may have major implications on ways in which current (and future) municipal water management infrastructure is designed, operated, and maintained. The simulations however, did not represent the future predictions. The climate change scenarios are in general obtained as outputs of GCM simulations and do not represent future forecasts, but simply offer possibilities of what might happen if the future development follows a certain course of action (i.e., continual growth of population, increased carbon dioxide emissions, increased urbanization, etc.). The authors recommended that the current IDF curves should be revised to reflect the potential impact of climate change.

Nguyen et al (2007) also presented technique for constructing IDF relations using outputs from two GCMs (HadCM3 A2 and CGCM2 A2) for future climate. A spatial-temporal downscaling methodology based on Statistical Downscaling Model (SDSM) was used to generate daily precipitation data for Dorval Station, Quebec. The temporal scaling (Nguyen et al., 2002) was performed for GEV distribution factors based on current historical rainfall distribution. The proposed downscaling approach was used to construct the IDF relations. The resulting design storms for Dorval Station

for the 1961-1994 period and for future periods (2020s, 2050s, and 2080s) using climate predictors given by the HadCM3 A2 and CGCM2 A2 simulations are shown in Figure 2.38. It was found that annual maximum precipitations downscaled from the HadCM3 A2 and the resulting design storm rainfall intensities displayed a small decreasing change in the future, while those values estimated from the CGCM2 A2 indicated a large increasing trend for future periods. The authors have demonstrated the presence of high uncertainty in climate simulations provided by different GCMs. In addition, the authors recommended further studies using more GCMs and data from regions with different climatic conditions to assess the feasibility and reliability of the suggested downscaling approach.

Similar methodology based on SDSM was used by Coulibaly and Shi (2005) to conduct a research project to identify the effect of climate change on future highway drainage infrastructures in Ontario. SDSM was used to downscale Canadian Global Circulation Model (CGCM) outputs for the current and future time periods and the downscaled outputs is used to develop IDF curves for Grand River, Kenora and Rainy River regions in Ontario. The IDF curves analysis and comparison based on the downscaled data at each station shows significant changes in the precipitation intensity between the current and the future time periods. Their study also found that similar increasing trends are shown in almost all stations from the current to the 2080s time period (Figure 2.39 and 2.40). The results showed that most of the highway infrastructures can be significantly affected by the heavy and more frequent rainfall intensity. An actual 10-year drainage system will be able to

withstand only 5-year storms by 2050s, whereas a current 50-year drainage structure will be able to handle only 20-year storms by 2050s.

An early research was done by Huntingford et al. (2003) to demonstrate RCM predictions of rainfall under changing climate. The study carried out with the second generation Hadley Centre coupled AOGCM (HadCM2), about 300km × 300km resolution. The Hadley Centre RCM (HadRM2), about 50km × 50km is nested within the HadCM2. The analyses focused on three regions near the towns of Lewes, Shrewsbury and York, all of which were very badly affected by the autumn-2000 floods. The authors interested in rainfall totals over 30 consecutive days, because sustained heavy rainfall was the main cause of the autumn-2000 floods. From the study they found out that the return periods of extreme 30-day rainfall for the three towns likely to reduce between pre-industrial times and the present (Figure 2.41). An event that had a 5% chance of occurring in any year may now have a 12% chance of happening.

Many studies indicate that rainfall magnitude as well as intensity will be different in the future. With climate change, one of the anticipated impacts is an increase in the intensity and frequency of extreme rainfall which will cause even much more casualties. Optimal mitigation measures can be taken only when projected rainfall is derived from high resolution regional climate models (RCM). From RCM, extremes can be analyzed and thus Intensity-Duration-Frequency (IDF) curves for the future which incorporate different climate change scenarios can be derived

2.6 SUMMARY

A review of the literature to-date on effects of climate change, impacts study and development of current and future IDF curves under changing climate are conducted in this chapter. An overview of the published modeling and field studies, climate modeling predictive methods and the development of future IDF curves with response to climate change are also presented. The short-comings from existing literature can be summarized as follows:

- Studies carried out, to develop rainfall IDF curves for ungauged sites, mainly focus on the identification of homogenous regions of rainfall zones. Most of these research works indicated the uncertainty related to homogeneity assumptions of the gauged and ungauged regions. Hence, the current study's proposed approach applying the simulation output of RCM, driven by Re-Analysis data, to derive IDF curves for ungauged sites is the first ever introduced and requires no homogeneity assumptions.

- Several studies used the GCMs' simulation output for rainfall extreme projection which should not be done due to the coarse spatial resolution of GCMs. Dynamical Downscaling (DD), with fine spatial resolution, is thus required to fully utilize GCMs' projected climate data.

- In most of the impacts studies, Statistical Downscaling (SD) approach has been the most commonly used (Onof and Arnbjeg-Nielsen, 2009; Prodanovic and Simonovic, 2007; Nguyen et al., 2007; Coulibaly and Shi, 2005). It is widely used for its simplicity and is computational inexpensive as compared with Dynamical Downscaling. SD approach is able to fill gap between large-scale climate change and local-scale hydrological response. However, the major weakness of SD is the assumption that the derived links between large-scale predictors and local predictands will remain unchanged (stationary relationship) with any changes in the future climate. In SD approach, each variable is typically handled independently, therefore, only specific variables are downscaled. DD approach (adopted in the present study) on the other hand is able to produce a dynamically consistent solution that includes all relevant variables throughout the designed domain.

- Limited study on RCM's future climate projection, for ungauged sites, on extreme rainfall intensities in general and on IDF curves in particular. Hence, the present study with regional climate modelling emerges as an alternative to solve such problem.

The following chapters aim to present the detailed model, data and methodologies used for the study and to discuss results related to some of the key issues raised in this chapter.

This page is intentionally left blank.

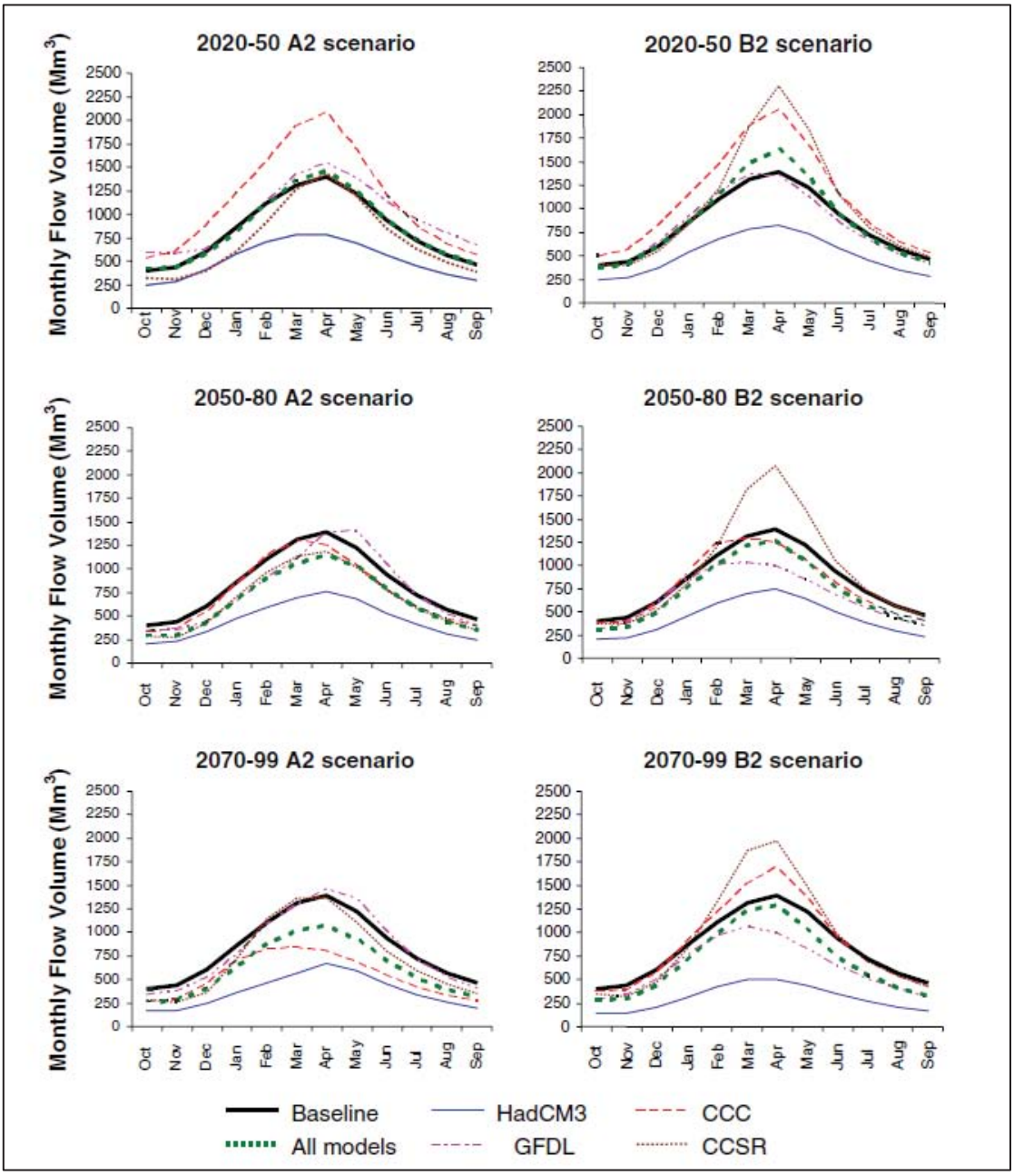

Figure 2.1: Mean monthly flow at Mukwe with baseline simulations and with assessment of changes of precipitation and evaporation derived from various GCMs, driven by the A2 and B2 greenhouse gas emission scenarios.
[Adapted from Andersson et al., 2006]

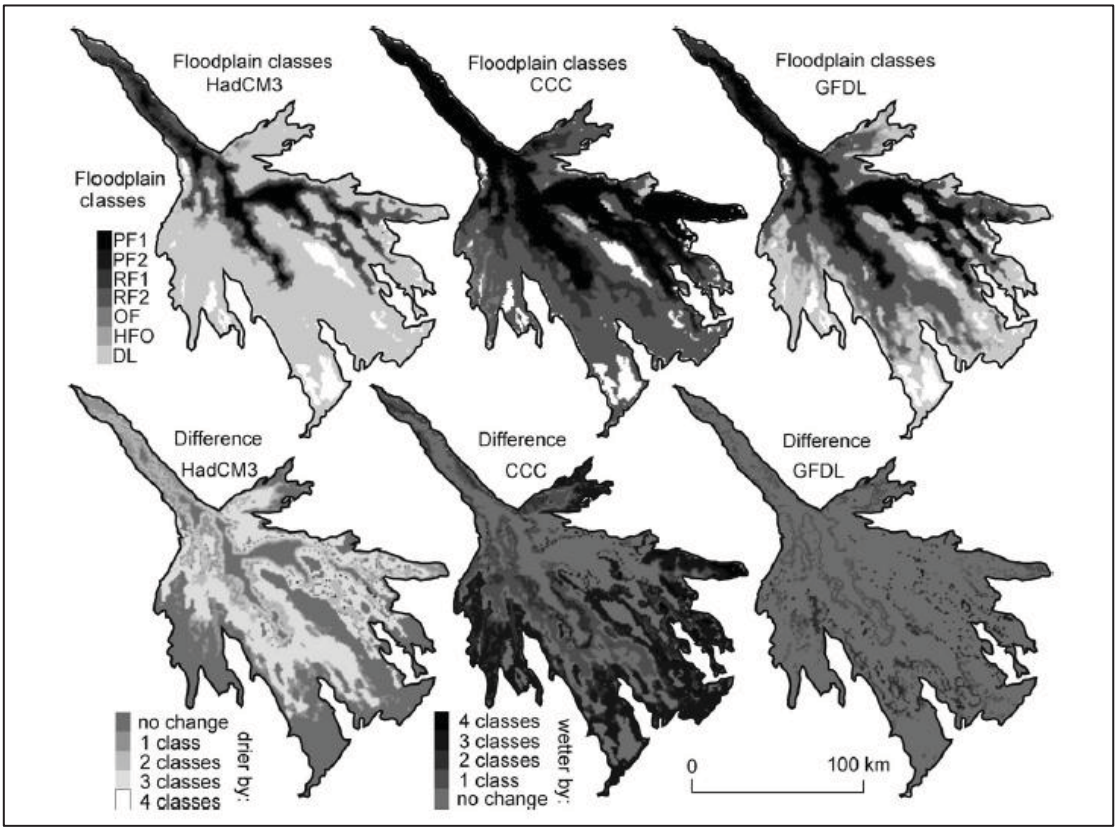

Figure 2.2: Effects of change in hydrological inputs on the Okavango Delta as obtained from various climate models (HadCM3, CCC and GFDL) under A2 greenhouse gases scenario for 2020–2050 period.
[Adapted from Murray-Hudson et al., 2006]

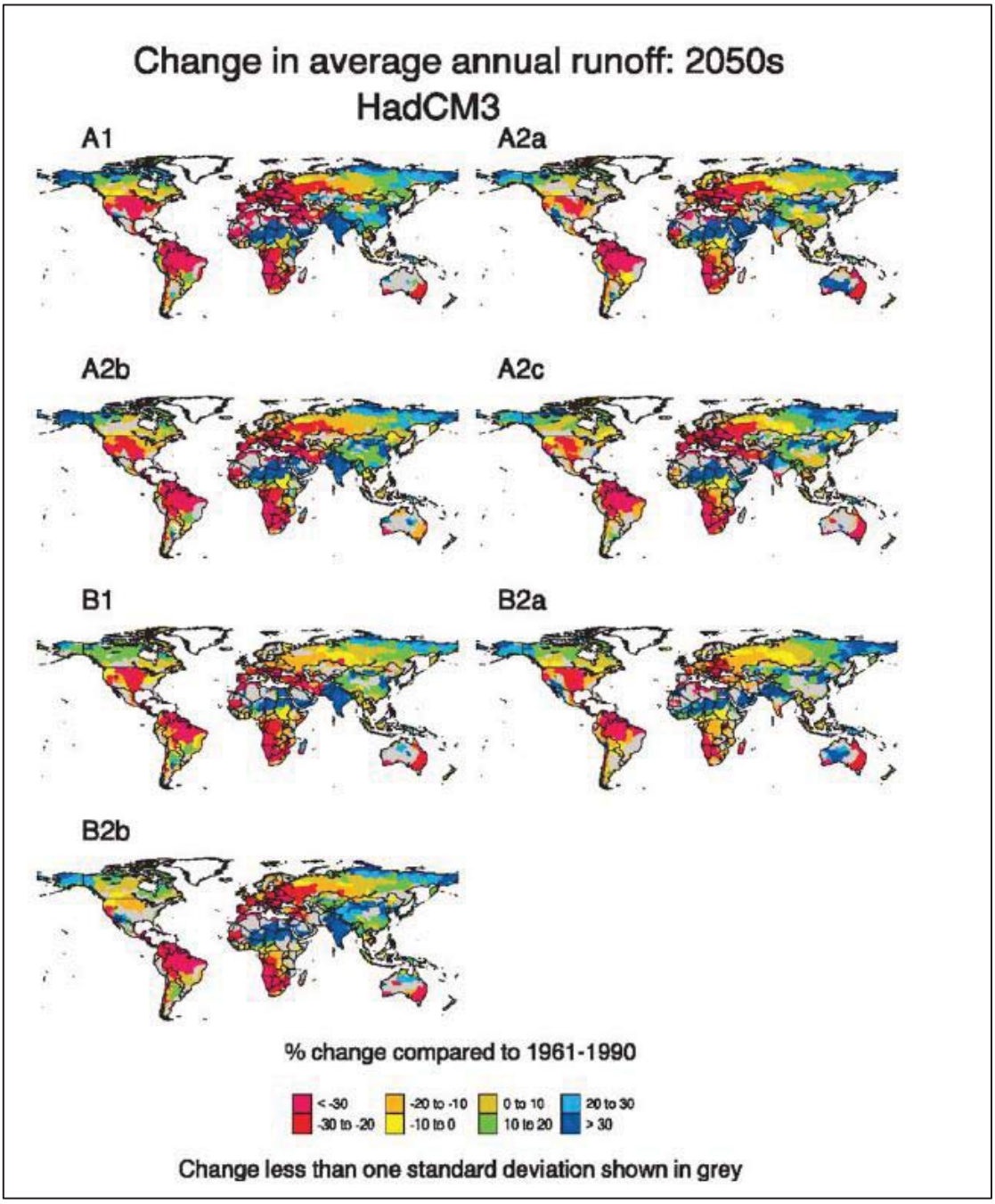

Figure 2.3: Changes in average annual runoff for 2050 using A2 IPCC Emission scenario shown by different GCMs. Percentage change compared to 1961-1990.
(GCMs HadCM3, ECHAM4, CGCM2, CSIRO, GFDL and CCSR/NIES)
[Adapted from Arnell, 2004]

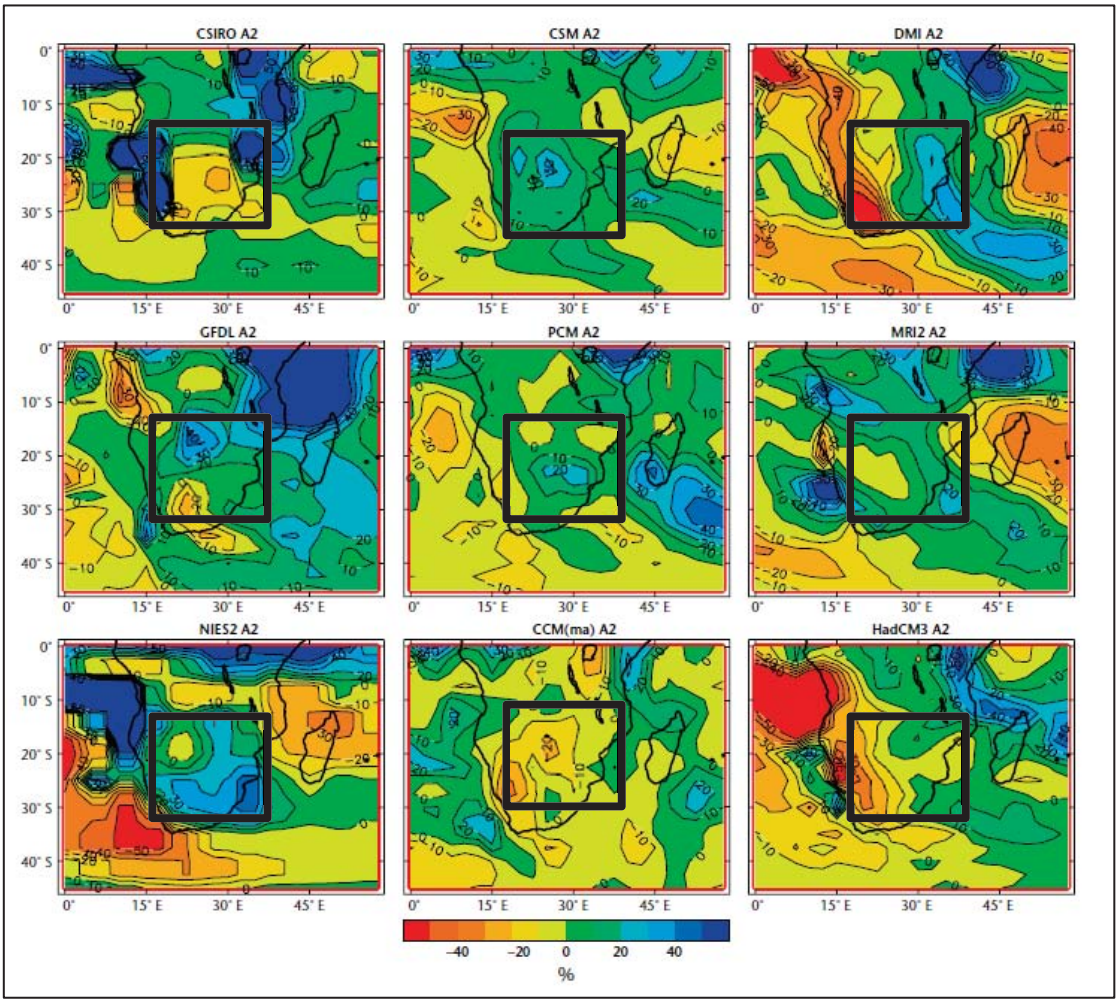

Figure 2.4: Thirty-year mean change in summer (DJF) precipitation (%) for the 2080s relative to the present-day under the A2 emissions scenario from nine different fully coupled ocean-atmosphere GCMs.
[GCMs: CSIRO, CSM, ECHAM4, GFDL, PCM, MRI2, NIES2, CGCM2 and HadCM3] [Adapted from PRECIS Handbook, Jones et al., 2004]

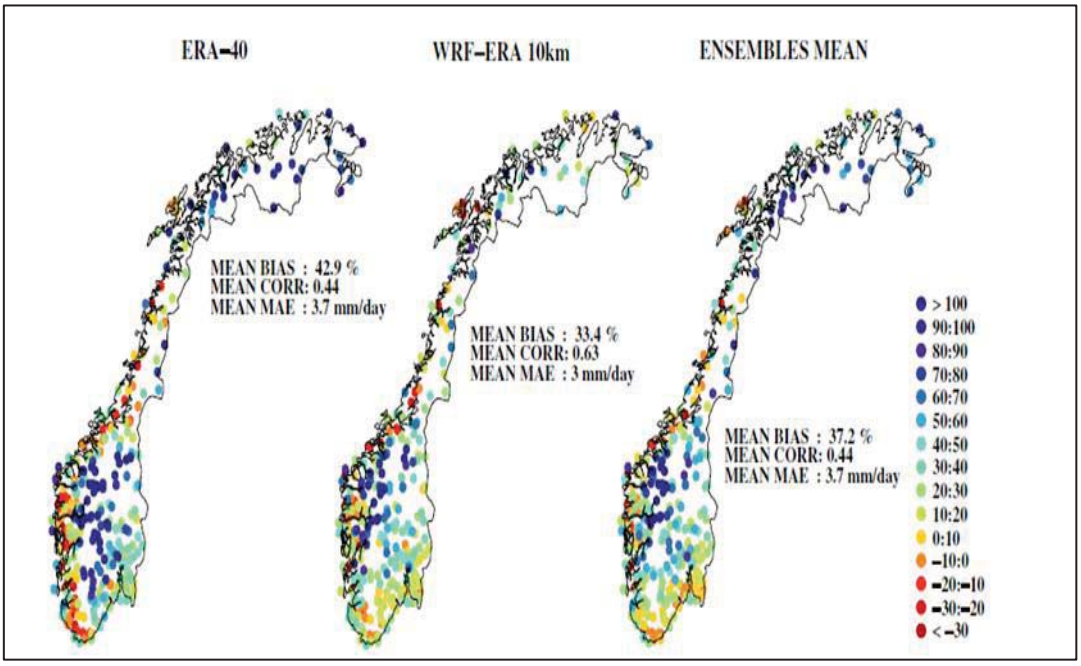

Figure 2.5: The 30-year total precipitation bias of the ERA-40 reanalysis, the WRF model (10km) and the 12 model mean of the ENSEMBLES project [Adapted from Heikkila et al., 2011].

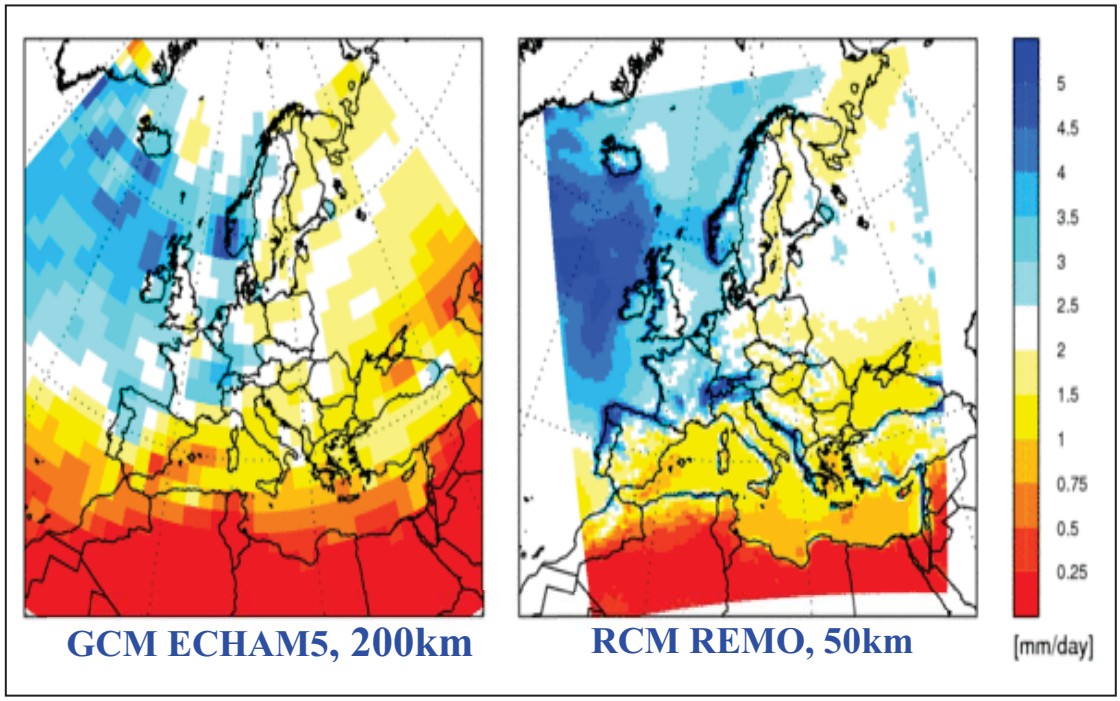

Figure 2.6: Precipitation fields from ECHAM5 (~200 km horizontal resolution, left) and REMO (~50 km, right) simulations over Europe [Adapted from Max Planck Institute for Meteorology, Hamburg, Germany, Sieck, 2008].

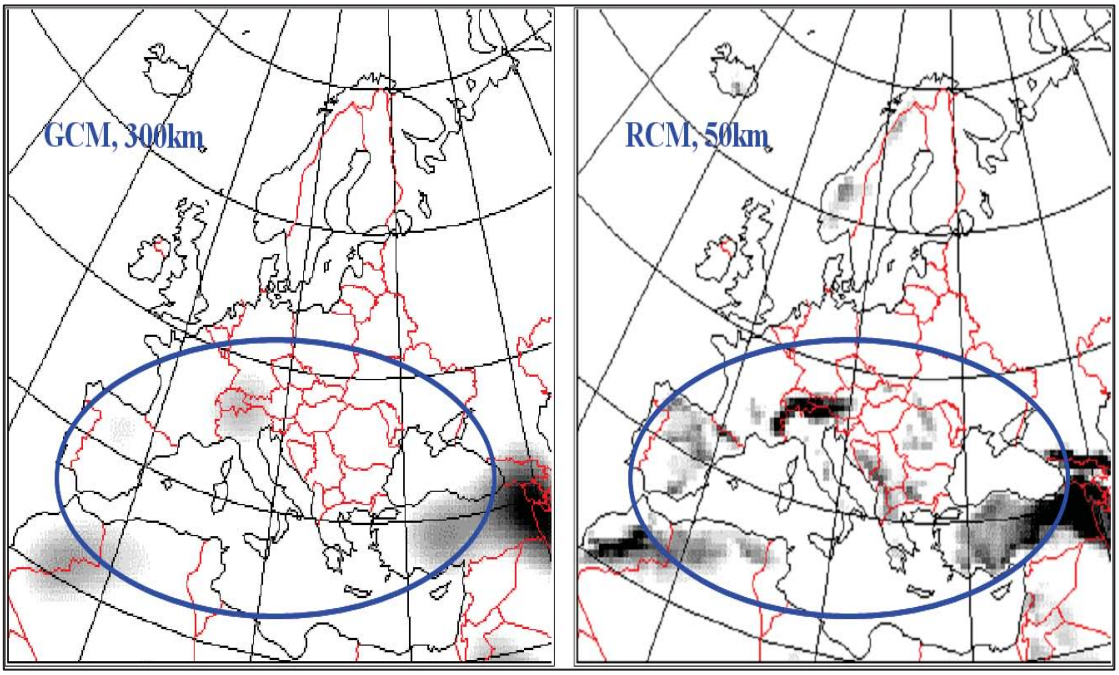

Figure 2.7: Topographic details over Europe seen in: (a) GCM (left) (b) RCM (right)
[Adapted from Christensen, 2001]

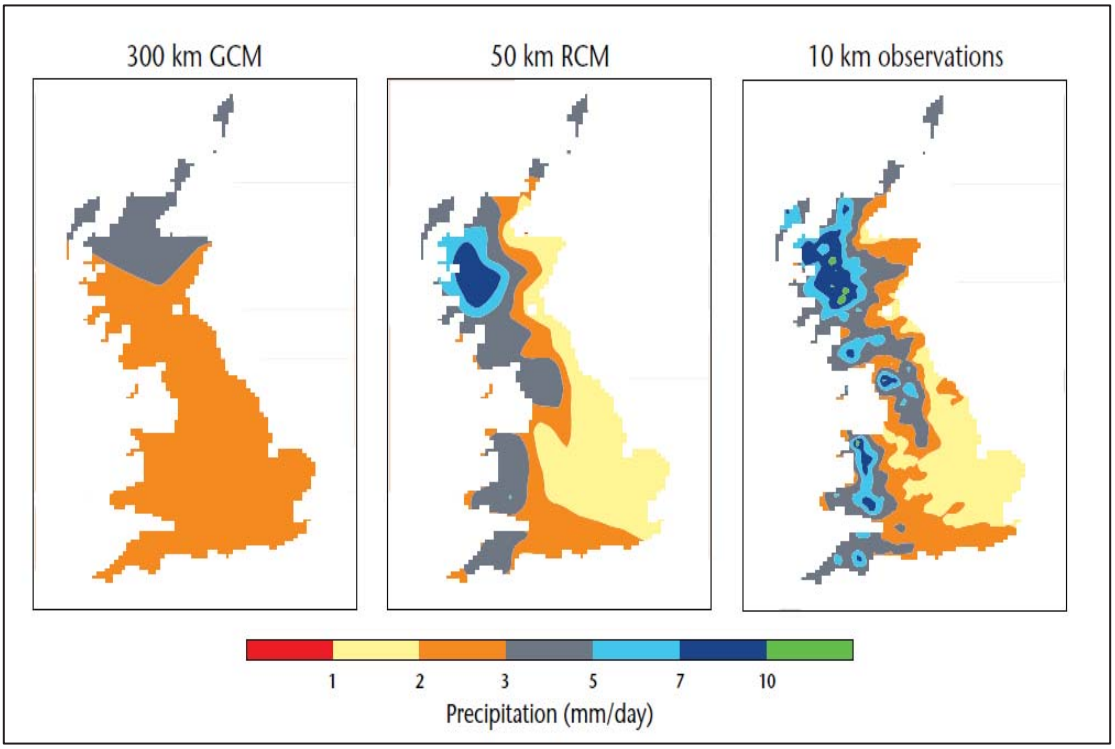

Figure 2.8: Precipitation over Great Britain as simulated by GCM and RCM compared to observations
[Adapted from Jones et al., 2004]

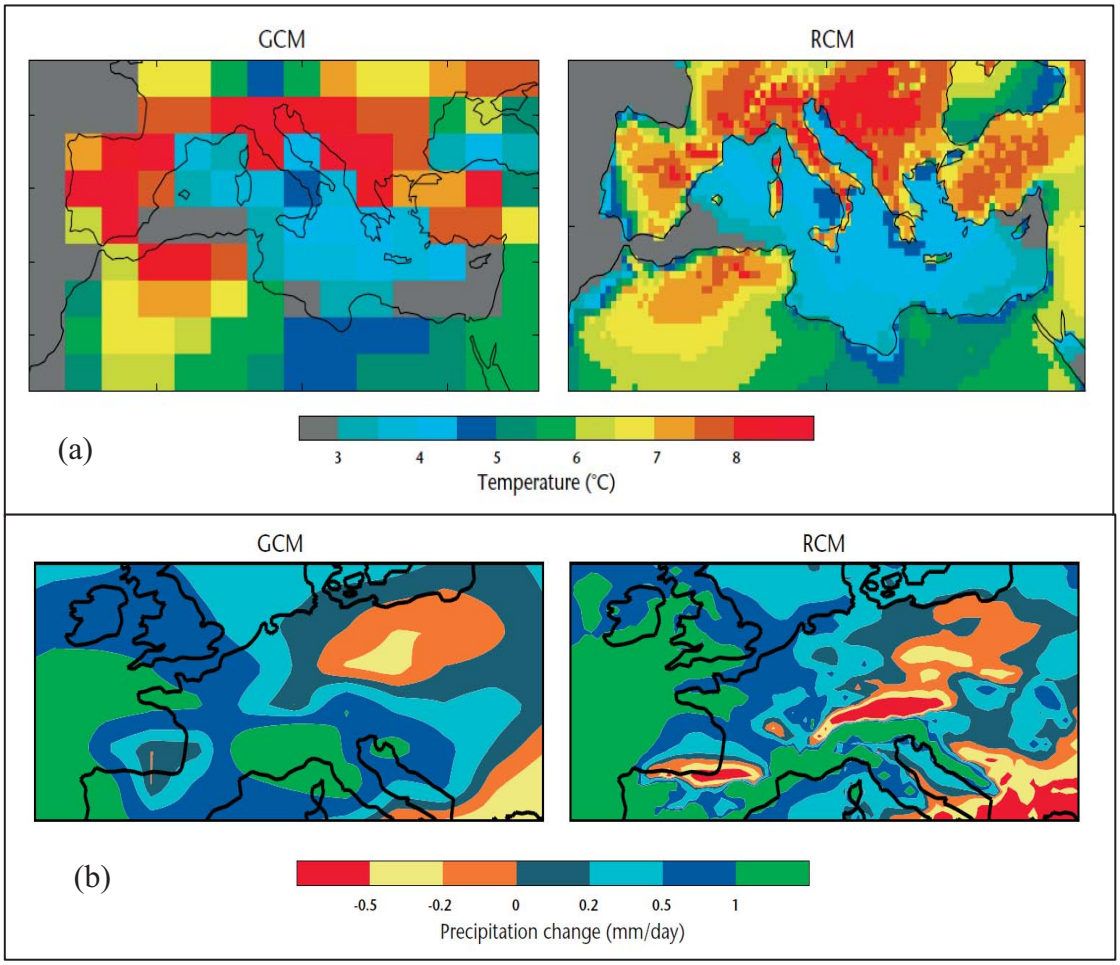

Figure 2.9: Hadley Centre GCM and RCM projection of (a) summer temperature change in and around the Mediterranean and (b) winter precipitation over the Pyrenees and Alps, two mountain ranges in Europe [Adapted from PRECIS Handbook, Jones et al., 2004]

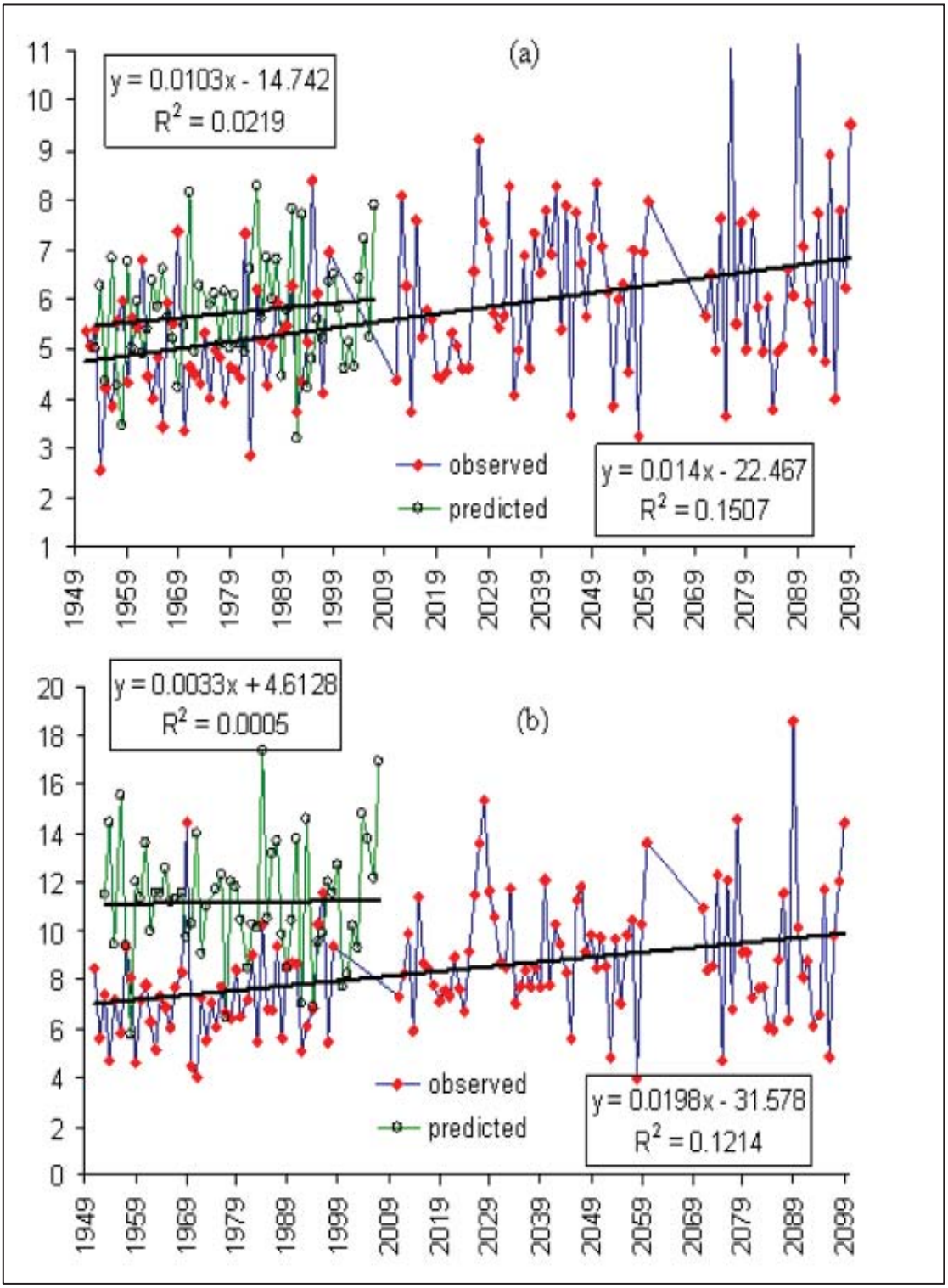

Figure 2.10: Daily RCM predicted rainfall over Dhaka city from 1951 to 2100 using A1B scenario for (a) whole year and (b) monsoon (June-September) [Adapted from Murshed et al., 2011]

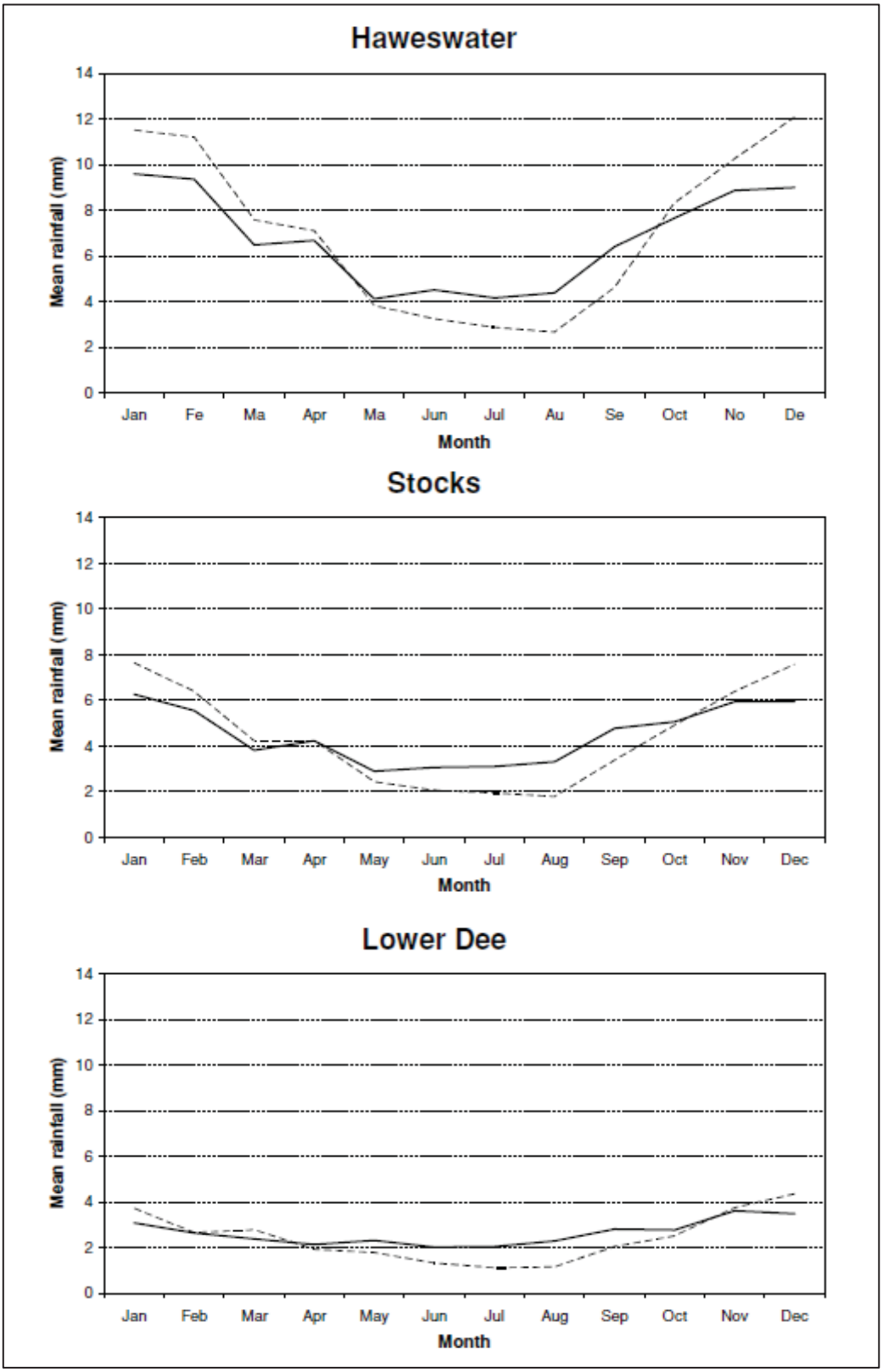

Figure 2.11: Comparison of catchment monthly mean rainfall (mm) for observed data (bold line), bias-corrected HadRM3H control scenario (bold line) and bias-corrected HadRM3H future scenario (dashed line)
[Adapted from Fowler and Kilsby, 2007]

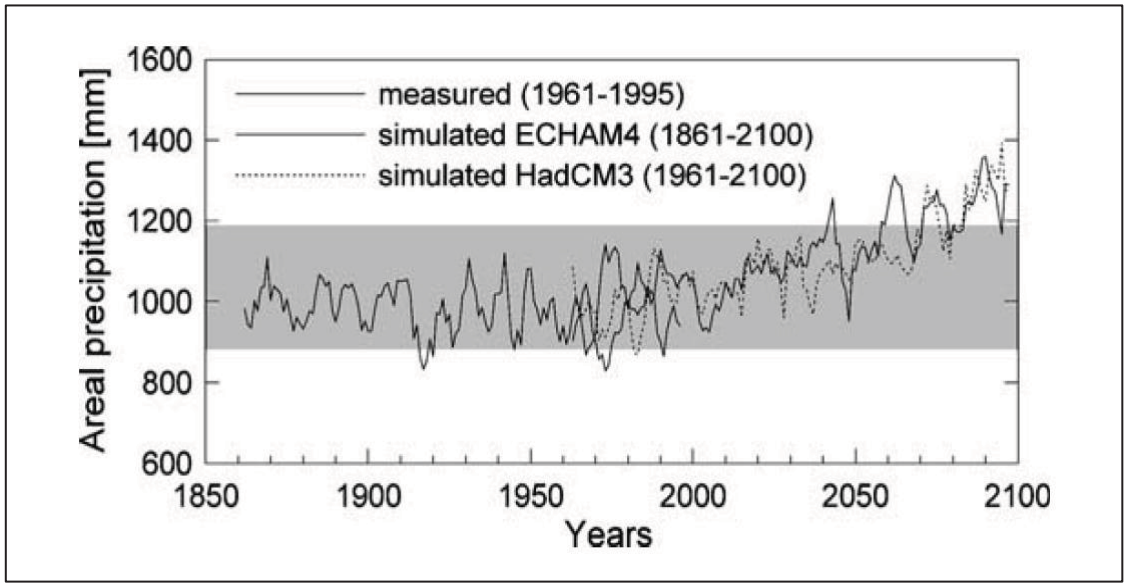

Figure 2.12: The temporal behaviour of areal precipitation in the Neckar catchment, constructed using measured and simulated station data.
The curves represent running averages over five consecutive years. The shaded area is the assumed natural variability as computed using downscaled data from the ECHAM4/OPYC3 control run. [Adapted from by Menzel et al., 2006]

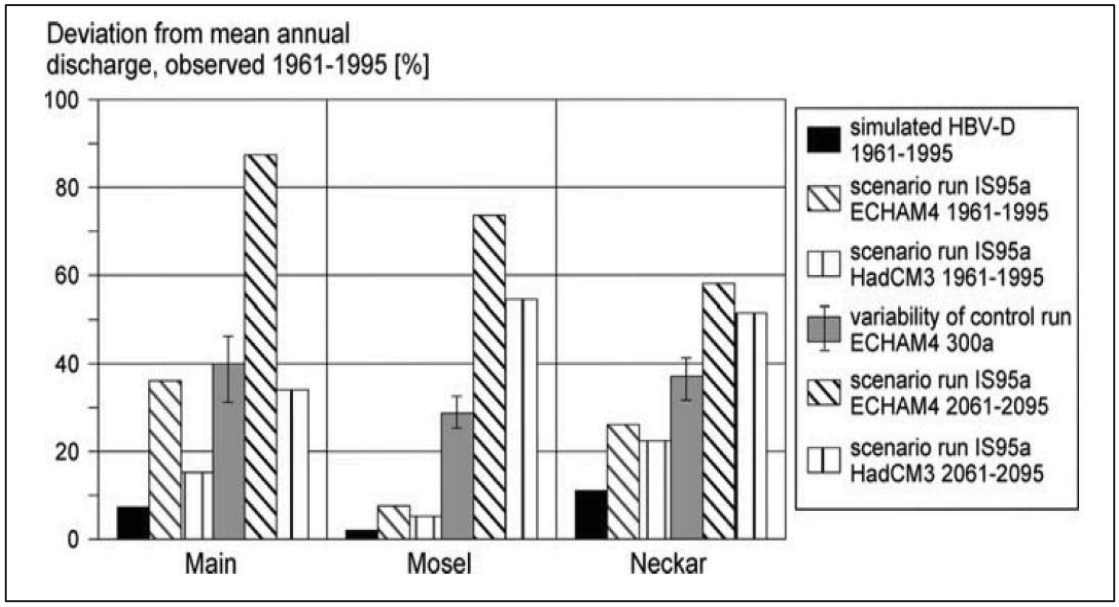

Figure 2.13: Deviations (in %) between mean annual discharge determined by measurements and simulations using HBV-D with measured (black bars) and downscaled climate input, respectively.
The reference periods are the years 1961–1995 and 2061–2095. The data represented by the ECHAM4/OPYC3 control run refer to the period 1961–1995 (grey bars), to which the whole variability of the control run computed over 300 years (error bars) is added. [Adapted from by Menzel et al., 2006]

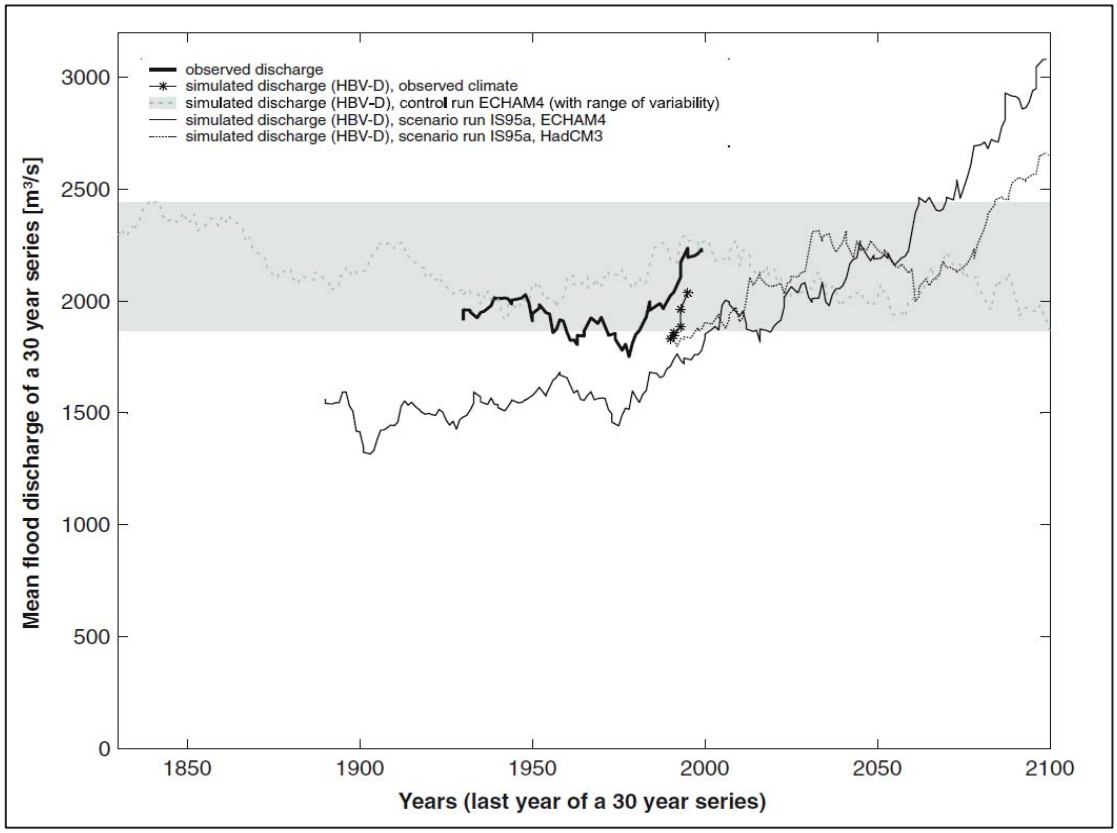

Figure 2.14: Development of the mean flood discharge at the Cochem gauge (River Mosel).
The data points represent running averages of annual maximum discharges over 30 consecutive years. The grey shaded box encloses the assumed natural variability as constructed using a 300-year ECHAM4/OPYC3 control run.
[Adapted from by Menzel et al., 2006]

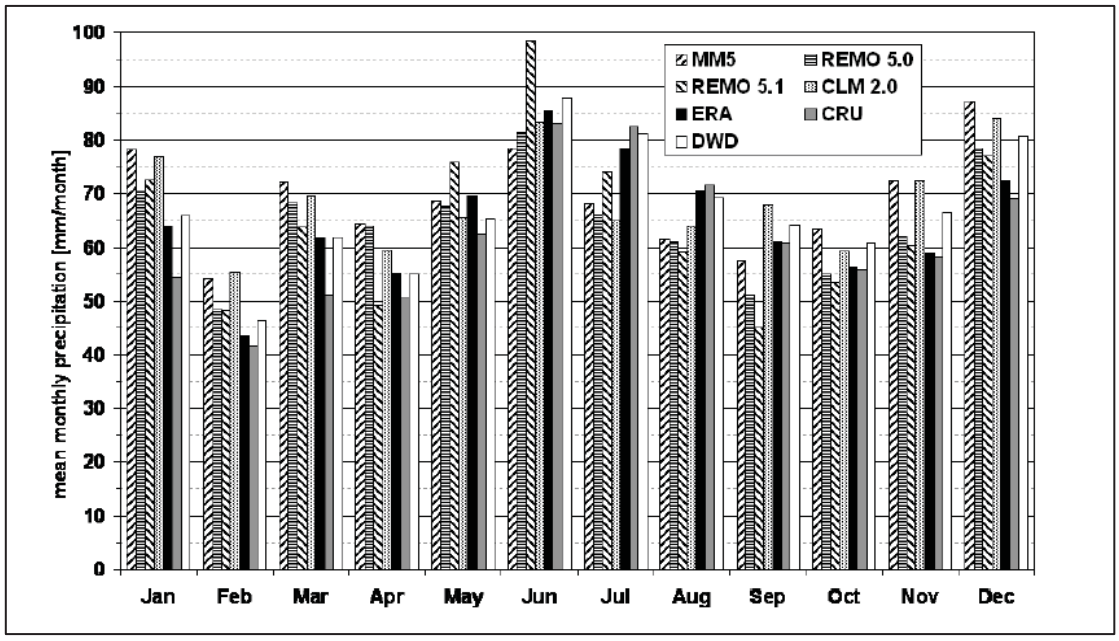

Figure 2.15: Mean annual cycle of total precipitation over Germany (RCM simulations and reference data sets) [mm/month].
[Adapted from Kotlarski et al., 2005]

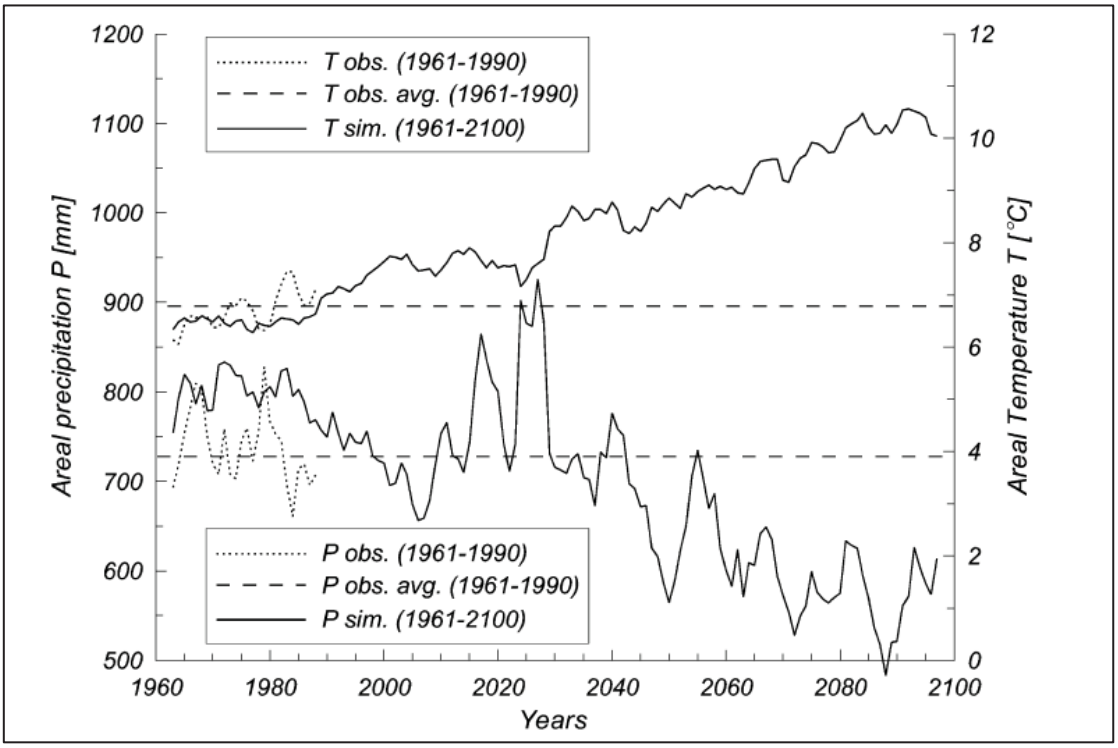

Figure 2.16: Annual areal temperature T and annual areal precipitation P for the Mulde catchment derived from observations
('obs.', period 1961–1990, dotted lines) and from simulations ('sim.', period 1961–2100, solid lines) using the downscaled output from a GCM climate change scenario run. The respective averages ('avg.', period 1961–1990) from observations are given as dashed lines. [Adapted from Menzel and Burger, 2002]

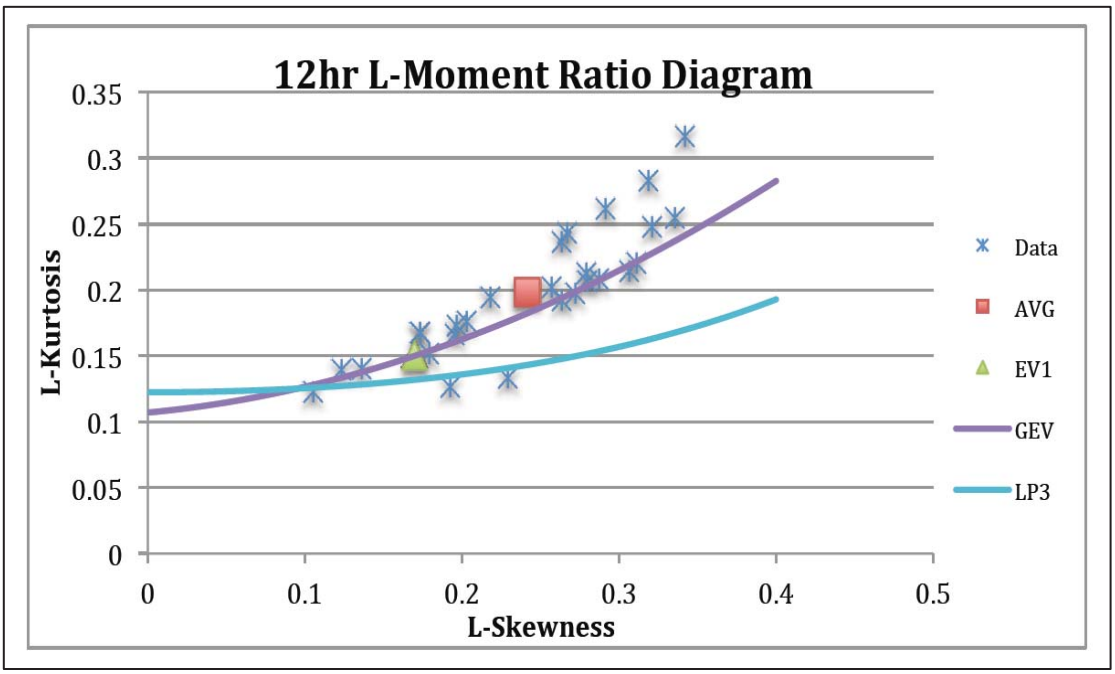

Figure 2.17: L-Moment Ratio Diagram for 12-hour storm duration
[Adapted from Millington et al., 2011]

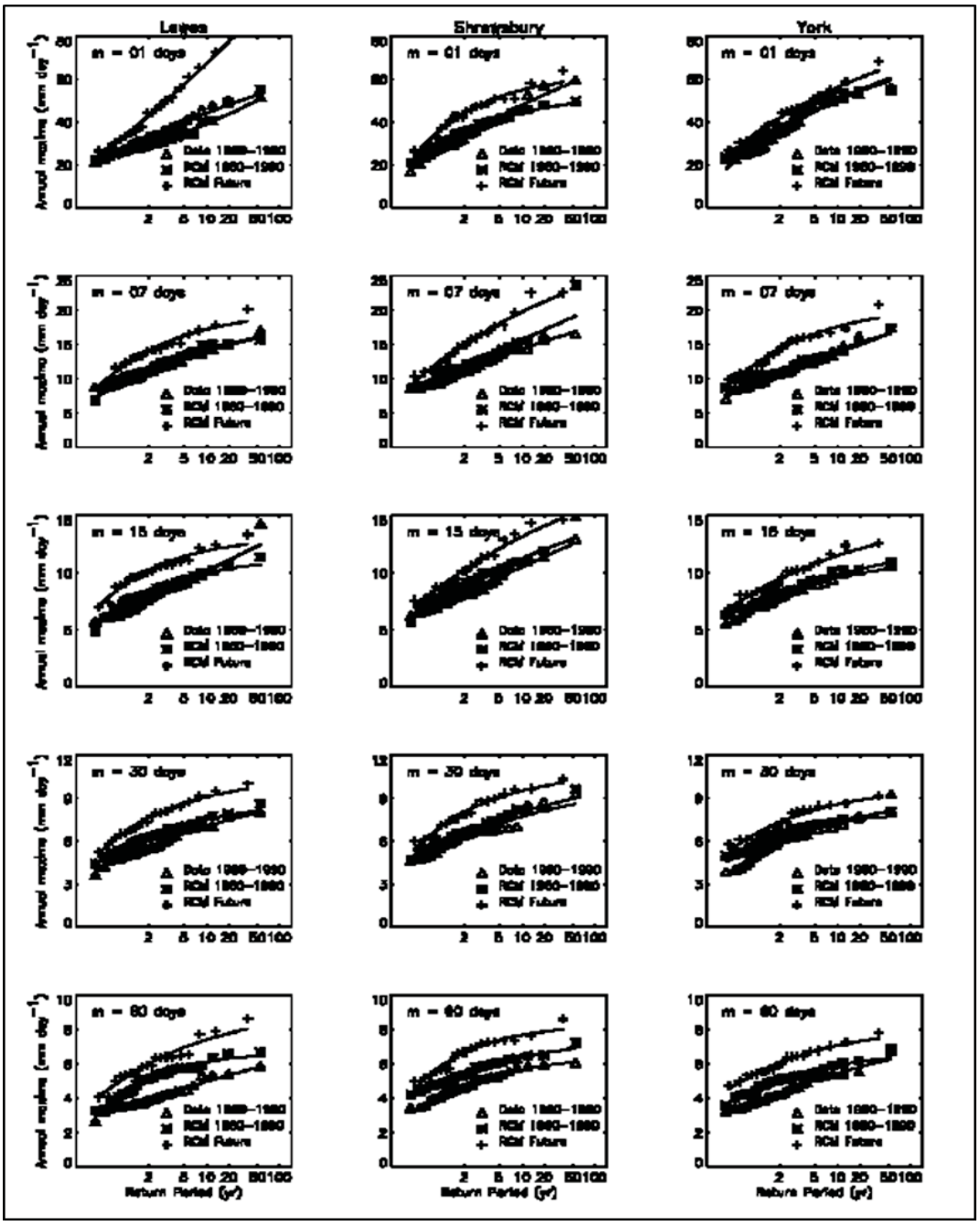

Figure 2.18: A plot of the annual maximum series (y-axis) from both measurements and regional climate model (RCM) output related to return period (x-axis).

The associated fitted generalized extreme-value frequency distributions (full lines) are also plotted. This is for (i) the raingauge data for the period 1961–1990 (triangles), (ii) the output from the RCM when nested within the control general-circulation model simulation with greenhouse-gas concentrations approximately at 1975 levels (stars), and (iii) the output from the RCM when nested within the last 20 years of the transient simulation which may, therefore, be representative of a future climate (crosses). The three columns of plots correspond to the three catchment areas of interest. The five rows correspond to different durations, m, in the calculation of the annual maximum series. [Adapted from Huntingford et al., 2003]

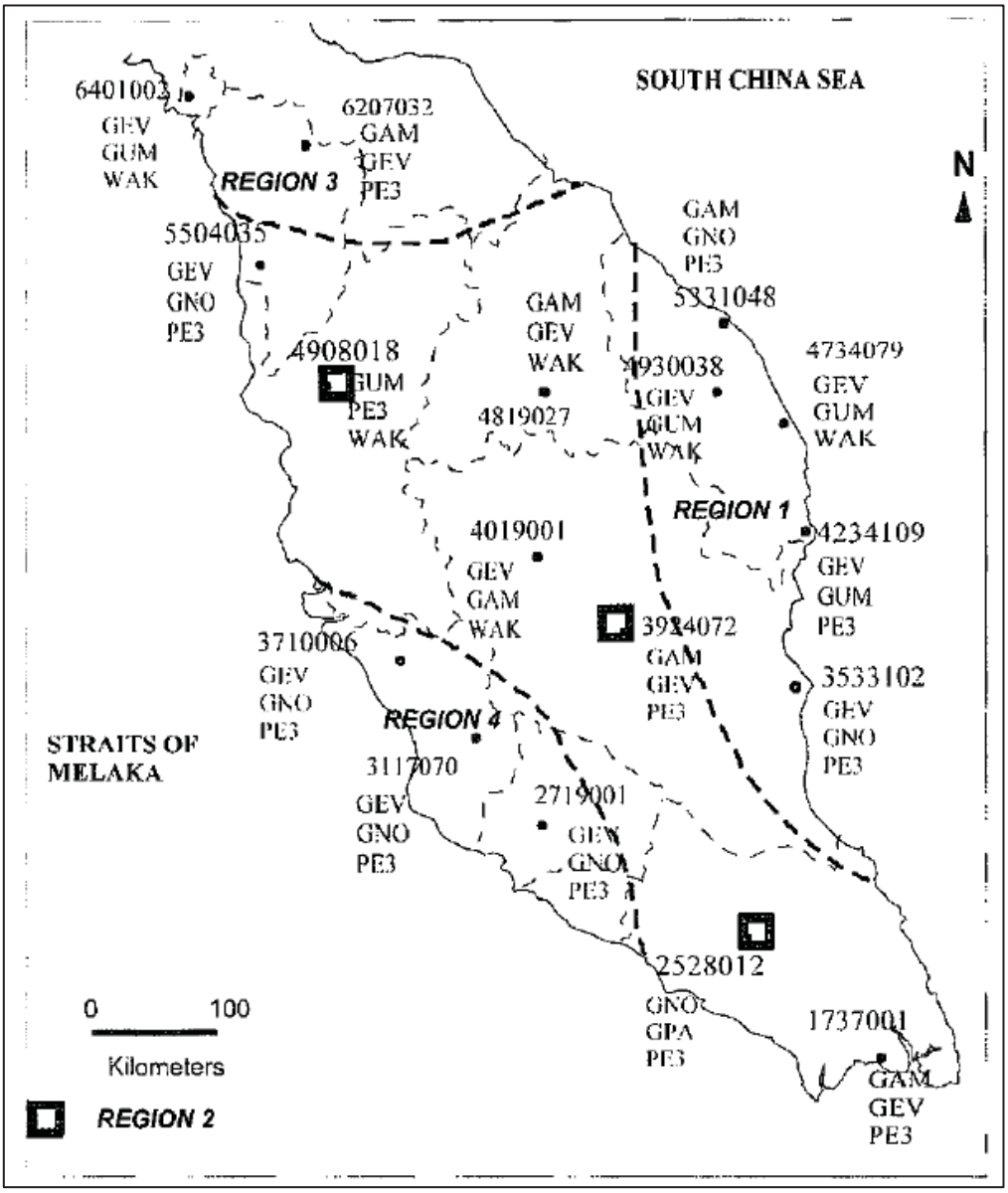

Figure 2.19: Map of Peninsular Malaysia showing the location of the stations, the three best fit distributions selected based on PPCC, RRMSE, RMSE and MAE values and the boundaries of the homogeneous regions.
[Adapted from Mohd Daud et al., 2002]

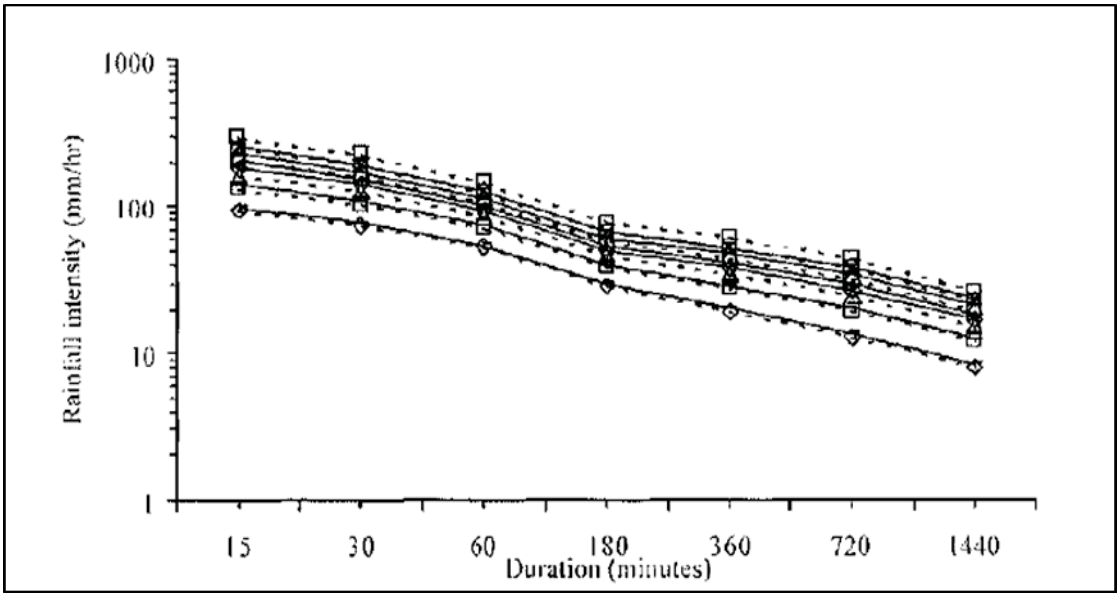

Figure 2.20: IDF curves produced from GEV (dotted line) and Gumbel (full lines) for Pekan station.
(Curves in descending order: 100, 50, 25, 10, 5 and 2-year return periods)
[Adapted from Mohd Daud et al., 2002]

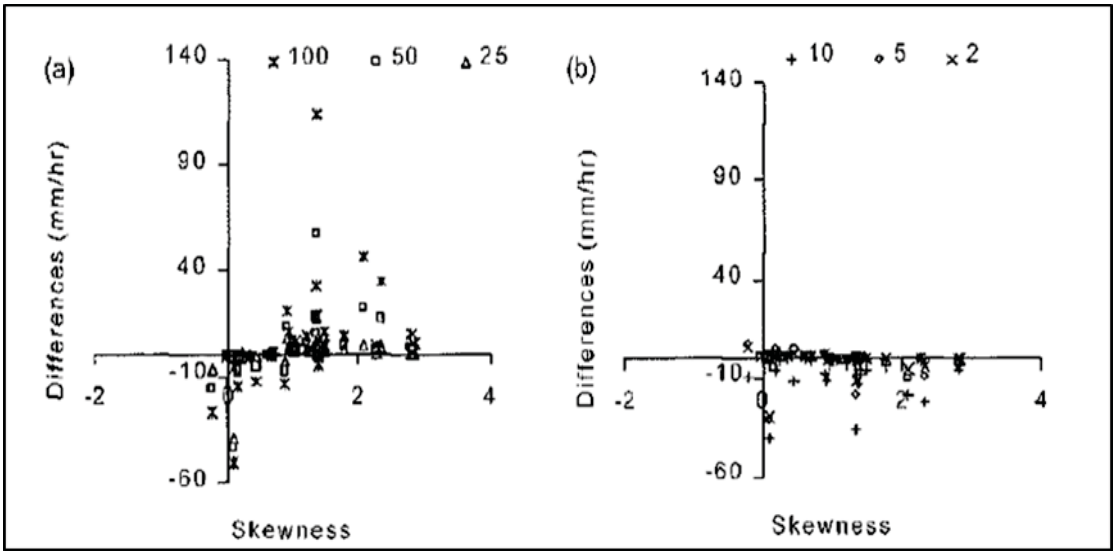

Figure 2.21: Plot of skewness vs the difference between GEV and Gumbel estimates
for (a) 100, 50, and 25-year return periods, and (b) 10, 5, and 2-return periods (GEV-Gumbel) [Adapted from Mohd Daud et al., 2002]

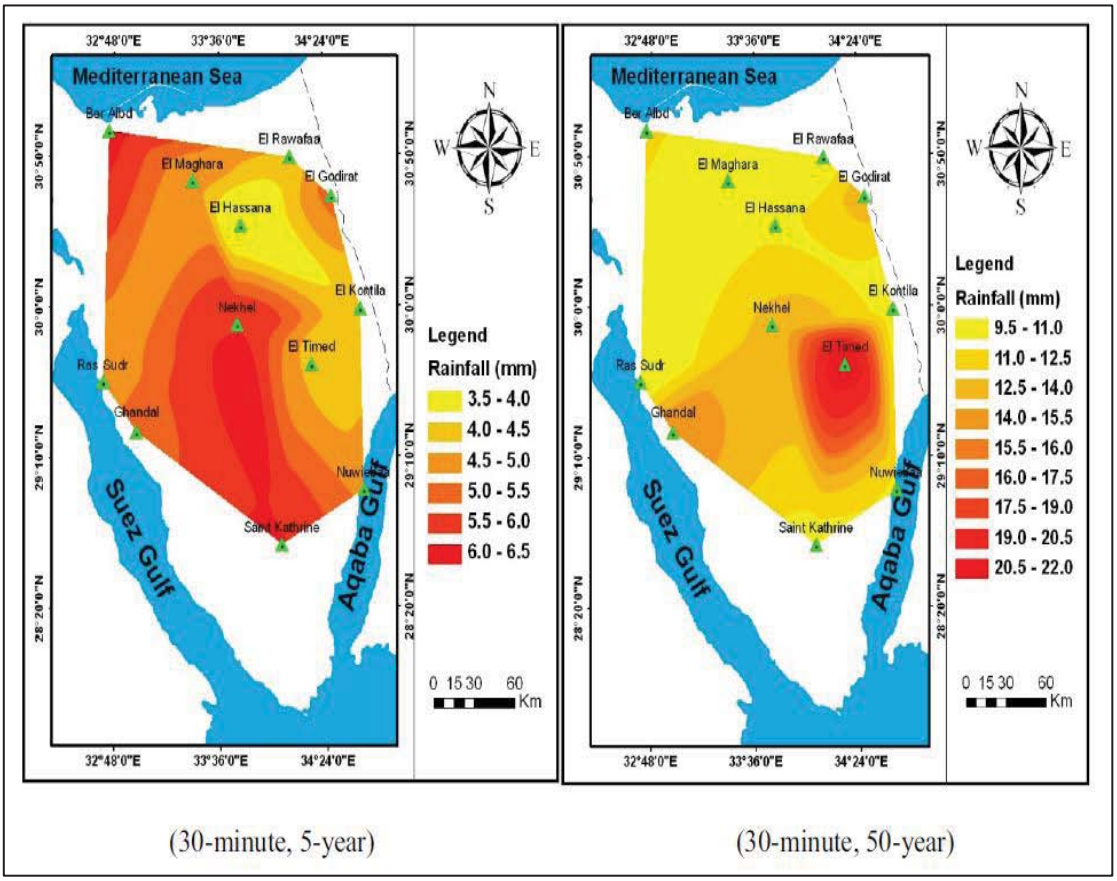

Figure 2.22: Typical Isopluvial Maps (mm) for 30 minute duration
[Adapted from El-Sayed, 2011]

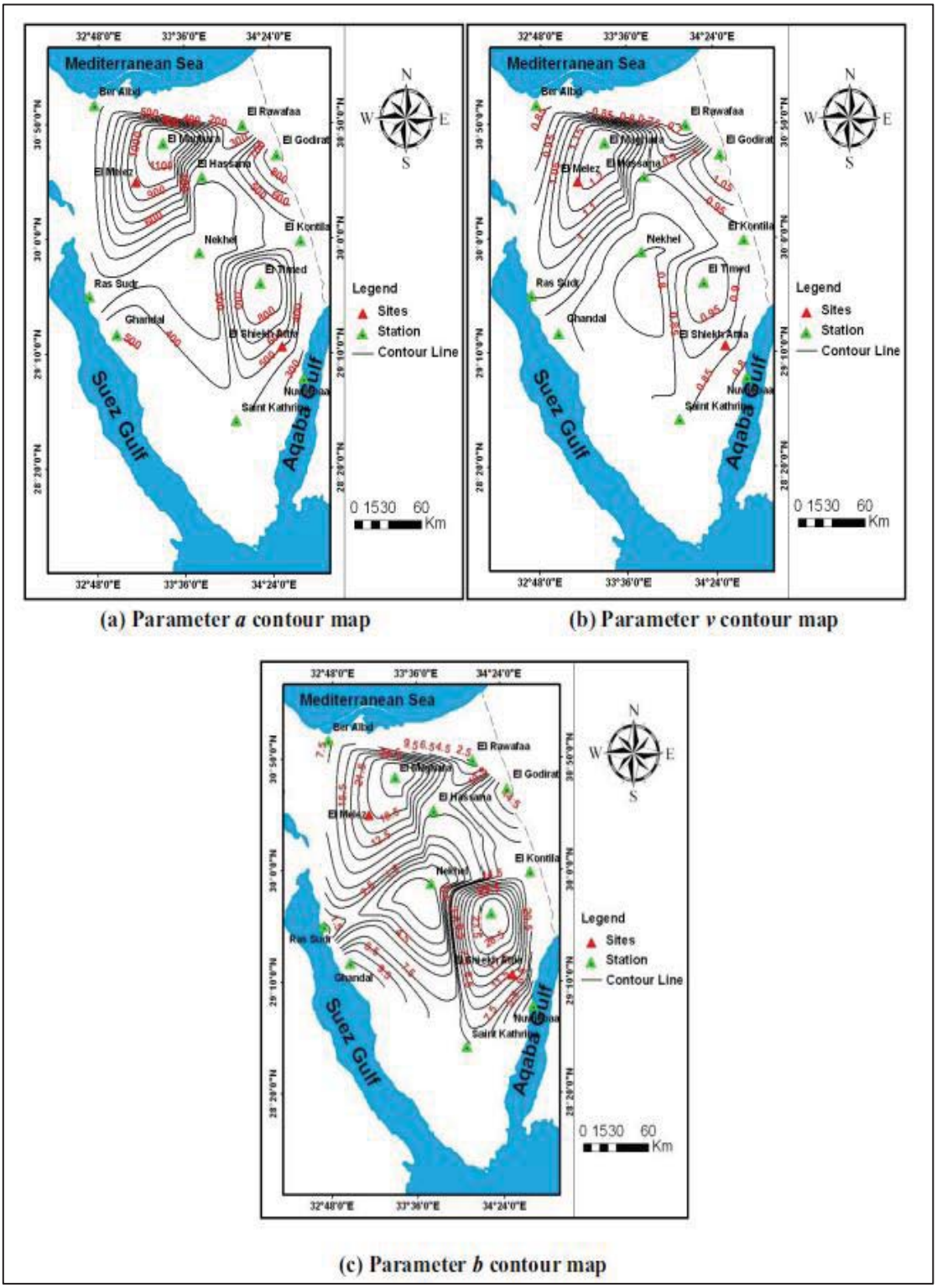

Figure 2.23: Parameters contour maps of Kimijima equation with 10-year return period
[Adapted from El-Sayed, 2011]

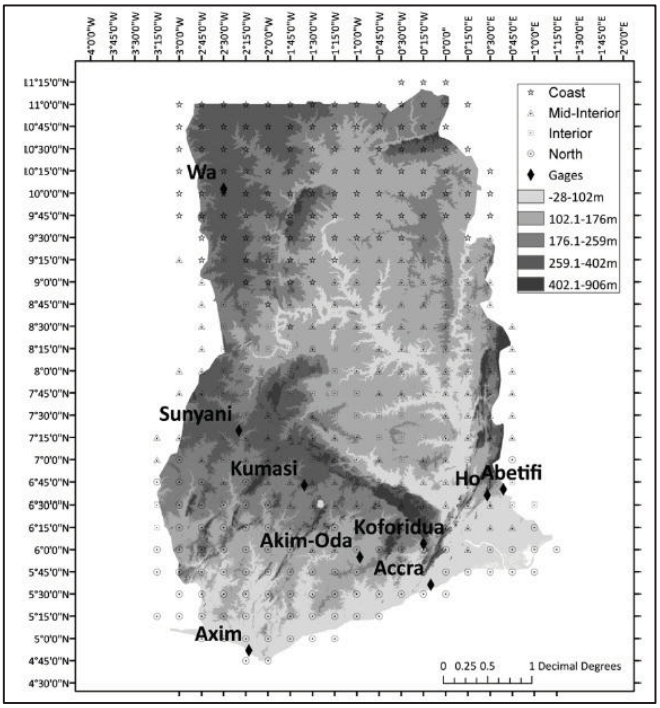

Figure 2.24: Map of Ghana showing 15-min TRMM bin coordinates, GMSD ground gauge station locations, ground elevation (meters), and rainfall regions. [Adapted from Endreny and Imbeah, 2009]

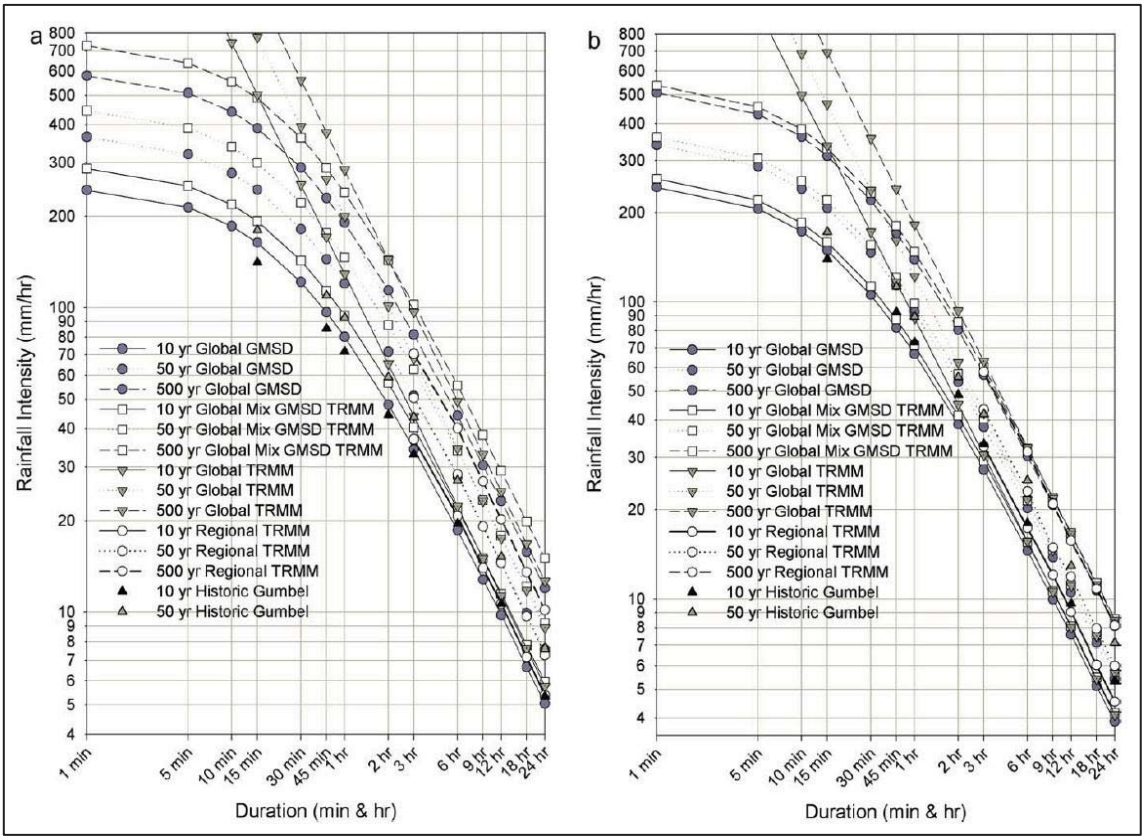

Figure 2.25: Rainfall intensity (mm/h) curves from the four IDF approaches and the 1974 Gumbel curve for 10–500 years return intervals for (a) Accra, and (b) Ho
[Adapted from Endreny and Imbeah, 2009]

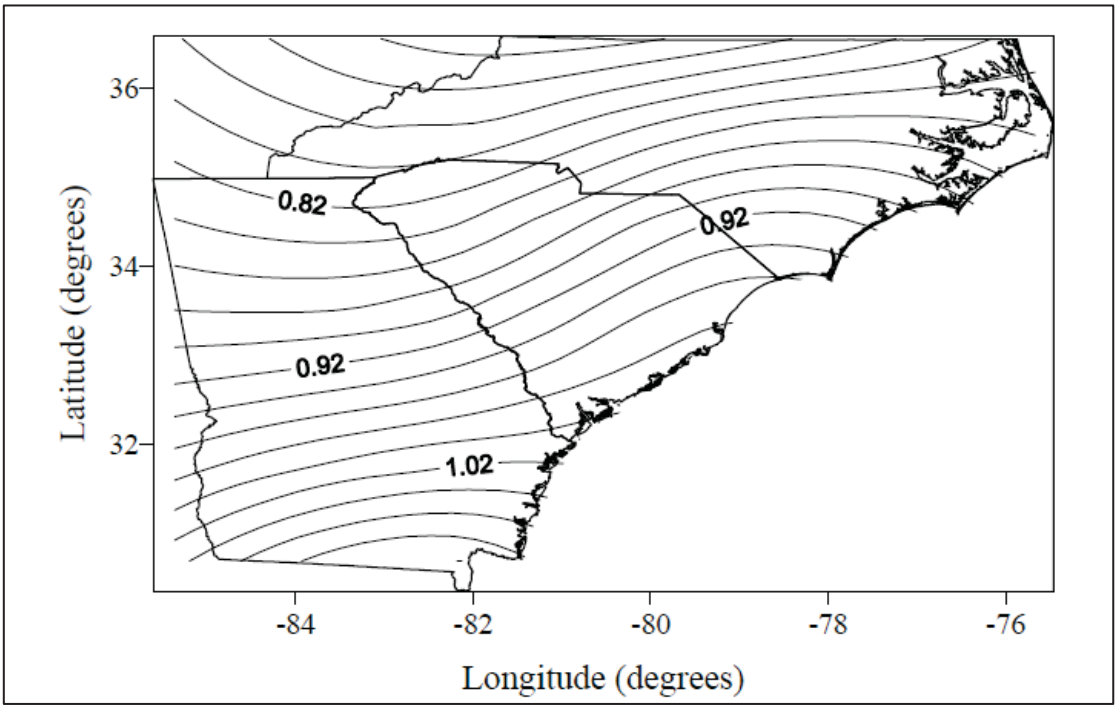

Figure 2.26: Typical Isopluvial Map (15-Minute, 2-Year)
[Adapted from Raiford et al., 2007]

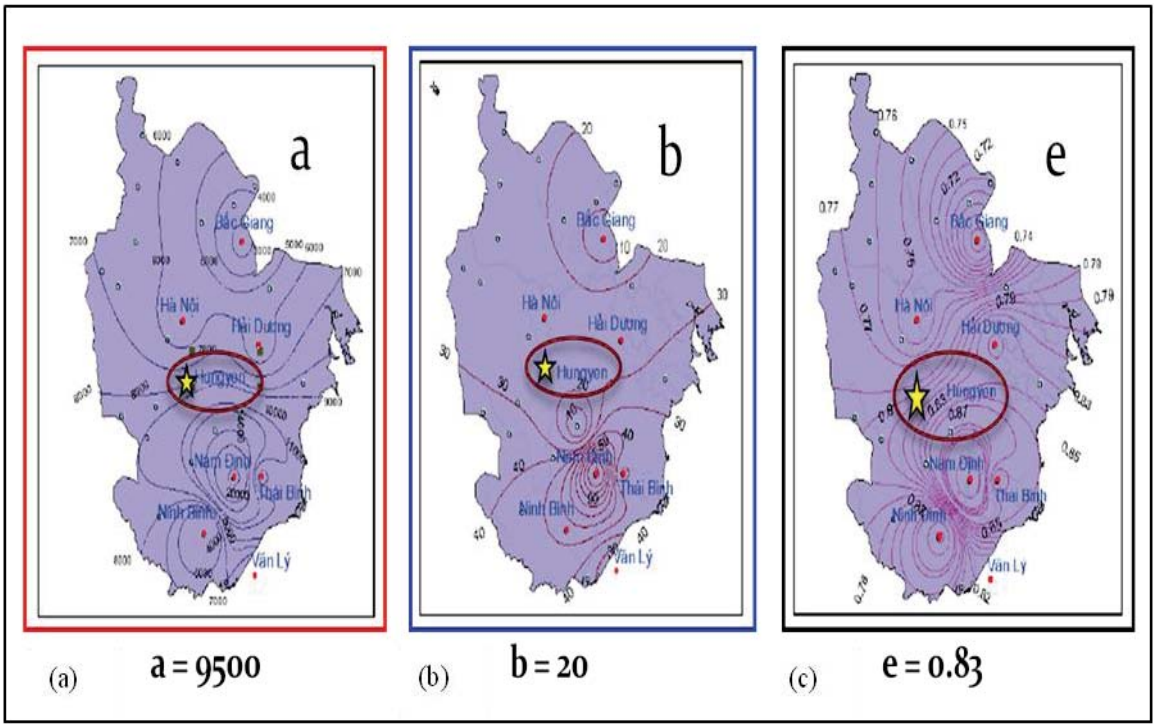

Figure 2.27: Contour map of parameter of Kimijima equation with 100 years returns period and IDF curves at un-gauged station
a) Parameter a contour map b) Parameter b contour map c) Parameter e contour map [Adapted from Nhat et al., 2006]

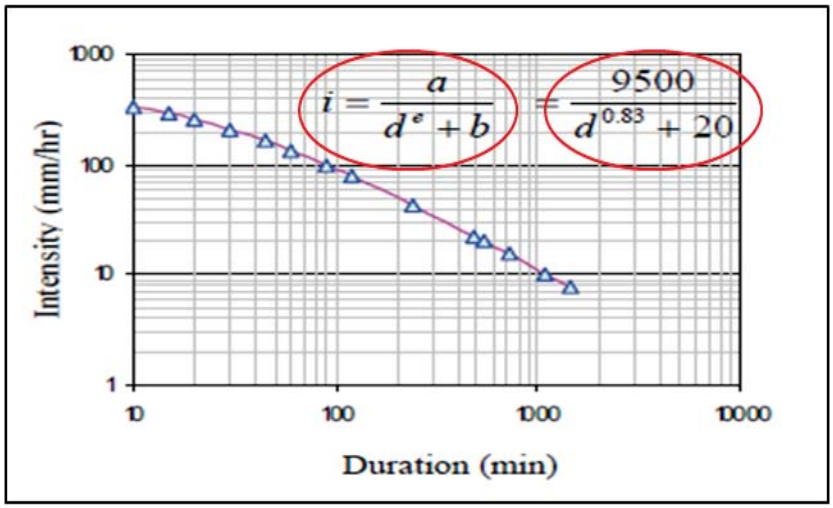

Figure 2.28: Rainfall IDF curves at Hungyen (ungauged location) using parameter contour maps
[Adapted from Nhat et al., 2006]

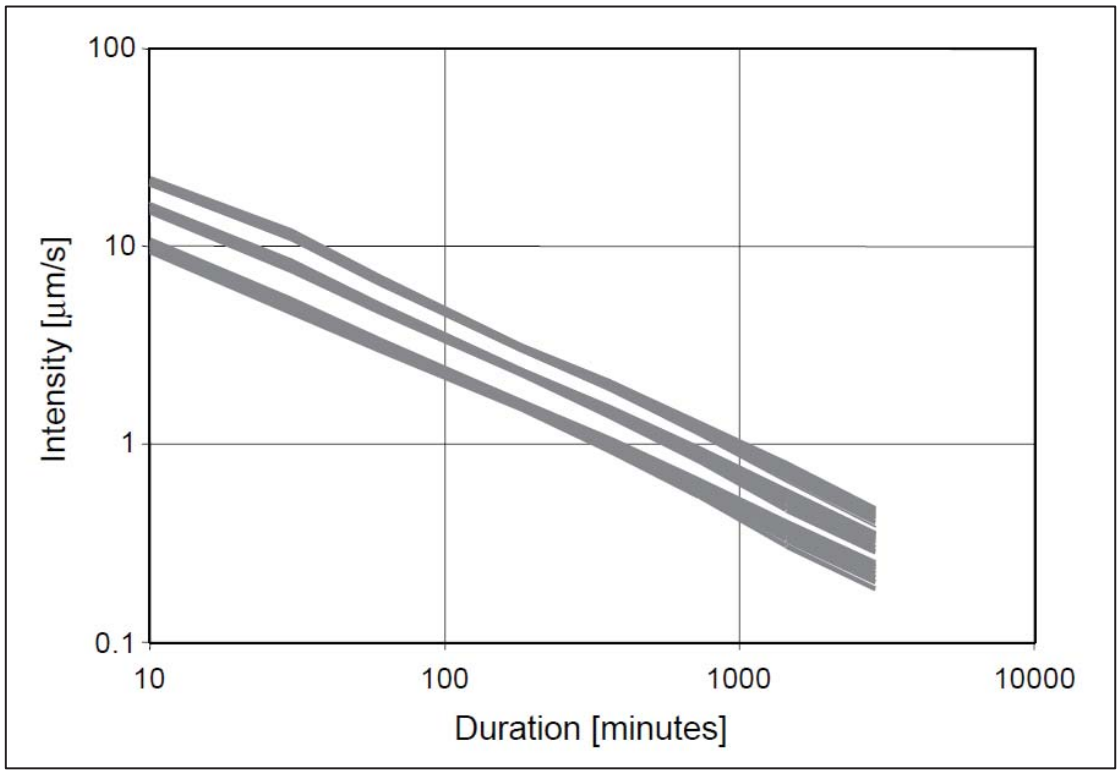

Figure 2.29: Regional intensity–duration–frequency (return periods T =1, 5 and 20 years) for the region 'outside Copenhagen'.
The grey shaded areas illustrate the effect of variations in Mean Annual Rainfall (MAR) within the region. [Adapted from Mikkelsen et al., 2005]

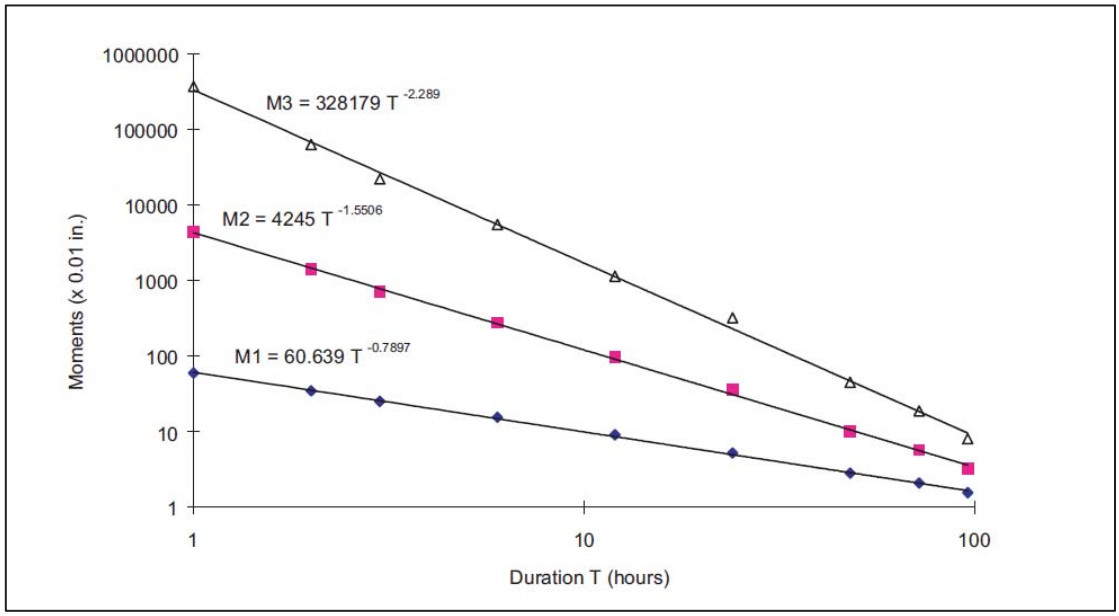

Figure 2.30: The log-log plot of maximum rainfall non-central moments (NCMs) versus rainfall duration for McGill station
[Adapted from Nguyen et al., 2002]

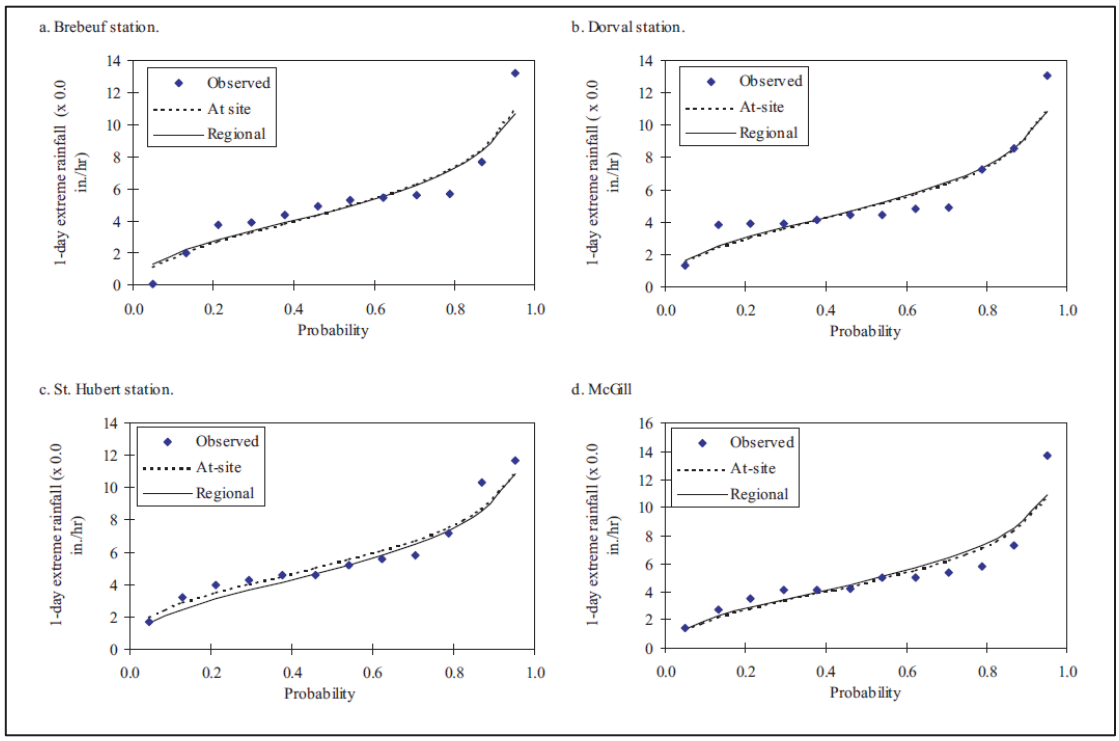

Figure 2.31: Empirical (observed) and estimated (at-site and regional) distributions of annual maximum daily rainfalls for Brebeuf, Dorval, St-Hubert, and McGill stations
[Adapted from Nguyen et al., 2002]

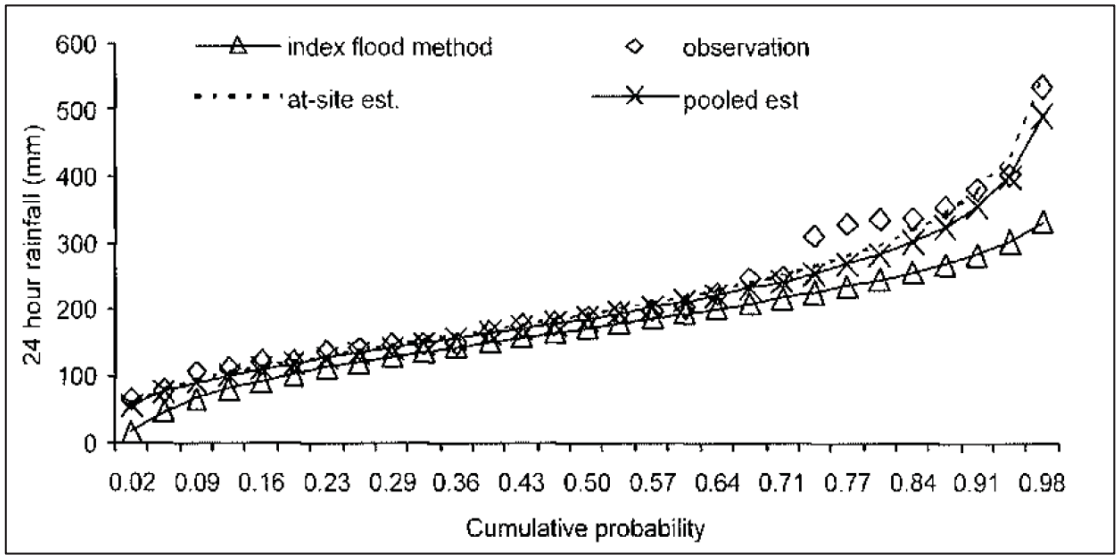

Figure 2.32: Comparison of index-flood method to the pooled station-year method for Pekan Station.
[Adapted from Mohd Daud et al., 2002]

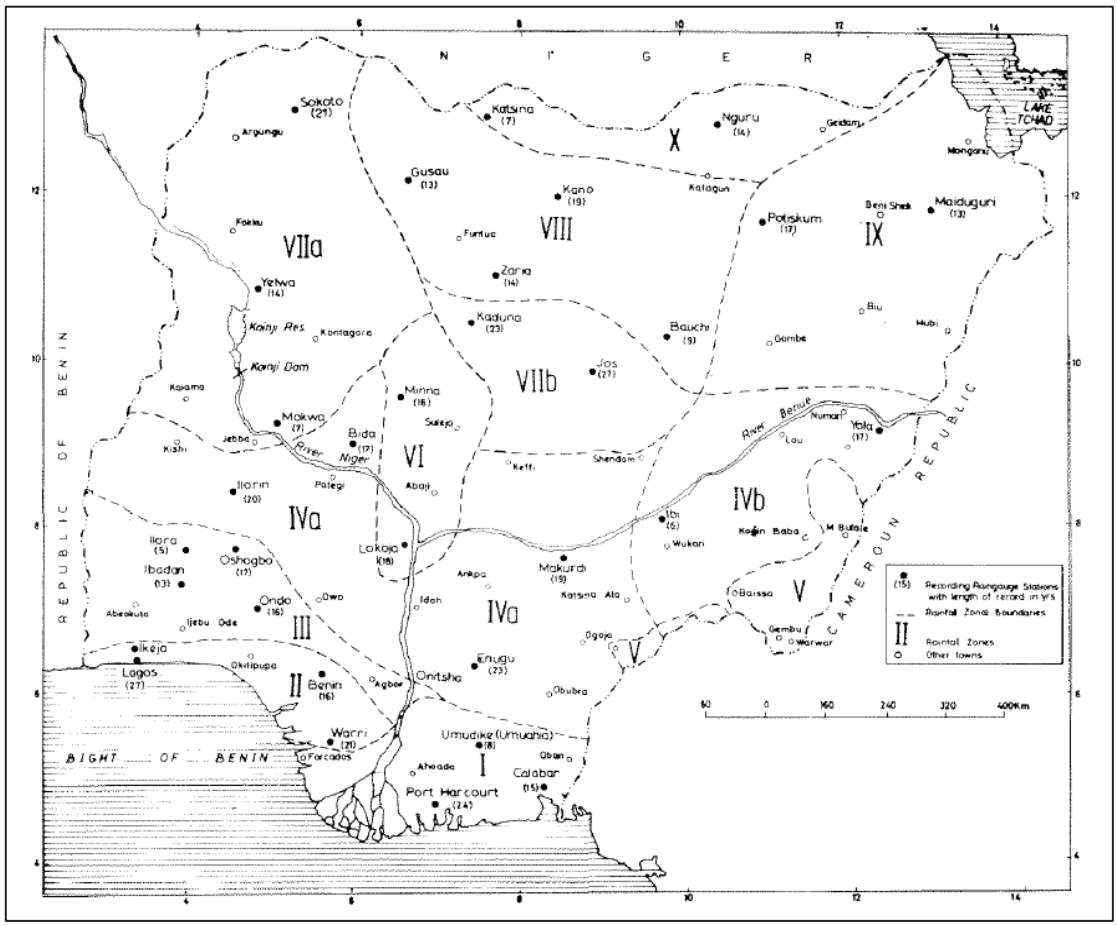

Figure 2.33: Rainfall zones in Nigeria
[Adapted from Oyebande, 1982]

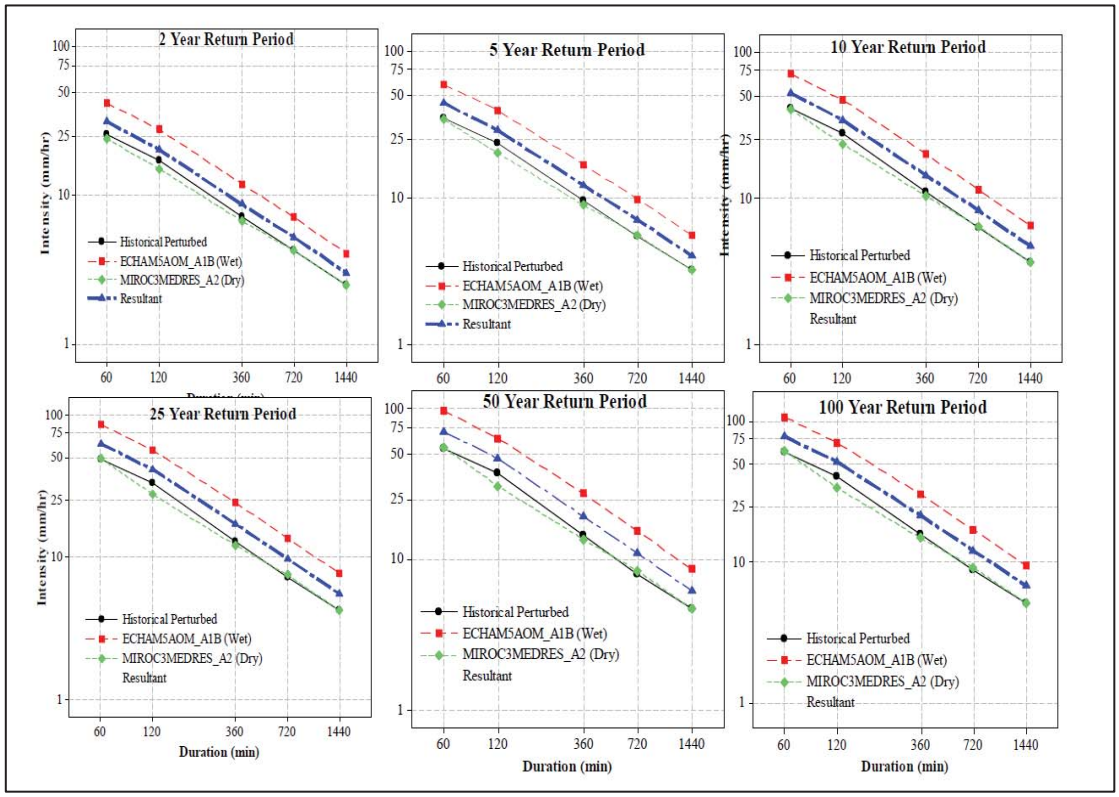

Figure 2.34: Comparison of IDF plots for different scenarios: 2071 – 2100 [Adapted from Solaiman and Simonovic, 2011]

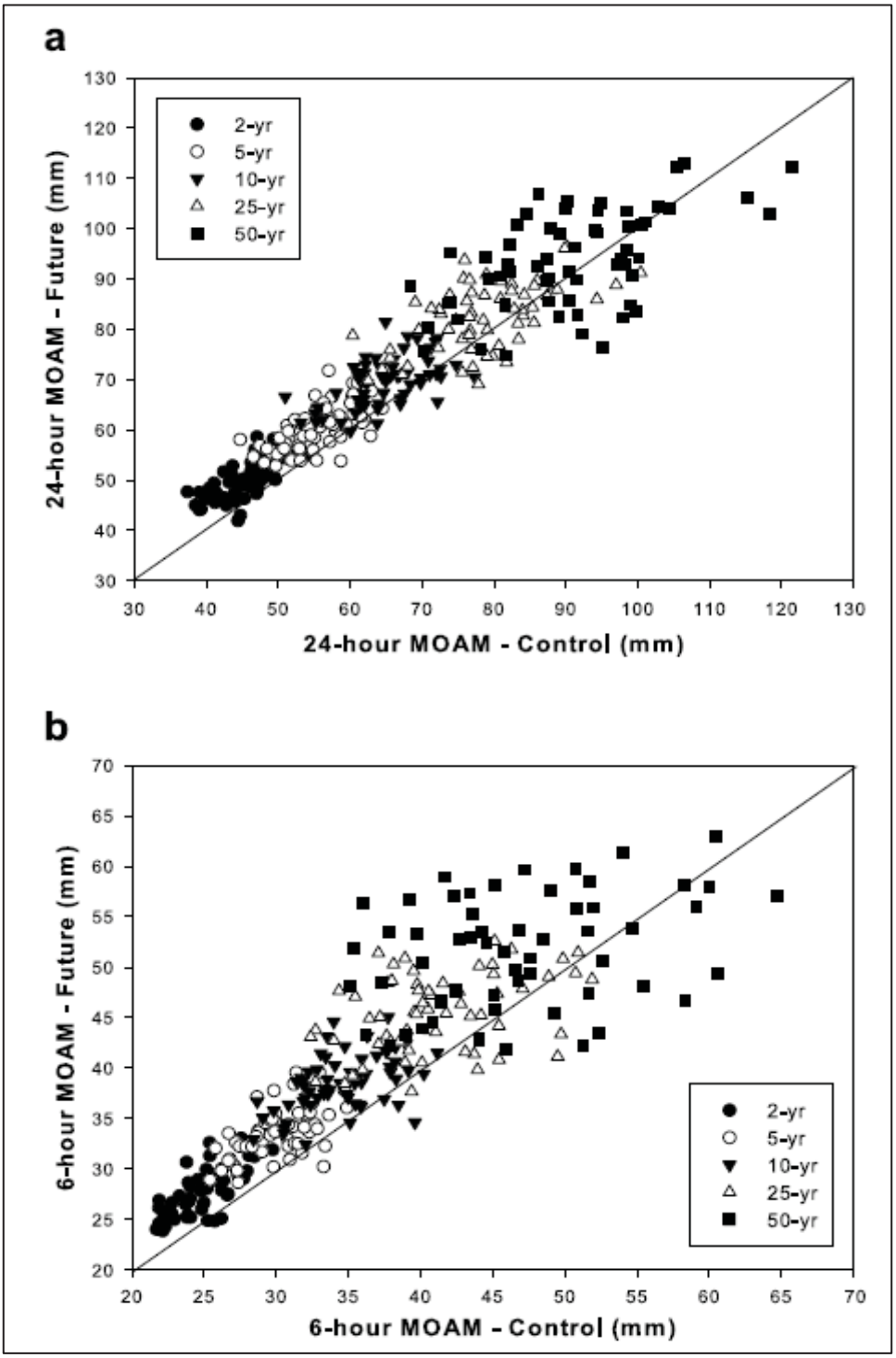

Figure 2.35: Comparison of 24-h (a) and 6-h (b) May-to-October Annual Maximum (MOAM) estimates obtained from CRCM simulations in control (x-axis) and future (y-axis) climates for the various return periods considered. [Adapted from Mailhot et al., 2007]

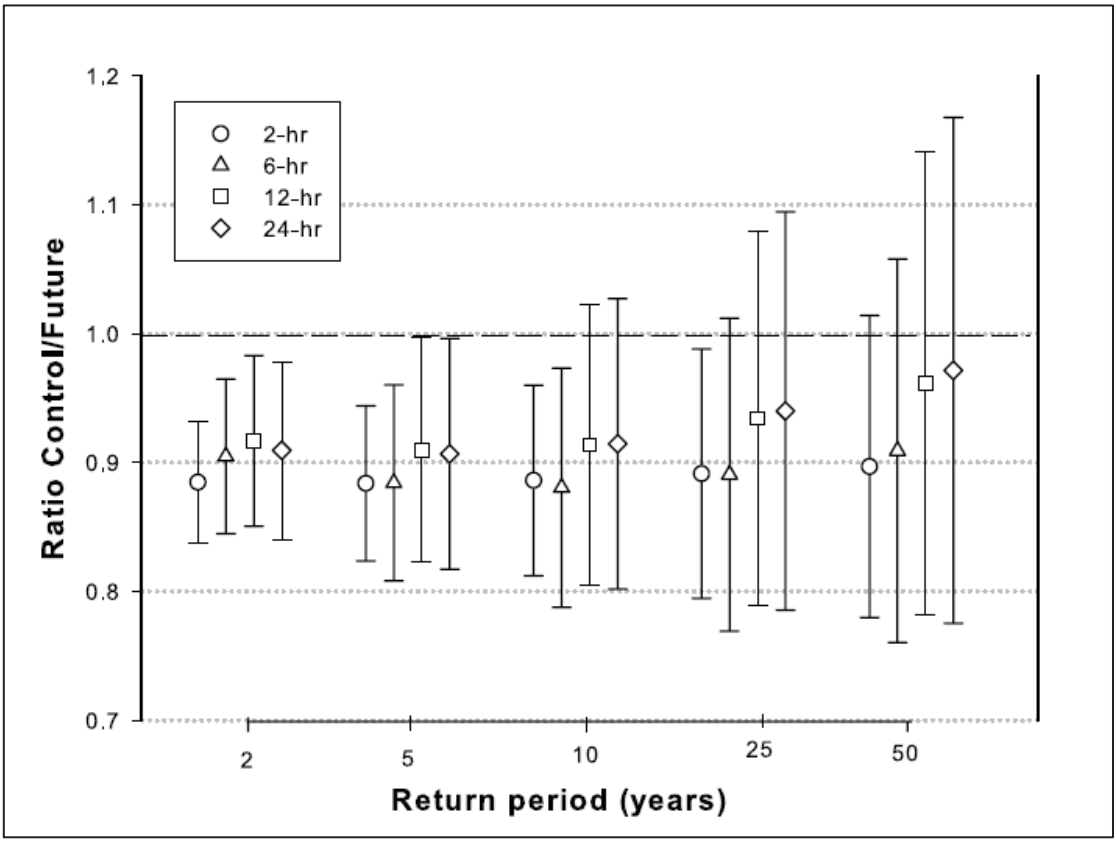

Figure 2.36: Ratio of regionally averaged MOAM estimates in control and future climates (control/future) at the grid box scale for the various durations and return periods. Vertical bars are 90% bootstrap confidence intervals. [Adapted from Mailhot et al., 2007]

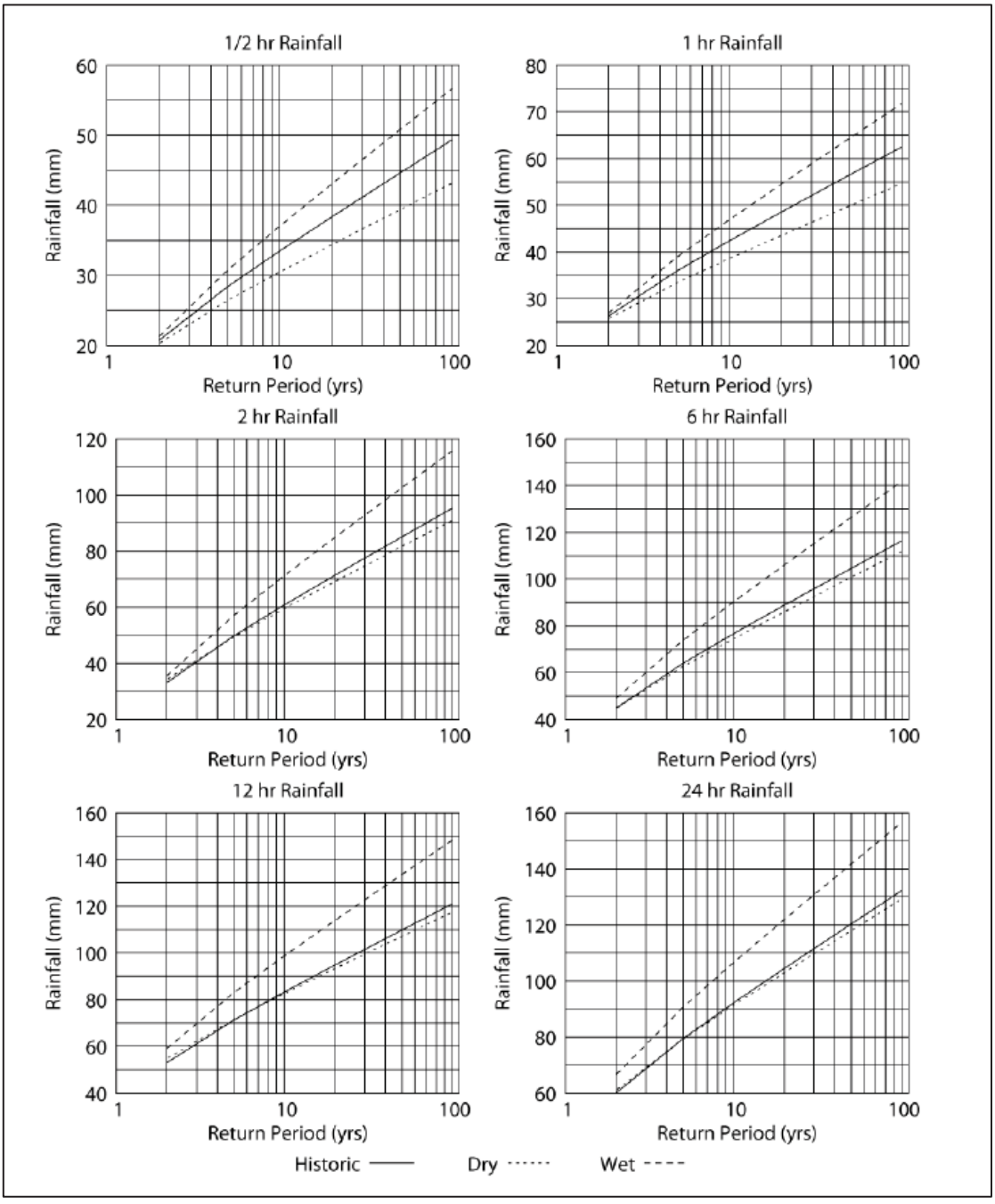

Figure 2.37: IDF curves for London: historic, dry and wet weather generator (WG) output
[Adapted from Prodanovic and Simonovic, 2007]

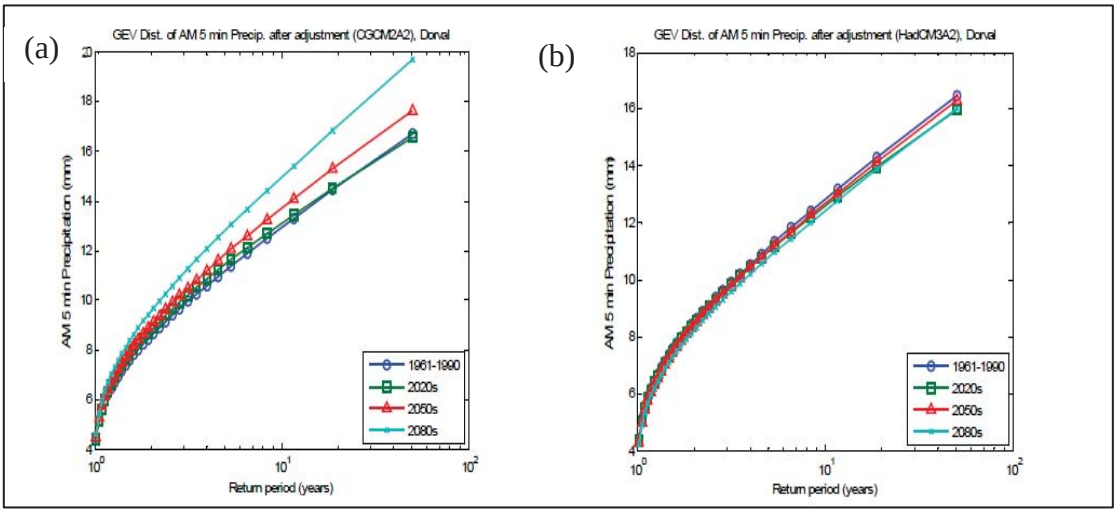

Figure 2.38: Probability plots of 5-minute annual maximum (AM) precipitations projected from (a) CGCM2A2 and (b) HadCM3A2 scenarios for the 1961-1990 period and for future periods (2020s, 2050s, and 2080s) for Dorval station. [Adapted from Nguyen et al., 2007]

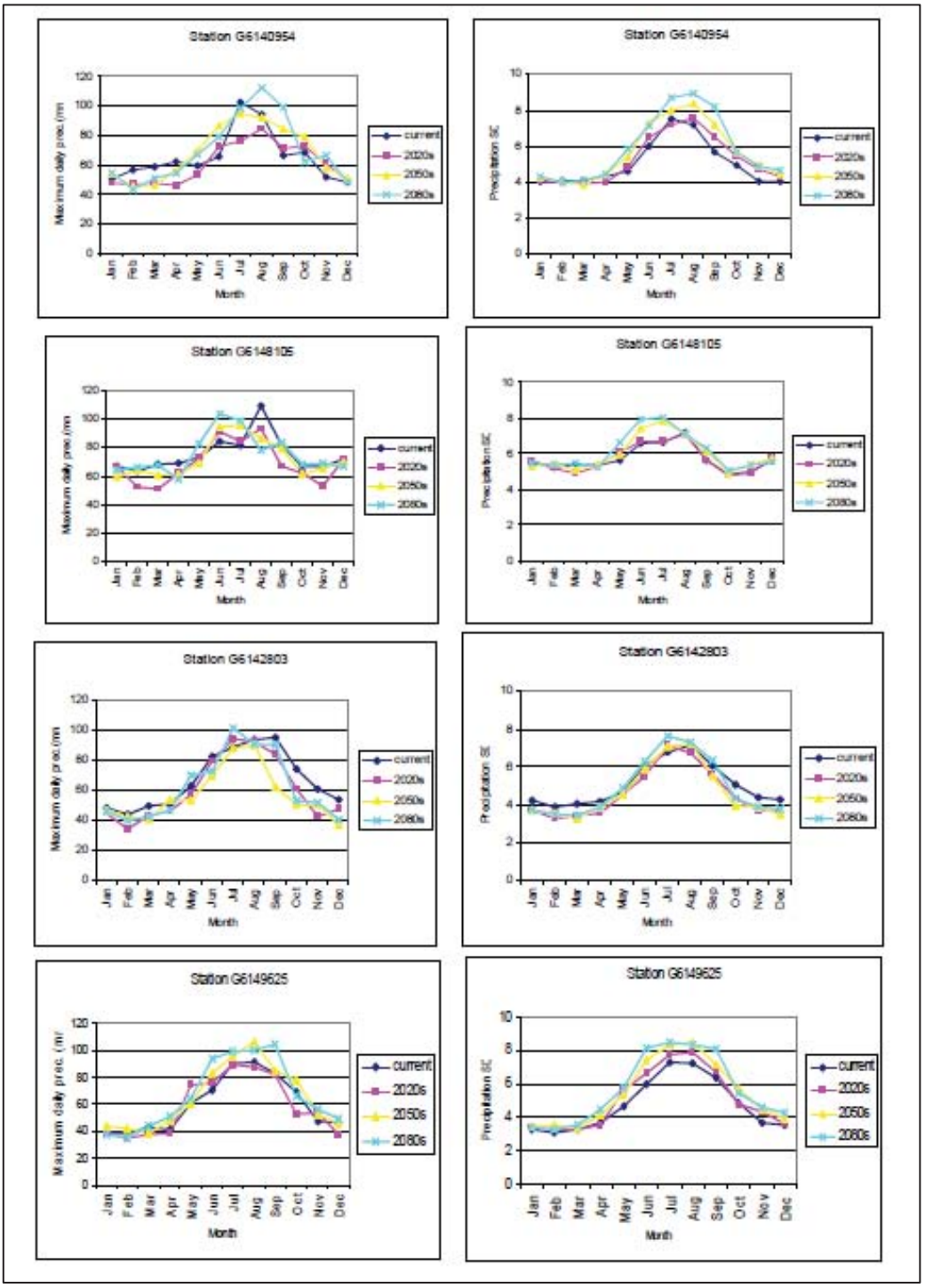

Figure 2.39: General Trend in Predicted Precipitation in the Grand River Region [Adapted from Coulibaly and Shi, 2005]

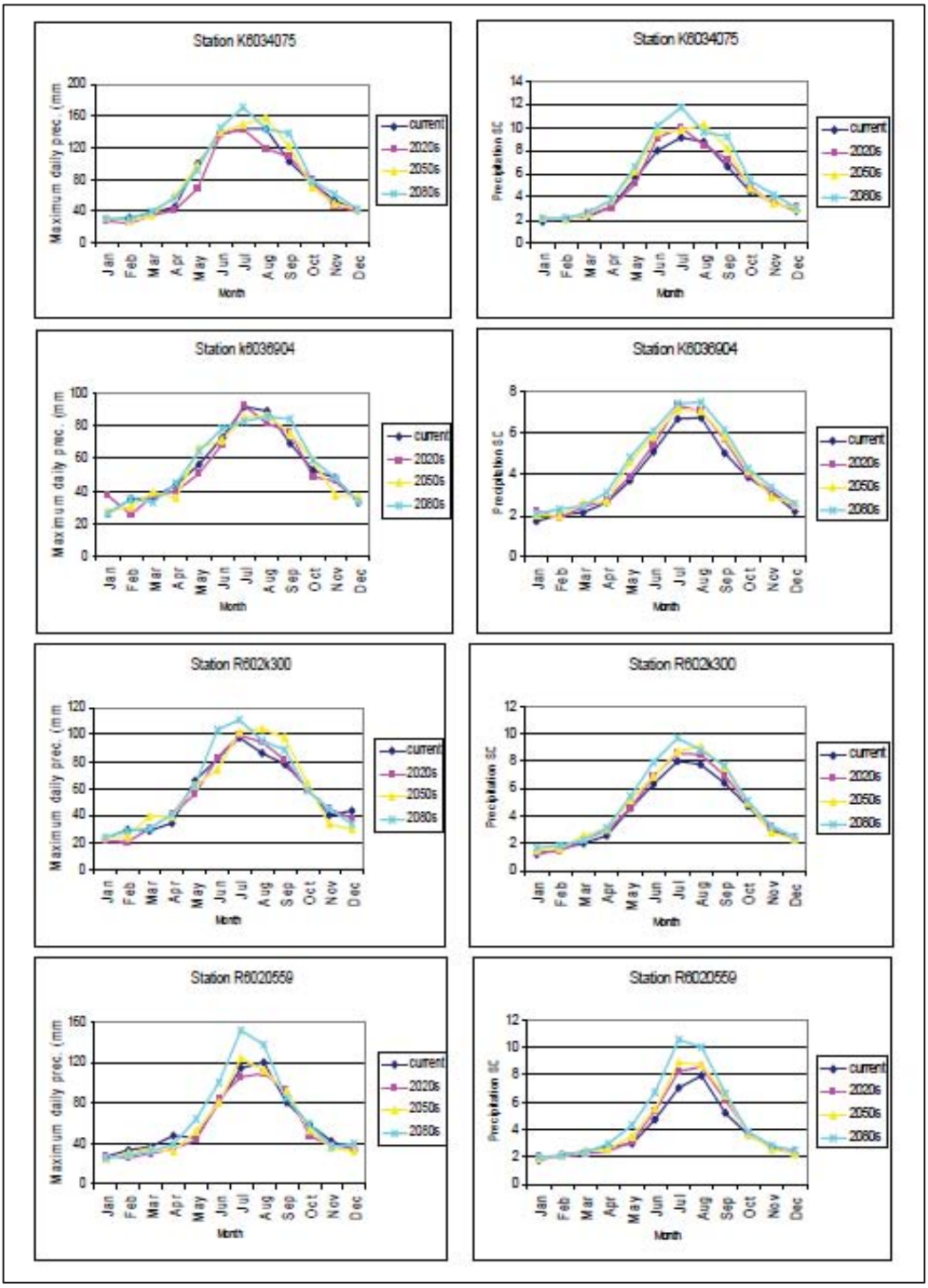

Figure 2.40: General Trend in Predicted Precipitation in the Kenora and Rainy River Region
[Adapted from Coulibaly and Shi, 2005]

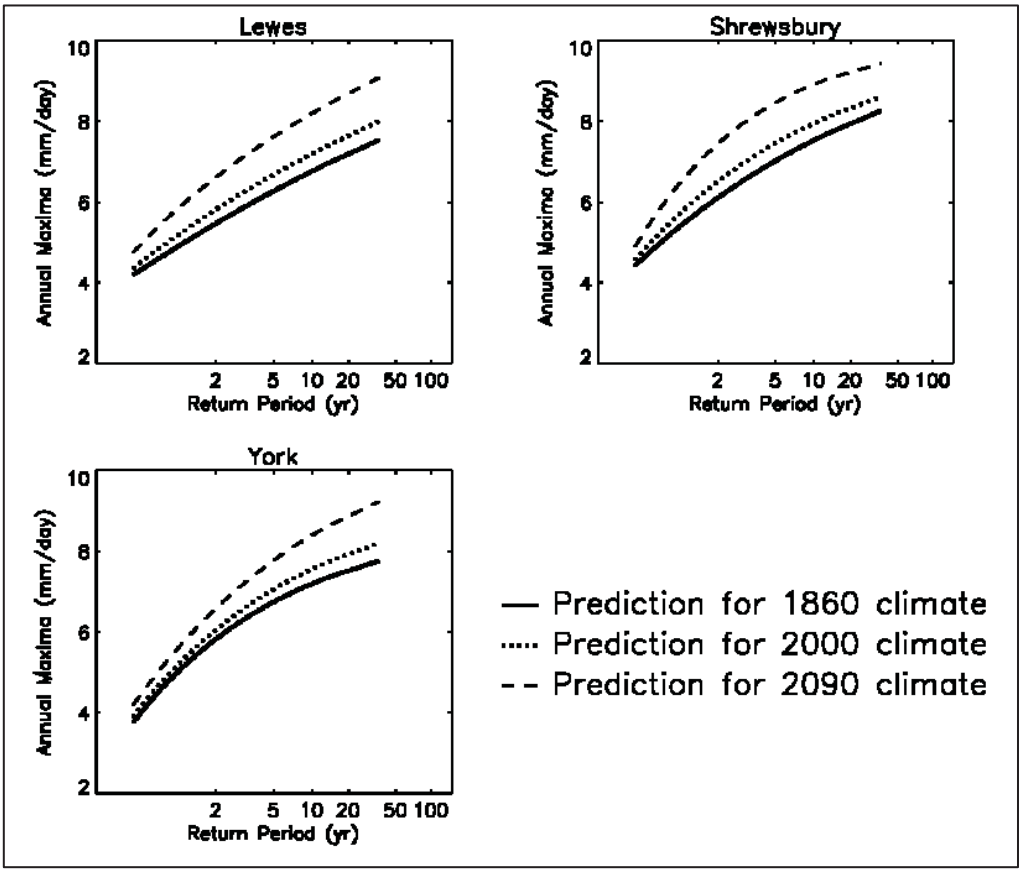

Figure 2.41: Plots of the generalized extreme-value frequency distributions, P1860(τ), P2000(τ) and P2090(τ) for 30-day durations and for the three regions of interest.
[Adapted from Huntingford et al., 2003]

Table 2-1 Projected Change in Mean Surface Air Temperature for Southeast Asia under A1FI and B1 (with respect to baseline period of 1961-1990), °C [Adapted from IPCC, 2007]

Table 3.2. Projected Change in Mean Surface Air Temperature for Southeast Asia under A1FI and B1 (with respect to baseline period of 1961–1990), °C

Season	2010–2039		2040–2069		2070–2099	
	A1FI	B1	A1FI	B1	A1FI	B1
December to February	0.86	0.72	2.25	1.32	3.92	2.02
March to May	0.92	0.80	2.32	1.34	3.83	2.04
June to August	0.83	0.74	2.13	1.30	3.61	1.87
September to November	0.85	0.75	1.32	1.32	3.72	1.90
Mean	0.87	0.75	2.01	1.32	3.77	1.96

Source: IPCC (2007).

Table 2-2 Summary of the Chi-Square and Kolmogorov-Smirnov Tests [Adapted from Rao and Kao, 2006]

	EV(1)		GEV		P(3)	
	χ^2	KS	χ^2	KS	χ^2	KS
total cases	639	666	639	666	639	666
not pass	165	9	200	4	240	25
(%)	25.82	1.35	31.30	0.60	37.56	3.75

	LP(3)		Pareto		Pareto (modified)	
	χ^2	KS	χ^2	KS	χ^2	KS
total cases	639	666	569	666	621	666
not pass	191	4	124	6	430	152
(%)	29.89	0.60	21.79	0.90	69.24	22.82

Table 2-3 Frequency results of rainfall depth (mm) at El Rawafaa station [Adapted from El-Sayed, 2011]

Return Period (year)	5-min	10-min	15-min	30-min	60-min	120-min	1440-min
2	1.12	1.75	2.02	2.82	3.66	4.96	6.69
5	1.80	2.70	3.25	4.46	5.67	7.60	12.52
10	2.34	3.43	4.38	5.90	7.46	10.01	18.63
20	2.93	4.21	5.71	7.57	9.53	12.85	26.51
25	3.14	4.47	6.19	8.16	10.26	13.86	29.48
50	3.83	5.34	7.83	10.17	12.75	17.37	40.22
100	4.62	6.28	9.75	12.47	15.61	21.45	53.56
200	5.51	7.32	11.96	15.09	18.87	26.16	69.90

Table 2-4 Kimijima parameters for Ghrandal, El Timid and El Godirat stations [Adapted from El-Sayed, 2011]

Return Period (yr)	Ghrandal station			El Timid station			El Godirat station		
	a	*v*	*b*	*a*	*v*	*b*	*a*	*v*	*b*
2	96.8	0.83	7.9	290.8	1.06	29.4	303.3	1.05	13.9
5	269.37	0.84	8.6	507.9	0.99	27.1	613.8	1.08	15.0
10	499.2	0.86	9.7	891.9	0.98	31.1	901.9	1.09	16.1
25	1002.6	0.89	11.5	2310.3	1.03	46.9	1364.1	1.11	17.5
50	1585.8	0.91	12.8	5098.4	1.10	68.6	1782.2	1.13	18.6
100	2398.7	0.93	14.1	11382.2	1.17	100.2	2271.6	1.14	19.6
200	3509.6	0.95	15.5	25329.6	1.26	144.9	2830.8	1.15	20.6

Table 2-5 Constant parameters with 4 empirical equations at the Hanoi station with 100 years return period
[Adapted from Nhat et al., 2006]

Function	*a*	*b*	*e*	RMSE	R
Talbot	32979	206.22	-	5.674	0.989
Bernard	697.77	0.453	-	4.536	0.961
Kimijima	5506.7	22.112	0.752	3.217	0.998
Sherman	38183	200.62	1.011	3.801	0.99

Table 2-6 Relative root mean square error (RRMSE) for the pooled estimation method and index flood method.
[Adapted from Mohd Daud et al., 2002]

	Sites	Pooled method RRMSE	Index-flood method RRMSE
Region 1	Pekan	0.1201 (0.1095)*	0.1572 (0.2520)
	K. Menerong	0.2165 (0.2147)	0.2444 (0.1654)
	K. Trengganu	0.1842 (0.1174)	0.2158 (0.3076)
	Kemaman	0.1187 (0.0635)	0.1583 (0.3264)
	Dungun	0.2184 (0.1103)	0.1787 (0.2268)
Region 2	P. Kangsar	0.2202 (0.3280)	0.1894 (0.3100)
	Segamat	0.1107 (0.1867)	0.0801 (0.2220)
	Batu Kurau	0.2004 (0.1696)	0.2152 (0.2240)
Region 4	Sikamat	0.1612 (0.0772)	0.1665 (0.1245)
	Ampang	0.1563 (0.1508)	0.1745 (0.1408)
	Bagan Terap	0.0492 (0.1468)	0.1479 (0.1734)

* Numbers in parentheses are for 24-h duration data, numbers without parentheses are for 60-min duration data.

Table 2-7 Derived zonal rainfall records
[Adapted from Oyebande, 1982]

Zone	Station names	No. of stations	Length of period (station years)	Period
I	Port, Harcourt, Calabar, Umudike	3	45	1951–78
II	Warri, Lagos, Ikeja, Oshodi, Benin, Aero & NIFOR	6	115	1948–78
III	Oshogbo, Ondo, Ilora, Ibadan	4	51	1956–75
IVa	Enugu, Ilorin, Bida, Makurdi	4	82	1956–78
IVb	Ibi, Yola	2	22	1956–73
V	—	—	—	—
VI	Lokoja, Minna	2	34	1956–75
VIIa	Mokwa, Yelwa, Sokoto	3	35	1956–76
VIIb	Kaduna, Jos Aero, Lamingo	3	60	1952–78
VIII	Bauchi, Zaria, Kano, Gusau, Samaru	5	61	1951–75
IX	Potiskum, Maiduguri, Aero & Water Works	3	38	1956–74
X	Nguru, Katsina	2	20	1960–75
		35		

Table 2-8 Estimates of parameters of the equation $x = \beta + (1/\alpha)\, y$ for zones
[Adapted from Oyebande, 1982]

Zone	0.2 h	0.4 h	1 h	3 h	6 h	12 h	24 h
I	23.52	19.19	12.10	6.63	3.74	1.87	0.98
	118.94	97.43	60.13	26.25	14.48	7.63	4.03
II	24.83	20.97	14.36	6.29	3.88	2.16	1.26
	113.16	85.74	55.06	23.58	13.30	7.03	3.81
III	19.57	14.99	11.32	5.59	2.94	1.49	0.85
	108.78	78.59	43.63	17.43	9.55	4.85	2.61
IVa	21.42	16.24	12.65	4.69	3.04	1.57	0.89
	111.83	83.38	49.13	20.03	10.56	5.61	2.83
IVb	20.15	15.87	12.70	6.30	3.56	1.84	0.92
	108.40	78.66	46.29	18.02	10.28	5.20	2.64
VI	32.95	21.76	13.49	6.03	3.13	2.26	0.57
	115.60	81.22	47.27	19.80	10.61	5.14	2.81
VIIa	19.40	15.62	9.21	3.52	1.60	0.88	0.39
	99.99	67.07	36.25	14.21	7.53	3.99	2.05
VIIb	23.28	17.95	9.83	3.87	3.13	1.14	0.68
	99.96	72.72	39.78	15.72	8.57	4.49	2.41
VIII	18.04	14.64	10.87	4.76	2.70	1.53	0.78
	95.65	69.79	40.67	15.92	8.46	4.47	2.28
IX	25.43	21.92	11.53	4.59	2.74	1.43	0.76
	98.23	73.30	40.32	15.85	8.65	4.39	2.23
X	21.53	17.65	9.35	3.86	2.09	1.08	0.57
	103.66	69.82	35.75	12.78	6.73	3.43	1.76

[The first row in each zone contains the value of α; the second row in each zone contains the value of β.]

Table 2-9 Estimates of parameters of the equation $x = \beta + (1/\alpha)\, y$ for individual stations
[Adapted from Oyebande, 1982]

Station	Zone	0.2 h	0.4 h	1 h	3 h	6 h	12 h	24 h
Port Harcourt*	I	26.43	15.22	14.00	6.45	3.70	1.61	0.85
		121.03	100.13	61.35	27.31	15.53	8.10	4.29
Warri*	II	29.33	22.65	14.57	4.85	3.44	1.68	1.04
		120.78	92.47	59.91	27.53	15.06	7.90	4.52
Lagos*	II	23.55	22.17	16.66	6.82	3.93	1.97	1.11
		105.69	80.18	55.97	25.06	15.03	8.04	4.12
Ikeja*	II	23.32	18.35	10.99	4.69	2.94	1.62	1.00
		109.99	86.64	53.59	22.27	12.24	6.63	3.58
Oshogbo	III	26.47	12.89	7.51	5.27	2.73	1.25	0.76
		109.59	81.64	44.60	18.55	10.25	4.90	2.62
Enugu*	IVa	17.95	14.52	13.30	4.20	2.36	1.21	0.62
		121.05	92.27	53.34	22.00	11.85	6.12	3.26
Makurdi	IVa	27.13	20.54	11.61	4.54	2.57	1.39	0.73
		113.81	86.25	50.08	20.38	11.35	5.88	2.97
Ilorin*	IVa	18.85	12.19	10.30	3.73	3.15	1.56	0.95
		105.81	80.68	39.74	18.25	8.75	4.93	2.38
Yola	IVb	16.89	13.12	12.91	6.27	3.58	1.85	0.94
		102.12	73.83	44.53	16.96	9.69	4.90	2.49
Lokoja	VI	20.54	19.23	10.58	4.90	2.46	1.38	0.68
		101.17	82.31	47.22	18.95	9.93	4.92	2.57
Sokoto	VIIa	14.89	12.80	7.74	3.05	1.33	0.85	0.39
		90.11	60.26	32.92	12.75	6.80	3.76	2.00
Jos Aero*	VIIb	23.63	18.92	9.66	3.14	1.84	1.04	0.63
		101.64	70.32	39.41	14.85	7.98	4.21	2.28
Kaduna*	VIIb	19.82	15.04	10.00	4.50	2.34	1.24	0.72
		99.79	73.17	39.95	16.25	9.04	4.67	2.43
Kano	VIII	16.61	17.05	14.13	6.05	3.41	1.78	0.92
		90.64	66.62	39.87	15.37	8.12	4.13	2.11
Potiskum	IX	17.55	13.54	10.57	4.74	2.52	1.29	0.70
		90.76	71.00	41.43	15.92	8.47	4.28	2.17
Nguru	X	19.16	18.25	10.16	3.89	2.18	1.15	0.61
		106.34	70.46	35.11	11.97	6.30	3.25	1.66

*Record length of 20–29 years.
Other records are 14–19 years.

[The first row in each zone contains the value of α; the second row in each zone contains the value of β.]

CHAPTER 3 MODELS, DATA AND METHODOLOGY

3.1 INTRODUCTION

This chapter deals with climate models used in this study, various types of data considered, and the methodologies employed for dynamical downscaling and the development of Intensity-Duration-Frequency (IDF) curves. A flowchart that summarizes the entire research approach is shown in Figure 3.1. The individual components are described in the following sections

3.2 REGIONAL CLIMATE MODEL (RCM)–WEATHER RESEARCH AND FORECASTING MODEL (WRF)

The Regional Climate Model Weather Research and Forecasting (RCM WRF) used in this study is discussed in this section.

The effort to develop WRF has been a collaborative partnership, principally among the National Center for Atmospheric Research (NCAR), the National Oceanic and Atmospheric Administration (NOAA), the National Centers for Environmental Prediction (NCEP) and the Forecast Systems Laboratory, the Air Force Weather Agency, the Naval Research Laboratory, Oklahoma University, and the Federal Aviation Administration, USA. WRF is suitable for a broad spectrum of applications across scales ranging from

meters to thousands of kilometres. The WRF model was specifically designed for high resolution applications, and provides an ideal tool for assessing the value of high resolution regional climate modeling. WRF has been widely used in climate research by several research groups around the world. The WRF model also contains a multitude of physical parameterizations. This model has been described and documented by Skamarock et al., 2005 and detailed information is also available at: http:/www.wrf-model.org. The WRF version 3.2.1 is used in this study.

3.3 GLOBAL REANALYSIS AND OBSERVED DATA

It has been mentioned in Chapter 1 that regional climate models need to be driven by large scale fields such as reanalysis or global climate models. In addition, regional climate models also need to be compared against observations (Table 3-1) for benchmarking. In this section, the global reanalysis that are used to drive the RCM WRF and the observational datasets that are used for comparing RCM WRF simulations are described.

3.3.1 The ERA-40 Global Reanalyses (ECMWF 40 Year Re-analysis) Datasets

ERA-40 (Uppala et al., 2005) is a re-analysis of meteorological observations from September 1957 to August 2002 produced by the European Centre for Medium-Range Weather Forecasts (ECMWF) in collaboration with many institutions. The ERA-40 reanalyses provide information about a suite of

climate variable (such as precipitation, humidity, temperature and pressure) every six hours, at a horizontal resolution of 2.5º × 2.5º. The data records span more than 40 years (1957-2002). The ERA40 reanalysis products use a global spectral grid model and assimilate part of the observational data from a wide variety of observed sources. Details of the reanalysis project can be found in the citation above and additional details can be obtained from: http://www.ecmwf.int/research/era/. In short, reanalysis essentially globally gridded products which take several long records of global weather measurements and employ quality control and data assimilation techniques to 'reanalyse' these observations. For this reason, they are termed 'global reanalyses'. Hence, it is primary that when such reanalyses are used to drive a climate model, the output of the climate model serves to establish the model performance.

In this thesis, the RCM WRF was driven using the ERA40 reanalysis for a 30-year period spanning from 1961-1990. The annual mean climatology temperature, annual mean seasonal winds and precipitation from the simulations of RCM are compared to this datasets to evaluate the performance of RCM WRF (dealt in detail in Chapter 4) as they envelope the main climate features of the study region. In addition, the high resolution outputs from RCM WRF driven using this datasets are also used in this thesis to derive present day IDF curves for sites with short or no rainfall records (also dealt in detail in Chapter 5).

3.3.2 APHRODITE (Asian Precipitation Highly Resolved Observational Data Integration Towards the Evaluation of Water Resources) Datasets

The APHRODITE project developed state-of-the-art daily precipitation datasets at high-resolution grids (0.25° and 0.5°) for Asia. This study uses the 0.25° dataset. The datasets were created primarily using data obtained from rain-gauge observations network. APHRODITE's Water Resources project was conducted by the Research Institute for Humanity and Nature (RIHN), Japan and the Meteorological Research Institute of Japan Meteorological Agency (MRI/JMA). This dataset of precipitation is available on a daily scale and available only for all land area covering all Asia and not available for oceanic areas. Further information on this datasets is available at its website, http://www.chikyu.ac.jp/precip/. Precipitation results from the simulations of RCM WRF are compared against this data over the period of 1961-1990 (Chapter 4, Sections 4.2.3) to evaluate the model performances. Moreover, the data are used in STARDEX indices (Table 3-2) also to evaluate the model performance; the results for the different indices are shown in Chapter 4. Temperature records are not yet available at the time of the study. The temperature dataset was released in July 2012.

3.3.3 CRU (Climatic Research Unit) Datasets

Developed at the Climatic Research Unit (CRU) at the University of East Anglia, UK, the CRU TS (Time-Series) version 3.0 dataset, used in this study,

comprises monthly grids of observed climate, for the period 1901-2006 covering only the global land surface at 0.5° × 0.5° horizontal spatial resolution. This dataset is one of the most extensively used dataset by the climate modeling community. The precipitation and temperature datasets used in this study consist of data obtained from many land based gauging stations only around the globe. Temperature and Precipitation variables from the simulations of the RCM WRF are compared against this data over the period of 1961-1990 (Chapter 4, Section 4.2) to evaluate the performance of RCM WRF. Further information on these datasets is available at http://www.cru.uea.ac.uk/cru/data and is also documented by New et al., (2000; 1999) and Mitchell and Jones (2005).

3.3.4 CPC (Climate Prediction Center) Datasets

This dataset is the first product of the CPC Unified Precipitation Project of the NOAA Climate Prediction Center (hereafter, CPC). The primary goal of the project is to create a suite of unified precipitation products with consistent quantity and improved quality by combining all information sources available at CPC and by taking advantage of the optimal interpolation (OI) objective analysis technique. The data records span mostly global land cover at 0.5° resolution. Although available initially from 1979, the datasets have now been extended from 1949 onwards until 2005. Further details are available from: http://www.cpc.ncep.noaa.gov/products. These datasets have been documented by Chen et al. (2002). Temperature and Precipitation variables

from the simulations of the RCM WRF are compared against this data over the period of 1961-1990 (Chapter 4, Sections 4.2.1 and 4.2.3).

3.3.5 VASClimO (Variability Analysis of Surface Climate Observations) Datasets

Variability **A**nalysis of **S**urface **Clim**ate **O**bservations (hereafter, VASClimO) was a joint climate research project of the German Weather Service (Global Precipitation Climatology Centre - GPCC) and the Johann Wolfgang Goethe-University Frankfurt (Institute for Atmosphere and Environment - Working Group for Climatology). One substantial part of GPCC's contribution to VASClimO is the creation of a gridded monthly 50-year precipitation dataset for the period of 1951-2000 covering the global land areas (Beck et al., 2005). The monthly data set for the global land areas gridded at 0.5° latitude/longitude resolutions was developed on the basis of the most comprehensive database of monthly observed global precipitation data that resides with the GPCC. The 50-year precipitation dataset (1951-2000) has been a contribution to the IPCC WGI Fourth Assessment Report (2007). Further information on these datasets is available at its website, http://iridl.ldeo.columbia.edu/SOURCES/.DEKLIM/.VASClimO/.PrcpClim/.

This study uses the precipitation results from the simulations of RCM WRF and compared against this data over the period of 1961-1990 (Chapter 4, Sections 4.2.3). Temperature records are not available from this source.

3.4 GCM DATA USED TO DRIVE RCM WRF

It has been mentioned earlier that RCMs need to be driven by GCMs. In this study a few GCMs were used to drive the RCM WRF. They are: (1) GCM CCSM3.0, Community Climate System Model (CCSM), a coupled Global Climate Model developed by the University Corporation for Atmospheric Research (UCAR); and (2) GCM ECHAM5, the fifth-generation coupled general circulation model developed at the Max Planck Institute for Meteorology (MPIM) (hereafter, ECHAM5). These GCMs provide the large scale boundary conditions that are required to run RCM WRF. The RCM WRF was run for the present day (1961-1990) and the future (e.g. 2071-2100) climate using the boundary conditions from these GCMs, forced under different emission scenarios. Further details of these GCMs are outlined in Sections 3.4.1 and 3.4.2

3.4.1 CCSM3.0 (Community Climate System Model, USA)

The components of Community Climate System Model (CCSM) include an atmospheric model (Community Atmosphere Model), a land-surface model (Community Land Model), an ocean model (Parallel Ocean Program), and a sea ice model (Community Sea Ice Model). The atmospheric component of CCSM is the Community Atmosphere Model which has a 256 × 128 regular longitude/latitude global horizontal grid (giving a 1.4°×1.4° resolution).

3.4.2 ECHAM5 (European Centre Hamburg Model, Max-Planck Institute, Germany)

The ECHAM5 model is the most recent version in a series of ECHAM models evolving originally from the spectral weather prediction model of the ECMWF. This model has been run at a range of horizontal spatial resolutions with Gaussian grids of T21 to T159. A detailed description of the model has been provided by Roeckner et al. (2006). This study uses the T63 resolution version (1.8°×1.8°) of the GCM.

3.5 IDF CURVES DERIVED FROM RAINGAUGE DATA

Existing IDF curves and rainfall records from Singapore (Singapore, 103° 50'E, 1° 18'N), Kuala Lumpur (Malaysia, 101° 41'E, 3° 09'N), Jakarta Meteorological Station (Indonesia, 106° 49'E, 6° 10'S), and Darmaga Station (Indonesia, 106° 45'E, 6° 33'S) are used in this study. Figure 3.2 shows the location of rainfall stations (Indonesia, Singapore and Malaysia) used in the study.

For Singapore and Kuala Lumpur stations, the design curves for 5, 10, 50 and 100 year return periods are available. For Jakarta Meteorological and Darmaga stations, however, only the design curves of 5, 10, 25 and 50-year return periods are presented on the IDF chart. Existing IDF curves for Jakarta Meteorological Station, Singapore and Kuala Lumpur are illustrated in Figure 3.3, 3.4 and 3.5 respectively and the rainfall durations presented are in 6, 12,

18 and 24-hour. It should be noted that RCM WRF simulation results are generated 6-hourly. Thus, rainfall durations considered in this study were of 6, 12, 18 and 24-hour.

This concludes the descriptions of models and data used in this study.

3.6 METHODOLOGY – CLIMATE DOWNSCALING

3.6.1 Climate Downscaling with Regional Climate Model

Dynamical downscaling technique was performed in this study to investigate the ability of the climate model to reproduce the present day climate and to determine the changes in future climate over the chosen study region. The usefulness of RCMs as dynamical downscaling tool is recognized from numerous studies done by the climate modeling community around the world and from the vast amount of literature available that bolsters this cause, as discussed in Chapter 1. In addition, this research work has been done at the Tropical Marine Science Institute (TMSI), National University of Singapore, where one of the main research foci is climate modelling and dynamical downscaling. Therefore, this PhD candidate's many years research experience gained in working on several climate change projects at TMSI also adds to the confidence in undertaking this research exercise and applies that experience with regard to understanding the model sensitivities and dynamics.

The dynamical downscaling using the RCM WRF was performed over the Southeast Asian region with a particular focus over Jakarta region. The domain area considered in this study is 93°E to 120°E, 12°S to 13°N for the model run (Figure 3.6). Before any climate models can be used to project future climate, their ability to simulate the current climate must be evaluated. As there is no direct verification of future changes in climate (Knutti et al., 2010), these evaluations of the present day climate simulations are necessary so as to place more confidence on the model simulated future climates. Thus, the initial work of the dynamical downscaling approach involved evaluating the inherent strengths and weaknesses of the RCM WRF model to reconstruct the observed climate regime with respect to key climate variables: precipitation, temperature and winds. The following section describes some statistical tests that were carried out in this study to evaluate the performance of RCM WRF.

To generate climate change projections, two time slices are used to drive the RCM. The first time slice may be when there are no increases in greenhouse gas emissions (i.e. to represent pre-industrial climate also called a 'control run') or can be for a recent climate period. Baseline period from 1961-1990 is often chosen as it is the recommended standard by World Meteorological Organization (WMO). The second time slice can be any period of the future, although mostly accounted for the end of the century (e.g., 2071-2100) when the climate change signal will be more pronounced. This study used 3 thirty year time slices of the future, namely, 2011-2040, 2041-2070 and 2071-2100.

The RCM WRF was first driven by ERA-40 reanalysis, GCM CCSM3.0 and GCM ECHAM5 for the present day climate spanning the period 1961-1990 for study region at a 30 × 30 km spatial resolution. The RCM WRF simulations results are compared with gridded observation data, CRU, CPC, VASClimO and APHRODITE. Due to time constraints, the RCM WRF was used to simulate future climate only from GCM CCSM3.0 (under A1FI, A2 and A1B emission scenarios), and GCM ECHAM5 (under A2 scenario) to determine climate changes over the future time slices 2011- 2040, 2041- 2070 and 2071-2100.

The climate response, otherwise termed as climate change signal, was computed as the difference in the climates of the future and present day conditions (e.g. (2071-2100) minus (1961-1990)). It is important to determine whether the sign of the climate change signal for model simulated precipitation is positive (wetter) or negative (drier) over the future. These experimental results are discussed in Chapter 4.

3.6.2 Performance Evaluation of Regional Climate Model

Some statistical metrics are needed to evaluate regional climate model performance. This thesis assesses the selected observed datasets (e.g. CRU, CPC, APHRODITE and VASClimO) as well as evaluates the ability of RCM WRF to simulate current climate. Bias, Root Mean Squared Anomaly (hereafter, RMSA) and Root Mean Squared Error (hereafter, RMSE) are some of the statistical measures that were commonly used for evaluation of model

performance. These statistical analyses were performed on temperature and precipitation as these are the most commonly observed climate variables. It is widely known that precipitation is the most difficult variable of all the climate variables to simulate (Legates, 2001) as the majority of precipitation processes occurring at scales much smaller than a grid box in a GCM. Hence, this section also includes extreme indices of precipitation (Table 3-2) to evaluate RCM WRF performances in the precipitation regime.

3.6.2.1 Bias

Bias is simply computed as the difference between the observed and modelled estimates. Precisely, it is a measure of the absolute magnitude of error between a domain averaged mean of the observed and the modelled estimates, given by the relation:

$$\boldsymbol{Bias = \sigma_{O-}\sigma_{M}} \qquad \textbf{(3-1)}$$

where $\boldsymbol{\sigma_O}$ is the domain averaged mean of the observations and $\boldsymbol{\sigma_M}$ is the domain averaged mean of the modelled estimates.

The biases for mean annual temperature and precipitation were carried out in Chapter 4, comparing observed (e.g. CRU, CPC, APHRODITE and VASClimO) and simulated means of temperature and precipitation (e.g. WRF/ERA40, WRF/CCSM and WRF/ECHAM). Results for temperature and

precipitation are presented later in Chapter 4 (Figure 4.2 to 4.3 and Figure 4.7 to 4.10 respectively).

3.6.2.2 Root Mean Squared Anomaly (RMSA) and Root Mean Squared Error (RMSE)

Root Mean Squared Anomaly (RMSA), known as root mean squared deviation is very similar to standard deviation except RMSA is more suitable for large sample sizes (i.e. divisor is n instead of n-1).

RMSA is expressed as follows:

$$\boldsymbol{S_N = \sqrt{\frac{1}{N}\sum_{i=1}^{N}(x_i - \bar{x})^2}} \qquad \textbf{(3-2)}$$

where $\bar{x}$ is the mean, $\mathbf{x_i}$ is each data value, and **N** is the number of observations. RMSA provides similar information into the dispersion of data as the standard deviation. It is often used as a measurement of error and more commonly used than the standard deviation function in the statistical analysis of climate data because climate-related datasets are generally quite large in size, in terms of number of data points.

The root mean square error (RMSE) is used to measure the errors not only in the mean value but also in the inter-annual variability of each simulated precipitation variable or index versus the observed one.

RMSE is expressed as follows:

$$\boldsymbol{RMSE} = \sqrt{\frac{\sum_{i=1}^{N}\left(X_{Sim,i,j} - X_{Obs,i,j}\right)^2}{N}} \qquad \textbf{(3-3)}$$

where $\mathbf{X_{Sim,i,j}}$ and $\mathbf{X_{Obs,i,j}}$ are the simulated and the observed values, and **N** is the number of observations.

3.6.2.3 Extreme Indices

One of the ways to characterize climate variability and extremes is to calculate climate indices based on daily time series of basic variables such as temperature and precipitation. In this study, APHRODITE, which is in daily frequency, was used to assess the performance of RCM WRF in the precipitation regime. This allows assessments of the capability of the RCM WRF, driven in reanalyses mode, whether it can capture the main weather meteorological sequence. Two (2) indices were considered: (1) mean intensity per wet day (hereafter, SDII) and (2) the 90th percentile of daily rainfall (hereafter, P90p), see Table 3-2. In addition, the indices were also used for future projection of precipitation to compare changes in frequency or intensity of extreme weather events, current vs. future climates. This information is very much of interest for applications in impacts and risk assessment studies, for examples, drainage designs (IDF curves), water resources, health, coastal and slope erosion, biodiversity.

It should be noted that the aforementioned indices are used by several international research groups who have developed a standard methodology for calculating such indices, e.g. ETCCDMI -Expert Team on Climate Change Detection and Indices (http://cccma.seos.uvic.ca/ETCCDMI/index.shtml), the European research project known as STARDEX (Statistical and Regional dynamical Downscaling of Extremes for European regions; www.cru.uea.ac.uk/cru/projects/stardex), and, in North America, the work of Yagouti et al. (2008), Vincent and Mekis (2006), Gachon et al. (2005), Peterson et al. (2001) and Karl et al. (1999). For the indices used in the present study, the methodology to define and compute those indices is defined in Gachon et al. (2005). Results of the evaluation study are presented in Chapter 4.

The second part of the methodology is the utilization of the output of RCM for the development of rainfall Intensity-Duration-Frequency curves for sites with short or no rainfall record. This methodology is described in Section 3.7.

3.7 METHODOLOGY – "DOWNSCALING – COMPARISON – DERIVATION" APPROACH FOR SITES WITH SHORT OR NO RAINFALL RECORD

A novel approach is presented in this study to develop Intensity-Duration-Frequency (IDF) curves for sites with short or no rainfall record. The approach comes in 3 steps (Figure 3.7),

Step 1: Dynamical Downscaling [D];

Step 2: Comparison [C]; and

Step 3: Derivation of IDF curves [D].

The approach is hence named as a (3-step) DCD approach. The 3 steps in the DCD approach are described below.

Step 1: Dynamical Downscaling and Performace Evaluation of RCM WRF driven by ERA-40

Dynamical downscaling of climate models, as described in Section 3.6, was first performed to obtain high resolution climate outputs. Subsequently, the performance evaluation of RCM WRF, driven by ERA-40, for the study region at 30 x 30 km spatial resolution was carried by comparing the simulation results with gridded observation data (e.g. CRU, CPC, VASClimO, APHRODITE). The evaluation of WRF continues until reasonably well fine-tuned WRF is achieved. Results of the evaluation study are presented in Chapter 4.

Step 2: Comparison Between WRF/ERA40 and Raingauge Data Derived IDF Curves

The annual maximum series resulting from the 6-hourly WRF/ERA40 simulation were used in the development of IDF curves. To generate annual maximum series, at first the **rainfall data aggregation** was done and followed

by determination of suitable **probability distribution function** for annual maximum rainfall.

Aggregation of Data and Extraction of Extremes: The present day 6-hourly precipitation datasets for 3 sites (with available IDF curves) in the study domain, Jakarta Meteorology Station, Singapore and Kuala Lumpur, were extracted from the simulations of WRF/ERA40 for the period 1961-1990. It should be noted that the time series extraction was done through bilinear interpolation. Data aggregation is based on selected design storm durations (6, 12, 18 and 24-hour) as only 6-hourly rainfall output was generated by WRF. Data aggregation for 12, 18 and 24-hour design storm durations, a time window of width equal to the respective duration is moved over the 6-hourly datasets. This also means that the selected annual maximum value may sometimes come from only a part of one storm and sometimes from parts of two or more consecutive storms (Singh and Zhang, 2007).

After the aggregation of the selected storm duration data, the identification of the extreme events (annual maximum) was performed. For the 6-hour raifall duration study, a total of 30 (1961-1990) annual maximum rainfall depths were then extracted from the 6-hourly rainfall data. The same processes were repeated for 12, 18 and 24 hour rainfall from their respective precipitation datasets simulated from WRF/ERA40. Thus, we now have extreme rainfall time series of 6, 12, 18, and 24 rainfall durations.

The above processes were then repeated on simulated data resulting from WRF/CCSM (A1FI, A2 and A1B emission scenarios) and WRF/ECHAM (A2 emission scenario).

Probability Distribution Function for Annual Maximum Rainfall: Selecting a suitable probability distribution function to fit extreme rainfall intensity dataset is an important step. There are many distribution functions (e.g. Generalized Extreme Value (GEV), Gumbel) and various fitting methods (e.g., the method of moments, the maximum likelihood and the least-squares error methods). Finding a suitable distribution function and fitting method is quite a challenge as the resulting IDF curves will affect the storm drainage network design.

The GEV distribution was adopted in this study mainly due to its high goodness-of-fit tests. The GEV distribution is also widely used in the last decade (Hlavcova et al., 2005).

The expected extreme value for rainfall intensities, $\boldsymbol{I_{max}}$, for any return periods, T, can be computed by using Equation 3-4. The quantile function for GEV distribution is obtained as **(1-1/T)** and the maximum rainfall intensity is expressed as:

$$\boldsymbol{I_{max} = \mu + \frac{\sigma}{k}\left\{\left[-ln\left(1-\frac{1}{T}\right)\right]^{-k} - 1\right\}} \qquad \textbf{(3-4)}$$

where k, μ and σ are shape, location and scale parameters, respectively.

A probability distribution function software, EasyFit (http://www.mathwave.com/products/easyfit.html), was used in this study to determine the GEV's three parameters (k, μ, σ).

Since the main objective of this study is to develop IDF curves for sites at which IDF curves are not available. The proof of concept analyses was first done on sites at which IDF curves are available. Three sites with IDF curves, mentioned earlier, are Jakarta Meteorological Station, Singapore and Kuala Lumpur; their IDF curves were used for comparison with the IDF curves derived from WRF/ERA40 and for the required bias correction measures at each station. The determined bias quantities will later serve as a guideline for derivation of IDF curves at sites with short or no rainfall record.

The idea is to assess how much the WRF/ERA40 derived IDF curves deviate from their observed counterparts. The baseline period considered was 1961-1990. The percentage differences between both IDF curves (Existing vs. WRF/ERA40 derived IDF curves) are computed and the upper and lower bounds (range of bias correction) from the three stations (Jakarta Meteorological, Singapore and Kuala Lumpur) were recorded. These were done for 5, 10, 25 and 50-year return periods for Jakarta Meteorological Station while for Singapore and Kuala Lumpur the validation was done for 5, 10, 50 and 100-year return periods due to their limited availability.

Step 3: Derivation of IDF Curves for Regions with Short or No Rainfall Record

Darmaga station, located southerly of Jakarta Meteorological Station, was selected as a site with "short or no rainfall record", thus, a validation site. Note that Darmaga station has existing IDF curves derived from raingauge data; however, it is used as a site to demonstrate the performance of the proposed (3-step) DCD approach. The IDF curves for Darmaga station were compared with the upper and lower bounds (range of bias correction) obtained from the 3 aforementioned locations.

IDF curves for Darmaga station was first derived from rainfall data simulated by WRF/ERA40. The lower and upper bounds (range of bias correction) obtained from Step 2 was then applied to the WRF/ERA40 derived IDF curve of respective return period. The final product of the present day WRF/ERA40 derived IDF curves is a pair of upper and lower bound IDF curves. This range will allow drainage designers to decide on a value within the upper and lower bounds; decision making is usually subjected to engineering, economic, social and environmental concerns.

A flowchart that describes and summarizes the entire (3-step) DCD approach to develop IDF curves for sites with short or no rainfall record is shown in Figure 3.7.

3.8 METHODOLOGY – PROJECTED FUTURE IDF CURVES

The above sections describe the (3-step) DCD approach proposed to derive present climate's IDF curves for sites with short or no rainfall record. For the anticipated changes in rainfall due to climate change, the study continues to propose the development of future IDF curves.

A simple "delta" method (Miller et al., 2003; Hamlet and Lettenmaier, 1999), developed for bias removal during the early days of climate change assessments and still widely used today, is adopted in this study. Climate model output is used to determine future change in climate with respect to the model's present-day climate, typically a difference in climate variables between the future and present day estimates. This change is referred to as the 'climate change signal' or 'change factor' (Δ_i). The climate change factor (climate responses, 'simulated future rainfall intensities minus present day rainfall intensities') (Wilby et al., 2009) is added to the present climate's lower and upper bounds of WRF/ERA40 derived IDF curves to form the range of each of the return periods for future rainfall extremes. It should be noted that should the site under consideration have existing IDF curves, the delta factor is simply applied directly to the respective existing IDF curves. Results of the development of present day and future IDF curves are presented in Chapter 5.

This page is intentionally left blank.

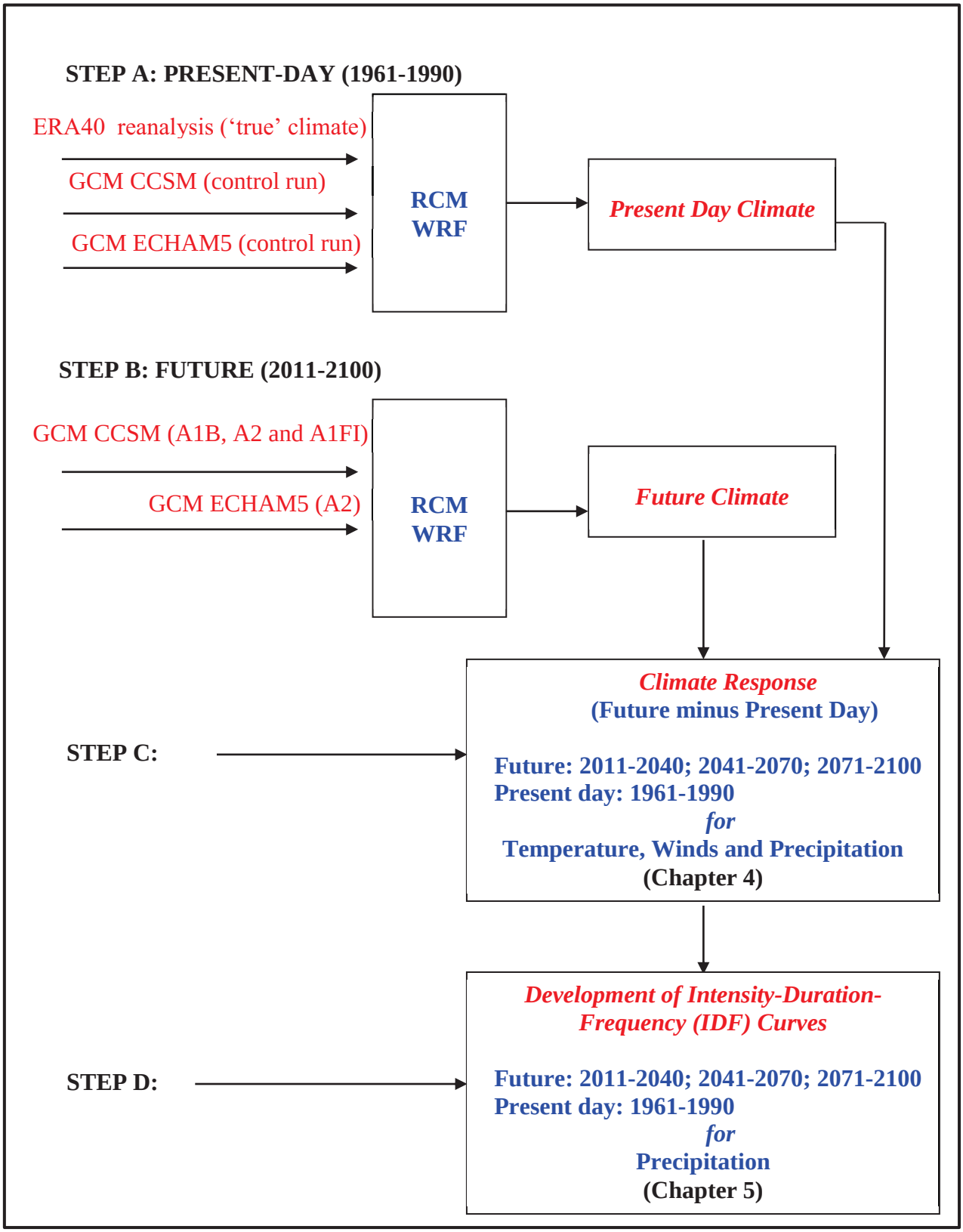

Figure 3.1: A flowchart that describes and summarizes the entire approach and objective of the proposed study

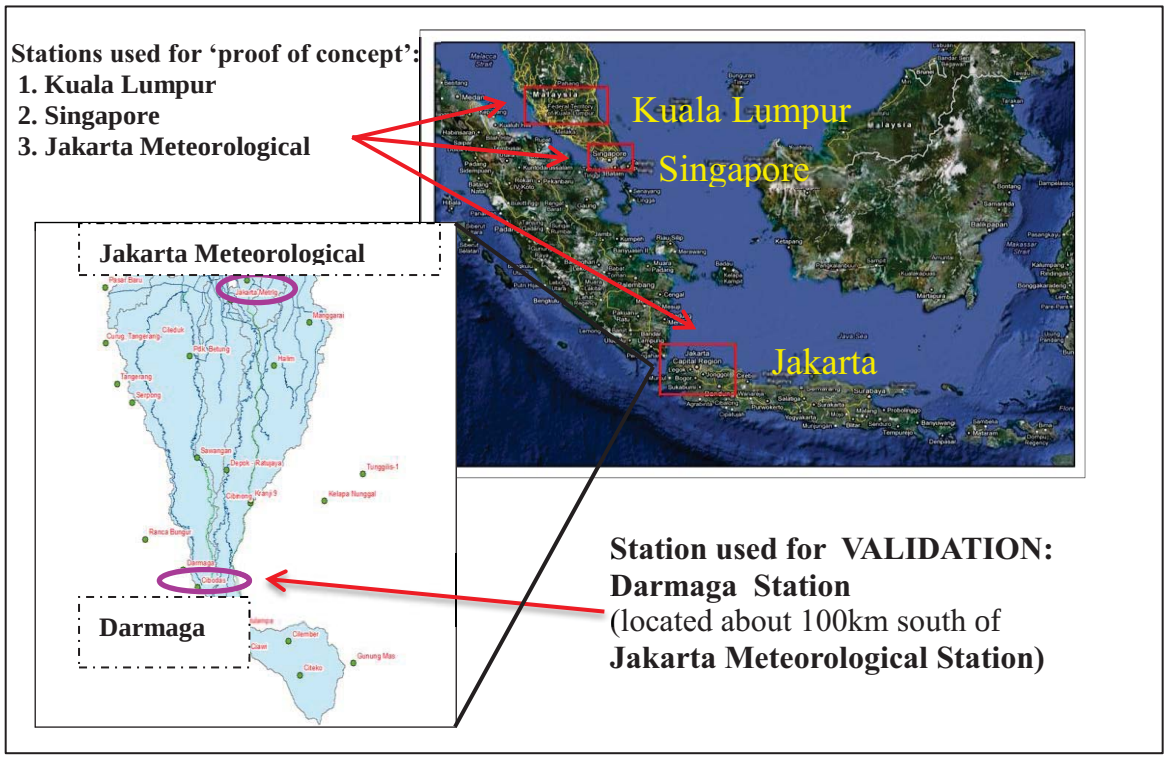

Figure 3.2: Location of rainfall stations used in the study: **Jakarta**, **Singapore** and **Kuala Lumpur**

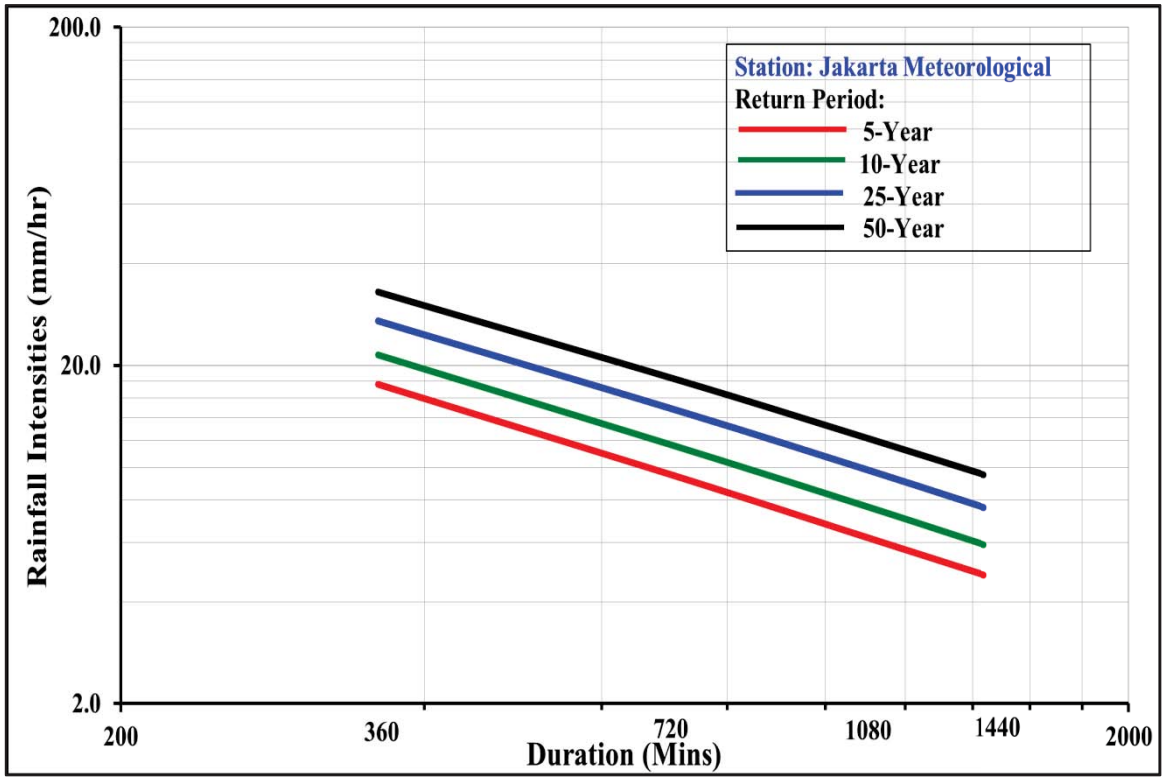

Figure 3.3: Existing IDF curves: **Jakarta Meteorological Station**

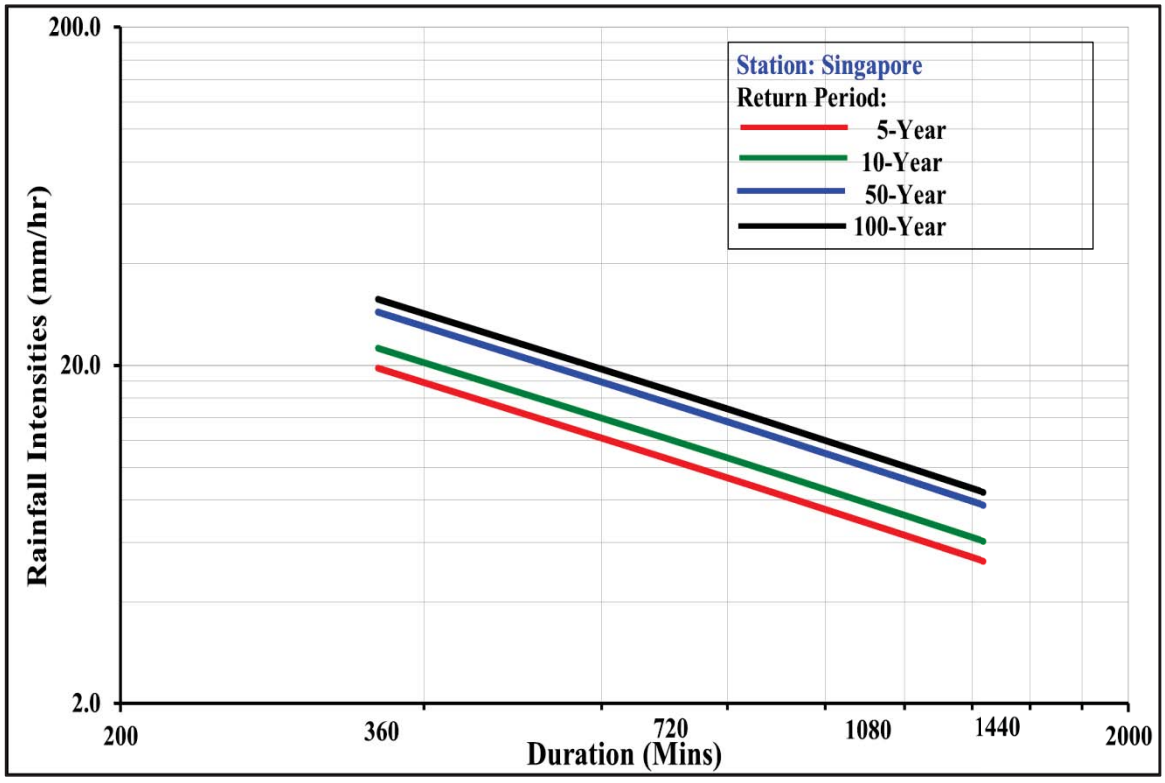

Figure 3.4: Existing IDF curves: **Singapore**

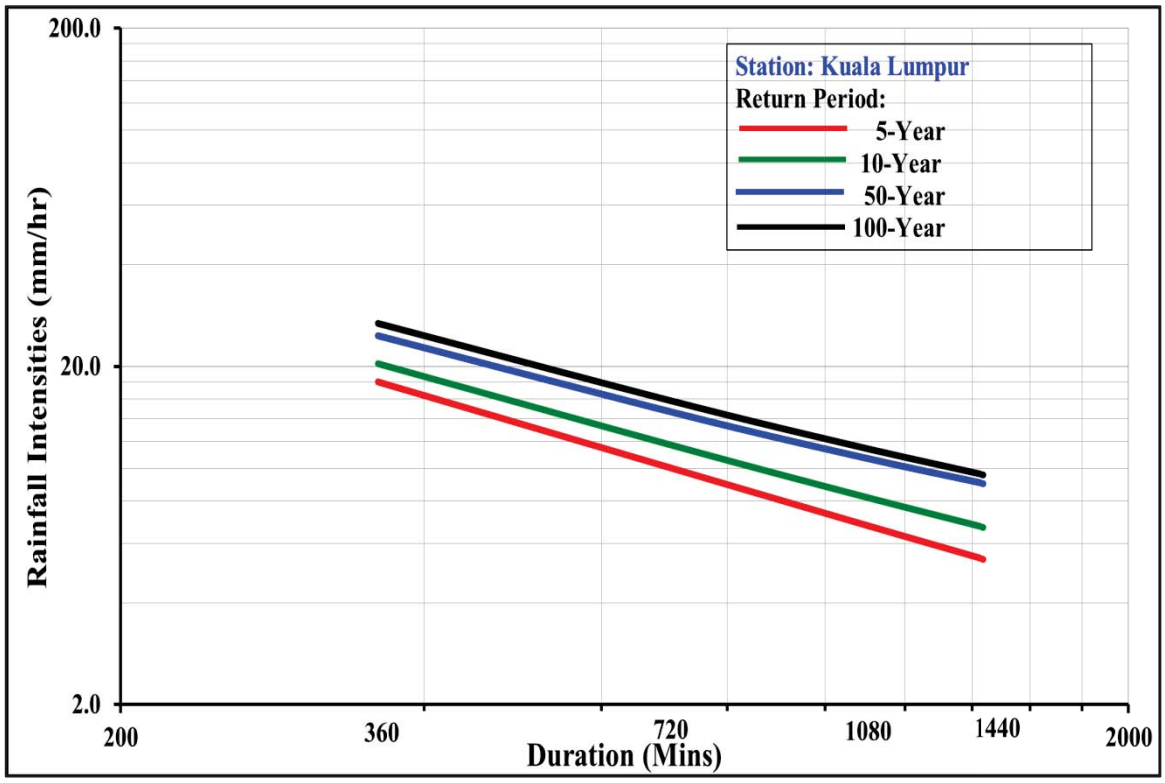

Figure 3.5: Existing IDF curves: **Kuala Lumpur**

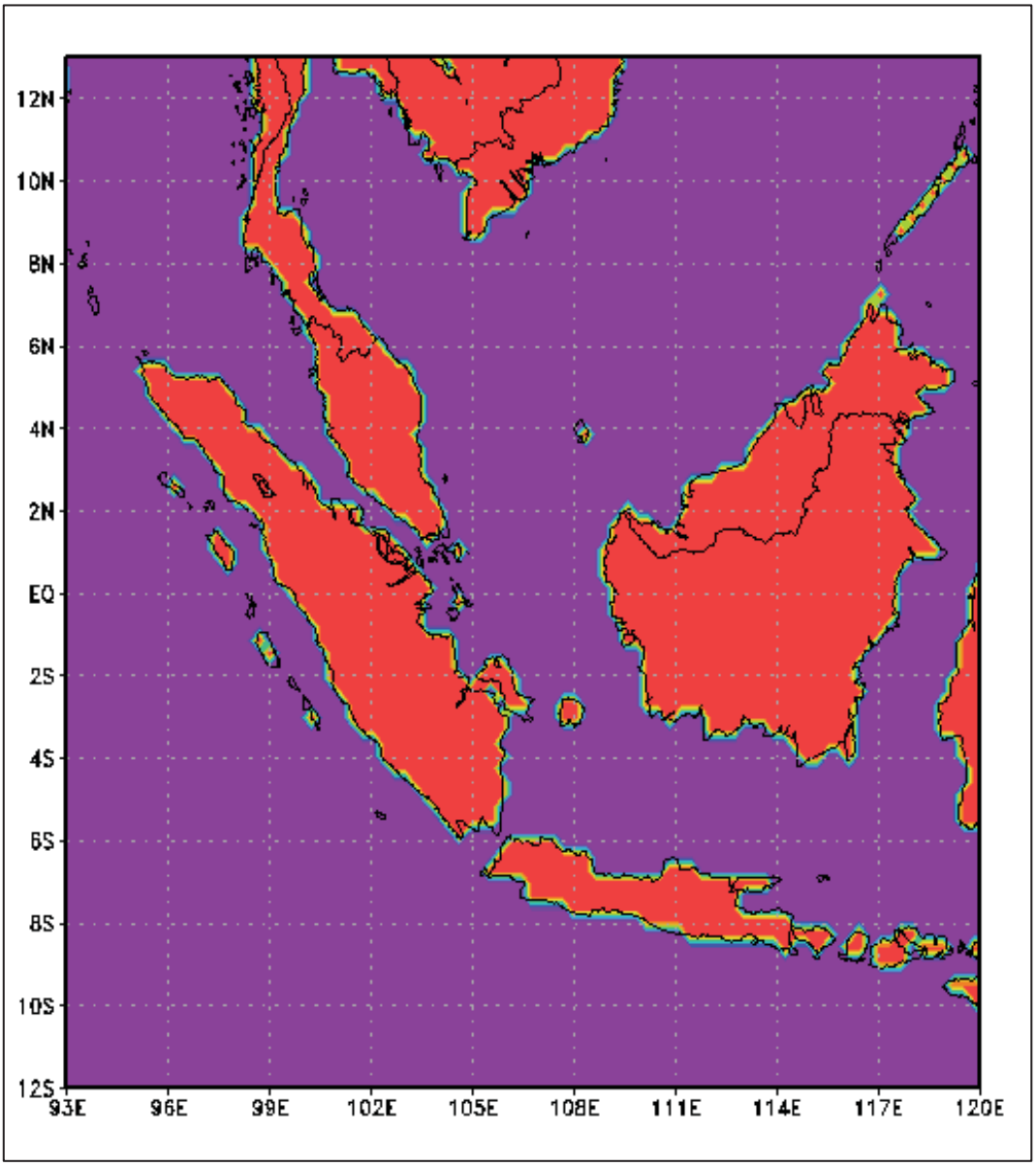

Figure 3.6: Study Domain: 93°E to 120°E, 12°S to 13°N

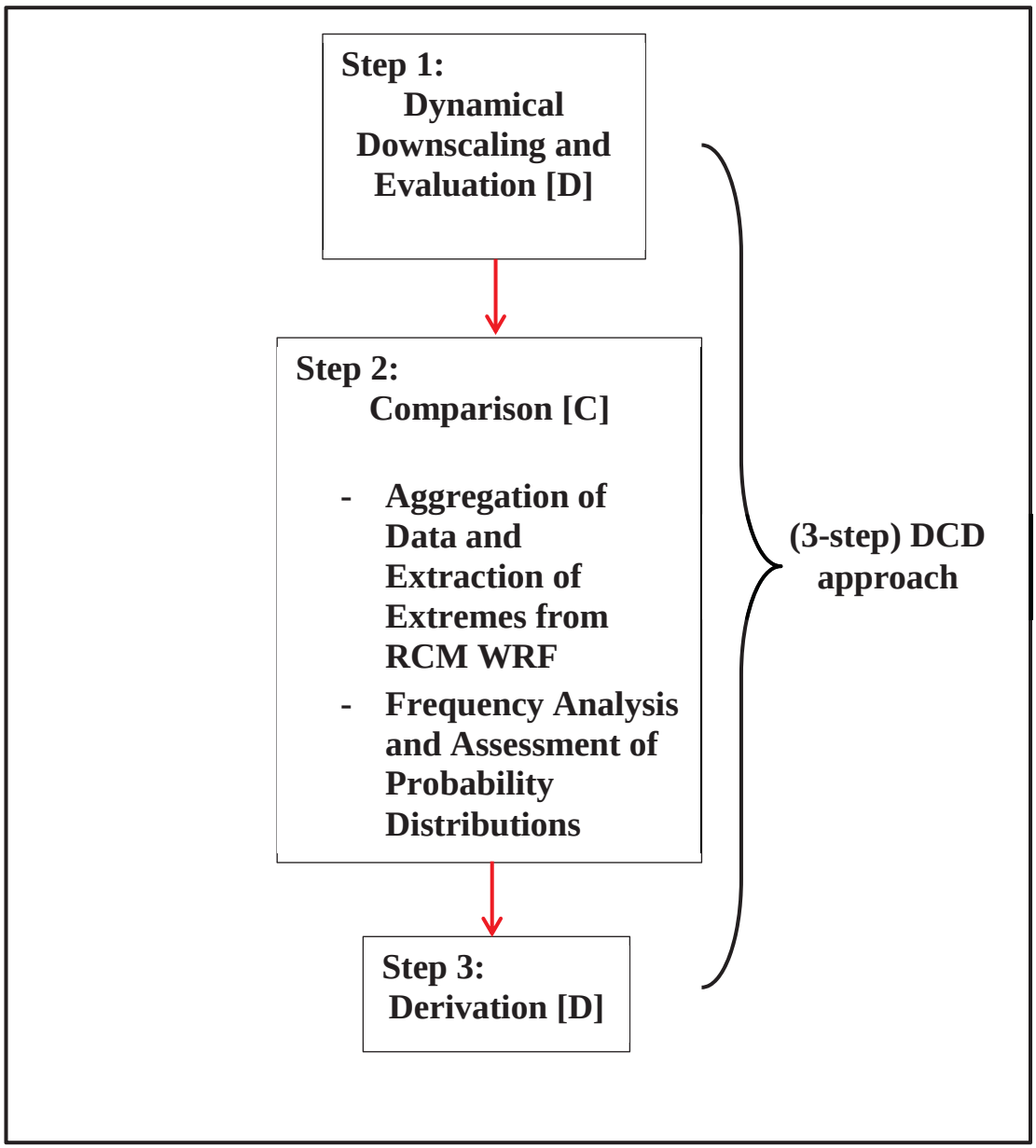

Figure 3.7: A (3-step) DCD approach to develop IDF curves for sites with short or no rainfall record

Table 3-1 List of Global reanalysis and observed datasets for precipitation used for validation of the RCM and their basic characteristics

SOURCE	GRID	RESOLUTION Lat × Lon	FREQUENCY	TIME WINDOW
ERA-40	**Global**	**2.5° × 2.5°**	**6 Hourly**	**1961-1990**
APHRODITE	**Global**	**0.25° × 0.25°**	**Daily**	**1961-1990**
CRU_TS3.0	**Global**	**0.5° × 0.5° (over land)**	**Monthly**	**1961-1990**
CPC	**Global**	**0.5° × 0.5°**	**Monthly**	**1961-1990**
VASClimO	**Global**	**0.5° × 0.5°**	**Monthly**	**1961-1990**

Table 3-2 Extreme indices of precipitation
(For further information about the methodology used to define and compute these indices, please refer to Frich et al. (2002), STARDEX (2004, see http://www.cru.uea.ac.uk/projects/stardex/), and Gachon et al. (2005)

INDICES	ABBREVIATION	DESCRIPTION [unit]	TIME WINDOW
INTENSITY	**SD II**	**Precipitation intensity (rain/wet day), [mm/day]**	**Annual, Seasonal**
DURATION & EXTREMES	**P90p**	**90^{th} percentile of daily rainfall [mm/day]**	**Annual, Seasonal**

CHAPTER 4 REGIONAL CLIMATE MODELING AND PROJECTIONS

4.1 INTRODUCTION

This chapter describes the results of the dynamical downscaling over the study region as mentioned in the methodology section (Chapter 3, Section 3.2). Before projections of future climate are undertaken, the ability, hence the performance, of the climate model to simulate the present day climate needs to be ascertained. In this study, the RCM WRF was first driven by the ERA40 reanalyses (hereafter, this simulation will be referred to as 'WRF/ERA40'). These reanalysis of meteorological observations are considered as 'near perfect boundary conditions' for all RCM simulations and hence the RCM simulations driven by these reanalyses serve as a benchmark for model performance and evaluations. To evaluate model performance, some of the gridded observations, CRU, CPC, VASClimO and APHRODITE datasets (discussed in Chapter 3) were used to compare model simulated surface air temperature and precipitation.

Later the RCM WRF was also driven by the GCMs CCSM3.0 (simulations hereafter, WRF/CCSM) and ECHAM5 (simulations hereafter, WRF/ECHAM) for the same period between 1961-1990 from the 20^{th} century control climate (without the influence of CO_2) experiments and is compared to the simulations of the model driven by the reanalysis as well as the

observations. This step is followed because the WRF/ERA40, essentially represents the 'true' climate whereas the WRF driven by the GCMs are climate estimates that duplicate the true climate. In short, it is also important to see how well the WRF driven by the GCMs represent the mean state of climate. For this reason, the WRF driven by GCMs are evaluated against both the observations and WRF/ERA40. The following sub-section starts with description of the surface air temperature simulation of the WRF model. It is then followed by descriptions of the winds and precipitation simulation of the WRF model.

4.2 PRESENT DAY CLIMATE

4.2.1 Simulation of Temperature

This section discusses the present climate simulations of WRF. The model simulated air surface temperature fields are compared with gridded observation data as shown Figure 4.1 to 4.3.

Figure 4.1 shows the climatological annual mean surface air temperatures of WRF/ERA40, WRF/CCSM and WRF/ECHAM compared to gridded observations, CRU and CPC over the period 1961-1990. The range of annual mean temperatures is from 21°C to 30°C over the study domain. Results show a very good agreement of surface air temperature distributions all over the region. This could be attributed to the confidence in model

estimates, where there is higher confidence in temperature projections due to their relatively homogeneous nature (IPCC, 2007).

Analysis of bias is an assessment of the model's ability to correctly estimate variables; largely independent of whether the actual process descriptions in the model are accurate. The analysis is performed to measure the magnitude of error between a domain averaged mean of the observed and the modeled estimates. The annual biases in the climatological mean surface air temperatures compared to gridded observations are shown in Figure 4.2 to 4.3. The model results are very reasonable with WRF/ERA40, WRF/CCSM while WRF/ECHAM exhibiting least biases (about -1°C to 1°C) over the whole domain except for some parts of Cambodia, Peninsula Malaysia, Northern Sumatra and Borneo Islands where the bias is about -3 °C. Figure 4.2 to 4.3 reflect generally cold bias in most of the regions, with Kalimantan, Indonesia, only being warmer than the observed climatology. Overall biases in WRF/ERA40 are less than that of WRF-CCSM and WRF/ECHAM, which could be a possible influence of the lateral boundaries of the driving GCM/CCSM3.0 and GCM/ECHAM5. As for WRF/CCSM and WRF/ECHAM compared with observed CRU and CPC, there is no significant difference in the overall biases, exhibiting consistent trend of RCM WRF performance for both GCMs.

4.2.2 Simulation of Winds

Of particular interest to study region and its surroundings, with reference to the climate variable wind, are the two monsoon seasons – the Northeast and the Southwest. The mean seasonal surface winds (Northeast and Southwest Monsoon periods) are shown in Figure 4.4 and Figure 4.5 respectively. The Northeast Monsoon spans over the months November through to February (simulations hereafter, NDJF) and the Southwest Monsoon spans over the months from June through to August (simulations hereafter, JJA). The WRF simulations of surface winds at 10 m (U10 and V10) are compared to the ERA40 reanalysis as no other complete global observations are available over land and ocean. This also serves to verify the simulation of WRF driven by ERA40 reanalysis.

The WRF simulations of the surface wind patterns driven by ERA40, GCM/CCSM3.0 and GCM/ECHAM5 (both magnitude and the direction shown by vectors of wind speeds) reveal very reasonable representation of the wind patterns with that of the ERA40 reanalysis (Figure 4.4 and 4.5). The patterns of winds simulated by the actual GCM/ECHAM5 are also shown for comparison. Note that as there are no U10 and V10 winds available from the actual GCM/CCSM3.0, it has not been possible to include them in the figures for comparison. From all the WRF simulations, it is observed that JJA has higher surface wind speed compared to NDJF; all the simulations agree well with each other.

4.2.3 Simulation of Precipitation

The resulting precipitation simulations are compared with gridded observation data as shown in Figure 4.6 to 4.13.

The mean annual climatological (1961-1990) precipitation of WRF/ERA40, WRF/CCSM and WRF/ECHAM compared with gridded observation data CRU, CPC, VASClimO and APHRODITE is presented in Figure 4.6. From Figure 4.6(e), it is clearly visible that the WRF/ERA40 results are very close to observations, particularly over the Java Island (Jakarta), Malaysian Peninsula (Kuala Lumpur) and Singapore.

The overall simulation on the study domain is highly reasonable when compared to the gridded observations (CRU, CPC, VASClimO and APHRODITE) during this same period (Figure 4.6). The spatial distribution of rainfall is fairly well represented. The simulations of WRF/CCSM as shown in Figure 4.6(f) slightly underestimate rainfall in some regions of the northern domain (by approximately 2 mm/day to 3 mm/day) compared to WRF/ERA40 (Figure 4.6(e)). Overestimation, as high as 6 mm/day is seen over Java Island and part of Borneo Island. However, the spatial distributions of rainfall over the regions of Malaysian Peninsula and Sumatra, Indonesia show good agreement against observations. Contrary to the simulations of WRF/CCSM, WRF/ECHAM (Figure 4.6(g)) overestimates rainfall in most of the regions over the domain. Malaysian Peninsula, western Sumatra, Java and Borneo islands are overestimated by 4 mm/day to 5 mm/day when compared to

WRF/ERA40. In particularly Java Island, the overestimation is approximately 5 mm/day as compared to WRF/ERA40 (7 mm/day). This overestimation of the WRF/ECHAM simulations is probably due to the GCM ECHAM boundary forcing itself that tends to simulate a wetter distribution by overestimating precipitation. It has been noted that the GCM ECHAM5 overestimates the frequency of heavy precipitation events (> 6 mm/day) in the tropics (Posselt and Lohmann, 2008), especially at higher vertical resolution, along steep mountain slopes and during the Asian summer monsoon season (Hagemann et al., 2006). Nevertheless, spatial distributions of rainfall simulated by WRF/ECHAM over southern Vietnam show good agreement against the observations. It is to be noted that high rainfall over mountains is well resolved and reflected in all high resolution WRF simulations; however, it is not being well resolved in the observed data (Figure 4.6(a) to 4.6(d)) due to its coarse resolution.

To determine differences between observed and modeled estimates, precipitation bias of the WRF/ERA40, WRF/CCSM and WRF/ECHAM against CRU, CPC, VASClimO and APHRODITE are presented in Figure 4.7 to 4.10. Overall biases in WRF/ERA40 are less than that of WRF/CCSM and WRF/ECHAM, which could be a possible influence of the lateral boundaries of the driving GCM/CCSM3.0 and ECHAM5. As for the comparison of WRF/CCSM and WRF/ECHAM with observed CRU, CPC, VASClimO and APHRODITE, WRF/ECHAM has lower bias than WRF/CCSM. Consequently, The RCM downscaling reduces significantly driving GCM/CCSM3.0 and GCM/ECHAM5 present-climate biases and narrows

inter-model differences in representing climate sensitivity and hence in simulating the present and future climates (Liang et al., 2008).

Calculating the true skill of any climate model is quite challenging because many types of statistical analysis can be used to evaluate the model performance. Generally, the analyses of skill compare the observed and the predicted time series of the parameters (DbLive Meteorological Group, 2010). In order to assess the ability to reproduce inter-annual variability of the model simulations as compared to the observed, Root Mean Square Anomaly (RMSA) is performed on all the datasets. Figure 4.11 provides information on the dispersion of datasets. RMSA is, however, very similar as standard deviation; it is more commonly used in the statistical analysis of climate data. The distribution of regional precipitation is again well simulated by the RCM WRF; relatively low RMSA values are found in Malaysian Peninsula and Java Island whereas higher RMSA values are obtained in some regions of the northern part of the domain. High RMSA values correspond to areas with higher variability as compared to the observed. Comparatively low RMSA value on Java Island has provided clear evidence that RCM simulations can demonstrate a satisfactory precipitation outputs consistent with observed.

The STARDEX indices, the simple daily precipitation intensity, SDII (mm/day) (hereafter, SDII) and 90^{th} percentile of daily precipitation, P90p (mm/day) (P90p), as shown in Table 4-1 (identical to Table 3-2 for readers' easy reference), are also used to evaluate the model performance. The results for the different indices are shown in Figure 4.12 to 4.13.

The precipitation intensity (SDII) for APHRODITE is approximately 10 mm/day higher than WRF/ERA40, WRF/CCSM and WRF/ECHAM. The comparison indicates that WRF simulations underestimate the actual precipitation intensity. However, WRF simulated precipitation resulting from WRF/ERA40, WRF/CCSM and WRF/ECHAM agree well with each other. All the three WRF simulated precipitation are able to capture about 18 mm/day to 20 mm/day of rainfall intensity in Borneo and Sumatra Islands. The 90^{th} percentile of rain (P90p) amounts is reasonable. Nevertheless, WRF/ERA40, WRF/CCSM and WRF/ECHAM overestimate P90p compared to the observation APHRODITE. WRF simulations estimated 25 mm/day to 30 mm/day of P90p (90% of rain falls below 25 mm/day to 30 mm/day) especially over the Malay Peninsula, Sumatra, Java and Borneo regions; APHRODITE on the other hand observed 90% of the rain falls below 15 mm/day to 20 mm/day.

One key contribution of the this study is the recognition of RCM WRF to resolve features on finer scales than those resolved by the GCM, particularly those related to improved resolution of the topography, as shown in Figure 4.1 and 4.13, WRF model is able to add significant detail to the representation of air surface temperature and precipitation of the ERA-40 reanalysis, CCSM3.0 and ECHAM5.

This study has provided conclusive evidence that RCM WRF driven by ERA-40, GCM/CCSM3.0 and GCM/ECHAM5 are able to capture current climate by comparing with the observation datasets (CRU, CPC, VASClimO

and APHRODITE). The study has also demonstrated the consistency of the model simulations (WRF/CCSM and WRF/ECHAM) as compared to the observed datasets. These findings are significant because it provides promising frameworks for future climate simulations. The results of present day climate simulations suggest that the temperatures and winds are very well reproduced while rainfall is reasonably well reproduced.

4.3 FUTURE CLIMATE RESPONSE FOR STUDY REGION

Since the main objective of this thesis is to determine the changes in climate over the future, and its impact on the IDF curves, the RCM WRF was then run for the future climate driven by GCM/CCSM3.0 forced under the IPCC emission scenarios A1FI, A2 and A1B and GCM/ECHAM5 forced under the A2 scenario, to determine climate changes over the future time slices 2011-2040, 2041-2070 and 2071-2100. The simulations results are shown in the following sections. The climate responses, including annual and seasonal climatologies for the larger domain and for study region are shown in sections 4.3.1 to 4.3.4 for the key climate variables – temperature, winds and precipitation. Additional analyses such as the extreme indices (STARDEX) of precipitation for larger domain and the study region, Jakarta were also discussed in the following sections. This section mainly describes the climate responses for the study region only, which is the key focus of the study. However, the figures for the larger domain (which include Kuala Lumpur and Singapore) are more representative for part of the Southeast Asian sub-

continent as such. The precipitation response simulated for Jakarta, Kuala Lumpur and Singapore are utilised in Chapter 5 to develop IDF curves for future climate.

Next two sections of this thesis discuss climate projections from WRF/CCSM and WRF/ECHAM under different climate change scenarios.

4.3.1 Climate Projections from WRF/CCSM driven under A1FI, A2 and A1B scenarios

Climate Projections from WRF/CCSM driven under A1FI scenario

The future temperature responses simulated by WRF/CCSM driven under A1FI scenario are shown in Figure 4.14 to 4.17. It can be seen that the annual temperature over study region, Jakarta, is poised to increase between 1°C - 1.3°C by 2011-2040 and nearly to 2.1°C during the mid-century, 2041-2070 and up to 3.7°C by the end of the century. The region will experience warming of about 0.4°C per decade by 2100. The WRF simulation results is quite in line with the best estimate by IPCC (IPCC, 2007) where for the high scenario, A1FI, the warming of 4°C (likely range is 2.4°C to 6.4°C) relative to pre-industrial is expected by the end of the 21st century.

Future projections of wind speeds (Figure 4.18 to 4.21) suggest no substantial increases during both monsoon seasons NDJF and JJA; nevertheless JJA wind speeds show slightly larger values than that of NDJF.

The simulation result of WRF/CCSM driven under A1FI scenario as presented in Figure 4.22 suggests that the overall trend for Jakarta, Singapore and Kuala Lumpur indicate a gradual increase in precipitation. The increase of approximately 30% to 50% may be expected for all the three regions by the end of 21st century. The NDJF monsoon season as shown in Figure 4.23 also show that the three regions will experience increase in the total annual rainfall throughout the 21st century; however, the results suggest decrease in future precipitation for Jakarta region during JJA monsoon season.

Figure 4.24 shows an annual precipitation increase of nearly 25% during the immediate future time slice 2011-2040 over study region, Jakarta. An increase of up to 40% or more may be expected during the mid-century and more than 45% likely by 2071-2100. The monsoon seasons, as shown in Figure 4.25, also suggest an increase in the rainfall over the future with NDJF season showing larger increases changes than the JJA season. Wet monsoon during the NDJF season shows an increase of +20% to +40% by 2100, whereas dry monsoon (JJA season) indicates a decrease in precipitation of about -10% to -25% by the end of the century. A possible reason could be due to global warming that resulted the dry season become drier and the wet season become wetter.

The STARDEX indices for WRF/CCSM driven under A1FI scenario are shown in Figure 4.26 to 4.33. Projections indicate that the rainfall intensity is likely to get stronger than the current climate, as high as 5 mm/day throughout the future periods until the end of the 21st century on the annual

scale. The results shown in Figure 4.30 to 4.33 indicate that the 90th percentile of rainfall shows marginal increases over the study domain, with relatively higher (more than 5 mm/day) during the wet monsoon during the NDJF season and drier (5 mm/day less than current climate) during the dry monsoon, JJA season by 2100.

The future changes in the rainfall for Jakarta Meteorological Station is also represented in Probability Density Function in Figure 4.34. The precipitation over the present day climate, the WRF model (red line) overestimates the dry spells and underestimates lower rainfall intensities. The extreme rainfall is reasonably well represented. For the future, the rainfall patterns simulated from WRF/CCSM driven by A1FI scenario closely follow the present day climate distribution.

Tables 4-2 and 4-3 show the summary of the temperature and precipitation response respectively projected by WRF/CCSM driven under A1FI scenario.

Climate Projections from WRF/CCSM driven under A2 scenario

Temperature projections from WRF/CCSM driven under A2 scenario (Figure 4.35 to 4.38), demonstrate that the annual temperature over Jakarta is likely to increase between 1.1°C by 2011-2040 and nearly up to 1.9°C during the mid-century 2041-2070 and up to 3.2°C by the end of the century. Generally, the

projections are slightly lower relative to the same period for projections by A1FI scenario.

Future projections of wind speeds as shown in Figure 4.39 to 4.42 suggest no substantial increases during both monsoon seasons NDJF and JJA, nevertheless JJA wind speeds show slightly larger values than that of NDJF.

Projections of annual increase in precipitation by WRF/CCSM driven under A2 scenario for Jakarta, Singapore and Kuala Lumpur are slightly lower as compared with precipitation increase simulated by scenario A1FI. WRF/CCSM A2 projected approximately 20% of increase rainfall during the immediate future time slice 2011-2040, whereas an increase of up to 35% or more may be expected during the mid-century for the three regions. However, the annual precipitation response for Singapore and Kuala Lumpur regions by the end of the 21st century is about 35% (Figure 4.43), slightly lower than Jakarta region which is more than 40% to 50% likely by 2100 (Figure 4.45).

Figure 4.46 indicates that the wet monsoon season (NDJF) for Jakarta region suggest an increase in the rainfall over the future for about 40% by 2100, while JJA season shows a 30% decrease in rainfall by 2100. Similar to Jakarta region, by 2100 the increase in the rainfall over the future with NDJF season for both Kuala Lumpur and Singapore regions (Figure 4.44) is about 40% to 50% relative to JJA season (-20 %).

As shown in Figure 4.47 to 4.48, the rainfall projections indicate that the annual and seasonal SDII for Jakarta, Singapore and Kuala Lumpur are likely to gradually get stronger (2 mm/day to 5 mm/day) throughout the future periods with larger increases towards the period 2071-2100. The projection is slightly lower than simulations by A1FI scenario which project 5 mm/day throughout the century. These results are particularly pronounced over the wet NDJF monsoon season as shown in Figure 4.48 and 4.50. Dry JJA monsoon season conversely indicates -1 mm/day to -2 mm/day less than the present day climate by the end of the 21st century. As for the P90p of rainfall in Figure 4.51 to 4.53 shows gradual increases over the Jakarta domain, as well as Singapore and Kuala Lumpur regions during the course of the future time slices. The simulations results for the study region, Jakarta, suggest that higher P90p relative to current climate during the NDJF monsoon season (nearly 5 mm/day) than the JJA monsoon season, where the P90p falls approximately 5 mm/day by 2070-2100 (Figure 4.54).

The future changes in the rainfall for Jakarta Meteorological Station is also represented in Probability Density Function in Figure 4.55. The precipitation over the present day climate, the WRF model (red line) overestimates the dry spells and underestimates lower rainfall intensities. However, the extreme rainfall patterns simulated from WRF/CCSM driven by A2 scenario closely follow the present day climate distribution, especially with respect to extremes.

Tables 4-2 and 4-3 show the summary for the temperature and precipitation response respectively projected by WRF/CCSM driven under A2 scenario.

Climate Projections from WRF/CCSM driven under A1B scenario

Model simulations as shown in Figure 4.56 to 4.59 clearly show that the surface temperatures are likely to be more than 1°C higher than the present day values by the period 2011-2040 all over Southeast Asia, while Jakarta region could experience a surge of 1.1°C by then. Up to a 3°C rise in Southeast Asia is likely by the end of the century with Jakarta likely to experience about a maximum of 2.3°C by 2100.

There are no substantial changes in wind speeds, although the JJA season is likely to see stronger wind speeds than NDJF season (Figure 4.60 to 4.63).

Projections from WRF/CCSM A1B suggest that the increases in annual and seasonal rainfall over Southeast Asia are more pronounced over the Malaysian Peninsula, Indonesia and Borneo over the future time slices (Figure 4.64 and 4.65). The increase of approximately 25% to 30% may be expected for both Kuala Lumpur and Singapore regions by the end of 21st century (Figure 4.64). Figure 4.66 shows a closer look at Java Island, where the main focus is Jakarta. Jakarta rainfall could see an increase of about 15% during 2011-2040 period, 30% by the mid-century. The last 30 years of the

century may expect up to a 40% increase in precipitation response. The NDJF monsoon seasons for Jakarta region also show an increase (15% to 40%) in the rainfall over the future by 2100; however the percentage of rainfall increment in A1B projections is lower than scenarios A1FI and A2. Overall, Jakarta region may experience 15% less rainfall as compared to current climate during the dry season (JJA) (Figure 4.67).

The STARDEX indices for WRF/CCSM driven under A1B scenario are shown in Figure 4.68 to 4.75. The SDII is likely to get stronger throughout the future periods until the end of the century both on the annual and seasonal scales (Figure 4.68 to 4.71). The annual and seasonal P90p of rainfall shows marginal increases over the study domain (Figure 4.72 and 4.73); however for Jakarta region, the results as shown in Figure 4.73 suggest decease by about 3 mm/day to 4 mm/day during the dry JJA season.

The future changes in the rainfall for Jakarta Meteorological Station is also represented as Probability Density Function in Figure 4.76. The precipitation over the present day climate, the WRF model (red line) overestimates the dry spells and underestimates lower rainfall intensities. Similar to WRF/CCSM A1FI and WRF/CCSM A2, the extreme rainfall simulated from WRF/CCSM A1B is reasonably well represented. For the future, the rainfall patterns simulated from WRF/CCSM driven by A1B scenario closely follow the present day climate distribution.

Table 4-2 and 4-3 summarize the temperature and precipitation response respectively projected by WRF/CCSM driven under A1B scenario.

4.3.2 Climate Projections from WRF/ECHAM driven under A2 scenario

Temperature projections simulated by WRF/ECHAM driven under A2 scenario (Figure 4.77) show that the surface temperatures are likely to be more than 0.8°C higher than the present day values by the period 2011-2040 in Southeast Asia. The simulations also show that, by 2100, Southeast Asia is likely to experience approximately 3.5°C increase in temperature as compared to the present day temperature. As for the study region, surface air temperature change in Jakarta is poised to increase between 0.4°C to 0.6°C by 2011-2040 (Figure 4.79(D1)) and nearly to 1.8°C during the mid-century 2041-2070 (Figure 4.79(D2)) and more than 3.5°C by the end of the century (Figure 4.79(D3)).

Future projections of wind speeds (Figure 4.81 to 4.84) illustrate that there is no substantial increases during both monsoon seasons NDJF and JJA; nevertheless JJA wind speeds are projected to be higher than NDJF.

As for precipitation change, Figure 4.85 and 4.86 illustrate increasing trends for rainfall over all the three future time slices over Southeast Asia. Kuala Lumpur and Singapore may experience about 30% increase in precipitation by 2100. Jakarta rainfall is on the increasing trend with more

than 45% of rainfall by the end of the century. Contrary to the WRF/CCSM projections, both NDJF and JJA seasons show approximately 20% to 50% increases in precipitation by 2100 (Figure 4.86 and 4.88).

SDII are likely to get stronger, approximately 5 mm/day compared to the current climate throughout the future periods until the end of the century both on the annual and seasonal scales (Figure 4.86 to 4.89). Figure 4.93 to 4.96 illustrate marginal increases of the P90p of rainfall over the Jakarta domain, where no significant differences after 2040s. The results also suggest relatively larger increases during the NDJF season as compared with JJA season (Figure 4.96).

The future changes in the rainfall for Jakarta Meteorological Station is also represented as Probability Density Function in Figure 4.97. The present day climate simulation from the WRF model (red line) follows the pattern of the present day climate from the station. In addition, the future extreme rainfall patterns simulated from WRF/ECHAM driven by A2 scenario closely follow the present day climate distribution, especially with respect to extremes. However, the WRF/ECHAM A2 2071-2100 show higher distribution for both the dry spells and high rainfall intensities.

The findings from Sections 4.3.1 and 4.3.2 are of crucial importance in term of providing information on future climate projections from different GCMs and climate change scenarios. The simulation results in Figure 4.98 show that the warming in Java Island in the immediate future could be

stronger than the global mean temperature increase of 0.75°C in the last 100 years (IPCC, 2007). The surface air temperature is projected to increase at least 1.1°C in the Jakarta region by 2011-2040. Climate scenarios project further warming of 2.3°C to 3.7°C increase until the end of this century depending on the emission scenario. Associated with changes in surface air temperature, precipitation changes are expected in the study region. The changes in precipitation, either increases or decreases compared to the present situation (1961-1990) are already significant in many regions for the first 30-year time slice (2011-2040) and become more intense by the end of the century (Figure 4.99).

4.3.3 Comparative study of different scenarios: WRF/CCSM A1FI, A2 and A1B

The RCM WRF simulations show that the differences in the IPCC SRES emission scenarios lead to significantly different temperature developments until the end of this century. The temperature increases only by about 2.3°C in the A1B scenario, while it increases between 3.2°C and 3.7°C in the A2 and A1FI simulations for 2071-2100 as compared with 1961-1990 (Figure 4.100 and Table 4-2). This is most likely related to the different developments of emissions which are prescribed in the simulations. However, before 2040s none of the scenarios is clearly higher than the others, where temperature increases about 1.1°C to 1.3°C as compared with the present climate (1961-1990) for all the three scenarios.

On the contrary, the future precipitation change for the three scenarios did not significant differences throughout the 21st century. Figure 4.101 and Table 4-3 suggest that the percentage increase of precipitation by the end of the 21st century is about the same (+40% to +45%), except for immediate future (2011-2040) where scenario A1B has the lowest increment (+15%) as compared with scenarios A2 and A1FI (+20% and +25 %).

One hypothesis that can be concluded in this study is that the intensification of the future precipitation happens until a warming of about 2°C is reached (Jacob and Lorenz, 2009), which happened during 2011-2070 (Figure 4.100 and 4.101, Table 4-2 and 4-3) and that further warming will only cause a slight increment in percentage precipitation change. Future analyses for which many more climate change scenarios and ensembles study are needed to further investigate this phenomenon.

Comparing the simulation results driven by different scenarios is important to create a better informed recommendation for policy makers. With the information of future emission and its effect on temperature and precipitation, the mitigation opportunities in each scenario as well as different policy perspective can be adopted.

Figure 4.102 indicates that adopting any of the scenarios did not appear have much impact on the temperature responses by 2040. The ratio of scenario A1FI to A1B is about 1.18 indicating that, by adopting scenario A1FI the immediate future will be exposed to a temperature rise at approximately

0.3°C higher than scenario A1B. As for precipitation (Figure 4.103), adopting a policy based on the emission scenario A1FI results will be subjected to an increase in the precipitation of 1.67 times higher than scenario A1B in the immediate future time period (2011-2040). However, adopting any of these three scenarios will have to be concerned of shows approximately the same amount of increase in precipitation by the end of the century.

Contrary to that of precipitation, by 2100 the warming very much depends on the scenarios adopted. Adopting A1FI scenario will have to be concerned with an increase in temperature as high as 1.61 times scenario A1B. In this study, scenario A2 falls in between A1FI and A1B scenarios. Scenario A2 indicates a moderate rate of precipitation and temperature increase to 2100. This study is the first to have provided clear illustration for the policy makers to justify their future policies. In addition, the results from this study also serves as guidelines to incorporate climate change issues into drainage design curves (Chapter 5).

4.3.4 Comparative study of different GCMs: WRF/CCSM A2 and WRF/ECHAM A2

It is worth to compare future climate response simulated by various climate models in order to reduce the climate model uncertainties. In this section, climate signals from two different climate models GCM/CCSM3.0 and GCM/ECHAM5 forced under IPCC A2 scenarios are compared (Figure 4.104 and Figure 4.105).

Table 4-4 shows the annual and seasonal changes for temperature responses. There is no significant difference in annual and seasonal warming for both climate models. This provides clear evidence that the future precipitation is more difficult to project, and changes are generally of lower statistical significance, than changes in temperature (Barrow et al., 2004).

As illustrated in Table 4-5, WRF/ECHAM A2 appears to be wetter than WRF/CCSM A2 during the immediate future; however, WRF/CCSM A2 shows slight increase in precipitation (+35%) as compared to WRF/ECHAM A2 (+30%) by 2070s. Both climate models project more than 45% increase in rainfall by the end of the 21st century. The difference in annual precipitation increase between these two models ranges from 17% to 25% indicating a range of possible change among climate models. As for seasonal change, both models agree that, over the Jakarta region, NDJF season will become wetter (Table 4-4). There is not quite the same agreement on changes in JJA season. WRF/CCSM A2 indicates a decrease in total rainfall for about 10% to 20% during JJA season, WRF/ECHAM A2 on the other hand project an increase in rainfall up to 45% by the end of the century. This finding has again shown that there are variations across different climate models.

Currently, the only way to appreciate this uncertainty is to look at results from the full range of global models that have been presented in the recent IPCC assessment. Whilst comparing different model results is important to illustrate uncertainty, there is no easy way to attach higher or lower confidence to the results of one model over another (Hulme and

Turnpenny, 2002). The GCM/CCSM3.0 and GCM/ECHAM5, however, perform quite well in reproducing current climate and this has added confidence level for the models to capture future climates.

4.4 CONCLUDING REMARKS

4.4.1 Present Day Climate

This study has provided an initial confidence level of RCM WRF in simulating credible quantitative estimates of future climate change. This confidence comes from the foundation of the models in accepted physical principles and from their ability to reproduce observed features of current climate and past climate changes (IPCC, 2007).

In the present day climate study, the present day simulations with the RCM WRF (1961-1990) is evaluated and compared with the observation datasets (CRU, CPC, VASClimO and APHRODITE), including an identification of biases in the RCM climate. One key contribution of the this study is the recognition of RCM WRF to resolve features on finer scales than those resolved by the GCM, particularly those related to improved resolution of the topography, such as its influence on surface air temperature and large-scale precipitation.

This study has provided conclusive evidence that RCM WRF driven by ERA-40, GCM/CCSM3.0 and GCM/ECHAM5 were able to capture current

climate depicted in the observation datasets. The study has also demonstrated the consistency of the model simulations (WRF/CCSM and WRF/ECHAM) as compared to the observed datasets. These findings are significant because it provides promising frameworks for future climate simulations and climate change projections.

RCM WRF has been extensively used and evaluated over many other regions and domain, but this first-of-its-kind study highlights the importance of evaluating RCM WRF over Southeast Asia domain. This helps in the identification of model errors and leads to the improvement of the climate models.

4.4.2 Main Findings: Future Climate Response for Study Region

Comparative studies have been performed to analyse the future climate response for precipitation, temperature and winds due to different climate change emission scenarios (A1FI, A2 and A1B) and different GCMs (CCSM3.0 and ECHAM5) for three future time slices (2011-2040, 2041-2070 and 2071-2100).

For comparative study of different IPCC SRES emission scenarios (A1FI, A2 and A1B), the WRF simulations show that the differences in the emission scenarios lead to significantly different in temperature increases until the end of 21st century. The analysis shows that before 2040s all scenarios project about the same moderate temperature increase of about 1.1°C to 1.3°C.

The precipitation, however, has the inverse trend; the percentage change of precipitation for different scenario is obvious during 2011-2070. Higher percentage of precipitation response for A1FI scenario, followed by A2 and A1B. However, by 2100, these three scenarios show approximately same amount of increase in precipitation. As mentioned in Section 4.3.3, one hypothesis could be that the increase of the future precipitation happens until a warming of about 2°C is reached (Jacob and Lorenz, 2009) and that further warming will only cause a slight increment in percentage precipitation change (Figure 4.100 and 4.101, Table 4-2 and 4-3).

By adopting scenario A1FI, the increase in the precipitation is 1.67 times higher than scenario A1B during the immediate future (2011-2040), and increase in temperature as high as 1.61 times by the end of 21st century. Higher warming and increase in precipitation in A1FI scenario are due to the greater total energy demand and carbon intensity. In this study, scenario A2 falls in between A1FI and A1B world. Scenario A2 indicates a moderate rate of precipitation and temperature increase to 2100.

This study is the first to have provided clear illustration for the policy makers to justify their future policies. Comparing the simulation results driven by different scenarios is essential to present a better informed recommendation to policy makers. With the information of future emission and its effect on temperature and precipitation, the mitigation opportunities in each scenario as well as different policy perspective can be more wisely adopted.

In addition, a comparative study of different GCMs has been performed. Both WRF/CCSM and WRF/ECHAM project approximate 45% increase in rainfall by the end of the 21st century. The difference in annual precipitation change between these two models ranges from 17% to 25% indicating a range of possible change among climate models. Although the GCM CCSM3.0 and ECHAM5 yielded different WRF simulations, both models perform quite well in reproducing current climate and this has added confidence level for the models to capture future climates. There is no significant difference in annual and seasonal warming for both climate models. This provides clear evidence that the future precipitation is more difficult to project, and precipitation changes are generally of lower statistical significance than changes in temperature (Barrow et al., 2004). It appears that climate models' uncertainties are foreseeable. One way to appreciate this uncertainty is to look at results from the full range of global models that have been presented in the recent IPCC assessment. Whilst comparing different model results is important to illustrate uncertainty, there is no easy way to attach higher or lower confidence to the results of one model over another (Hulme and Turnpenny, 2002).

In conclusion, the results from this study have provided important insight that many of the severe impacts projected under high A1FI and mid high A2 scenarios could be avoided by adopting mid-range A1B scenario; a scenario that balanced emphasis on a wide range of energy sources. However, even if global emissions stay below the A1B emissions scenario, some impacts from climate change are inevitable. Evidence shows that even if actions could

be taken to immediately limit the GHG emissions, the GHGs that have already built up and their long atmospheric lifetimes could result in average global temperatures rising at an additional 0.6°C (1.1°F) (Wigley, 2005; Meehl et al. 2005; Cayan et al. 2008). As a result, some impacts from climate change, in Jakarta region, and across the globe, are seemingly unavoidable. Climate change signals have shown significant increase in rainfall intensities and frequencies in many regions. Therefore, a revisit of the existing IDF curves is called for to re-examine the adequacy of the current drainage system and capacity to meet the projected future rainfall extremes. With regard to data sparse or ungauged sites, developing IDF curves is a challenge for both present and future climate. Mitigation measures can be taken only when projected rainfall is available. In this study, the projected rainfall is derived from a high resolution regional climate model (RCM) which enables rainfall extremes to be analyzed for derivation of IDF curves. Thus, the modeling outputs from this chapter are fully utilised in Chapter 5 to develop present day and future IDF curves.

This page is intentionally left blank.

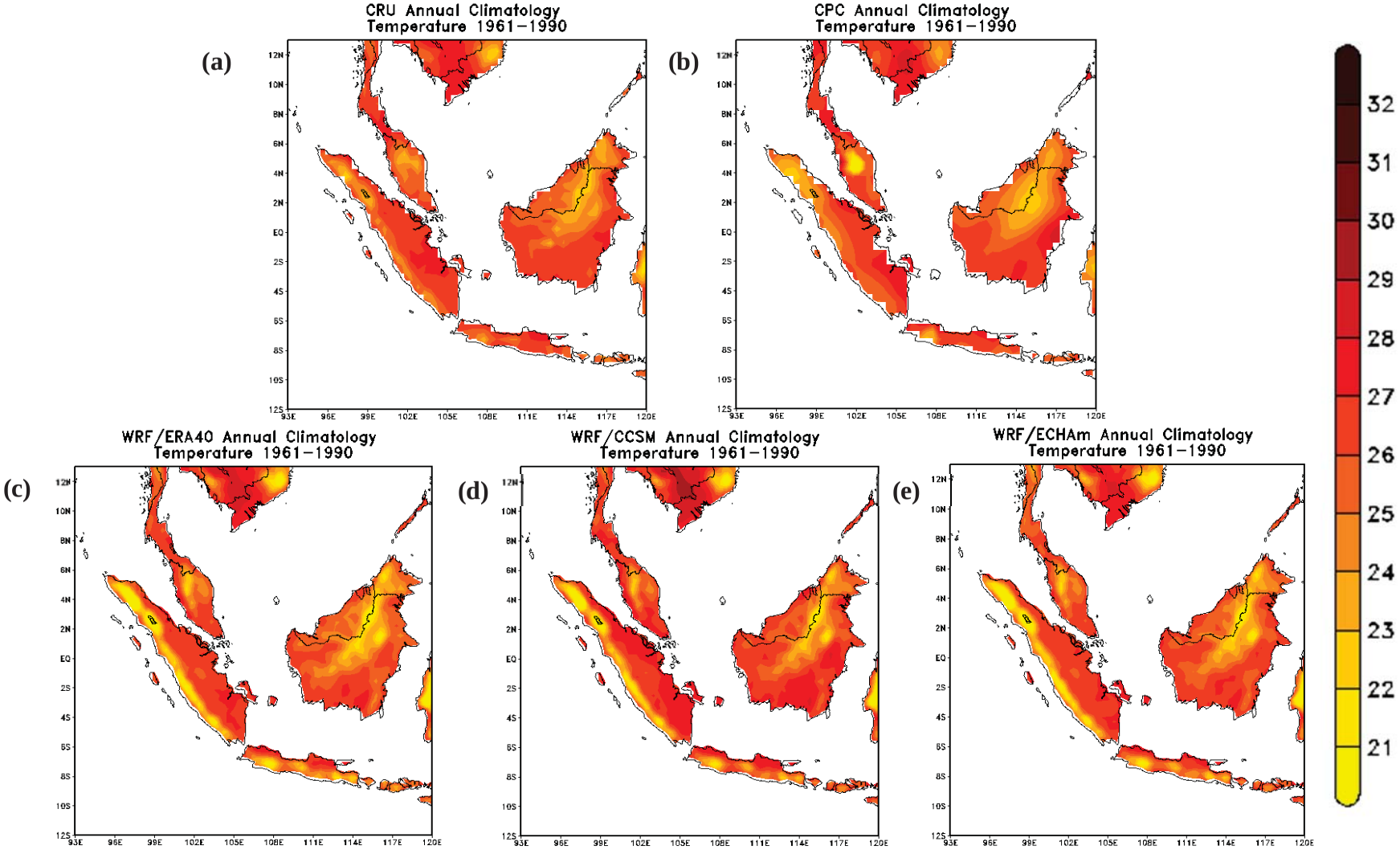

Figure 4.1: Mean **Annual** Surface Air Temperatures (T2), °C, 1961-1990
(a) CRU (b) CPC (c) WRF/ERA40 (d) WRF/CCSM (e) WRF/ECHAM

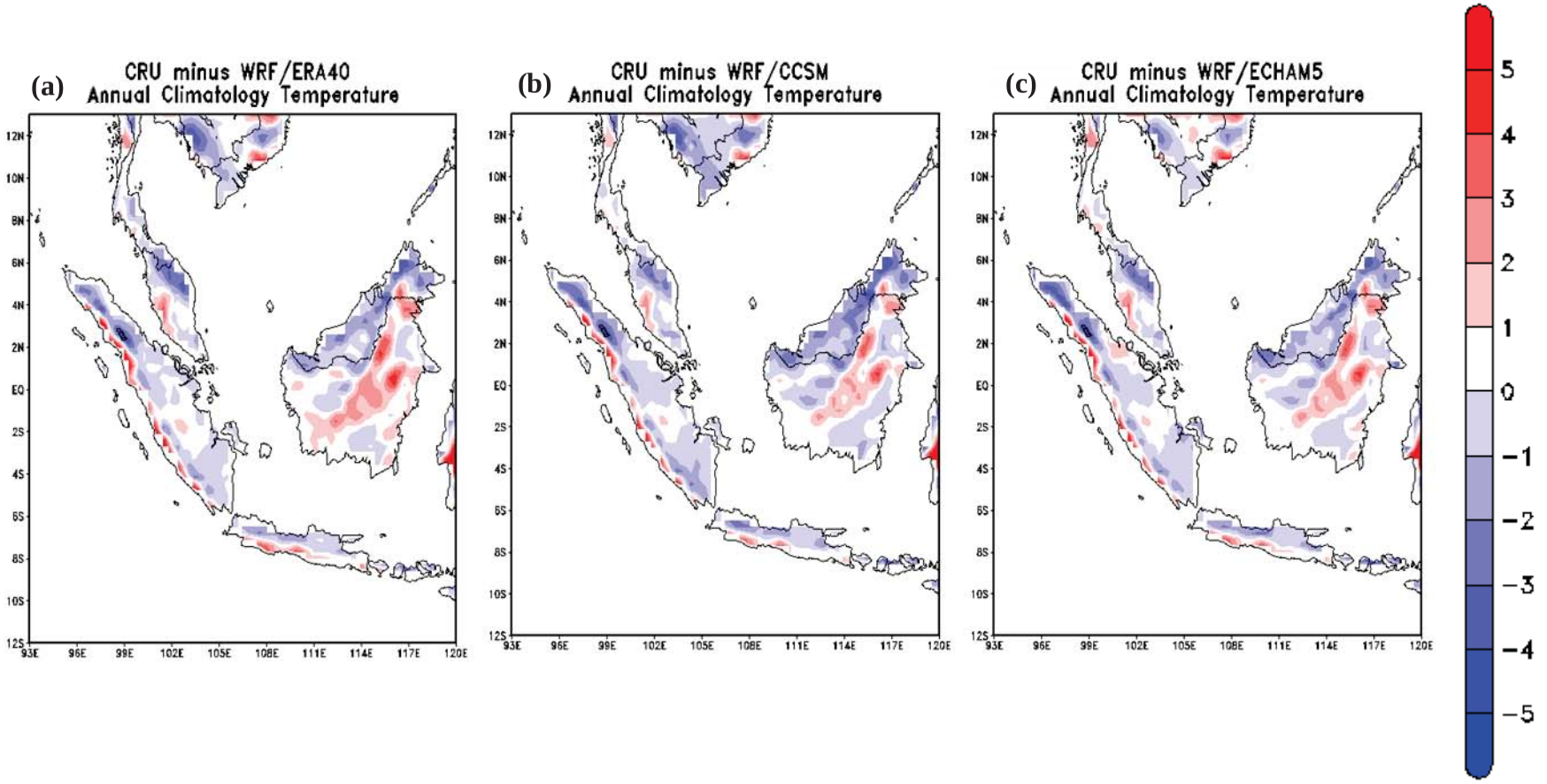

Figure 4.2: Mean **Annual** Bias in Surface Air Temperature, °C, 1961-1990
(a) CRU minus WRF/ERA40 (b) CRU minus WRF/CCSM (c) CRU minus WRF/ECHAM

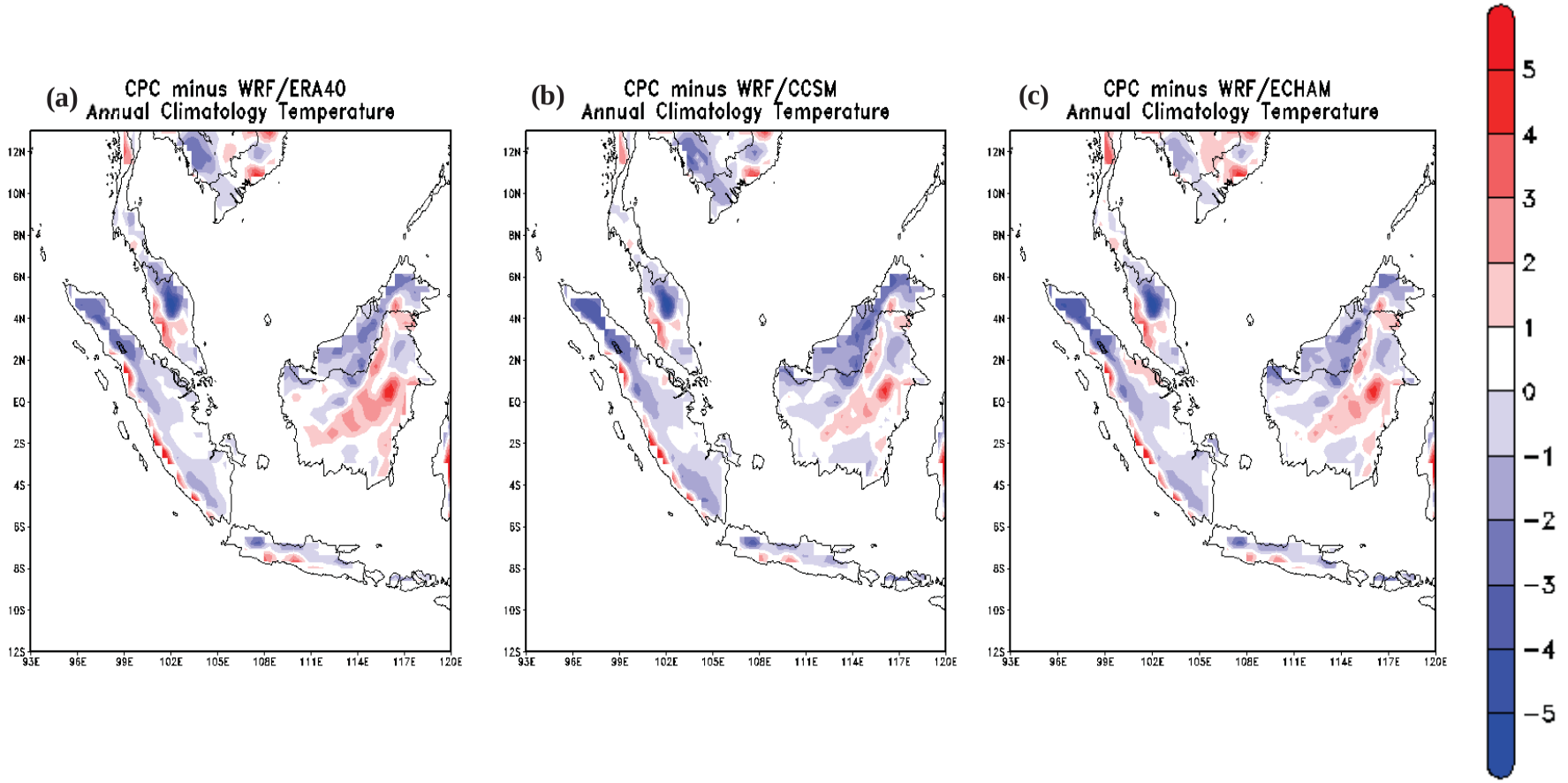

Figure 4.3: Mean Annual Bias in Surface Air Temperature, °C, 1961-1990
(a) CPC minus WRF/ERA40 (b) CPC minus WRF/CCSM (c) CPC minus WRF/ECHAM

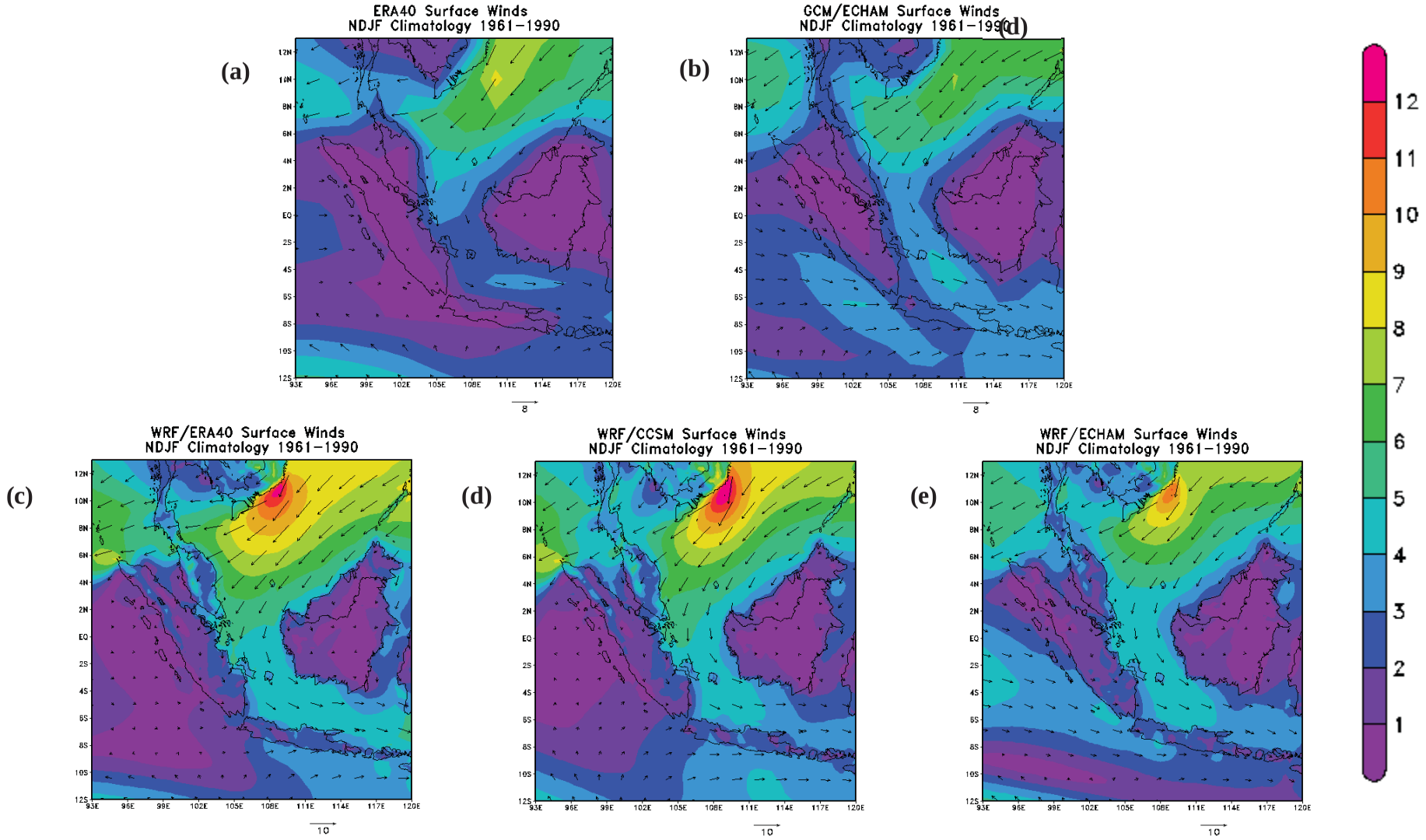

Figure 4.4: Mean Seasonal **Northeast Monsoon (NDJF)** Surface Winds, m/s, 1961-1990
(a) ERA40 (b) GCM/ECHAM (c) WRF/ERA40 (d) WRF/CCSM (e) WRF/ECHAM

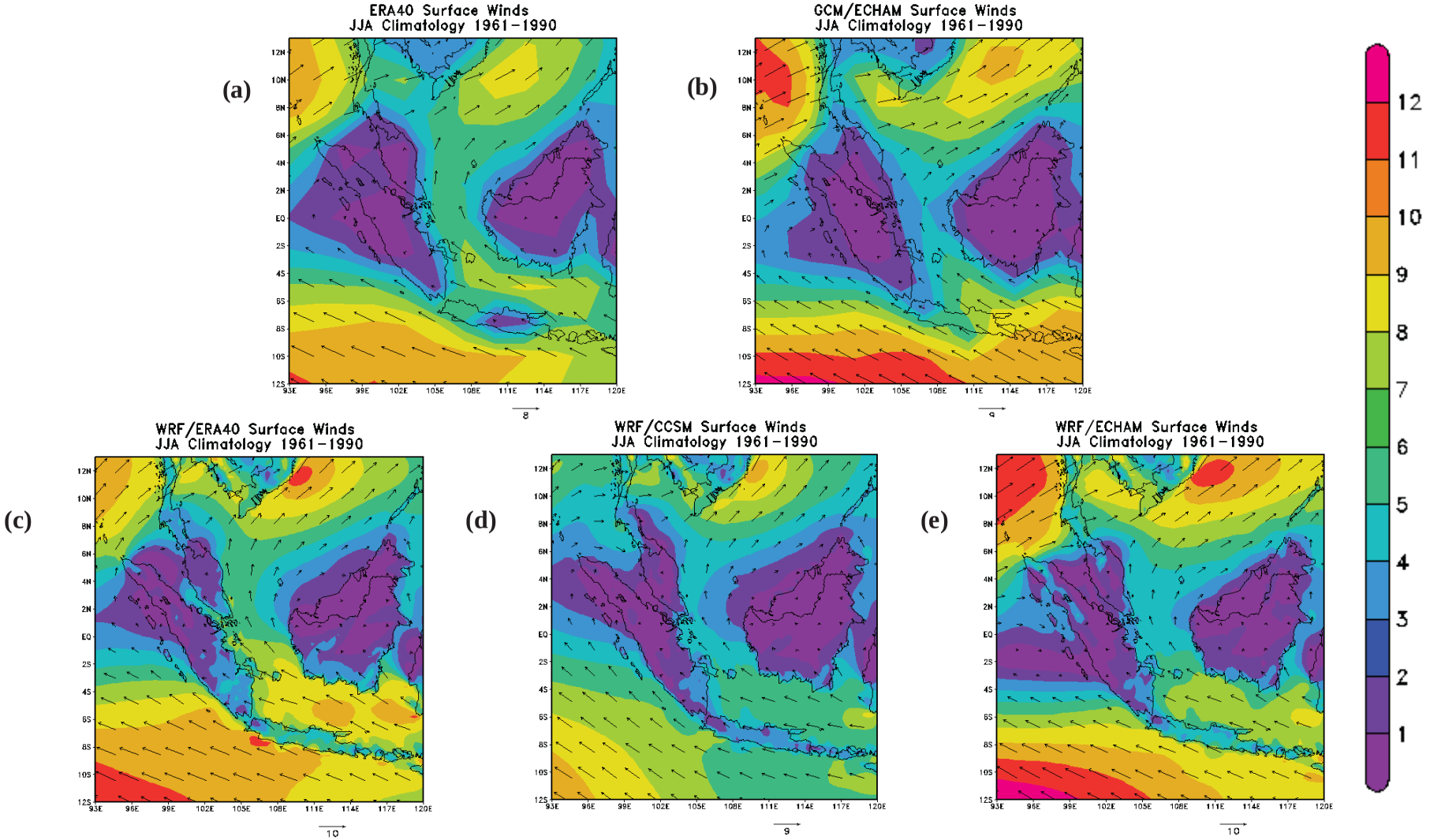

Figure 4.5: Mean Seasonal **Southwest Monsoon (JJA)** Surface Winds, m/s, 1961-1990
(a) ERA40 (b) GCM/ECHAM (c) WRF/ERA40 (d) WRF/CCSM (e) WRF/ECHAM

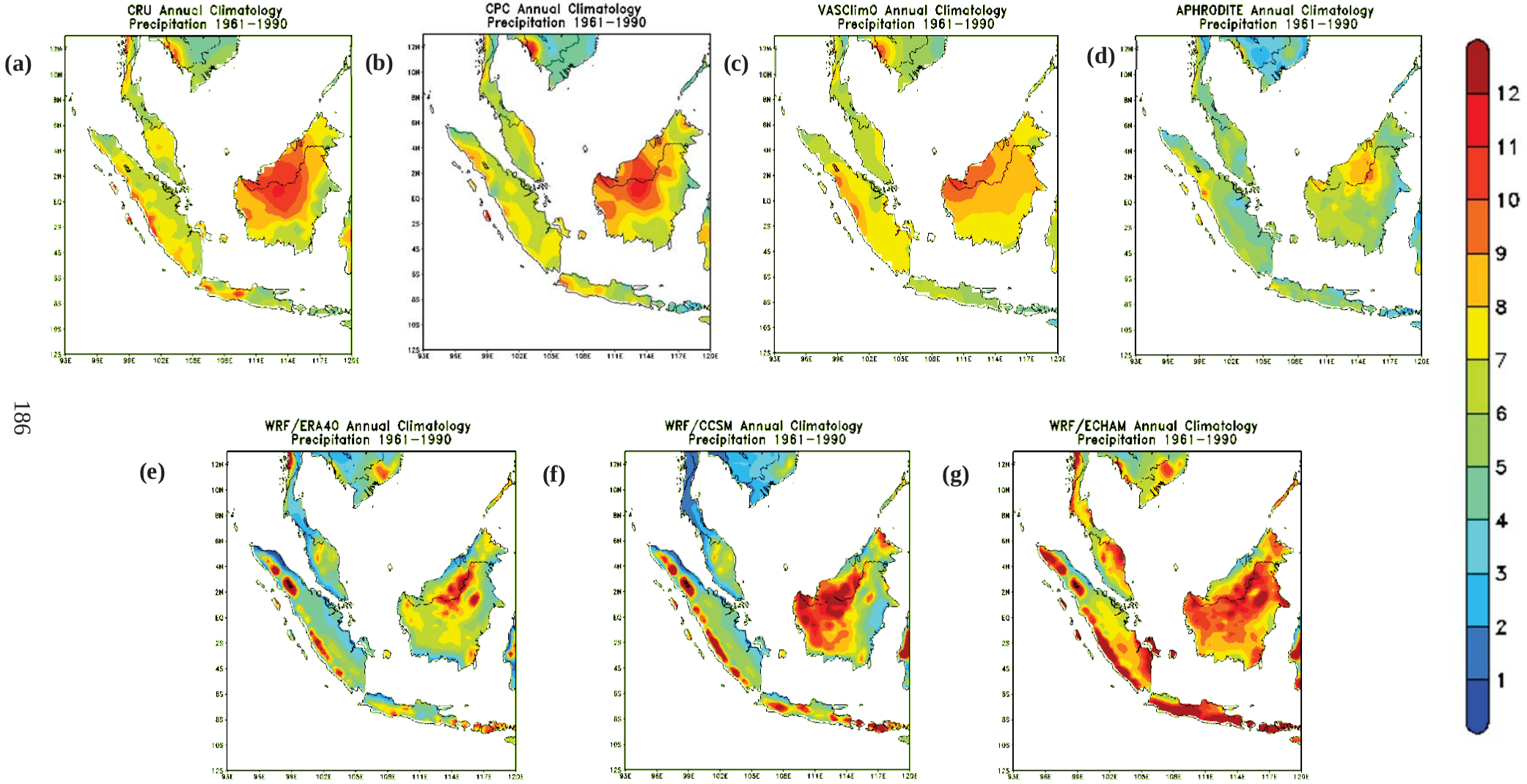

Figure 4.6: Mean **Annual** Precipitation, mm/day, 1961-1990
(a) CRU (b) CPC (c) VASClimO (d) APHRODITE (e) WRF/ERA40 (f) WRF/CCSM (g) WRF/ECHAM

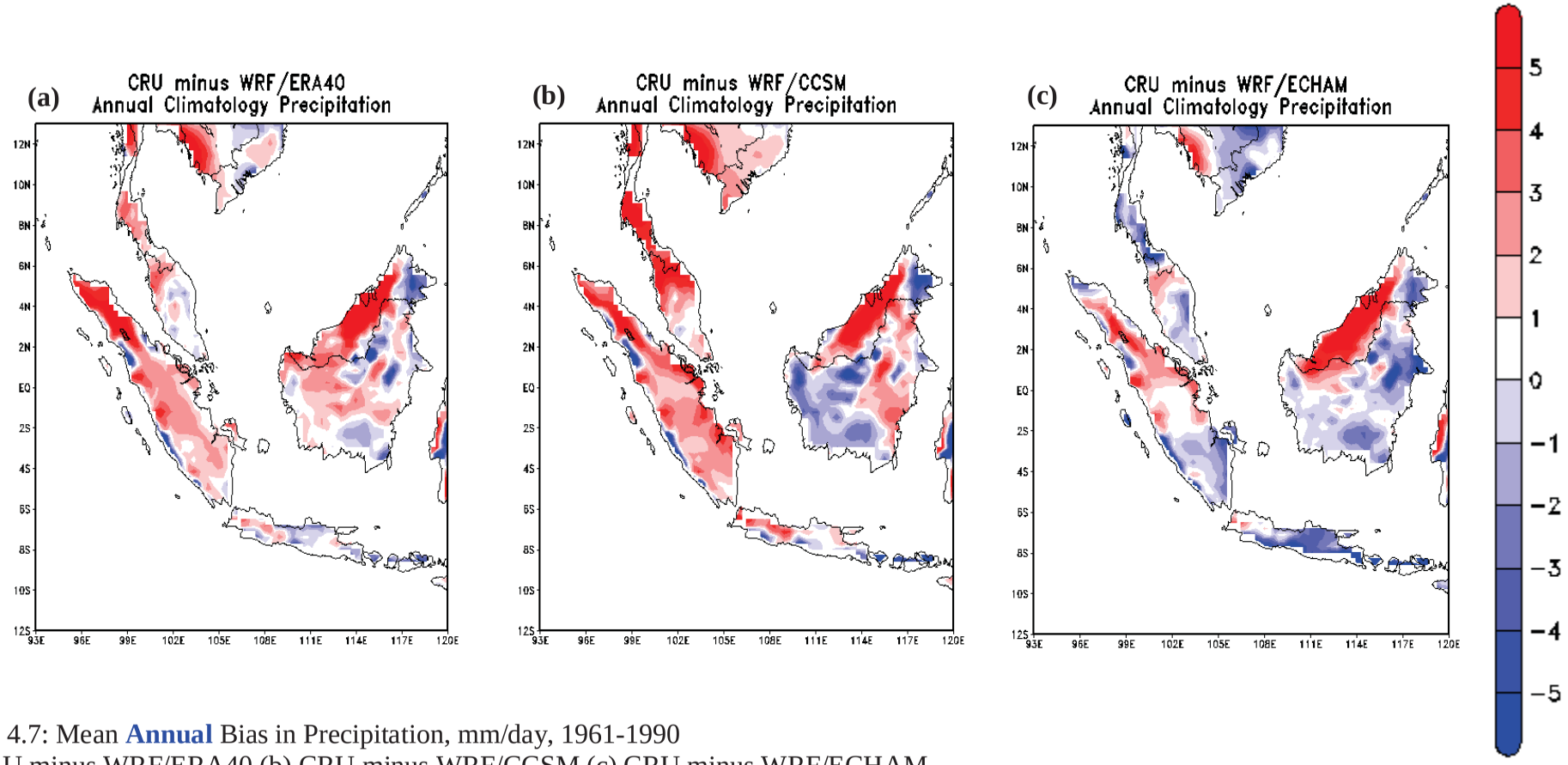

Figure 4.7: Mean **Annual** Bias in Precipitation, mm/day, 1961-1990
(a) CRU minus WRF/ERA40 (b) CRU minus WRF/CCSM (c) CRU minus WRF/ECHAM

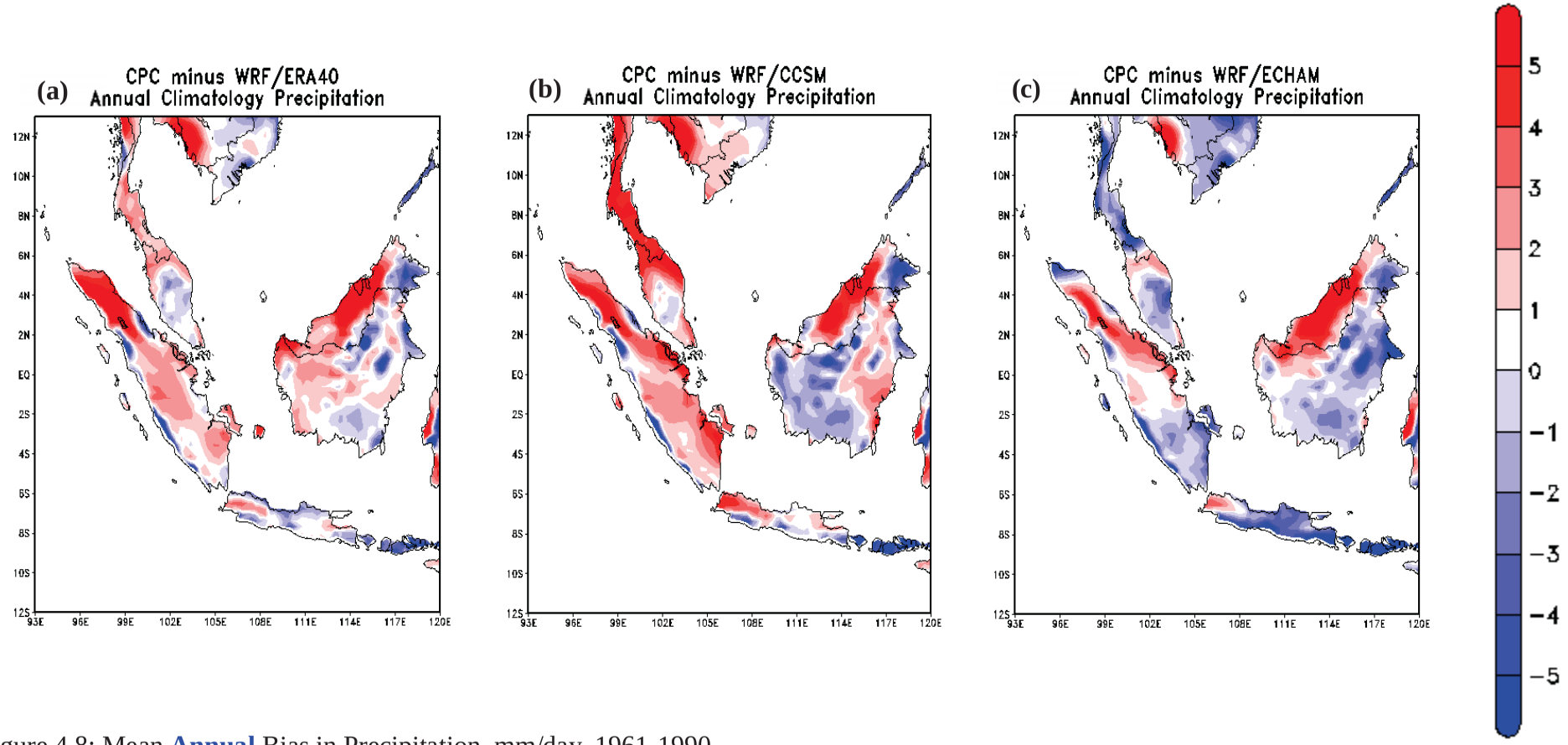

Figure 4.8: Mean **Annual** Bias in Precipitation, mm/day, 1961-1990
(a) CPC minus WRF/ERA40 (b) CPC minus WRF/CCSM (c) CPC minus WRF/ECHAM

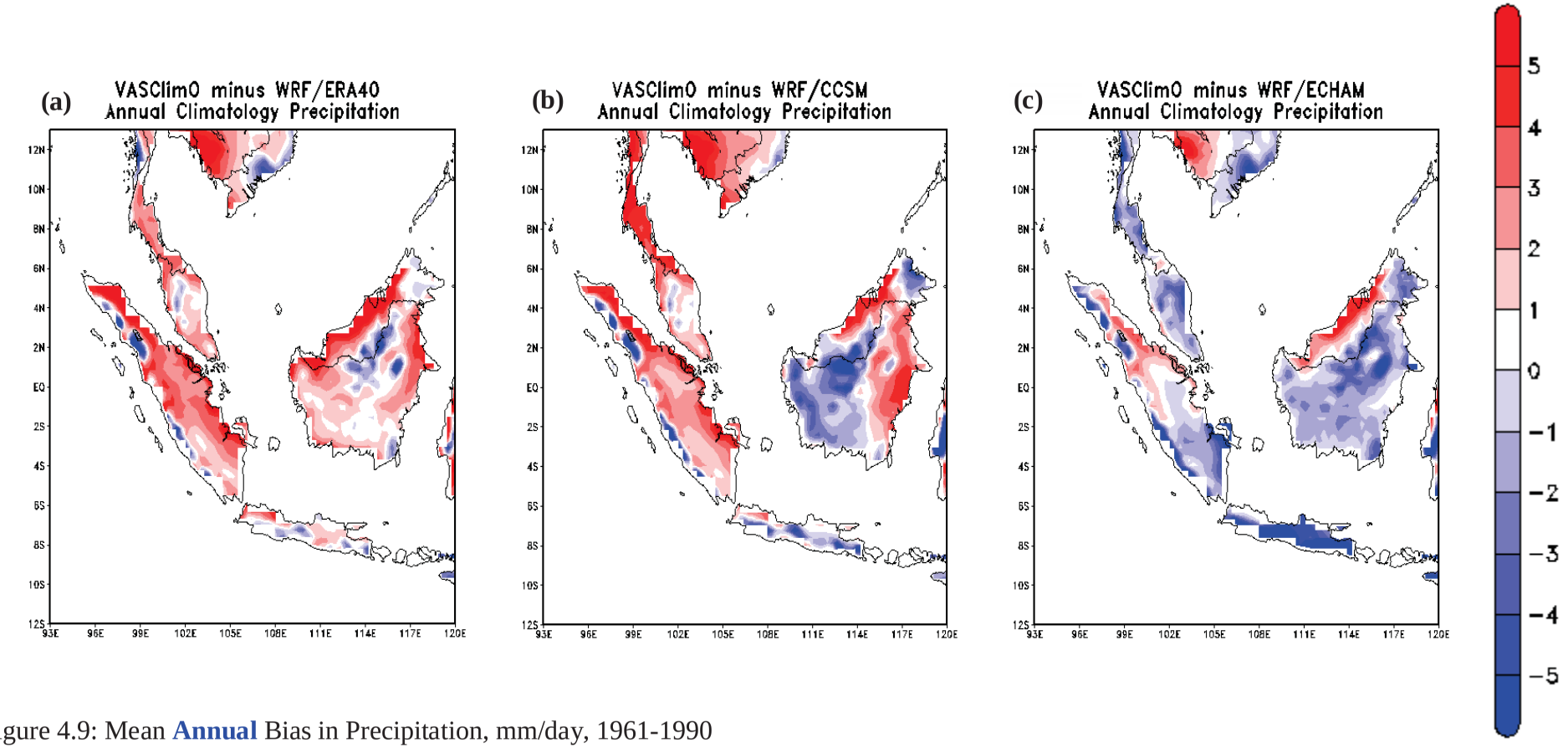

Figure 4.9: Mean **Annual** Bias in Precipitation, mm/day, 1961-1990
(a) VASClimO minus WRF/ERA40 (b) VASClimO minus WRF/CCSM (c) VASClimO minus WRF/ECHAM

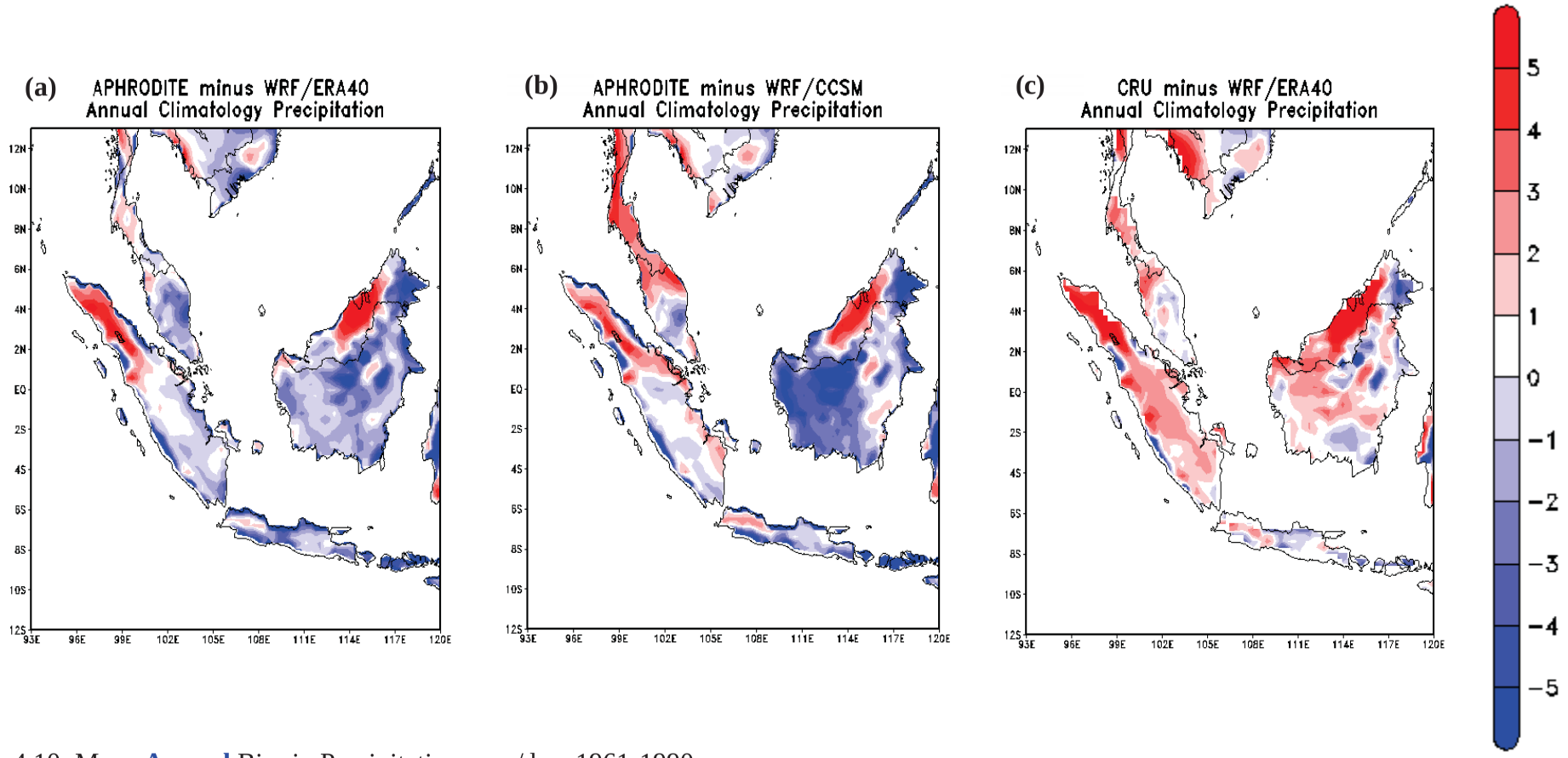

Figure 4.10: Mean **Annual** Bias in Precipitation, mm/day, 1961-1990
(a) APHRODITE minus WRF/ERA40 (b) APHRODITE minus WRF/CCSM (c) APHRODITE minus WRF/ECHAM

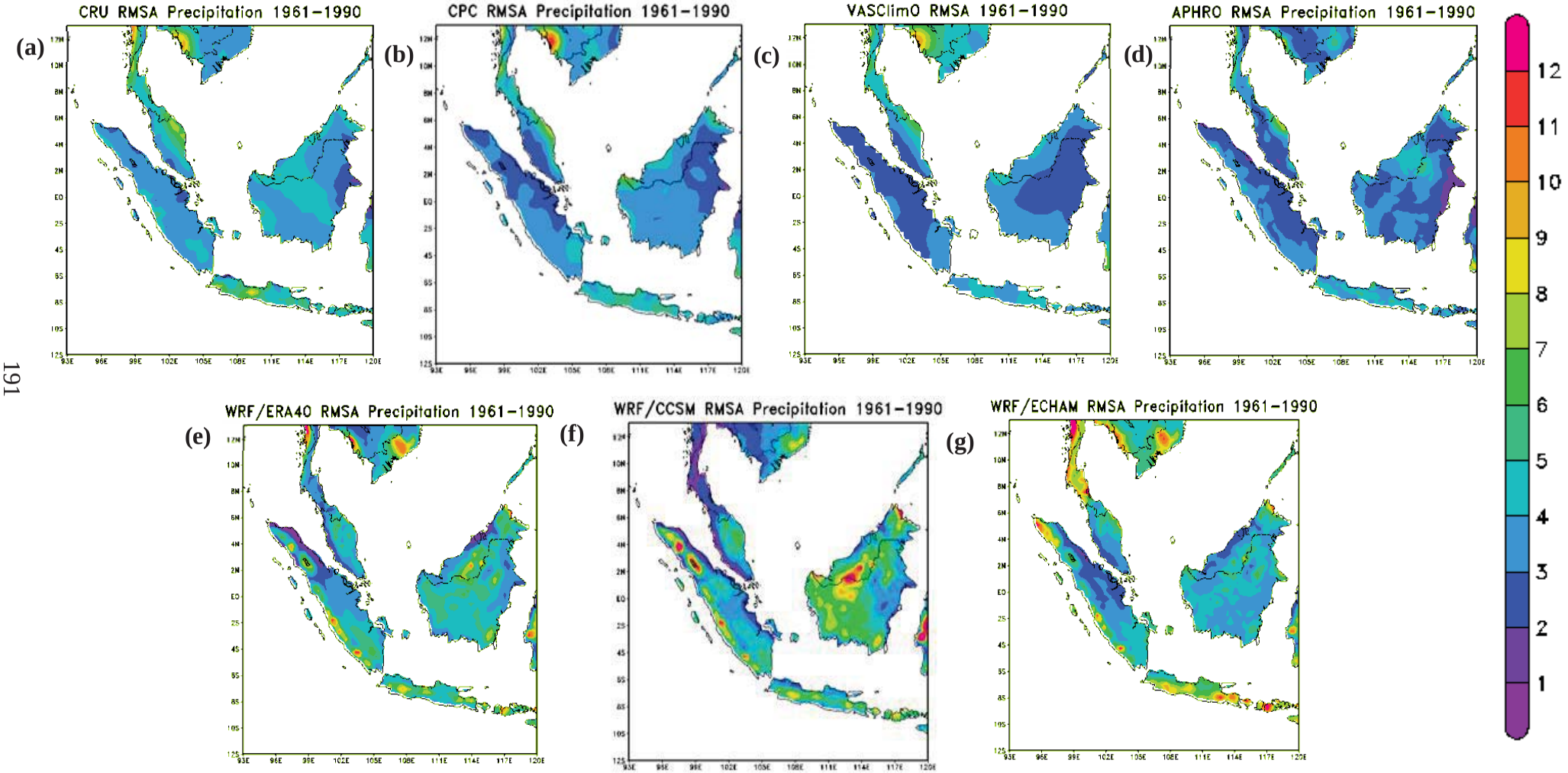

Figure 4.11: Root Mean Square Anomaly **(RMSA)** Precipitation, mm/day, 1961-1990
(a) CRU (b) CPC (c) VASClimO (d) APHRODITE (e) WRF/ERA40 (f) WRF/CCSM (g) WRF/ECHAM

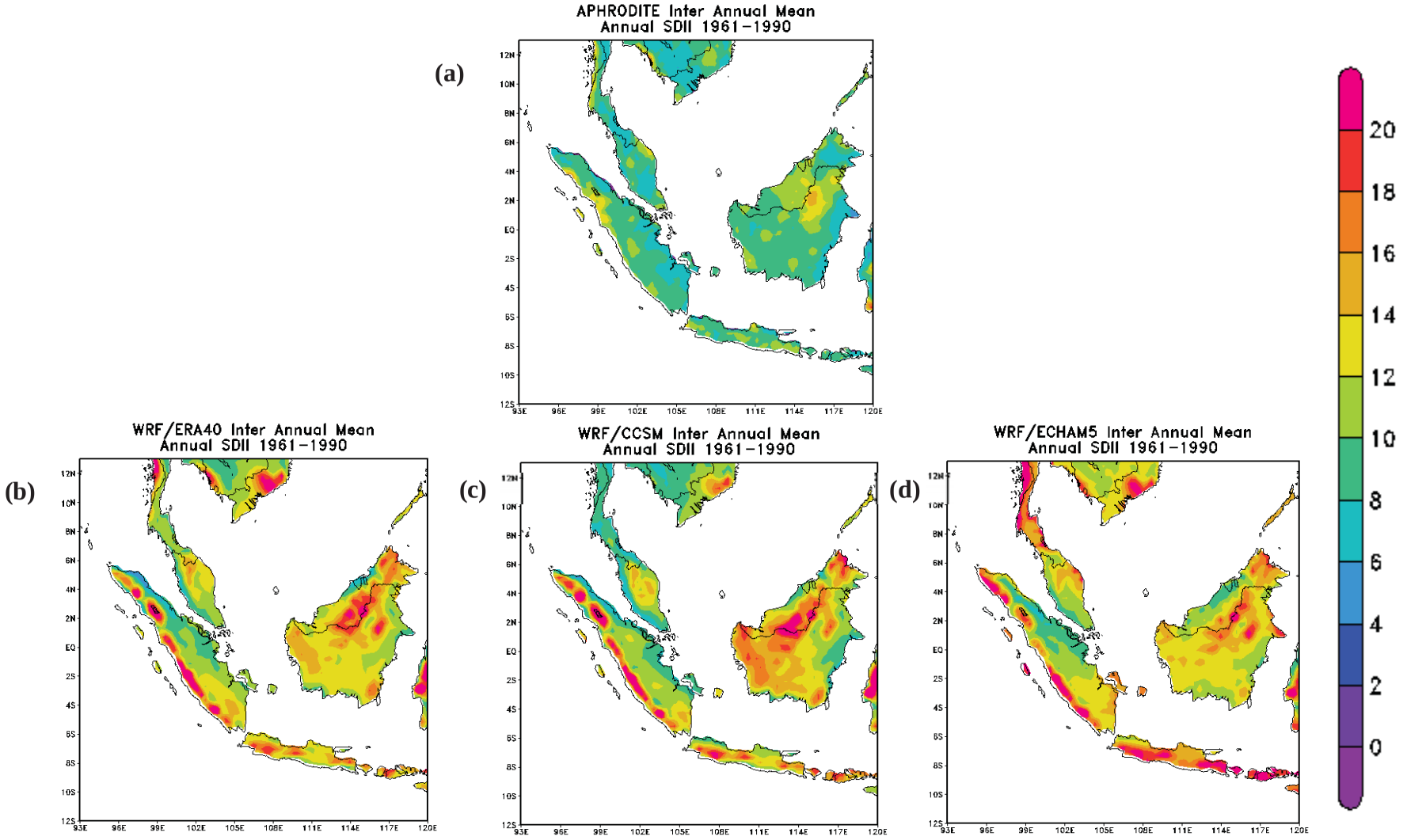

Figure 4.12: Mean **Annual** Climatology of STARDEX Indices, 1961-1990 for **SDII, mm/day**
(a) APHRODITE (b) WRF/ERA40 (c) WRF/CCSM (d) WRF/ECHAM

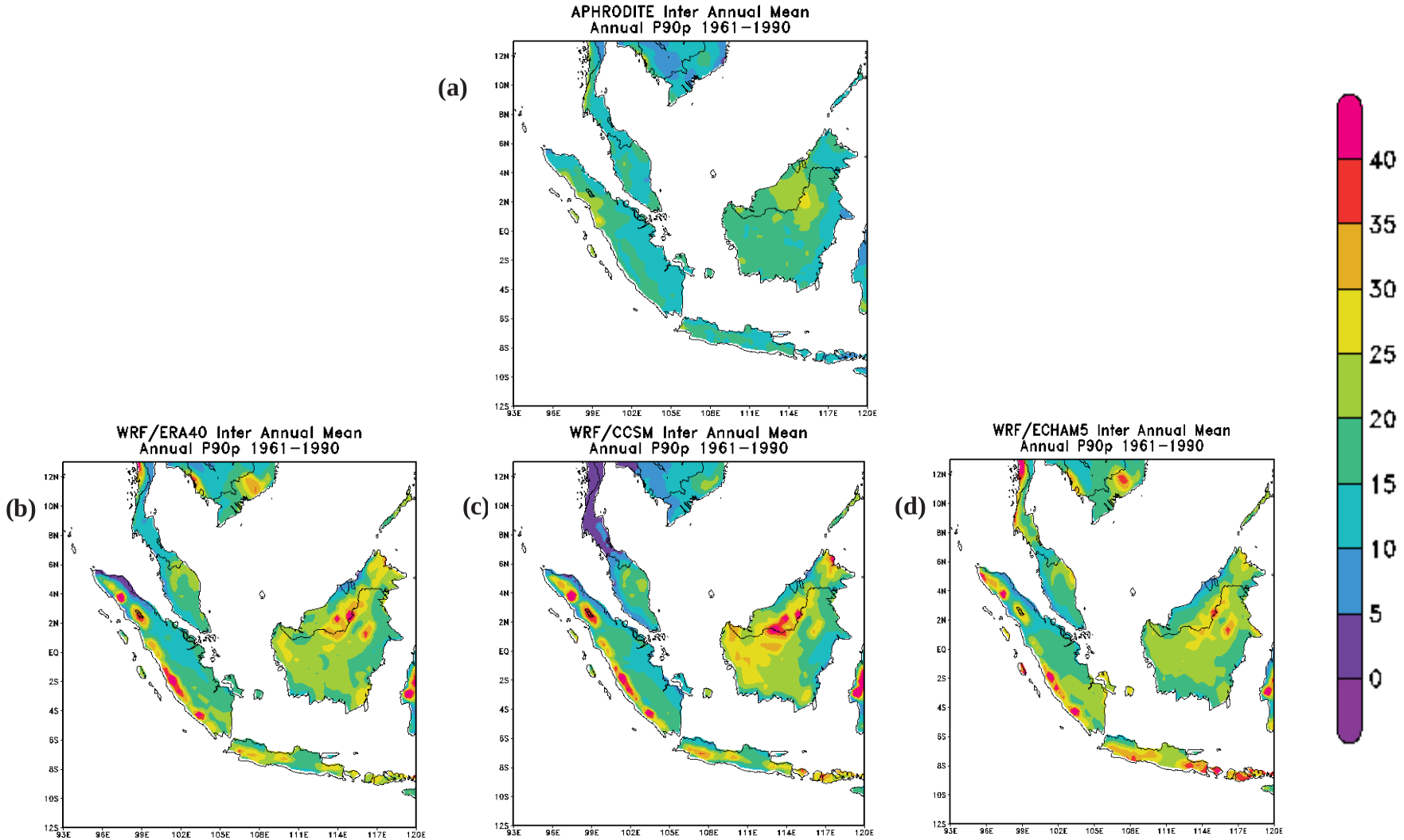

Figure 4.13: Mean **Annual** Climatology of STARDEX Indices, 1961-1990 for **P90p, mm/day**
(a) APHRODITE (b) WRF/ERA40 (c) WRF/CCSM (d) WRF/ECHAM

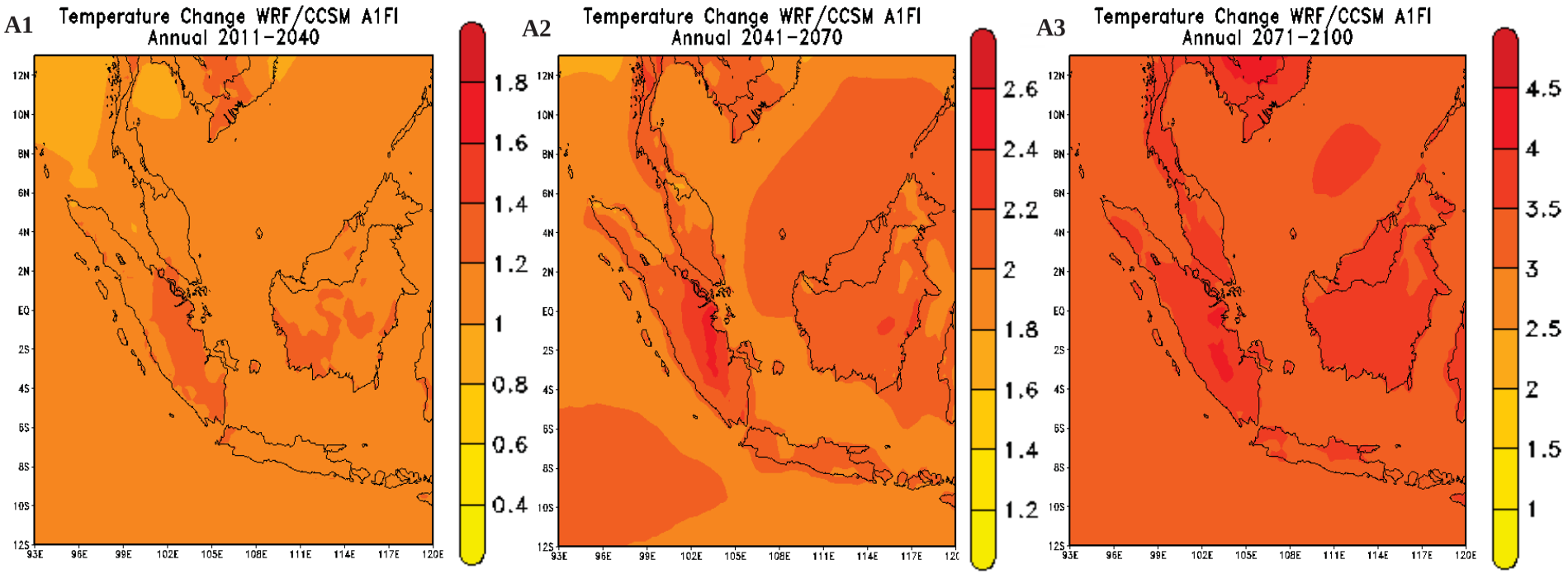

Figure 4.14: WRF/CCSM **A1FI** Climate Response for Temperature (Abs. Anomaly in ºC) relative to 1961-1990
A1: 2011-2040, A2: 2041-2070, A3: 2071-2100 **Annual Change**

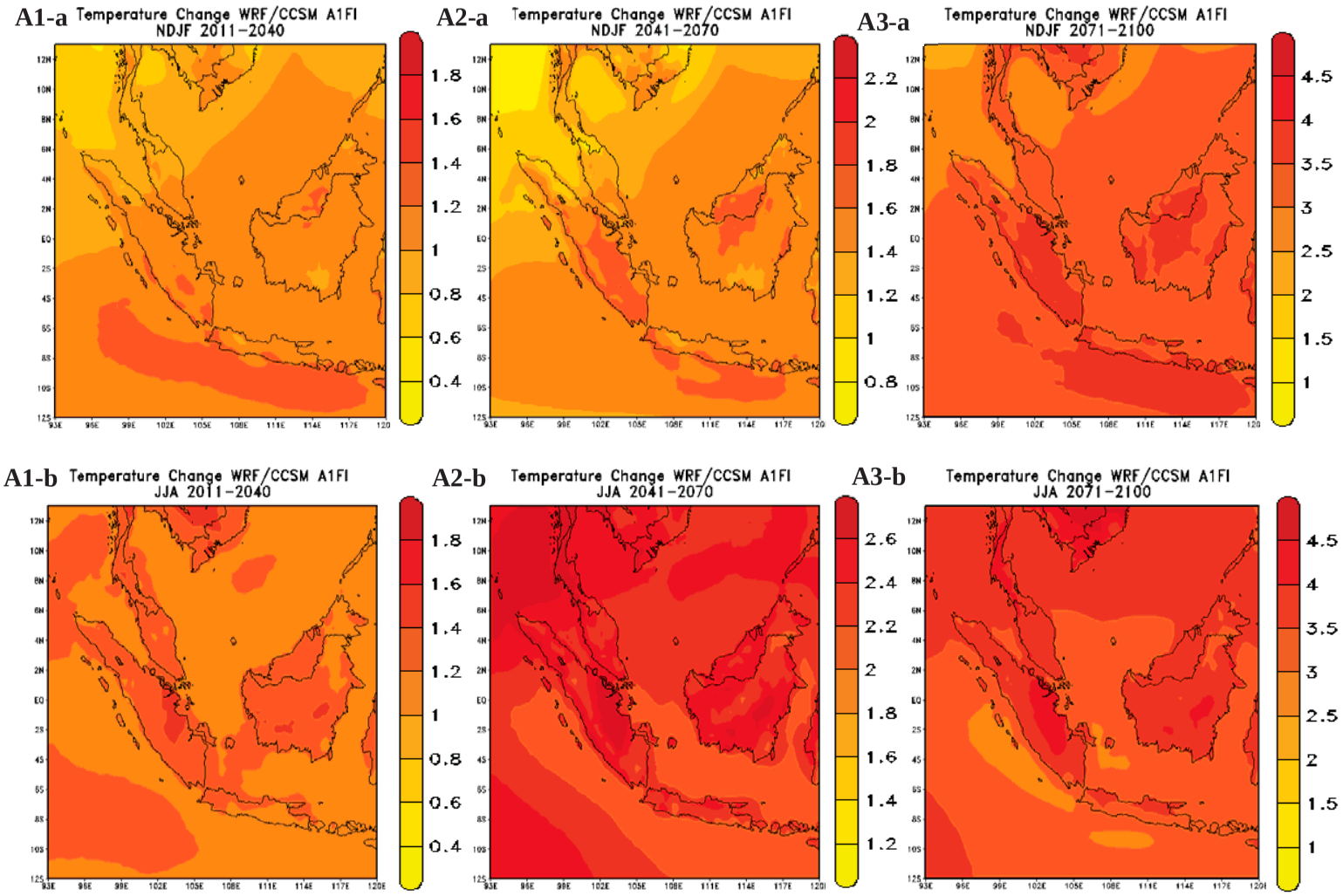

Figure 4.15: WRF/CCSM **A1FI** Climate Response for Temperature (Abs. Anomaly in ºC) relative to 1961-1990
A1: 2011-2040, A2: 2041-2070, A3: 2071-2100 (a) **NDJF Change** (b) **JJA Change**

A1

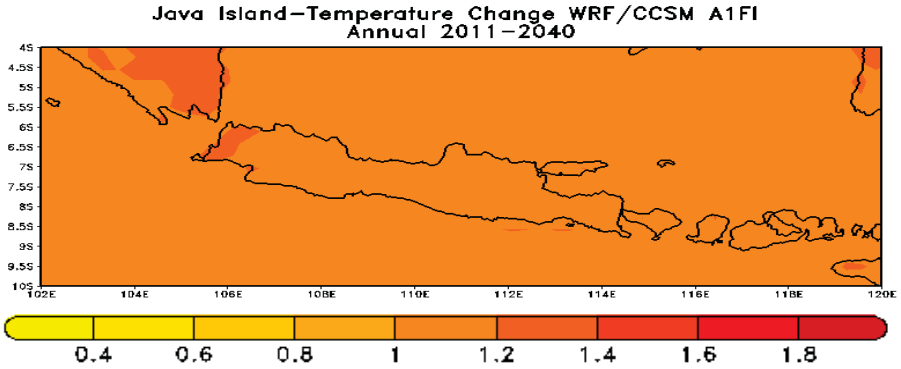

A2

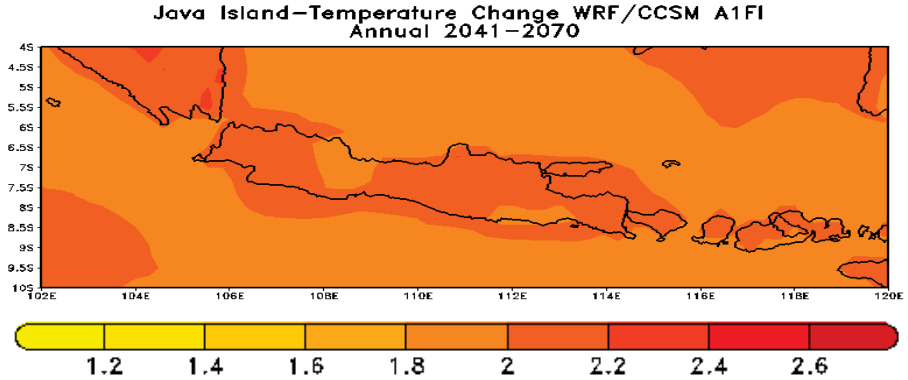

A3

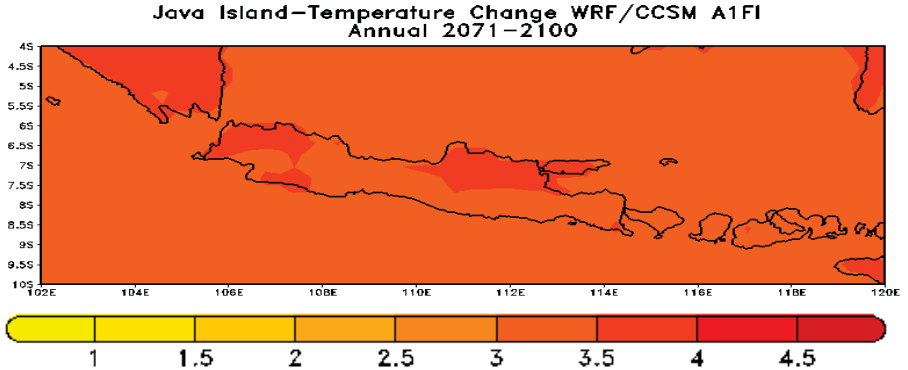

Figure 4.16: WRF/CCSM **A1FI** Climate Response for Temperature (Absolute Anomaly in ºC) relative to 1961-1990, **Jakarta**
A1: 2011-2040, A2: 2041-2070, A3: 2071-2100 **Annual Change**

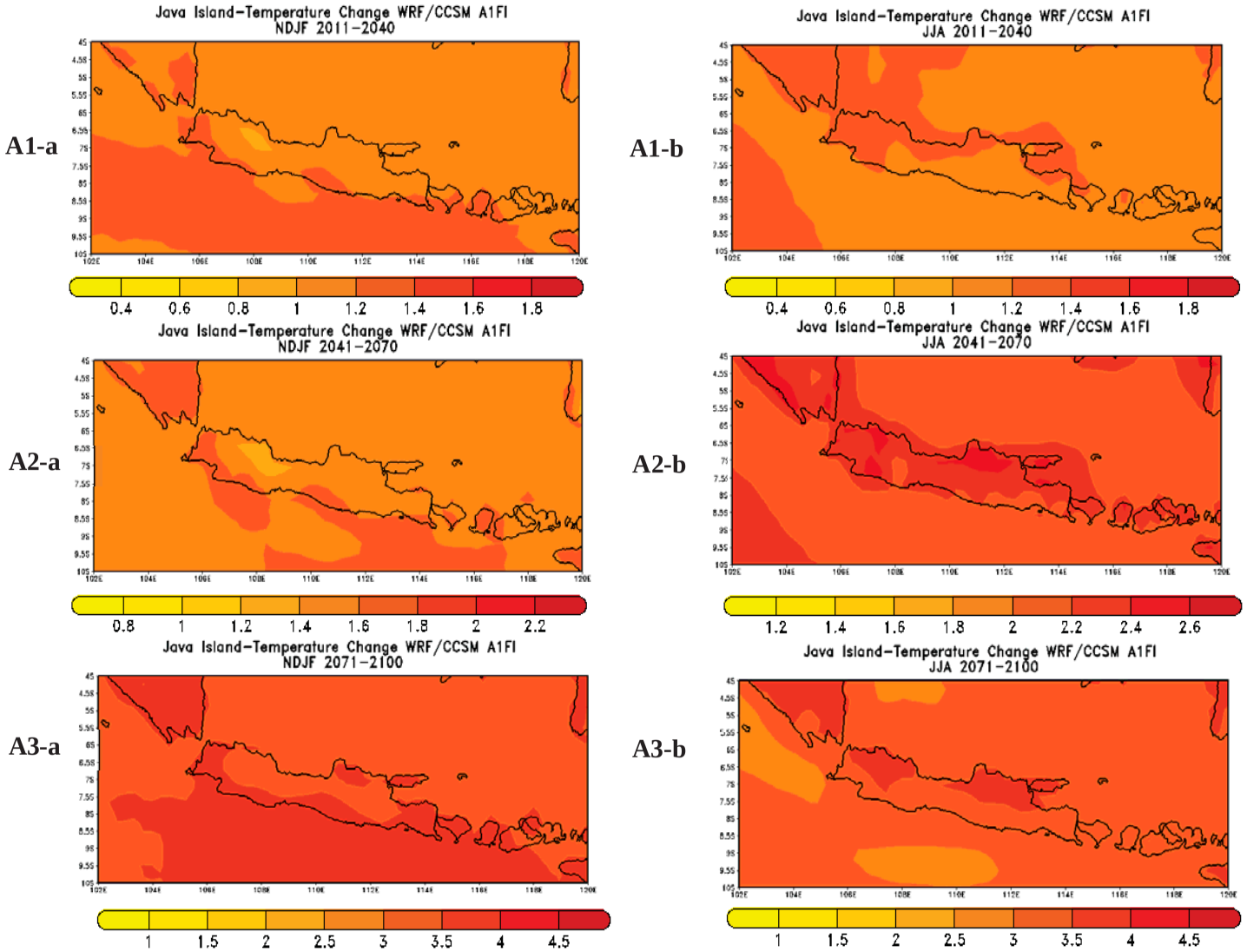

Figure 4.17: WRF/CCSM **A1FI** Climate Response for Temperature (Absolute Anomaly in ºC) relative to 1961-1990, **Jakarta**
A1: 2011-2040, A2: 2041-2070, A3: 2071-2100 (a) **NDJF Change** (b) **JJA Change**

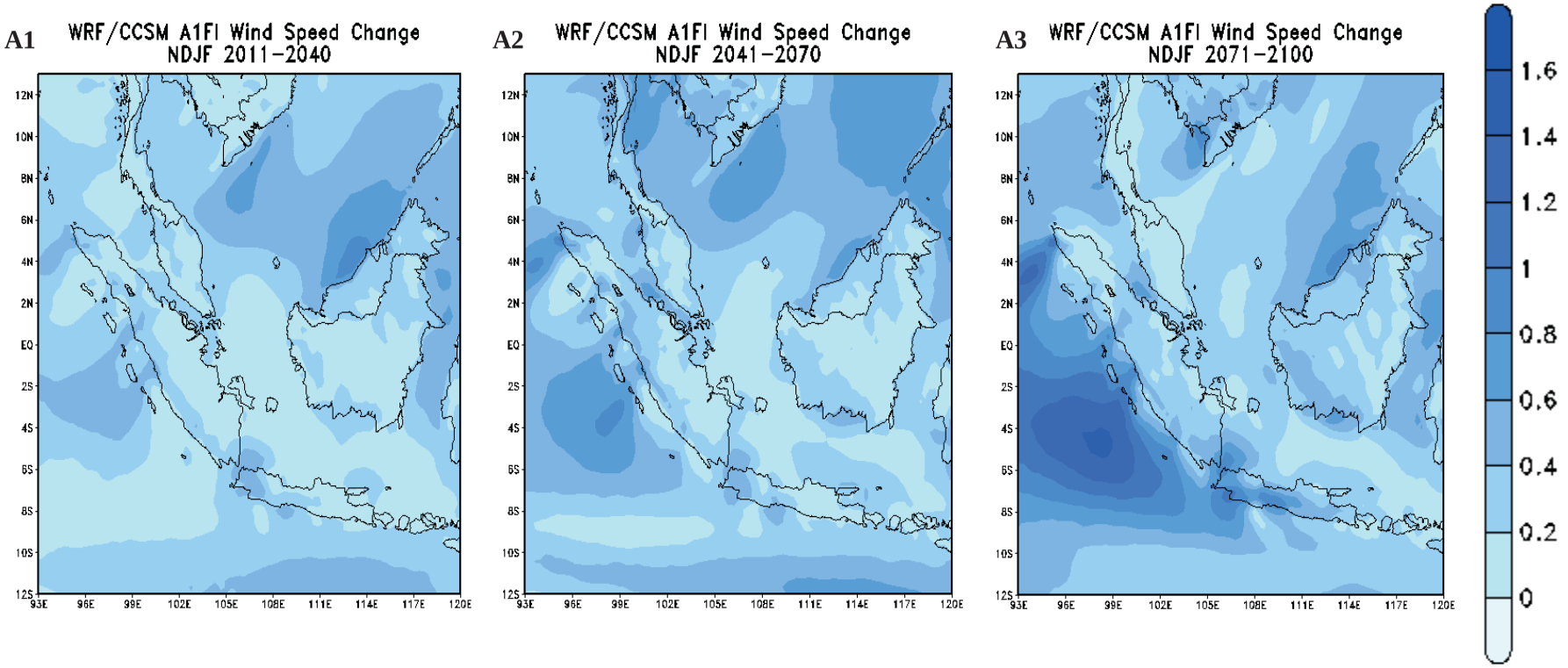

Figure 4.18: WRF/CCSM **A1FI** Climate Response for **NDJF** Wind Speed Change (Absolute Anomaly in m/s) relative to 1961-1990
A1: 2011-2040, A2: 2041-2070, A3: 2071-2100

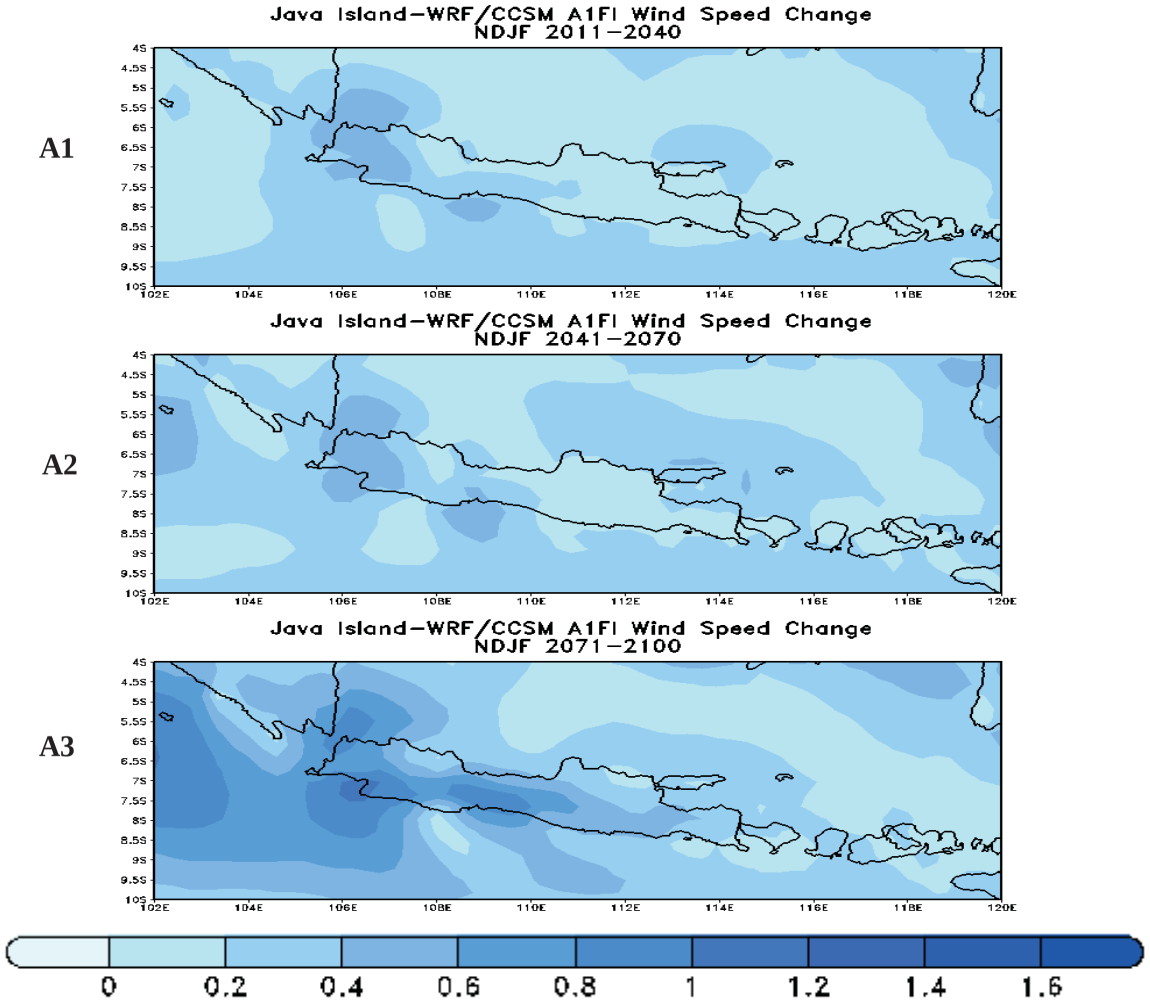

Figure 4.19: WRF/CCSM **A1FI** Climate Response for **NDJF** Wind Speed Change (Absolute Anomaly in m/s) relative to 1961-1990
A1: 2011-2040, A2: 2041-2070, A3: 2071-2100: **Jakarta**

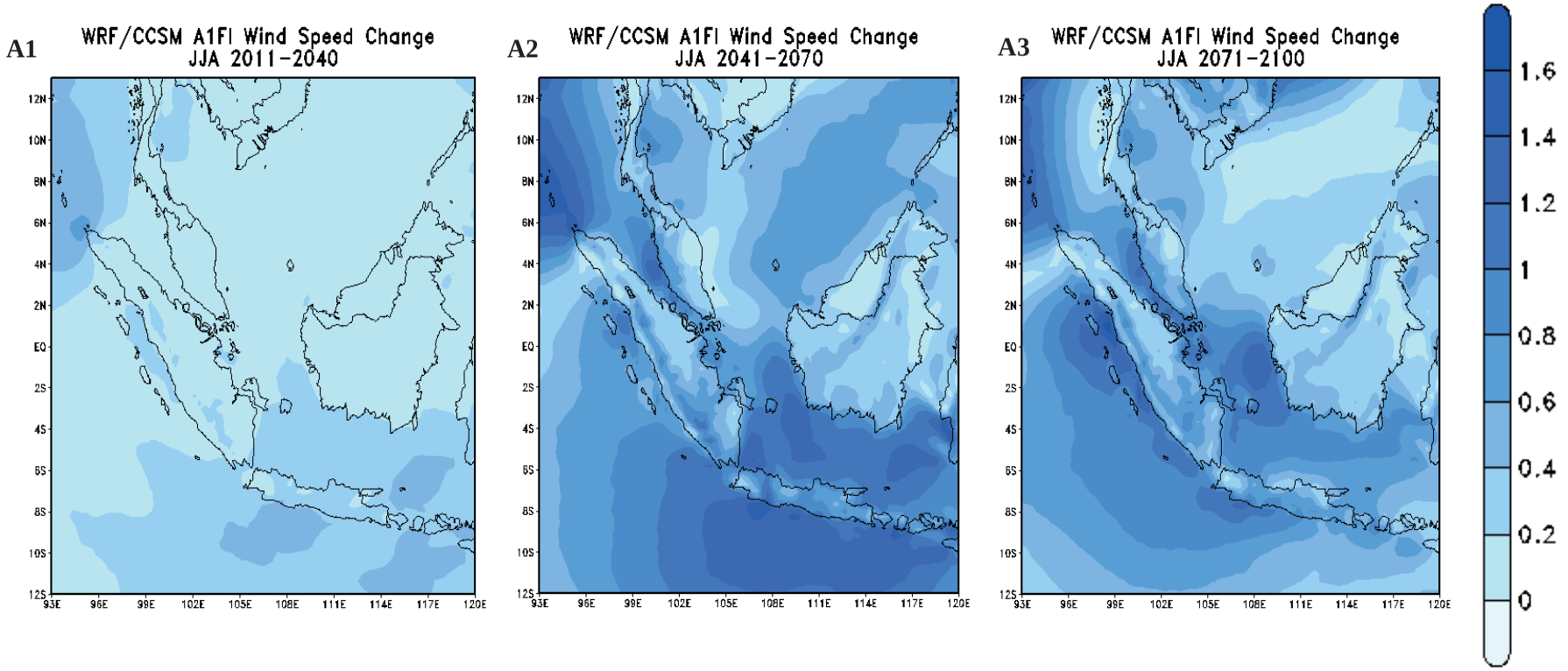

Figure 4.20: WRF/CCSM **A1FI** Climate Response for **JJA** Wind Speed Change (Absolute Anomaly in m/s) relative to 1961-1990
A1: 2011-2040, A2: 2041-2070, A3: 2071-2100

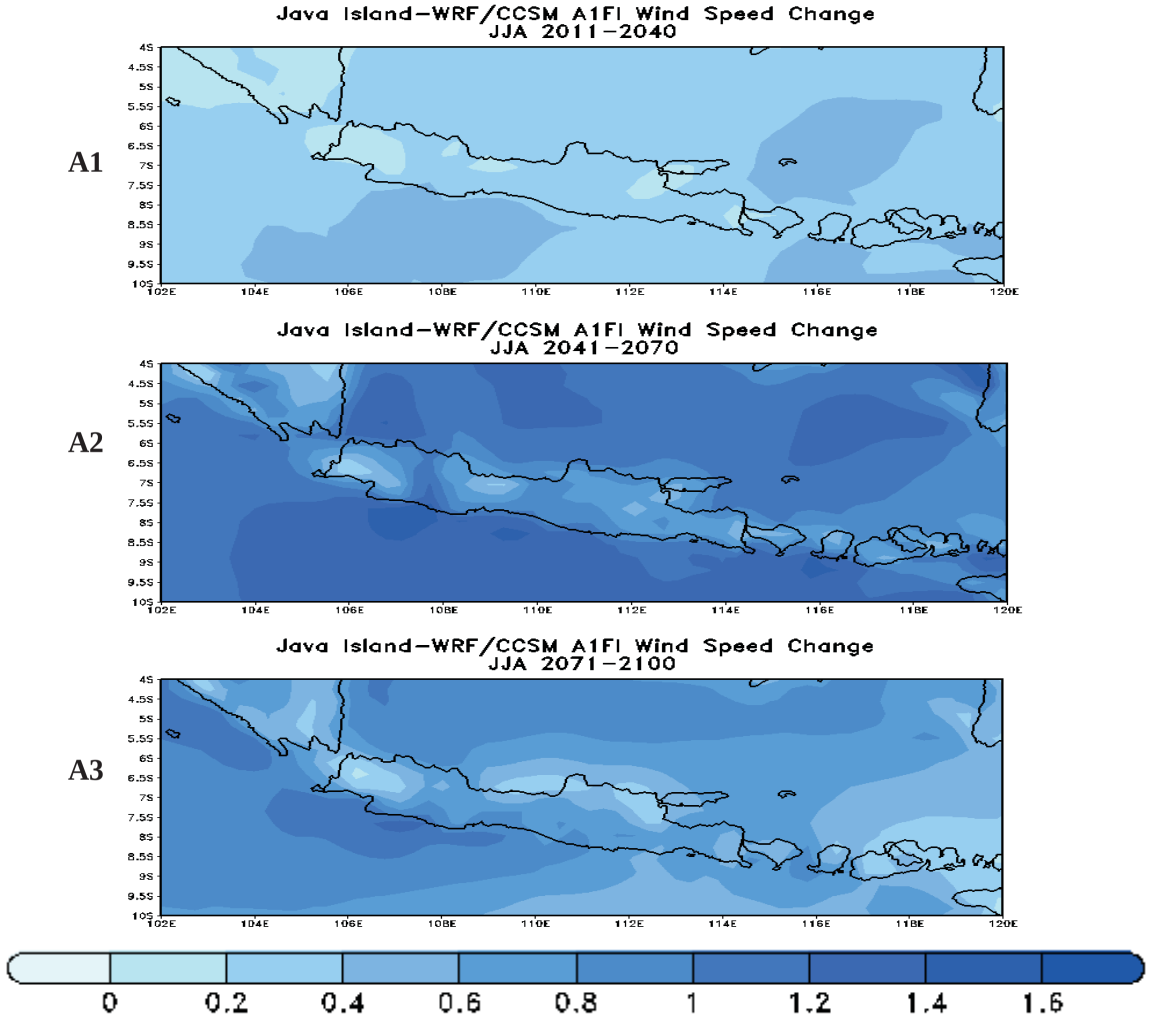

Figure 4.21: WRF/CCSM **A1FI** Climate Response for **JJA** Wind Speed Change (Absolute Anomaly in m/s) relative to 1961-1990
A1: 2011-2040, A2: 2041-2070, A3: 2071-2100: **Jakarta**

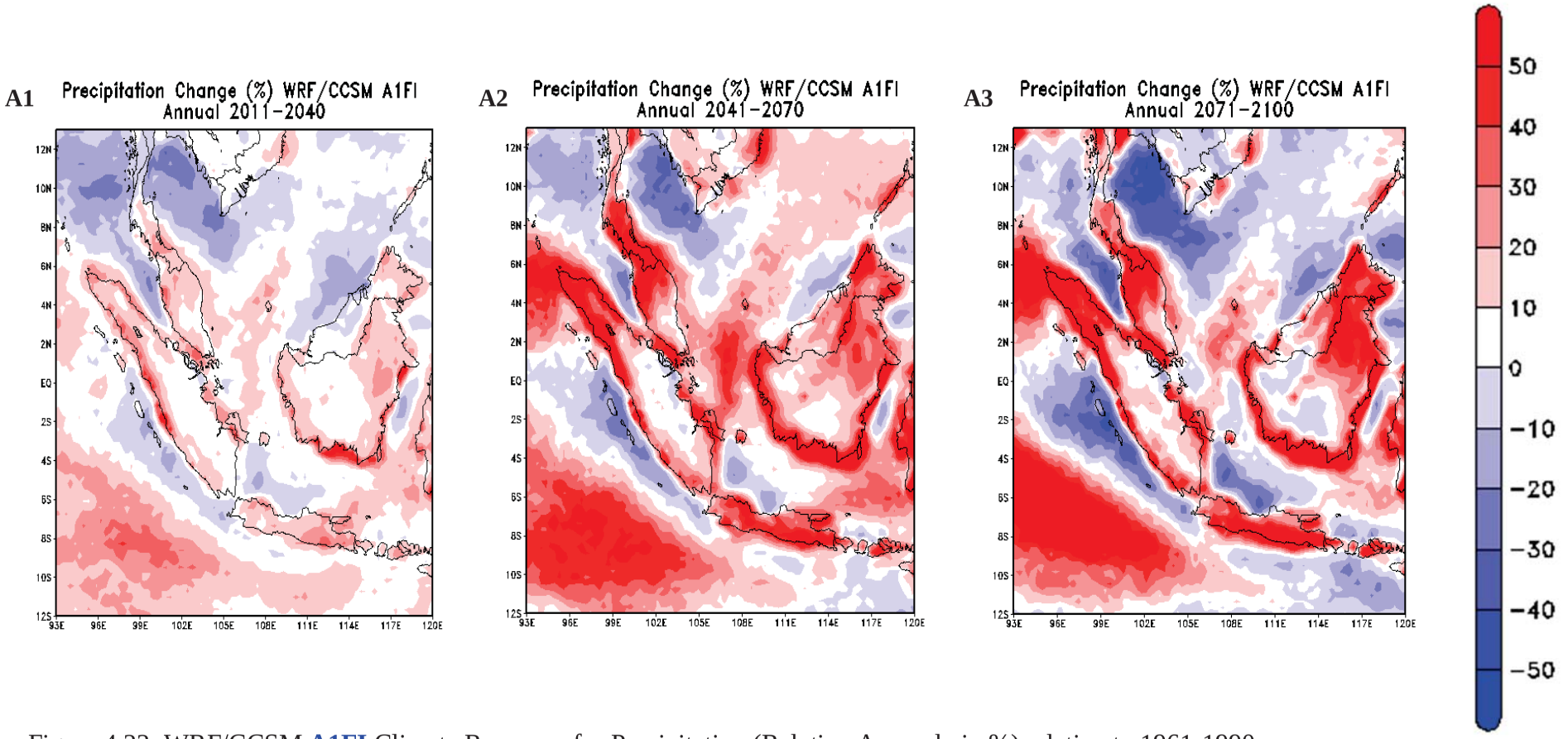

Figure 4.22: WRF/CCSM **A1FI** Climate Response for Precipitation (Relative Anomaly in %) relative to 1961-1990
A1: 2011-2040, A2: 2041-2070, A3: 2071-2100 **Annual Change**

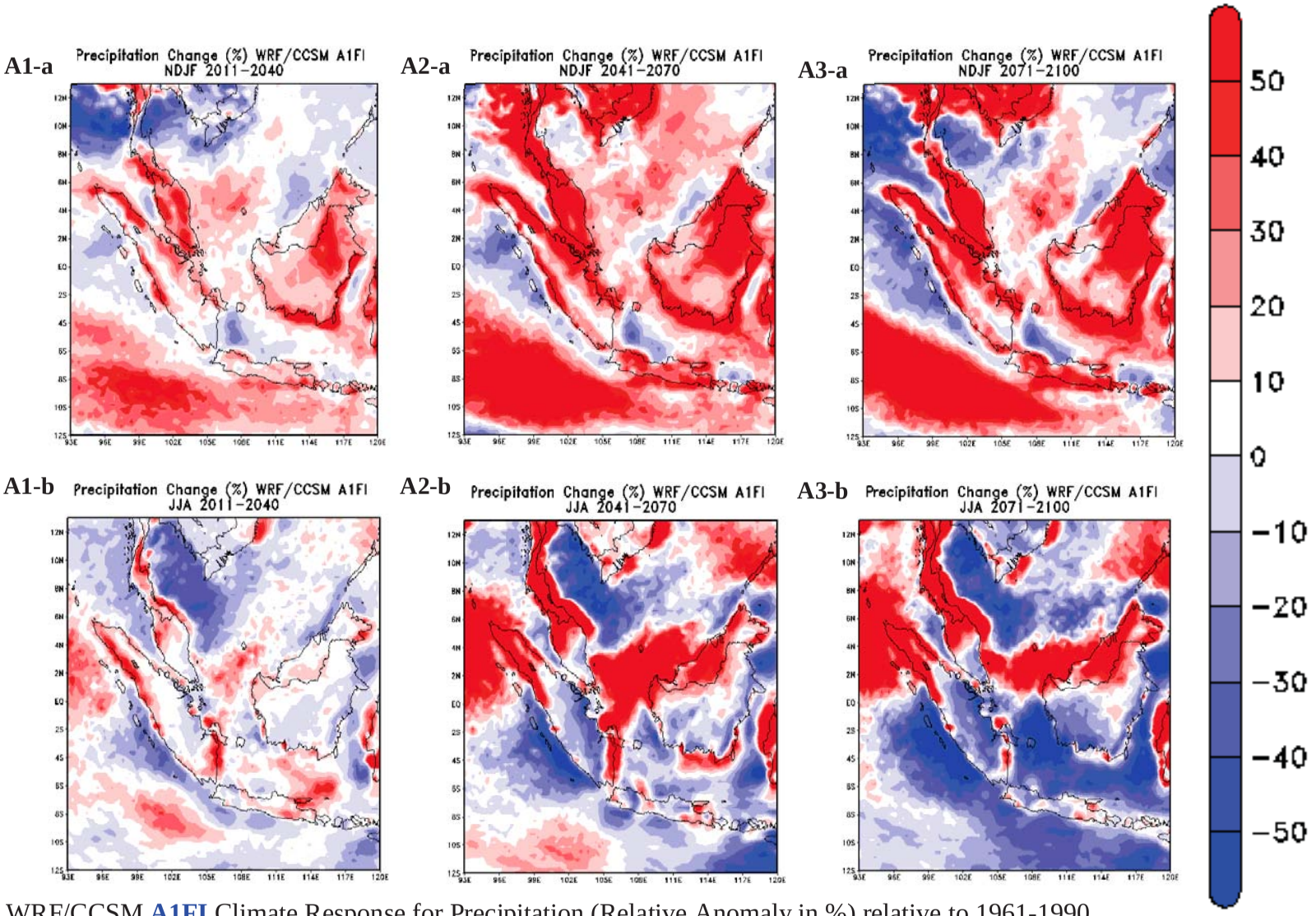

Figure 4.23: WRF/CCSM **A1FI** Climate Response for Precipitation (Relative Anomaly in %) relative to 1961-1990
A1: 2011-2040, A2: 2041-2070, A3: 2071-2100 (a) **NDJF Change** (b) **JJA Change**

A1

A2

A3

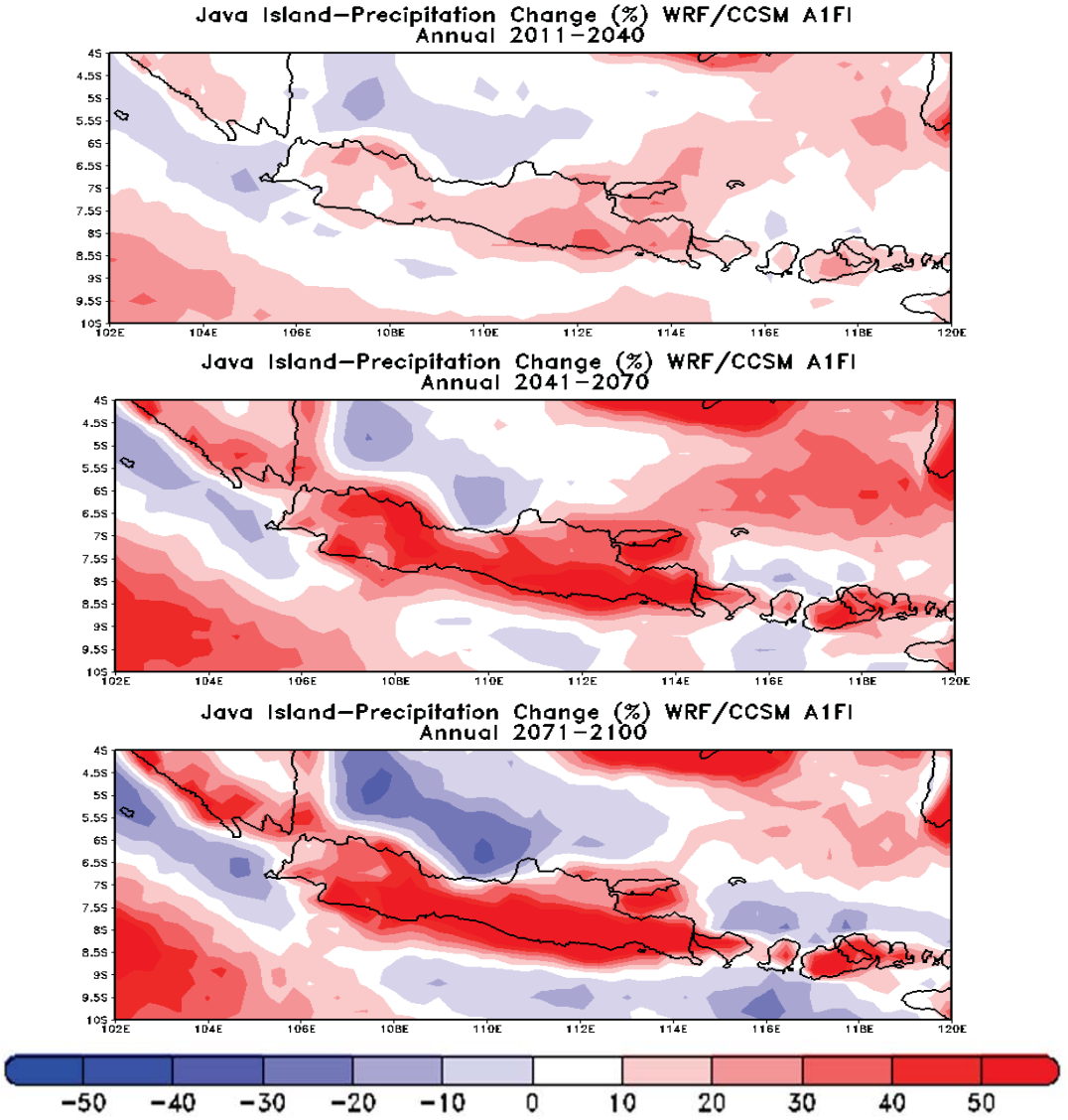

Figure 4.24: WRF/CCSM **A1FI** Climate Response for Precipitation (Relative Anomaly in %) relative to 1961-1990, **Jakarta**
A1: 2011-2040, A2: 2041-2070, A3: 2071-2100 **Annual Change**

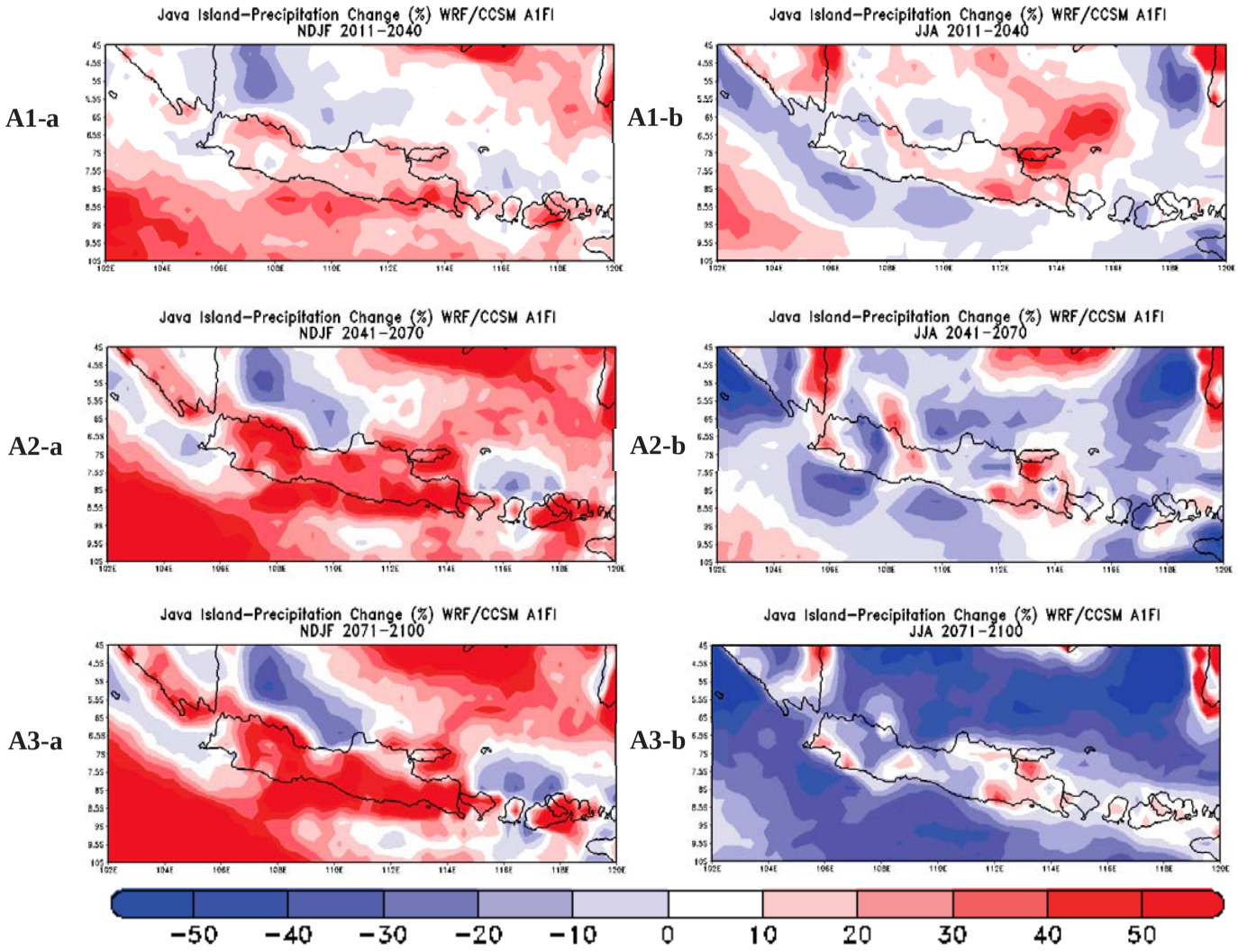

Figure 4.25: WRF/CCSM **A1FI** Climate Response for Precipitation (Relative Anomaly in %) relative to 1961-1990, **Jakarta** A1: 2011-2040, A2: 2041-2070, A3: 2071-2100 (a) **NDJF Change** (b) **JJA Change**

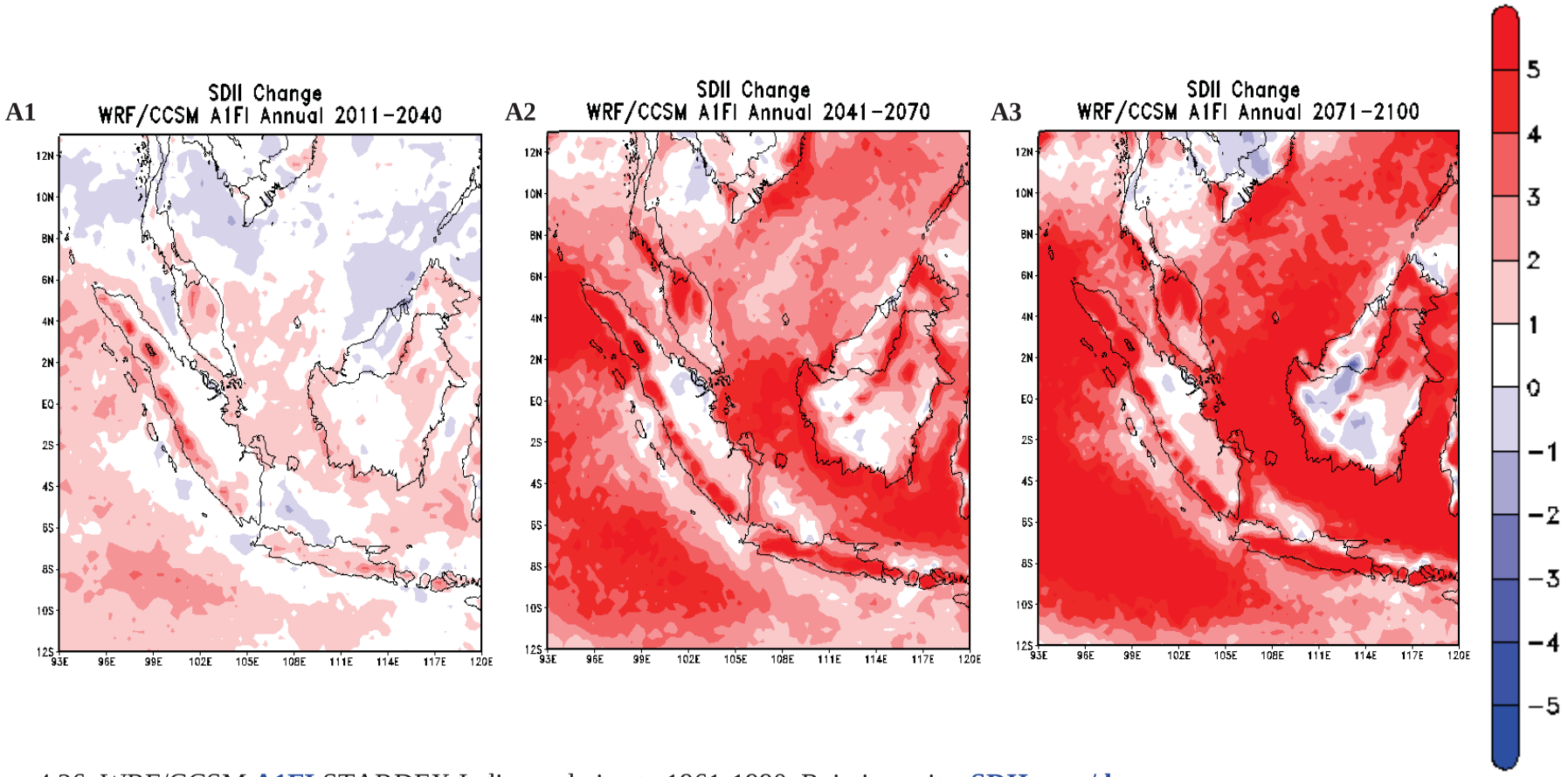

Figure 4.26: WRF/CCSM **A1FI** STARDEX Indices relative to 1961-1990, Rain intensity, **SDII, mm/day**
A1: 2011-2040, A2: 2041-2070, A3: 2071-2100 **Annual Change**

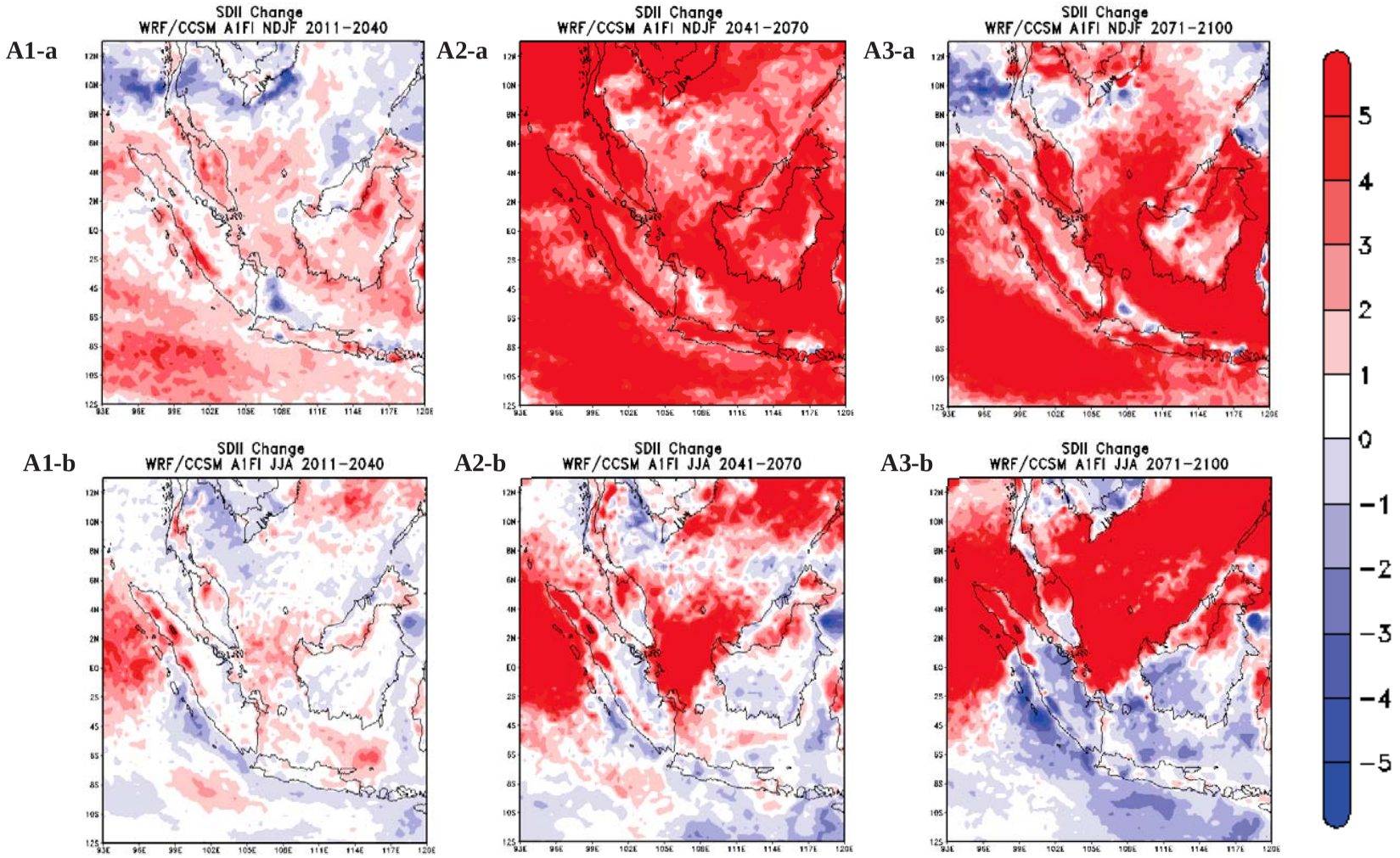

Figure 4.27: WRF/CCSM **A1FI** STARDEX Indices relative to 1961-1990, Rain intensity, **SDII, mm/day**
A1: 2011-2040, A2: 2041-2070, A3: 2071-2100 (a) **NDJF Change** (b) **JJA Change**

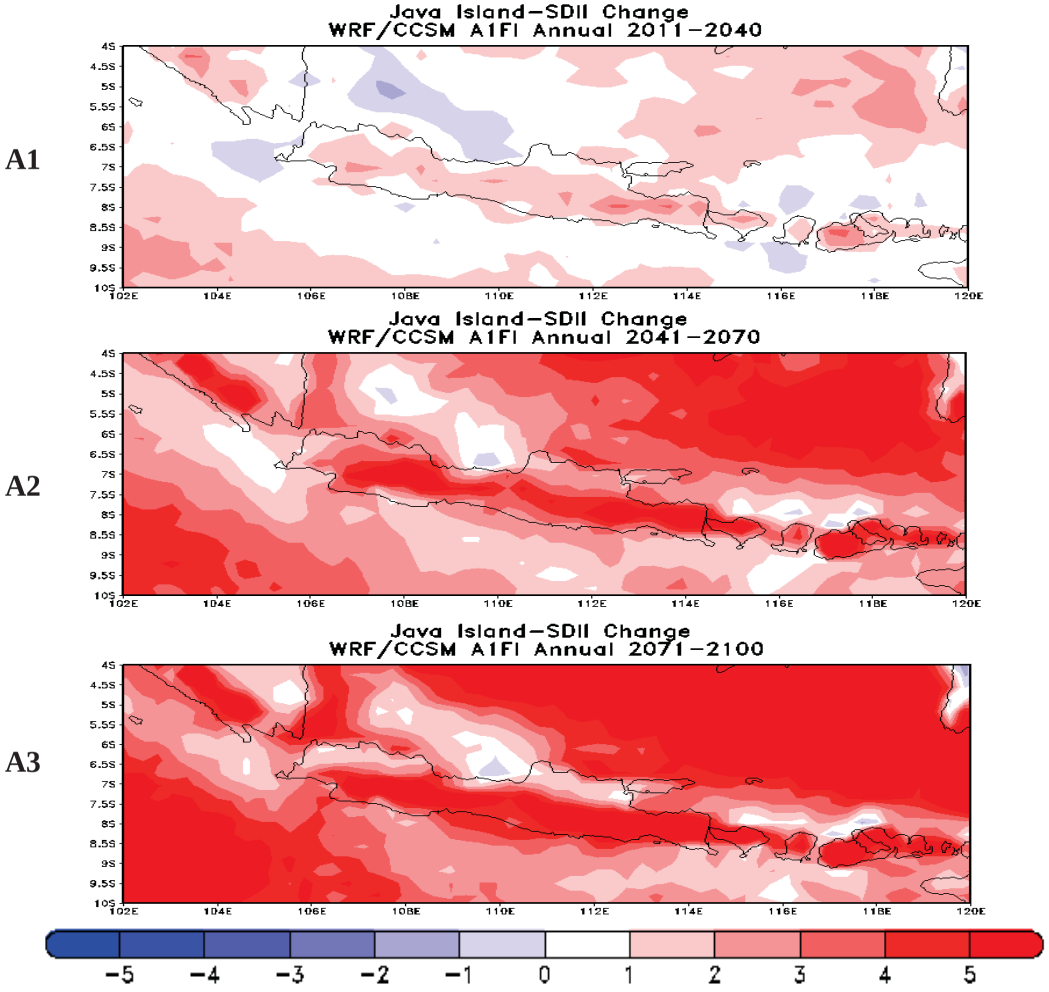

Figure 4.28: WRF/CCSM **A1FI** STARDEX Indices relative to 1961-1990, Rain intensity, **SDII, mm/day, Jakarta**
A1: 2011-2040, A2: 2041-2070, A3: 2071-2100 **Annual Change**

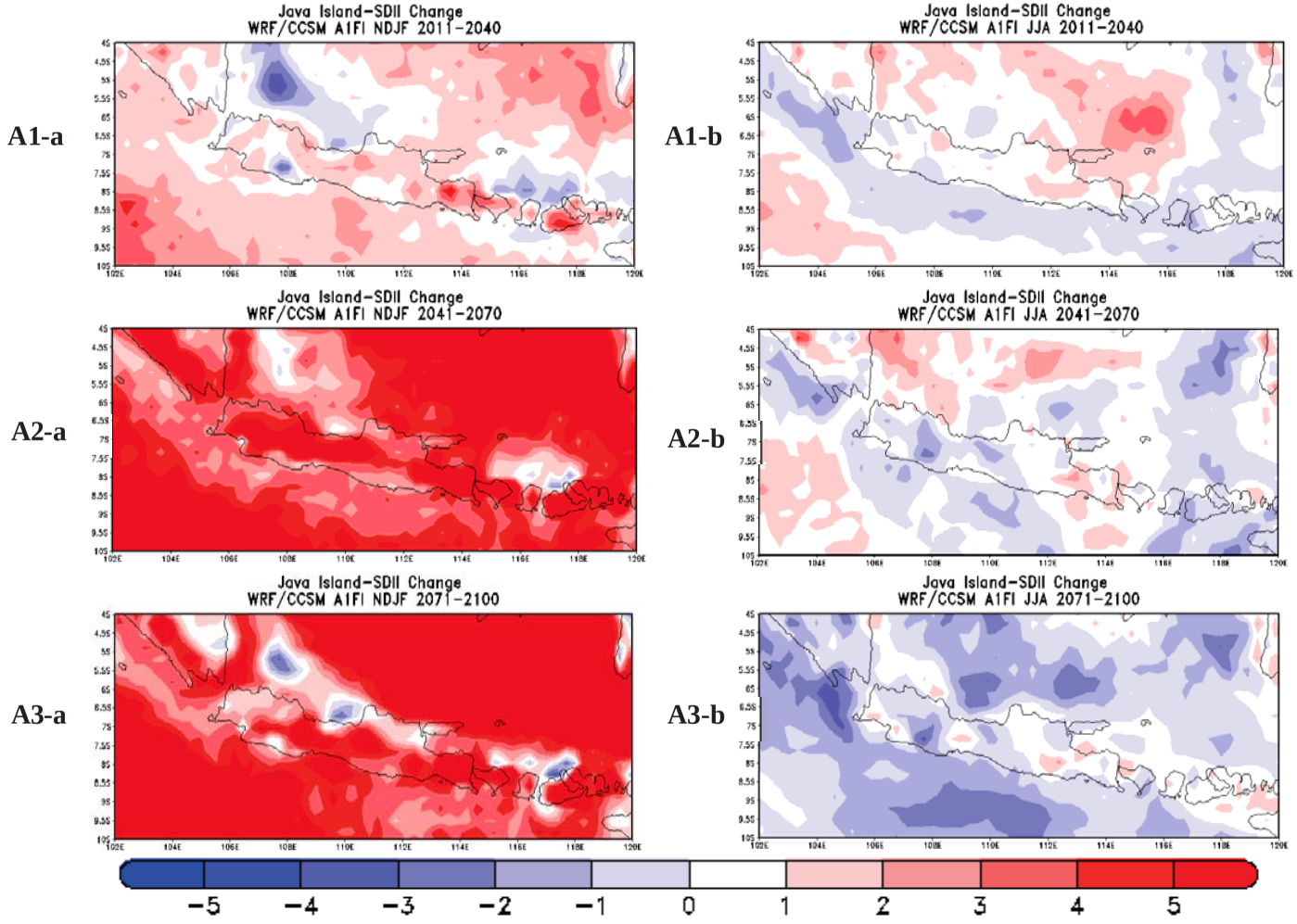

Figure 4.29: WRF/CCSM **A1FI** STARDEX Indices relative to 1961-1990, Rain intensity, **SDII, mm/day**, **Jakarta**
A1: 2011-2040, A2: 2041-2070, A3: 2071-2100 (a) **NDJF Change** (b) **JJA Change**

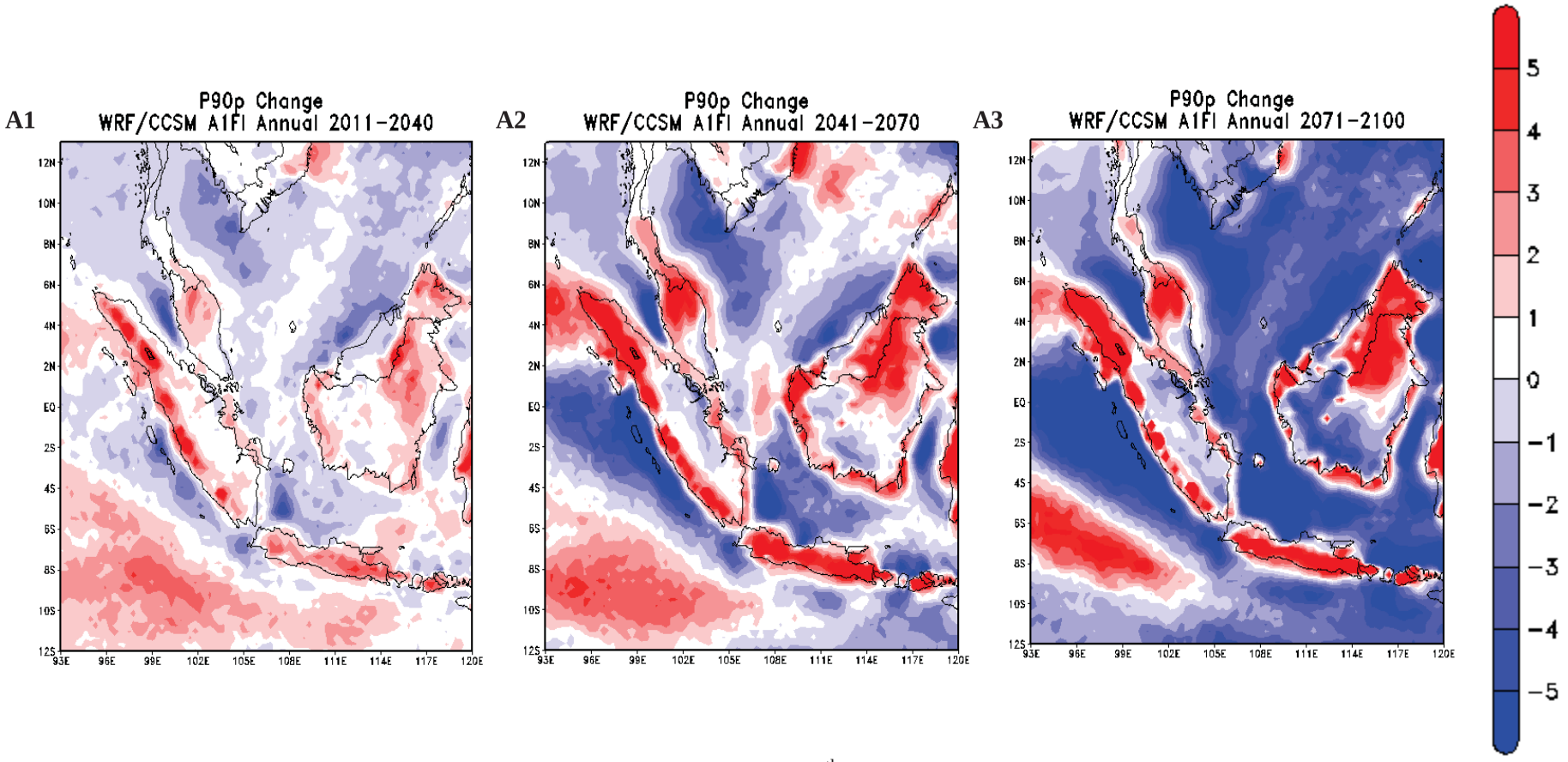

Figure 4.30: WRF/CCSM **A1FI** STARDEX Indices relative to 1961-1990, 90th percentile of rain amounts, **P90p, mm/day**
A1: 2011-2040, A2: 2041-2070, A3: 2071-2100 **Annual Change**

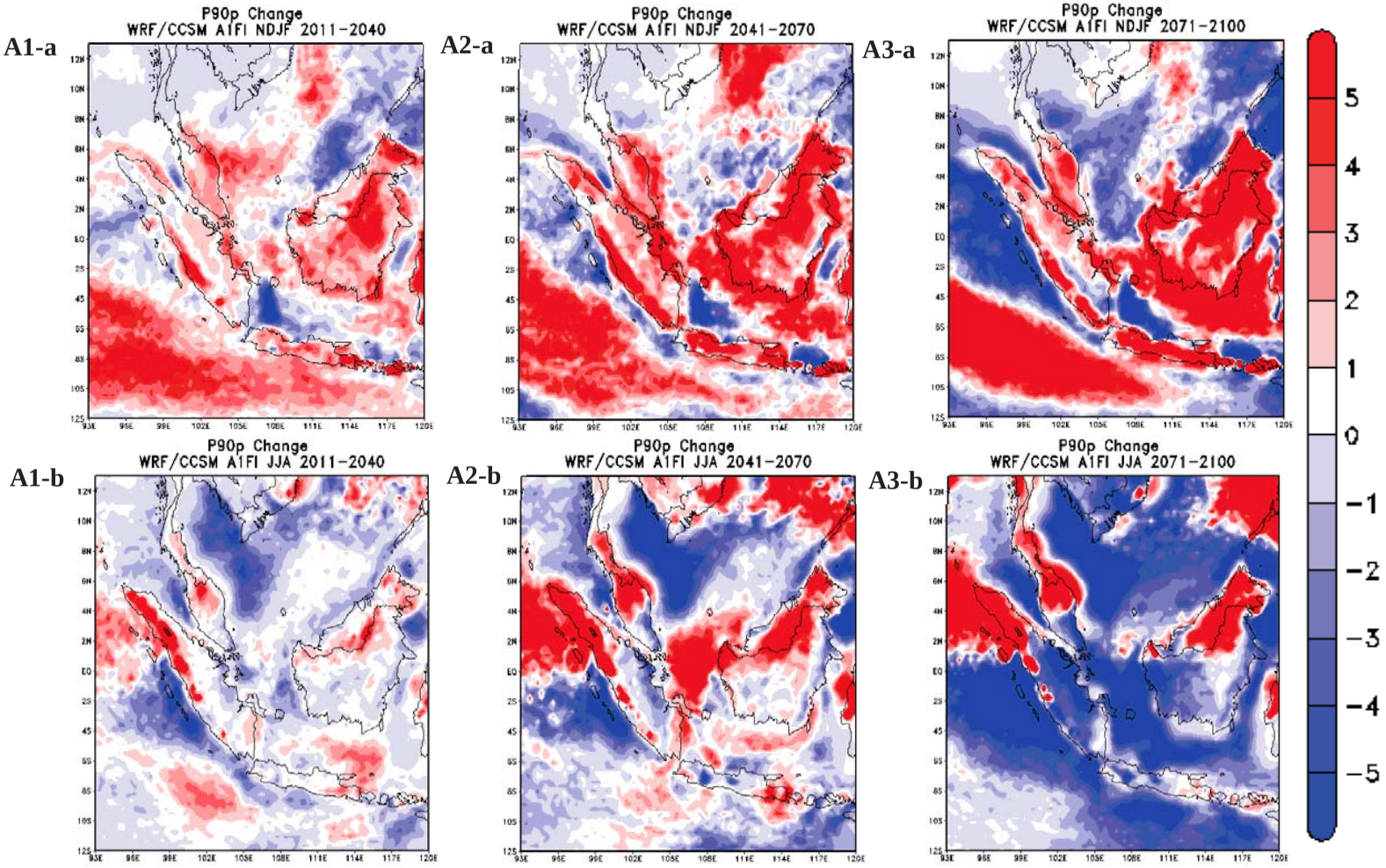

Figure 4.31: WRF/CCSM **A1FI** STARDEX Indices relative to 1961-1990, 90th percentile of rain amounts, **P90p, mm/day**
A1: 2011-2040, A2: 2041-2070, A3: 2071-2100 (a) **NDJF Change** (b) **JJA Change**

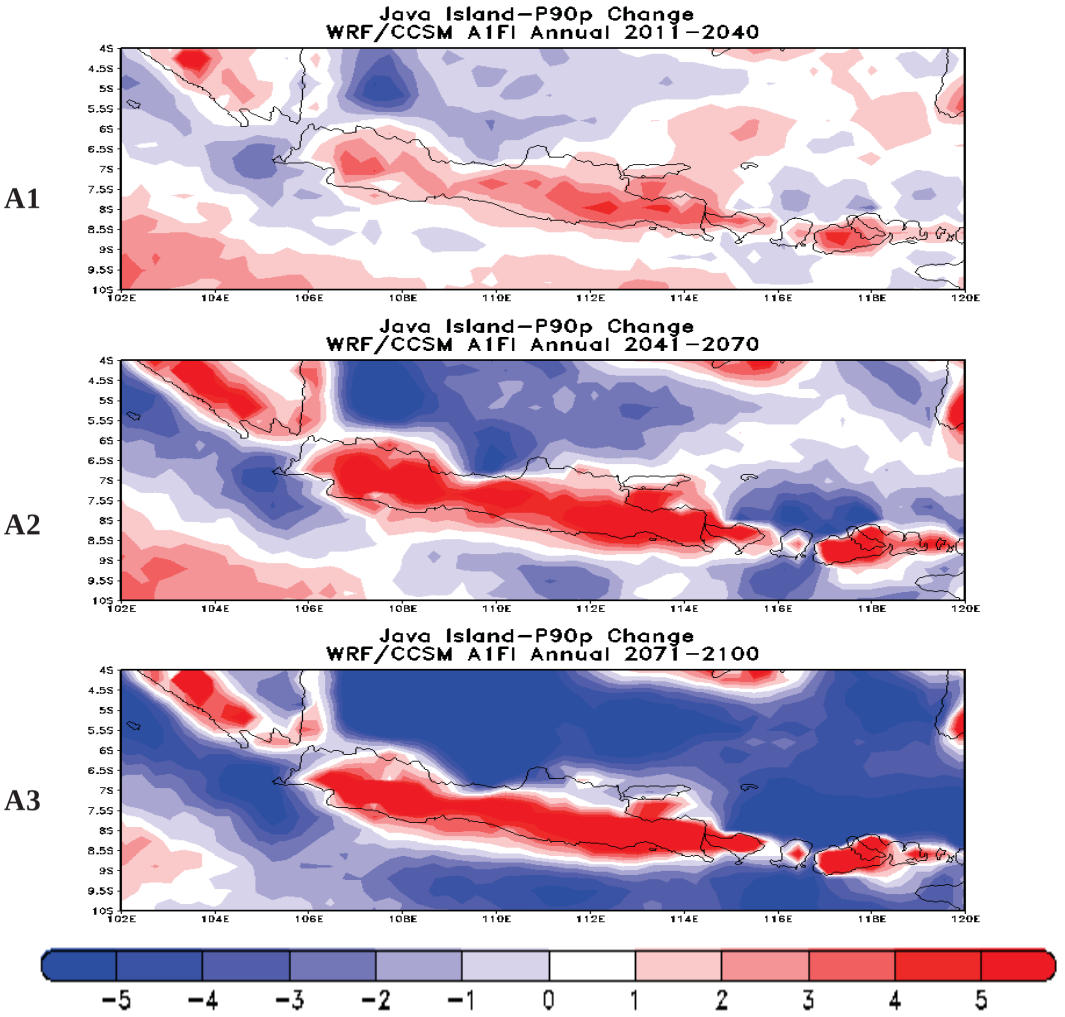

Figure 4.32: WRF/CCSM **A1FI** STARDEX Indices relative to 1961-1990, 90th percentile of rain amounts, **P90p, mm/day**, **Jakarta**
A1: 2011-2040, A2: 2041-2070, A3: 2071-2100 **Annual Change**

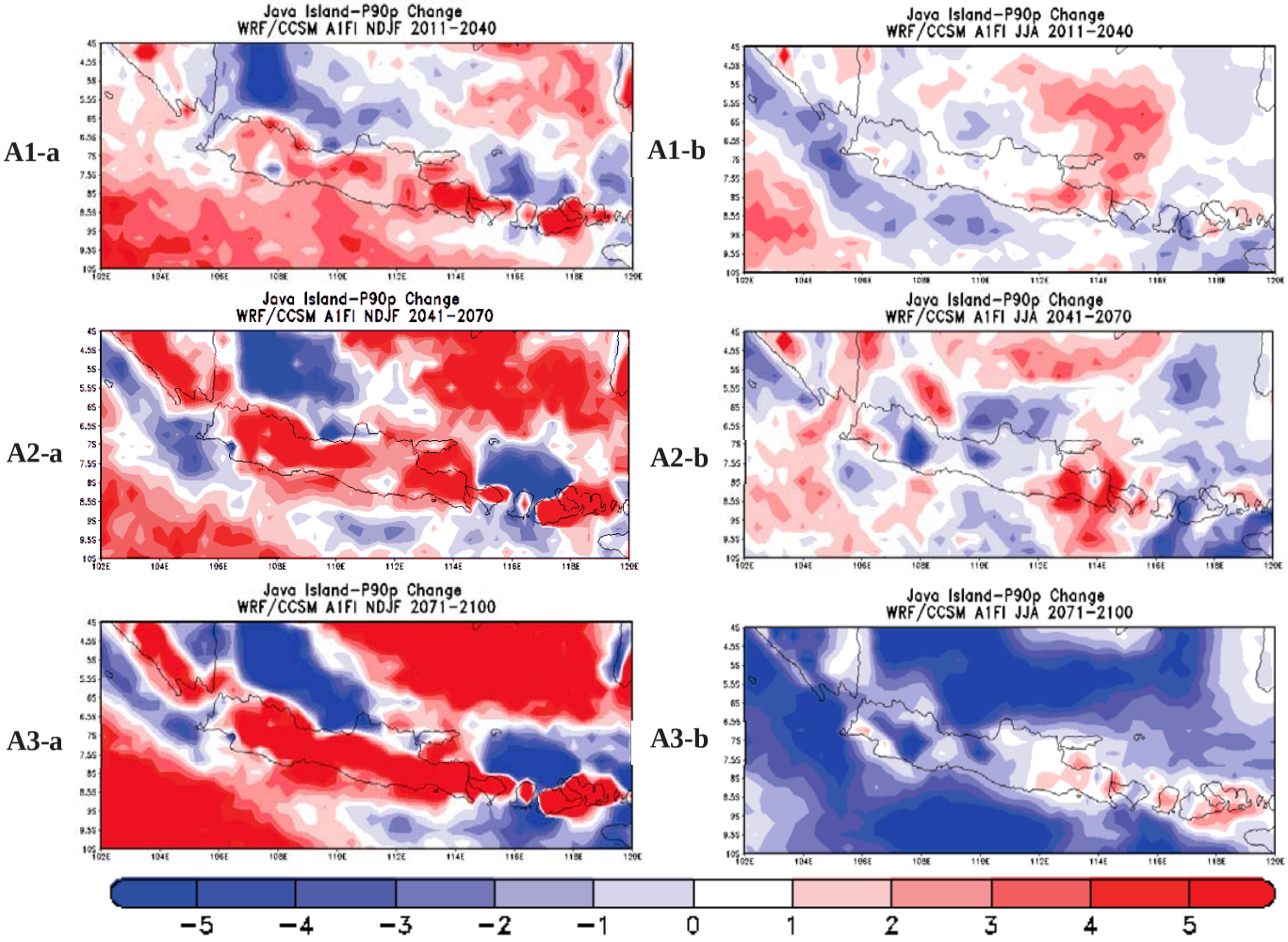

Figure 4.33: WRF/CCSM **A1FI** STARDEX Indices relative to 1961-1990, 90th percentile of rain amounts, **P90p, mm/day**, **Jakarta**
A1: 2011-2040, A2: 2041-2070, A3: 2071-2100 (a) **NDJF Change** (b) **JJA Change**

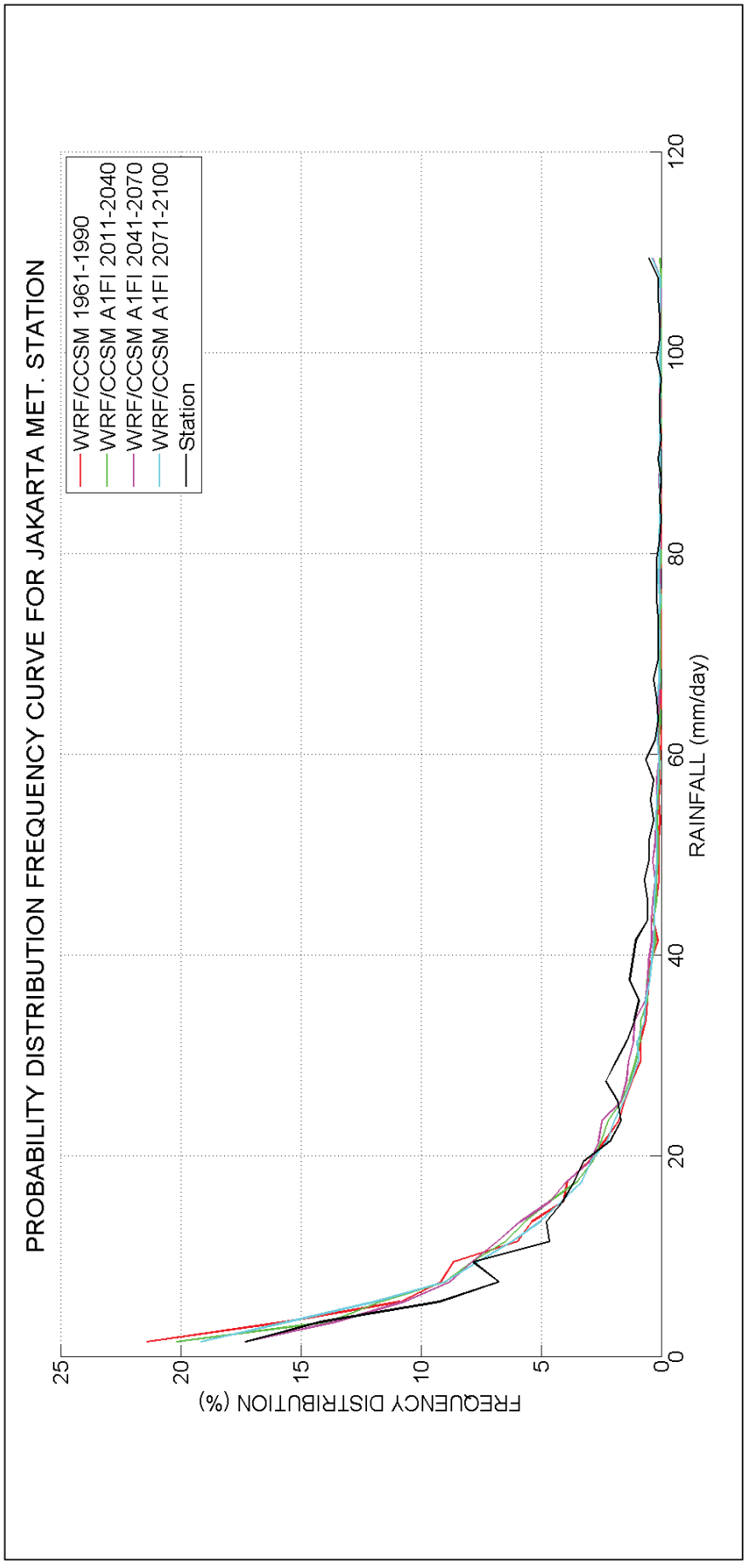

Figure 4.34: Precipitation Probability Density Function (PDF) for **WRF/CCSM (2011-2100) A1FI scenario**

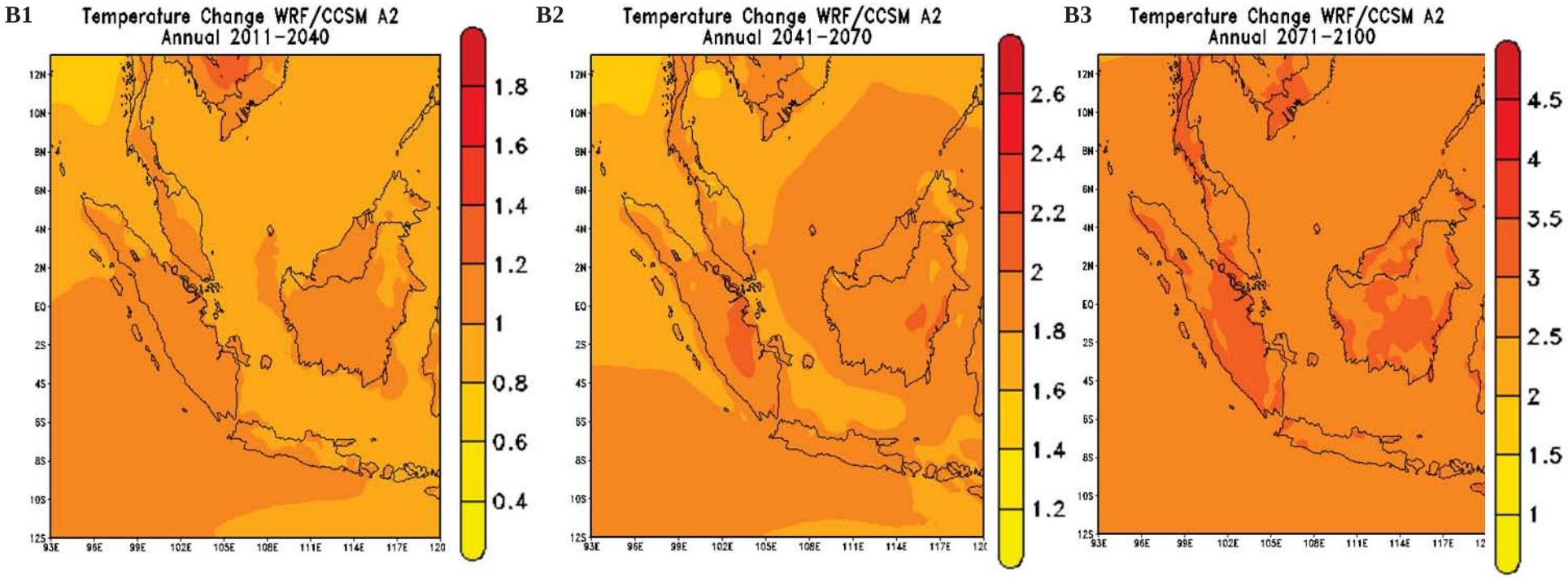

Figure 4.35: WRF/CCSM **A2** Climate Response for Temperature (Absolute Anomaly in ºC) relative to 1961-1990
B1: 2011-2040, B2: 2041-2070, B3: 2071-2100 **Annual Change**

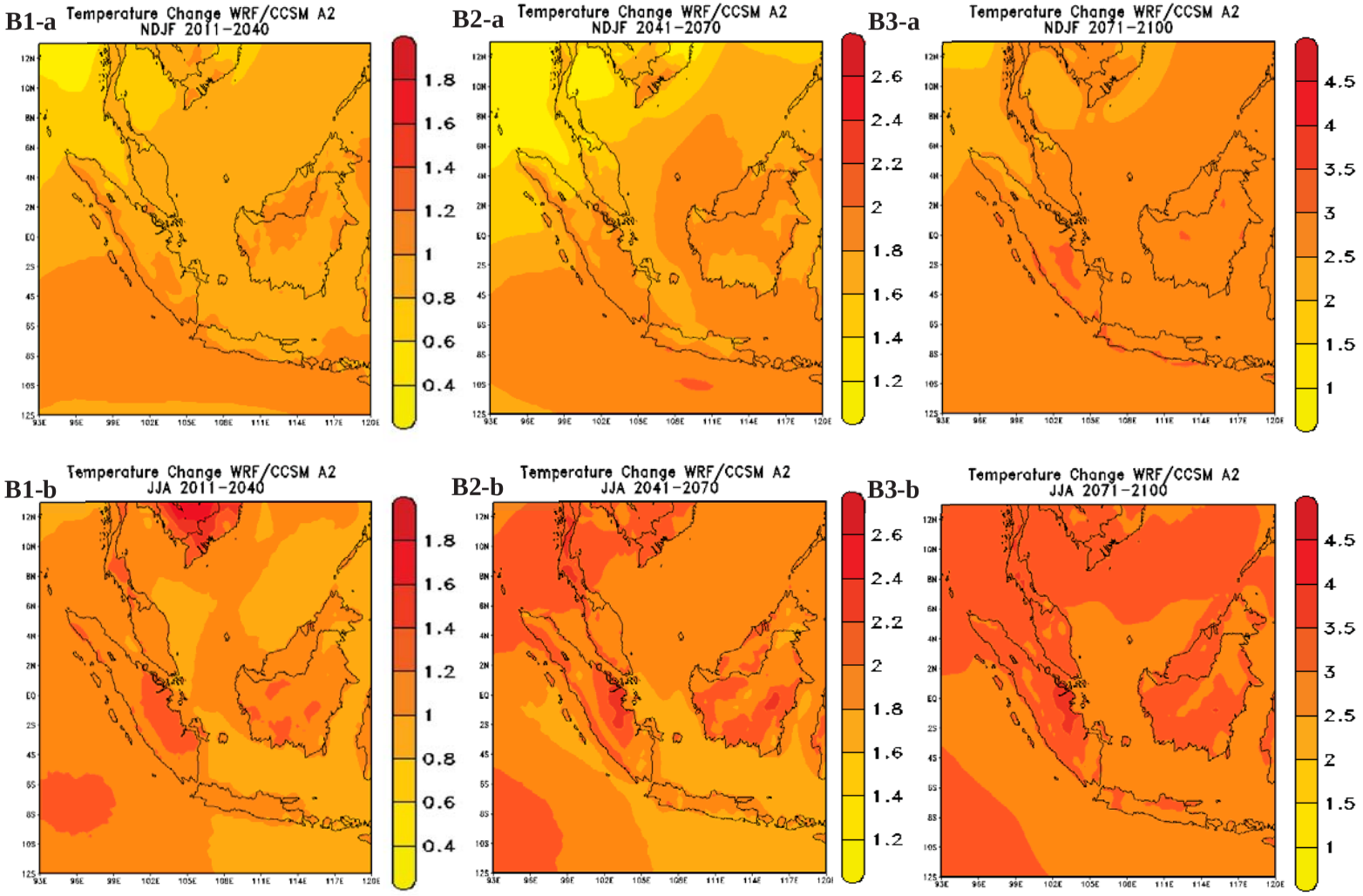

Figure 4.36: WRF/CCSM **A2** Climate Response for Temperature (Absolute Anomaly in ºC) relative to 1961-1990
B1: 2011-2040, B2: 2041-2070, B3: 2071-2100 (a) **NDJF Change** (b) **JJA Change**

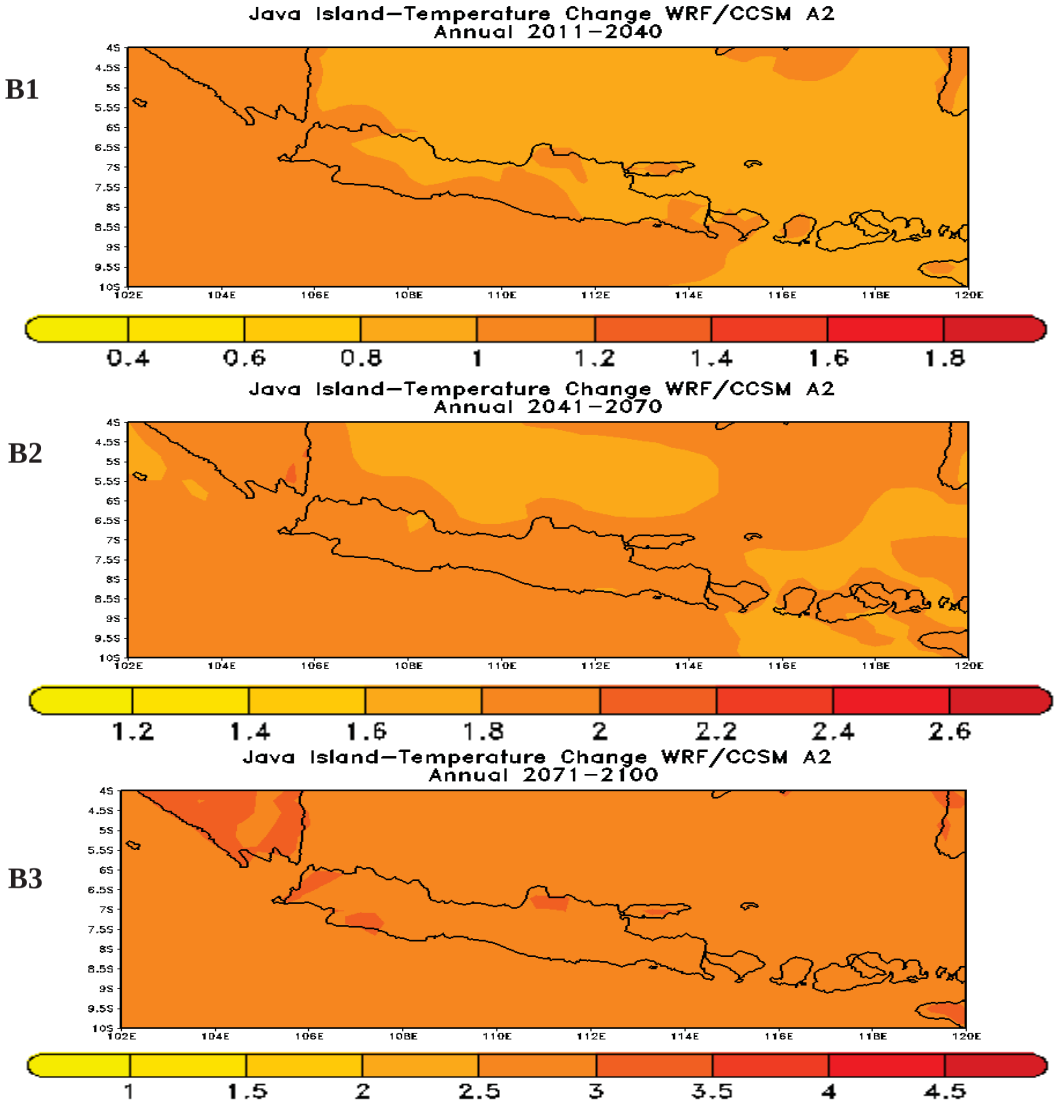

Figure 4.37: WRF/CCSM **A2** Climate Response for Temperature (Absolute Anomaly in ºC) relative to 1961-1990, **Jakarta**
B1: 2011-2040, B2: 2041-2070, B3: 2071-2100 **Annual Change**

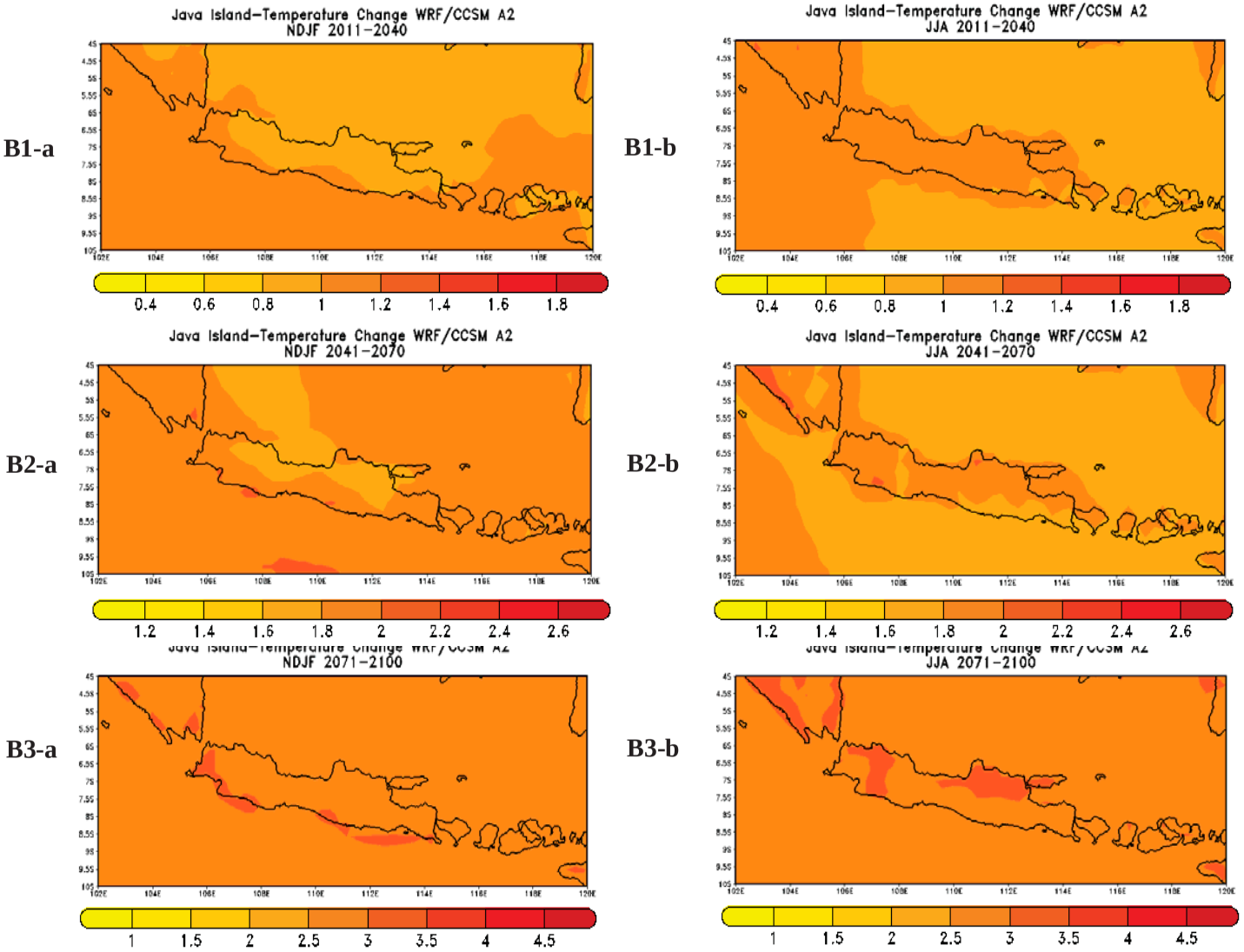

Figure 4.38: WRF/CCSM **A2** Climate Response for Temperature (Absolute Anomaly in ºC) relative to 1961-1990, **Jakarta**
B1: 2011-2040, B2: 2041-2070, B3: 2071-2100 (a) **NDJF Change** (b) **JJA Change**

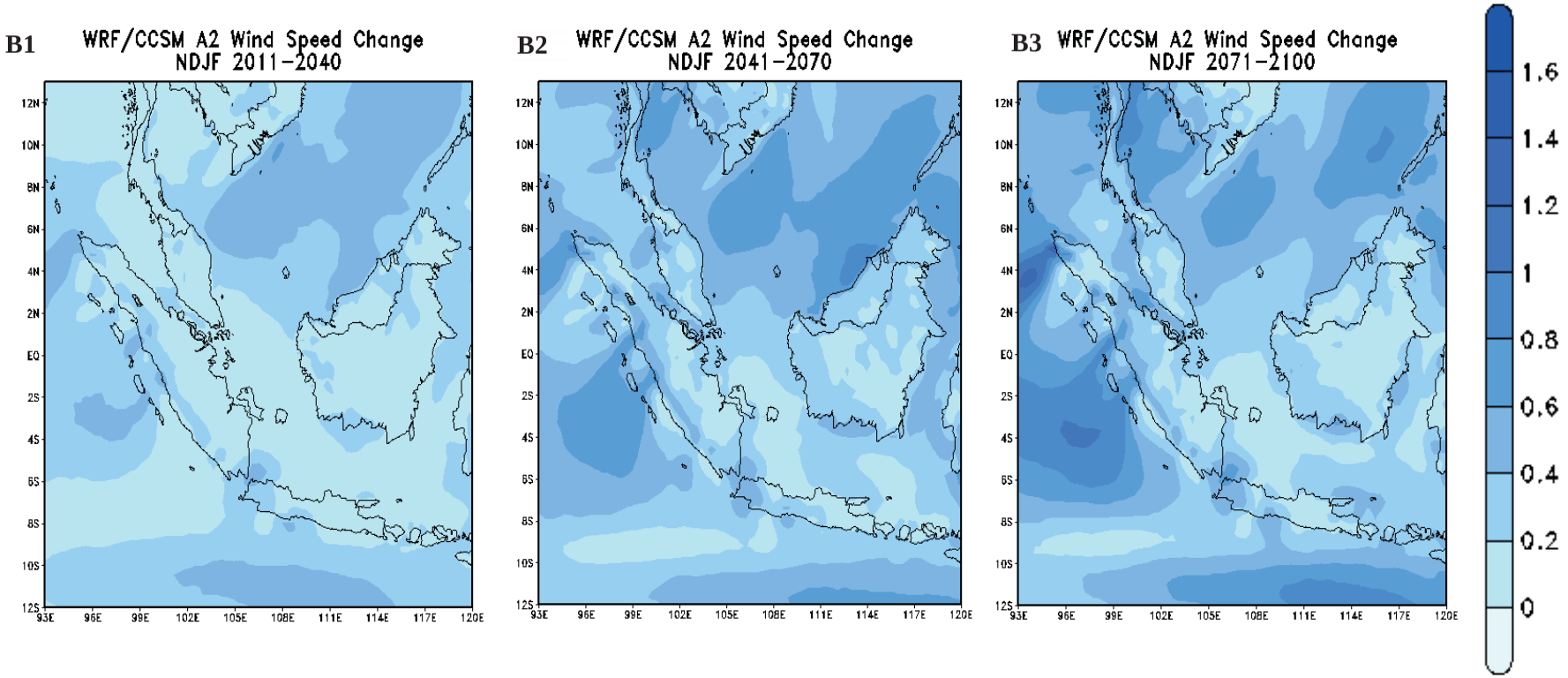

Figure 4.39: WRF/CCSM **A2** Climate Response for **NDJF** Wind Speed Change (Absolute Anomaly in m/s) relative to 1961-1990
B1: 2011-2040, B2: 2041-2070, B3: 2071-2100

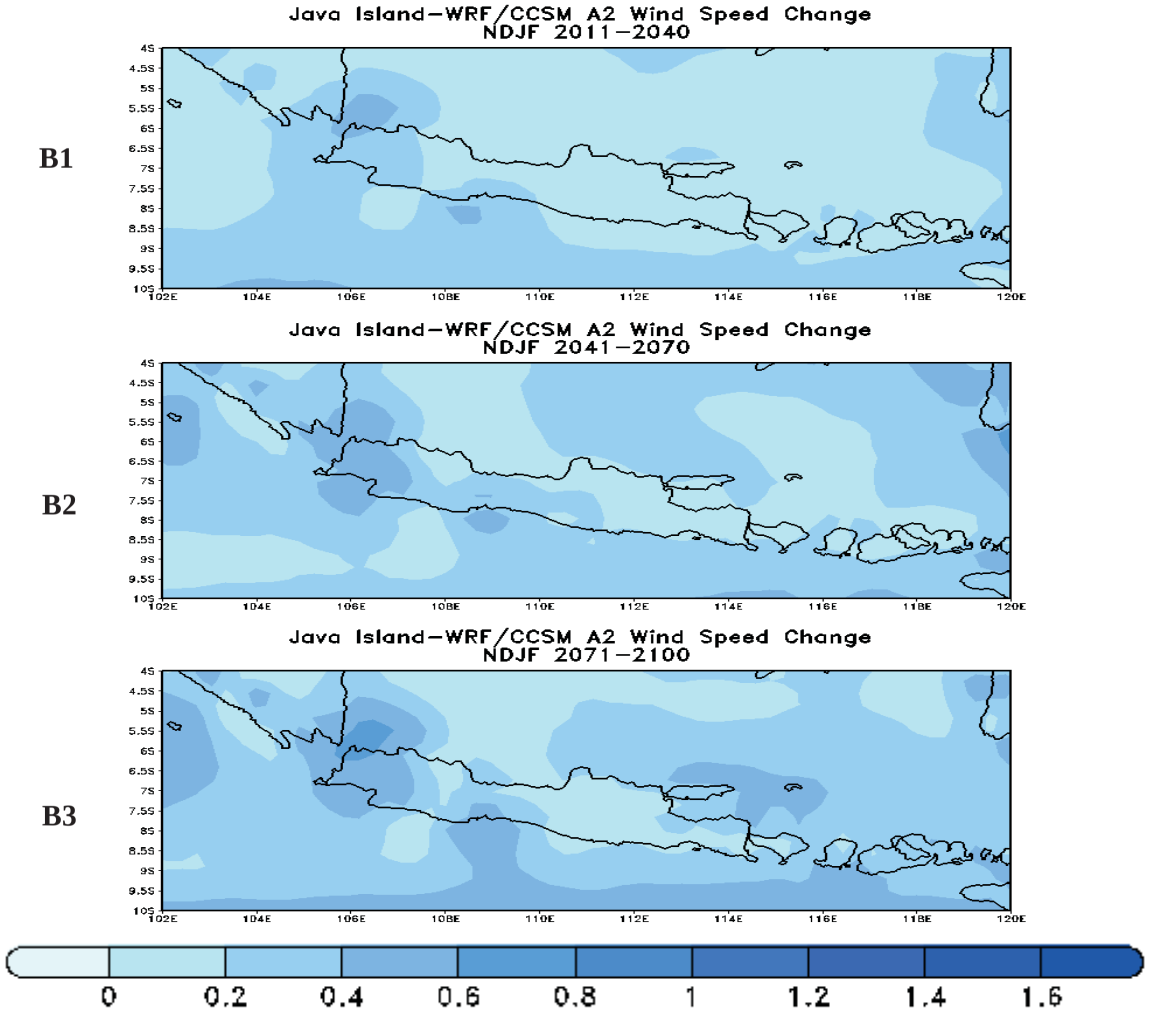

Figure 4.40: WRF/CCSM **A2** Climate Response for **NDJF** Wind Speed Change (Absolute Anomaly in m/s) relative to 1961-1990
B1: 2011-2040, B2: 2041-2070, B3: 2071-2100: **Jakarta**

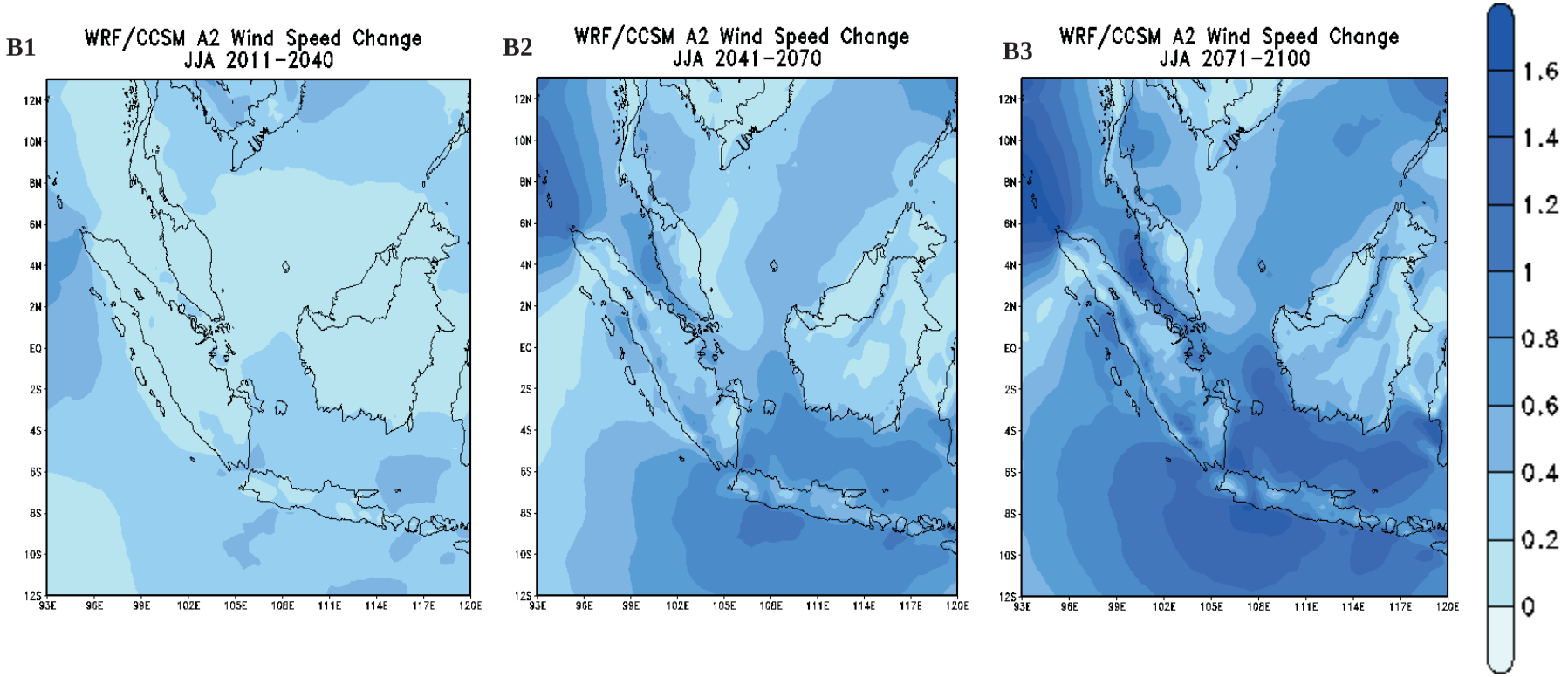

Figure 4.41: WRF/CCSM **A2** Climate Response for **JJA** Wind Speed Change (Absolute Anomaly in m/s) relative to 1961-1990
B1: 2011-2040, B2: 2041-2070, B3: 2071-2100

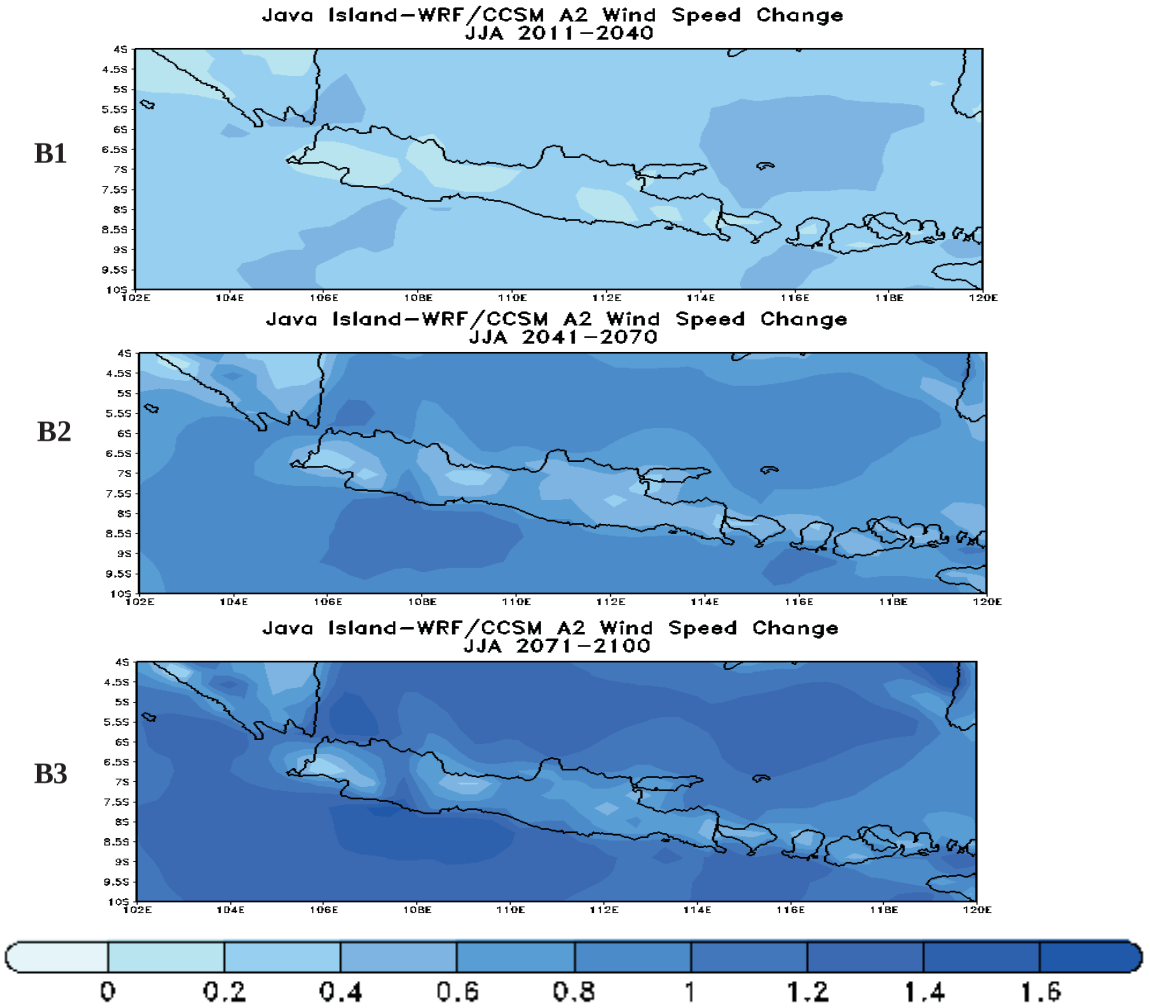

Figure 4.42: WRF/CCSM **A2** Climate Response for **JJA** Wind Speed Change (Absolute Anomaly in m/s) relative to 1961-1990
B1: 2011-2040, B2: 2041-2070, B3: 2071-2100: **Jakarta**

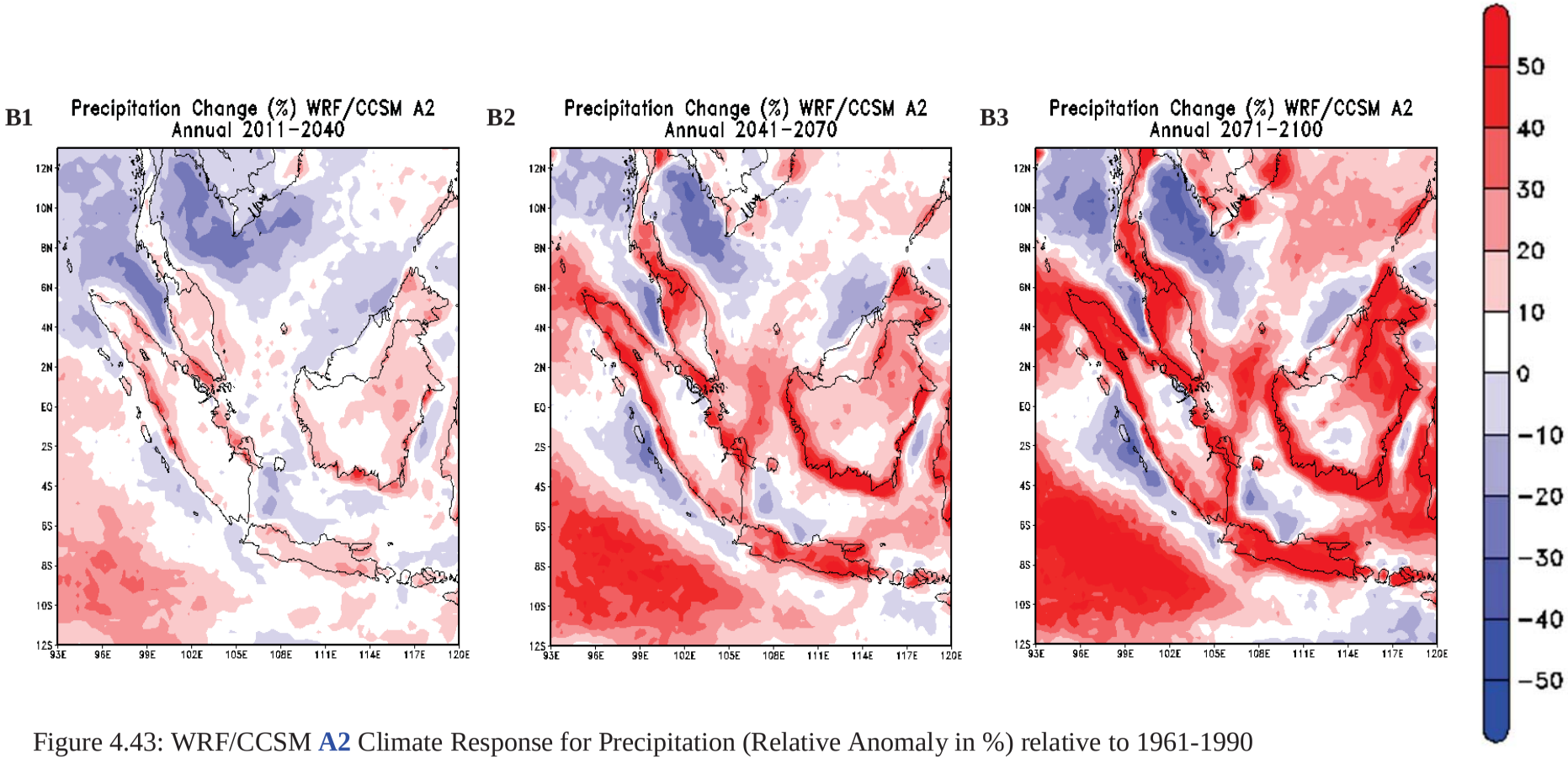

Figure 4.43: WRF/CCSM **A2** Climate Response for Precipitation (Relative Anomaly in %) relative to 1961-1990
B1: 2011-2040, B2: 2041-2070, B3: 2071-2100 **Annual Change**

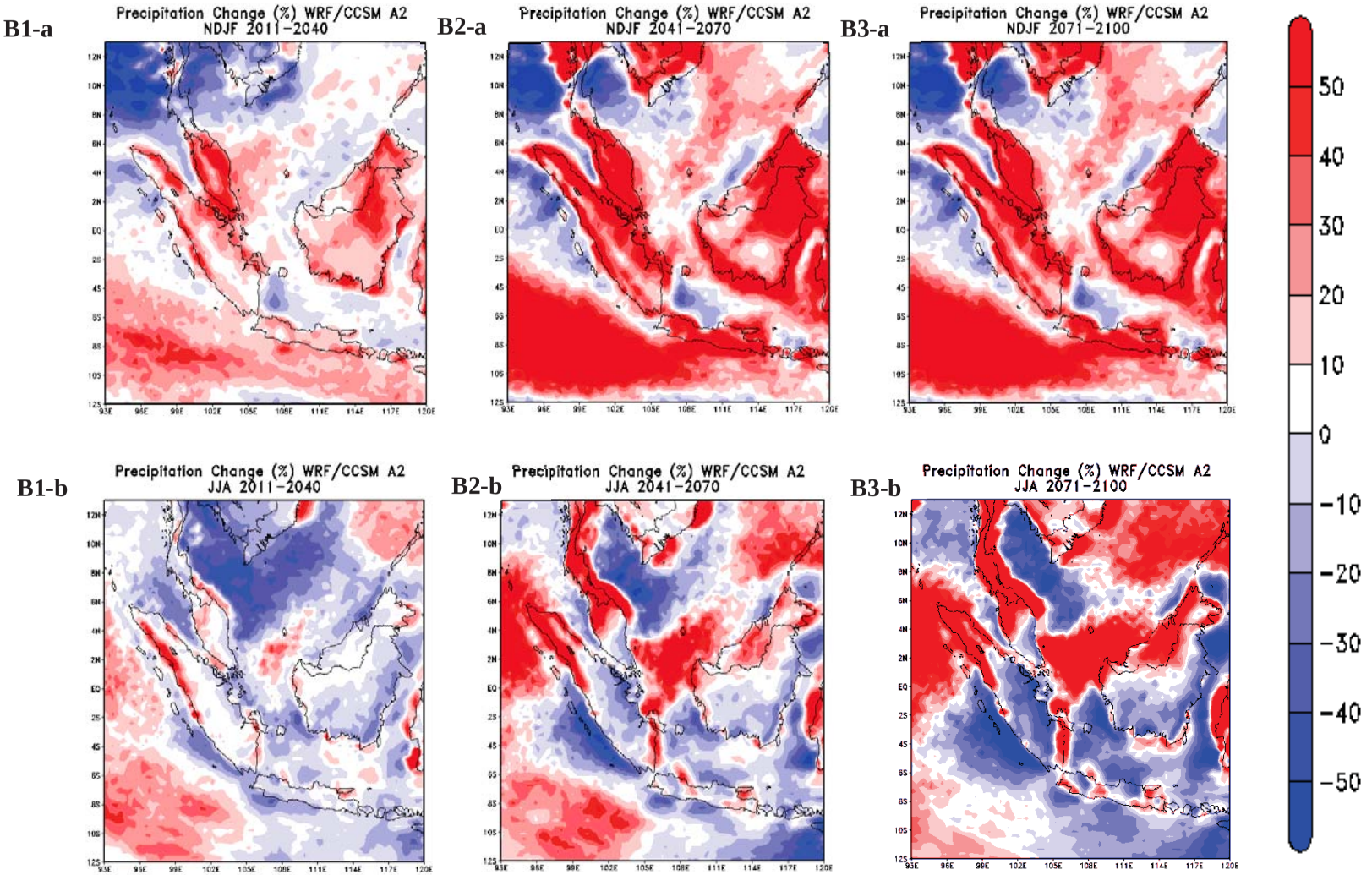

Figure 4.44: WRF/CCSM **A2** Climate Response for Precipitation (Relative Anomaly in %) relative to 1961-1990
B1: 2011-2040, B2: 2041-2070, B3: 2071-2100 (a) **NDJF Change** (b) **JJA Change**

B1

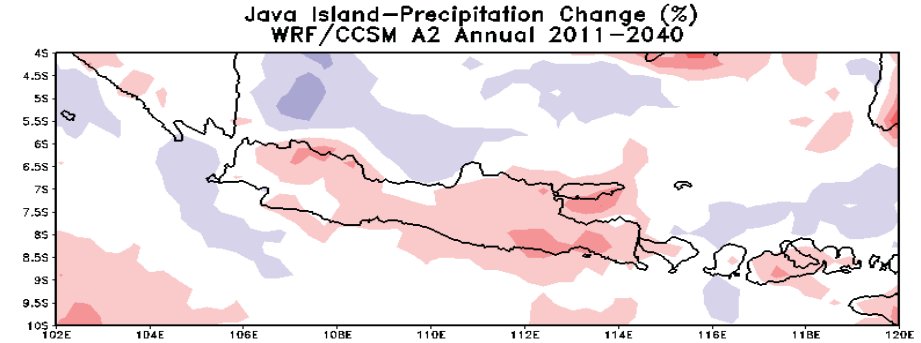

B2

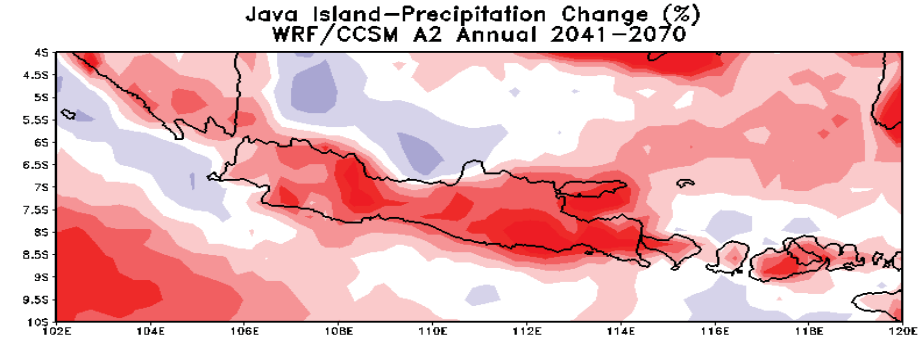

B3

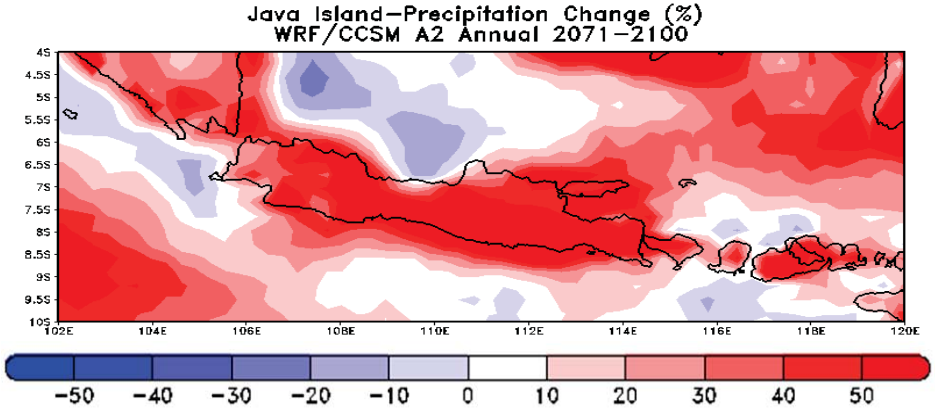

Figure 4.45: WRF/CCSM **A2** Climate Response for Precipitation (Relative Anomaly in %) relative to 1961-1990, **Jakarta**
B1: 2011-2040, B2: 2041-2070, B3: 2071-2100 **Annual Change**

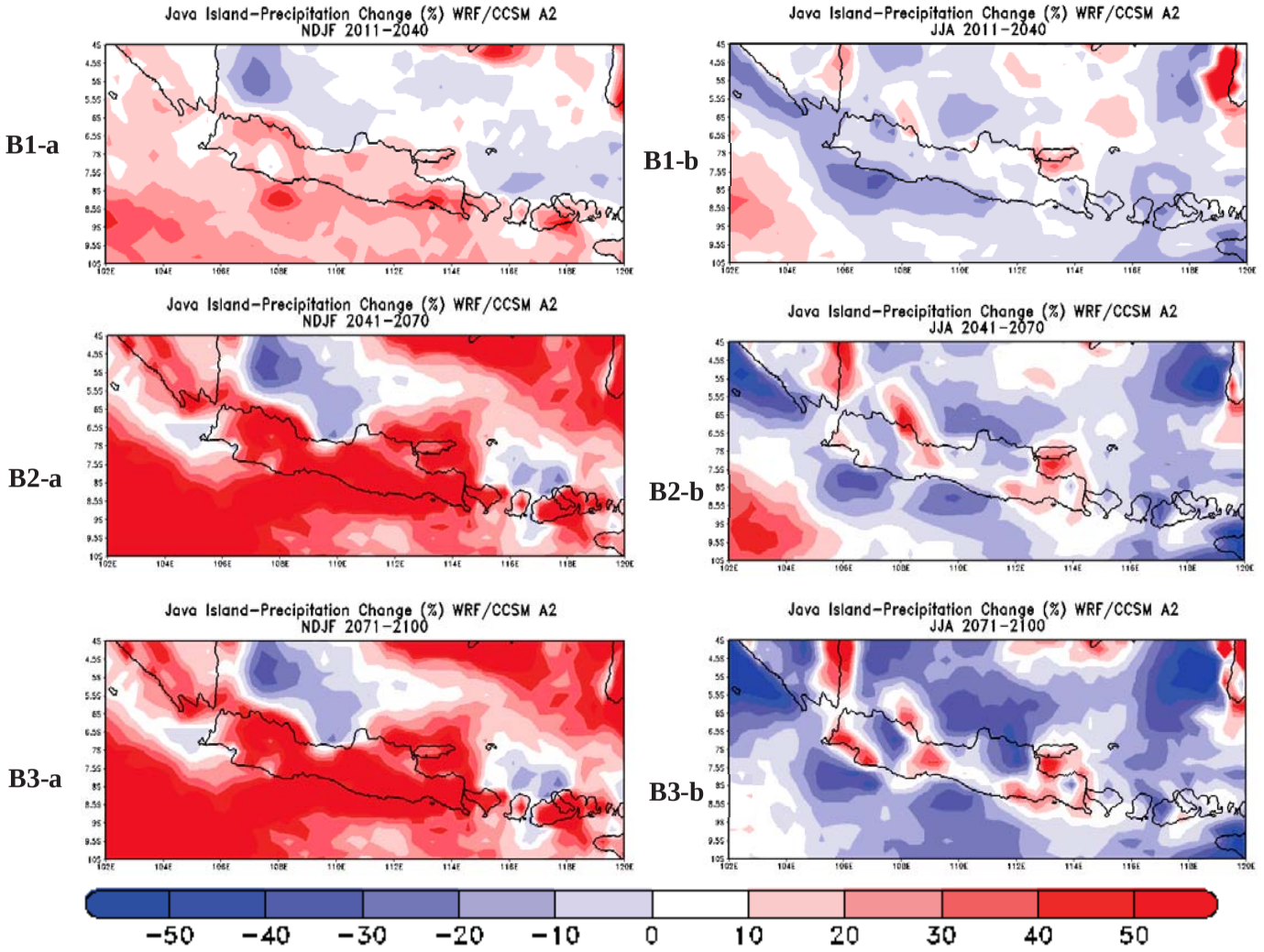

Figure 4.46: WRF/CCSM **A2** Climate Response for Precipitation (Relative Anomaly in %) relative to 1961-1990, **Jakarta**
B1: 2011-2040, B2: 2041-2070, B3: 2071-2100 (a) **NDJF Change** (b) **JJA Change**

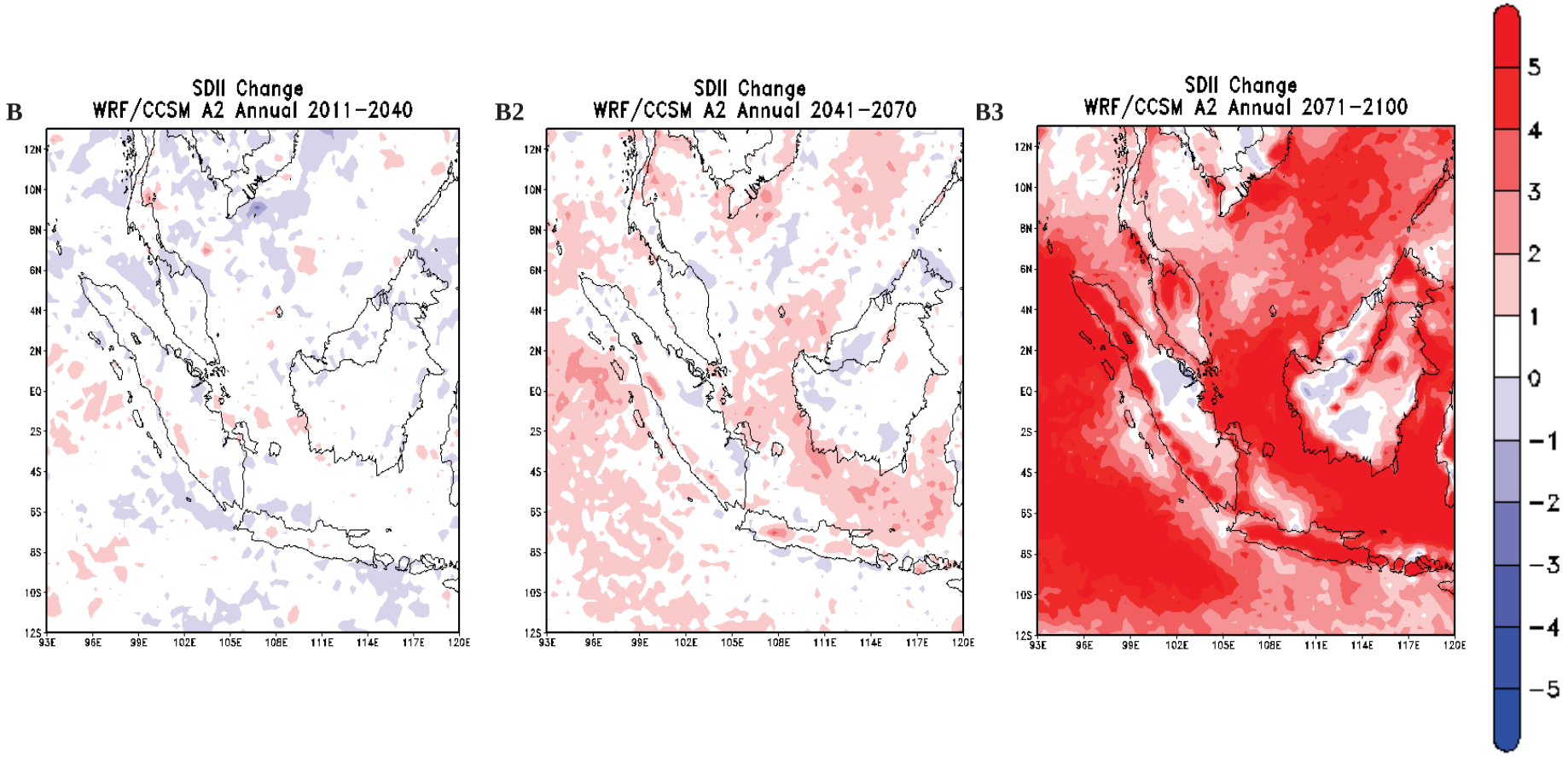

Figure 4.47: WRF/CCSM **A2** STARDEX Indices relative to 1961-1990, Rain intensity, **SDII, mm/day**
B1: 2011-2040, B2: 2041-2070, B3: 2071-2100 **Annual Change**

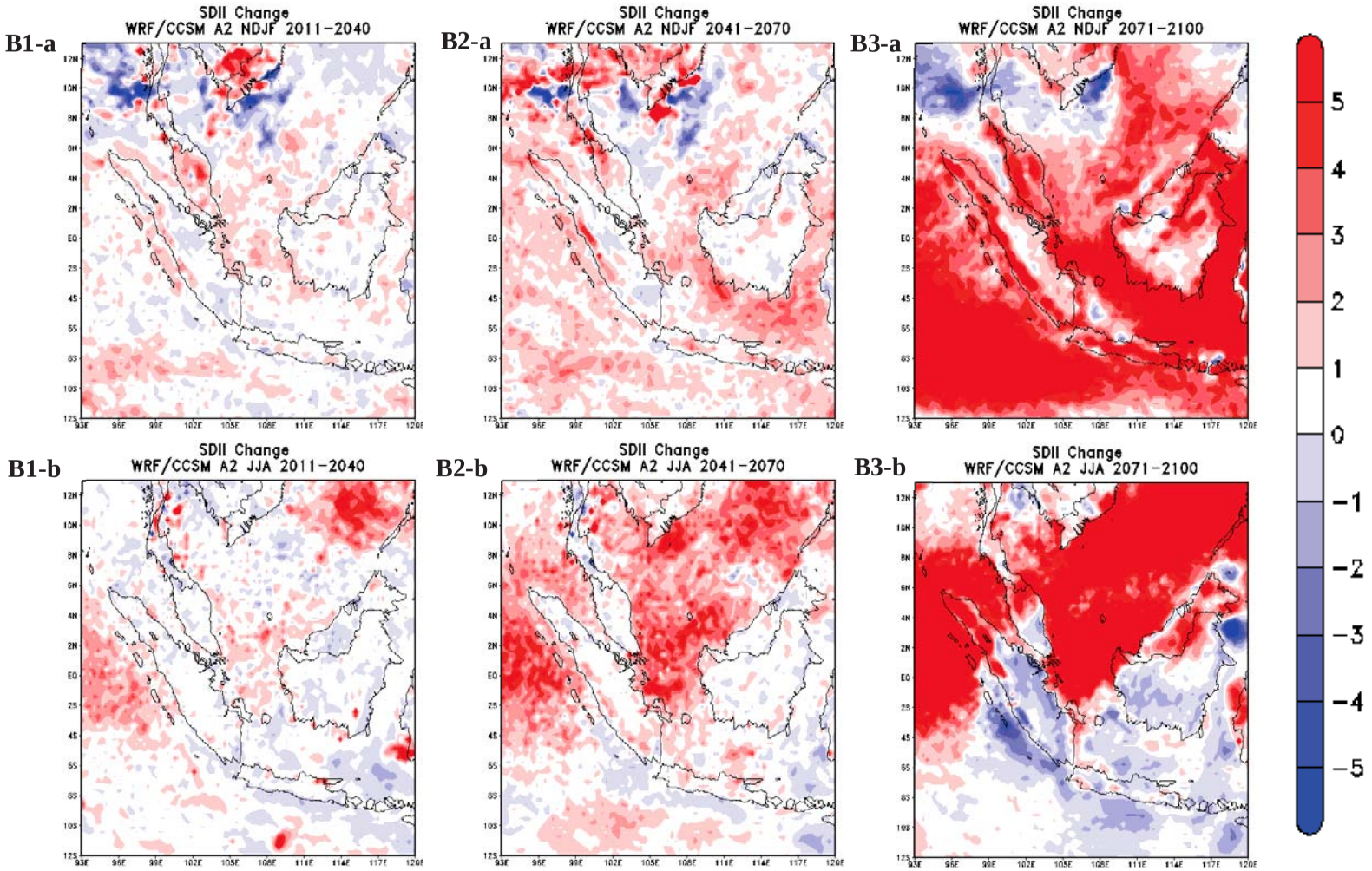

Figure 4.48: WRF/CCSM **A2** STARDEX Indices relative to 1961-1990, Rain intensity, **SDII, mm/day**
B1: 2011-2040, B2: 2041-2070, B3: 2071-2100 (a) **NDJF Change** (b) **JJA Change**

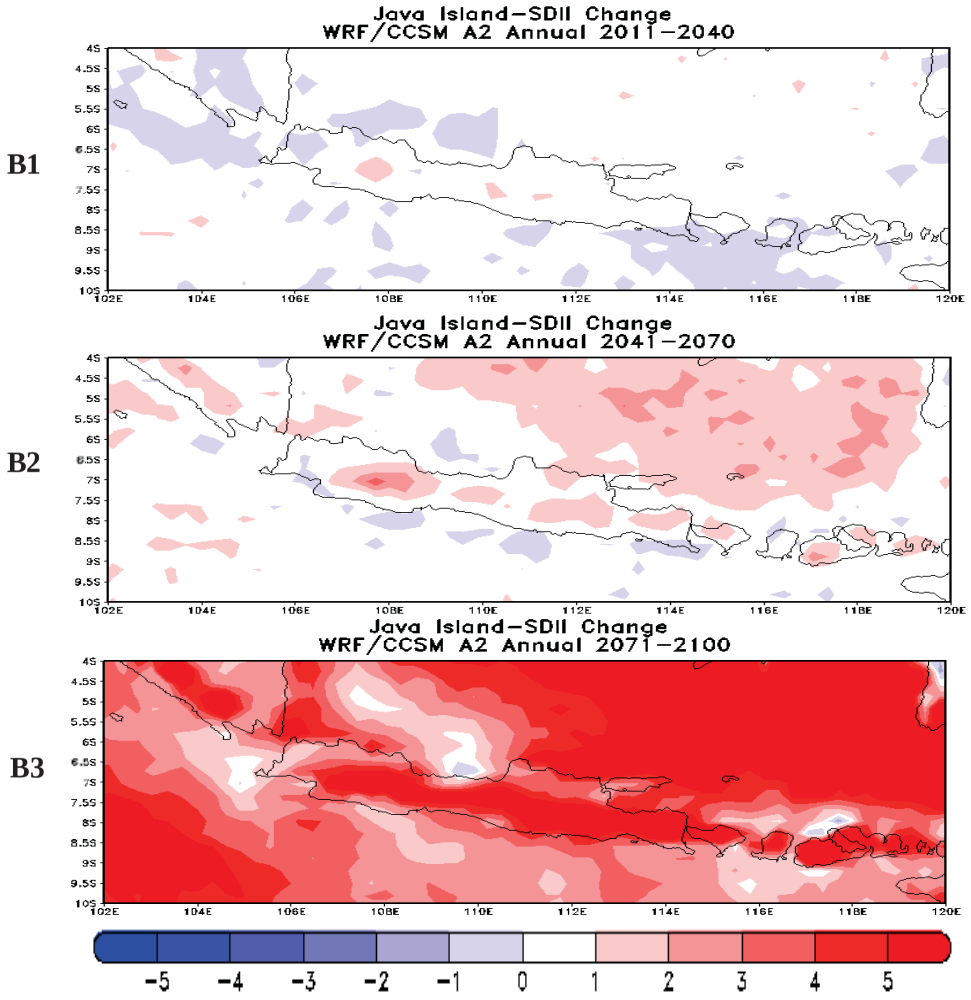

Figure 4.49: WRF/CCSM **A2** STARDEX Indices relative to 1961-1990, Rain intensity, **SDII, mm/day, Jakarta**
B1: 2011-2040, B2: 2041-2070, B3: 2071-2100 **Annual Change**

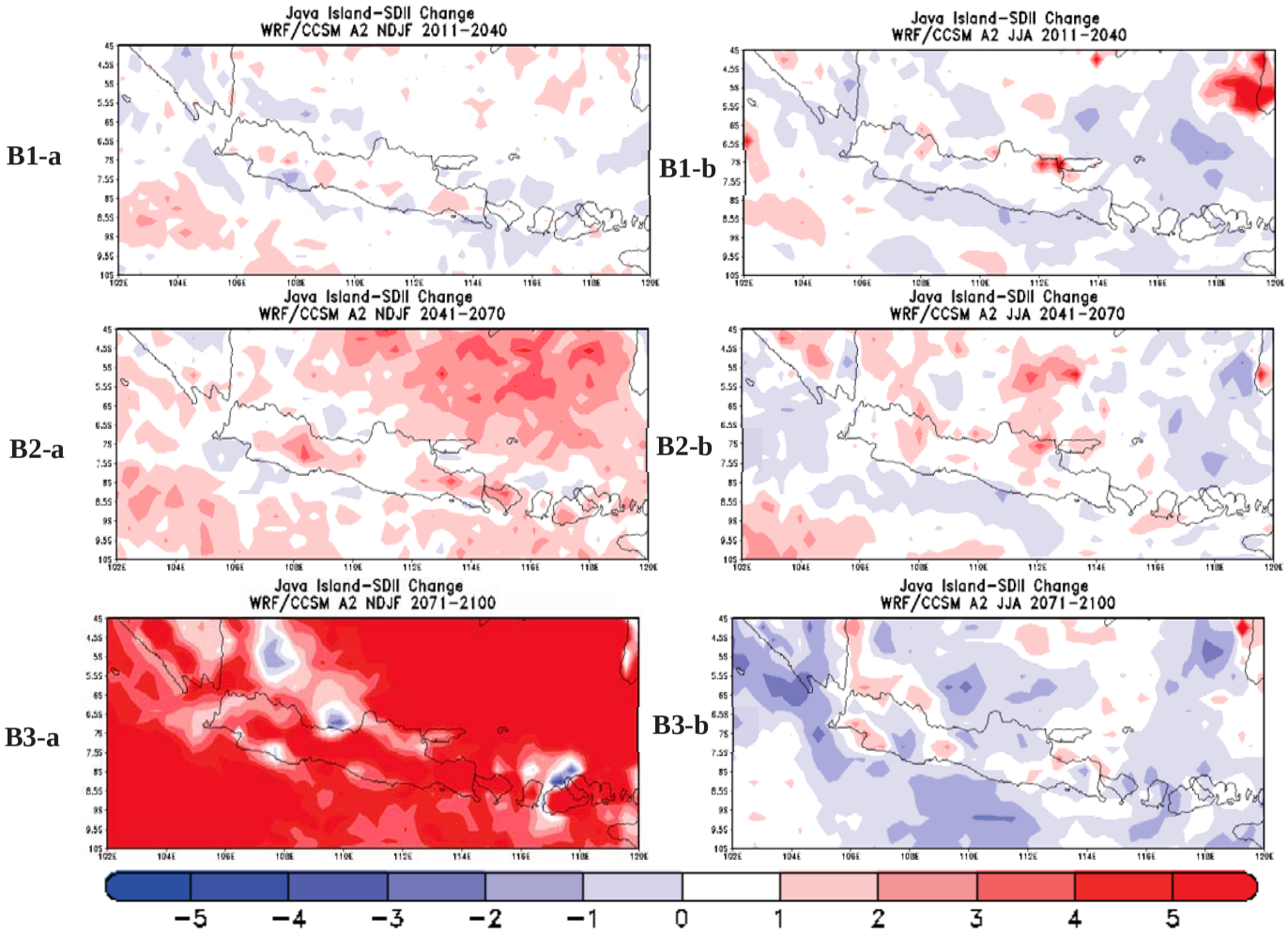

Figure 4.50: WRF/CCSM **A2** STARDEX Indices relative to 1961-1990, Rain intensity, **SDII, mm/day, Jakarta**
B1: 2011-2040, B2: 2041-2070, B3: 2071-2100 (a) **NDJF Change** (b) **JJA Change**

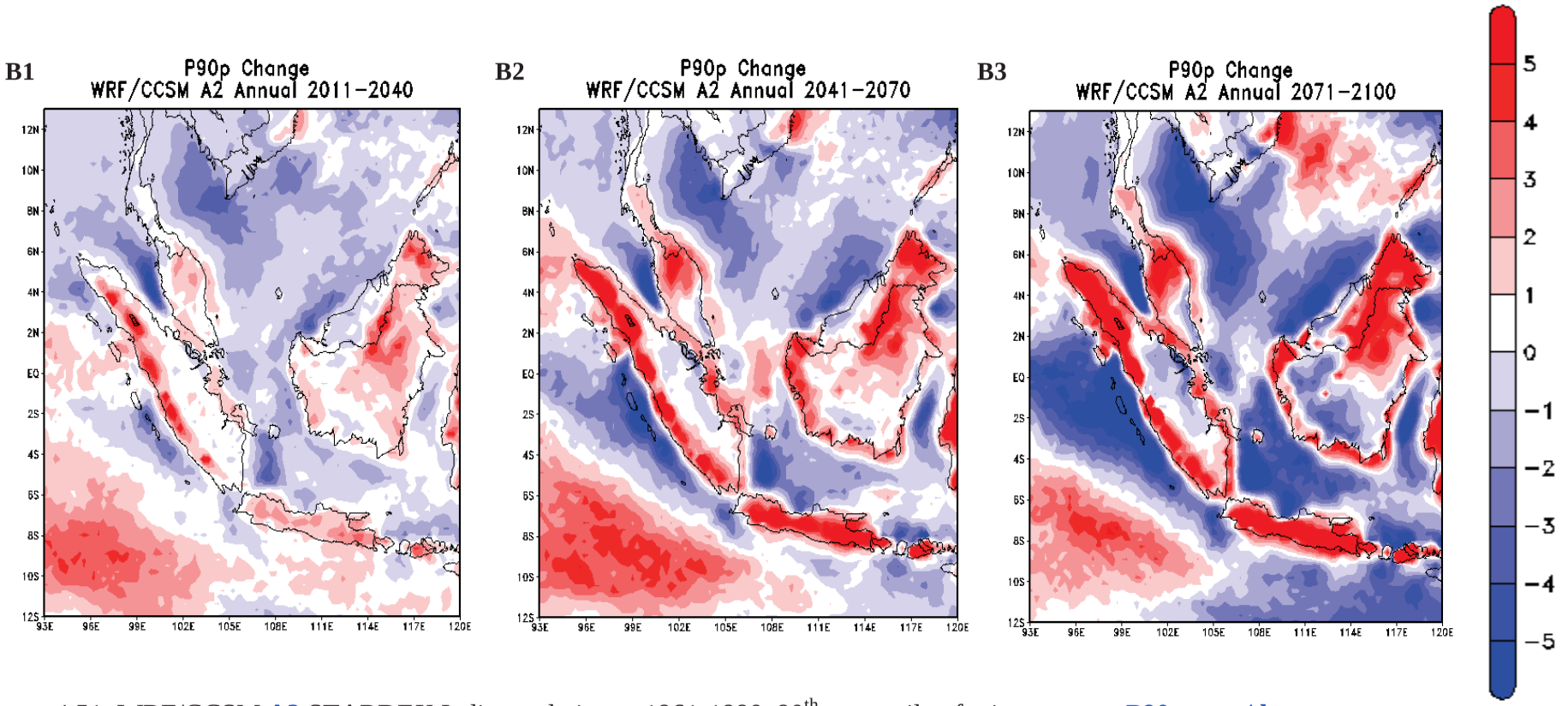

Figure 4.51: WRF/CCSM **A2** STARDEX Indices relative to 1961-1990, 90th percentile of rain amounts, **P90p, mm/day**
B1: 2011-2040, B2: 2041-2070, B3: 2071-2100 **Annual Change**

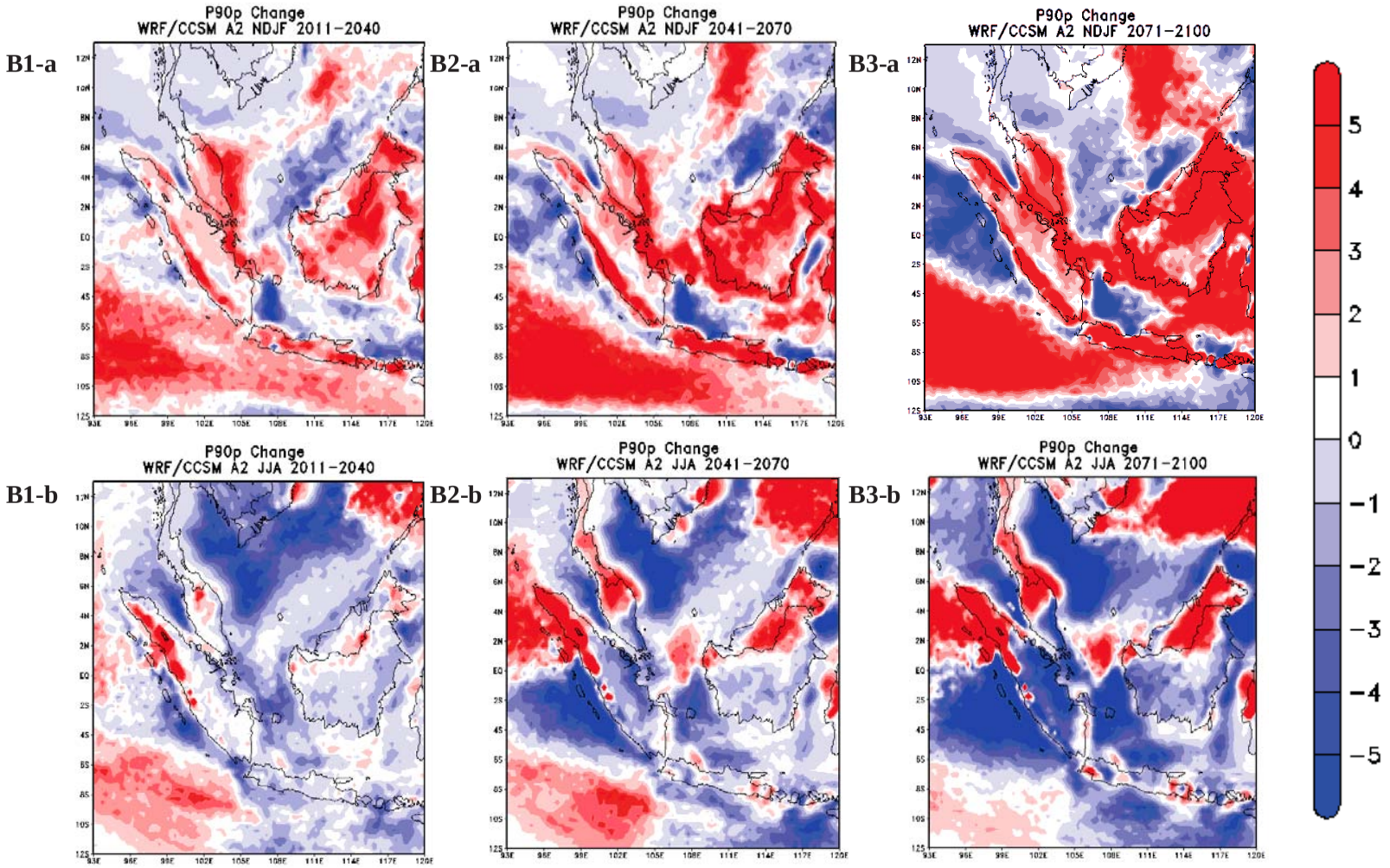

Figure 4.52: WRF/CCSM **A2** STARDEX Indices relative to 1961-1990, 90th percentile of rain amounts, **P90p, mm/day**
B1: 2011-2040, B2: 2041-2070, B3: 2071-2100 (a) **NDJF Change** (b) **JJA Change**

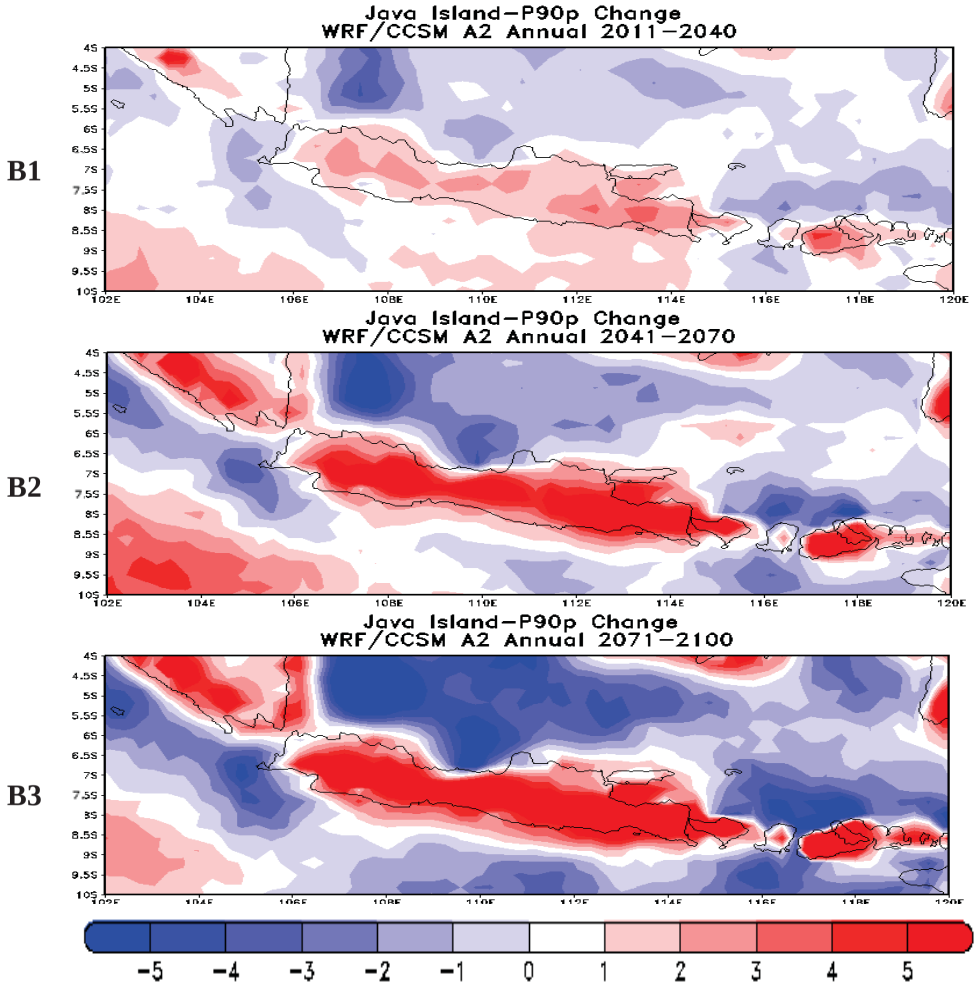

Figure 4.53: WRF/CCSM **A2** STARDEX Indices relative to 1961-1990, 90th percentile of rain amounts, **P90p, mm/day**, **Jakarta**
B1: 2011-2040, B2: 2041-2070, B3: 2071-2100 **Annual Change**

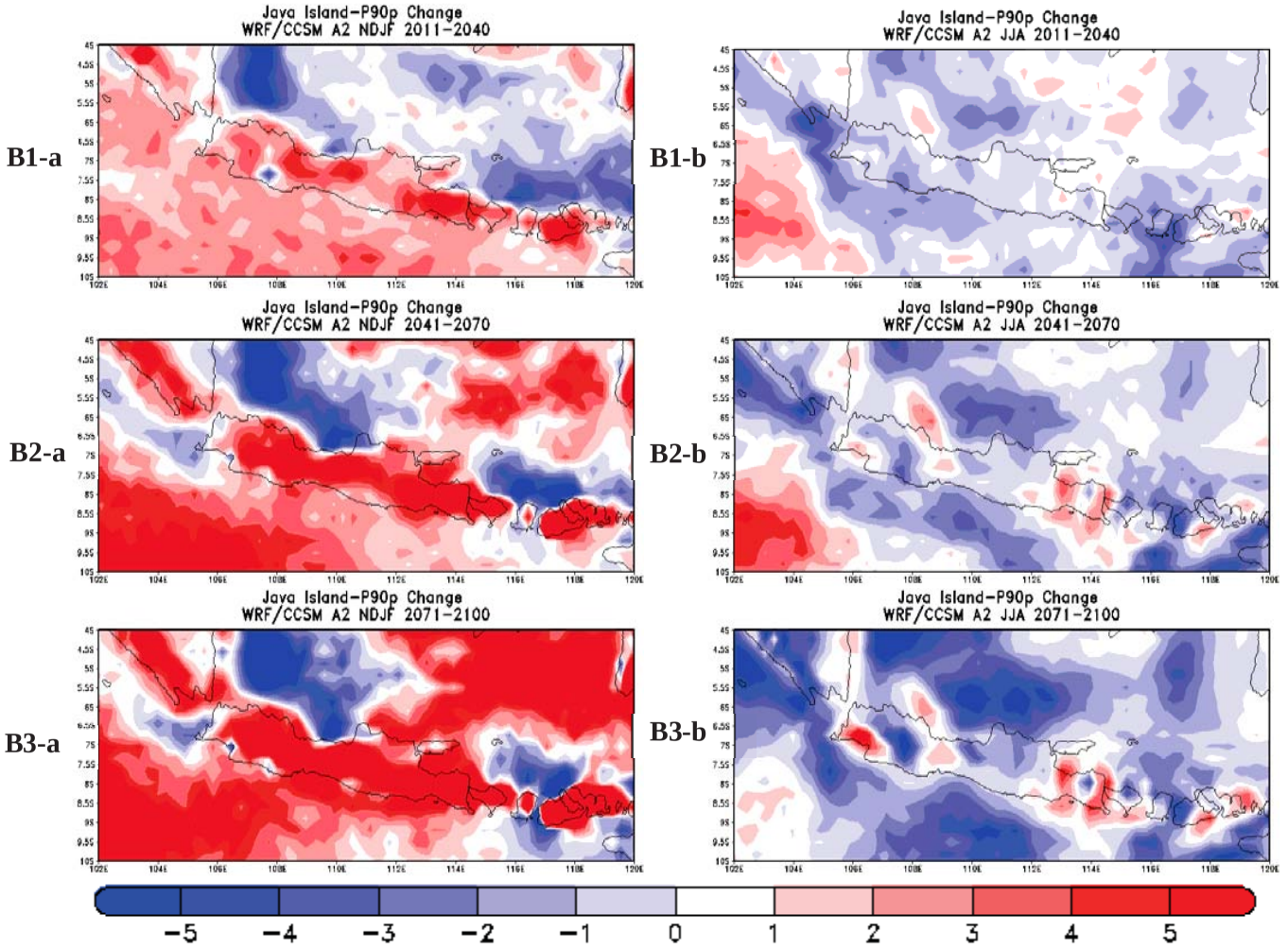

Figure 4.54: WRF/CCSM **A2** STARDEX Indices relative to 1961-1990, 90th percentile of rain amounts, **P90p, mm/day**, **Jakarta**
B1: 2011-2040, B2: 2041-2070, B3: 2071-2100 (a) **NDJF Change** (b) **JJA Change**

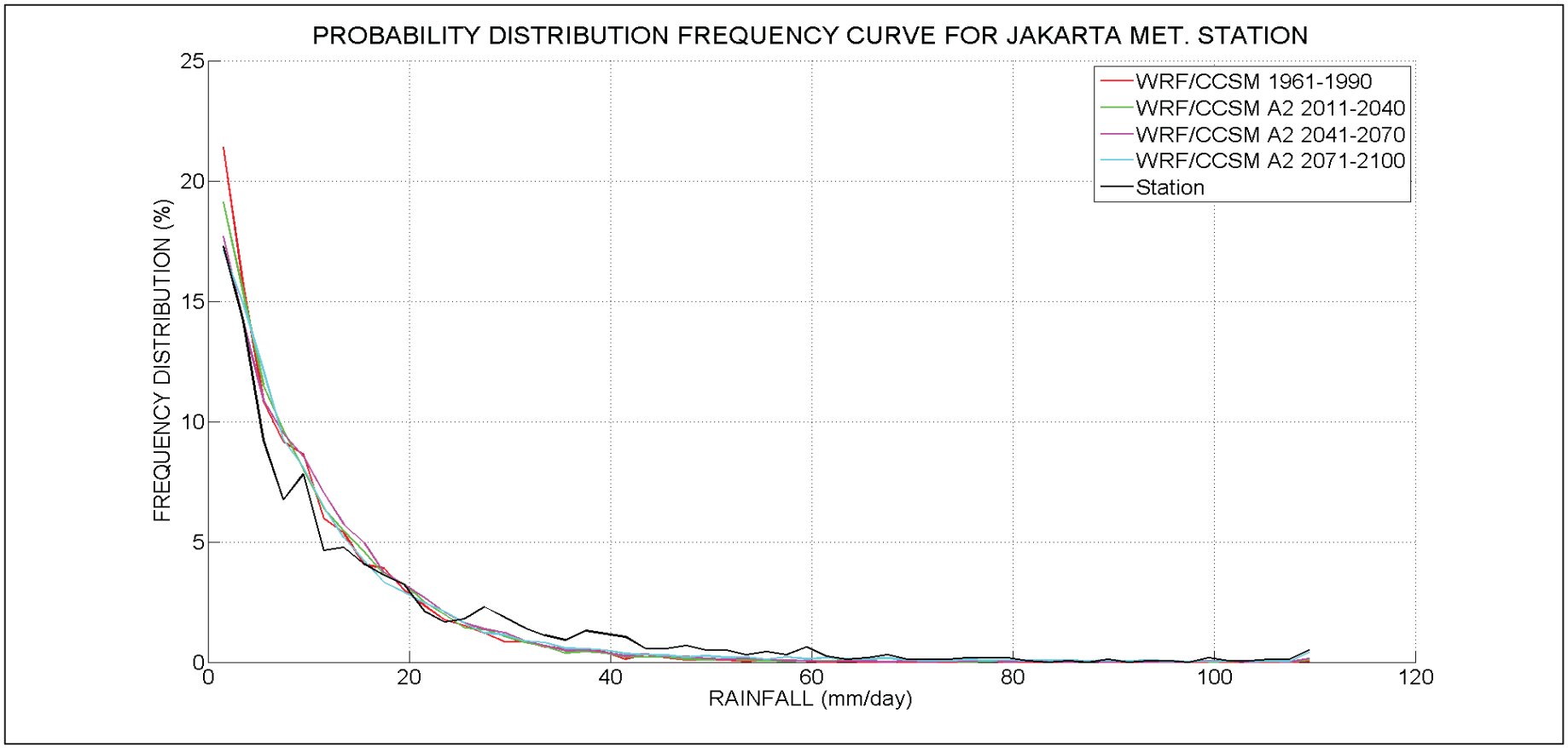

Figure 4.55: Precipitation Probability Density Function (PDF) for **WRF/CCSM (2011-2100) A2 scenario**

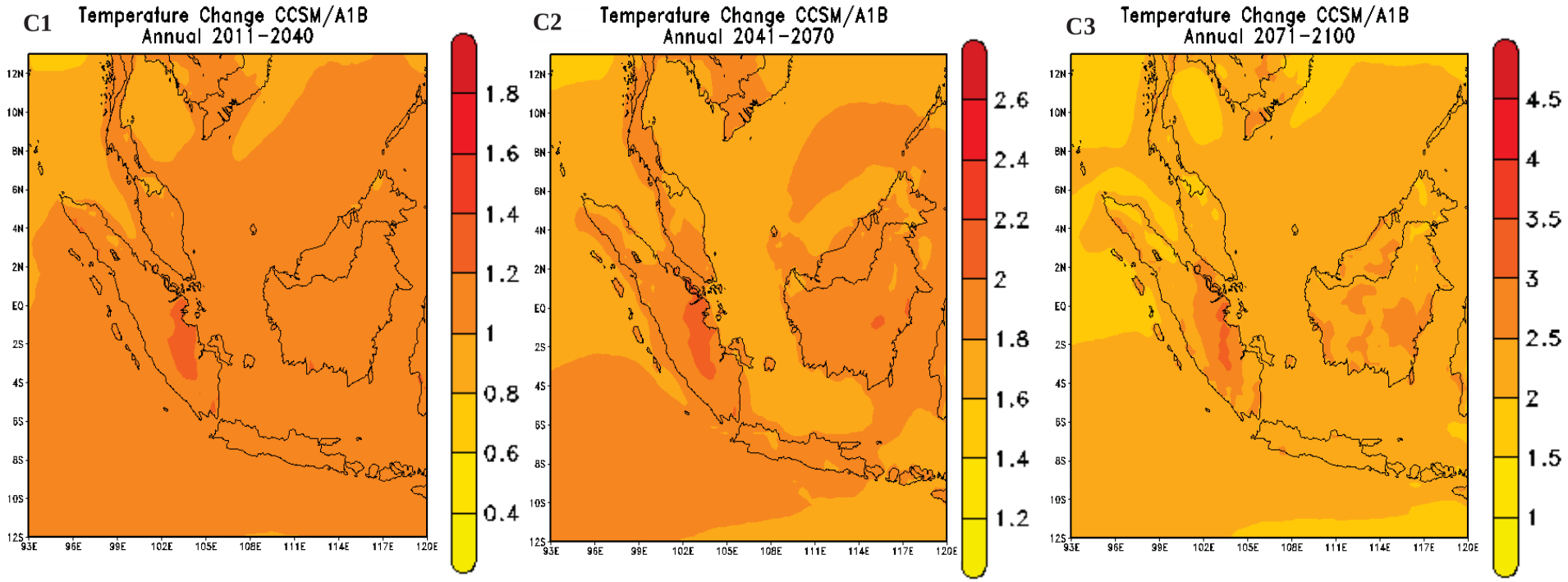

Figure 4.56: WRF/CCSM **A1B** Climate Response for Temperature (Absolute Anomaly in ºC) relative to 1961-1990
C1: 2011-2040, C2: 2041-2070, C3: 2071-2100 **Annual Change**

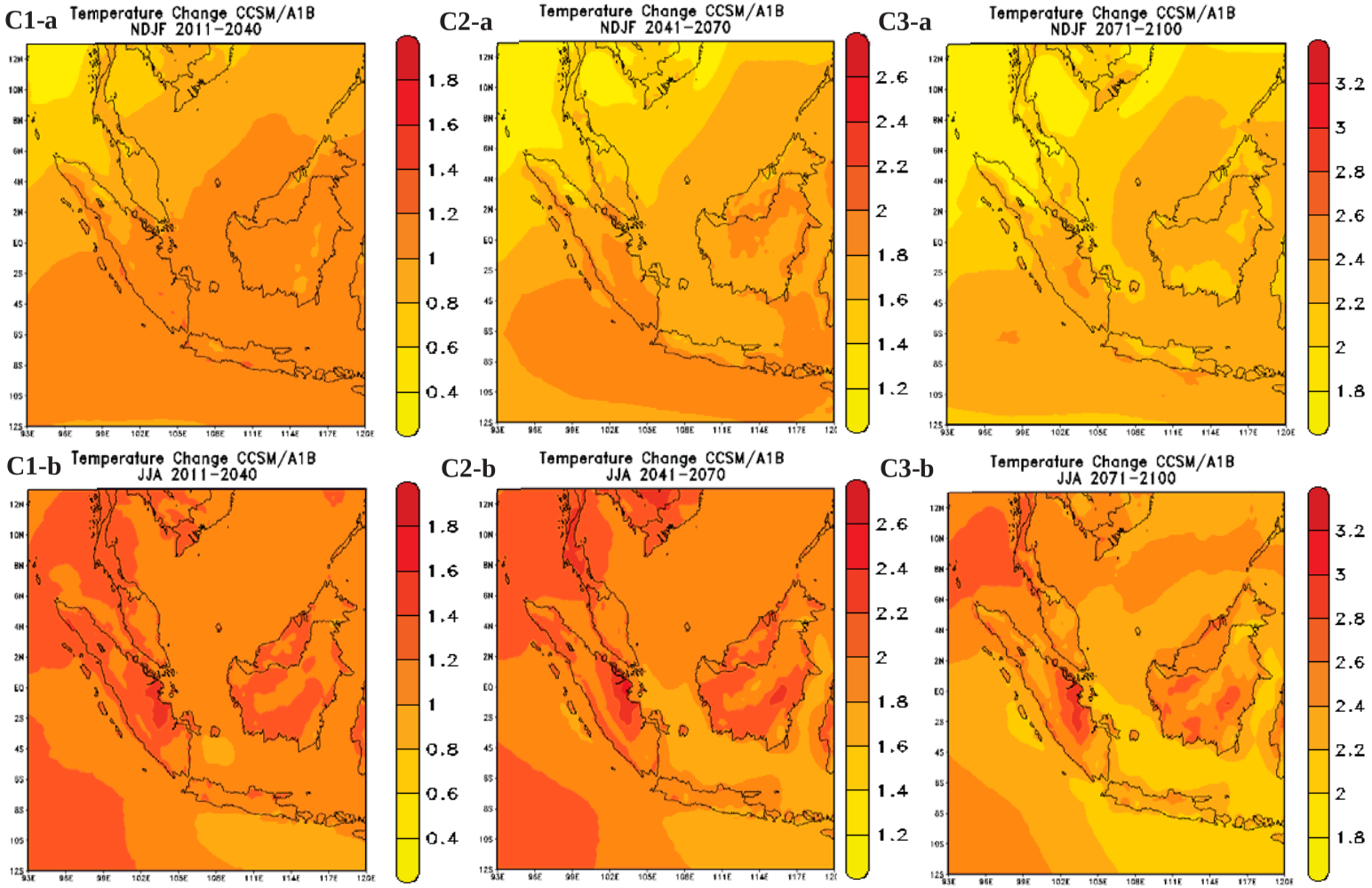

Figure 4.57: WRF/CCSM **A1B** Climate Response for Temperature (Absolute Anomaly in ºC) relative to 1961-1990
C1: 2011-2040, C2: 2041-2070, C3: 2071-2100 (a) **NDJF Change** (b) **JJA Change**

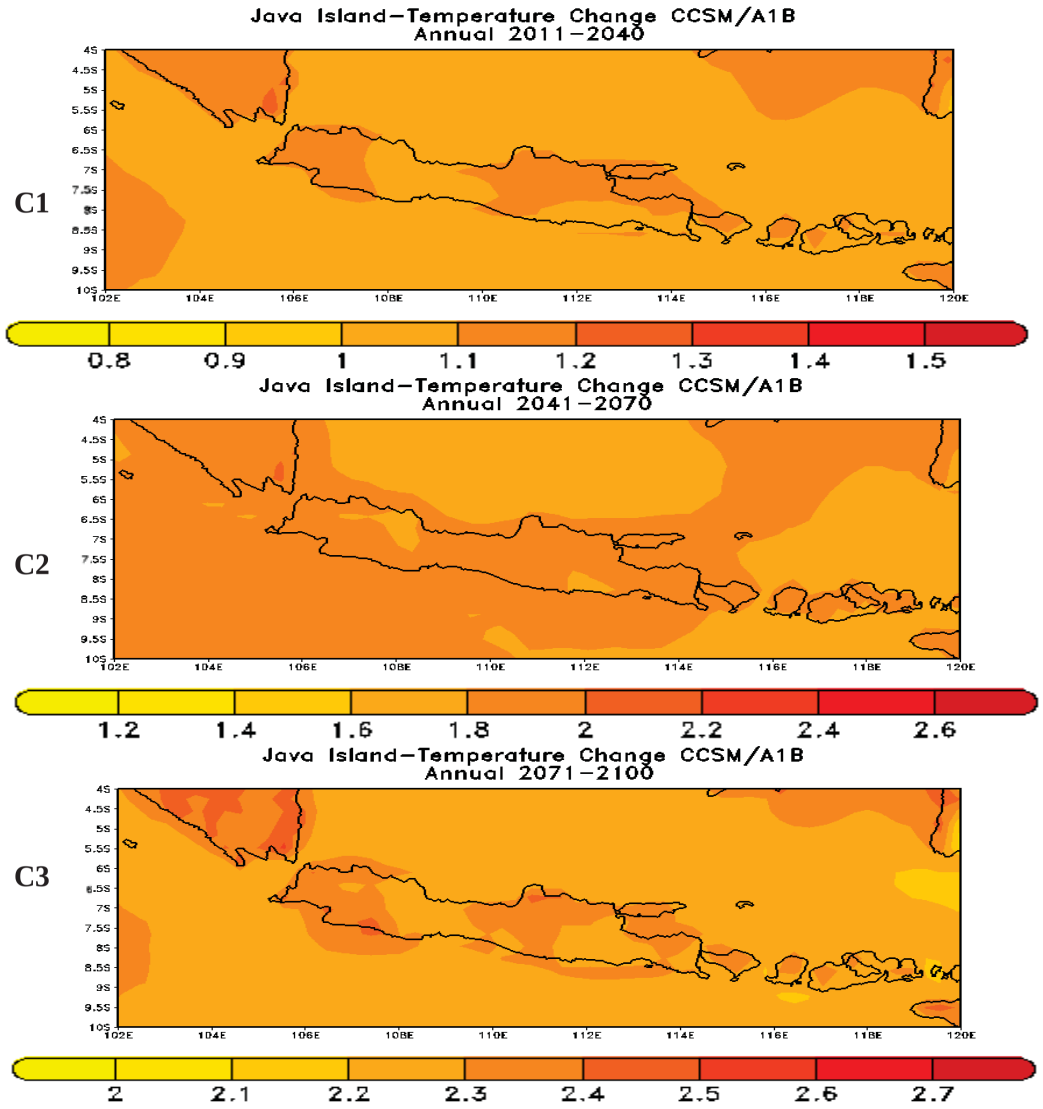

Figure 4.58: WRF/CCSM **A1B** Climate Response for Temperature (Absolute Anomaly in ºC) relative to 1961-1990, **Jakarta**
C1: 2011-2040, C2: 2041-2070, C3: 2071-2100 **Annual Change**

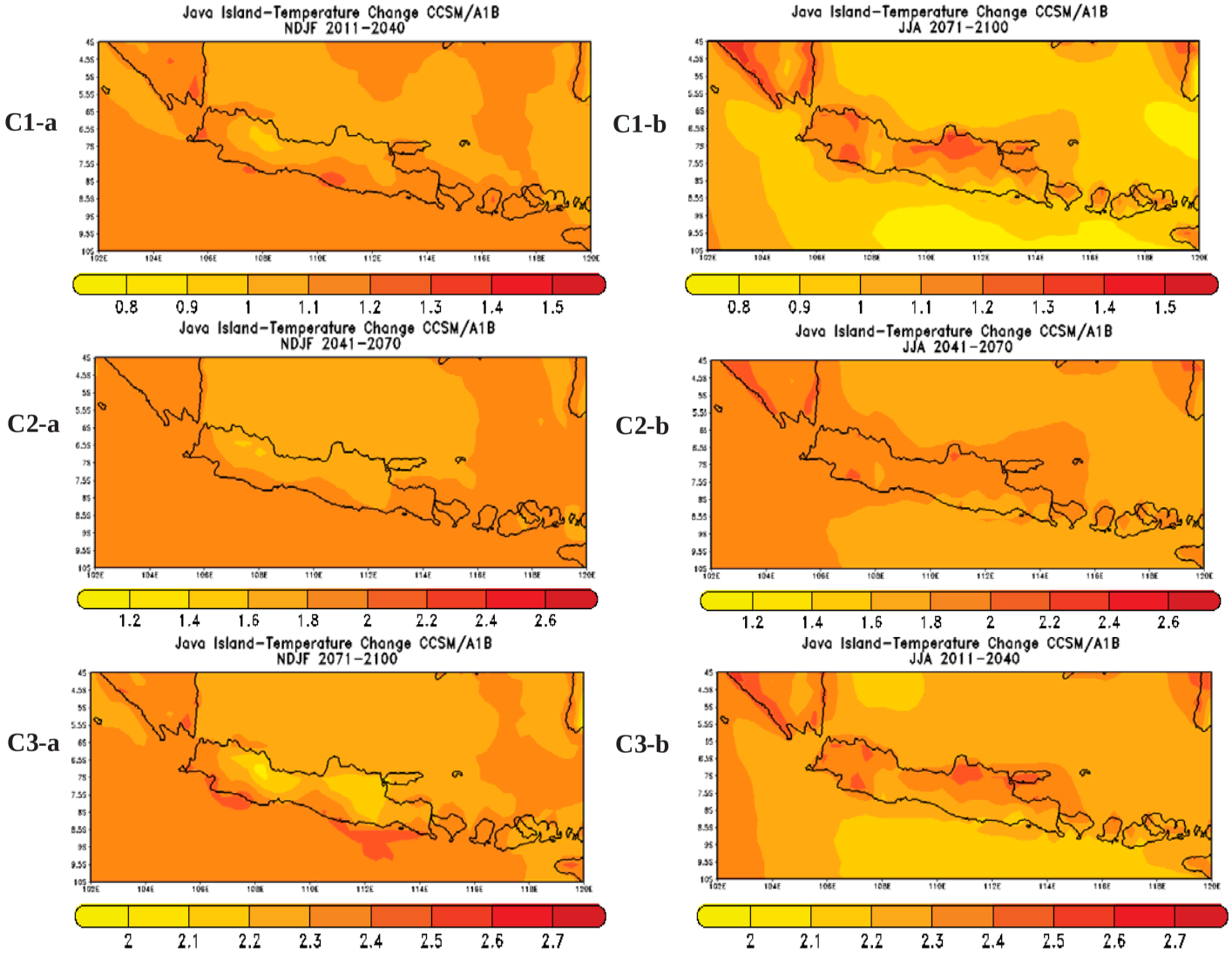

Figure 4.59: WRF/CCSM **A1B** Climate Response for Temperature (Absolute Anomaly in ºC) relative to 1961-1990, **Jakarta**
C1: 2011-2040, C2: 2041-2070, C3: 2071-2100 (a) **NDJF Change** (b) **JJA Change**

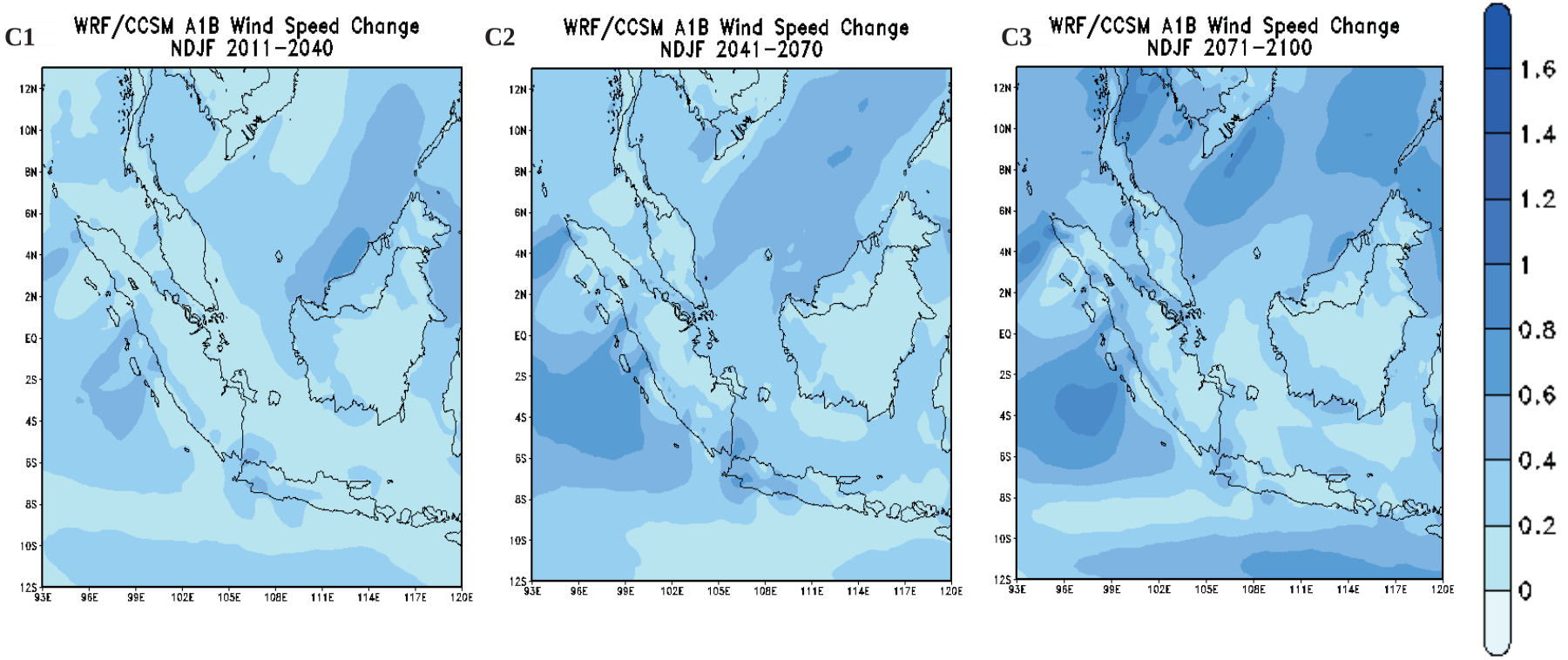

Figure 4.60: WRF/CCSM **A1B** Climate Response for **NDJF** Wind Speed Change (Absolute Anomaly in m/s) relative to 1961-1990
C1: 2011-2040, C2: 2041-2070, C3: 2071-2100

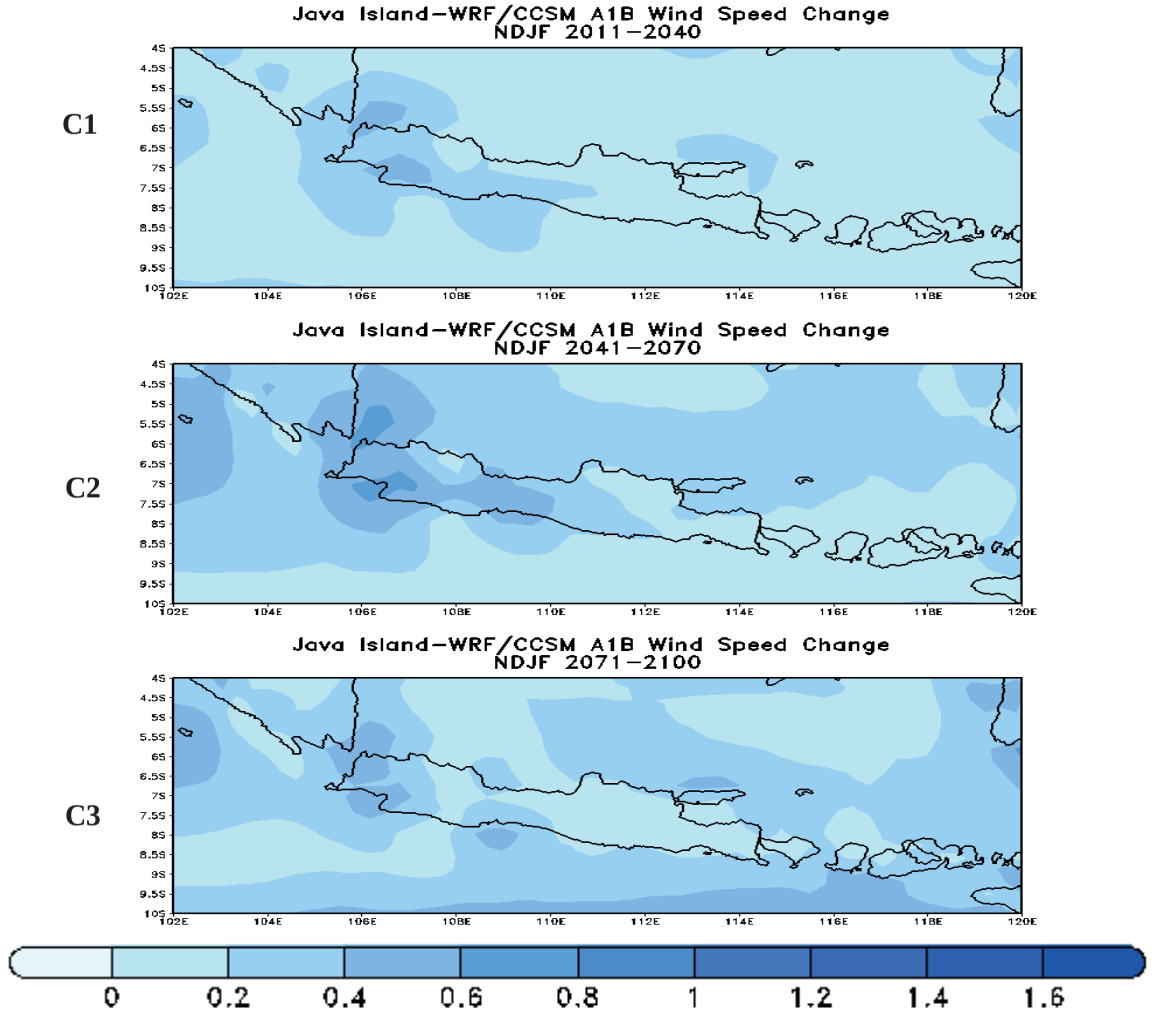

Figure 4.61: WRF/CCSM **A1B** Climate Response for **NDJF** Wind Speed Change (Absolute Anomaly in m/s) relative to 1961-1990
C1: 2011-2040, C2: 2041-2070, C3: 2071-2100: **Jakarta**

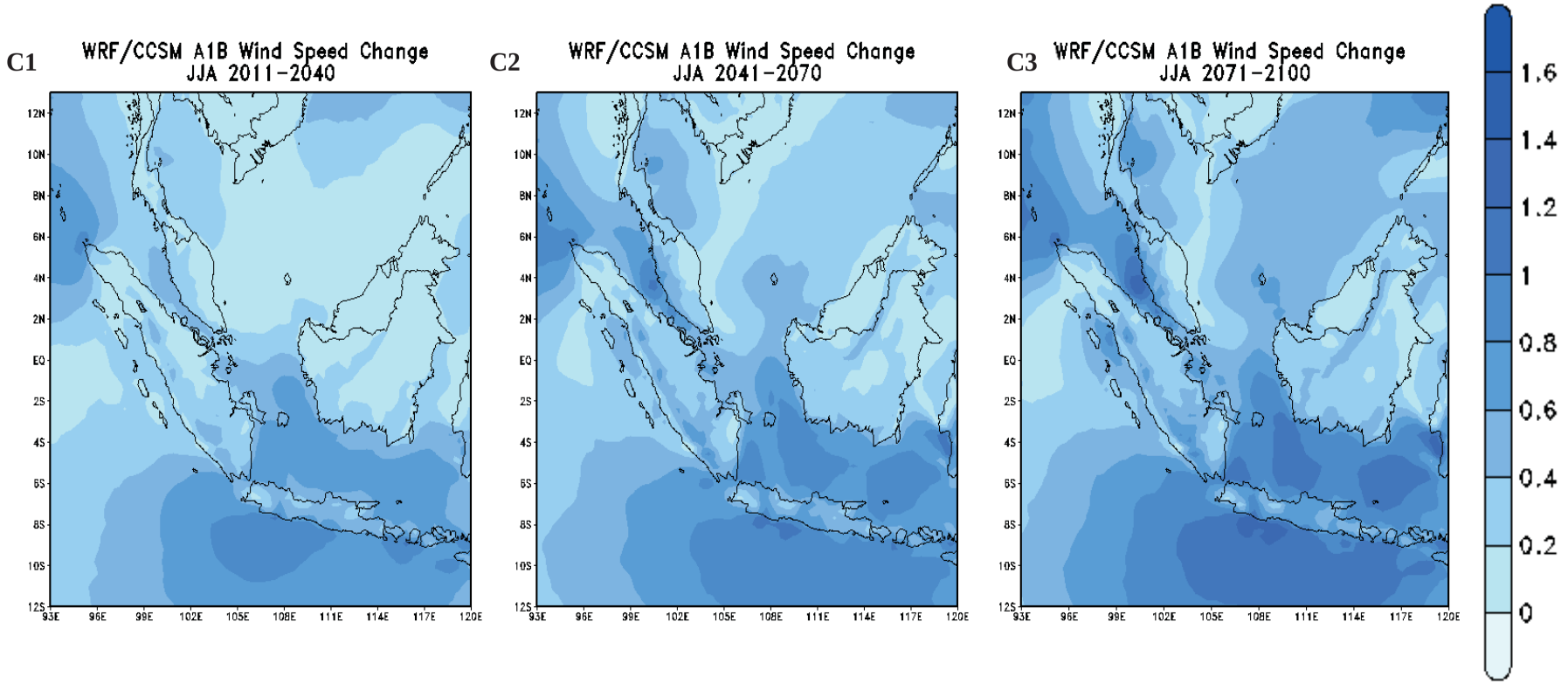

Figure 4.62: WRF/CCSM **A1B** Climate Response for **JJA** Wind Speed Change (Absolute Anomaly in m/s) relative to 1961-1990
C1: 2011-2040, C2: 2041-2070, C3: 2071-2100

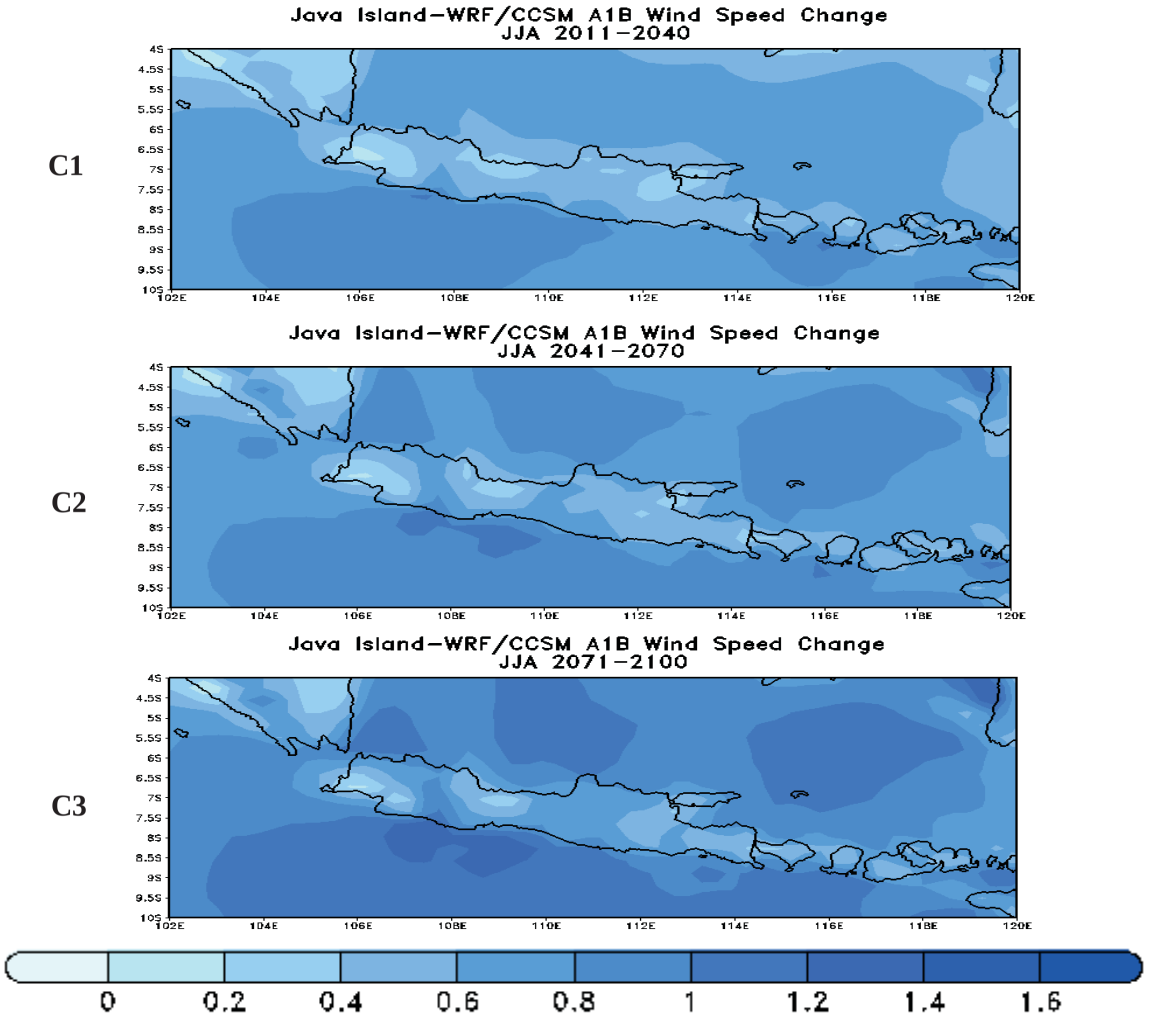

Figure 4.63: WRF/CCSM **A1B** Climate Response for **JJA** Wind Speed Change (Absolute Anomaly in m/s) relative to 1961-1990
C1: 2011-2040, C2: 2041-2070, C3: 2071-2100: **Jakarta**

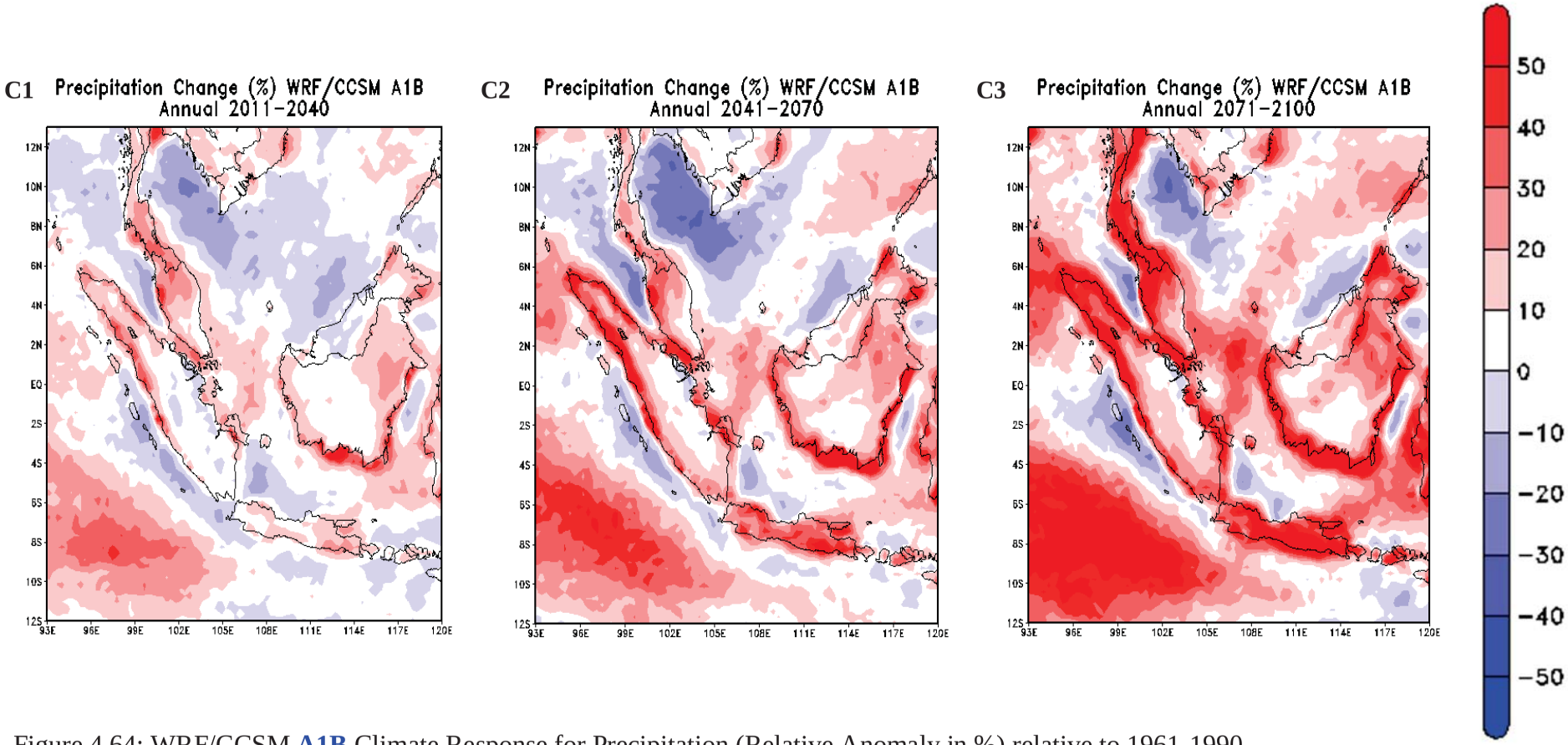

Figure 4.64: WRF/CCSM **A1B** Climate Response for Precipitation (Relative Anomaly in %) relative to 1961-1990
C1: 2011-2040, C2: 2041-2070, C3: 2071-2100 **Annual Change**

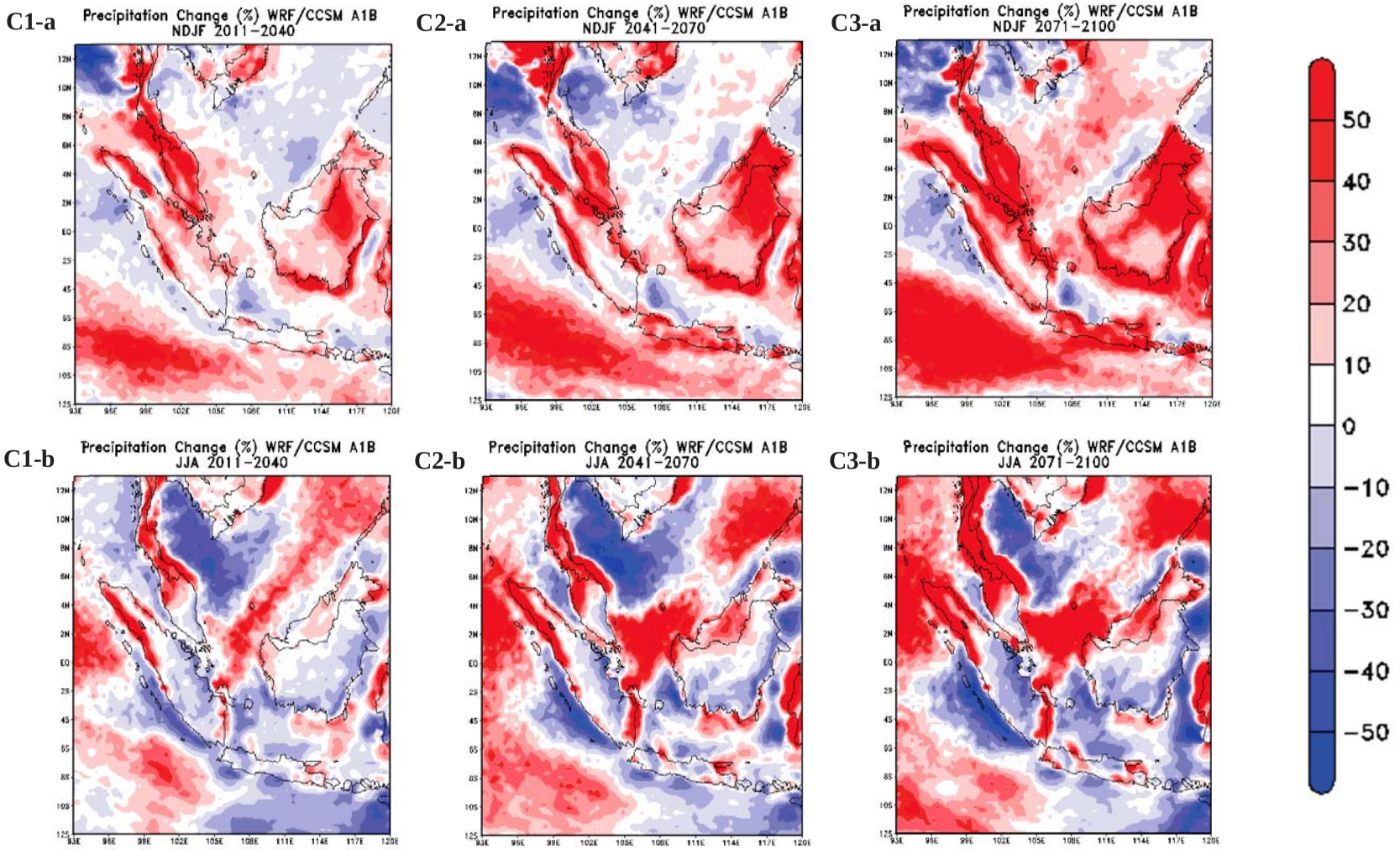

Figure 4.65: WRF/CCSM **A1B** Climate Response for Precipitation (Relative Anomaly in %) relative to 1961-1990
C1: 2011-2040, C2: 2041-2070, C3: 2071-2100 (a) **NDJF Change** (b) **JJA Change**

C1

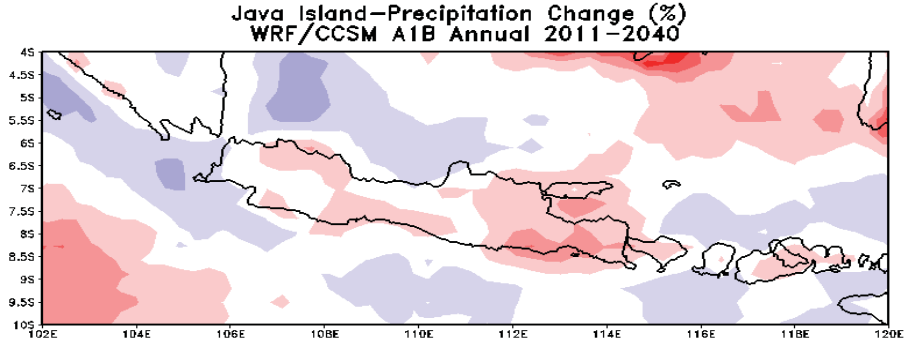

C2

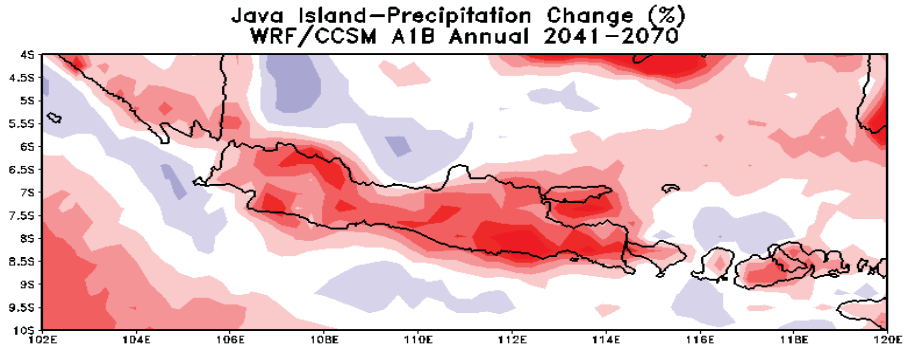

C3

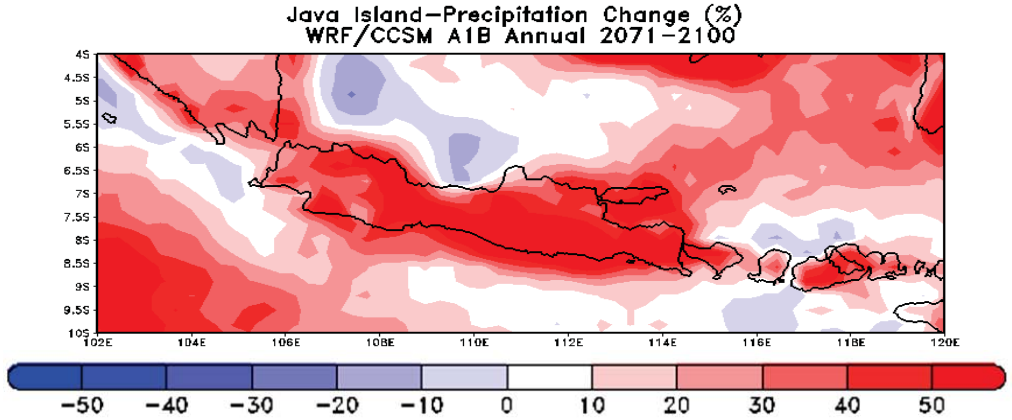

Figure 4.66: WRF/CCSM **A1B** Climate Response for Precipitation (Relative Anomaly in %) relative to 1961-1990, **Jakarta**
C1: 2011-2040, C2: 2041-2070, C3: 2071-2100 **Annual Change**

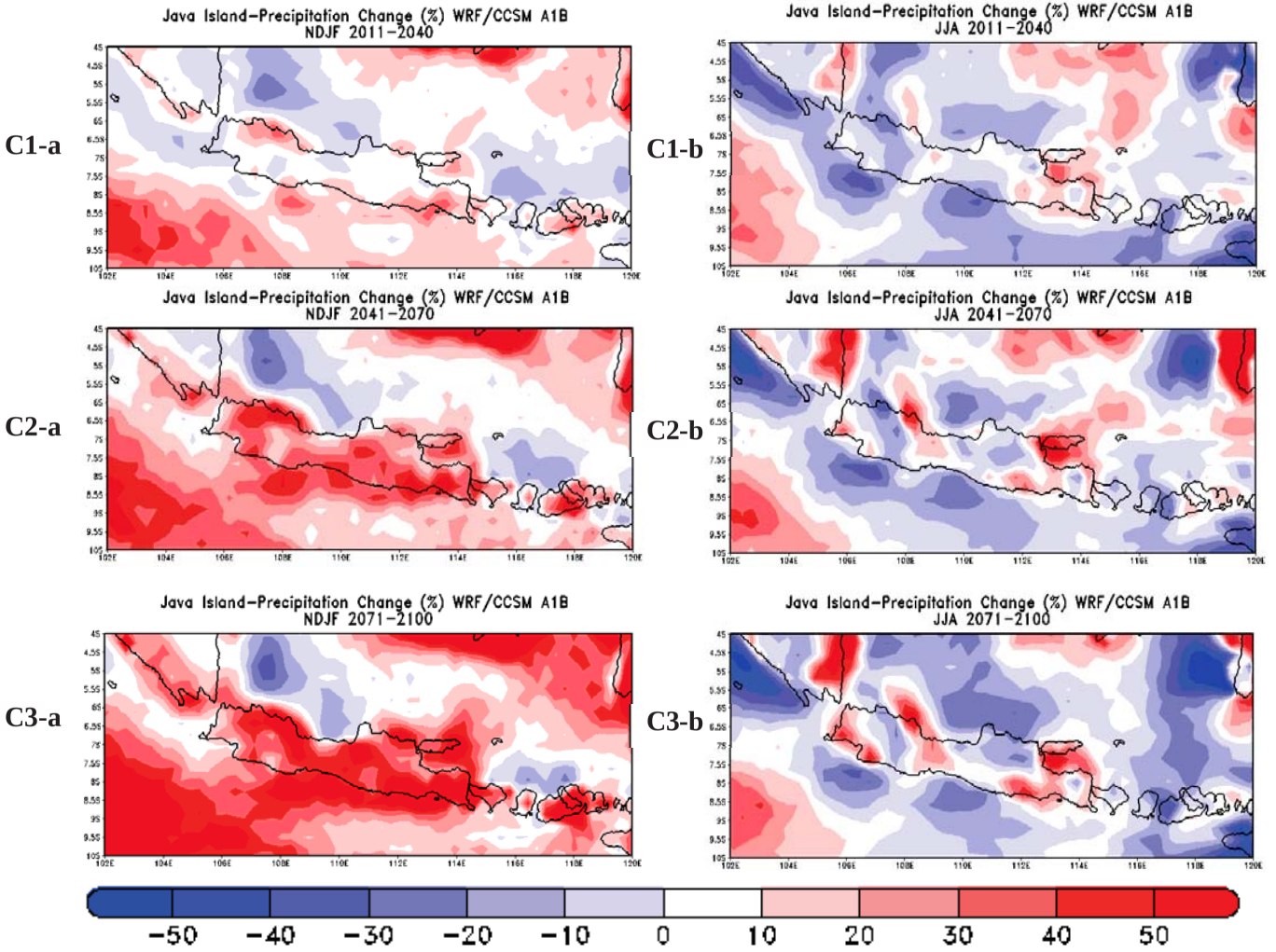

Figure 4.67: WRF/CCSM **A1B** Climate Response for Precipitation (Relative Anomaly in %) relative to 1961-1990, **Jakarta**
C1: 2011-2040, C2: 2041-2070, C3: 2071-2100 (a) **NDJF Change** (b) **JJA Change**

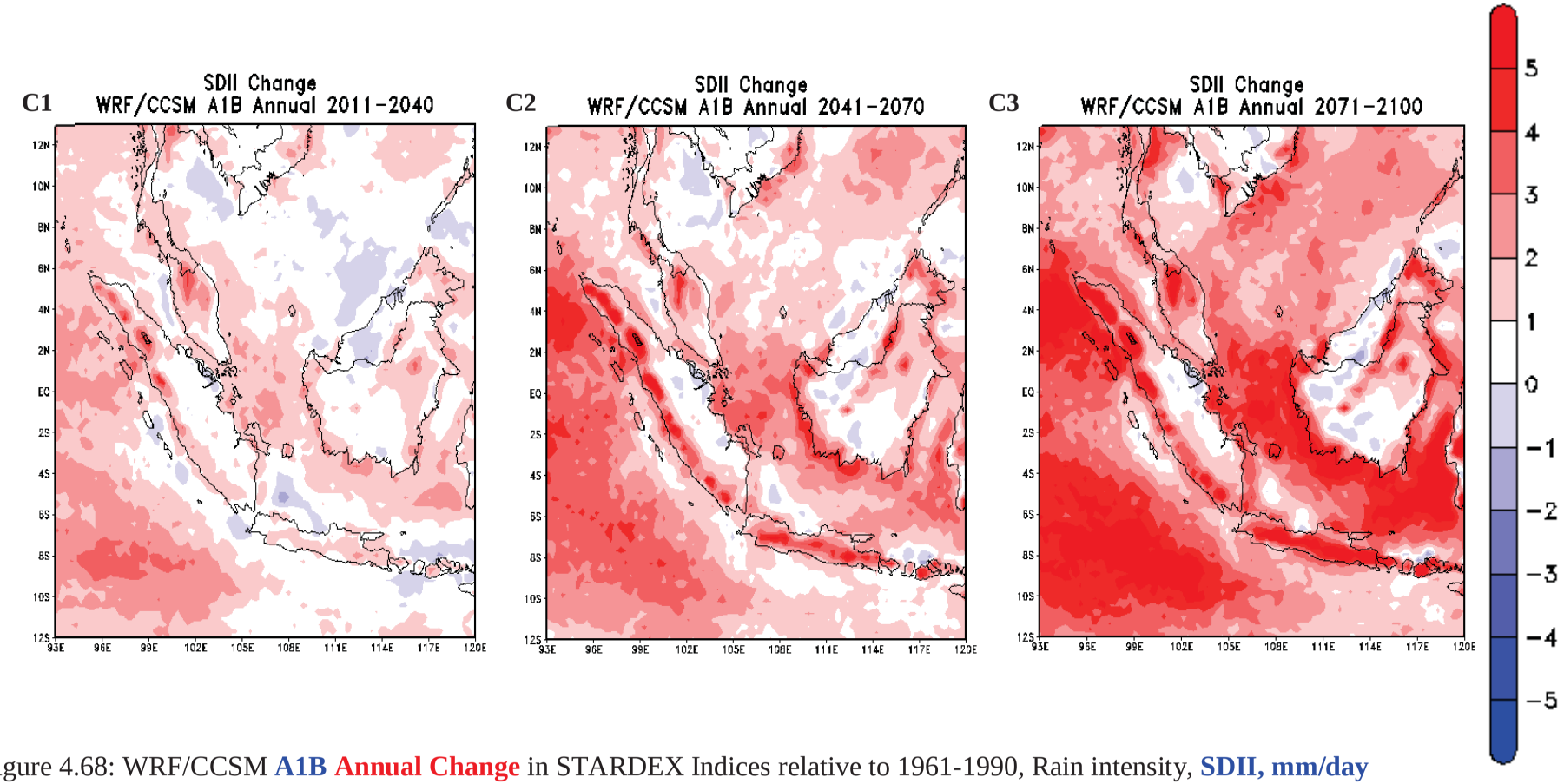

Figure 4.68: WRF/CCSM **A1B Annual Change** in STARDEX Indices relative to 1961-1990, Rain intensity, **SDII, mm/day**
C1: 2011-2040, C2: 2041-2070, C3: 2071-2100

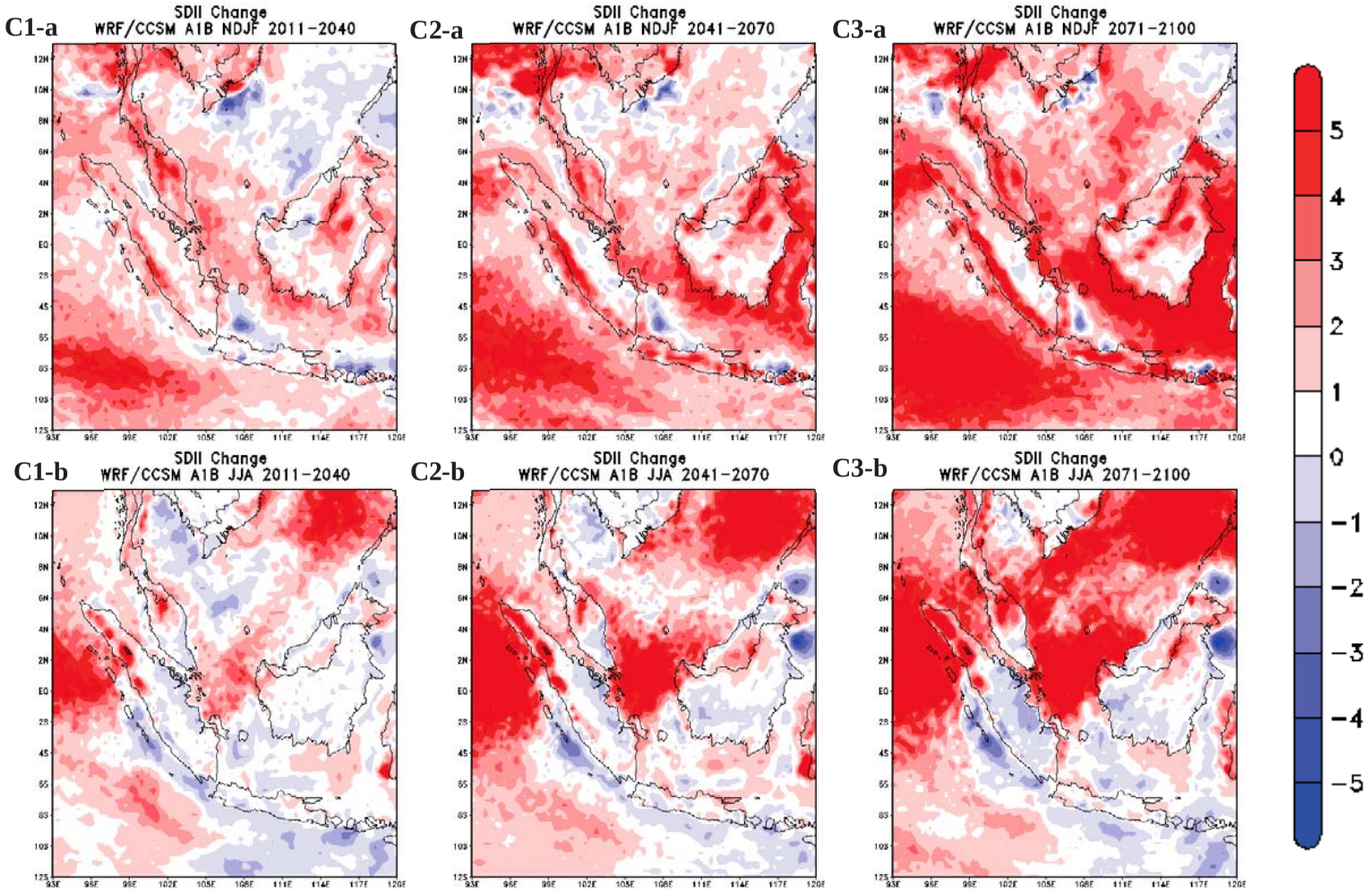

Figure 4.69: WRF/CCSM **A1B** STARDEX Indices relative to 1961-1990, Rain intensity, **SDII, mm/day**
C1: 2011-2040, C2: 2041-2070, C3: 2071-2100 (a) **NDJF Change** (b) **JJA Change**

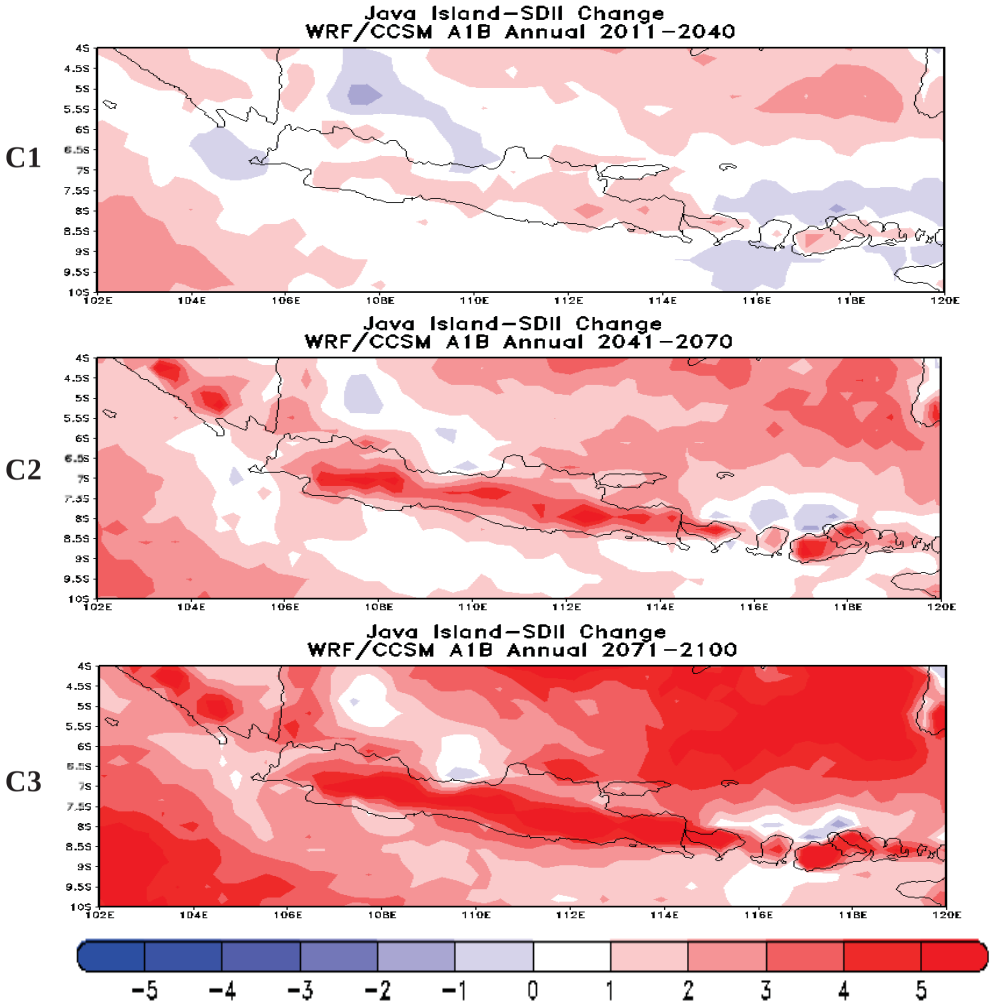

Figure 4.70: WRF/CCSM **A1B** STARDEX Indices relative to 1961-1990, Rain intensity, **SDII, mm/day**, **Jakarta**
C1: 2011-2040, C2: 2041-2070, C3: 2071-2100 **Annual Change**

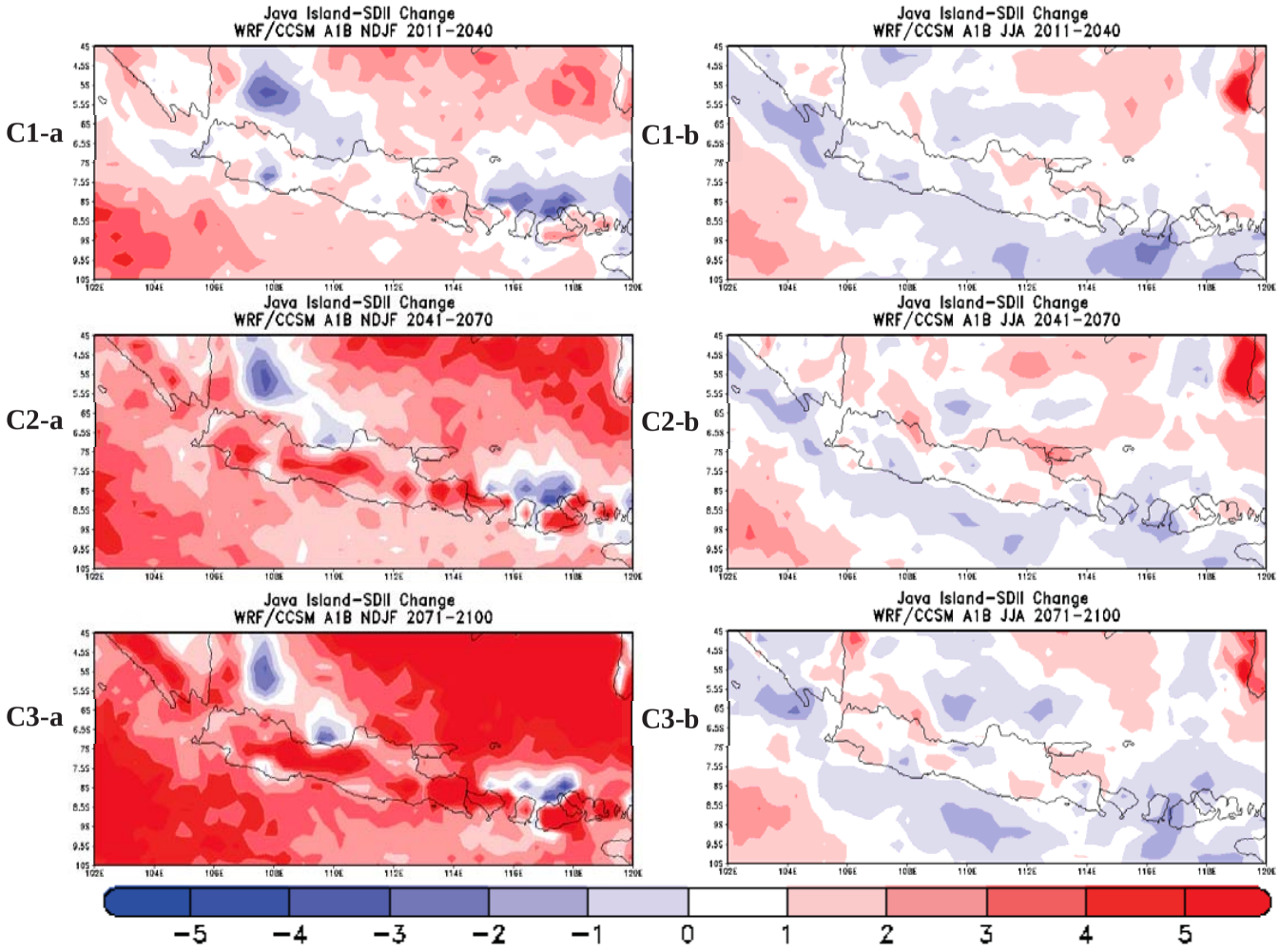

Figure 4.71: WRF/CCSM **A1B** STARDEX Indices relative to 1961-1990, Rain intensity, **SDII, mm/day, Jakarta**
C1: 2011-2040, C2: 2041-2070, C3: 2071-2100 (a) **NDJF Change** (b) **JJA Change**

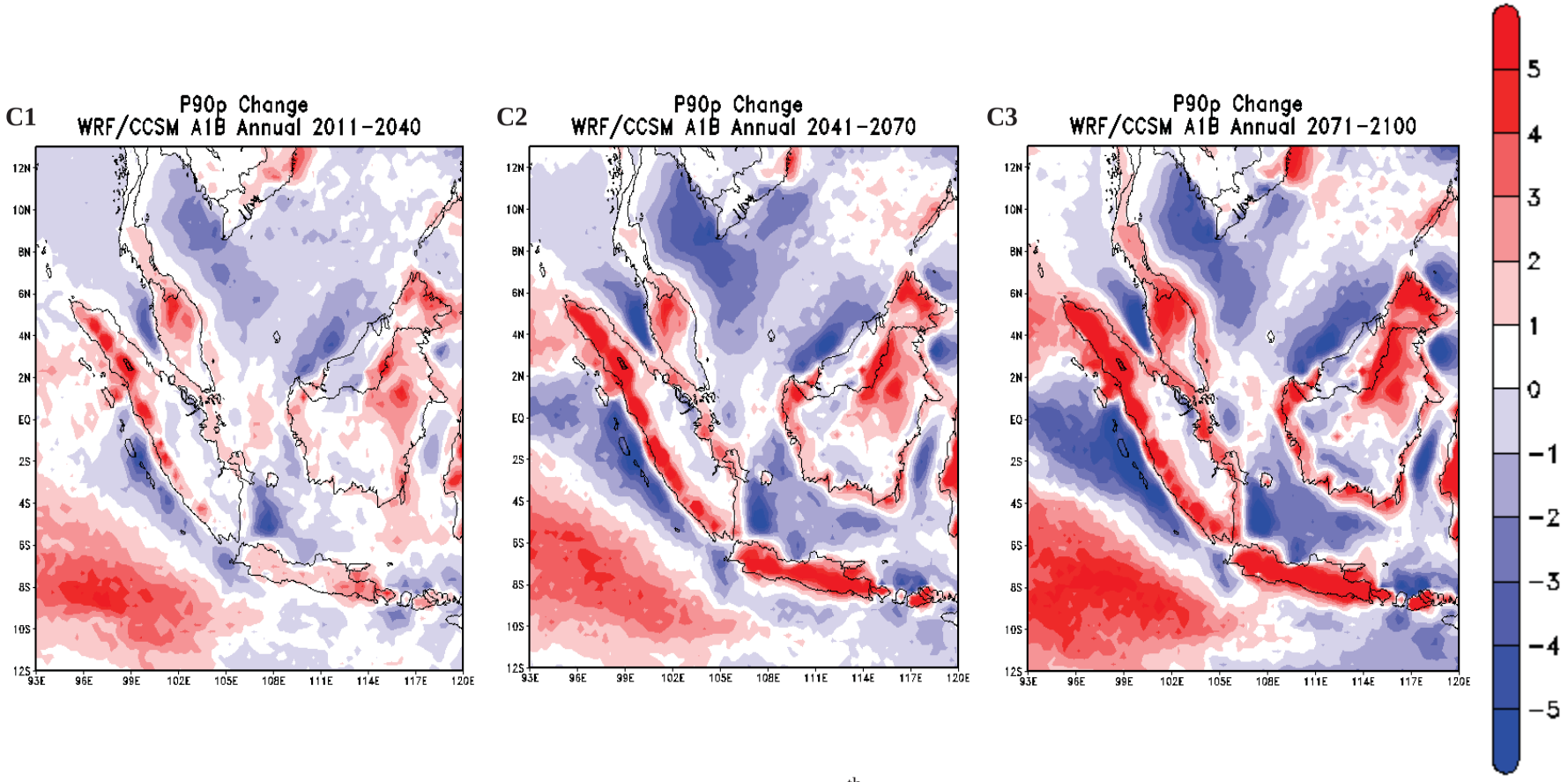

Figure 4.72: WRF/CCSM **A1B** STARDEX Indices relative to 1961-1990, 90th percentile of rain amounts, **P90p, mm/day**
C1: 2011-2040, C2: 2041-2070, C3: 2071-2100 **Annual Change**

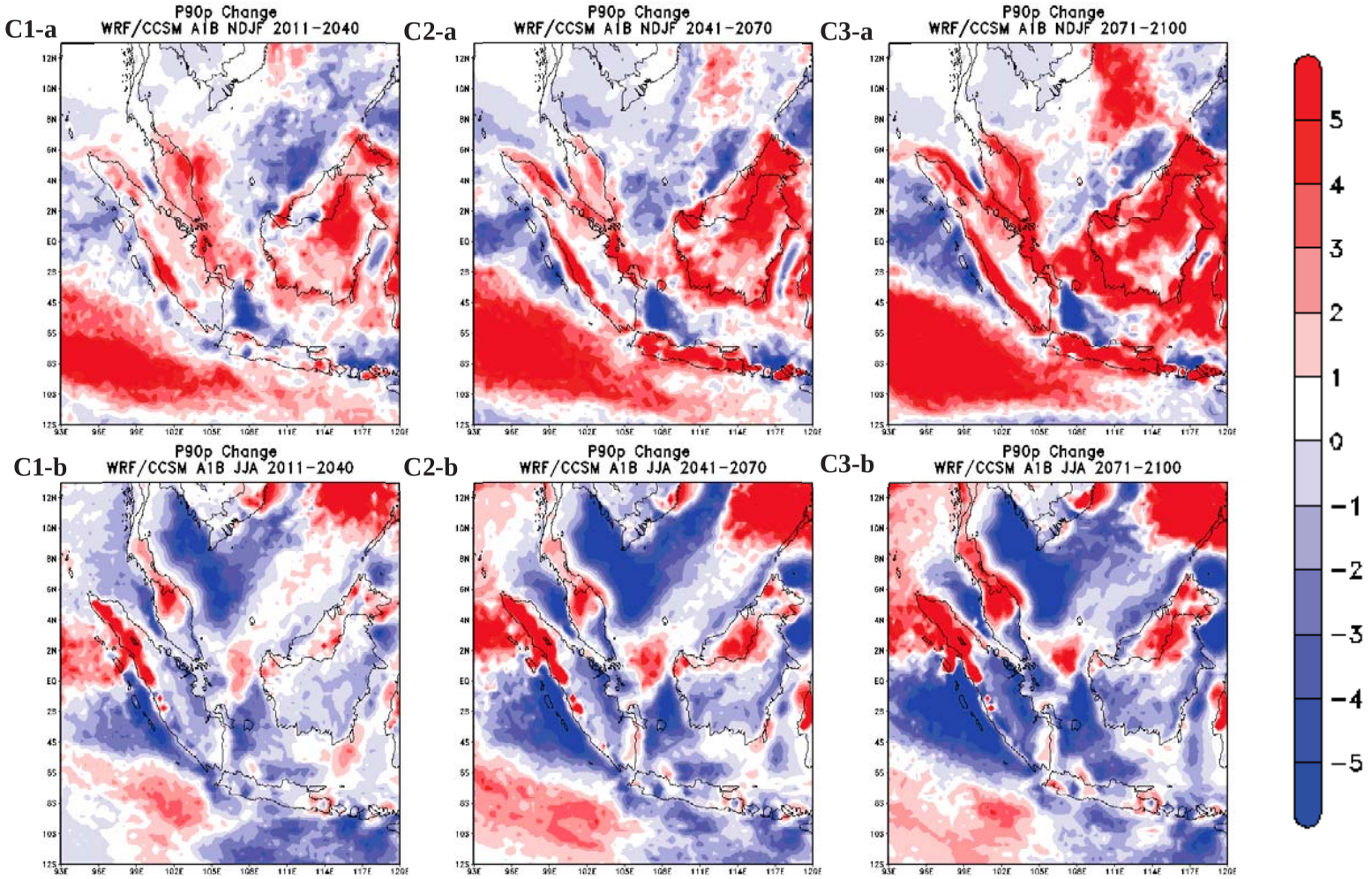

Figure 4.73: WRF/CCSM **A1B** STARDEX Indices relative to 1961-1990, 90th percentile of rain amounts, **P90p, mm/day**
C1: 2011-2040, C2: 2041-2070, C3: 2071-2100 (a) **NDJF Change** (b) **JJA Change**

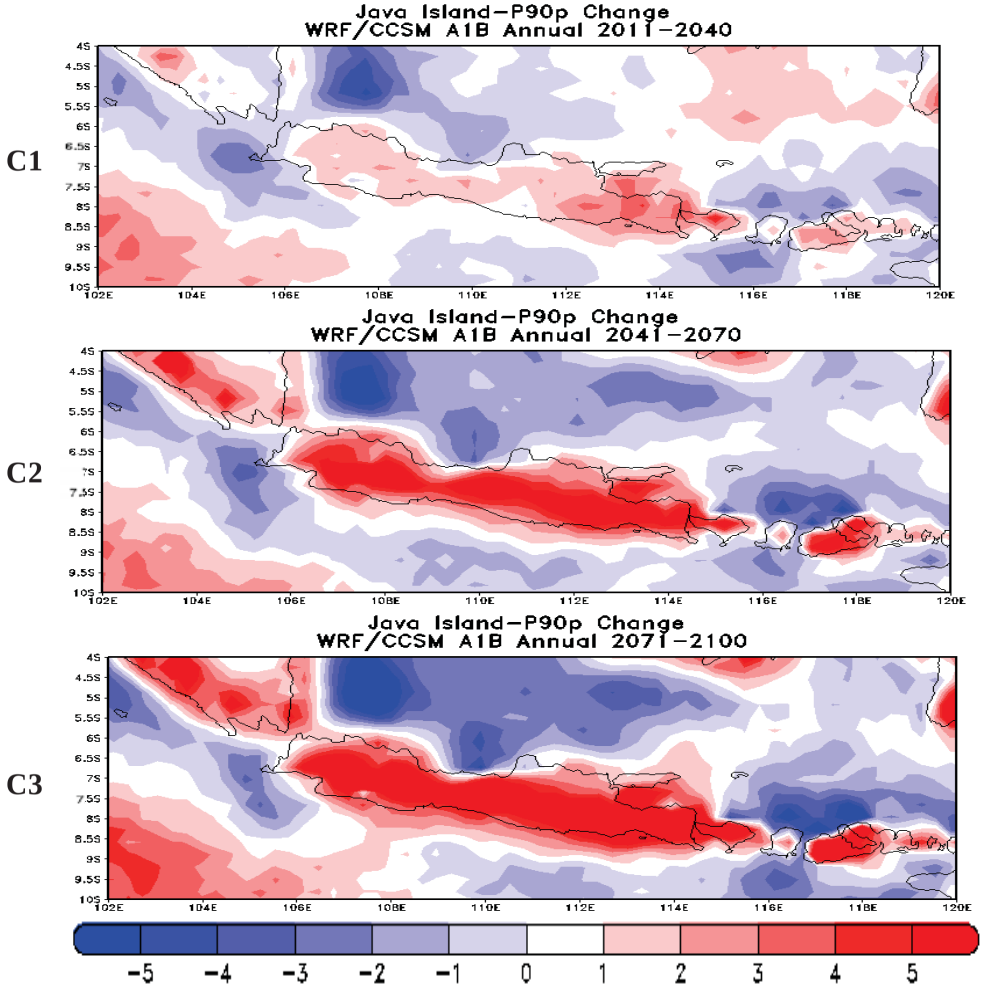

Figure 4.74: WRF/CCSM **A1B** STARDEX Indices relative to 1961-1990, 90th percentile of rain amounts, **P90p, mm/day, Jakarta**
C1: 2011-2040, C2: 2041-2070, C3: 2071-2100 **Annual Change**

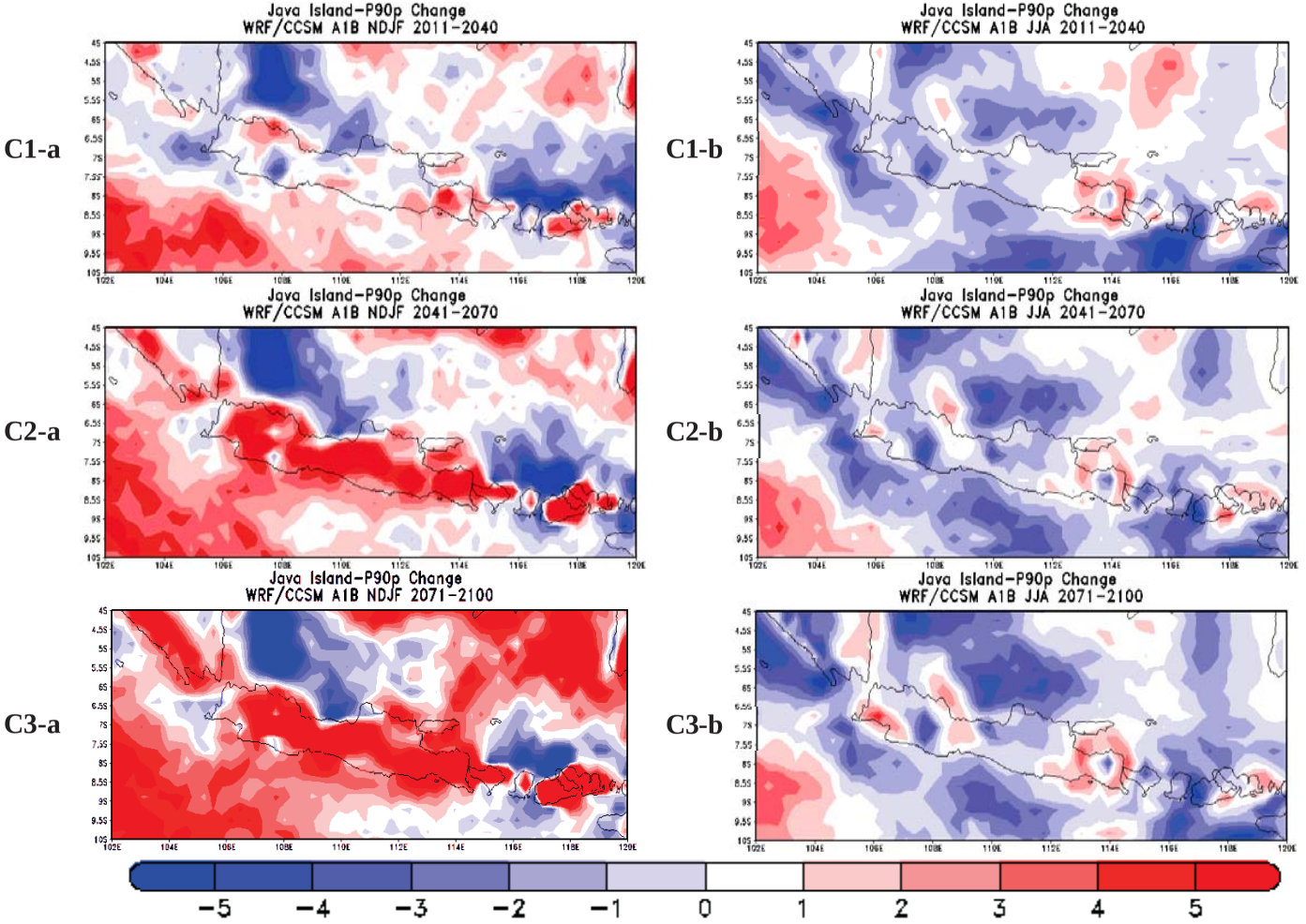

Figure 4.75: WRF/CCSM **A1B** STARDEX Indices relative to 1961-1990, 90th percentile of rain amounts, **P90p, mm/day**, **Jakarta**
C1: 2011-2040, C2: 2041-2070, C3: 2071-2100 (a) **NDJF Change** (b) **JJA Change**

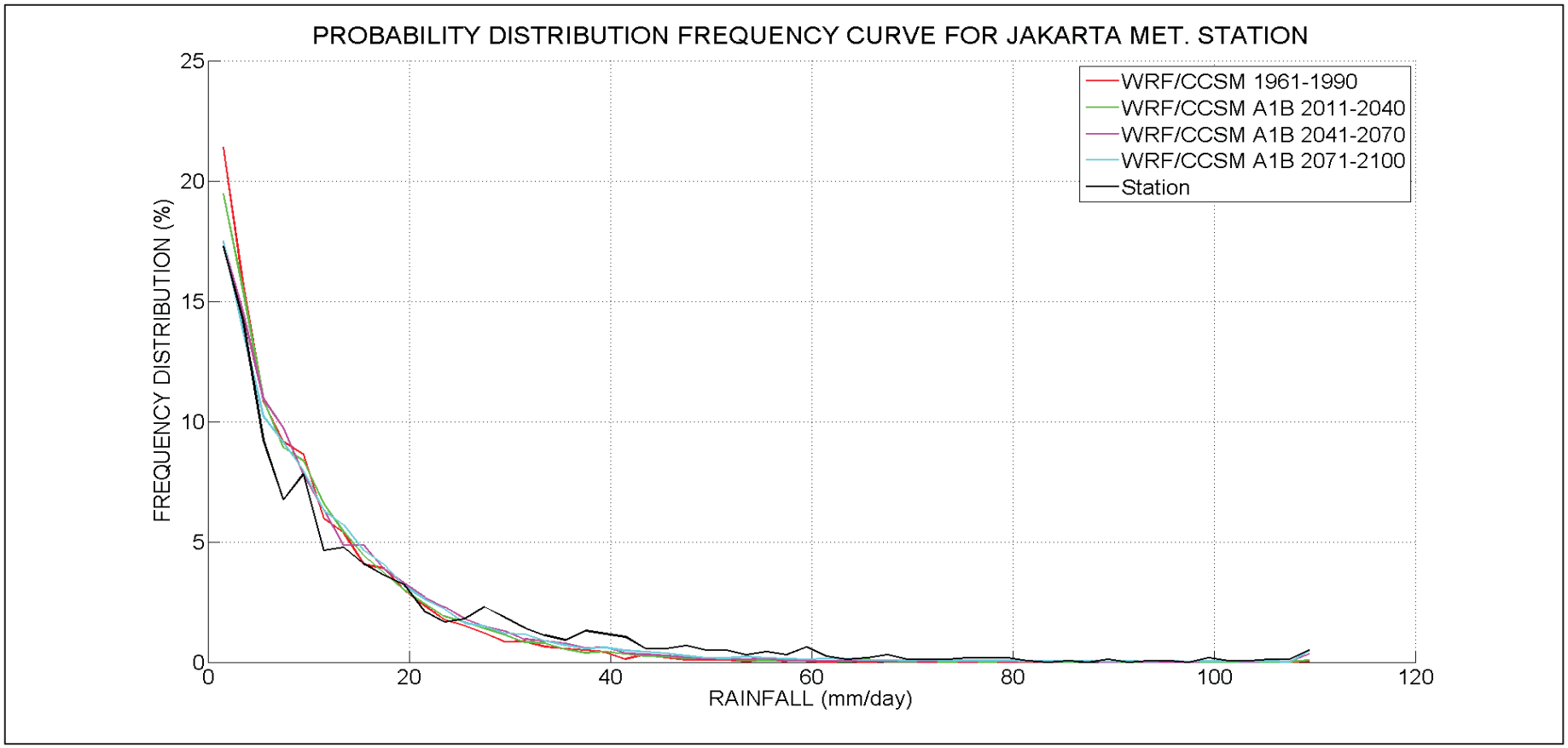

Figure 4.76: Precipitation Probability Density Function (PDF) for **WRF/CCSM (2011-2100) A1B scenario**

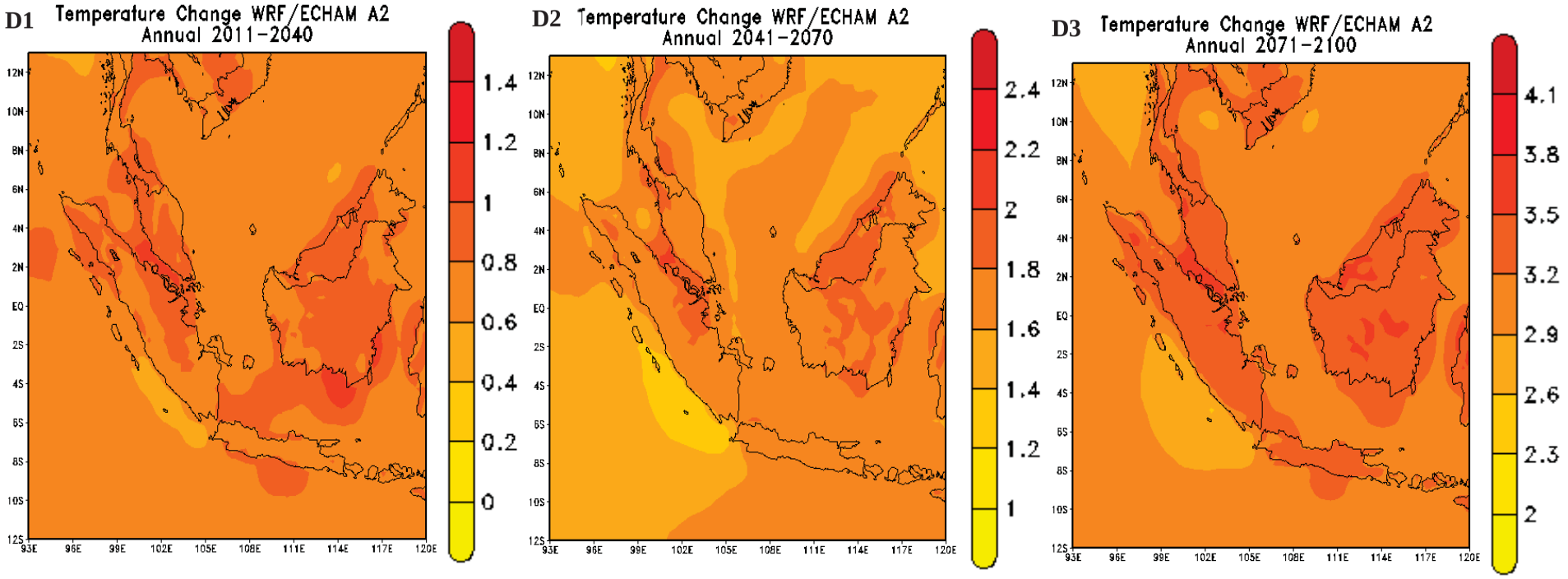

Figure 4.77: WRF/ECHAM **A2** Climate Response for Temperature (Absolute Anomaly in ºC) relative to 1961-1990
D1: 2011-2040, D2: 2041-2070, D3: 2071-2100 **Annual Change**

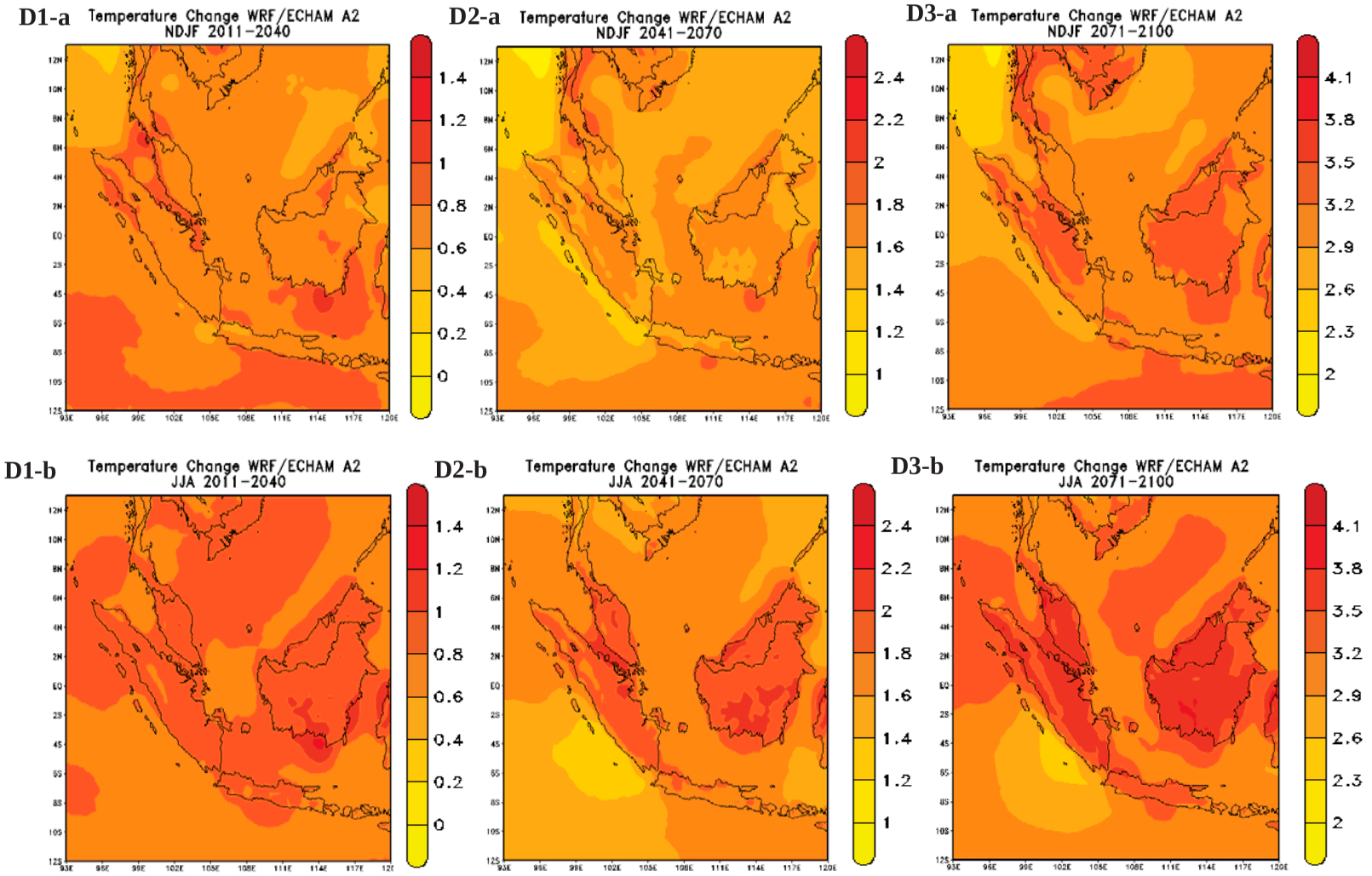

Figure 4.78: WRF/ECHAM **A2** Climate Response for Temperature (Absolute Anomaly in ºC) relative to 1961-1990
D1: 2011-2040, D2: 2041-2070, D3: 2071-2100 (a) **NDJF Change** (b) **JJA Change**

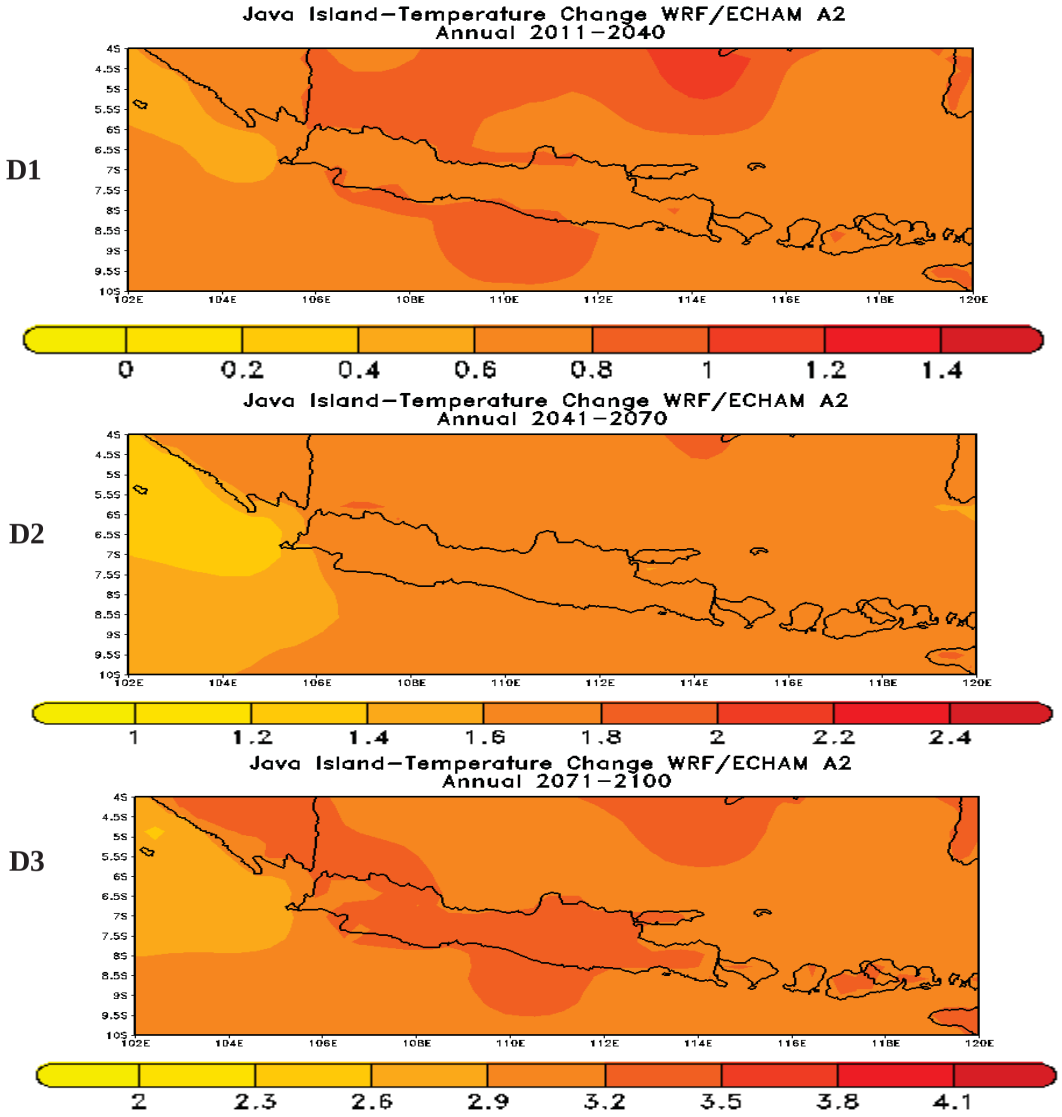

Figure 4.79: WRF/ECHAM **A2** Climate Response for Temperature (Absolute Anomaly in ºC) relative to 1961-1990, **Jakarta**
D1: 2011-2040, D2: 2041-2070, D3: 2071-2100 **Annual Change**

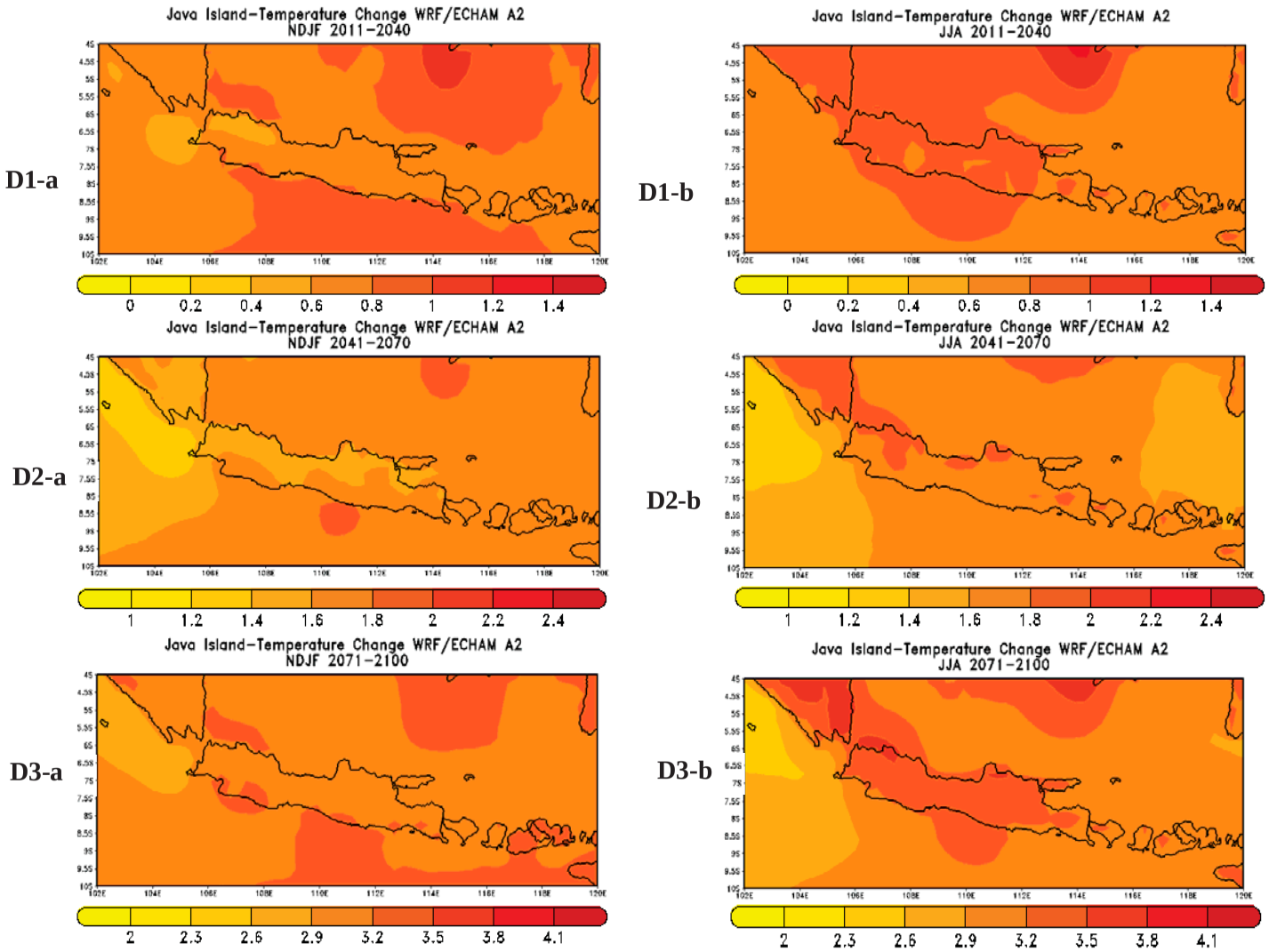

Figure 4.80: WRF/ECHAM **A2** Climate Response for Temperature (Absolute Anomaly in ºC) relative to 1961-1990, **Jakarta**
D1: 2011-2040, D2: 2041-2070, D3: 2071-2100 (a) **NDJF Change** (b) **JJA Change**

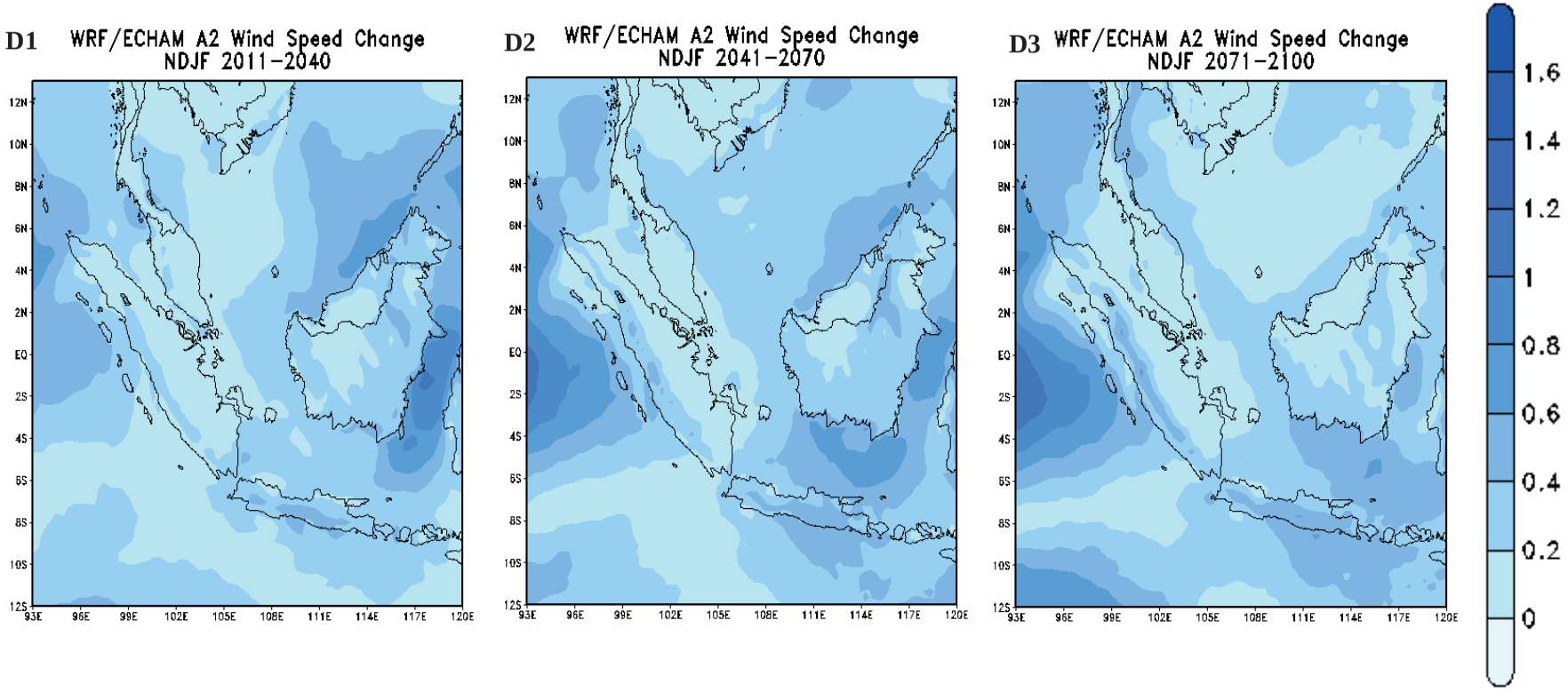

Figure 4.81: WRF/ECHAM **A2** Climate Response for **NDJF** Wind Speed Change (Absolute Anomaly in m/s) relative to 1961-1990
D1: 2011-2040, D2: 2041-2070, D3: 2071-2100

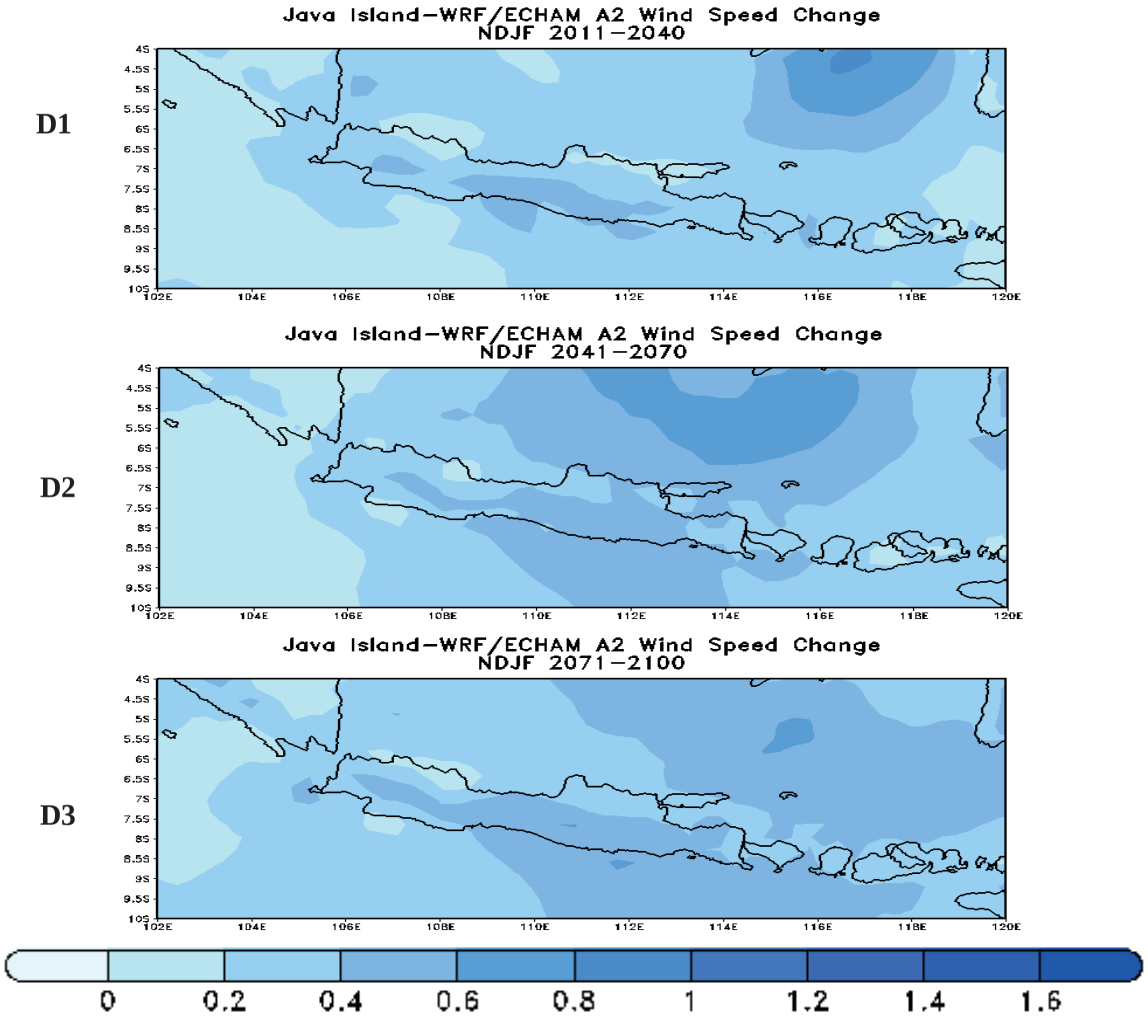

Figure 4.82: WRF/ECHAM **A2** Climate Response for **NDJF** Wind Speed Change (Absolute Anomaly in m/s) relative to 1961-1990
D1: 2011-2040, D2: 2041-2070, D3: 2071-2100: **Jakarta**

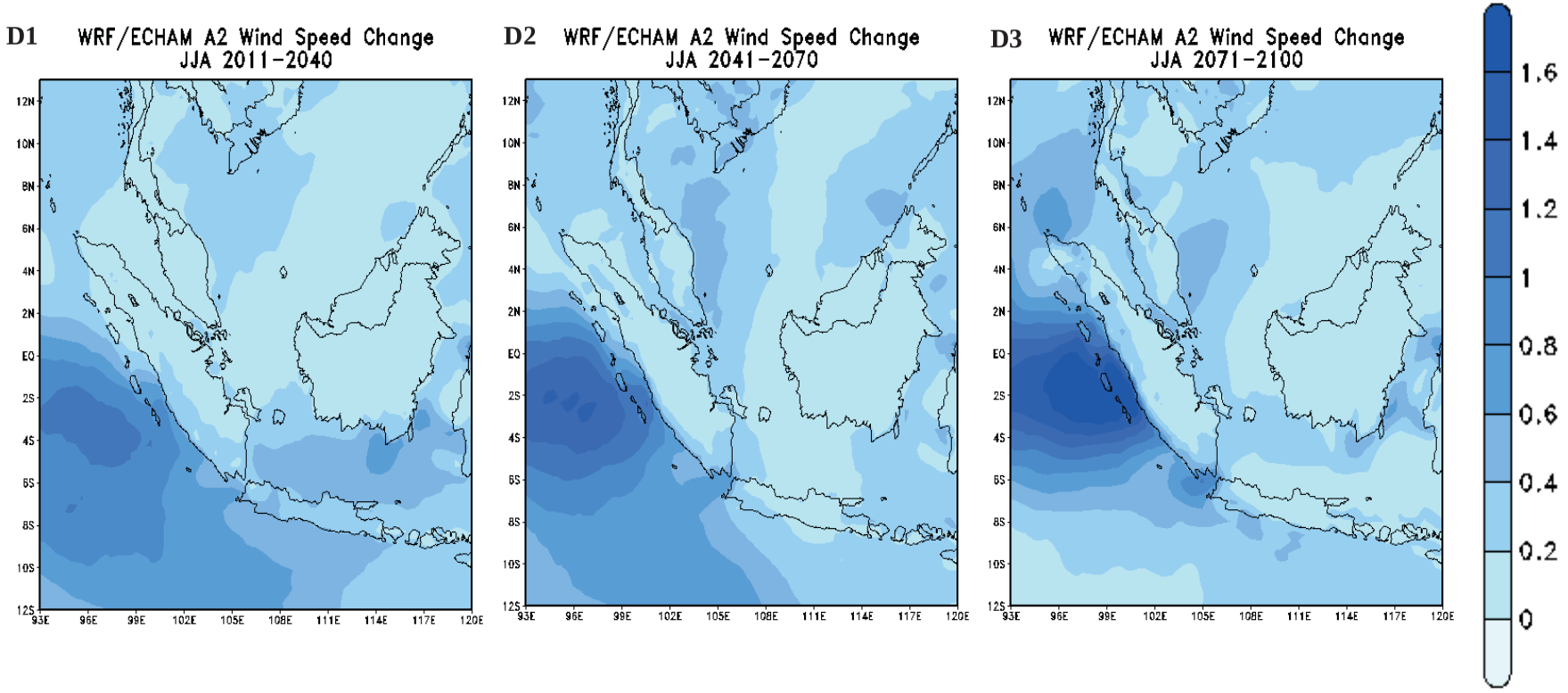

Figure 4.83: WRF/ECHAM **A2** Climate Response for **JJA** Wind Speed Change (Absolute Anomaly in m/s) relative to 1961-1990
D1: 2011-2040, D2: 2041-2070, D3: 2071-2100

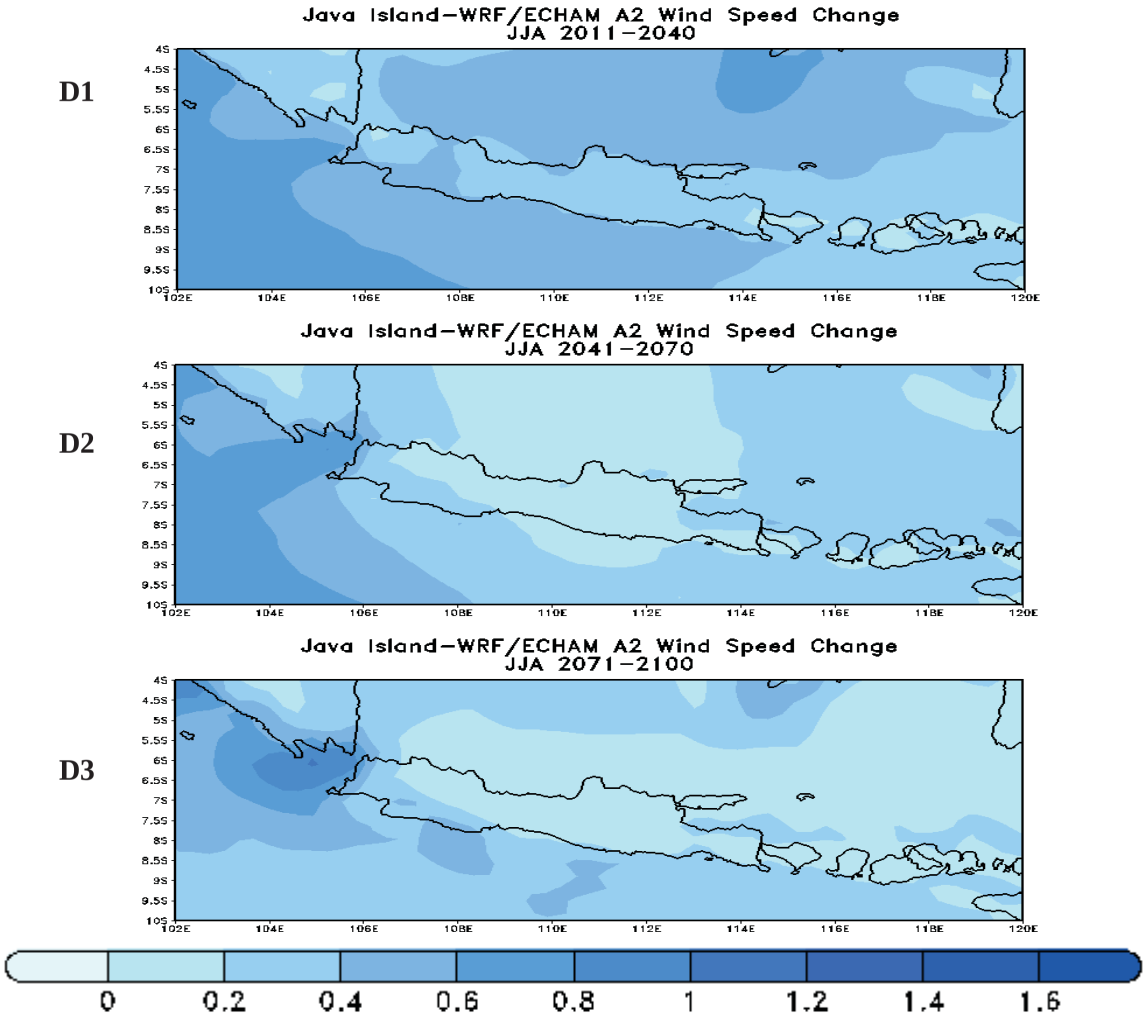

Figure 4.84: WRF/ECHAM **A2** Climate Response for **JJA** Wind Speed Change (Absolute Anomaly in m/s) relative to 1961-1990
D1: 2011-2040, D2: 2041-2070, D3: 2071-2100: **Jakarta**

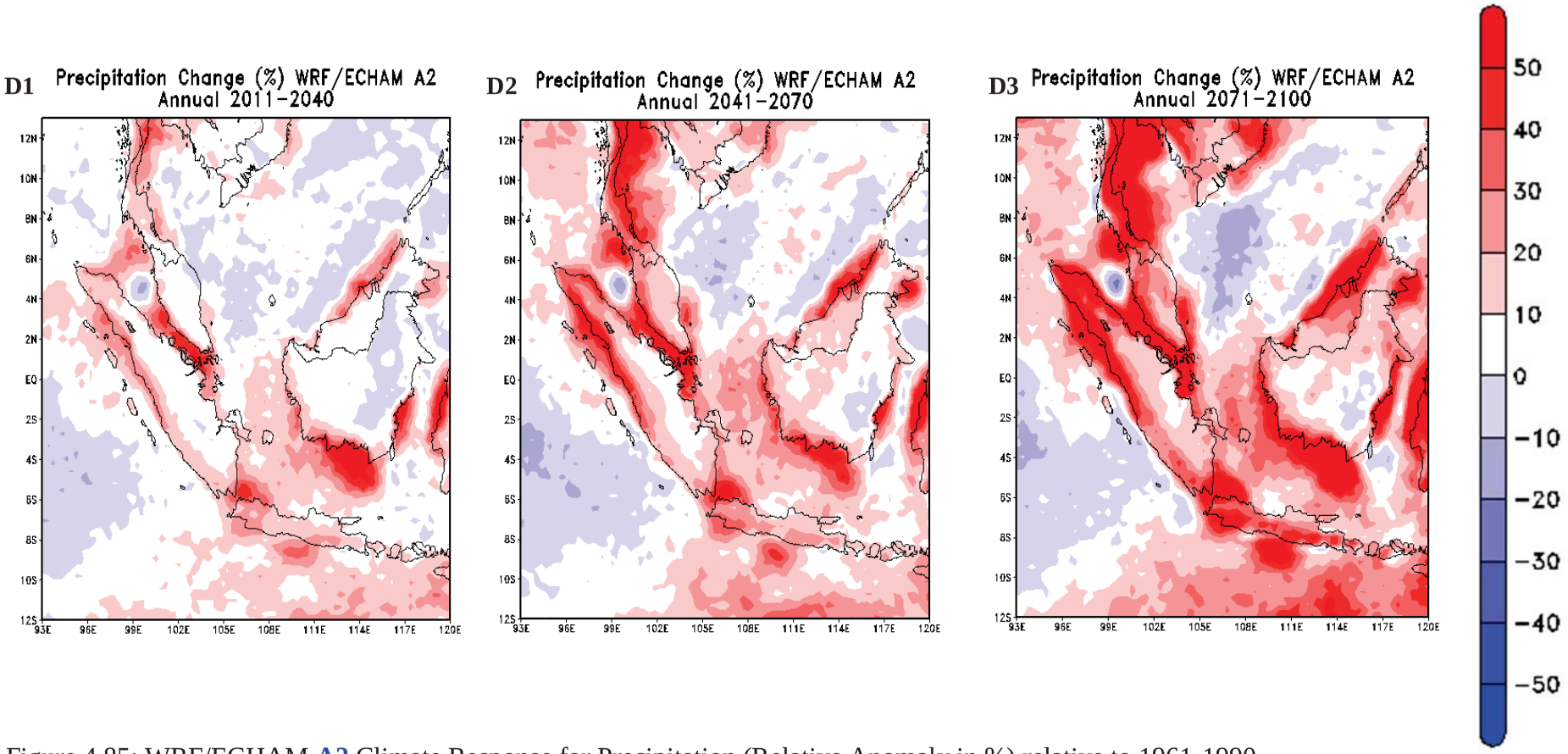

Figure 4.85: WRF/ECHAM **A2** Climate Response for Precipitation (Relative Anomaly in %) relative to 1961-1990
D1: 2011-2040, D2: 2041-2070, D3: 2071-2100 **Annual Change**

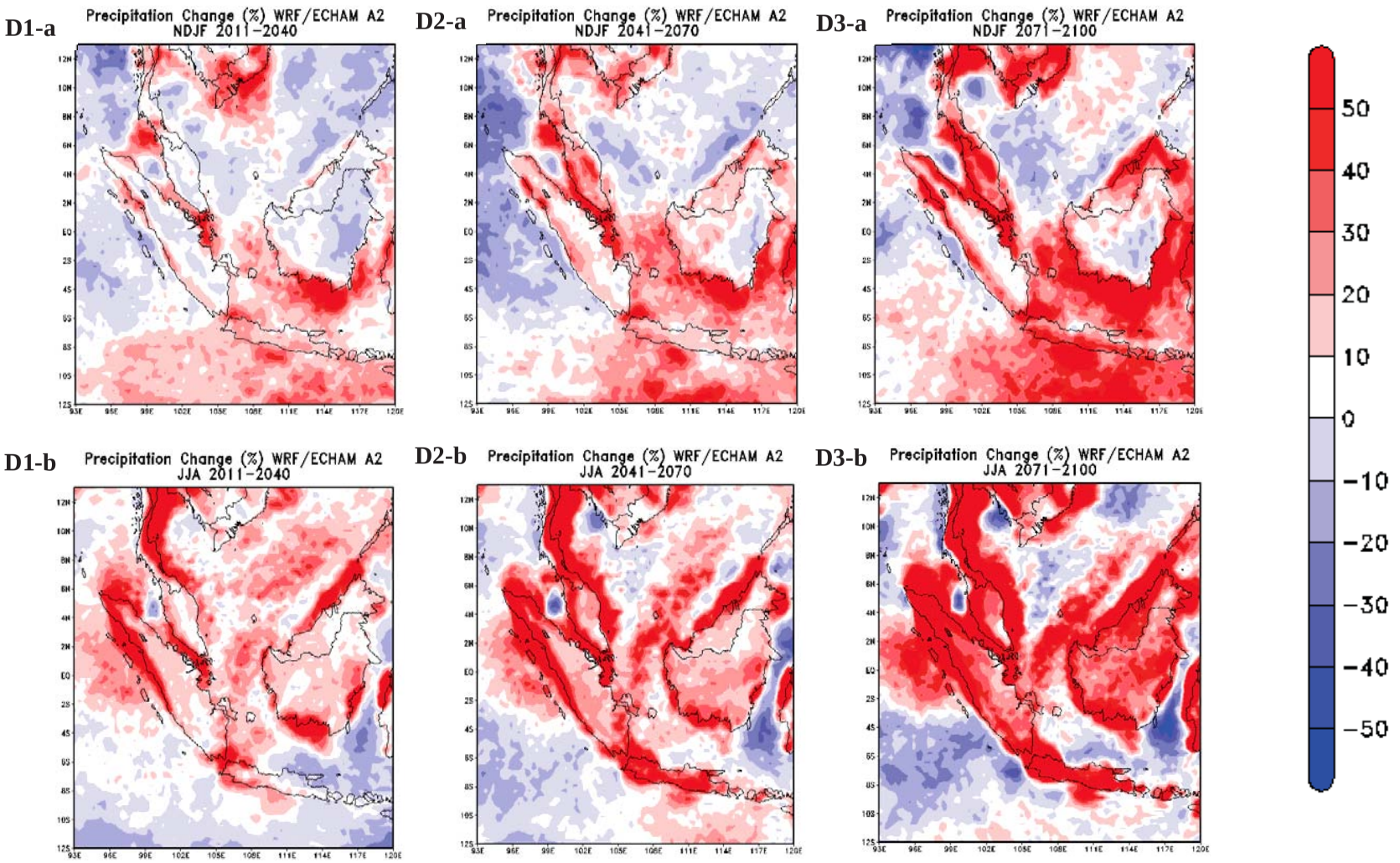

Figure 4.86: WRF/ECHAM **A2** Climate Response for Precipitation (Relative Anomaly in %) relative to 1961-1990
D1: 2011-2040, D2: 2041-2070, D3: 2071-2100 (a) **NDJF Change** (b) **JJA Change**

D1

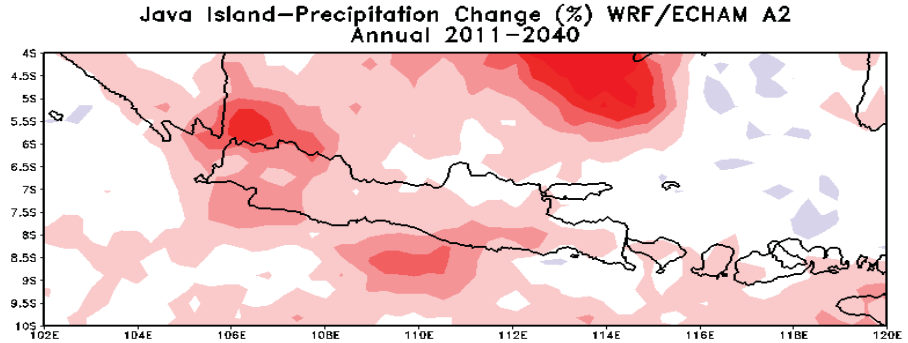

D2

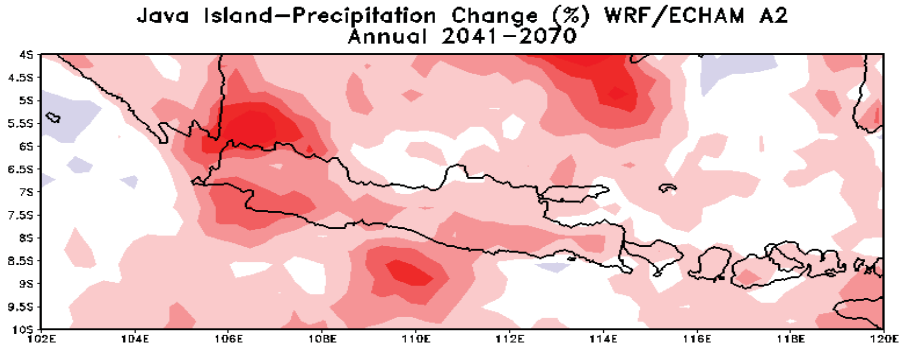

D3

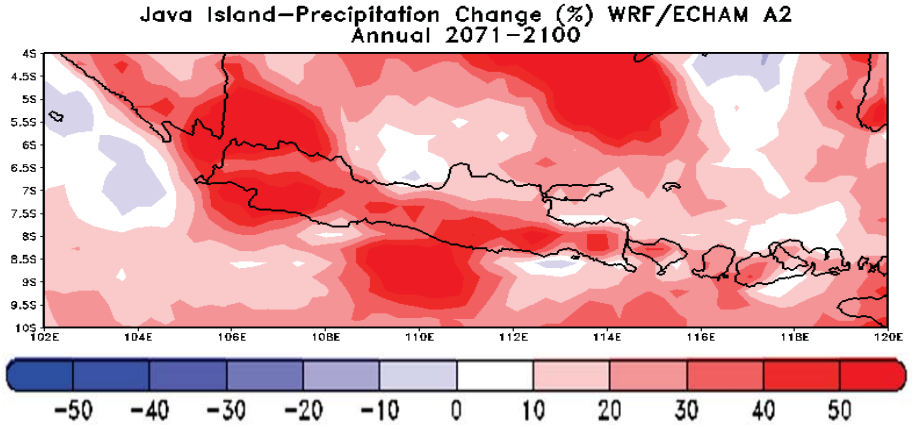

Figure 4.87: WRF/ECHAM **A2** Climate Response for Precipitation (Relative Anomaly in %) relative to 1961-1990, **Jakarta**
D1: 2011-2040, D2: 2041-2070, D3: 2071-2100 **Annual Change**

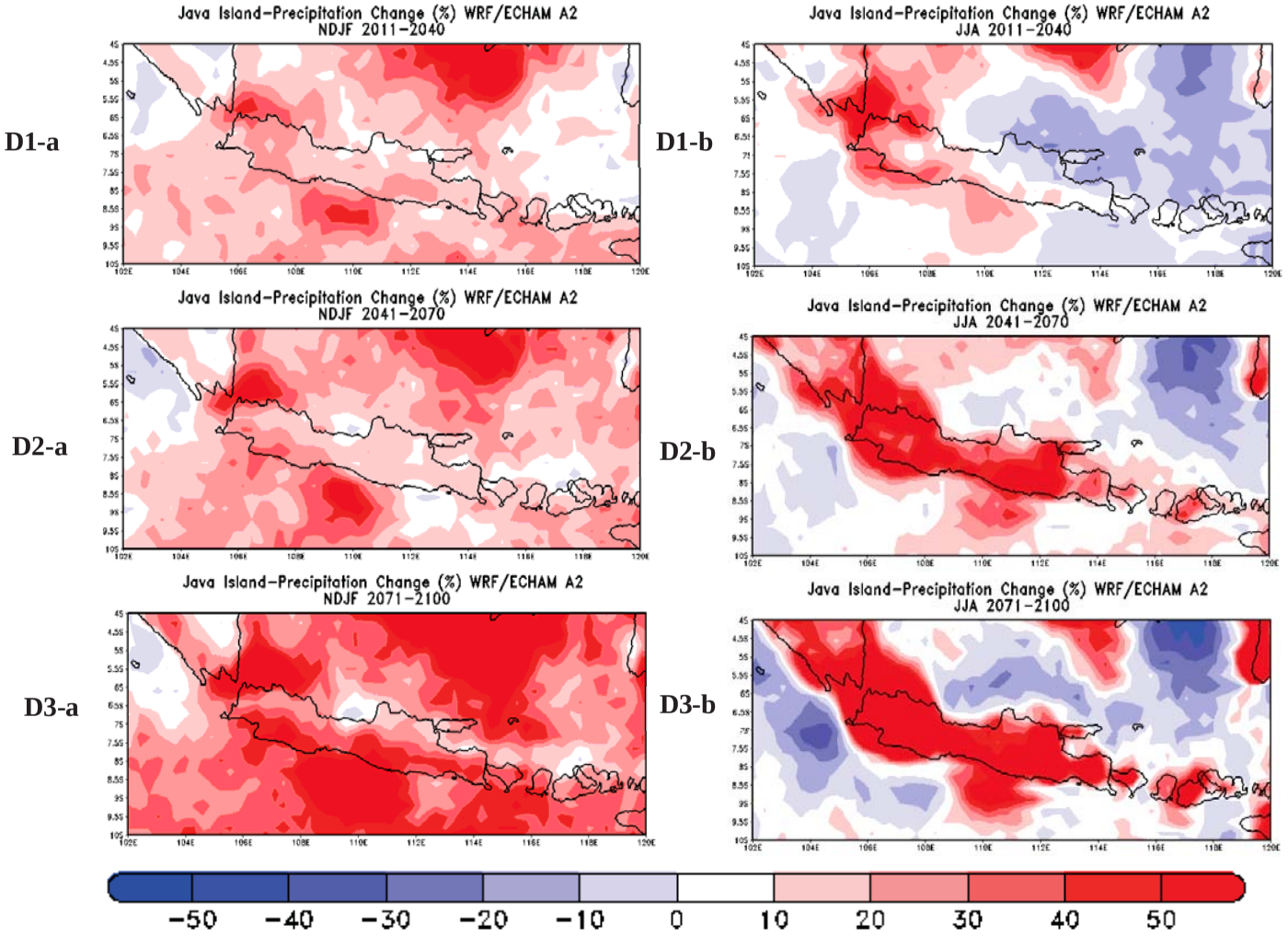

Figure 4.88: WRF/ECHAM **A2** Climate Response for Precipitation (Relative Anomaly in %) relative to 1961-1990, **Jakarta**
D1: 2011-2040, D2: 2041-2070, D3: 2071-2100 (a) **NDJF Change** (b) **JJA Change**

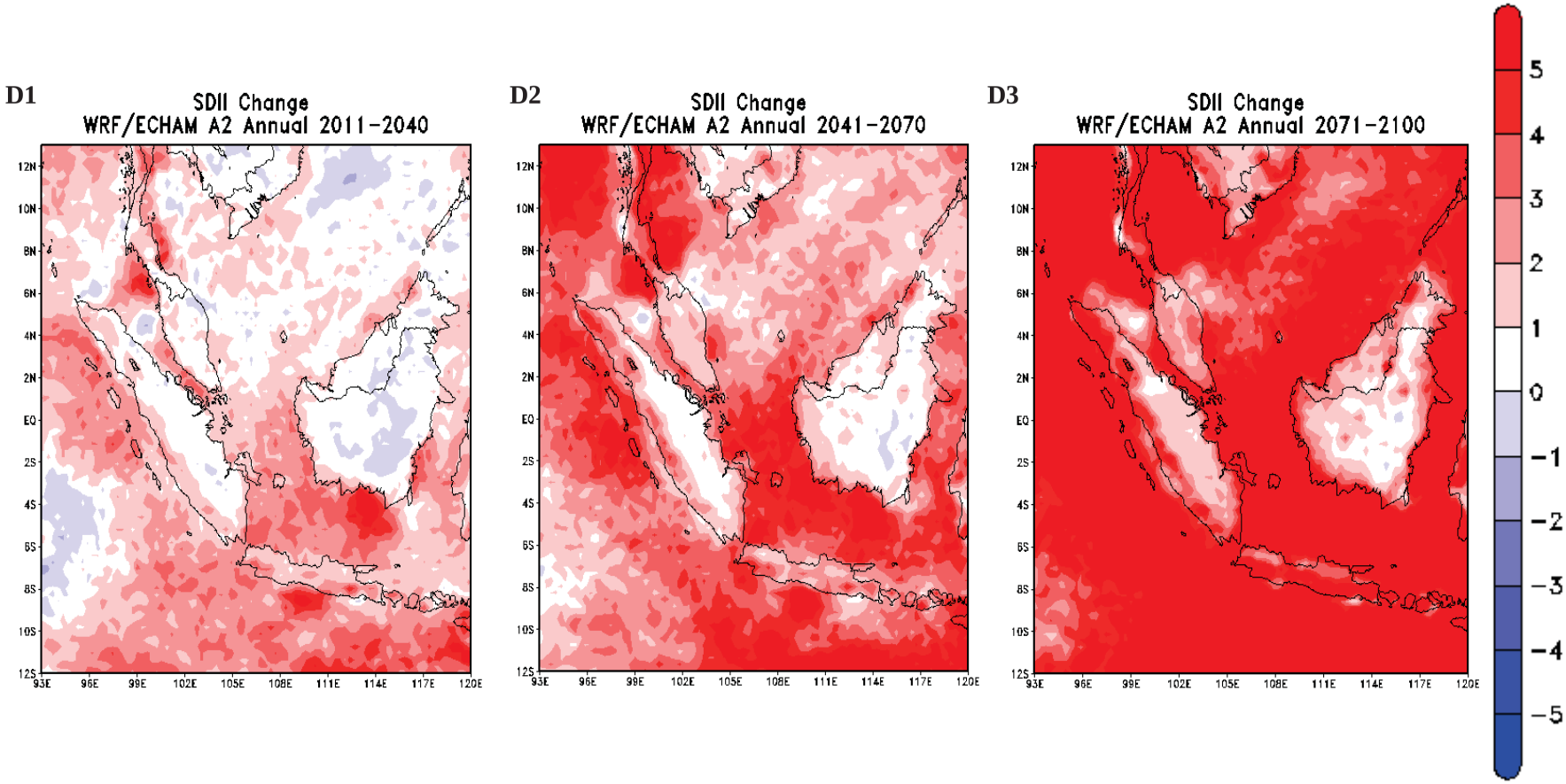

Figure 4.89: WRF/ECHAM **A2** STARDEX Indices relative to 1961-1990, Rain intensity, **SDII, mm/day**
D1: 2011-2040, D2: 2041-2070, D3: 2071-2100 **Annual Change**

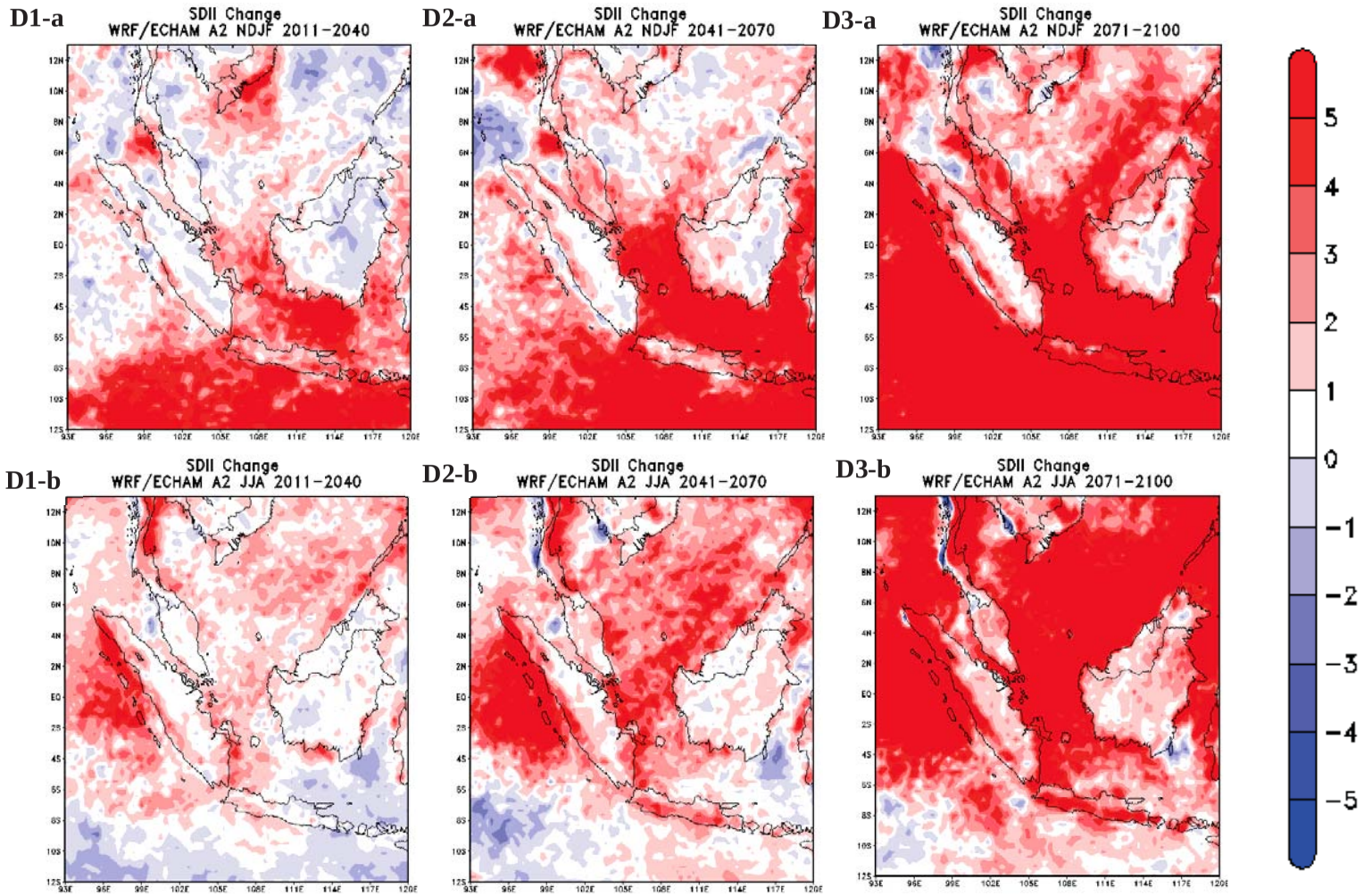

Figure 4.90: WRF/ECHAM **A2** STARDEX Indices relative to 1961-1990, Rain intensity, **SDII, mm/day**
D1: 2011-2040, D2: 2041-2070, D3: 2071-2100 (a) **NDJF Change** (b) **JJA Change**

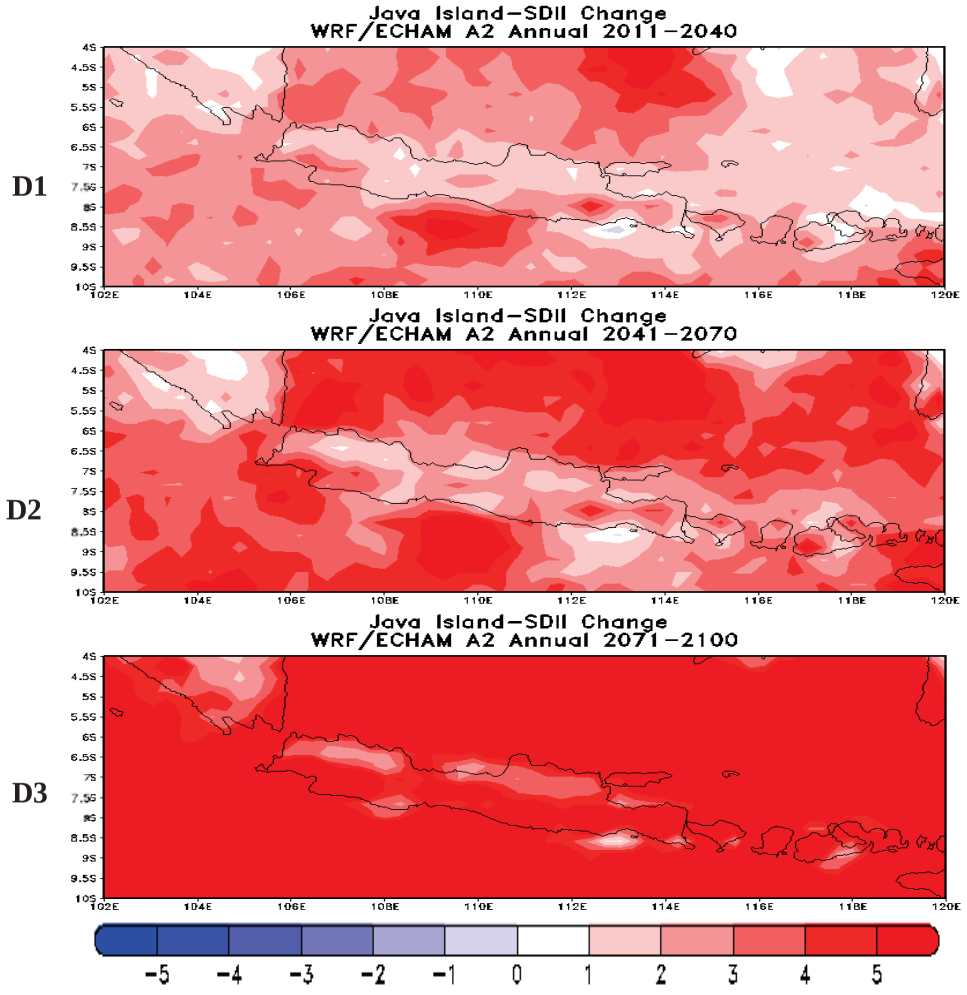

Figure 4.91: WRF/ECHAM **A2** STARDEX Indices relative to 1961-1990, Rain intensity, **SDII, mm/day**, **Jakarta**
D1: 2011-2040, D2: 2041-2070, D3: 2071-2100 **Annual Change**

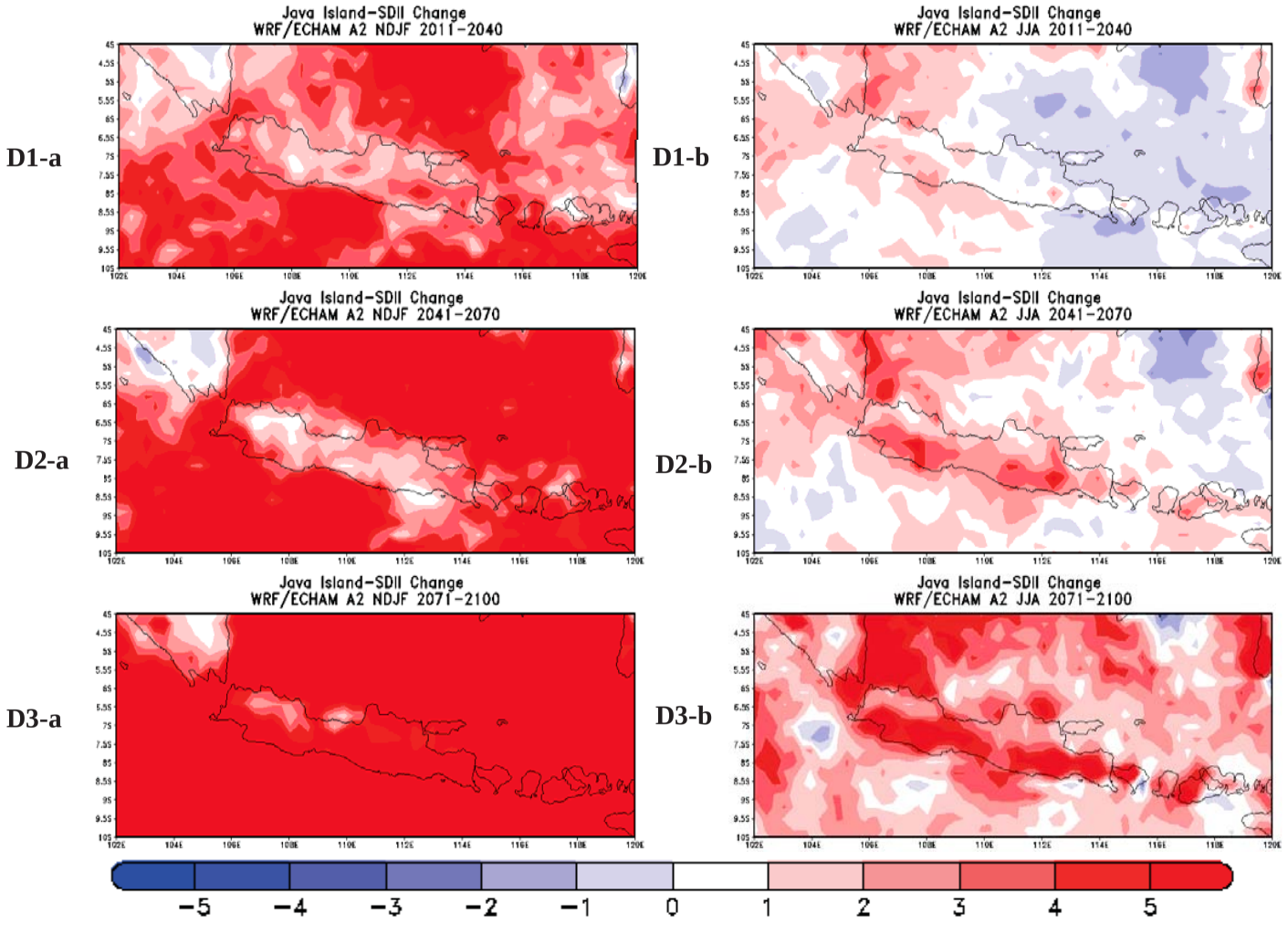

Figure 4.92: WRF/ECHAM **A2** STARDEX Indices relative to 1961-1990, Rain intensity, **SDII, mm/day**, **Jakarta**
D1: 2011-2040, D2: 2041-2070, D3: 2071-2100 (a) **NDJF Change** (b) **JJA Change**

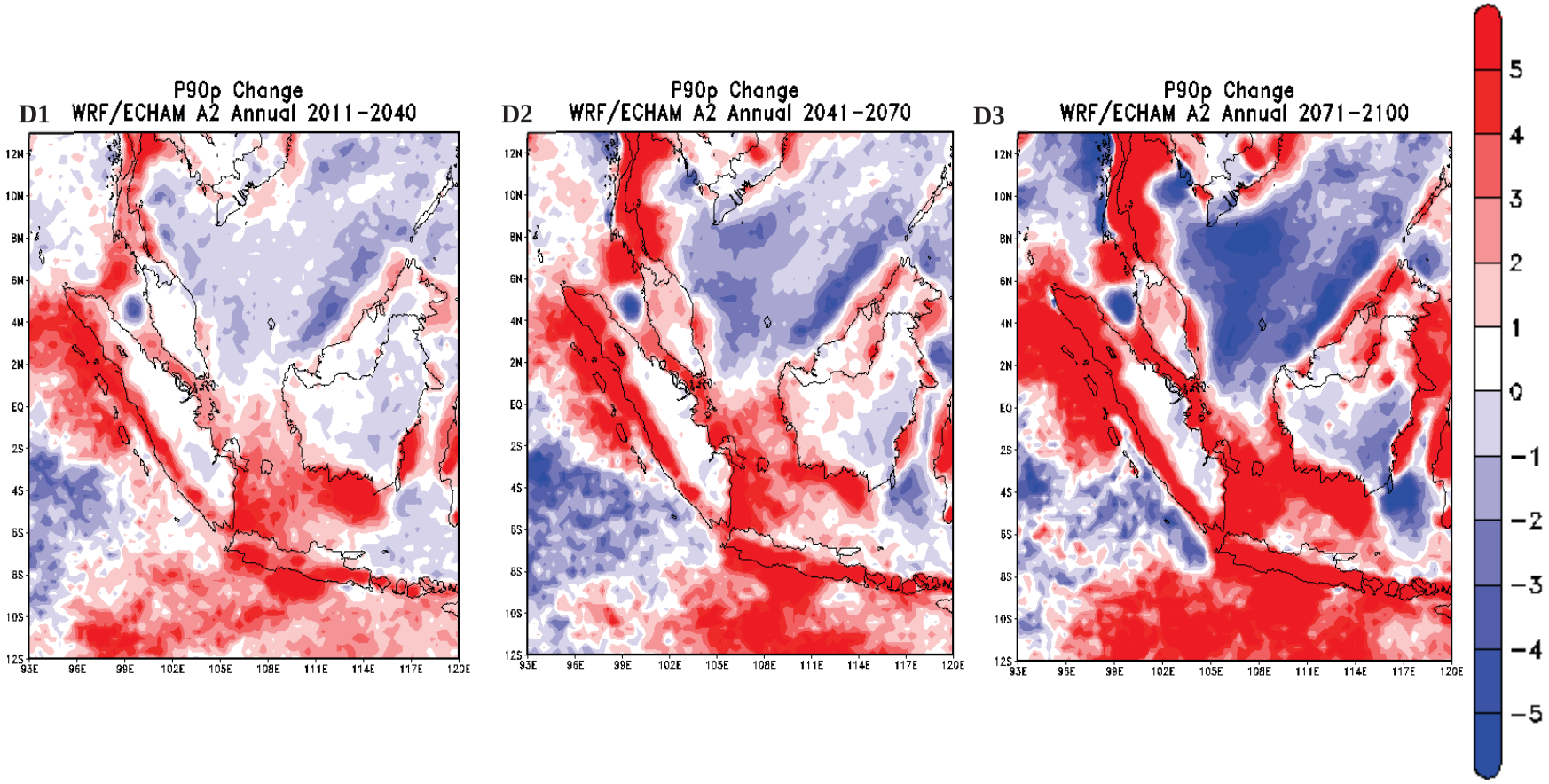

Figure 4.93: WRF/ECHAM **A2** STARDEX Indices relative to 1961-1990, 90th percentile of rain amounts, **P90p, mm/day**
D1: 2011-2040, D2: 2041-2070, D3: 2071-2100 **Annual Change**

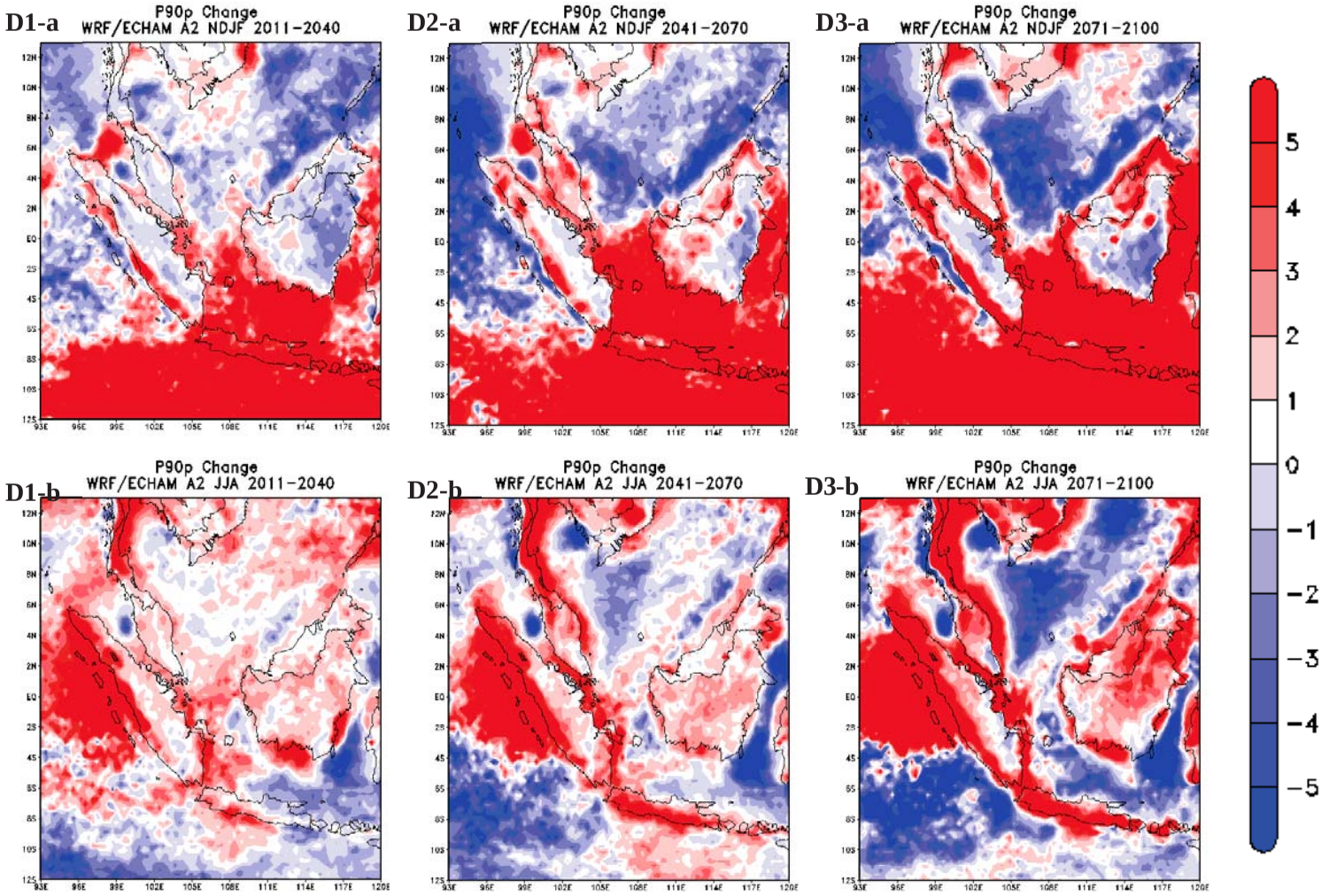

Figure 4.94: WRF/ECHAM **A2** STARDEX Indices relative to 1961-1990, 90th percentile of rain amounts, **P90p, mm/day**
D1: 2011-2040, D2: 2041-2070, D3: 2071-2100 (a) **NDJF Change** (b) **JJA Change**

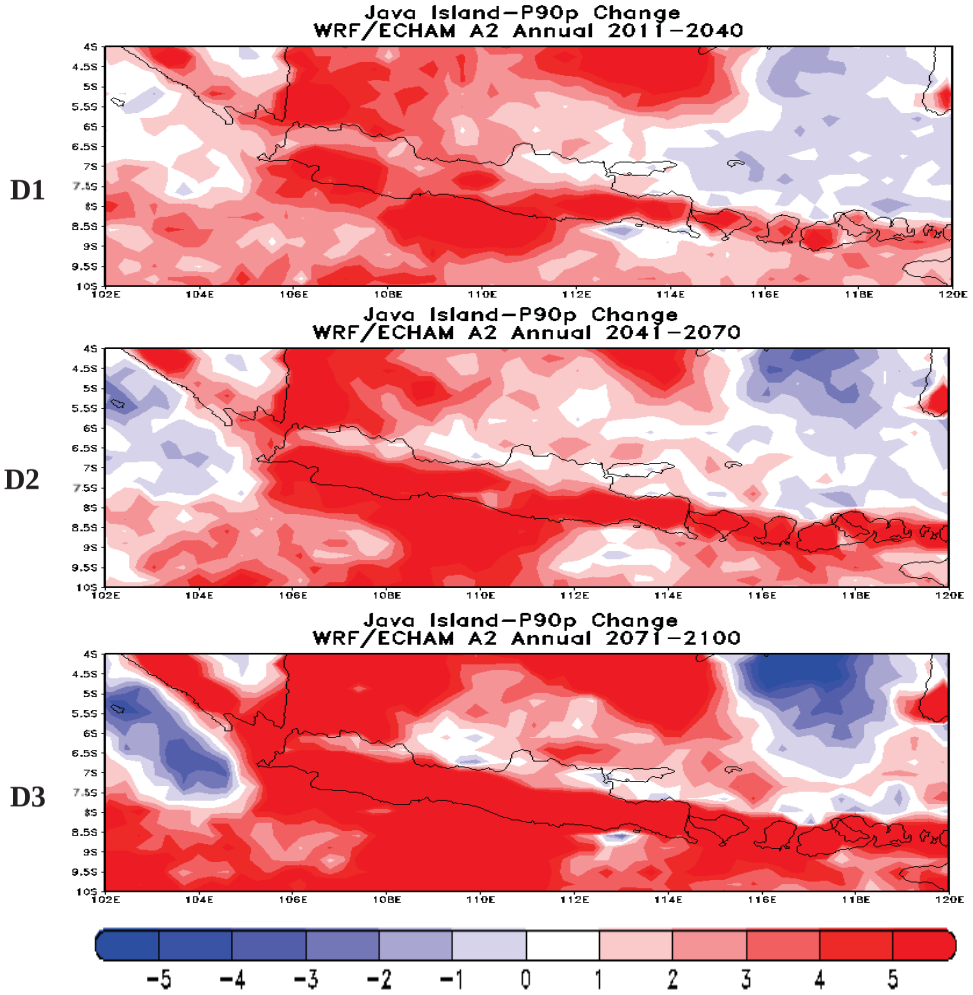

Figure 4.95: WRF/ECHAM **A2** STARDEX Indices relative to 1961-1990, 90th percentile of rain amounts, **P90p, mm/day**, **Jakarta**
D1: 2011-2040, D2: 2041-2070, D3: 2071-2100 **Annual Change**

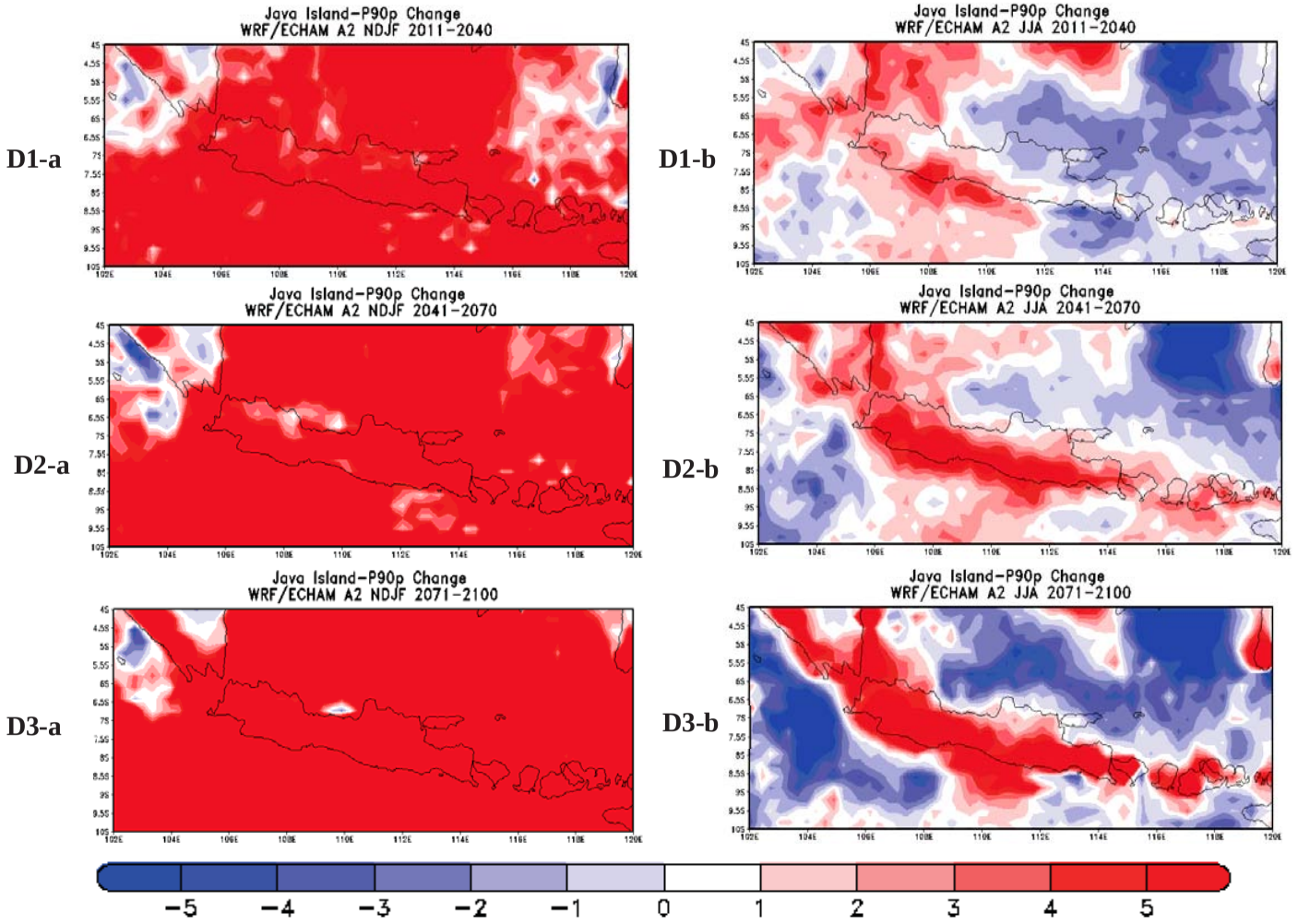

Figure 4.96: WRF/ECHAM **A2** STARDEX Indices relative to 1961-1990, 90th percentile of rain amounts, **P90p, mm/day**, **Jakarta**
D1: 2011-2040, D2: 2041-2070, D3: 2071-2100 (a) **NDJF Change** (b) **JJA Change**

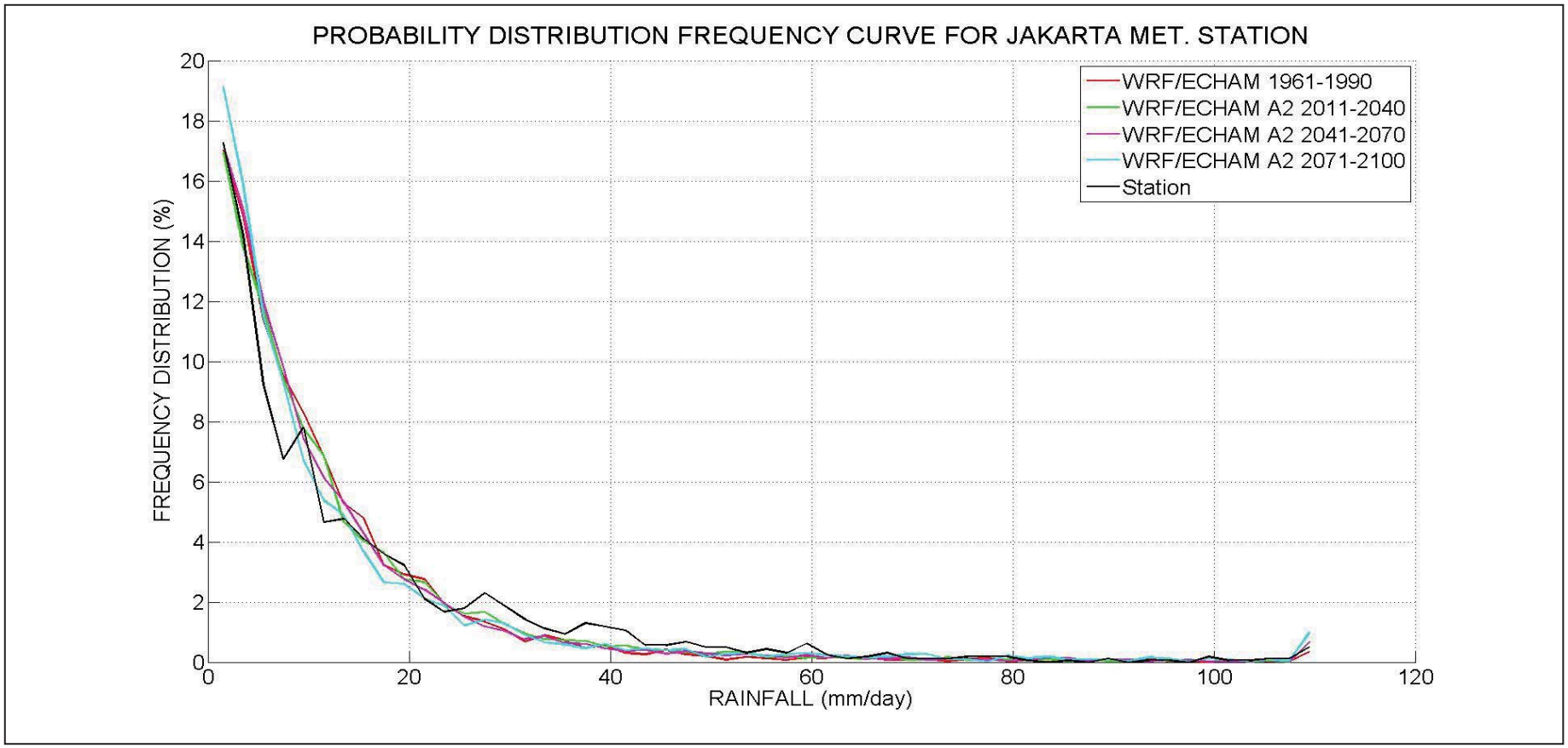

Figure 4.97: Precipitation Probability Density Function (PDF) for **WRF/CCSM (2011-2100) A1B scenario**

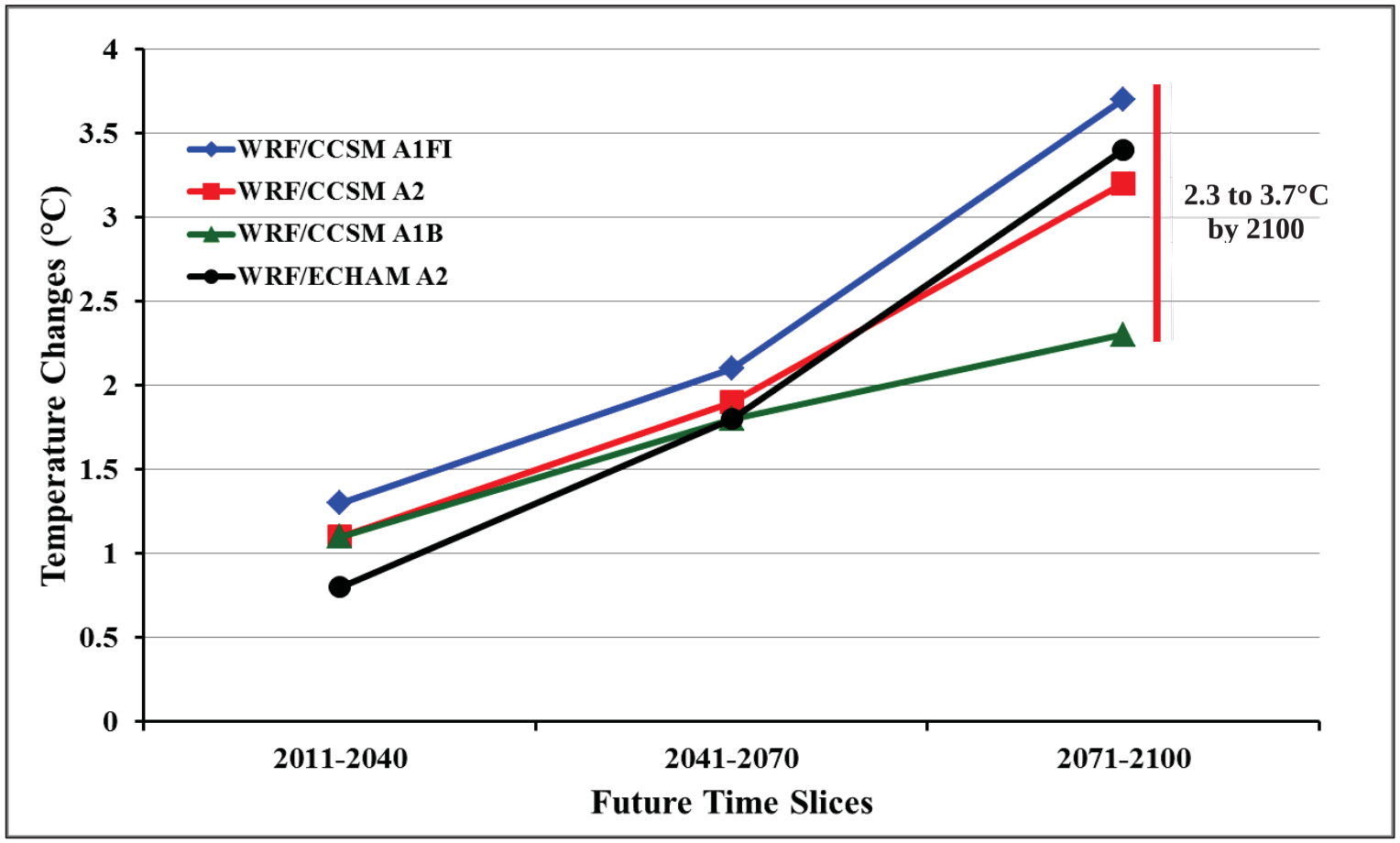

Figure 4.98: Bandwidth of Responses from different future climate scenarios: Temperature (°C), **Jakarta**

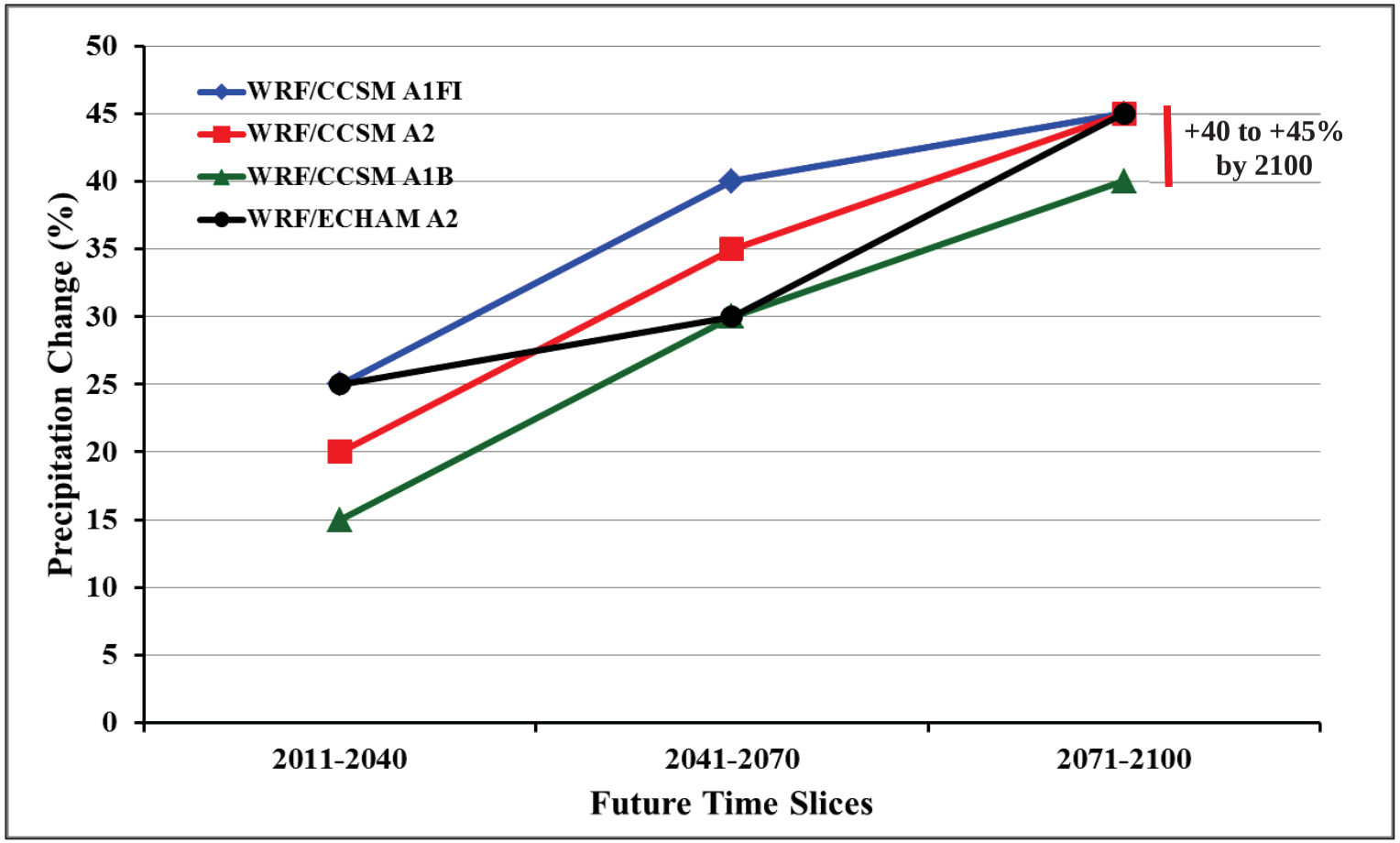

Figure 4.99: Bandwidth of Responses from different future climate scenarios: Precipitation (%), **Jakarta**

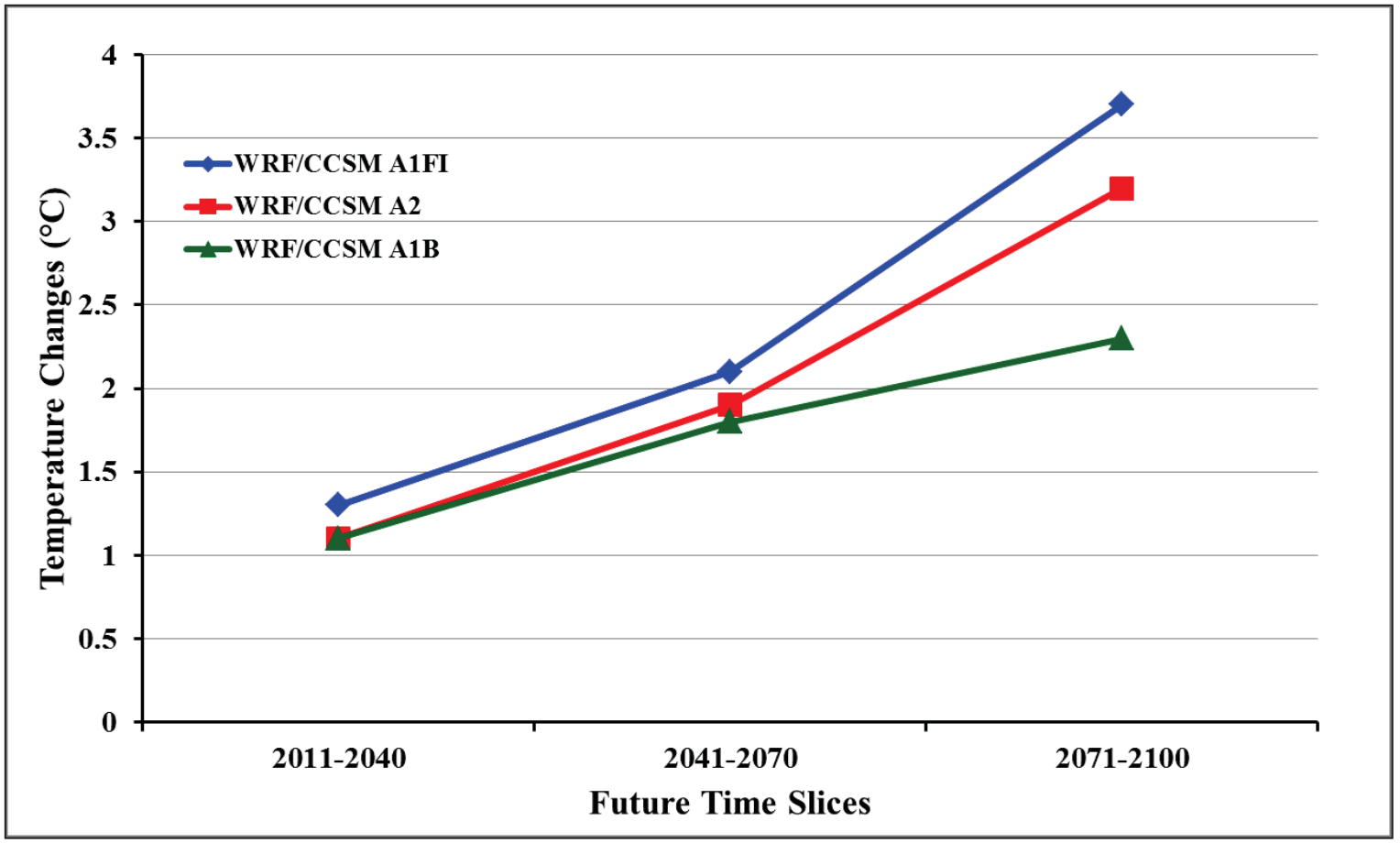

Figure 4.100: Temperature (°C) Responses from WRF driven by CCSM forced under different IPCC future climate change scenarios: A1FI, A2 and A1B, **Jakarta**

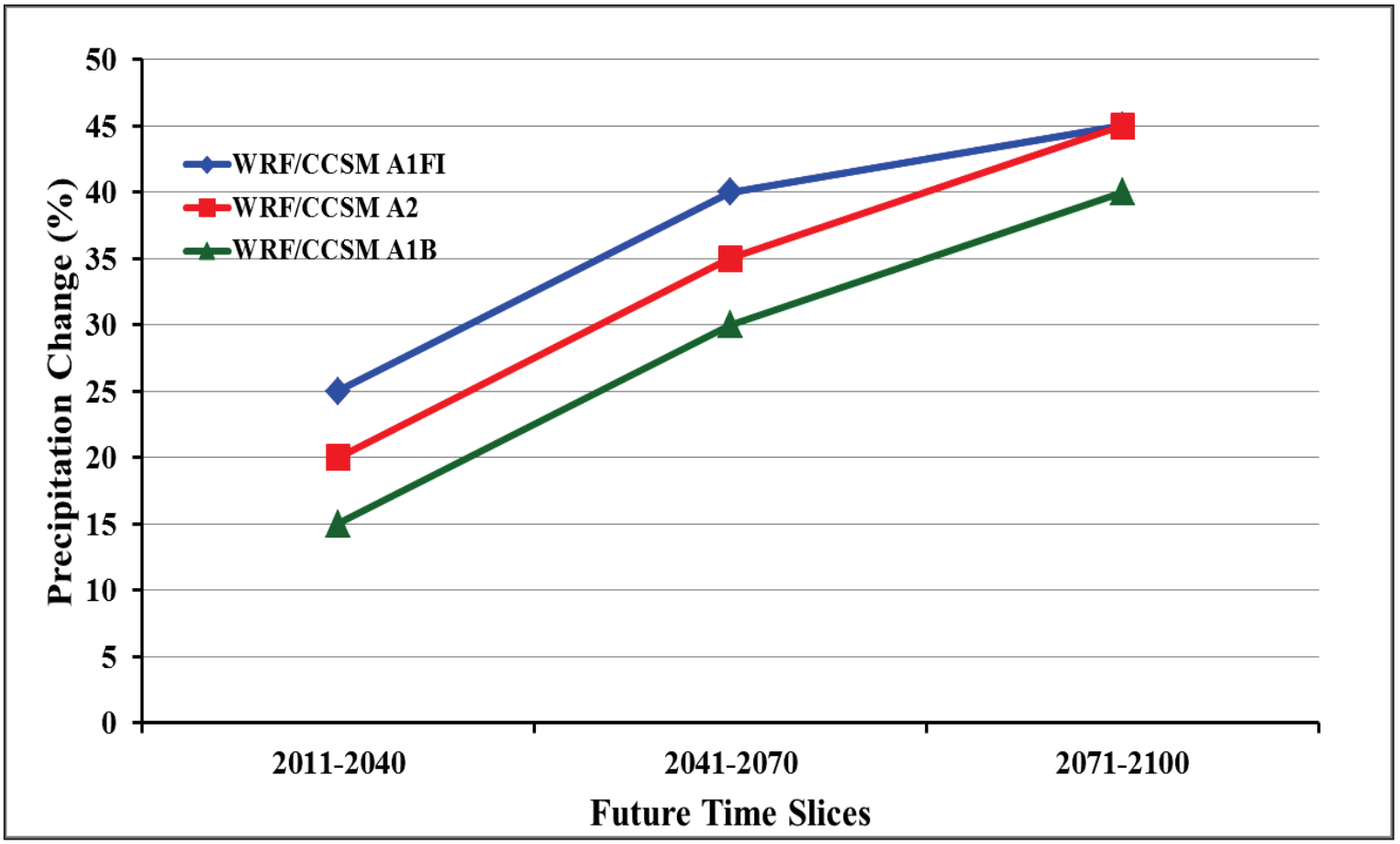

Figure 4.101: Precipitation (%) Responses from WRF driven by CCSM forced under different future climate change scenarios: A1FI, A2 and A1B, **Jakarta**

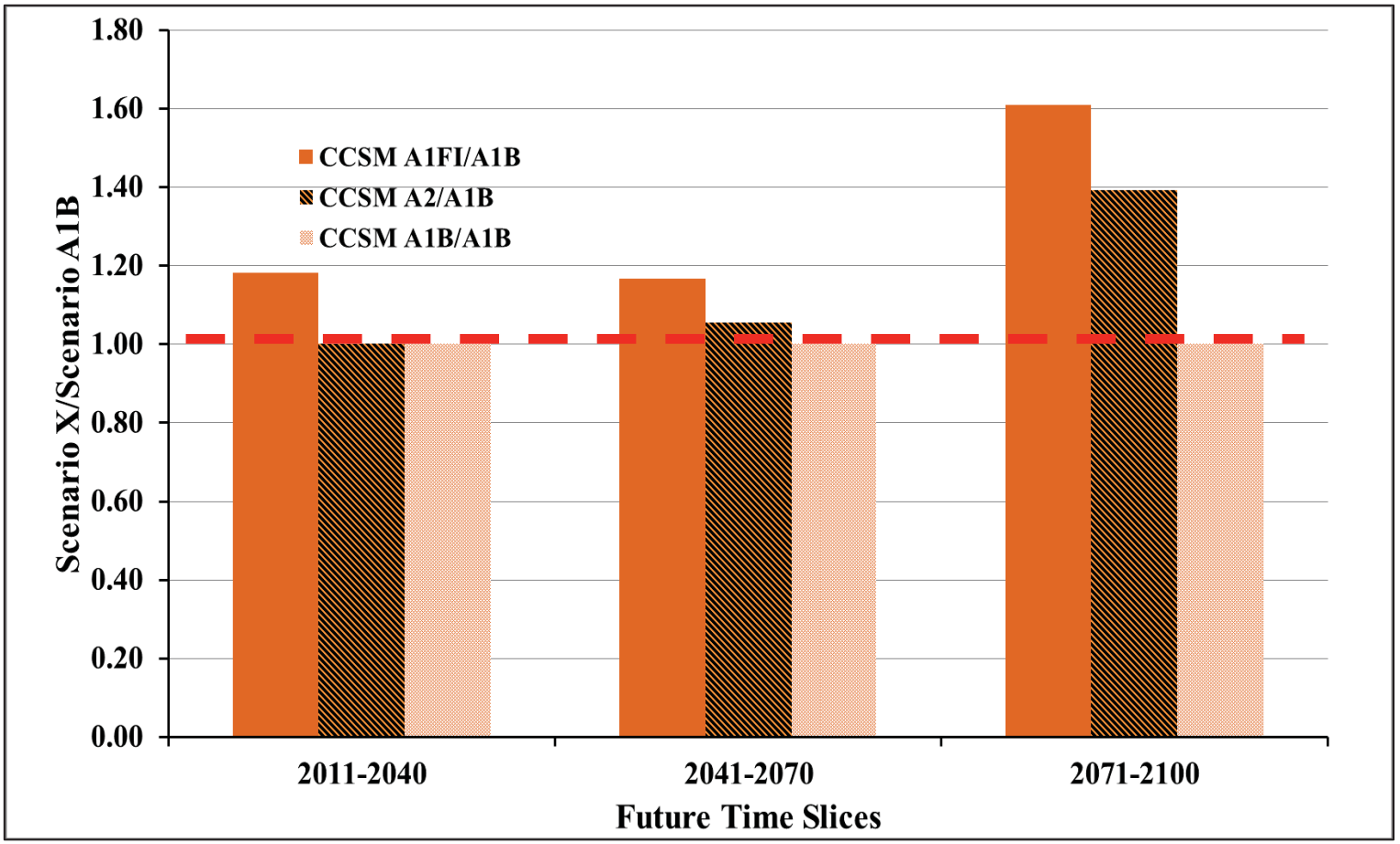

Figure 4.102: Scenario X to Scenario A1B ratio for Temperature (°C) Response (Scenario X, X= A1FI, A2 and A1B), WRF driven by CCSM, **Jakarta**

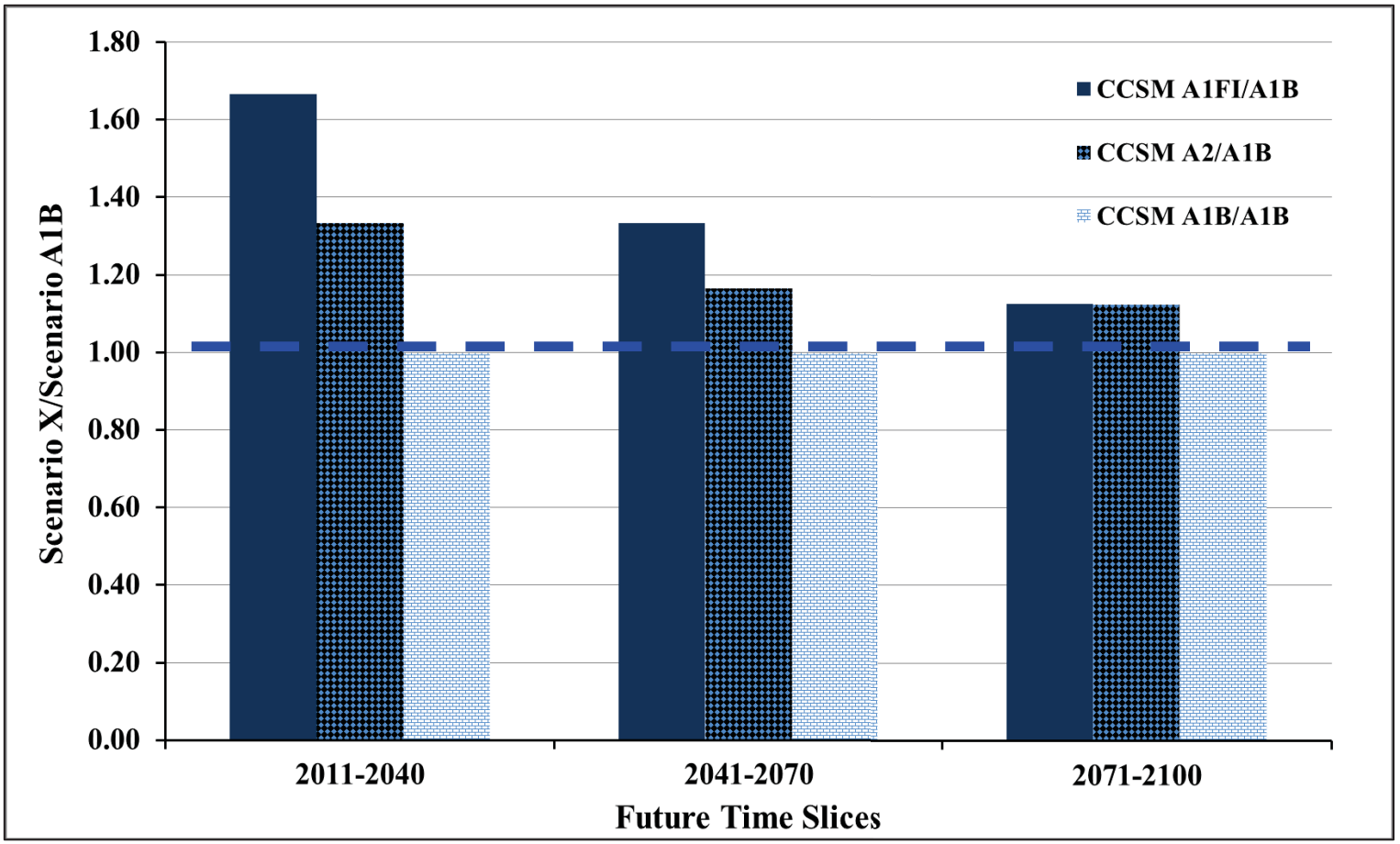

Figure 4.103: Scenario X to Scenario A1B ratio for Precipitation (%) Response (Scenario X, X=A1FI, A2 and A1B), WRF driven by CCSM, **Jakarta**

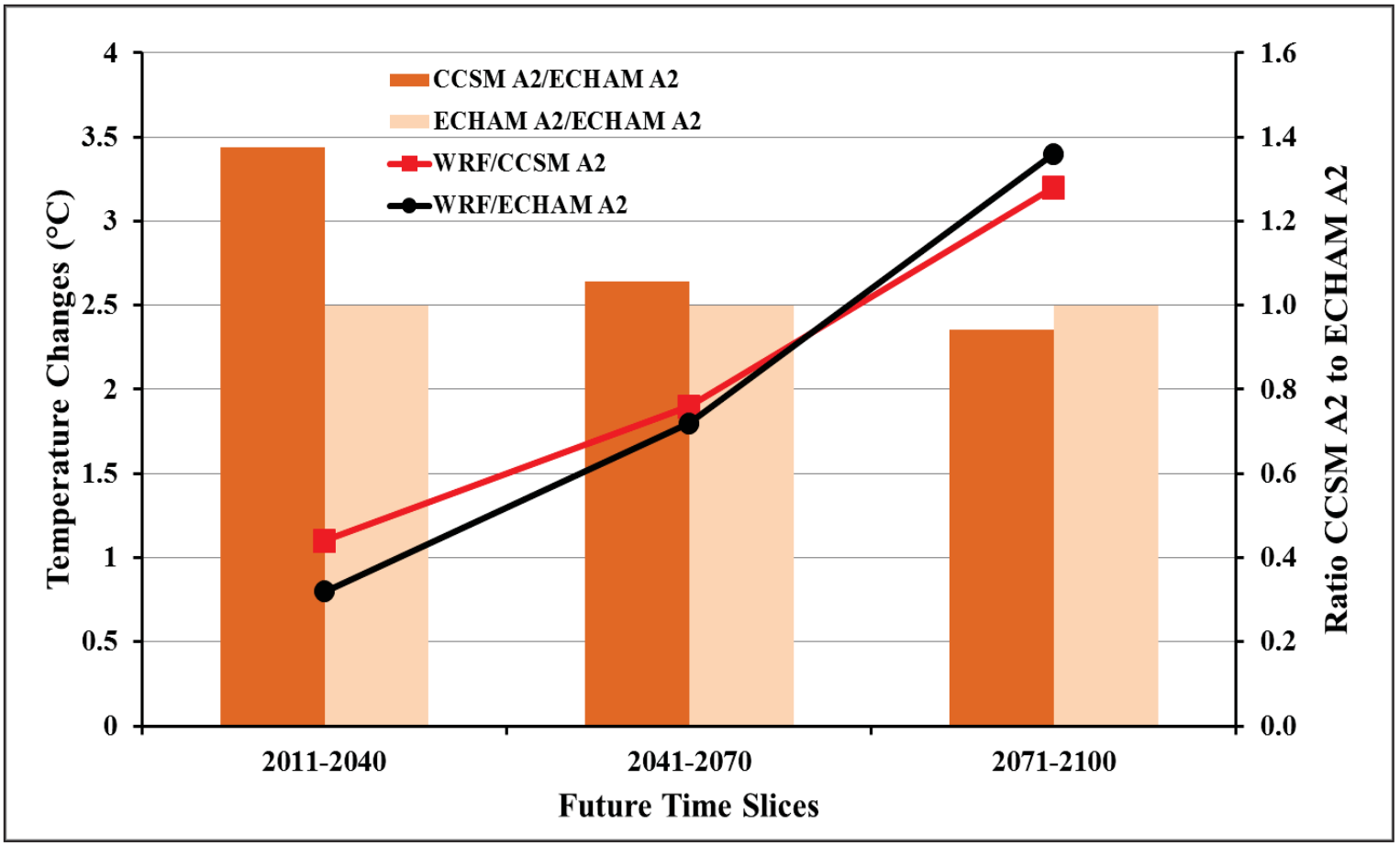

Figure 4.104: Temperature (°C) Responses and WRF/CCSM A2 to WRF/ECHAM A2 ratio: **Jakarta**

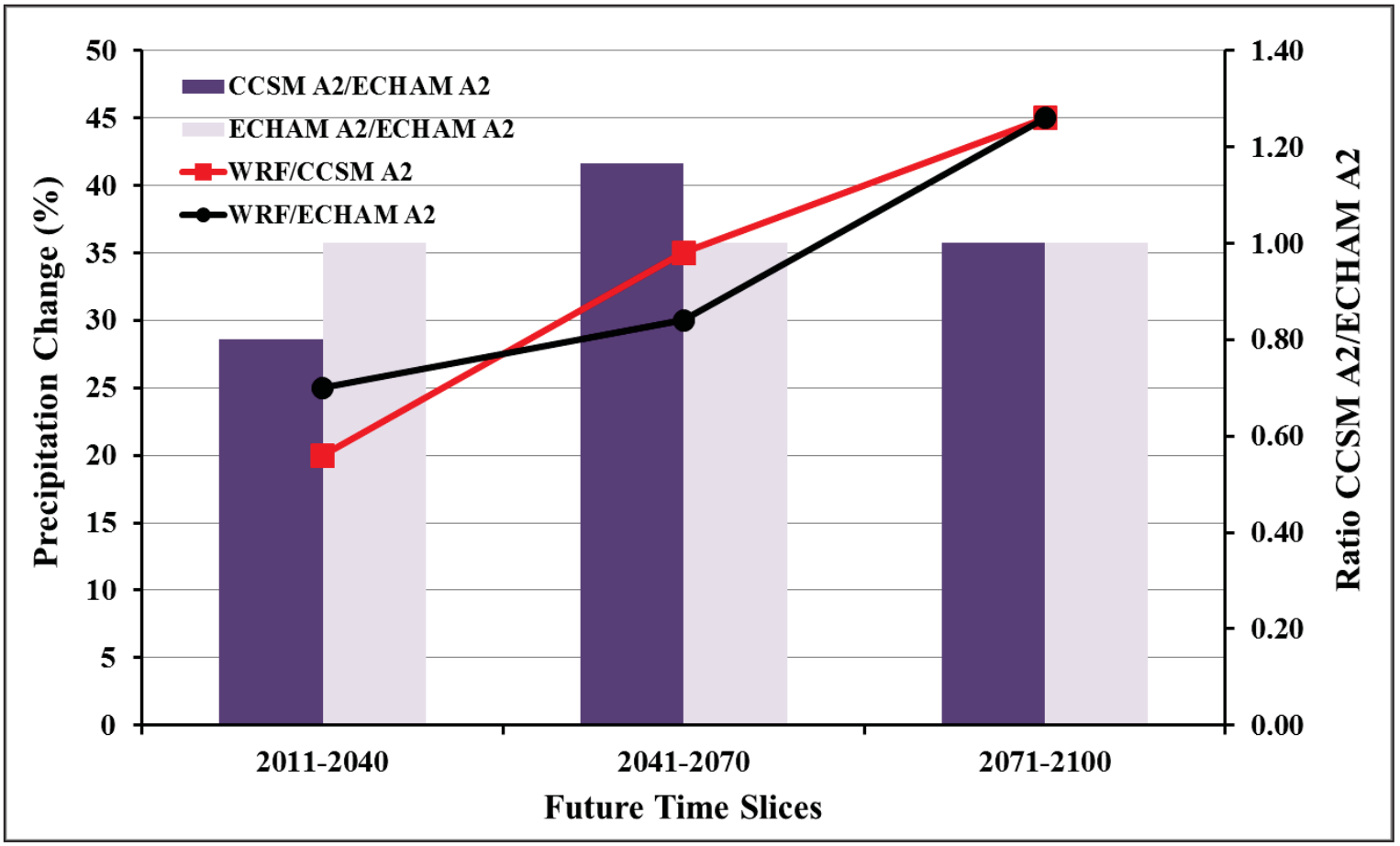

Figure 4.105: Precipitation (%) Responses and WRF/CCSM A2 to WRF/ECHAM A2 ratio: **Jakarta**

Table 4-1 Extreme indices of precipitation
(For further information about the methodology used to define and compute these indices, please refer to Frich et al. (2002), STARDEX (2004, see http://www.cru.uea.ac.uk/projects/stardex/), and Gachon et al. (2005)

INDICES	ABBREVIATION	DESCRIPTION [unit]	TIME WINDOW
INTENSITY	SD II	Precipitation intensity (rain/wet day), [mm/day]	Annual, Seasonal
DURATION & EXTREMES	P90p	90th percentile of daily rainfall [mm/day]	Annual, Seasonal

Table 4-2 Summary of temperature (°C) responses from different future climate change scenarios: A1FI, A2 and A1B, **Jakarta**

Time Slice	WRF/CCSM Scenarios	Annual	Seasonal: NDJF	Seasonal: JJA
Projected Changes (2011-2040) minus (1961-1990)	A1FI	1.3	1.2	1.4
	A2	1.1	1.2	1.2
	A1B	1.1	1.1	1.3
Projected Changes (2041-2070) minus (1961-1990)	A1FI	2.1	1.6	2.3
	A2	1.9	1.9	1.8
	A1B	1.8	1.8	2
Projected Changes (2071-2100) minus (1961-1990)	A1FI	3.7	3.5	3.5
	A2	3.2	3	3.5
	A1B	2.3	2.3	2.5

Table 4-3 Summary of percentage precipitation responses from different future climate change scenarios: A1FI, A2 and A1B, **Jakarta**

Time Slice	WRF/CCSM Scenarios	Annual	Seasonal: NDJF	Seasonal: JJA
Projected Changes (2011-2040) minus (1961-1990)	**A1FI**	**+25**	**+20**	**-10**
	A2	**+20**	**+30**	**-10**
	A1B	**+15**	**+15**	**-15**
Projected Changes (2041-2070) minus (1961-1990)	**A1FI**	**+40**	**+45**	**-20**
	A2	**+35**	**+45**	**-20**
	A1B	**+30**	**+40**	**-15**
Projected Changes (2071-2100) minus (1961-1990)	**A1FI**	**+45**	**+40**	**-25**
	A2	**+45**	**+45**	**-20**
	A1B	**+40**	**+40**	**-15**

Table 4-4 Summary of temperature (°C) responses from WRF driven by different GCMs: CCSM A2 and ECHAM A2, **Jakarta**

Time Slice	WRF/Scenarios	Annual	Seasonal: NDJF	Seasonal: JJA
Projected Changes (2011-2040) minus (1961-1990)	**WRF/CCSM A2**	**1.1**	**1.2**	**1.2**
	WRF/ECHAM A2	**0.8**	**0.7**	**1**
Projected Changes (2041-2070) minus (1961-1990)	**WRF/CCSM A2**	**1.9**	**1.9**	**1.8**
	WRF/ECHAM A2	**1.8**	**1.7**	**1.9**
Projected Changes (2071-2100) minus (1961-1990)	**WRF/CCSM A2**	**3.2**	**3**	**3.5**
	WRF/ECHAM A2	**3.4**	**3.2**	**3.5**

Table 4-5 Summary of percentage precipitation responses from WRF driven by different GCMs: CCSM A2 and ECHAM A2, **Jakarta**

Time Slice	WRF/Scenarios	Annual	Seasonal: NDJF	Seasonal: JJA
Projected Changes (2011-2040) minus (1961-1990)	**WRF/CCSM A2**	**+20**	**+30**	**-10**
	WRF/ECHAM A2	**+25**	**+25**	**+20**
Projected Changes (2041-2070) minus (1961-1990)	**WRF/CCSM A2**	**+35**	**+45**	**-20**
	WRF/ECHAM A2	**+30**	**+20**	**+45**
Projected Changes (2071-2100) minus (1961-1990)	**WRF/CCSM A2**	**+45**	**+45**	**-20**
	WRF/ECHAM A2	**+45**	**+20**	**+50**

CHAPTER 5 A PROPOSED APPROACH TO DERIVE PRESENT AND FUTURE IDF CURVES

5.1 INTRODUCTION

This chapter presents a novel approach to develop the present day and future climate Intensity-Duration-Frequency (IDF) curves for regions with short or no rainfall station data records (i.e. ungauged basins). How the extreme rainfall values from the climate model results were obtained were discussed in Chapter 3. There, discussed also how their values were fitted with GEV distribution function and then used to derive present and future IDF curves.

As urbanization has been taking place rapidly since 1980s in many places severe flooding, particularly in the developing countries, have been witnessed and reported. Many of these newly urbanized areas often do not have or have short rainfall records which are not sufficient to construct IDF curves essential in the storm drainage design. As a rule of thumb, at least 20 years of datasets is needed to derive a rainfall of 100-year return period. Thus, deriving present day climate's IDF curves is absolutely essential steps for these areas (ungauged basins). Only then it is more meaningful in deriving and presenting future climate's IDF curves. In this study, Darmaga Station, a site in Java, Indonesia, is used as the proof-of-concept of the proposed approach to derive present IDF curves using simulated data from RCM (WRF) driven by reanalysis data, e.g. ERA40, WRF/ERA40.

In this study, the extremes from projected rainfall, from WRF/ERA40, are used to derive IDF curves for sites (Singapore, Kuala Lumpur and Jakarta Meteorological Stations) in the 'vicinity' where IDF curves exist; bias quantities resulting from these sites are captured, identified and serve as very useful information in deriving present IDF curves for sites (e.g. Darmaga Station) with short or no rainfall records. The detailed approach is presented in Section 5.2.

For the anticipated extremes in future rainfall due to climate change, Section 5.3 demonstrates the development of future IDF curves by incorporating climate change projections. Results and comparison of the future IDF curves for 3 different time periods 2011-2040, 2041-2070 and 2071-2100 under different GCMs (CCSM3.0 and ECHAM5) and emission scenarios (A1FI, A2 and A1B) are presented in detail in Section 5.3 as well. This study is probably the first of its kind to incorporate the application of a regional climate model which provides high resolution information on both the present day and future IDF curves under different emission scenarios of climate change.

Section 5.4 presents extended studies of the climate change impacts on future IDF curves for mega-cities under different emission scenarios. This extended study contributes significant information for impacts assessment, adaptation and mitigation strategies for climate change. Figure 5.1 shows the flowchart for the development of present and future climate IDF curves, using regional climate model (RCM) and incorporating climate change projections.

5.2 DEVELOPMENT OF PRESENT DAY IDF CURVES

The proposed approach of deriving the present day climate IDF comes in 3 steps: Step 1: Dynamical Downscaling [D]; Step 2: Comparison [C]; and Step 3: Derivation [D]. This approach is named as a (3-step) DCD approach. A flowchart that describes and summarizes the entire (3-step) DCD approach, to develop IDF curves for sites with short or no rainfall records is shown in Chapter 3, Figure 3.7 and for the reader's convenience the same flowchart is shown in Figure 5.2.

Step 1: <u>Dynamical Downscaling and Performance Evaluation of RCM WRF driven by ERA-40</u>

This step has been detailed in Chapter 4. The RCM WRF was first parameterized with boundary forcing originating from the perfect climate model (reanalysis) data, ERA-40. Each parameterization experiment was compared with the gridded oberservational data such as CRU; this iterative process continues until a reasonably well comparison is achieved. After achieving acceptable match with the gridded observational data, the WRF/ERA40 results were then ready for its consideration in Step 2 detailed below.

Step 2: Comparison Between WRF/ERA40 and Gauge Data Derived IDF Curves

For generating IDF curves, aggregation of datasets from RCM WRF was first performed; followed by identification and extraction of the annual maximum rainfall series and subsequently, frequency analysis and assessment of suitable probability distribution function for annual maximum rainfall series.

Since the main objective of this chapter is to develop IDF curves for sites with short or no rainfall record, the proof of concept analyses was first done on locations at which IDF curves are available. Three locations with IDF curves considered are Singapore, Kuala Lumpur and Jakarta Meteorological Stations (Chapter 3, Figure 3.2 and for the reader's convenience the same figure is shown in Figure 5.3). Their existing IDF curves, as shown in Figures 5.4 (a to c), were used for comparison with the IDF curves derived from WRF-ERA40 and for obtaining the bias correction quantity for each station. The bias quantities will later serve as a guideline for derivation of IDF curves at sites with short or no rainfall records. The coordinates of the sites considered can be found in Table 5-1. Methodology required in Step 2 has been discussed in Section 3.7.

The idea is to assess how much the WRF/ERA40 derived IDF curves deviate from their observed counterparts. The baseline period considered was 1961-1990. The percentage differences between both IDF curves (Existing vs. WRF/ERA40 derived IDF curves) are computed and the upper and lower

bounds (range of bias correction) from the three stations (Singapore, Kuala Lumpur and Jakarta Meteorological Stations) were noted. These were done for 5, 10, 25 and 50 year return periods for Jakarta Meteorological Station while for Singapore and Kuala Lumpur the comparison was done only for 5, 10, 50 and 100-year return periods due to their availability. The results are shown in Figure 5.5 (a to c) and the percentage difference between the existing and the WRF/ERA40 derived IDF curves are presented in Table 5-2 (a to c). Despite the relatively high percentage of underestimation of WRF model driven by reanalysis data ERA-40, when compared to the existing IDF curves for Singapore, Kuala Lumpur and Jakarta Meteorological Stations, it can be seen that the IDF curves, derived from WRF/ERA40, fairly consistently underestimate their counterparts, the raingauge derived IDF curves; the underestimations range, in average, from 38 % (lower bound) to 45 % (upper bound).

This finding is significant because: (a) it appears that RCM WRF driven by ERA40 has the tendency to underestimate rainfall intensities in this area; and (b) it quantifies the range of bias correction which serves as a guideline for derivation of present climate's IDF curves for sites with short or no rainfall records. Figure 5.6 shows bias correction on the present day's IDF curves derived from WRF/ERA40 with lower and upper bounds derived earlier.

Step 3: Derivation of IDF Curves for Regions with Short or No Rainfall Records

Darmaga station (106° 45'E, 6° 33'S), located about 100 km southerly of Jakarta Meteorological Station, was selected as a site for proof of concept, thus, a validation site. Note that Darmaga station has raingauge data derived IDF curves. The IDF curves for Darmaga station were compared with the upper and lower bounds (range of bias correction) obtained from the 3 aforementioned sites.

The present climate IDF curves for Darmaga station was first derived from rainfall data simulated by WRF/ERA40. The lower (+38%) and upper (+45%) bounds (range of bias correction) obtained from Step 2 were then applied to the WRF/ERA40 derived IDF curve of respective return period. Thus, the present day WRF/ERA40 derived IDF curves of each return period for Darmaga Station are a pair of upper and lower bound IDF curves. The existing (raingauge data derived) IDF curves for Darmaga station were then compared with the lower and upper bounds (range of bias correction) obtained earlier corresponding with the selected return periods. The results for 5, 10, 25 and 50-year return periods are shown in Figure 5.7a, b, c and d respectively. Table 5-3 lists the lower and upper bound values for 5, 10, 25 and 50 year return periods and their counterparts from Darmaga station data. The figures indicated that the existing IDF curves for 5, 10, 25 and 50-year return periods very much lie within the lower and upper bounds resulting from the proposed approach; the exception is for rainfall duration of 360 minutes (6-hour) which

lie slightly above the upper bound. The slight exceedance is expected as the upper bound suggested is an average value from the 3 stations. The same can be expected for the lower bound when the approach is applied to other ungauged basins. Nevertheless, the results clearly prove that the proposed approach is able to develop the IDF curves for the ungauged basin reasonably accurate.

In summary, to develop present climate IDF curves for sites with short or no rainfall records, IDF curves for region of interest are first derived from WRF driven with ERA-40. The lower and upper bounds (range of bias correction) obtained from Section 5.2 (Step 2) are then applied to the WRF/ERA40 derived IDF curve of relevant return period. The final product of the present climate WRF/ERA40 derived IDF curves are a pair of IDF curves which consists of a lower and upper bounds (Figure 5.7) for each return period. This range of bias correction allows drainage designers to decide on a value within the lower and upper bounds; decision making is usually subjected to engineering, economic, social and environmental concerns.

It should be noted that RCM WRF simulations are in 6-hour time step, thus, rainfall durations considered were of 6, 12, 18 and 24-hours. These, however, do not constrain the application of the findings to Jakarta as flooding there was mainly caused by long rainfall durations. Shorter duration rainfall can be obtained for further analyses; however, it is not in the scope of this thesis.

One of the main contributions of this study is to provide a solution to derive present climate IDF curves for regions with short or no rainfall records, e.g. Darmaga Station, by applying the (3-step) DCD approach, incorporating regional climate modeling. The approach has also been tested successfully to a number of Meteorological stations (Ipoh, Seremban, Melaka and Johor Bahru) in Peninsula Malaysia. Results are shown in Appendix B1.

In short, by comparing the reliable raingauge data derived IDF curves with the RCM WRF/ERA40 (or any re-analysis datasets) derived IDF curves, a range of bias correction, a pair of IDF curves which consist of a lower and upper bounds, can be obtained for ungauged basins in the vicinity. Thus, the approach provides a range of rainfall intensity of a particular rainfall duration and return period in a data sparse region of interest.

To further assess the future rainfall intensities due to climate change, next section discusses the approach to derive future climate IDF curves.

5.3 DEVELOPMENT OF FUTURE CLIMATE IDF CURVES

IDF curves are developed using historical rainfall time series data, where annual extreme rainfall data are fitted with a suitable probability distribution function from which rainfall intensities, corresponding to particular durations, are obtained. In the use of this procedure an assumption is made that historic extremes can be used to characterize extremes of the future (i.e., the historical

records are assumed to be stationary). In other words, the present day IDF curves were developed based on already altered GHG concentrations in the atmosphere, thus, ignoring any future change in the GHG emissions. This assumption is not valid under changing climatic conditions as well as the consequences of human induced climate change that may bring shifts in magnitude and frequency of extreme rainfall (Prodanovic and Simonovic, 2007). Projected future climate change impacts for the study region, e.g. Jakarta, include higher temperatures and increase in rainfall intensity, leading to an amplification of the hydrologic cycle. One of the expected consequences of change is an increase in the magnitude and frequency of extreme events (e.g. high intensity rainfall, flash flooding, etc.). Changes in extreme events are of particular importance to the design, operation and maintenance of stormwater infrastructure.

Section 5.2 demonstrated a (3-step) DCD approach to derive present climate IDF curves for sites with short or no rainfall record. For the anticipated changes in rainfall due to climate change, this section continues to propose the development of future climate IDF curves. RCM WRF simulations presented in Chapter 4 for the future climate driven by GCM/CCSM3.0 forced under the IPCC emission scenarios A1FI, A2 and A1B and GCM/ECHAM5 forced under the A2 scenario were used in the subsequent sections to determine climate changes over the future time slices 2011- 2040, 2041- 2070 and 2071-2100 (Figure 5.1).

The following Section 5.3.1 demonstrates, in detail, the development of future climate IDF curves application on Darmaga Station, a validation station. Presentation focuses only on the period of 2071-2100 and the emission scenario A2 while the other two 30-year periods (2011-2040 and 2041-2070) and other emission scenarios (A1FI AND A1B) are presented in Appendix B2. Similar to Section 5.3.1, Section 5.3.2 presents future climate IDF curves for Jakarta Meteorological Station, a site with existing present climate IDF curves. Section 5.3.2 also focuses on the time period of 2071-2100 and emission scenario A2 while the other two time periods and other scenarios (A1FI AND A1B) are shown in Appendix B3.

A simple "delta" method (Hamlet and Lettenmaier, 1999; Miller et al., 2003), discussed in Section 3.8 of Chapter 3, is adopted in this study. The climate change factor or climate responses, 'simulated future rainfall intensities minus simulated present day rainfall intensities' (Wilby et al., 2009), is added to the present climate's lower and upper bounds of WRF/ERA40 derived IDF curves to form the range of each of the return periods for future rainfall extremes. It should be noted that should the site under consideration have existing IDF curves, the delta factor is simply applied directly to the respective existing IDF curves.

5.3.1 Future Climate IDF Curves for Stations with short or no rainfall record

The emission scenario A2 from GCM/ECHAM5 is used in this section to present the approach. Outputs from GCM/ECHAM5 for 1961-1990 represent baseline climate against which the future climate change scenario 2071-2100 was computed. To derive future climate's IDF curves, average climate change delta factor, Δ_i (simulated future (2071-2100) rainfall intensities minus simulated present day (1961-1990) rainfall intensities), is added to the present day's lower and upper bounds of WRF/ERA40 derived IDF curves to form the range of each of the return periods for future rainfall extremes. In this case, average delta (Δ_i, i = 6, 12, 18 and 24-hours) were derived and added on to the lower (+38%) and upper (+45%) bounds of the corrected present climate.

Figure 5.8 (a to d) showcases the lower and upper bounds of Darmaga station's 5, 10, 25, and 50-year return periods for the period of 2071-2100. Table 5-4 lists the lower and upper bounds for 5, 10, 25 and 50-year return periods for the period 2071-2100. By 2071-2100, the rainfall intensity is expected to increase between 49% and 82 % for the upper bound, and between 55% and 92% for the lower bound for 5-, 10-, 25- and 50-year return periods relative to their counterparts of the present climate. The results for the future climate IDF curves indicate that there is at least 49% to 55% increase in rainfall intensities by the end of the century. Table 5-5 shows summary of projected percentage future rainfall increase that can be expected for different time slices in the 21st century. The projections show a 'wetter' future for the

study region, Darmaga station by 2100; approximately 82% to 93% increase in rainfall intensity as compared to the present day climate. In the study, for proof-of-concept of the proposed approach, WRF simulations was only driven with GCM ECHAM5 forced under IPCC A2 emission scenario for 3 time slices (2011-2040, 2041-2070 and 2071-2100) of the 21st century; similar steps can, however, be implemented for other GCMs and climate scenarios.

Similarly, the approach was applied on 5, 10, 25 and 50-year return periods for the time periods of 2011-2040 and 2041-2070. Results are shown in Appendix B2.

This approach has provided a new perspective for developing future IDF curves in data sparse regions. The future IDF curves derived in this study incorporate different climate change scenarios with a range of upper and lower bounds which minimizes the uncertainties of the estimated future rainfall intensity. The delta approach will also be demonstrated in Section 5.3.2 on a site, Jakarta Meteorological Station, which has existing IDF curves.

5.3.2 Future Climate IDF Curves for Sites with Raingauge Data Derived IDF Curves

This section further demonstrates the derivation of IDF curves for future climate for sites with existing IDF curves. However, it only considers the Jakarta Meteorological Station to demonstrate the approach. A WRF driven by GCM/ECHAM5 under IPCC climate change emission A2 was used in this

section. The changes in the projected precipitation intensity as compared with the present day precipitation intensity were computed. The average delta (Δ_i, i = 6, 12, 18 and 24-hour) were derived and added on to the existing IDF curves. The approach was shown on precipitation intensities of 5, 10, 25 and 50-year return periods for the time period 2071-2100. Results are shown in Figure 5.9. WRF/ECHAM A2 projected highest increase in rainfall intensities for the 50-year return period as compared to 5, 10 and 25-year return periods (Figure 5.9) by 2071-2100. The precipitation response indicates that there is a projected increase in rainfall intensity as high as 201% for the 50-year return period of 24-hour rainfall duration (Figure 5.9b) toward the end of the 21st century. This finding is of crucial importance because the current stormwater infrastructures are not designed for twofold increases in rainfall intensity; thus, this provides essential information for future drainage design and mitigation measures.

The developed future climate IDF curves are of crucial importance for Jakarta region. It has provided a set of future IDF curves for early adaptation frameworks in view of the recent mapping vulnerability assessment (WWF, 2009) where Jakarta regions are at particular threat to droughts, floods, landslides and sea level rise. Recent floods, such as the flood of February 2007 can partly be explained by the inadequacy of drainage design capacity of the sewage system. Thus, a proper IDF curves which incorporated future climate change projections should be seriously considered for the future development of the region.

Table 5-6 and Figure 5.10 show that the precipitation intensity with the same duration and return period continue to increase from the 2011-2040 to 2041-2070 periods, except for 25 and 50-year return period where WRF/ECHAM A2 projected a slight decrease in rainfall intensity during the period 2011-2040. A significant increase is clearly projected in the 2071-2100 periods. These findings help to recognize the consequences of the anticipated changes in the rainfall intensity of the future climate rainfall events on the existing drainage facilities and suggest upgrading in the existing design standards so as to maintain the present level of capability and avoid an increase in the risk of flooding due to infrastructure failure.

Complete sets of Jakarta future IDF curves derived by WRF/ECHAM A2 for the time period of 2071-2100 is shown in Figure 5.11. The future IDF curves were derived for 6, 12, 18 and 24-hour durations for 5, 10, 25 and 50-year return periods. The complete sets of WRF/ECHAM A2 for the other two time period of 2011-2040 and 2041-2070 IDF curves are shown in Appendix B3.

The future climate IDF curves of WRF CCSM forced under different A1FI, A2 and A1B scenarios for all durations for specific durations are presented in Appendix B3. Similarly, the above demonstrated approach was applied on 5, 10, 25 and 50-year return periods for the time periods of 2011-2040, 2041-2070 and 2071-2100. All the results are shown in Appendix B3.

5.3.3 Ensemble Climate Change Simulations of An Emission Scenario: Jakarta Meteorological Station

This section aims to provide an insight on how to deal with uncertainties into the future changes and trends in the intensities of extreme rainfall of, say, A2 emission scenario; Jakarta Meteorological Station is selected for its demonstration. Two GCMs have been also used for projecting future climate.

It is well understood that in the presence of significant uncertainties, utilization of a single GCM may be one of many possible realizations and hence cannot be representative of the future. So, for a comprehensive assessment of the future changes, it is important to use collective information by utilizing all available or as many GCM models as possible, synthesizing the projections and uncertainties in a probabilistic manner (Solaiman and Simonovic, 2011).

This section analyses future precipitation change of A2 scenario driven by two different GCMs, WRF/CCSM and WRF/ECHAM. The analyses were carried out only for the 50-year return period to present the concept of GCMs' simulation uncertainties.

Figure 5.12 to 5.15 illustrate the 50-year return period precipitation change of 21st century for Jakarta Meteorological Station under two aforementioned GCMs. Projections for both WRF/CCSM A2 and WRF/ECHAM A2 show similar trend in the future precipitation change

projection for all rainfall durations (6, 12, 18 and 24-hour). As shown in Figure 5.12 to 5.13, WRF/ECHAM A2 projects decrease of rainfall intensity in the immediate future; about 7% to 26% less than the present day value of 33 mm/hr. However, the simulations for WRF/ECHAM A2 project show consistent increasing trend throughout the century. Projections for both WRF/CCSM A2 and WRF/ECHAM A2 were in very close agreement with each other during the period 2041-2070 for all rainfall durations.

Figure 5.12 reveals the difference between the two models for 6-hour duration storm. WRF/CCSM A2 projects higher intensity than WRF/ECHAM A2 at approximately 12% and 4% for immediate future and mid of the century respectively. By 2100, the projection of rainfall intensity by WRF/ECHAM A2 is about 44% more intense than that of WRF/CCSM A2. Nevertheless, the two models agree that precipitation will be more intense by 2100, approximately from 38 mm/hr (14%) to 52 mm/hr (58%) in comparison to the present day 6-hour rainfall intensity, at 33 mm/hr.

A common trend has been observed for 12, 18 and 24-hour rainfall durations. Figure 5.13 and 5.14 demonstrates similar trend for 12 and 18-hour rainfall but with a higher magnitude. There are evidence of increasing trend in the future rainfall intensity. This is more pronounced in WRF/ECHAM A2 than WRF/CCSM A2 where the 12 and 18-hour rainfall projection from WRF/ECHAM A2 were as high as 37 mm/hr (106%) and 32 mm/hr (154%) by the end of 21st century, relative to 18 mm/hr and 12 mm/hr present day intensity respectively.

Overall results show that WRF/CCSM A2 anticipates small increase in precipitation throughout the 21st century; a marginal increase of 4 to 18% for each time slice. WRF/ECHAM A2, however, shows more significant precipitation increase throughout the 21st century; approximately 201% by 2071-2100 period for 24-hour duration storm relative to present day climate (Figure 5.15).

Figure 5.16 to 5.18 present the WRF/CCSM A2 and WRF/ECHAM A2 projected future 50-year return period IDF curves, for Jakarta Meteorological Station, for the time periods of 2011-2040, 2041-2070, and 2071-2100 respectively. The difference between the two simulations shows the range of uncertainty. Different projection results could be due uncertainties arising from model simulations.

Simulations based on the WRF/ECHAM A2 demonstrate a mixed result for the future precipitation change. A slight decrease during the period 2011-2040 and also significant increases in future precipitation by 2100. The simulations show that rainfall intensities for the 50-year storm during the immediate future will decrease relative to present day values, hence runoff values will also decrease; this implies that the infrastructure systems designed for 50-year storm would not require to be retrofitted for the immediate future (2011-2040). However, by the 2041-2070, the high rainfall intensities simulated from the WRF/ECHAM A2 suggest a potential future overwhelming of the drainage network. These results are consistent with the findings reported by ADB (ADB, 2009). ADB reported that Indonesia could

experience a decrease in precipitation toward the middle of this century with the pattern reversing beyond 2050. On the contrary, WRF/CCSM A2 projects a consistent increase in precipitation for Jakarta region. Uncertainties remain on the future percentage increase in precipitation and the capacity of the drainage system to carry out runoff water. These uncertainties seem due to the inherent uncertainties in the downscaling results using different GCMs. Hence, the proposed procedure appears to provide clear signal about the increase in future precipitation but actual amount of increase cannot be exploited due to the inherent uncertainties of the GCMs.

These findings have provided important conclusion that multi-model ensemble systems need to be analyzed in order to quantify uncertainties. These multi-model ensemble systems must include the use of the output of different GCMs, as well as different RCMs to estimate how model results can simulate extremes in future climate. Climate models and knowledge about of how the earth's atmosphere works are continuously being improved, which will lead to better projections in the future. Therefore, in addition to the multi-model ensemble systems, it is encouraged to always having up-to-date data from the climate models is important. More parameters are also needed in the impact analysis (Olofsson, 2007).

5.3.4 Ensemble Climate Change Simulations of Different Emission Scenarios: Jakarta Meteorological Station

In contrast to Section 5.3.3, this section quantifies uncertainties of projected IDF curves resulting from different emission scenarios. Again, the analysis is demonstrated on Jakarta Meteorological Station; however, it is only for the 50-year return period.

Figure 5.19 to 5.22 illustrate the 50-year return period precipitation change of the 21st century for Jakarta Meteorological Station. The simulations for all the scenarios in the immediate future do not show significant increase in rainfall intensity. Figure 5.19 reveals less than 9% precipitation increase for the 6-hour duration rainfall. The results are fairly consistent with ADB (2009) findings as mentioned above.

The results for all rainfall durations indicate that WRF/CCSM A1B and A2 projected higher percentage precipitation increase as compared to WRF/CCSM A1FI during the 2011-2040 period. Opposite trend is observed for the simulation results of the period 2011-2040 as compared with the simulations result by IPCC (IPCC, 2007) and CCSM simulations by ORNL (http://www.ornl.gov/). According to both IPCC and ORNL, A1FI has the highest precipitation increase in the immediate future, followed by A2 and A1B scenarios; in this study, however, the immediate future rainfall intensity projected by WRF/CCSM A1FI was the lowest amongst the 3 scenarios. However, by the end of the 21st century, the projected rainfall intensity for

WRF/A1FI is more pronounced and is in agreement with the IPCC and ORNL findings. By 2100, all the three scenarios investigated show approximately 48% to 94% increase in rainfall intensity relative to present day. WRF/A1FI has the most significant increase relative to A2 and A1B. This provides a higher certainty on what has been reported by ADB (2009). According to ADB, by 2100, under the A1FI scenario, most countries in Southeast Asia would experience an increase in precipitation.

As shown in Figure 5.19 to 5.22, WRF/CCSM A1FI projected a consistent increase of rainfall intensity from the immediate future to mid of the 21st century and thereafter a significant increase in 2100. WRF/CCSM A2 also demonstrated a consistent increasing trend throughout all the 3 time slices; however, the percentage increase is much lower relative to WRF/CCSM A1FI. The A1FI scenario shows more than 94% increase in rainfall intensity relative to present day intensity for the 24-hour duration rainfall. This value is significantly high as compared to the increase of rainfall intensities simulated by WRF/CCSM A2 (48%) and A1B (50%) by the end of the 21st century. This result could be due to the nature of A1FI scenario that assumes very high GHG emission and total energy demand, rapid economic growth and carbon concentration. Thus, should the A1FI scenario occur, Jakarta is likely to anticipate more intense precipitation by 2100. The results also reveal that WRF/CCSM A2 and A1B have similar increasing trend in the future precipitation (Figure 5.19 to 5.22). The precipitation changes, especially during the 2071–2100 period are quite closely clustered together. This finding is useful in adaptation measures as to which scenario to adopt in the climate

change planning. Changes in rainfall intensities are very similar for both A2 and A1B; adopting scenario A2 or A1B do not show significant difference on all rainfall durations for the 50-year return period throughout the 21st century.

Figure 5.23 to 5.25 show the projected rainfall intensities of different climate change scenarios for the 50-year return period at three different time slices, 2011-2040, 2041-2070, and 2071-2100 respectively. Figure 5.23 shows that WRF/CCSM A1FI projected a smaller increase in precipitation as compared to WRF/CCSM A2 and A1B for the 50-year return period in the immediate future. As shown in Figure 5.25, the effect of high emission scenario (A1FI) is more pronounced during the last time slice of the 21st century. By the end of 21st century, WRF/CCSM A2 and A1B projected approximately the same rainfall intensities for the 50-year return period.

Although the rainfall intensities developed from different scenarios indicate large uncertainty, all the scenarios demonstrate increase of future rainfall intensities with a varying degree. The projections of different climate change scenarios in the future may be useful to capture the upper and lower bounds of the future climate change. From the results of all the 3 scenarios, it can be concluded that the emission scenario that produced the most intense rainfall was A1FI, and the least intense rainfall was A1B.

A warmer atmosphere can hold more moisture, about 8% more for every 1°C increase in temperature (NIWA, 2008). Chapter 4 discussed the temperature increase for all the 3 time slices in the 21st century, therefore the

potential for heavier rainfall certainly exists. The IPCC in its Third Assessment Report (IPCC, 2001) announced that more intense rainfall events are "very likely over most areas" (Wratt and Mullan, 2008). Thus, this study has provided conclusive projections that Jakarta (the region under consideration in this study) will experience heavier rainfall. The effects from different climate change scenarios are more pronounced by the end of 2100. These findings reinforce the crucial importance of future climate change projection for Jakarta's adaptation measures.

5.4 PROJECTED FUTURE IDF CURVES FOR SINGAPORE, KUALA LUMPUR AND JAKARTA

This section is a "by-product" of the research work. The main purpose is to show the changes in and comparisons between extreme rainfalls of the 3 mega cities, Singapore, Kuala Lumpur and Jakarta. Section 5.4.1 showcases only the assessment of projected extreme rainfall, resulting from different GCMs and emission scenarios, for the 50-year return period of the period 2071-2100. Section 5.4.2 compares the IDF curves, resulting only from WRF/ECHAM and A2 scenarios of the 3 cities; however, again just for the 50-year return period and the time slice of 2071–2100. Finally, Section 5.4.3 presents the complete IDF curves for each of the 3 cities for the time slice 2071–2100 resulting from WRF/ECHAM and A2 emission scenario.

5.4.1 Comparison between extreme rainfalls of 3 cities for the 50-year Return Period (2071-2100): different GCMs and emission scenarios

Figure 5.26 to 5.29 illustrate the projections of rainfall intensity, resulting from different GCMs and emission scenarios, for the 3 cities under different emission scenarios by the end of the 21st century. Presentation is conducted only for the 50-year return period.

For the WRF/CCSM simulations, Kuala Lumpur experiences highest percentage precipitation increase under A1FI scenario, followed by A2 and A1B scenarios. The intensity of the 24-hour rainfall duration for Kuala Lumpur is approximately 20 mm/hr as compared to 9 mm/hr for the present day. Jakarta also demonstrates highest precipitation increase under A1FI, followed by A1B and A2 scenario; however, the difference between percentage increase for simulations under A2 and A1B is insignificant. The results for both Kuala Lumpur and Jakarta city are quite consistent with the expected trend where very high emission scenario, A1FI, is substantially greater than the A2 and A1B scenarios (IPCC, 2007; ADB, 2009). This trend, however, was not apparent for Singapore. The results for Singapore reveal highest precipitation increase under A2 scenario, followed by A1B and A1FI.

With WRF/ECHAM A2 simulations, Jakarta will experience highest percentage precipitation change among the three cities examined. By 2100, the 24-hour rainfall intensity projected for Jakarta is 29 mm/hr relative to

present day intensity of 9.5 mm/hr. This amount is significant as it represents an increase of about 200%. This poses serious issue for Jakarta where flooding has been an annual event in the recent decades. Adaptation measures, though costly, will have to be taken at the earliest.

5.4.2 Comparison between IDF Curves of 3 cities for 50-year Return Period: WRF/ECHAM and A2 emission scenario

Figure 5.30 to 5.32 compare future climate IDF curves of the 50-year return period and for all three time slice (2011-2040, 2041-2070 and 2071-2100) for Singapore, Kuala Lumpur and Jakarta Meteorological Stations. They are, however, derived only from simulation results from WRF/ECHAM and A2 emission scenario. A comparison of the three cities indicates that Singapore projected highest rainfall intensity for the 50-year return period for 2011-2040 and 2041-2070 followed by Jakarta and Kuala Lumpur. However, for the period of 2071-2100 (Figure 5.32), Jakarta projected higher rainfall intensity than the other two cities. There is no clear signal contributes significantly to the sudden change in trend; nevertheless, the difference is not that significant, about 10 mm/hr relative to Singapore's intensity for the same rainfall duration and future time slice.

Generally, the projected rainfall intensities for Singapore, Kuala Lumpur and Jakarta show a consistent increase from immediate future to mid of 21st century, and significantly more (about 50% more than 2041-2070) by the end of the century. Increased precipitation intensity and variability would

result in an increase in the flood risks in these cities. Similar simulations were done for 5 and 10-year return periods for all the 3 time slices of the 21st century. The simulation results are, however, presented in Appendix B4.

5.4.3 Comparison between IDF Curves of 3 cities under WRF/ECHAM and A2 emission scenario (2071-2100)

Figure 5.33 to 5.35 present the projected future IDF curves (2071-2100) for Singapore, Kuala Lumpur and Jakarta Meteorological Stations respectively. Note that, for easy reference and comparison, Figure 5.35 is identical to Figure 5.11 presented earlier. The curves were derived from WRF/ECHAM A2 for 6, 12, 18 and 24-hour rainfall durations. The complete future IDF curves for Singapore and Kuala Lumpur are presented for 5, 10, 50 and 100-year return periods while for Jakarta the complete future IDF curves are presented in 5, 10, 25 and 50-year return periods based on their availability. Similar simulations were also applied for the derivation of future climate IDF curves for period 2011-2040 and 2041-2070 and the results are presented in Appendix B5.

5.5 CONCLUDING REMARKS

The main objective of this chapter was to demonstrate the (3-step) DCD proposed approach to derive the present day and the future climate IDF curves particularly for regions with short or no rainfall records (Darmaga Station in Indonesia was used as a validation station). However, the derivation of future climate IDF curves for regions with long rainfall records (Singapore, Kuala

Lumpur and Jakarta Meteorological Stations) were demonstrated as well. This study is probably the first of its kind to apply the results of a regional climate model's results to derive the present and future IDF curves for sites with short or no rainfall records.

The proposed approach was relatively simple and yet has been proven effective. Simulation results from a RCM (WRF) driven by Re-Analysis data (ERA40) was first used to derived the present day IDF curves for sites with long rainfall records; these IDF curves were compared with their counterparts, IDF curves derived from raingauge data. Bias correction quantities (38% to 45%) were noted. These bias correction quantities form the basis in the construction of the present day IDF curves for sites where the rainfall record is short or non-existent.

Another contribution of this study is the development of future climate IDF curves. To demonstrate the development of future IDF curves, two sites (Jakarta Meteorological Station and Darmaga Station) were selected; one with long rainfall record while the other is from an ungauged basin. The derivation of future IDF curves was done by applying the 'simple delta' method on the high resolution dynamical downscaling outputs. In this study two GCMs (CCSM3.0 and ECHAM5) and three emission scenarios (A1FI, A2 and A1B) were considered. This study focuses only on IDF curves with rainfall durations of 6, 12, 18 and 24-hour. For a rather large catchment like Jakarta, partially urban and partially rural with a rather long time of concentration (12 hours at least), the presented approach and results are thus applicable.

However, for catchments with shorter than 6-hour time of concentration, results derived from 6-hourly have to be scaled down to sub-6 hourly. The approach suggested by Nguyen et al. (2007), where they demonstrated an approach as to how to correlate sub-daily IDF information from daily IDF data. For this study, the same approach may be used to extract 6-hourly IDF data by correlating the existing sub-6 hourly IDF and the 6-hourly IDF.

Results presented in this study were based on the output from only two climate models. It is essential that subsequent applications use a greater number of climate models. This way, the average of future precipitation change can be obtained and potentially reduce the uncertainty in future scenarios by down weighting underperforming climate models (Leith, 2008; Chandler et al., 2006). Nevertheless, the future climate IDF curves developed from this study has been a significant contribution, in particular, for adaptation measures to the climate change for Jakarta where flooding has been annual events in recent decades.

For all the cities considered (Singapore, Kuala Lumpur and Jakarta), the study has shown that the intensity of extreme rainfall is projected to increase significantly in particular towards the end of the 21st Century.

This page is intentionally left blank.

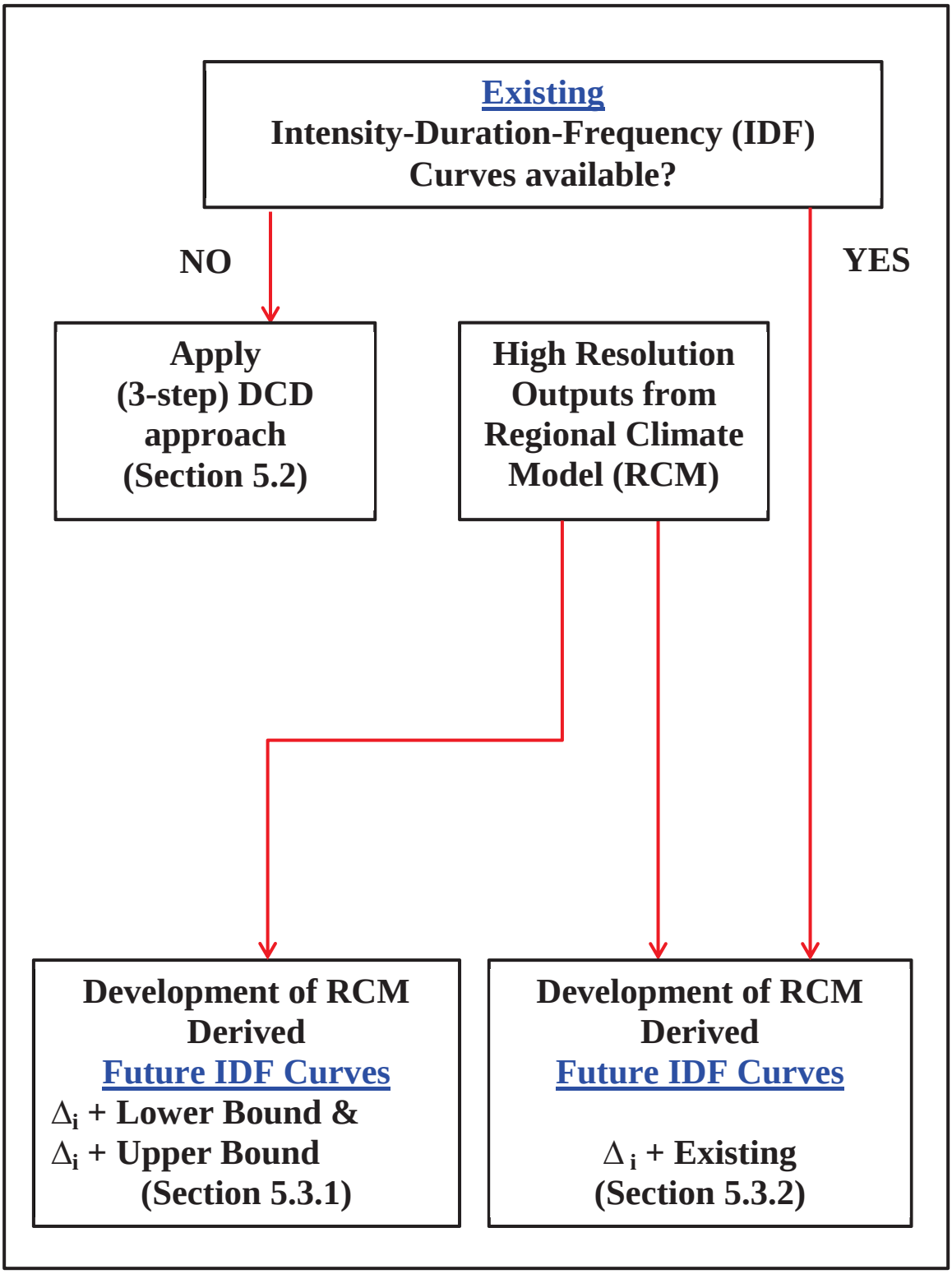

Figure 5.1: Development of present and future IDF curves, using regional climate model and incorporating climate change projections

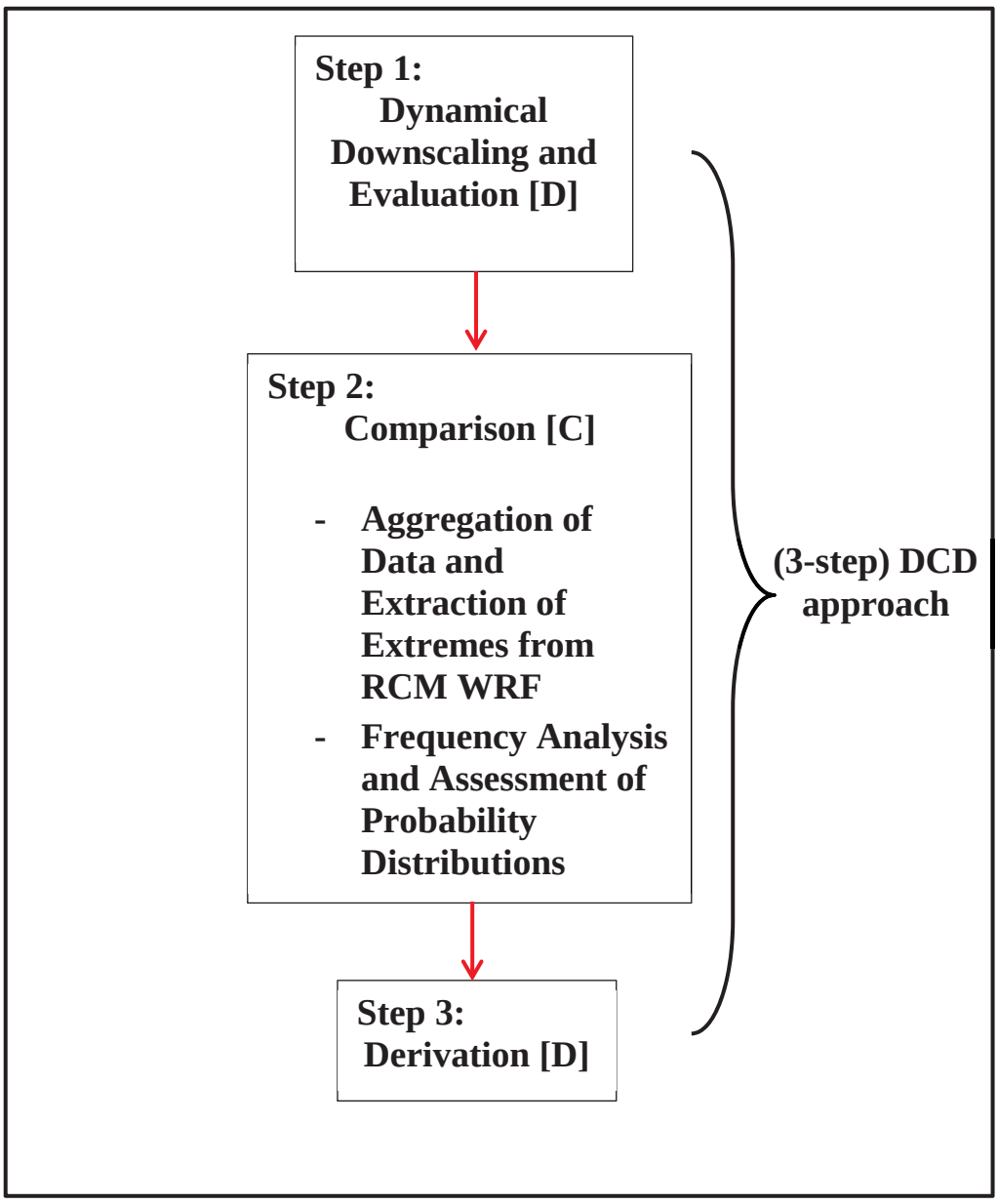

Figure 5.2: A (3-step) DCD approach to develop present climate IDF curves for sites with short or no rainfall data

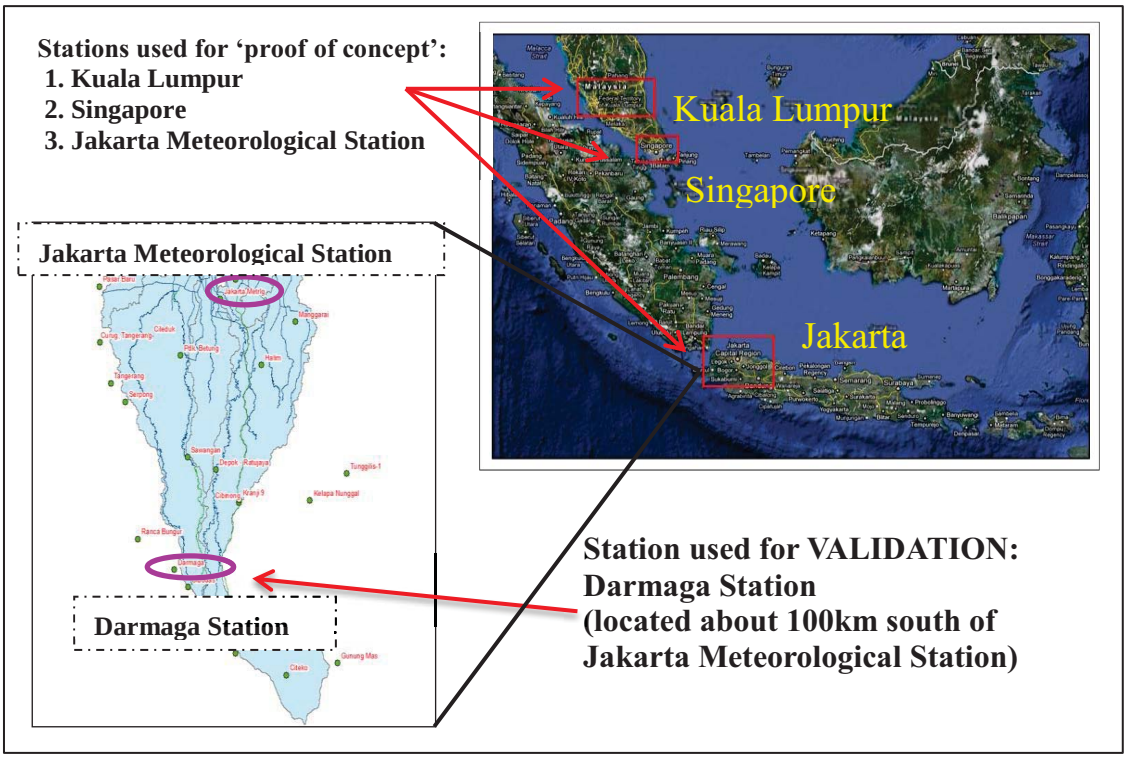

Figure 5.3: Location of rainfall stations used for 'proof of concept' and for validation

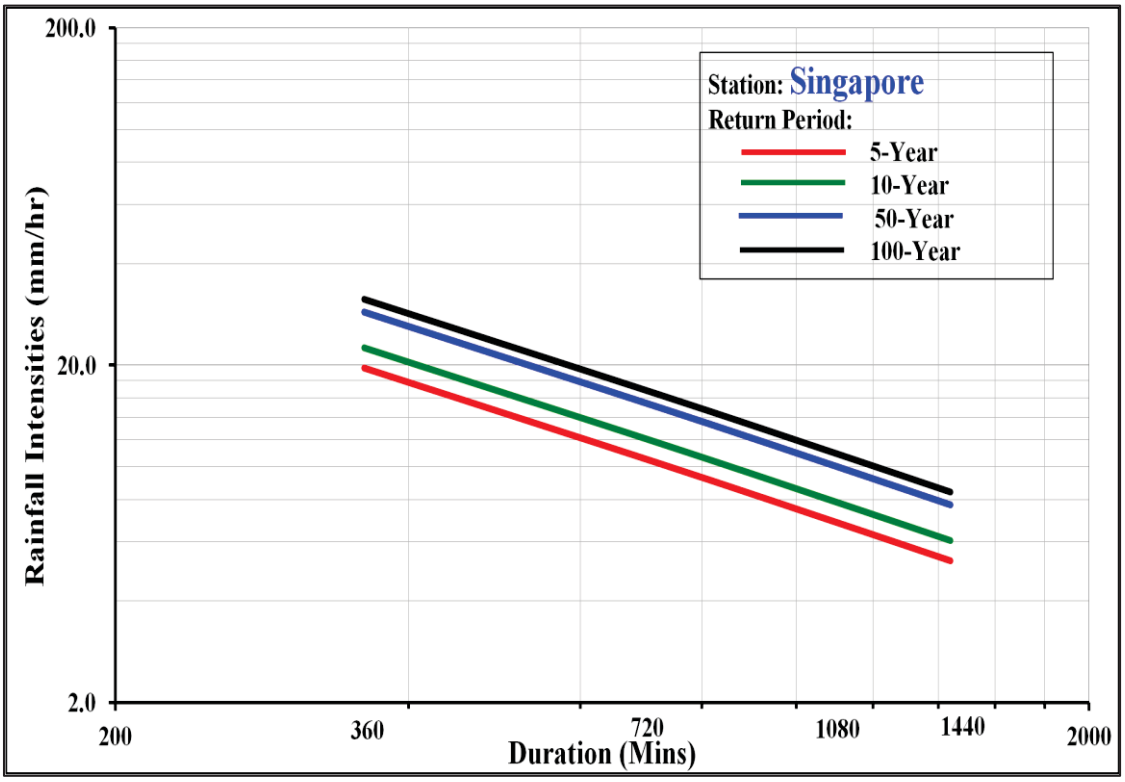

Figure 5.4: Existing IDF curves

(a) Singapore

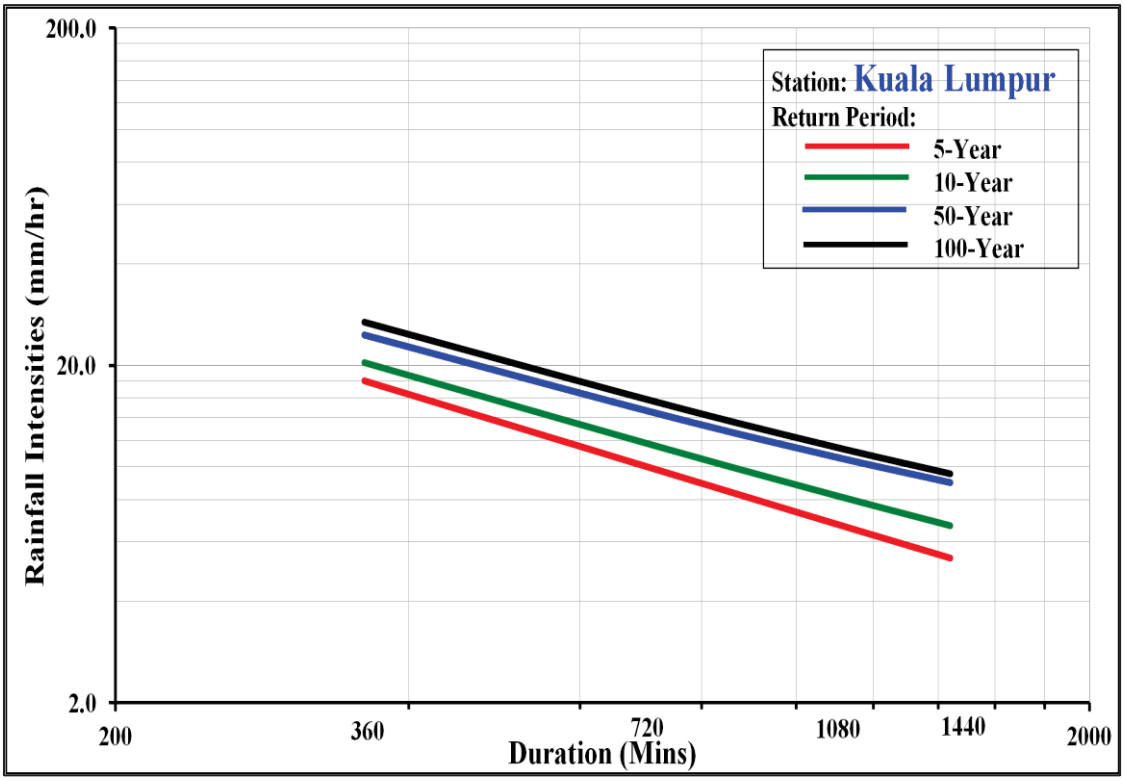

Figure 5.4: (contd) for **(b) Kuala Lumpur**

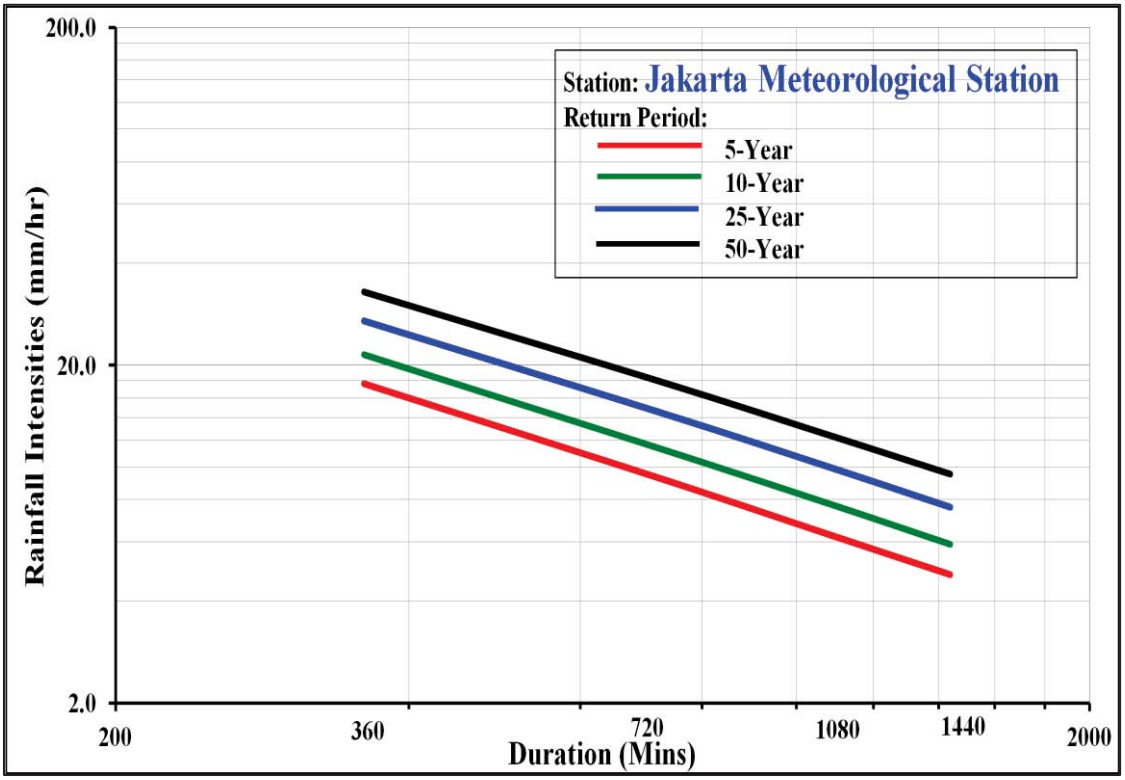

Figure 5.4: (contd) for **(c) Jakarta Meteorological Station**

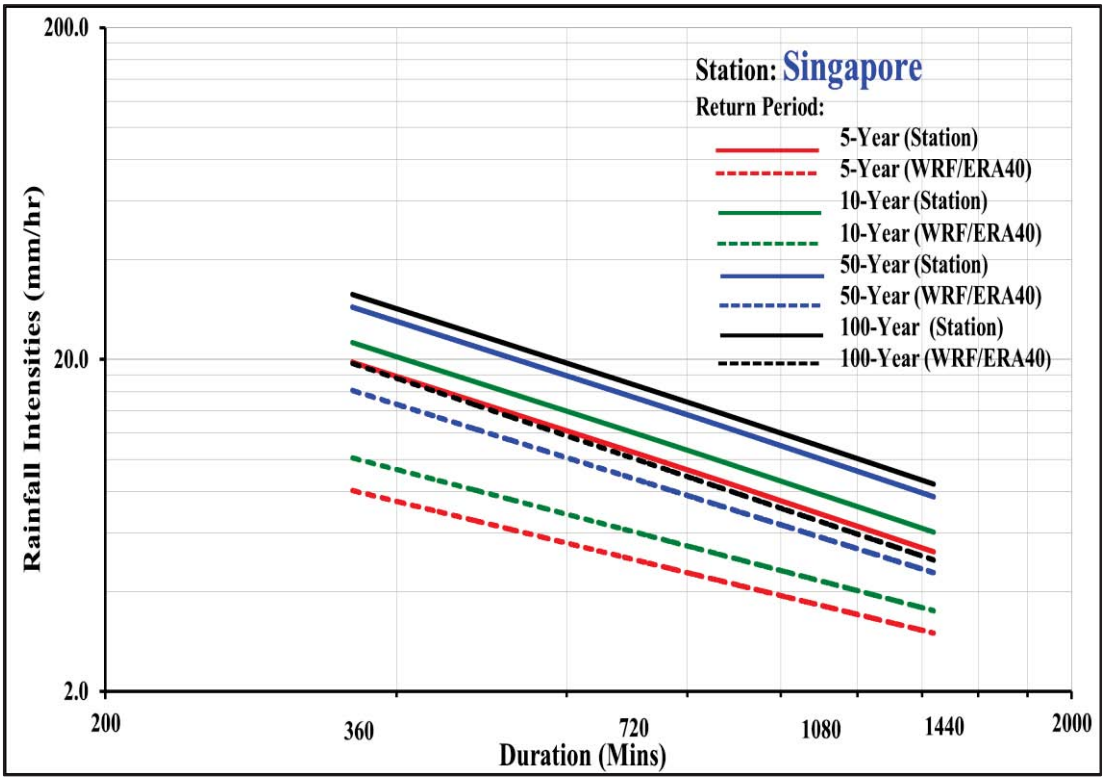

Figure 5.5: Comparison between existing and WRF/ERA40 derived IDF curves **(a) Singapore**

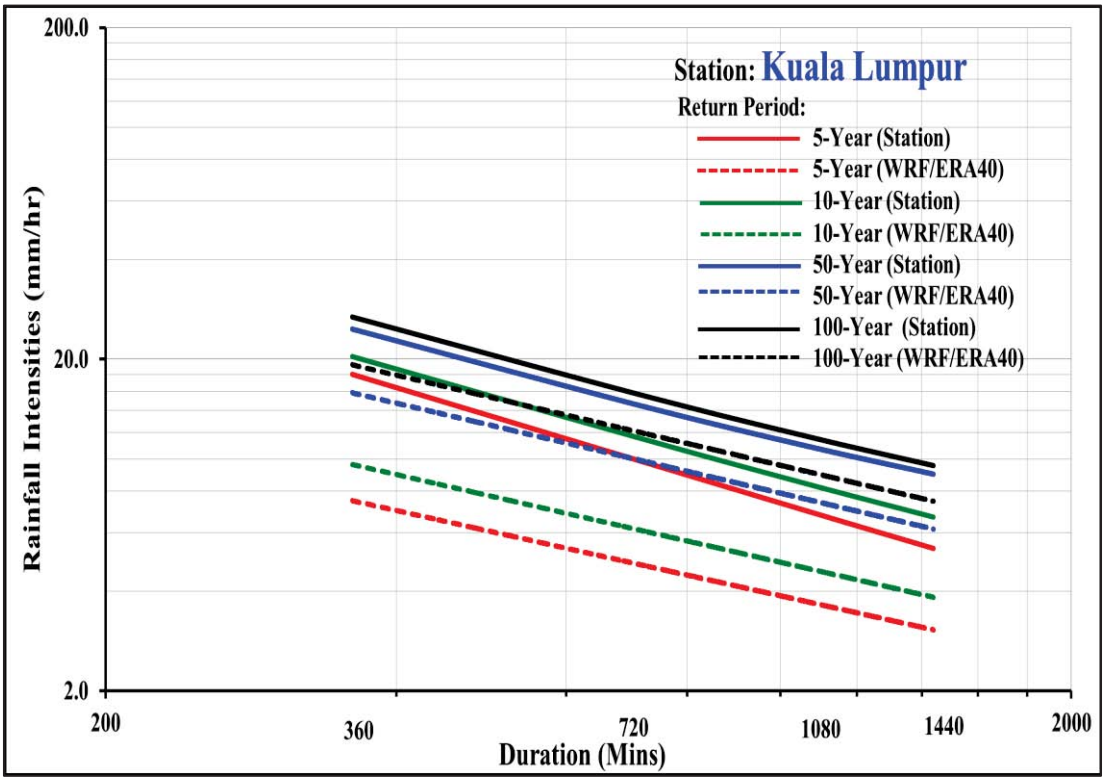

Figure 5.5: (contd) for **(b) Kuala Lumpur**

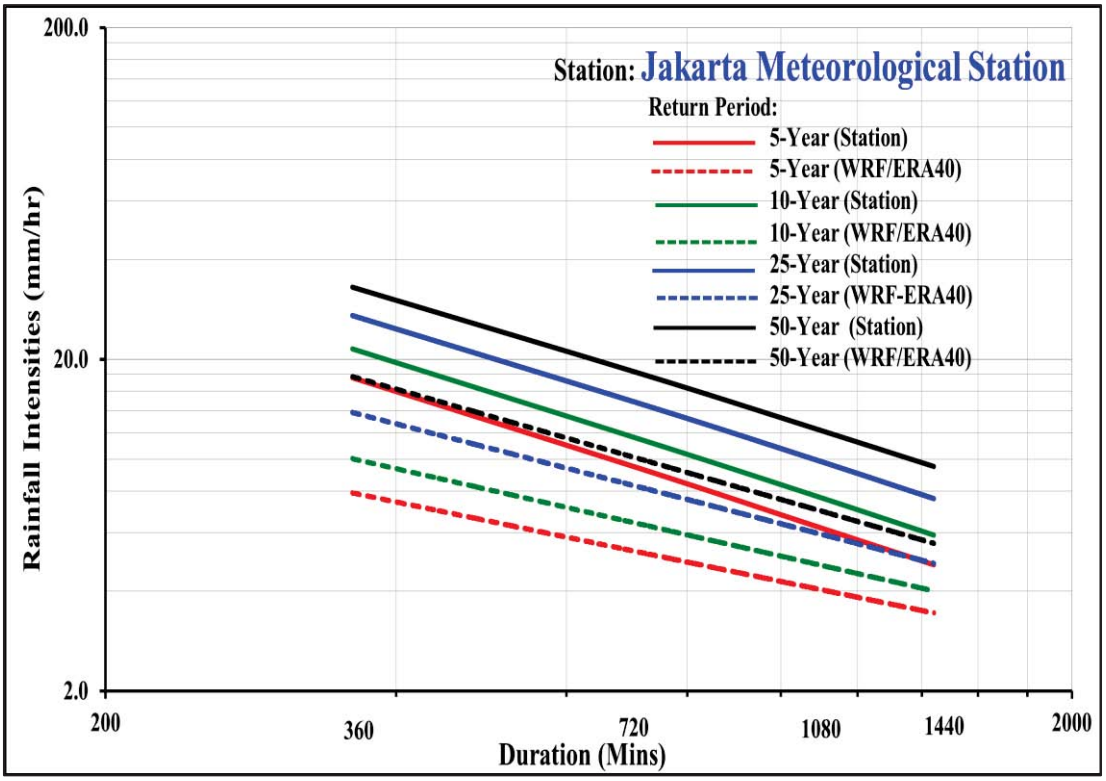

Figure 5.5: (contd) for **(c) Jakarta Meteorological Station**

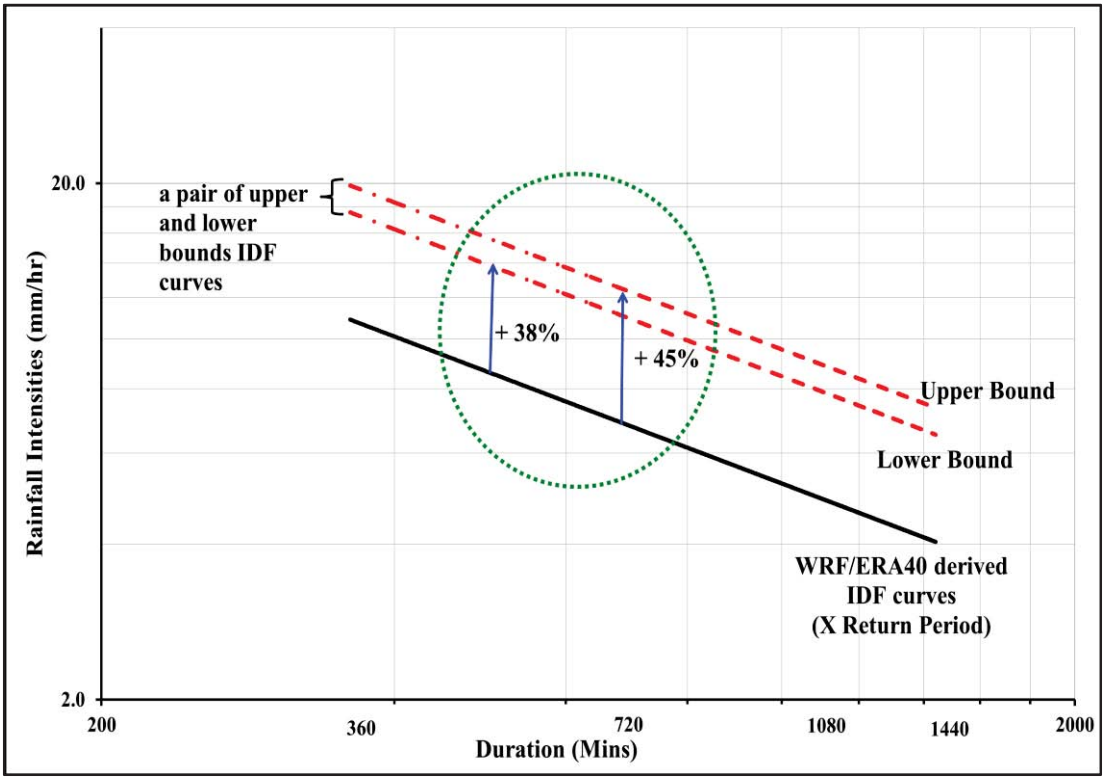

Figure 5.6: Proposed IDF curve of any return period at sites with short or no rainfall record: Solid line is derived from WRF/ERA40, dashed lines are the lower and upper bounds of the IDF curve after bias corrections

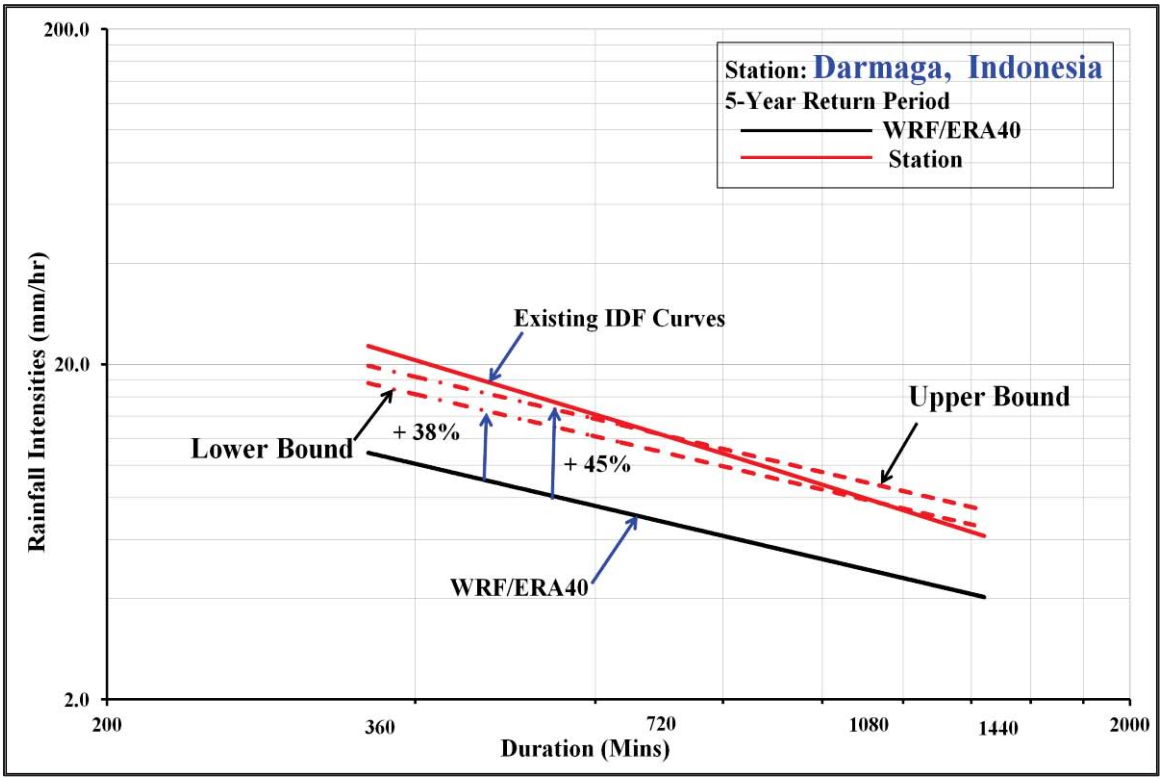

Figure 5.7: WRF/ERA40 projected present day rainfall intensities anomalies from the existing IDF curve: Darmaga Station

(a) 5-year return period

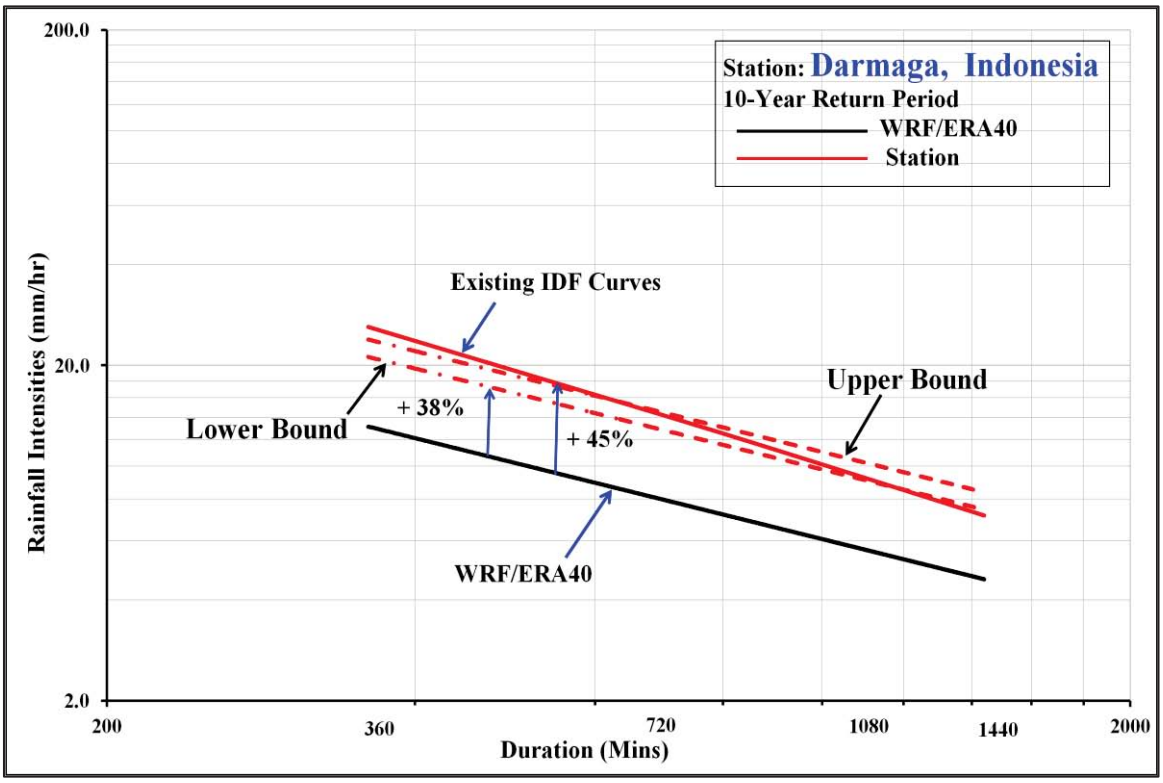

Figure 5.7: (contd) for **(b) 10-year return period**

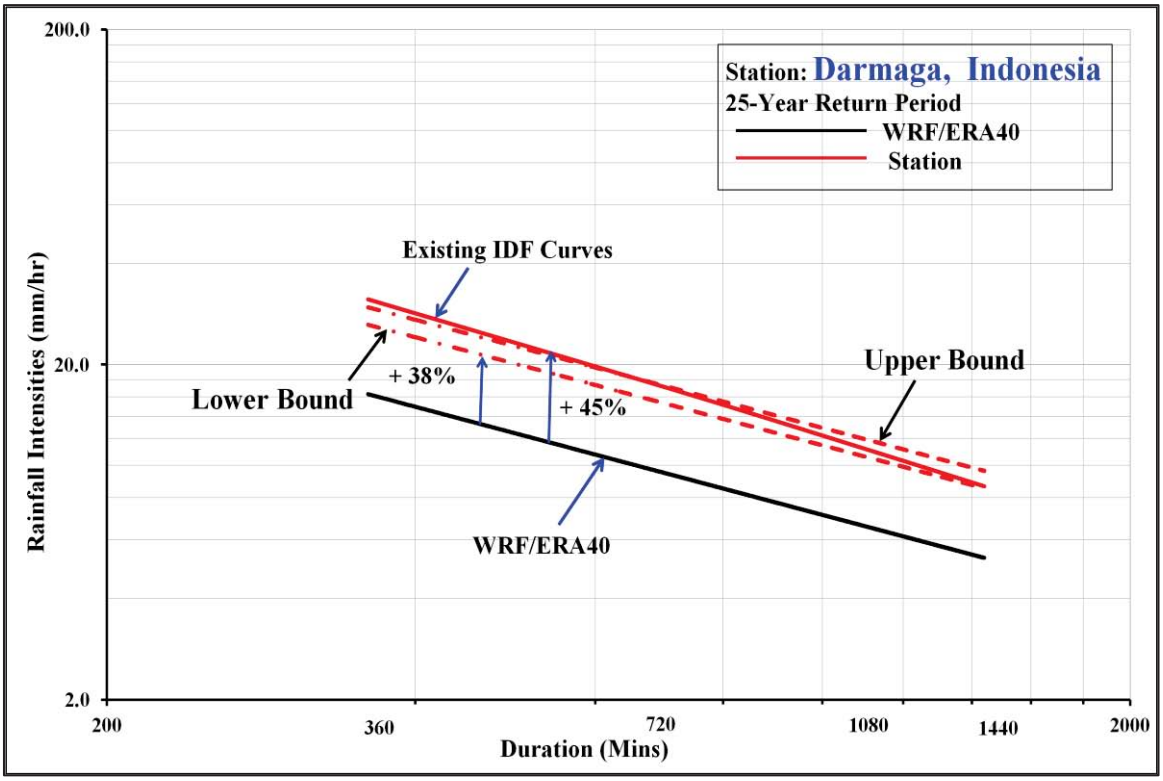

Figure 5.7: (contd) for **(c) 25-year return period**

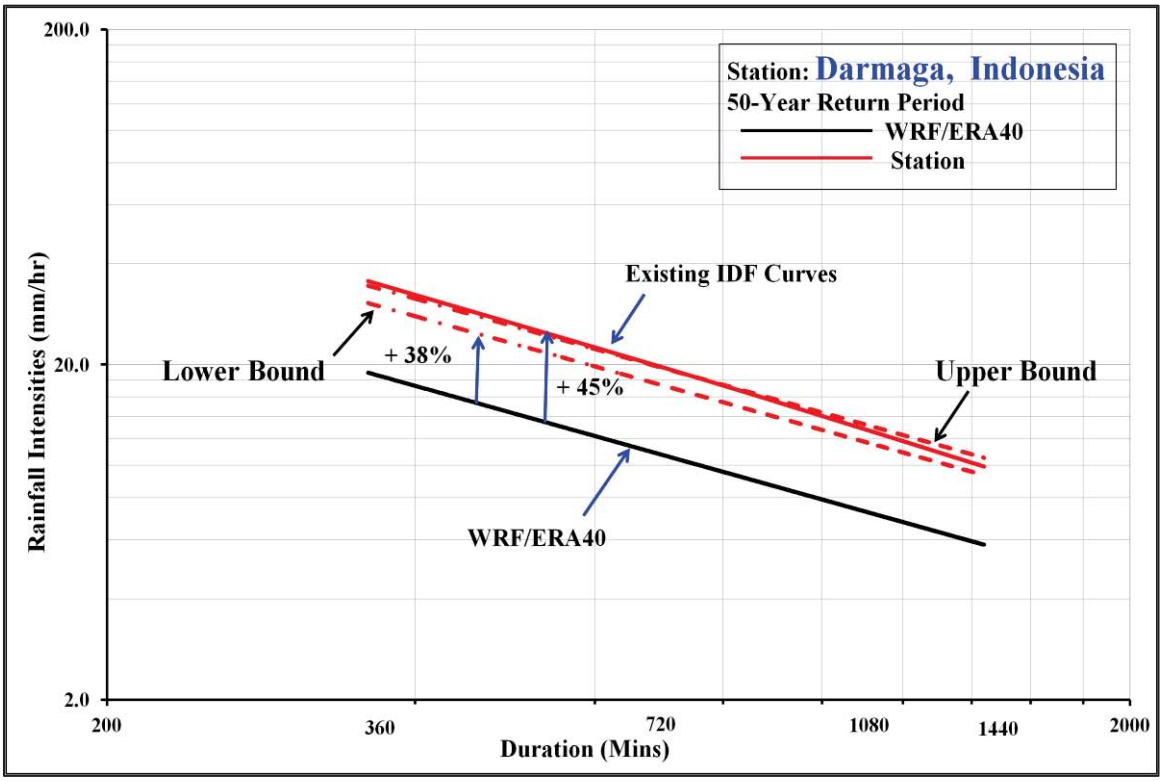

Figure 5.7: (contd) for **(d) 50-year return period**

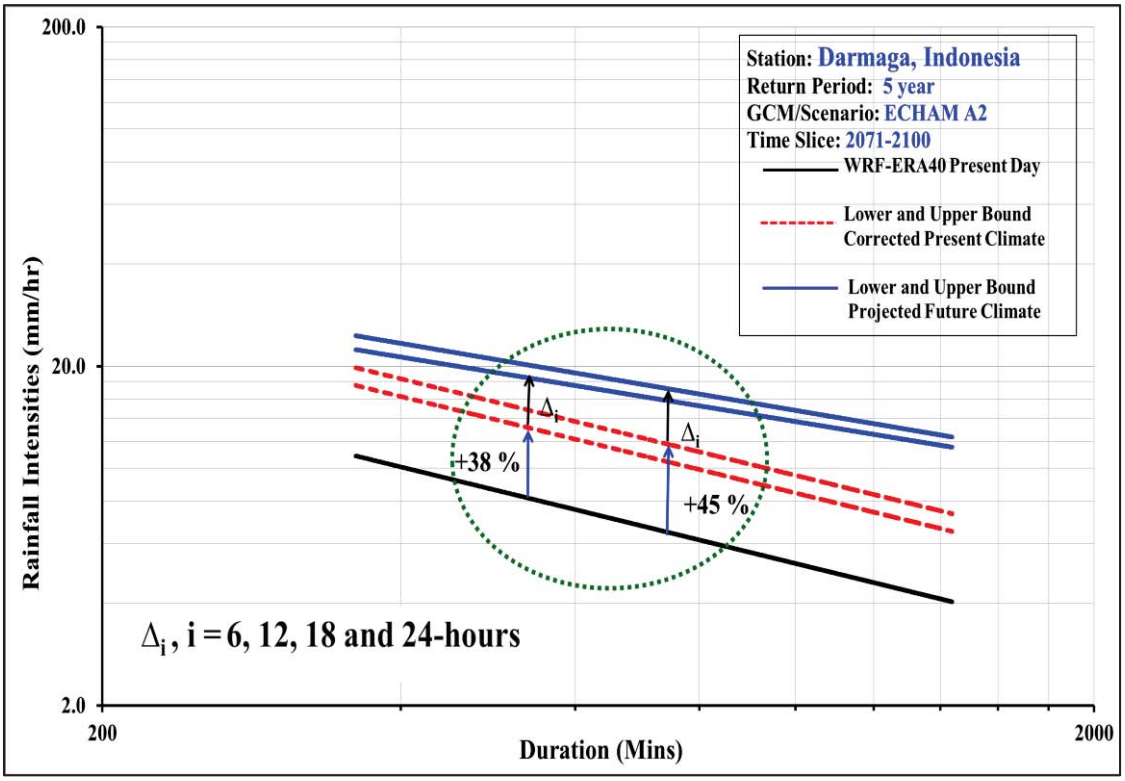

Figure 5.8: Projected future climate IDF curves **2071-2100, WRF/ECHAM A2**: Darmaga Station

(a) 5-year return period

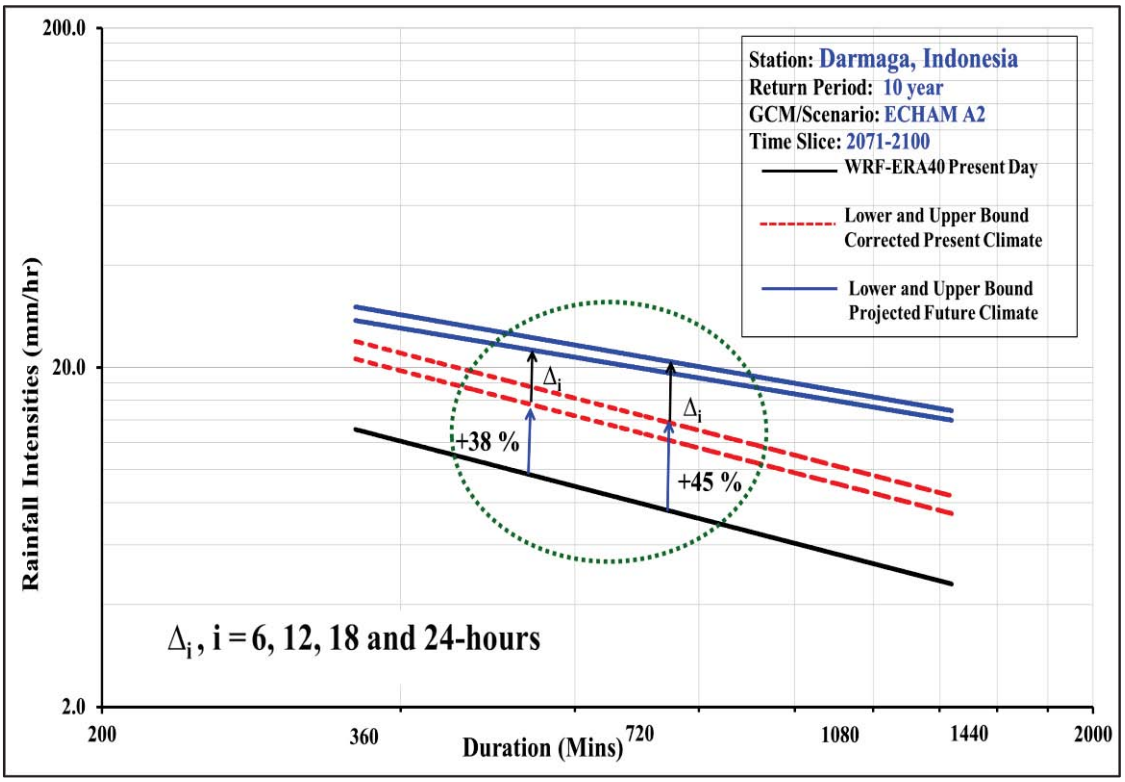

Figure 5.8: (contd) for **(b) 10-year return period**

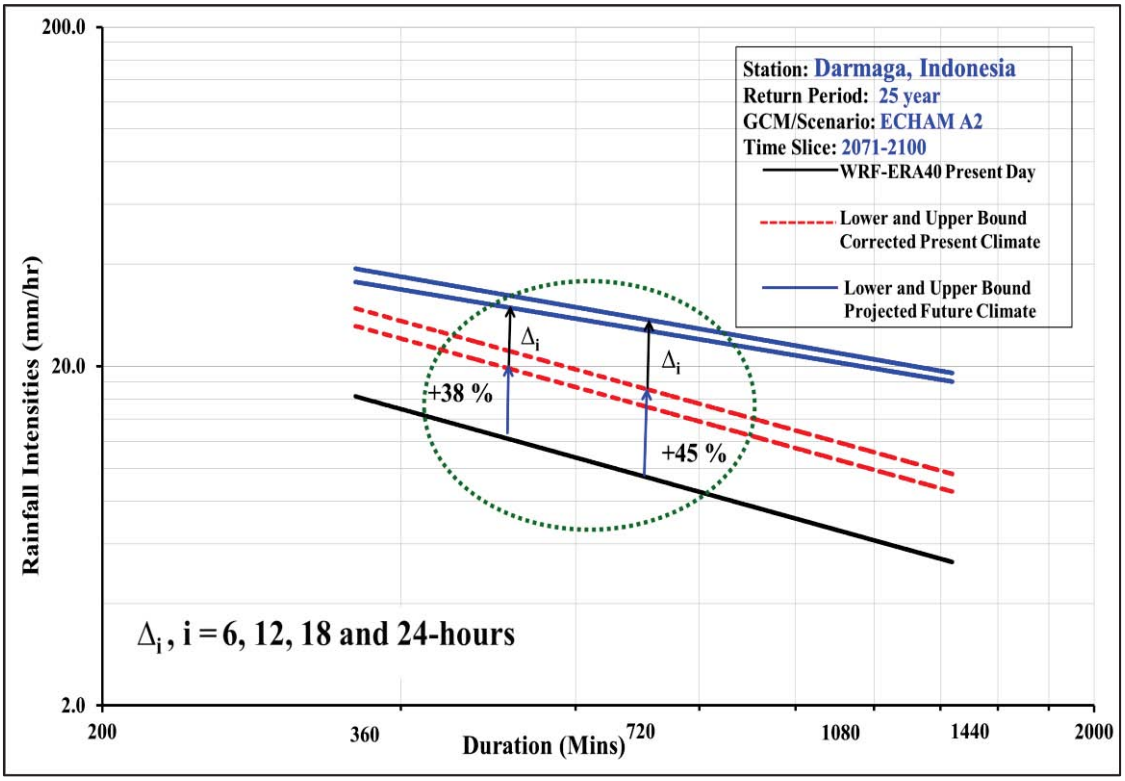

Figure 5.8: (contd) for **(c) 25-year return period**

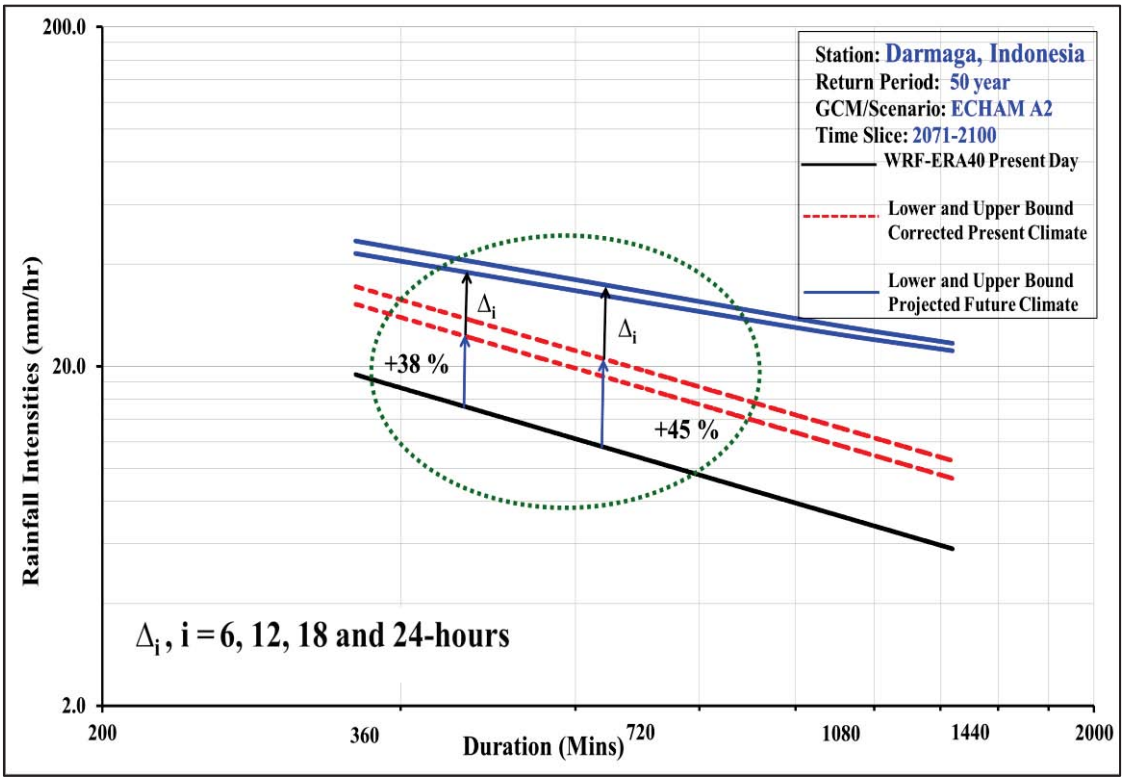

Figure 5.8: (contd) for **(d) 50-year return period**

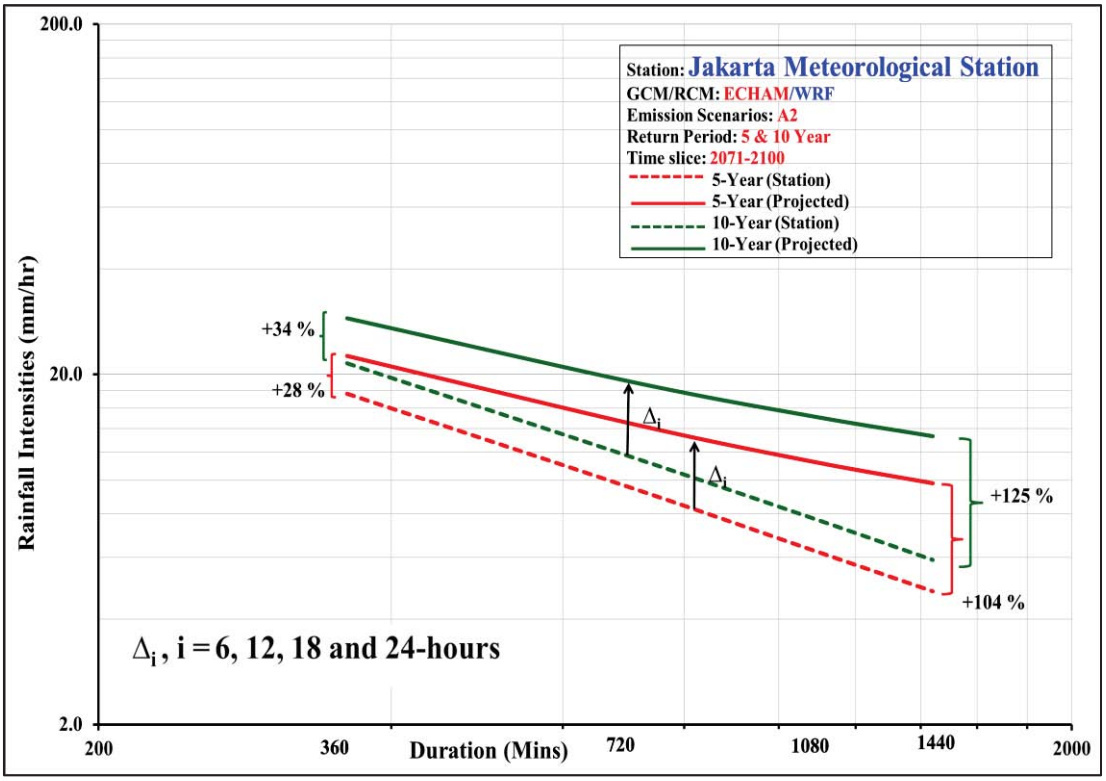

Figure 5.9: Projected future climate IDF curves **2071-2100, WRF/ECHAM A2**: **Jakarta Meteorological Station**
(a) 5 and 10-year return periods

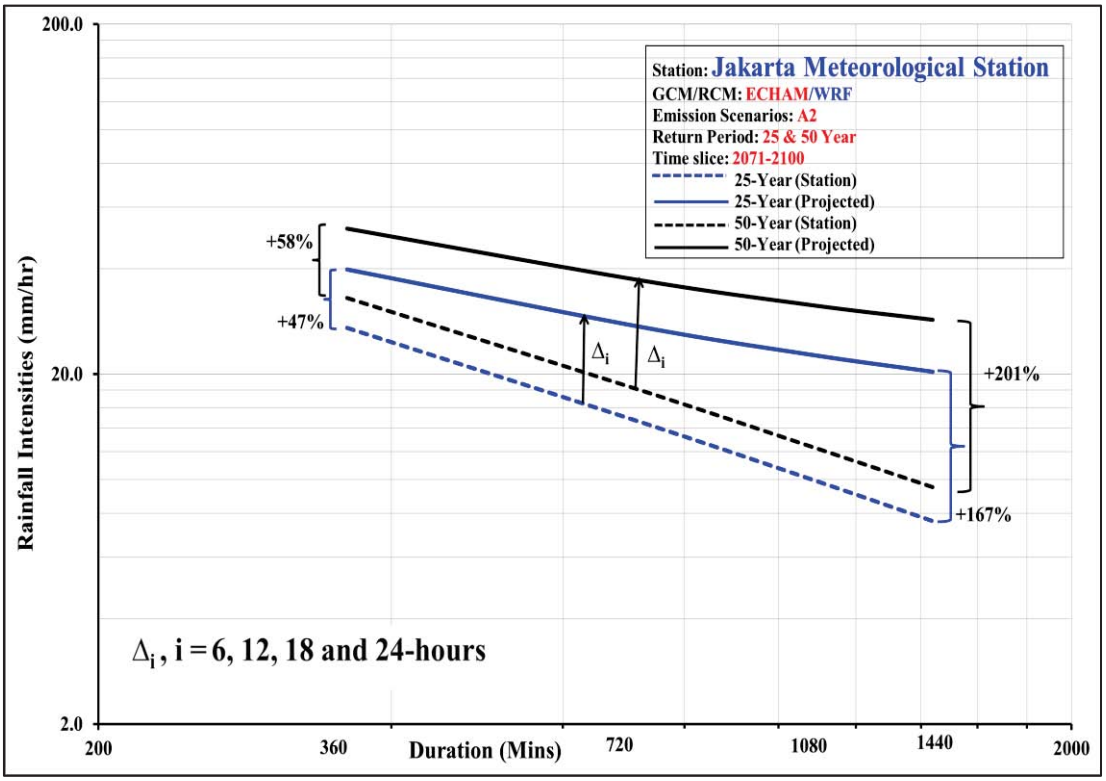

Figure 5.9: (contd) for **(b) 25 and 50-year return period**

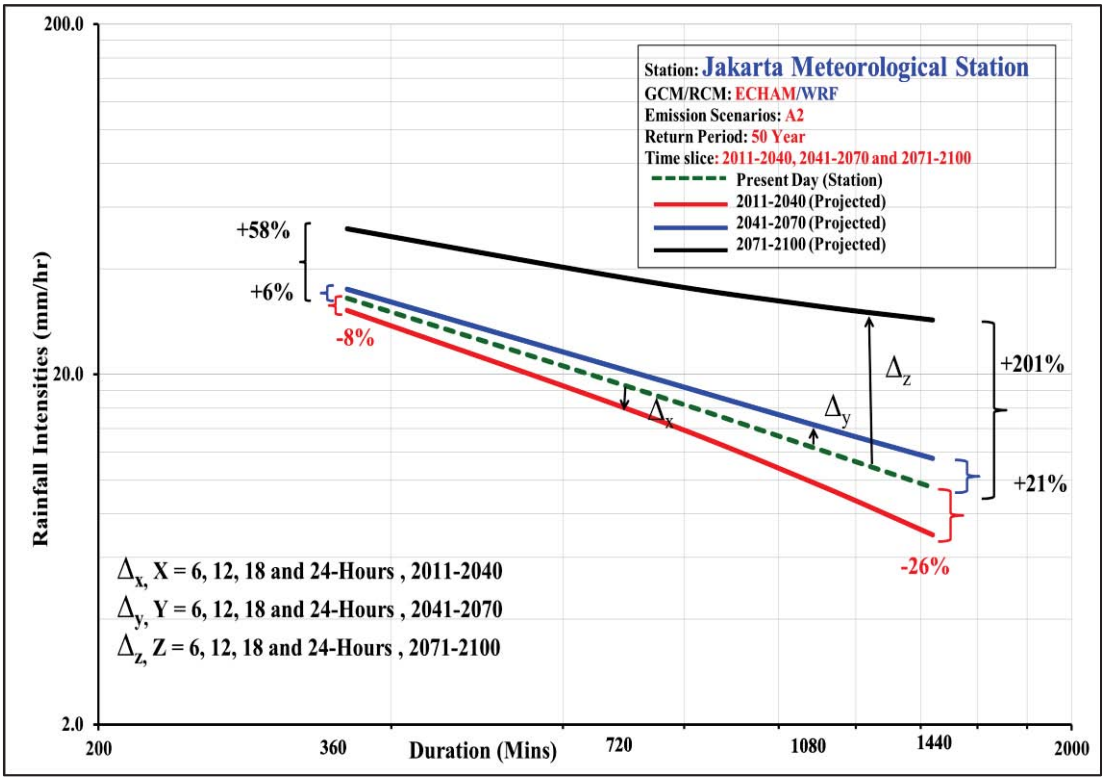

Figure 5.10: Projected future climate IDF curves **(50-year return period, 2011-2040, 2041-2070 and 2071-2100, WRF/ECHAM A2)**: **Jakarta Meteorological Station**

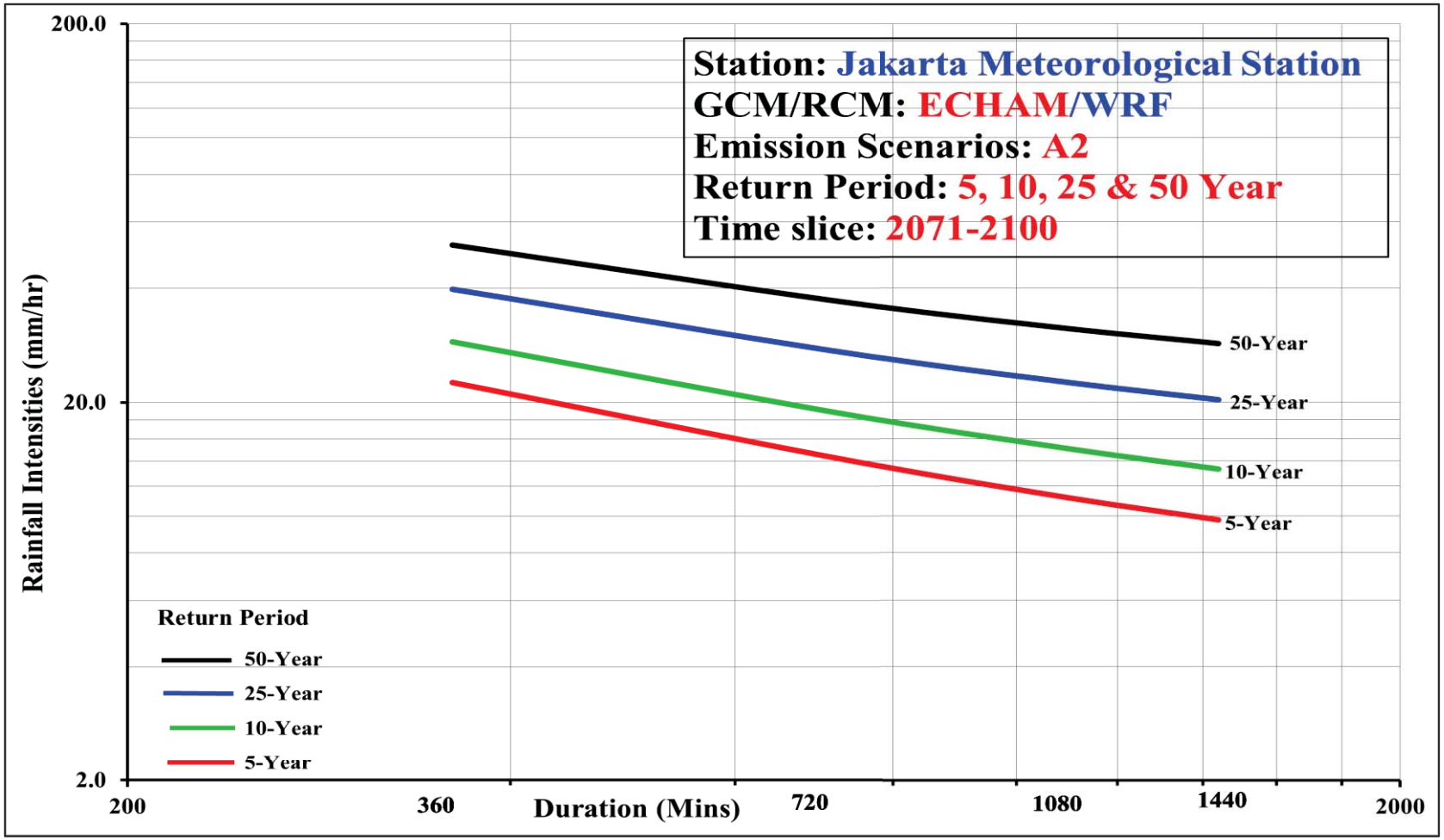

Figure 5.11: Future climate IDF Curves (2071-2100) derived from **WRF/ECHAM A2**: **Jakarta Meteorological Station**

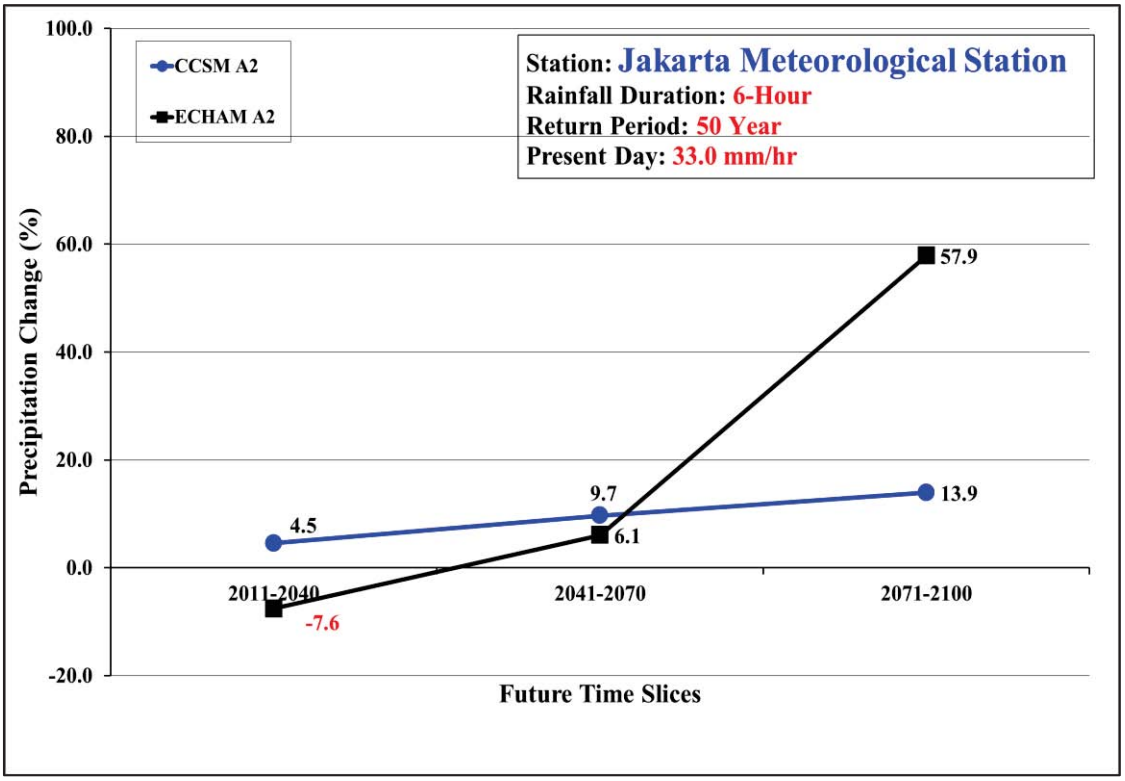

Figure 5.12: Comparison between **WRF/CCSM A2** and **WRF/ECHAM A2** projected 50-year return period for Jakarta Meteorogical Station: **6-hour rainfall duration**

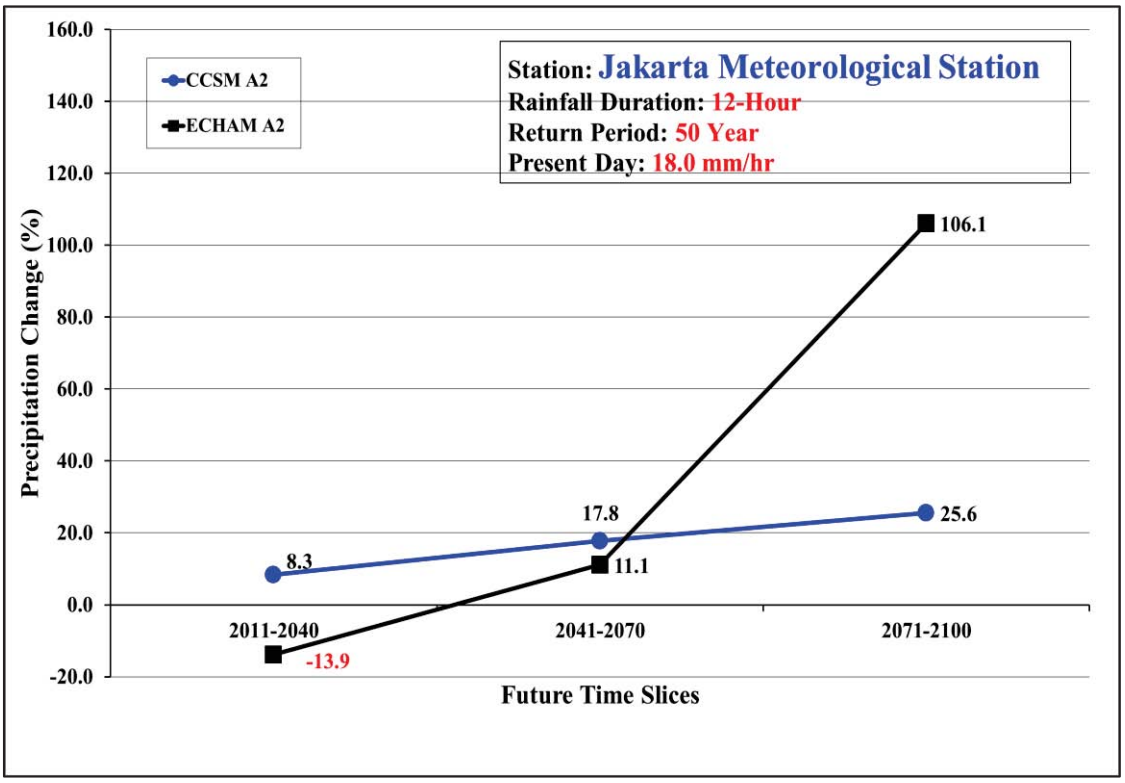

Figure 5.13: Comparison between **WRF/CCSM A2** and **WRF/ECHAM A2** projected 50-year return period for Jakarta Meteorogical Station: **12-hour rainfall duration**

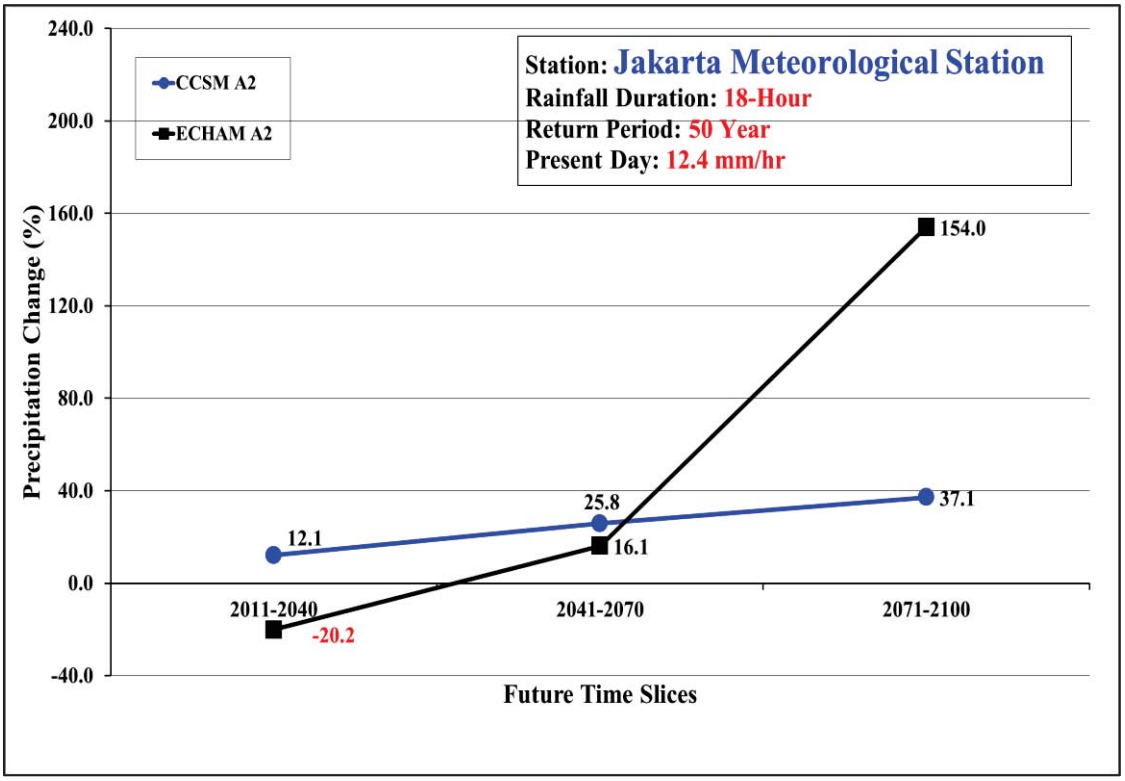

Figure 5.14: Comparison between **WRF/CCSM A2** and **WRF/ECHAM A2** projected 50-year return period for Jakarta Meteorogical Station: **18-hour rainfall duration**

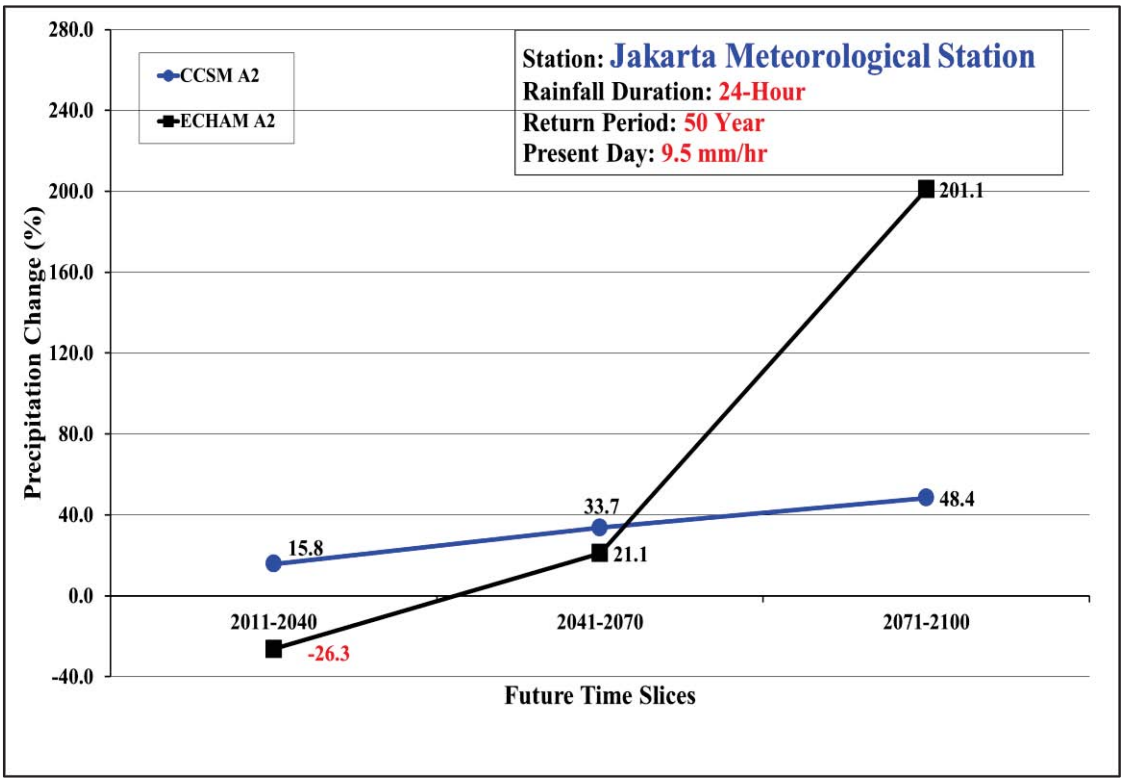

Figure 5.15: Comparison between **WRF/CCSM A2** and **WRF/ECHAM A2** projected 50-year return period for Jakarta Meteorogical Station: **24-hour rainfall duration**

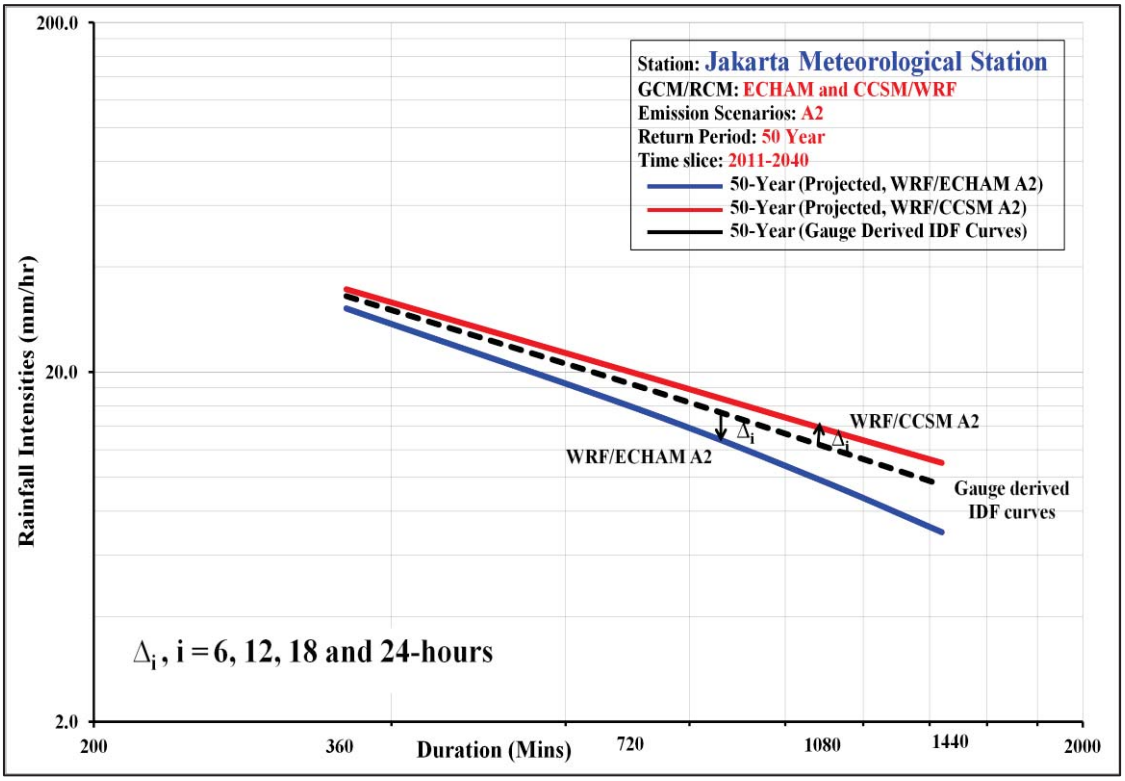

Figure 5.16: Quantifying uncertainties of projected 50-year return period, for Jakarta Meteorological Station, with **WRF/CCSM A2** and **WRF/ECHAM A2**: **2011-2040**

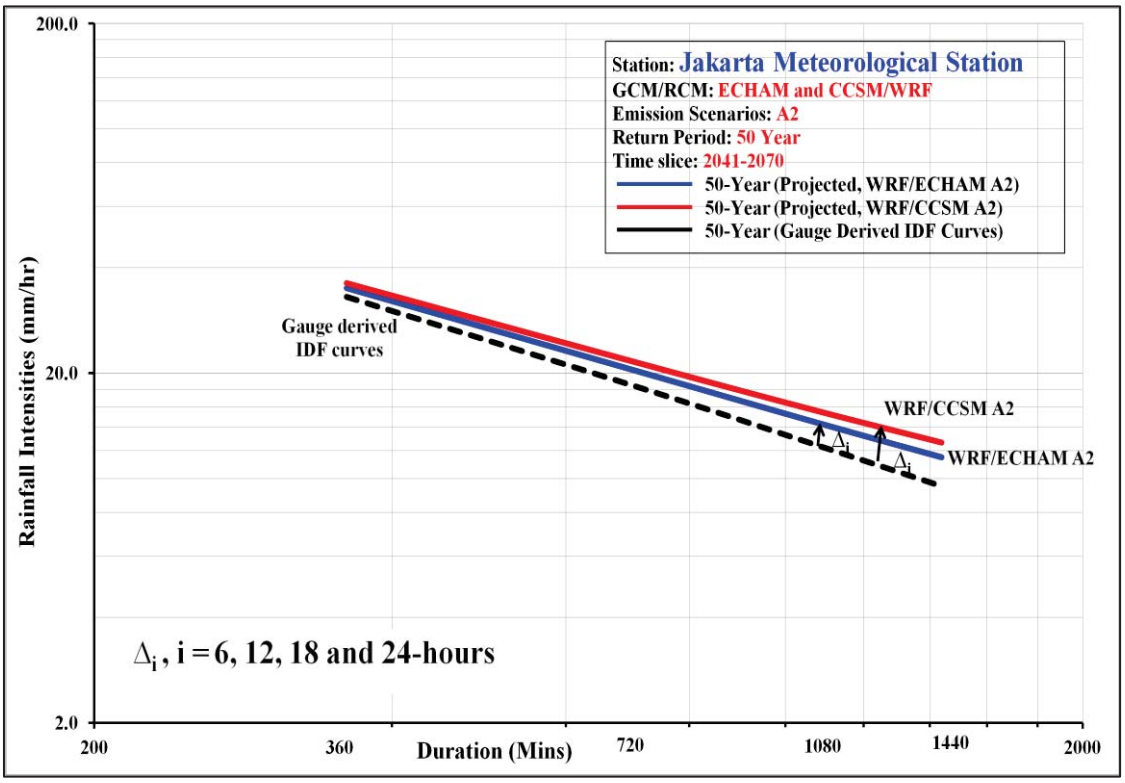

Figure 5.17: Quantifying uncertainties of projected 50-year return period, for Jakarta Meteorological Station, with **WRF/CCSM A2** and **WRF/ECHAM A2**: **2041-2070**

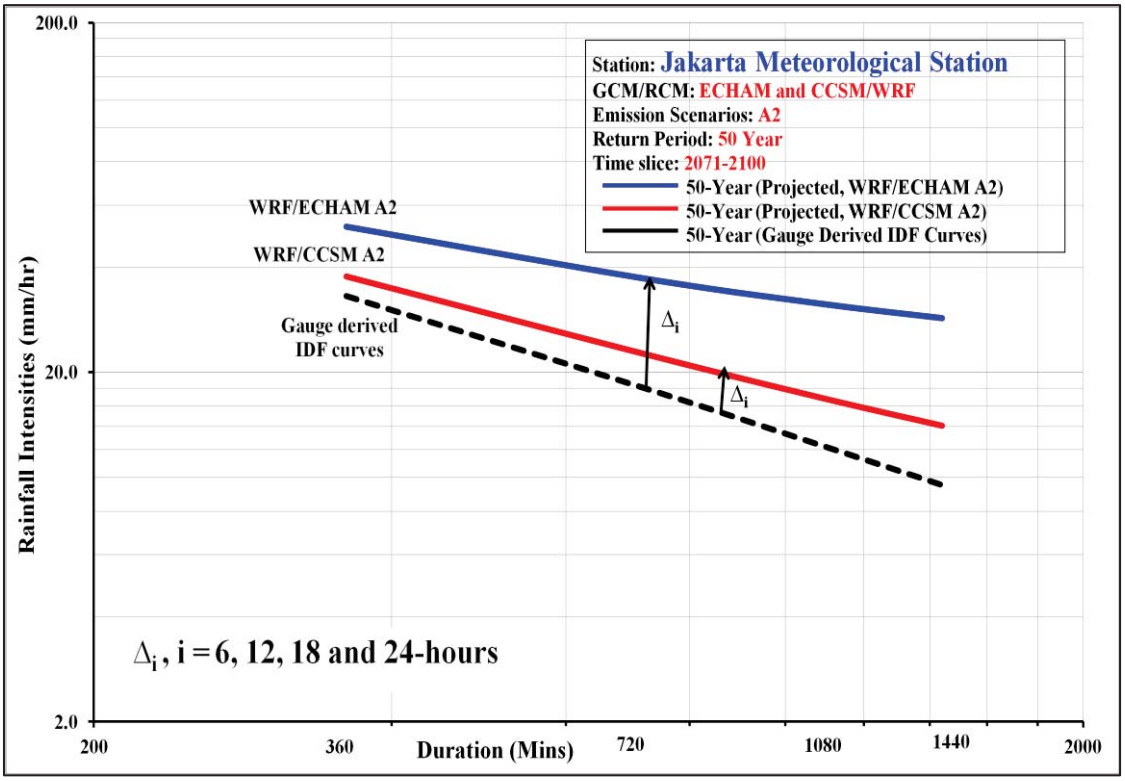

Figure 5.18: Quantifying uncertainties of projected 50-year return period, for Jakarta Meteorological Station, with **WRF/CCSM A2** and **WRF/ECHAM A2**: **2071-2100**

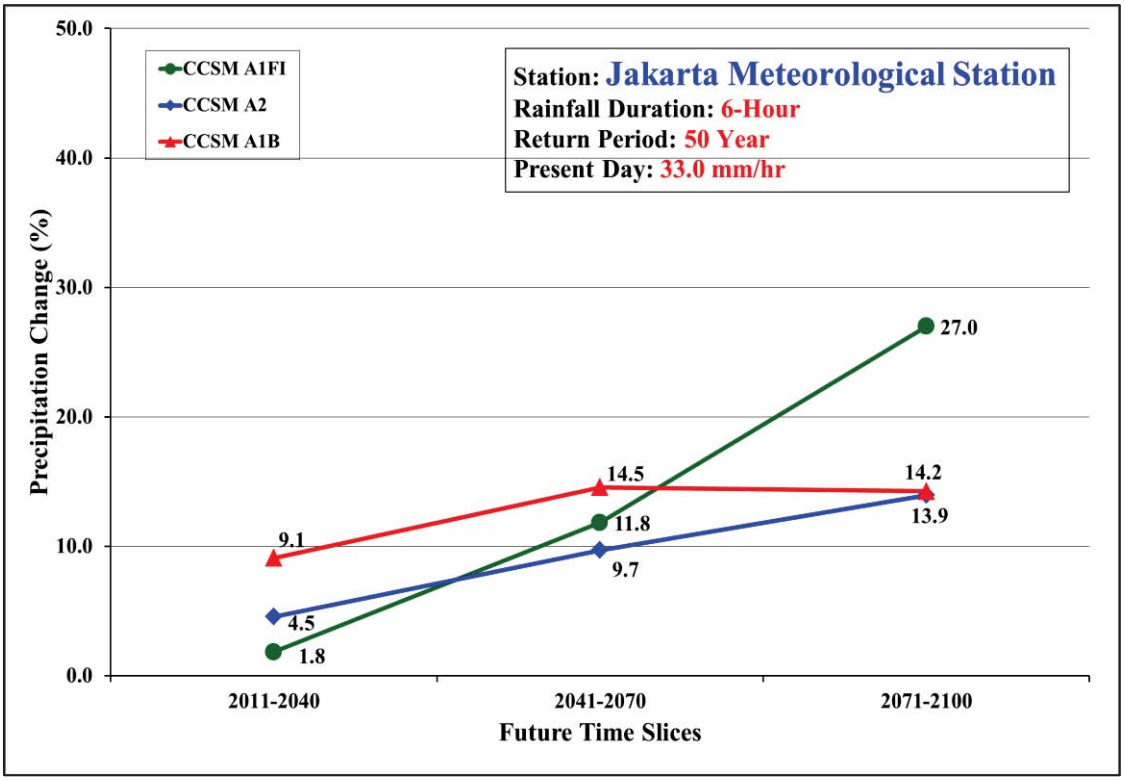

Figure 5.19: Comparison between **WRF/CCSM A1FI, A2** and **A1B** projected 50-year return period for Jakarta Meteorological Station: **6-hour rainfall duration**

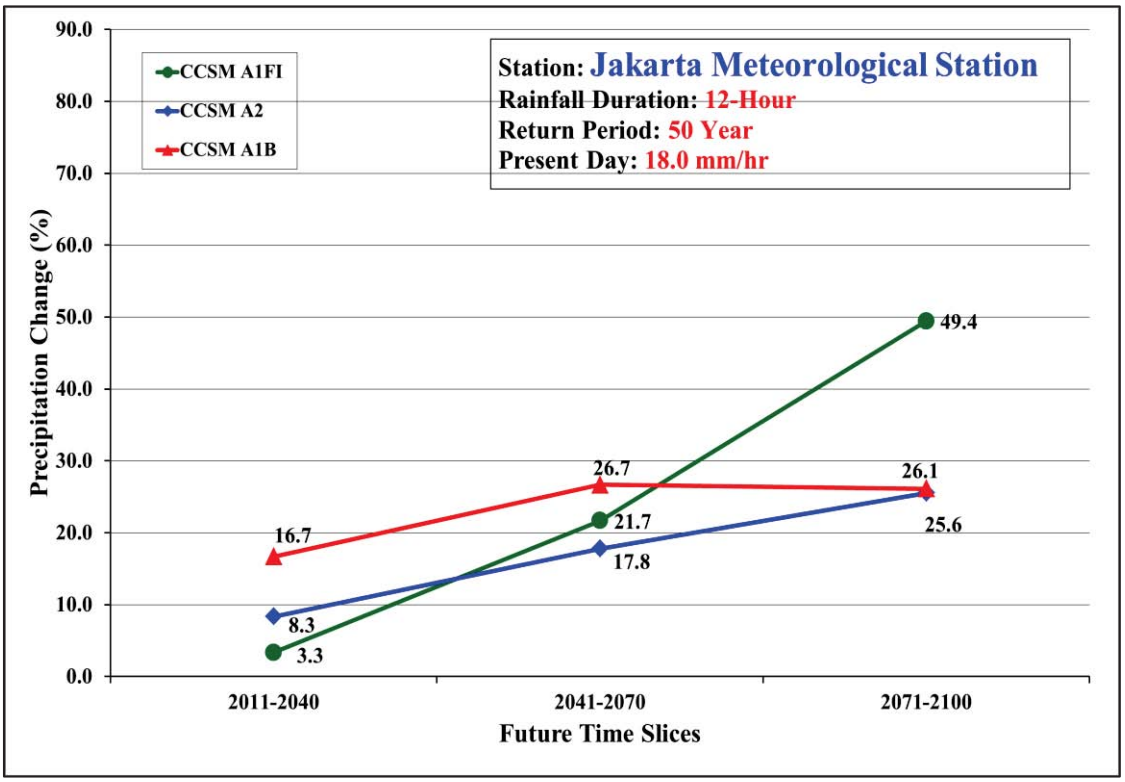

Figure 5.20: Comparison between **WRF/CCSM A1FI, A2** and **A1B** projected 50-year return period for Jakarta Meteorological Station: **12-hour rainfall duration**

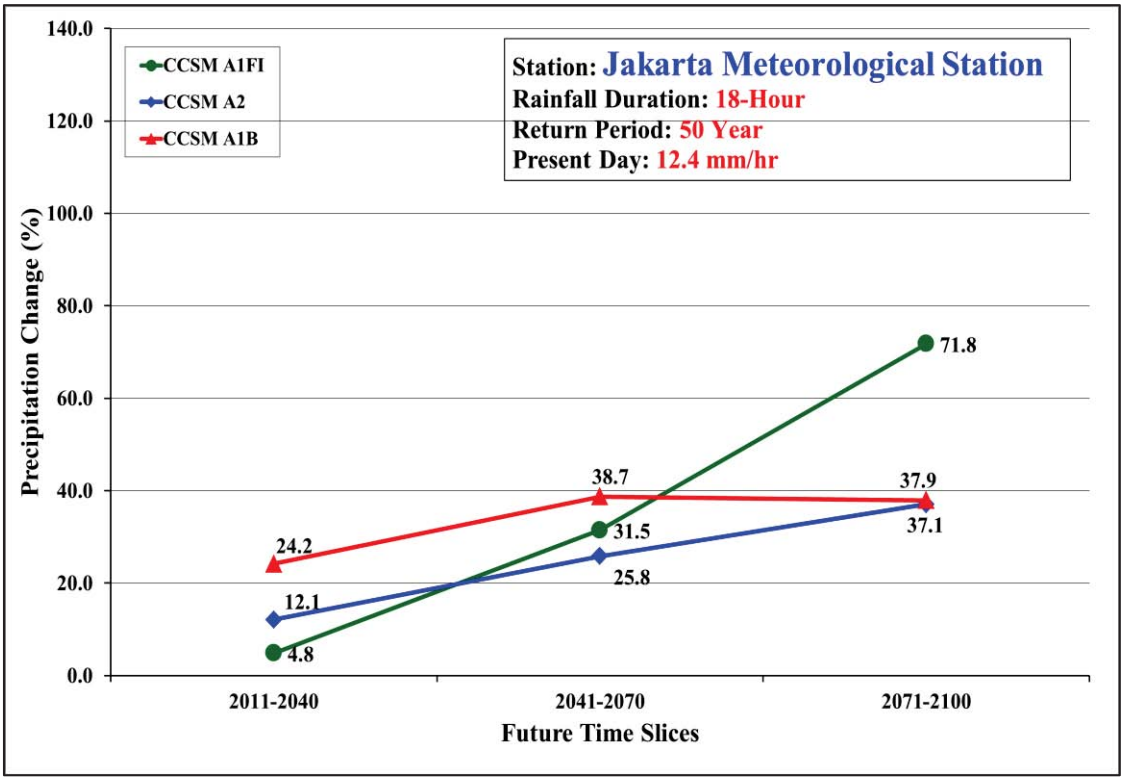

Figure 5.21: Comparison between **WRF/CCSM A1FI, A2** and **A1B** projected 50-year return period for Jakarta Meteorological Station: **18-hour rainfall duration**

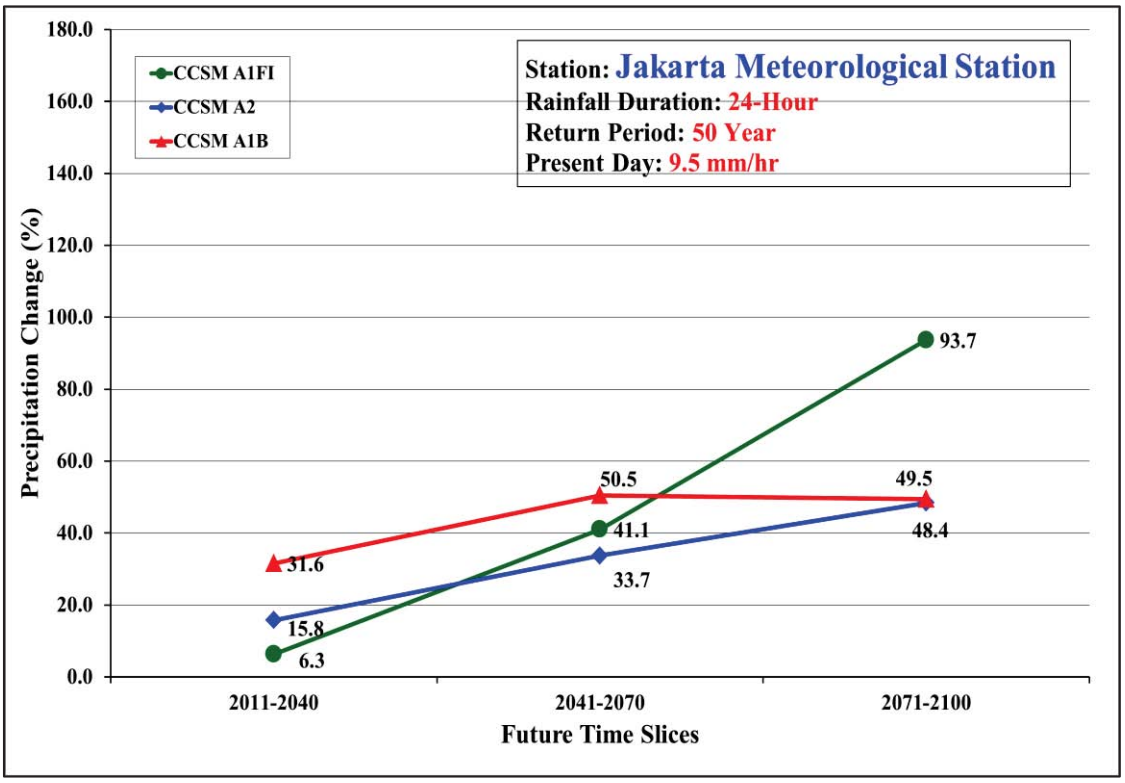

Figure 5.22: Comparison between **WRF/CCSM A1FI, A2** and **A1B** projected 50-year return period for Jakarta Meteorological Station: **24-hour rainfall duration**

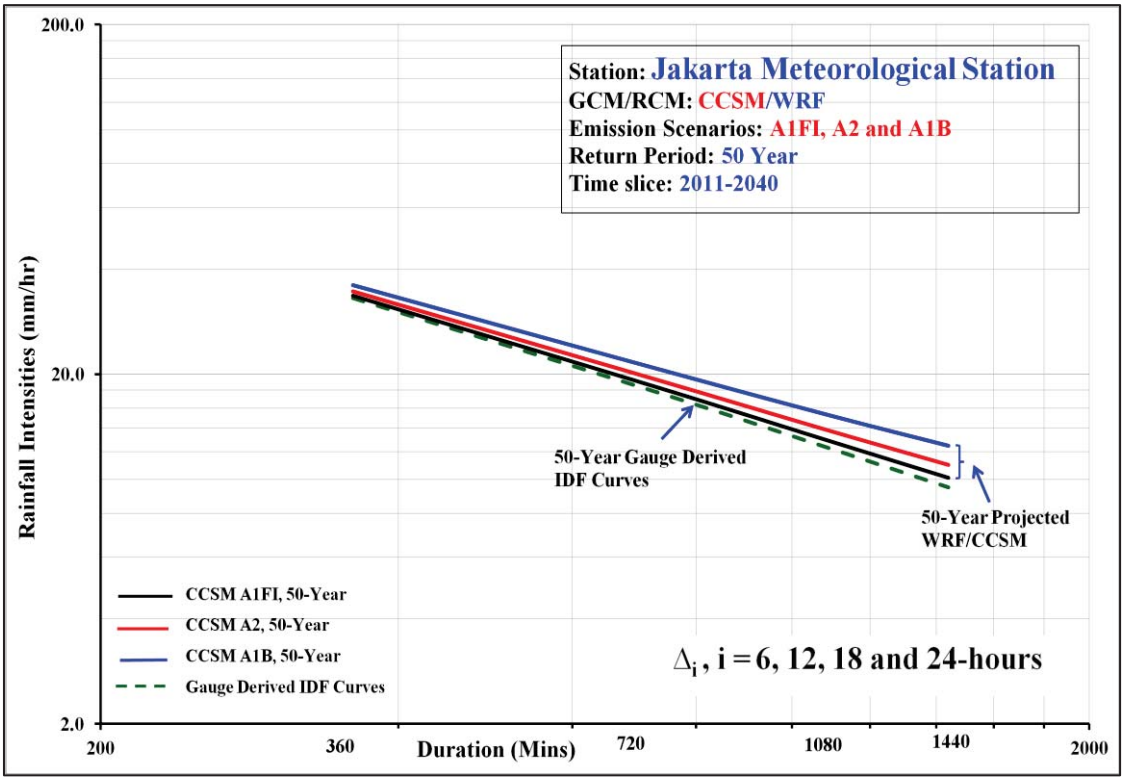

Figure 5.23: Quantifying uncertainties of projected 50-year return period, for Jakarta Meteorological Station, with **WRF/CCSM A1FI, A2** and **A1B**: **2011-2040**

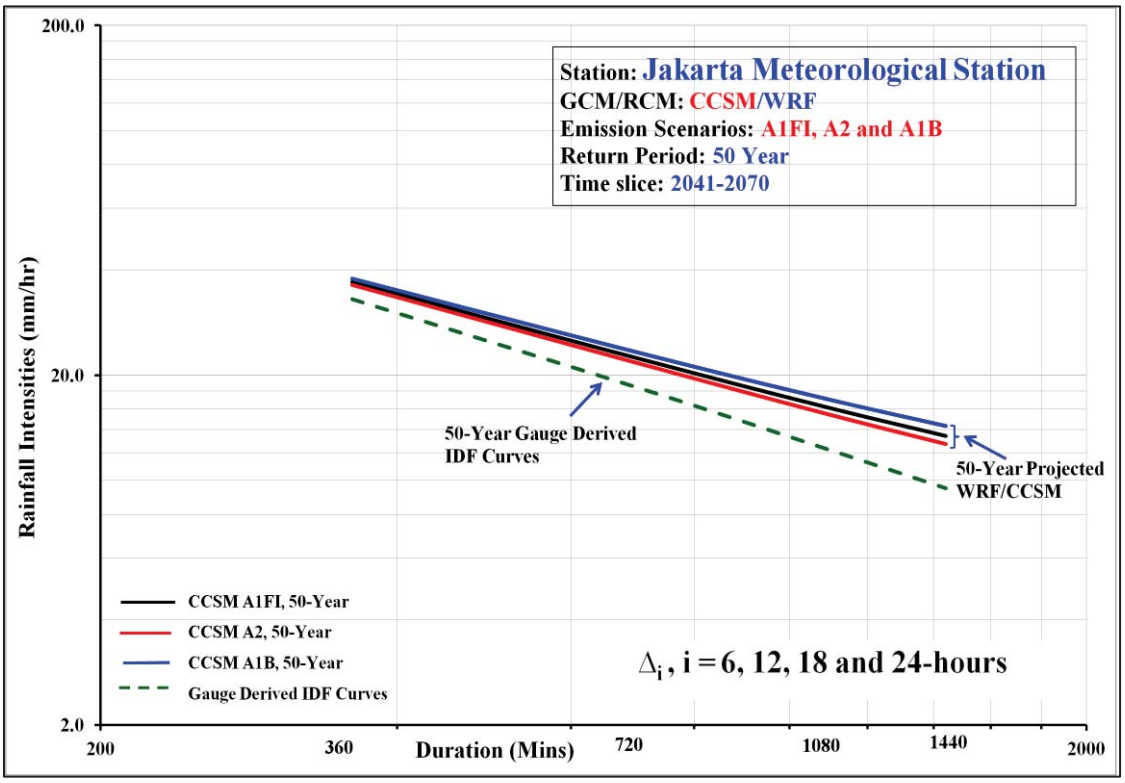

Figure 5.24: Quantifying uncertainties of projected 50-year return period, for Jakarta Meteorological Station, with **WRF/CCSM A1FI, A2** and **A1B**: **2041-2070**

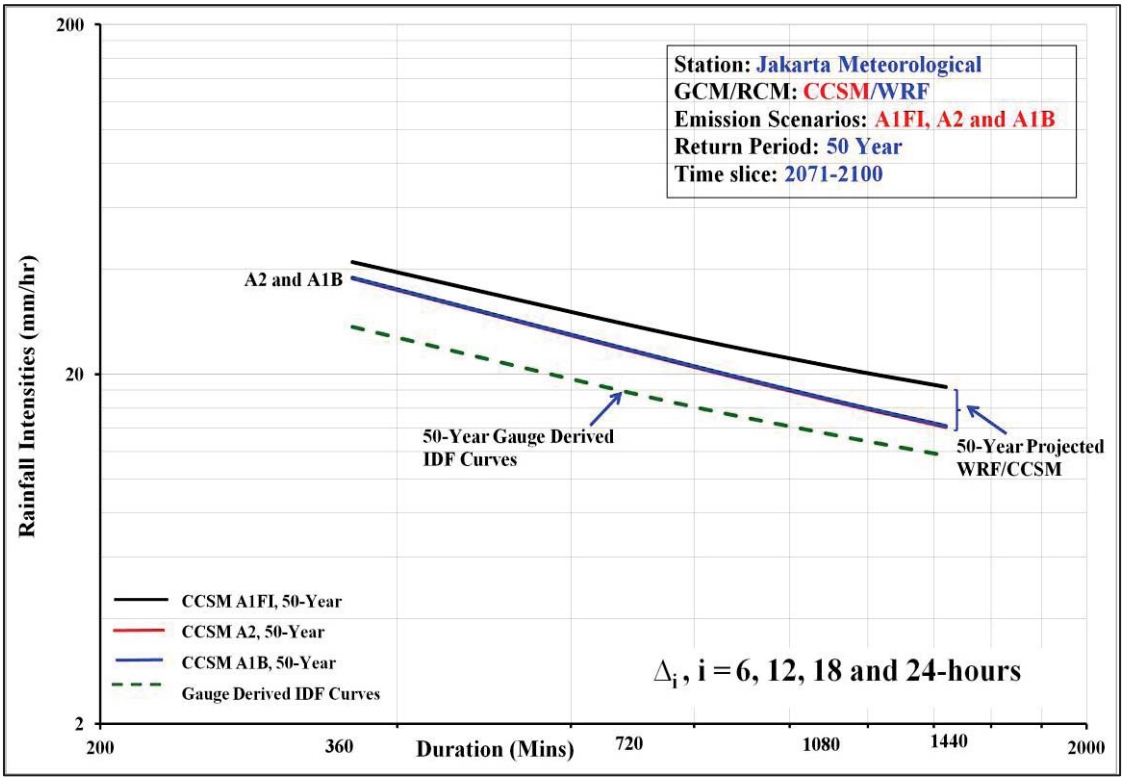

Figure 5.25: Quantifying uncertainties of projected 50-year return period, for Jakarta Meteorological Station, with **WRF/CCSM A1FI, A2** and **A1B**: **2071-2100**

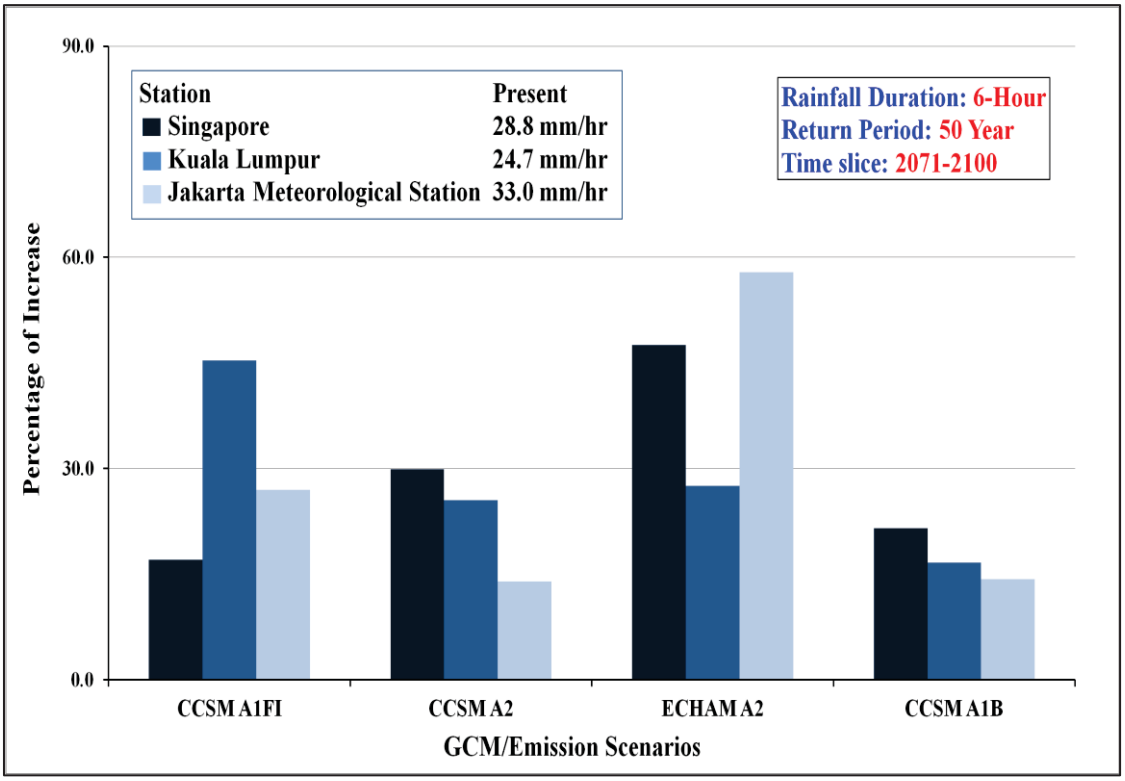

Figure 5.26: Comparison between projected percentages of future extreme rainfall intensities resulting from different GCMs and emission scenarios (6-Hour rainfall duration, 50 year return period, 2071-2100): Singapore, Kuala Lumpur and Jakarta Meteorological Station

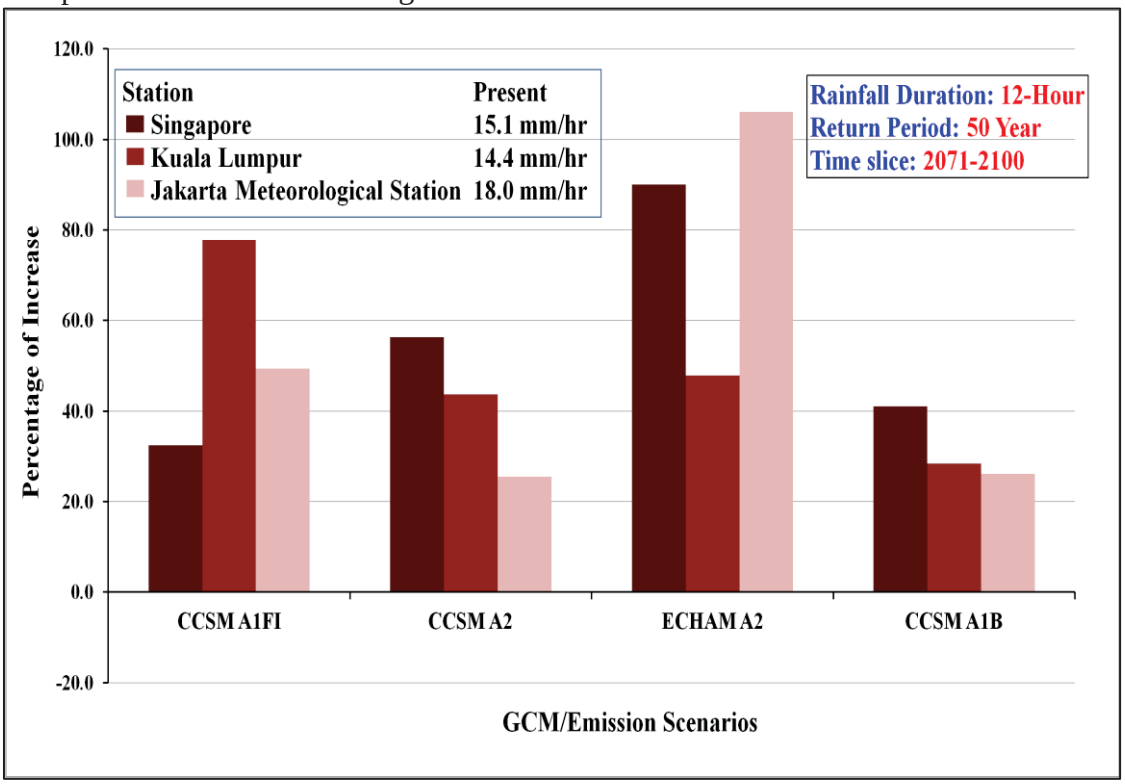

Figure 5.27: Comparison between projected percentages of future extreme rainfall intensities resulting from different GCMs and emission scenarios (12-Hour rainfall duration, 50 year return period, 2071-2100): Singapore, Kuala Lumpur and Jakarta Meteorological Station

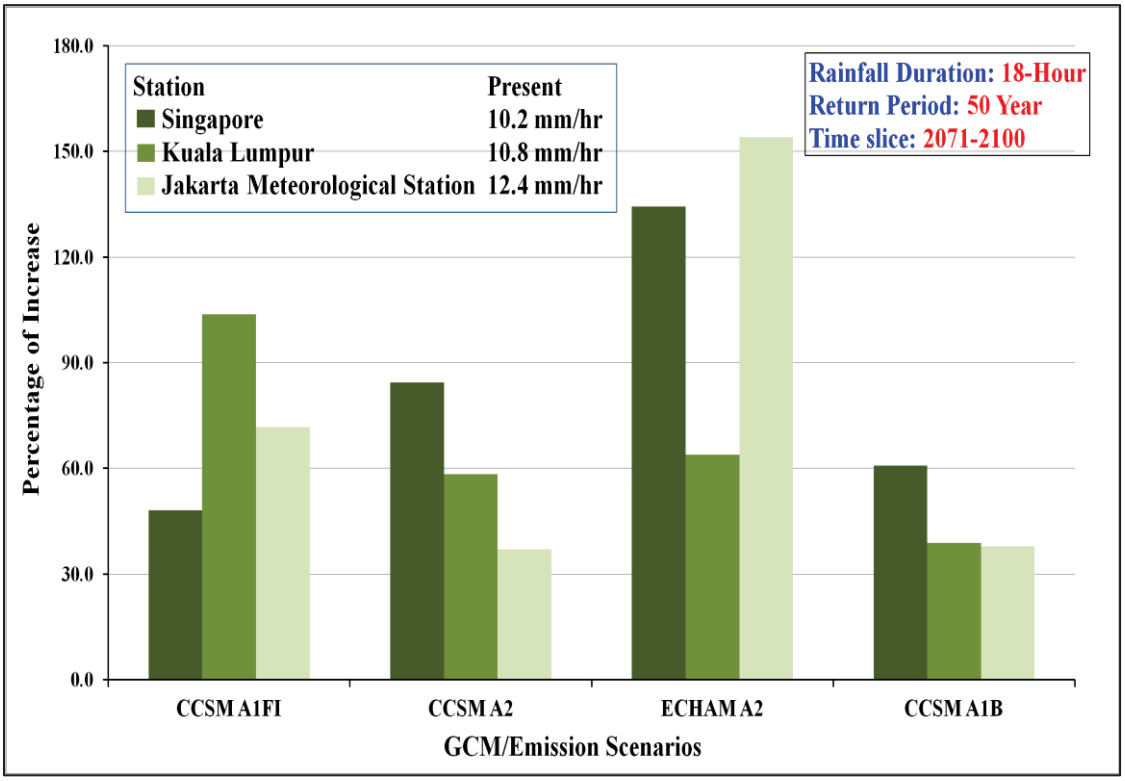

Figure 5.28: Comparison between projected percentages of future extreme rainfall intensities resulting from different GCMs and emission scenarios (18-Hour rainfall duration, 50 year return period, 2071-2100): Singapore, Kuala Lumpur and Jakarta Meteorological Station

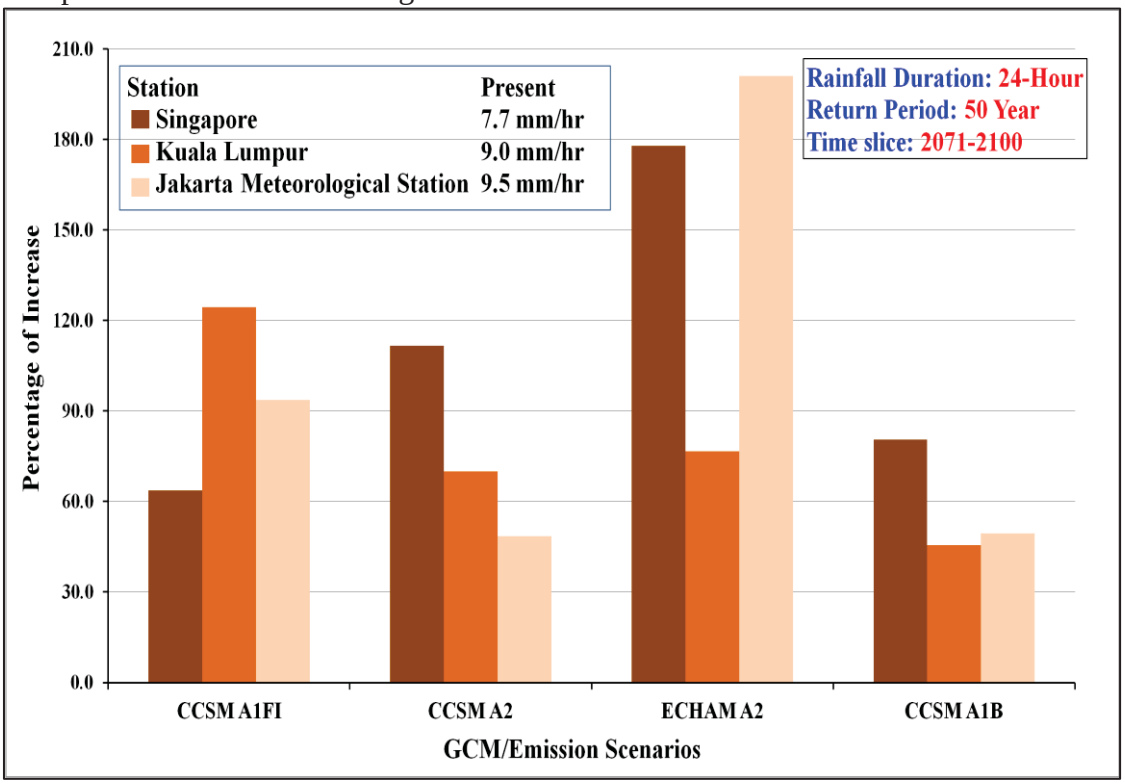

Figure 5.29: Comparison between projected percentages of future extreme rainfall intensities resulting from different GCMs and emission scenarios (24-Hour rainfall duration, 50 year return period, 2071-2100): Singapore, Kuala Lumpur and Jakarta Meteorological Station

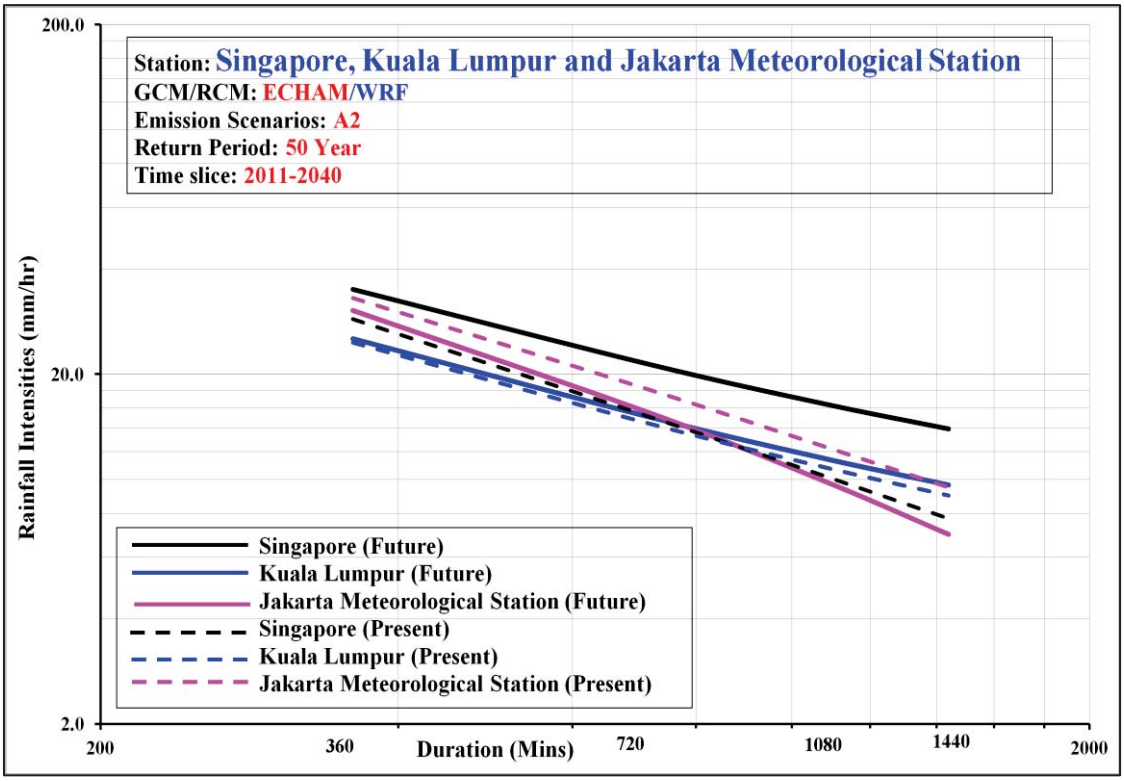

Figure 5.30: Comparison between projected IDF curves for different cities (50 year return period, WRF/ECHAM A2) in time slice 2011-2040: Singapore, Kuala Lumpur and Jakarta Meteorological Station

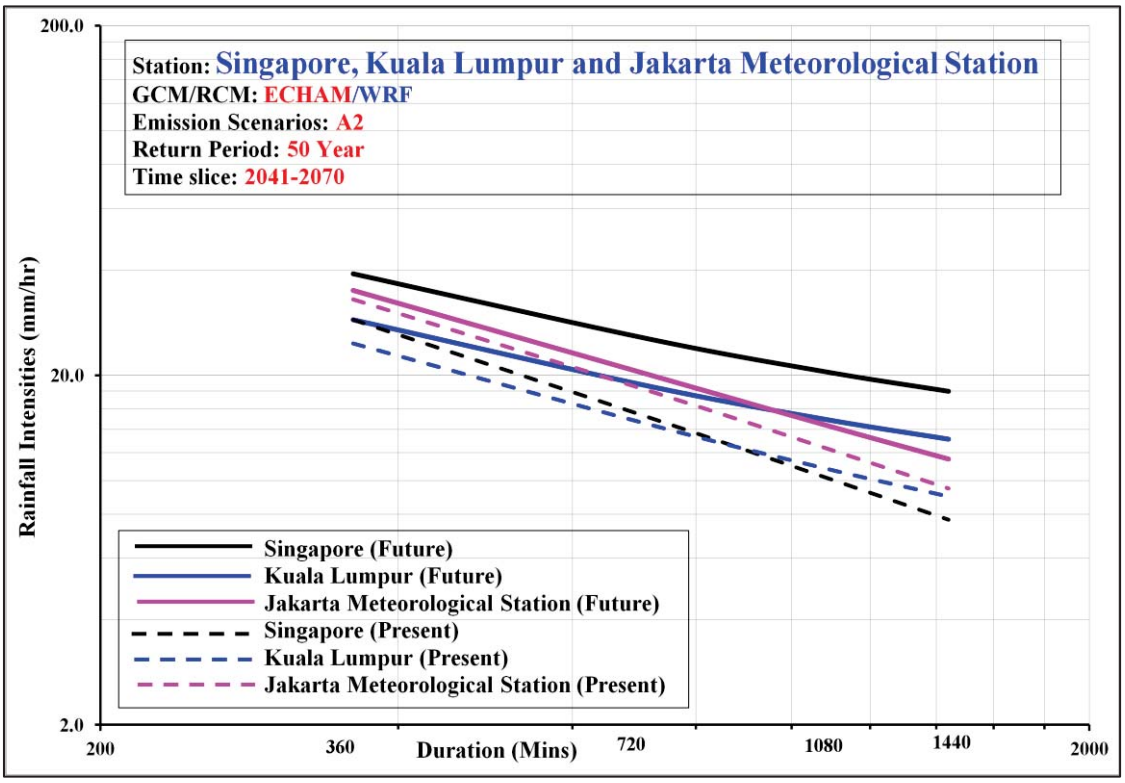

Figure 5.31: Comparison between projected IDF curves for different cities (50 year return period, WRF/ECHAM A2) in time slice 2041-2070: Jakarta Meteorological Station, Singapore and Kuala Lumpur

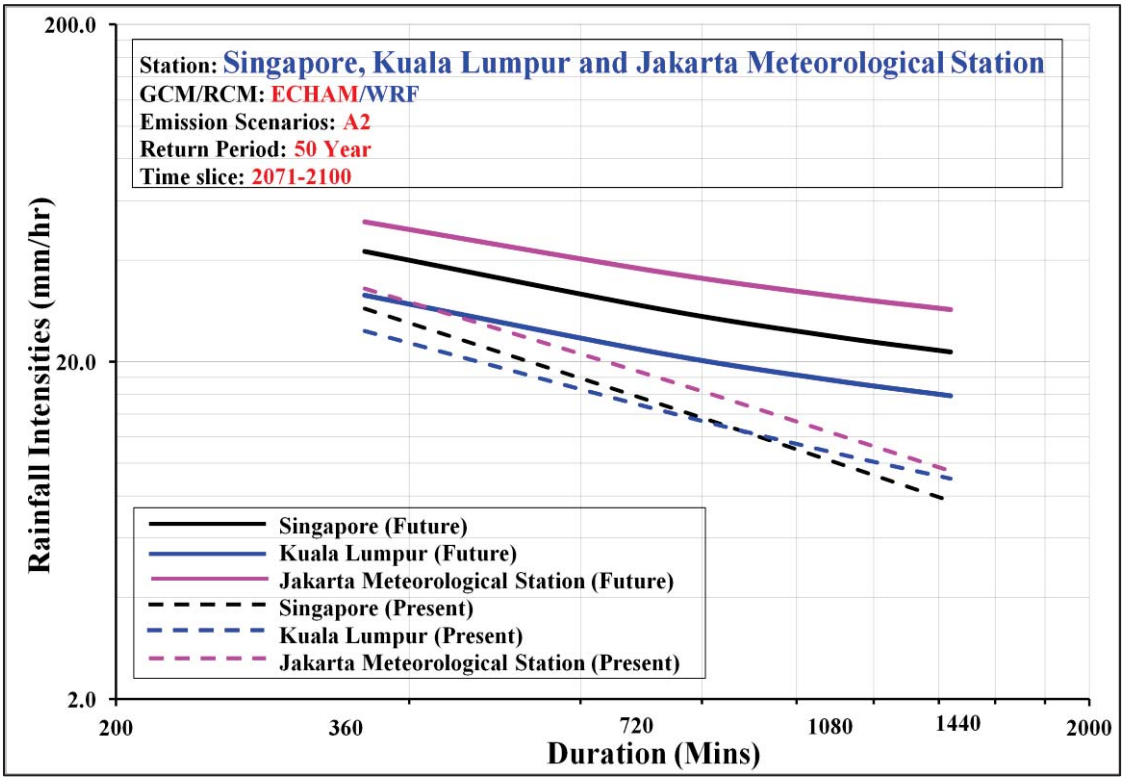

Figure 5.32: Comparison between projected IDF curves for different cities **(50 year return period, WRF/ECHAM A2) in time slice 2071-2100: Singapore, Kuala Lumpur and Jakarta Meteorological Station**

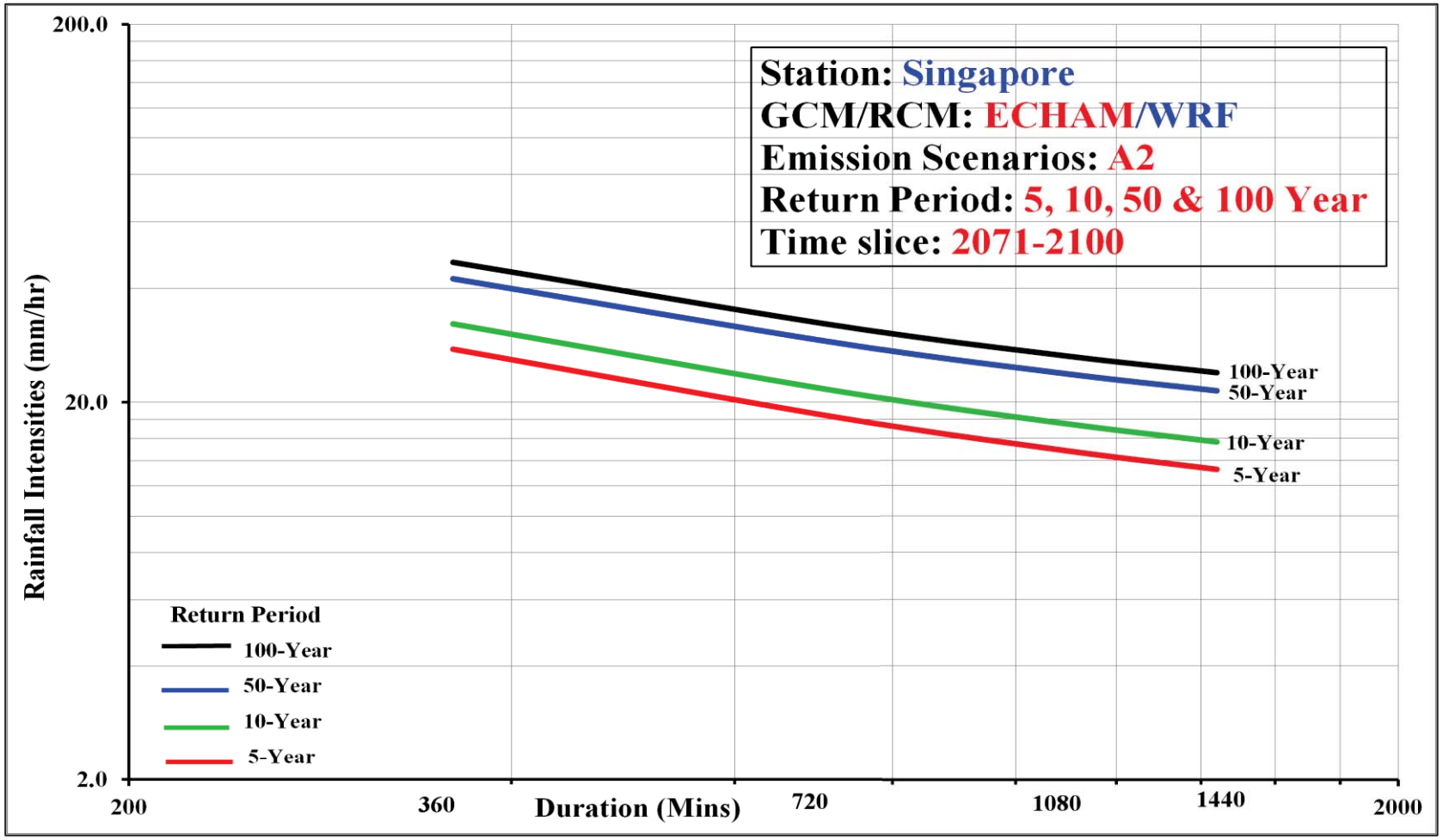

Figure 5.33: Future climate IDF Curves (2071-2100) derived from **WRF/ECHAM A2**: **Singapore**

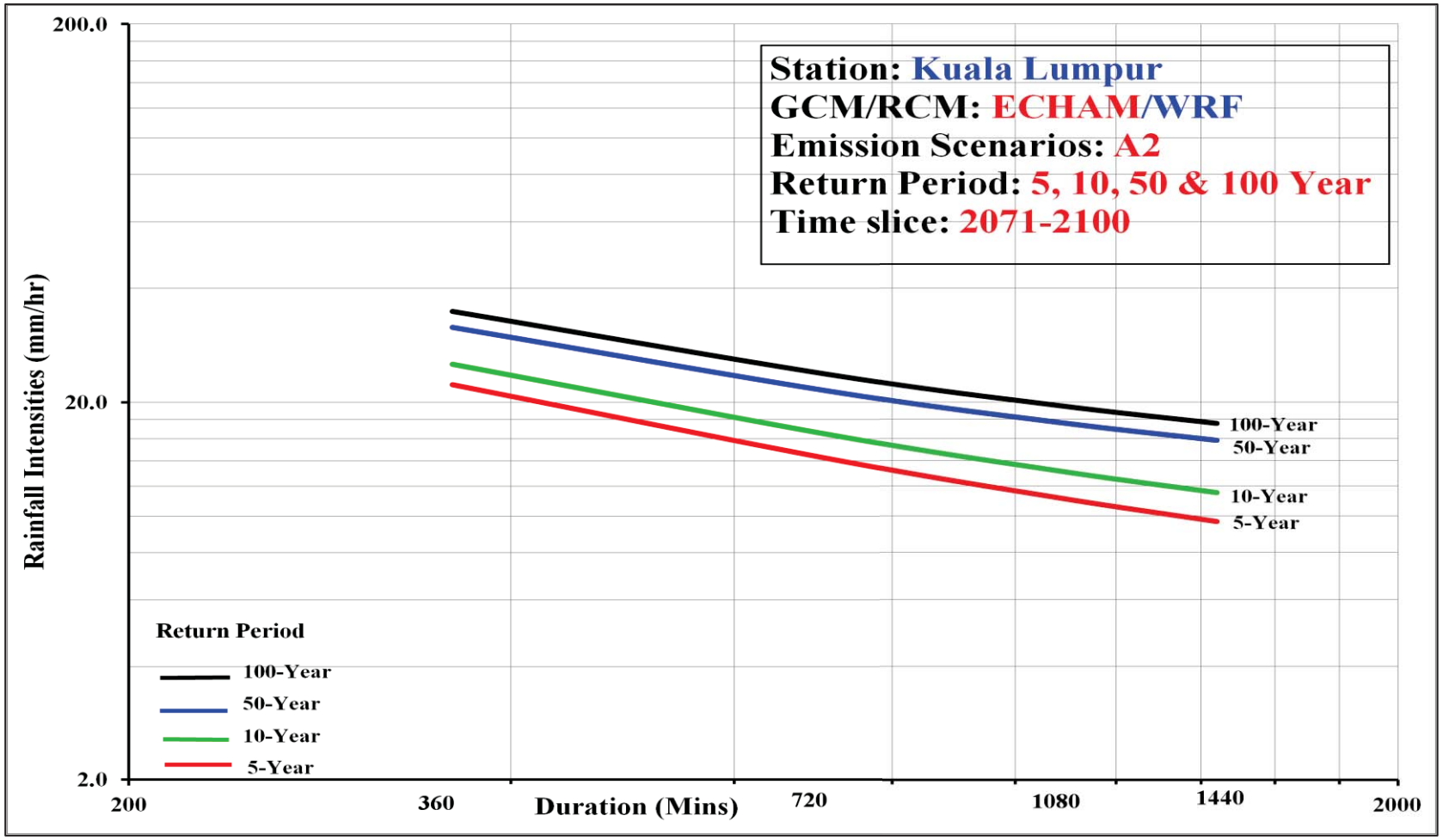

Figure 5.34: Future climate IDF Curves (2071-2100) derived from **WRF/ECHAM A2**: **Kuala Lumpur**

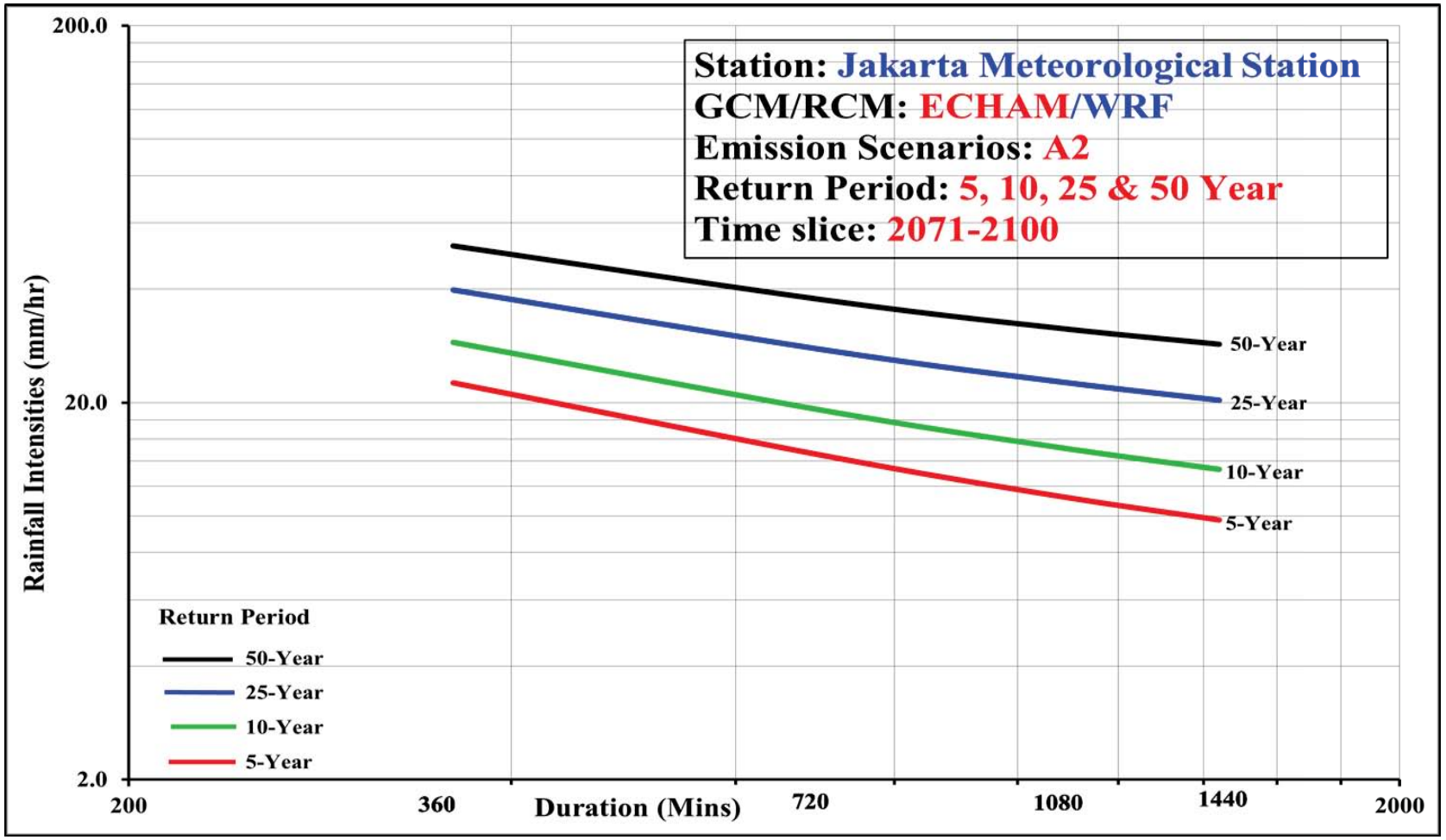

Figure 5.35: Future climate IDF Curves (2071-2100) derived from **WRF/ECHAM A2**: **Jakarta Meteorological Station**

Table 5-1 Coordinates of meteorological stations considered in the study

STATION	LONGITUDE	LATITUDE	COUNTRY
Jakarta Meteorological	**106° 49’ E**	**6° 10’ S**	**Indonesia**
Darmaga	**106° 45’E**	**6° 33’ S**	**Indonesia**
Singapore	**103° 50’ E**	**1° 18’ N**	**Singapore**
Kuala Lumpur	**101° 41’ E**	**3° 09’ N**	**Malaysia**

Table 5-2 Percentage difference between existing and WRF-ERA40 derived IDF curves

(a) Jakarta Meteorological Station

Jakarta Met. Station (1961-1990)	Duration (Min)	Return Period (Year)			
		5	10	25	50
$(IDF)_{Existing} - (IDF)_{WRF-ERA40}$ (%)	360	57	55	51	49
	720	39	40	39	40
	1080	36	38	39	42
	1440	31	35	39	45
Average %-age Difference		41	42	42	44

Table 5-2 (contd) for **(b) Singapore**

Singapore (1961-1990)	Duration (Min)	Return Period (Year)			
		5	10	50	100
$(IDF)_{Existing} - (IDF)_{WRF-ERA40}$ (%)	360	60	56	45	39
	720	51	48	40	37
	1080	47	46	43	42
	1440	44	43	42	41
Average %-age Difference		50	48	42	40

Table 5-2 (contd) for **(c) Kuala Lumpur**

Kuala Lumpur (1961-1990)	Duration (Min)	Return Period (Year)			
		5	10	50	100
$(IDF)_{Existing} - (IDF)_{WRF-ERA40}$ (%)	360	59	53	38	31
	720	50	46	27	17
	1080	47	44	30	20
	1440	43	43	34	26
Average %-age Difference		50	47	32	24

Table 5-3 Comparison between existing and WRF/ERA40 derived IDF curves (lower and upper bounds): **Darmaga Station**

Darmaga Station	Duration (Min)	Existing 1961-1990 (mm/hr)	Projected derived IDF 1961-1990 (mm/hr)		
			WRF/ERA40	Lower Bound	Upper Bound
5-Year Return Period	360	22.7	10.4	16.8	18.9
	720	12.0	7.3	11.7	13.2
	1080	8.1	4.9	8.0	9.0
	1440	6.2	3.9	6.3	7.1
10-Year Return Period	360	26.1	12.6	20.4	23.0
	720	13.8	8.4	13.6	15.3
	1080	9.4	5.7	9.2	10.4
	1440	7.1	4.4	7.2	8.1
25-Year Return Period	360	31.3	15.9	25.6	28.8
	720	16.7	9.8	15.8	17.8
	1080	11.4	6.7	10.8	12.2
	1440	8.7	5.1	8.3	9.4
50-Year Return Period	360	35.5	18.6	29.9	33.8
	720	19.1	10.8	17.5	19.7
	1080	13.1	7.5	12.0	13.6
	1440	9.9	5.7	9.1	10.3

Table 5-4 Projected lower and upper bounds of future rainfall intensities for **2071-2100**: **Darmaga Station**

Return Period (Year)	Duration (Min)	Adjusted WRF-ERA40 derived IDF 1961-1990; mm/hr		Projected future derived IDF 2071-2100; mm/hr (%)	
		Lower Bound	Upper Bound	Lower Bound	Upper Bound
5	360	16.8	18.9	21.9 (31)	24.1 (27)
	720	11.7	13.2	16.9 (44)	18.4 (39)
	1080	8	9.0	13.1 (64)	14.1 (57)
	1440	6.3	7.1	11.4 (82)	12.2 (73)
Average Percentage				55	49
10	360	20.4	23.0	27.1 (33)	29.7 (29)
	720	13.6	15.3	20.3 (50)	22.0 (44)
	1080	9.2	10.4	15.9 (73)	17.1 (65)
	1440	7.2	8.1	13.9 (94)	14.8 (83)
Average Percentage				62	55
25	360	25.6	28.8	35.3 (38)	38.6 (34)
	720	15.8	17.8	25.6 (62)	27.6 (55)
	1080	10.8	12.2	20.6 (90)	21.9 (80)
	1440	8.3	9.4	18.0 (118)	19.1 (104)
Average Percentage				77	68
50	360	29.9	33.8	43.0 (44)	46.9 (39)
	720	17.5	19.7	30.6 (75)	32.8 (66)
	1080	12	13.6	25.1 (109)	26.7 (97)
	1440	9.1	10.3	22.2 (143)	23.4 (127)
Average Percentage				93	82

Table 5-5 Projected Percentage Increase in Future Rainfall Intensities for difference time slices: **Darmaga Station (WRF/ECHAM A2)**

Darmaga Station (WRF/ECHAM A2)	Projected Increase in Future Rainfall Intensities (%)		
Time Slices	2011-2040	2041-2070	2071-2100
Lower Bound (+38 %)	18 % - 30 %	21 % - 34 %	49 % - 82 %
Upper Bound (+45 %)	21 % - 33 %	24 % - 38 %	55 % - 93 %

Table 5-6 Summary of percentage precipitation responses from different rainfall durations **(WRF/ECHAM A2)**: **Jakarta Meteorological Station**

Return Period (Year)	Duration (Min)	Projected future derived IDF 2011-2040; (%)	Projected future derived IDF 2041-2070; (%)	Projected future derived IDF 2071-2100; (%)
5-Year	360	5.1	8.5	28.4
	720	9.7	16.1	53.8
	1080	14.3	25.4	79.4
	1440	18.8	31.3	104.2
Average Percentage		12	20	66
10-Year	360	1.4	7.4	34.4
	720	2.6	14	64.9
	1080	3.8	20.5	94.9
	1440	5.1	27.1	125.4
Average Percentage		3	17	80
25-Year	360	-4.1	6.6	46.9
	720	-7.5	12.3	87
	1080	-11	18	127
	1440	-14.5	23.7	167.1
Average Percentage		-9	15	107
50-Year	360	-7.6	6.1	57.9
	720	-13.9	11.1	106
	1080	-20.2	16.1	154
	1440	-26.3	21.1	201.1
Average Percentage		-17	14	130

This page is intentionally left blank.

CHAPTER 6 SUMMARY AND CONCLUSIONS

6.1 INTRODUCTION

The main aims of the present study are to develop the present and future IDF curves for sites with short or no rainfall record with the use of simulation results from high spatial resolution regional climate model. The approach suggested in this study is the first of its kind and by far superior than the existing approaches in deriving the present climate IDF curves for ungauged sites. The objectives were achieved through (a) downscale of regional climates at high spatial resolution (30 km), for Southeast Asia, using a state-of-the-art Regional Climate Model WRF driven by Re-Analysis data (ERA-40), different GCMs (CCSM 3.0 and ECHAM5) and emission scenarios (A1B, A2 and A1FI) for the 21st century and determine the RCM simulated climate responses (temperature, winds and precipitation) over the study region, Jakarta inclusive; (b) the development of (3-step) Downscaling-Comparison-Derivation (DCD) approach in deriving present climate IDF curves for ungauged sites, e.g. Darmaga Station, using downscaled simulation output from RCM; and (c) the development of future IDF curves (periods: 2011-2040, 2041-2070 and 2071-2100), for both ungauged and gauged sites, using different GCMs under different emission scenarios.

The following Sections 6.2 and 6.3 summarize and conclude the main work and findings in the thesis. Section 6.4 present recommendations for future work.

6.2 REGIONAL CLIMATE MODELING AND PROJECTIONS

6.2.1 Present Day Climate

In the present study, the RCM WRF was first driven by the ERA40 reanalyses, which is considered as 'near perfect boundary conditions' for all RCM simulations. RCM simulations driven by ERA40 reanalyses serve as a benchmark for model performance and evaluations and to evaluate model performance. The gridded observations, CRU, CPC, VASClimO and APHRODITE datasets were used to compare model simulated surface air temperature and precipitation. The RCM WRF was also driven by the GCMs CCSM3.0 (WRF/CCSM) and ECHAM5 (WRF/ECHAM) for the same period 1961-1990 and is compared to the simulations of the model driven by the WRF/ERA40 as well as the observations, including identification of biases in the RCM climate. This step is important to see how well the WRF driven by the GCMs represent the mean state of climate. The results from RCM simulations presented in Chapter 4 have provided an initial confidence level of RCM WRF in simulating credible quantitative estimates of future climate change.

One key contribution of the this study is the recognition of RCM WRF to resolve features on finer scales than those resolved by the GCM, particularly those related to improved resolution of the topography, such as its influence on surface air temperature and large-scale precipitation.

This study has provided conclusive evidence that RCM WRF driven by ERA-40, GCM/CCSM3.0 and GCM/ECHAM5 were able to capture current climate by comparing with the observation datasets. The study has also demonstrated the consistency of the model simulations (WRF/CCSM and WRF/ECHAM) as compared to the observed datasets. These findings are significant because it provides promising frameworks for future climate simulations and climate change projections.

6.2.2 Future Climate Response for Study Region

Comparison studies have been performed to analysis the future climate response for temperature, winds and precipitation due to different climate change emission scenarios (A1FI, A2 and A1B) and different GCMs (CCSM3.0 and ECHAM5) for three future time slices (2011-2040, 2041-2070 and 2071-2100).

As discussed in Chapter 4, WRF simulation shows that the differences in the emission scenarios (A1FI, A2 and A1B) lead to significantly different temperature developments until the end of 21st century. By adopting scenario A1FI, for climate change adaptation strategies, measures will have to deal with the projected increase in the precipitation which is 1.67 times higher than that of scenario A1B in the immediate future period (2011-2040), and an increase in temperature as high as 1.61 times by the end of 21st century. Higher warming and increase in precipitation in A1FI scenario are due to the greater total energy demand and carbon intensity. In this study, scenario A2

falls in between A1FI and A1B scenarios. Scenario A2 indicates a moderate rate of precipitation and temperature increase to 2100.

This study is the first to have provided clear illustration for the policy makers to justify their future policies. Comparing the simulation results driven by different scenarios is crucial to create a better informed recommendation for policy makers. With the information of future emission and its effect on temperature and precipitation, the mitigation opportunities in each scenario as well as different policy perspective can better be decided.

In addition, a comparative study of different GCMs has been performed and presented. Both WRF/CCSM and WRF/ECHAM project approximate 45% increase in rainfall by the end of the 21st century. The difference in annual precipitation change between these two models ranges from 17% to 25% indicating a range of possible change among climate models. Although the GCM CCSM3.0 and ECHAM5 demonstrated different WRF simulation results, both models perform quite well in reproducing current climate and this has added confidence level for the models to capture future climates. There is no significant difference in annual and seasonal warming for both climate models. This provides clear evidence that the future precipitation is more difficult to project, and changes are generally of lower statistical significance than changes in temperature (Barrow et al., 2004). It appears that climate models uncertainties are foreseeable. One way to appreciate this uncertainty is to look at results from the full range of global models that have been presented in the recent IPCC assessment. Whilst

comparing different model results is important to illustrate uncertainty, there is no easy way to attach higher or lower confidence to the results of one model over another (Hulme and Turnpenny, 2002).

In conclusion, the results from this study have provided important insight that many of the severe impacts projected under high A1FI and mid high A2 scenarios could be avoided by adopting mid-range A1B scenario; a scenario that balanced emphasis on a wide range of energy sources. However, even if global emissions stay below the A1B emissions scenario, some impacts from climate change are inevitable. Evidence shows that even if actions could be immediately taken to limit the GHG emissions, the GHGs that have already built up and their long atmospheric lifetimes could result in average global temperatures rising an additional 0.6°C (1.1°F) (Wigley, 2005; Meehl et al. 2005). As a result, some impacts from climate change, in Jakarta region and across the globe, are now unavoidable. Climate change signals have shown significant increase in rainfall intensities and frequencies in many regions. In this context, a revisit of the existing IDF curves is called for to re-examine the adequacy of the current drainage system and capacity to meet the projected future rainfall extremes. With regard to data sparse or ungauged sites, developing IDF curves is a challenge for both present and future climate. Optimal mitigation measures can be taken only when the IDF curves for the current climate can be reasonably constructed. The study presented an approach to derive IDF curves for ungauged sites using projected precipitation resulting from a high spatial resolution RCM driven by Re-Analysis data, as presented in Chapter 5.

6.3 DERIVATION OF PRESENT DAY AND FUTURE IDF CURVES

Another significant contribution of this study is the development of present day IDF curves for ungauged sites. Chapter 5 gave detailed procedures and results on the proposed approach to derive the present day and the future climate IDF curves particularly for regions with short or no rainfall records or ungauged sites. The derivation of future climate IDF curves for regions with long rainfall records (Singapore, Kuala Lumpur and Jakarta Meteorological Stations) were demonstrated as well. This study is significant because it is the first of its kind to apply the results of a regional climate model's results to derive the present and future IDF curves for ungauged sites.

6.3.1 Development of Present Day IDF Curves

A novel approach is presented in this thesis to develop Intensity-Duration-Frequency (IDF) curves for ungauged sites. The approach comes in 3 steps, Step 1: Dynamical Downscaling [D]; Step 2: Comparison [C]; and Step 3: Derivation of IDF curves [D]. The 3 steps in the DCD approach are summarized below, where detailed description is presented in Section 3.7.

Simulation results from a RCM (WRF) driven by Re-Analysis data (ERA40) was first used to derived the present day IDF curves for sites with long rainfall records; these IDF curves were then compared with their counterparts, IDF curves derived from raingauge data. This proof-of-concept

analyses showed that the IDF curves derived from WRF/ERA40 fairly consistently underestimate each IDF curves ranging from +38% (lower bound) to +45% (upper bound). The range of bias correction showed reasonable results when applied to and compared with the validation site, Darmaga Station, Jakarta. These bias correction quantities form the basis in the construction of the present day IDF curves for sites where the rainfall record is short or non-existent (e.g. Darmaga station, Indonesia).

The proposed approach was relatively simple and yet has been proven effective to provide feasible solution for designs of urban drainages and stormwater infrastructure systems.

6.3.2 Development of Future Climate IDF Curves

For the anticipated changes in rainfall intensities due to climate change, this study continues to propose the development of future climate IDF curves (periods: 2011-2040, 2041-2070 and 2071-2100) for ungauged sites. The developed future IDF curves are essential for policy-makers to decide on appropriate and effective adaptation strategies/measures in addressing impacts of climate change.

To demonstrate the development of future IDF curves, two sites (Darmaga Station and Jakarta Meteorological Station) were selected; one is an ungauged site while the other is a site with long rainfall record. The derivation of future IDF curves was done by applying the ‘delta’ method (Hamlet and

Lettenmaier, 1999; Miller et al., 2003) on the high resolution dynamical downscaling outputs. Climate model output is used to determine future change in climate with respect to the model's present-day climate, typically a difference in climate variables between the future and present day estimates. This change is referred to as the 'climate change signal' or 'change factor'. The climate change factor, (Δi) (climate responses, 'simulated future rainfall intensities minus present day rainfall intensities') (Wilby et al., 2009), is added directly to the existing IDF curves' respective return periods.

For the development of future climate IDF curves for ungauged sites (e.g. Darmaga station), the climate change factor (Δi) is added to the present day's lower and upper bounds of WRF/ERA40 derived IDF curves to form the range of each of the return periods for future rainfall extremes. Should the site under consideration have existing IDF curves (Jakarta Meteorological Station), the delta factor, as mentioned earlier is simply applied directly to the respective existing IDF curves.

In this study two GCMs (CCSM3.0 and ECHAM5) and three emission scenarios (A1FI, A2 and A1B) were considered. Results presented in this study were based on the output from only two climate models. It is essential that subsequent applications use a greater number of climate models. This way, an ensemble of future precipitation changes can be obtained and potentially minimizes the uncertainty in future scenarios by down weighting underperforming climate models (Leith, 2006; Leith 2008). Nevertheless, the future climate IDF curves developed from this study has been a significant

contribution, in particular, for adaptation measures to the climate change for Jakarta where flooding has been annual events in recent decades.

The study also considered climate change impacts on future IDF curves on some Asia mega-cities (Singapore, Kuala Lumpur and Jakarta) under different emission scenarios. This extended study contributes significant information for impacts assessment, adaptation and mitigation strategies for climate change. The study showed projected changes in and comparisons between extreme rainfalls of the 3 mega cities. For all the cities considered, the study has provided clear evidence that the intensity of extreme rainfall is projected to increase significantly in particular towards the end of the 21st Century.

6.4 RECOMMENDATIONS FOR FUTURE STUDIES

This thesis has presented a novel approach to derive IDF curves for present climate using dynamically downscaled data (RCM driven by ReAnalysis data) for ungauged sites. In addition, deriving future IDF curves for stations with existing IDF curves and ungauged sites with simulation data from RCM driven by GCM has also been presented. The approach has demonstrated the importance of the data from the nearest meteorological stations to determine the required bias correction values for the derivation of present climate IDF curves at ungauged regions. However, more tests at other ungauged sites are required to increase the confidence level of the proposed approach.

The following are some possible areas that could be explored further:

- Select another ungauged sites, in Vietnam for example. Search for some meteorological stations in the region to determine the required bias correction values for Vietnam site.

- Conduct a larger ensemble of GCMs and apply even higher spatial resolution RCM for simulations. These might yield enhanced local information and reduce uncertainties that could be used for adaptation measures.

- The proposed 3-step DCD approach to derive IDF curves for ungauged sites can be extended to other emission scenarios so that a bandwidth of uncertainties can be assessed to create appropriate and effective adaptation strategies/measures to better address climate change impacts.

- The study focused only on IDF curves with rainfall durations of 6, 12, 18 and 24-hours. For a rather large catchment like Jakarta, partially urban and partially rural with a rather long time of concentration (12 hours at least), the presented approach and results are applicable. However, for catchments with shorter than 6-hour time of concentration (such as Singapore), the study can be extended further to derive sub-6 hourly information in the IDF curves. The approach presented in Nguyen et al. (2007) can be considered; in that study they derived sub-daily information from daily information.

BIBLIOGRAPHY

Allen, M.R. and Ingram, W.J. 2002. Constraints on future changes in climate and the hydrologic cycle. Nature, 419, pp. 224-232.

Andersson, L., Wilk, J., Todd, M.C., Hughes, D.A., Earle, A., Kniveton, D., Layberry, R. and Savenije, H.H.G. 2006. Impact of climate change and development scenarios on flow patterns in the Okavango river. Journal of Hydrology, 331, pp. 43-57.

Arnell, N. W. 2004. Global change and global water resources: SRES emissions and socio-economic scenarios. Global Environmental Change, 14, pp. 31–52.

Asian Development Bank (ADB). 2009. The Economics of Climate Change in Southeast Asia: A Regional Review. Asian Development Bank, Manila.

Badan Pusat Statistik (BPS) Jakarta. 2007. Jakarta dalam angka 2007. Katalog BPS: 1403.31, Badan Pusat Statistik Propinsi DKI Jakarta, pp. 520.

Badan Pusat Statistik (BPS) Jakarta. 2010. Jakarta dalam angka 2010. Katalog BPS: 1403.31, Badan Pusat Statistik Propinsi DKI Jakarta, pp. 607.

Bara, M., Kohnova, S., Gaal, L., Szolgay, J. and Hlavcova, K. 2009. Estimation of IDF curves of extreme rainfall by simple scaling in Slovakia. Contributions to Geophysics and Geodesy, Vol. 39/3, pp. 187–206.

Bardossy, A. and Plate, E.J. 1992. Space-time model for daily rainfall using atmospheric circulation patterns. Water Resources Research, 28, pp. 1247– 1259.

Barrow, E., Maxwell, B. and Gachon, P. 2004. Climate variability and change in Canada: past, present and future. Meteorological Service of Canada, Environment Canada, ACSD Science Assessment Series No. 2, pp. 114.

Barstad, I, Sorteberg, A., Flatoy, F. and Deque, M. 2008. Precipitation, temperature and wind in Norway: dynamical downscaling of ERA40. Climate Dynamics, DOI: 10.1007/s00382-008-0476-5.

Basher, M.A., Liu, T., Kabir, M.A., Ntegeka, V. and Willems, P. 2010. Climate change impact on the hydrological extremes in the Kaidu river basin, China. Collaborative Management of Integrated Watersheds, pp. 637-651.

Beck, C., Grieser, J. and Rudolf, B. 2005. A New Monthly Precipitation Climatology for the Global Land Areas for the Period 1951 to 2000. Climate Status Report 2004, German Weather Service, Offenbach, Germany, pp. 181 – 190. http://iridl.ldeo.columbia.edu/SOURCES/.DEKLIM/.VASClimO/.PrcpClim/.

Beckmann, B.R. and Buishand, T.A. 2002. Statistical downscaling relationships for precipitation in the Netherlands and north Germany. International Journal of Climatology, 22, pp. 15–32.

Bendjoudi, H., Hubert, P., Schertzer, D. and Lovejoy, S. 1997. Multifractal explanation of rainfall intensity-duration-frequency curves. EGS 24th General Assembly European Geophysical Society, The Hague, Netherlands.

Bergstrom, S., Carlsson, B., Gardelin, M., Lindstrom, G., Pettersson, A. and Rummukainen, M. 2001. Climate change impacts on runoff in Sweden - assessments by global climate models, dynamical downscaling and hydrological modelling. Climate Research, 16(2), pp. 101–112.

Bernard, M.M. 1932. Formulas for rainfall intensities of long durations. Transactions ASCE, 96, pp. 592–624.

Blazkova, S and Beven, K. 1997. Flood frequency prediction for data limited catchments in the Czech Republic using a stochastic rainfall model and TOPMODEL. Journal of Hydrology, 195(1-4). pp. 256-278.

Boer, R. and Faqih, A. 2004. Current and Future Rainfall Variability in Indonesia. An intergrated Assessment of Climate Change Impacts, Adaptation and Vulnerability in Watershed Areas and Communities in Southeast Asia, Report from AIACC Project No. AS21 (Annex C, 95-126). International START Secretariat, Washington, District of Columbia. http://sedac.ciesin.org/aiacc/progress/

Bormann, H. 2009. Analysis of possible impacts of climate change on the hydrological regimes of different regions in Germany, Advances in Geosciences, 21, pp. 3–11.

Caldwell, P., Chin, S.H.N., Bader, D.C. and Bala, G. 2009. Evaluation of a WRF dynamical downscaling simulation over California. Climate Change, 95, pp. 499-521.

Case, M., Ardiansyah, F. and Spector, E. 2007. Climate change in Indonesia: Implications for human and nature. World Wildlife Fund, pp. 1-13.

Cayan D.R., Luers, A.L., Franco, G., Hanemann, M., Croes, B. and Vine, E. 2008. Overview of the California climate change scenarios project. Climatic Change, 87(Suppl 1), S1–S6, DOI: 10.1007/s10584-007-9352-2.

Chandler, R.E., Isham, V.S., Wheater, H.S., Onof, C.J., Leith, N., Frost, A.J. and Segond, M-L. 2006. Joint Defra/EA Flood and Coastal Erosion Risk Management R&D Programme Spatial-temporal rainfall modelling with climate change scenarios. R&D Technical Report FD2113/TR.

Charles, S.P., Bates, B.C., Whetton, P.H. and Hughes, J.P. 1999. Validation of downscaling models for changed climate conditions: case study of southwestern Australia. Climate Research, Vol. 12, pp. 1-14.

Chen, C.L. 1983. Rainfall intensity-duration-frequency formulas. Journal of Hydraulic Engineering, 109, pp. 1603-1621.

Chen, M.Y., Xie, P.P., Janowiak, J.E. and Arkin, P.A. 2002. Global Land Precipitation: A 50-yr Monthly Analysis Based on Gauge Observations. Journal of Hydrometeorology, Vol 3, pp. 249-266. http://www.cpc.ncep.noaa.gov/products

Chow, V.T. 1964. Handbook of Applied Hydrology. McGraw-Hill, New York, pp. 1- 1450.

Chow, V.T., Maidment, D.R. and Mays, L.W. 1988. Applied Hydrology, McGraw-Hill.

Christensen, J.H. and Christensen, O.B. 2003. Climate Modeling: Severe summertime flooding in Europe. Nature, 421, pp. 805–806.

Christensen, J.H. and Christensen, O.B. 2007. A summary of the PRUDENCE model projections of changes in European climate by the end of this century. Climatic Change, 81, pp. 97-122, DOI: 10.1007/s10584-006-9210-7.

Christensen, O.B. and Christensen, J.H. 2008. Climate Models: An Assessment of Strengths and Limitations. A Report by the U.S. Climate Change Science Program (CCSP) and the Subcommittee on Global Change Research Department of Energy. Office of Biological and Environmental Research, Washington, D.C., USA, pp. 124.

Christensen, O.B., Christensen, J.H., Machenhauer, B. and Botzet, M. 1998. Very high-resolution regional climate simulations over Scandinavia–Present climate. Journal of Climate, 11, pp. 3204–3229.

Christensen, J., Hulme, M., von Storch, H., Whetton, P., Jones, R., Mearns, L. and Fu, C. 2001. Regional climate information—Evaluation and projections. Climate Change 2001: The Scientific Basis. Contribution of Working Group I to the Third Assessment Report of the Intergovernmental Panel on Climate Change, Cambridge University Press, pp. 583–638.

Christensen, J.H., Carter, T.R. and Rummukainen, M. 2007. Evaluating the performance and utility of regional climate models: the PRUDENCE project. Climatic Change, 81, pp. 1-6. DOI: 10.2007/s10584-006-9211-6.

Cocke, S.D. and LaRow, T.E. 2000. Seasonal prediction using a regional spectral model embedded within a coupled ocean-atmosphere model. Monthly Weather Review, 128, pp. 689–708.

Cole, S. and McCarthy, L. 2011. NASA – NASA research finds 2010 tied for warmest year on record (Feature). http://www.nasa.gov/topics/earth/features/2010-warmest-year.html.

Collischonn, B., Collischonn, W. and Tucci, C.E.M. 2008. Daily hydrological modeling in the Amazon basin using TRMM rainfall estimates. Journal of Hydrology, 360, pp. 207-216.

Connecting Delta Cities (CDC). 2009. Coastal cities, flood risk management and adaptation to climate change. VU University Press, Amsterdam, Netherlands.

Coulibaly, P. and Shi, X. 2005. Identification of the Effect of Climate Change on Future Design Standards of Drainage Infrastructure in Ontario. Report prepared by McMaster University with funding from the Ministry of Transportation of Ontario, pp. 82.

Cruz, R.V., Harasawa, H., Lal, M., Wu, S., Anokhin, Y., Punsalmaa, B., Honda, Y., Jafari, M., Li, C. and Huu Ninh, N., 2007. Asia. Climate Change 2007: Impacts, Adaptation and Vulnerability. Contribution of Working Group II to the Fourth Assessment Report of the Intergovernmental Panel on Climate Change, M.L. Parry, O.F. Canziani, J.P. Palutikof, P.J. van der Linden and C.E. Hanson, Eds., Cambridge University Press, Cambridge, United Kingdom, pp. 469-506.

DbLive Meteorological Group. 2010. Meteorological Intelligence Accuracy & Skill in Forecasting the Weather.

Dickinson, R.E., Errico, R.M., Giorgi, F. and Bates, G.T., 1989. A regional climate model for the western united states. Climate Change, 15, pp. 383-422.

Dupont, B.S. and Allen D.L. 2000. Revision of the Rainfall Intensity Duration Curves for the Commonwealth of Kentucky. Kentucky Transportation Center Lexington.

El-Sayed, E.A.H. 2011. Generation of Rainfall Intensity Duration Frequency Curves For Ungauged Sites. Nile Basin Water Science & Engineering Journal, 4(1), pp. 112-124.

Emanuel, K. 2011. Rethinking Climate Change: The Past 150 Years and the Next 100 Years. Massachusetts Institute of Technology (MIT).

Endreny, T.A. and Imbeah, N. 2009. Generating robust rainfall intensity–duration frequency estimates with short-record satellite data. Journal of Hydrology, 371, pp. 182–191.

Fennessy M.J., Shukla J. 2000. Seasonal prediction over North America with a regional model nested in a global model. Journal of Climate, 13, pp. 2605– 2627

Filliben, J.J. 1975. The probability plot correlation test for normality. Technometrics, 17(1), pp. 111-117.

Forest, C., Stone, P., Sokolov, A., Allen, M. and Webster, M. 2002. Quantifying uncertainties in climate system properties with the use of recent climate observations. Science, 295, pp. 113-117.

Fowler, H.J. and Kilsby, C.G. 2007. Using regional climate model data to simulate historical and future river flows in northwest England. Climatic Change, 80(3-4), pp. 337-367

Fowler, H.J., Kilsby, C.G. and Stunell, J. 2007. Modelling the impacts of projected future climate change on water resources in northwest England. Hydrology and Earth System Sciences, 11(3), pp. 1115–1126.

Framji, K.K., Garg, B.C. and Luthra, S.D.L. 1982. Irrigation and drainage in the world – A global review. The International Commission on Irrigation and Drainage (ICID).

Francisco, H.A. 2008. Adaptation to Climate Change: Needs and Opportunities in Southeast Asia. Asean Economic Bulletin, 25 (1).

Fuller, W.E. 1914. Flood flows. Transactions ASCE, 77, pp 564-617.

Gachon, P., St-Hilaire, A., Ouarda, T.B.M.J., Nguyen, V.T.V., Lin, C., Milton, J., Chaumont, D., Goldstein, J., Hessami, M., Nguyen, T.D., Selva, F., Nadeau, M., Roy, P., Parishkura, D., Major, N., Choux, M. and Bourque, A. 2005. A First Evaluation of the Strength and Weaknesses of Statistical Downscaling Methods for Simulating Extremes over Various Regions of Eastern Canada. Sub-component, Climate Change Action Fund (CCAF), Environment Canada, Montreal, Quebec, Canada, pp. 209.

Gan, T.Y., Dlamini, E.M. and Biftu, G.F. 1997. Effects of model complexity and structure, data quality and objective functions on hydrologic modeling. Journal of Hydrology, 192, pp. 81–103.

Gellens, D. 2002. Combining regional approach and data extension procedure for assessing GEV distribution of extreme precipitation in Belgium. Journal of Hydrology, Vol. 268, pp. 113-126.

Gibson, J.K., Kallberg, P., Uppala, S., Hernandez, A., Nomura, A. and Serrano, E. 1997. ERA Description. ECMWF Re-Analysis Project Series 1.

Giorgi, F. 1990. Simulation of regional climate using a limited area model nested in a general circulation model. American Meteorological Society, 3, pp. 941-963.

Giorgi, F. and Marinucci, M.R. 1991. Validation of a regional atmospheric model over Europe: sensitivity of wintertime and summertime simulations to selected physics parameterizations and lower boundary conditions, Quarterly Journal of the Royal Meteorological Society, 117, pp. 1171–1207.

Giorgi, F., Hewitson, B., Christensen, J.H., Hulme, M., von Storch, H., Whetton, P., Jones, R., Mearns, L.O., Fu, C. 2001. Regional climate information – evaluation and projections The Scientific Basis, Climate Change 2001. Cambridge University Press, Cambridge, UK, pp. 583–638.

Gordon, C., Cooper, C., Senior, C.A., Banks, H., Gregory, J.M., Johns, T.C., Mitchell, J.F.B. and Wood, R.A. 2000. The simulation of SST, sea ice extents and ocean heat transport in a version of the Hadley Centre coupled model without flux adjustments, Climate Dynamics, 16(2–3), pp. 147–168.

Graham L.P., Hagemann, S., Jaun, S. and Beniston, M. 2007. On interpreting hydrological change from regional climate models. Climatic Change, 81, pp. 97–122, DOI: 10.1007/s10584-006-9217-0.

Grimaldi, S., Kao, S.C., Castellarin, A., Papalexiou, S.M., Viglione, A., Laio, F., Aksoy, H. and Gedikli, A. 2011. Statistical Hydrology. In: Peter Wilderer (ed.). Treatise on Water Science, Vol. 2, Oxford: Academic Press, pp. 479–517.

Gumbel, E.I. 1958. Statistics of Extremes. Columbia University Press, New York.

Gyalistras, D., Schar, C., Davies, H.C. and Wanner, H. 1998. Future Alpine climate. Views from the Alps. Regional Perspectives on Climate Change. Cambridge, Massachusetts: MIT Press, pp. 171-223.

Hagemann, S. Arpe, K. and Roeckner, E. 2006. Evaluation of the Hydrological Cycle in the ECHAM5 Model. Journal of Climate – Special Section, 19, pp. 3810-3827.

Hamlet, A.F. and Lettenmaier, D.P. 1999. Effects of climate change on hydrology and water resources in the Columbia river basin. Journal of the American Water Resources Association, 36(6), pp. 1597-1623.

Hansen, J., Ruedy, R., Sato, M. and Lo., K. 2006. Goddard Institute for Space Studies, GISS Surface Temperature Analysis. NASA Goddard Institute for Space Studies, http://data.giss.nasa.gov/gistemp/2005/

Hara, M., Yoshikane, T., Kawase, H. and Kimura, F. 2008. Estimation of the impact of global warming on snow depth in Japan by the Pseudo-Global-Warming method. Hydrological Research Letters, 2, pp. 61-64.

Hay, L.E., Clark, M.P., Wilby, R.L., Gutowski, W.J., Leavesley, G.H., Pan, Z., Arritt, R.W. and Takle, E.S. 2002. Use of regional climate model output for hydrologic simulations. Journal of Hydrometeorology, 3(5), pp. 571–590.

Heikkila, U., Sandvik, A and A. Sorteberg, A. 2011. Dynamical downscaling of ERA-40 in complex terrain using the WRF regional climate model. Climate Dynamics, 37, pp. 1551-1564.

Hewitson, B.C. and Crane, R.G. 1996. Climate downscaling: Techniques and application, Climate Research, 7, pp. 85-95.

Hlavcova, K., Kohnova, S., Kubes, R., Szolgay, J. and Zvolensky, M. 2005. An empirical method for estimating future flood risks for flood warning. Hydrology and Earth Sciences, Vol. 9(4), pp. 431-448.

Hong, S.Y., Juang, H.M.H. and Lee, D.K. 1999. Evaluation of a regional spectral model for the East Asian monsoon case studies for July 1987 and 1988. Journal of the Meteorological Society of Japan, 77, pp. 553–572.

Hosking, J.M.R. 1990. L-moments: analysis and estimation of distributions using linear combinations of order statistics. Journal of the Royal Statistical Society, B 52(1), pp. 105-124.

Hosking, J.R. and Wallis, J.R. 2005. Regional Frequency Analysis: An Approach Based on L-Moments. Cambridge University Press: Cambridge, United Kingdom.

Hossain, F. and Katiyar, N. 2006. Improving flood forecasting in international river basins. EOS Transactions (American Geophysical Union), 87(5), pp. 49–50.

Houghton, J.T., Jenkins, G.J. and Ephraums, J.J. 1990. Climate Change. The IPCC Assessment, Cambridge University Press.

Huang, Q., Chen, Y.F., Xu, S., Liu, Y. and Li, X.K. 2010. Scaling Models of a Rainfall Intensity – Duration - Frequency Relationship. Sixth International Conference on Natural Computation (ICNC).

Hulme, M. and Turnpenny, J. 2002. Climate Change Scenarios for the United Kingdom The UKCIP02 Briefing Report.

Huntingford, C., Jones, R.G., Prudhomme, C., Lamb, R., Gash, J.H.C. and Jones, D.A. 2003. Regional climate-model predictions of extreme rainfall for a changing climate. Quarterly Journal of the Royal Meteorological Society, 129, pp. 1607-1621.

Indonesia Country Report (ICR). 2007. Climate variability and climate changes, and their implication. Ministry of Environment, Indonesia.

Intergovernmental Panel on Climate Change (IPCC). 2001. Climate Change 2001: The Scientific Basis. Contribution of Working Group I to the Third Assessment Report of the Intergovernmental Panel on Climate Change [Houghton, J.T., et al. (eds.)]. Cambridge University Press, Cambridge, United Kingdom and New York, USA

Intergovernmental Panel on Climate Change (IPCC). 2007. Climate change 2007. Contribution of Working Groups I and II to the Fourth Assessment Report of the Intergovernmental Panel on Climate Change, Cambridge University Press Cambridge, Cambridge, United Kingdom and New York, USA.

Intergovernmental Panel on Climate Change (IPCC). 2007a. Summary for policymakers. In: Climate change 2007: The physical science basis. Contribution of Working Group I to the Fourth Assessment Report of the Intergovernmental Panel on Climate Change, Cambridge, United Kingdom and New York, USA: Cambridge University Press.

Intergovernmental Panel on Climate Change (IPCC). 2007b. Summary for policymakers. In: Climate change 2007: Impacts, adaptation and vulnerability. Contribution of Working Group II to the Fourth Assessment Report of the Intergovernmental Panel on Climate Change, Cambridge, United Kingdom: Cambridge University Press

Jacob, D. and Lorenz, P. 2009. Future trends and variability of the hydrological cycle in diff IPCC SRES emission scenarios - a case study of Baltic Sea Region. Boreal Environment Research, 14, pp. 100-113.

Jones, P. 2011. CRU Information Sheet no. 1: Global Temperature Record. Climatic Research Unit, School of Environmental Sciences, University of East Anglia. http://www.cru.uea.ac.uk/cru/info/warming/.

Jones, R.G., Noguer, M., Hassell, D.C., Hudson, D., Wilson, S.S., Jenkins, G.J. and Mitchell, J.F.B. 2004. Generating high resolution climate change scenarios using PRECIS. Met Office Hadley Centre, Exeter, United Kingdom, pp. 40.

Kalnay, E., Kanamitsu, M., Kistler, R., Collins, W., Deaven, D., Gandin, L., Iredell, M., Saha, S., White, G., Woollen, J., Zhu, Y., Chelliah, M., Ebisuzaki, W., Higgins, W., Janowiak, J. Mo, K.C., Ropelewski, C., Wang, J., Leetmaa, A., Reynolds, R., Jenne, R. and Joseph, D. 1996. The NCEP/NCAR 40-Year reanalysis project. Bulletin of the American Meteorological Society, 77, pp. 437– 471.

Kanamitsu, M., Juang H.M.H. 1994. Simulation and analysis of an Indian Monsoon by the NMC nested regional spectral model. Proceedings of the International Conference on Monsoon Variability and Prediction, International Centre for Theoretical Physics, Trieste, Italy, 9–13 May 1994, vol II, WMO.TD-No. pp. 619

Karl, T.R., Nicholls, N. and Ghazi, A. 1999. Weather and climate extremes: Changes, variations and a perspective from the insurance industry. Climatic Change, 42, pp. 1-349.

Keikkila, U., Sandvik, A. and Sorteberg, A. 2011. Dynamical downscaling of ERA-40 in complex terrain using the WRF regional climate model. Climate Dynamics, 37, pp. 1551–1564.

Kilsby, C.G., Tellier, S.S., Fowler, H.J. and Howels, T.R. 2007. Hydrological impacts of climate change on the Tejo and Guadiana Rivers, Hydrology and Earth System Sciences, 11(3), pp. 1175-1189.

Klemes, V. 1993. Probability of extreme hydrometeorological events - a different Approach, Extreme Hydrological Events: Precipitation, Floods and Droughts. Proceedings of the Yokohama Symposium, IAHS PubI. no. 213.

Knutti, R., Furrer, R., Tebaldi, C., Cermak, J. and Meehl, G.A. 2010. Challenges in combining projections from multiple models. Journal of Climate, 23, pp. 2739-2758.

Kotlarski, S., Block, A., Bohm, U., Jacob, D., Keuler, K., Knoche, R., Rechid, D. and Walter, A. 2005. Regional climate model simulations as input for hydrological applications: evaluation of uncertainties. Advances in Geosciences, 5, pp. 119-125.

Koutsoyiannis, D. 2004. Statistics of extremes and estimation of extreme rainfall: I. Theoretical investigation. Hydrological Sciences Journal, 49(4), pp. 575-590.

Koutsoyiannis, D. 2007. A critical review of probability of extreme rainfall: principles and models. Advances in Urban Flood Management, Taylor and Francis, London, pp. 139-166.

Koutsoyiannis, D., Kozonis, D. and Manetas, A. 1998. A mathematical framework for studying rainfall intensity-duration-frequency relationships. Journal of Hydrology 206, pp. 118–135.

Labat, D., Godderis, Y., Probst, J.L. and Guyot, J.L. 2004, Evidence for global runoff increase related to climate warming. Advances in Water Resources, 27, pp. 631–642.

Lateckova, J., Kohnova, S., Gaal, L. and Szolgay, J. 2011. Estimation of IDF curves of monthly rainfall intensities in the western part of Slovakia. 7th Symposium: Development in Hydrological Sciences, Conference of the Danube Countries, Budapest, University of Technology and Economics.

Leclerc, M. and Ouarda, T.B.M.J. 2007. Non-stationary regional flood frequency analysis at ungauged sites. Journal of Hydrology, 343, pp. 254– 265.

Legates, D.R. 2001. Climate models and the National Assessment: Report to the George C. Marshall Institute, http://www.marshall.org/Legatesclimatemodels.htm.

Leith, N. A. 2008. Single-site rainfall generation under scenarios of climate change. PhD thesis, University College London.

Leung, L.R., Mearns, L.O., Giorgi, F. and Wilby R.L. 2003. Regional climate research – needs and opportunities. Bulletin of the American Meteorological Society, 84, pp. 89–95.

Liang, X-Z., Kunkel, K.E., Meehl, G.A., Jones, R.G. and Wang, J.X.L. 2008. Regional climate models downscaling analysis of general circulation models present climate biases propagation into future change projections. Geophysical Research Letters, 35, L08709, DOI: 10.1029/2007GL032849.

Lindstrom, G., Johansson, B., Persson, M., Gardelin, M. and Bergström, S. 1997. Development and test of the distributed HBV-96 hydrological model, Journal of Hydrology, 201, pp. 272-288.

Lu, L.H. and Jery R. Stedinger, J.R. 1992. Sampling variance of normalized GEV/PWM quantile estimators and a regional homogeneity test. Journal of Hydrology, 138, pp. 223-245.

Ma, X., Yoshikane, T., Hara, M., Wakazuki, Y., Takahashi, H.G. and Kimura, F. 2010. Hydrological response to future climate change in the Agano River basin, Japan. Hydrological Research Letters, 4, pp. 25-29.

Madsen, H. and Rosbjerg, D. 1997. Generalized least squares and empirical Bayes estimation in regional partial duration series index-flood modeling. Water Resources Research, 33 (4), pp. 771– 781.

Madsen, H., Mikkelsen, P.S., Rosbjerg, D. and Harremoe¨s, P. 1998. Estimation of regional intensity–duration–frequency curves for extreme precipitation. Water Sciences and Technology, 37 (11), pp. 29– 36.

Madsen, H., Mikkelsen, P.S., Rosbjerg, D. and Harremoe¨s, P. 2002. Regional estimation of rainfall intensity–duration–frequency curves using generalized least squares regression of partial duration series statistics. Water Resources Research, 38 (11), 21-1–21-11.

Maidment, D.R. 1993. Handbook of Hydrology. McGraw-Hill, New York.

Mailhot, A., Duschesne, S., Caya, D. and Talbot, G. 2007. Assessment of future change in intensity–duration–frequency (IDF) curves for Southern Quebec using the Canadian Regional Climate Model (CRCM). Journal of Hydrology, 347, pp. 197-210.

Manton, M.J., Della-Marta, P.M., Haylock, M.R., Hennessy, K.J., Nicholls, N., Chambers, L.E., Collins, D.A., Daw, G., Finet, A., Gunawan, D., Inape, K., Isobe, H., Kestin, T.S., Lefale, P., Leyu, C.H., Lwin, T., Maitrepierre, L., Ouprasitwong, N., Page, C.M., Pahalad, J., Plummer, N., Salinger, M.J., Suppiah, R., Tran, V.L., Trewin, B., Tibig, I. and Yee, D. 2001. "Trends in Extreme Daily Rainfall and Temperature in Southeast Asia and the South Pacific (1961–1998)." International Journal of Climatolology, 10(1002), pp. 610.

Mastrangelo, D., Horvath, K., Riccio, A. and Miglietta, M.M. 2011. Mechanisms for convection development in a long-lasting heavy precipitation event over southeastern Italy. Atmospheric Research, 100, pp. 586–602.

Mearns, L.O., Giorgi, F., McDaniel, L. and Shields, C. 1995. Analysis of daily variability of precipitation in a nested regional climate model: comparison with observations and doubled CO2 results. Global Planet Change, 10, pp. 55–78.

Mearns, L., Hulme, M., Carter, T., Leemans, R., Lal, M. and Whetton, P. 2001. Climate scenario development. Climate Change 2001: The Scientific Basis. Contribution of Working Group I to the Third Assessment Report of the Intergovernmental Panel of Climate Change, Houghton, J.T., Ding, Y., Griggs, D., Noguer, M., van der Linden, P.J., Dai, X., Maskell, K. and Johnson, C.A. Eds., Cambridge University Press, Cambridge, pp. 739-768.

Meehl, G.A., Washington, W.M., Collins, W.D., Arblaster, J.M., Hu, A., Buja, L.E., Strand, W.G. and Teng, H. 2005. How much more global warming and sea level rise? Science, 307(5716), pp. 1769–1772.

Meehl, G.A., Stocker, T.F., Collins, W.D., Friedlingstein, P., Gaye, A.T., Gregory, J.M., Kitoh, A., Knutti, R., Murphy, J.M., Noda, A., Raper, S.C.B., Watterson, I.G., Weaver, A.J. and Zhao, Z.-C. 2007. Global Climate Projections. In 'Climate Change 2007: The Physical Science Basis. Contribution of Working Group I to the Fourth Assessment Report of the Intergovernmental Panel on Climate Change'.(Eds Solomon, S., Qin, D., Manning M., Chen, Z., Marquis, M., Averyt, K.B., Tignor M. and Miller, H.L.), Cambridge, pp. 747-845.

Menzel, L. and Burger, G. 2002. Climate change scenarios and runoff response in the Mulde catchment (Southern Elbe, Germany). Journal of Hydrology, 267, pp. 53–64.

Menzel, L. and Schwandt, D. 2004. Hydrologische Modellierung von Klima- und Landnutzungsszenarien im Rheingebiet (hydrological modelling of climate and land use change scenarios in the Rhine basin). In: B. Merz and H. Apel (eds), Risiken durch Naturgefahren in Deutschland. Final Report, German Research Network Natural Disasters, GeoForschungsZentrum Potsdam, STR04/01, pp. 36–48.

Menzel, L., Thieken, A.H., Schwandt, D. and Burger, G. 2006. Impact of climate change on the regional hydrology – scenario-based modeling studies in the german rhine catchment. Natural Hazards, Vol. 38, pp. 45-61.

Mikkelsen, P.S., Madsen, H., Rosbjerg, D. and Harremoes, P. 1996. Properties of extreme rainfall: III. Identification of spatial inter-site correlation structure. Atmospheric Research, 40, pp. 77– 98.

Mikkelsen, P.S., Madsen, H., Arnbjerg-Nielsen, K., Jorgensen, H.K., Rosbjerg, D. and Harremoes, P. 1998. A rationale for using local and regional rainfall data for design and analysis of urban storm drainage systems. Water Science and Technology, 37(11), pp. 7 – 14.

Mikkelsen, P.S., Madsen, H., Arnbjerg-Nielsen, K., Rosbjerg, D. and Harremoes, P. 2005. Selection of regional historical rainfall time series as input to urban drainage simulations at ungauged locations. Atmospheric Research 77, pp. 4– 17.

Miller, N.L., Bashford, K.E. and Strem, E. 2003. Potential impacts of climate change on California hydrology. Journal of the American Water Resources Association 39(4): 771-784.

Millington, N., Das, S. and Simonovic, S.P. 2011. The Comparison of GEV, Log-Pearson Type 3 and Gumbel Distributions in the Upper Thames River Watershed under Global Climate Models. Water Resources Research Report, No. 077, Facility for Intelligent Decision Support, Department of Civil and Environmental Engineering, London, Ontario, Canada.

Mitchell, T.D. and Jones, P.D. 2005. An improved method of constructing a database of monthly climate observations and associated high-resolution grids. International Journal of Climatology, 25, pp. 693-712.

Mo, K., Kanamitsu, M., Juang, H.M.H. and Hong, S.-Y. 2000. Ensemble regional and global climate prediction for the 1997/1998 winter. Journal of Geophysical Research, 105, pp. 29609–29623.

Mohd Daud, Z., Kassim, A.H.M., Desa, M.N.M. and Nguyen, V.T.V. 2002. Statistical analysis of at-site extreme rainfall processes in Peninsular Malaysia. Regional Hydrology: Bridging the Gap between Research and Practice, Proceedings of the Fourth International FRIEND Conference held at Cape Town. South Africa.

Murphy, J. 1999. An evaluation of statistical and dynamical techniques for downscaling local climate. Journal of Climate, 12, pp. 2256–2284.

Murray-Hudson, M., Wolski, P. and Ringrose, S. 2006. Scenarios of the impact of local and upstream changes in climate and water use on hydro-ecology in the Okavango Delta, Botswana. Journal of Hydrology, 331, pp. 73– 84.

Murshed, S. Islam, A.K.M.S. and Khan, M.S.A. 2011. Impact of climate change on rainfall intensity in Bangladesh. 3rd International Conference on Water & Flood Management (ICWFM).

National Center for Atmospheric Research (NCAR), USA. 2003 http://www.eo.ucar.edu/basics/

National Climatic Data Center (NCDC). 2011. www.ncdc.noaa.gov

New, M., Hulme, M. and Jones, P.D. 1999. Representing twentieth century space time climate variability. Part 1: development of a 1961-90 mean monthly terrestrial climatology. Journal of Climate, 12, pp. 829-856.

New, M., Hulme, M., Jones, P.D. 2000. Representing twentieth century space-time climate variability. Part 2: development of 1901-96 monthly grids of terrestrial surface climate. Journal of Climate, 13, pp. 2217-2238.

Nguyen, V.T.V., Nguyen, T.D. and Ashkar, F. 2002. Regional frequency analysis of extreme rainfalls. Water Science and Technology, Vol 45, No. 2, pp 75-81.

Nguyen, V.T.V., Nguyen, T.D. and Cung, A. 2007. A Statistical approach to downscaling of sub-daily extreme rainfall processes for climate-related impact studies in urban areas. Water Sciences and Technology: Water Supply 7(2), pp. 183-192.

Nhat, L.M., Tachikawa, Y. and Takara, K. 2006. Establishment of Intensity-Duration Frequency Curves for Precipitation in the Monsoon Area of Vietnam. Annuals of Disaster Prevention Research Institute Kyoto University, No. 49 B.

Nobre, P., Moura, A.D., Sun L. 2001. Dynamical downscaling of seasonal climate prediction over Nordeste Brazil with ECHAM3 and NCEP's regional spectral models at IRI. Bulletin of the American Meteorological Society, 82, pp. 2787–2796.

Nozawa, T., Nagashima, T., Ogura, T., Yokohata, T., Okada, N. and Shiogama, H. 2007. Climate change simulations with a coupled ocean-atmosphere GCM called the model for interdisciplinary research on climate: MIROC, CGER's Supercomputer Monograph Report 12. Center for Global Environmental Research, National Institute for Environmental Studies, Tsukuba, Japan.

Oak Ridge National Laboratory (ORNL), http://www.ornl.gov/.

Olofsson, M. 2007. Climate Change and Urban Drainage: Future precipitation and hydraulic impact.

Onof, C. and Arnbjerg-Nielsen, K. 2009. Quantification of anticipated future changes in high resolution design rainfall for urban areas. Atmospheric Research 92, pp. 350 363, DOI: 10.1016/j.atmosres.2009.01.014.

Oyebande, L. 1982. Deriving rainfall intensity-duration-frequency relationships and estimates for regions with inadequate data, Hydrological Sciences - Journal – des Sciences Hydrologiques, 27.

Pakeh, M.I., Ria, P.G., Indra, H.T. and Wibowo, A. 2007. Jakarta flood control system: Modeling. Proceedings of the International Conference on Electrical Engineering and Informatics, Institut Teknologi Bandung, Indonesia.

Peterson, T.C., Folland, C., Gruza, G., Hogg, W., Mokssit, A. and Plummer, N. 2001. Report on the activities of the working group on climate change detection and related rapporteurs 1998–2001. Report WCDMP-47, WMOTD 1071, Geneva, Switzerland, pp. 143.

Posselt, R. and Lohmann, U. 2008. Introduction of prognostic rain in ECHAM5: design and single column model simulations. Atmospheric Chemistry and Physics, 8, pp. 2949–2963.

Prodanovic, P. and Simonovic, S.P. 2007. Development of rainfall intensity duration frequency curves for the City of London under the changing climate. Department of Civil and Environmental Engineering, The University of Western Ontario London, Ontario, Canada.

Prudhomme, C., Jakob, D. and Svensson, C. 2003. Uncertainty and climate change impact on the flood regime of small UK catchments. Journal of Hydrology, 277, pp. 1–23.

Quenouille, M.H. 1949. Approximate tests of correlation in time series. Journal of the Royal Statistical Society, Series B, 11, pp. 18-44.

Quenouille, M.H. 1956. Notes on bias in estimation. Biometrika, 61, pp. 353-360.

Raiford, J.P., Aziz, N.M., Khan, A.A. and Powell, D.N. 2007. Rainfall Depth Duration-Frequency Relationships for South Carolina, North Carolina, and Georgia. American Journal of Environmental Sciences, 3(2), pp. 78-84.

Rao, A.R. and Kao, S. 2006. Statistical Analysis of Indiana Rainfall Data. Joint Transportation Research Program, Indiana Department of Transportation and Purdue University, West Lafayette, Indiana, DOI: 10.5703/1288284313446.

Roads, J.O. 2000. The second international RSM workshop: meeting summary. Bulletin of the American Meteorological Society, 81, pp. 2979–2980.

Roeckner, E., Arpe, K., Bengtsson, L., Christoph, M., Claussen, M., Dümenil, L, Esch, M., Giorgetta, M., Schlese, U. and Schulzweida, U. 2006. The atmospheric general circulation model ECHAM-4: Model description and simulation of present-day climate. Report No.218, MPI, ISSN 0937-1060.

Rojas, M. and Seth, A. 2003. Simulation and sensitivity in a nested modeling system for South America. Part II: GCM boundary forcing. Journal of Climate, 16, pp. 2454-2471.

Sailor, D.J., Hu, T., Li, X. and Rosen, J.N. 2000. A neural network approach to local downscaling of GCM output for assessing wind power implications of climate change. Renewable Energy, 19, pp. 359-378.

Salathe E.P., Leung L.R., Qian, Y. and Zhang Y. 2010. Regional climate model projections for the state of Washington. Climatic Change, 102, pp. 51–75.

Schulla, J. 1997. Hydrologische Modellierung von Flussgebieten zur Abscha¨tzung der Folgen von Klimaa¨nderungen, Zu¨rcher Geographische Schriften, Heft, vol. 69. Geographisches Institut dur ETH Zurich, pp. 1–187.

Schulze, R. E. 1997. Impacts of global climate change in a hydrologically vulnerable region: challenges to South African hydrologists. Progress in Physical Geography, 21, pp. 113–36.

Seth, A. and Rojas, M. 2003. Simulation and sensitivity in a nested modeling system for South America. Part I: Reanalyses boundary forcing. Journal of Climate 15, pp. 2437–2453.

Shaefer, M.G. 1990. Regional analyses of precipitation annual maxima in Washington State. Water Resources Research, 26(1), pp. 119– 131.

Sherman, C.W. 1931. Frequency and intensity of excessive rainfalls at Boston, Massachusetts. Transactions ASCE, 96, pp. 951-960.

Shiklomanov, A.I., Lammers, R. B., and Vörösmarty, C. J. 2002. Widespread decline in hydrological monitoring threatens pan-arctic research. EOS Transactions, 83(2), pp. 16–17.

Sieck, K. 2008. Investigation of the "added value" to seasonal forecasts by dynamical downscaling, Max Planck Institute for Meteorology, Hamburg, Germany.

Simonovic, S.P. and Peck, A. 2009. Updated rainfall intensity duration frequency curves for the City of London under the changing climate. Water Resources Research Report, No. 065, Facility for Intelligent Decision Support, Department of Civil and Environmental Engineering, London, Ontario, Canada.

Singh, V.J. and Zhang, L. 2007. Discussion of IDF Curves Using the Frank Archimedean Copula. Journal of Hydrologic Engineering, Vol. 12, No. 6, pp. 651-662, DOI: 10.1061/ASCE1084-0699200712:6651.

Skamarock, W.C., Klemp J.B., Dudhia J., Gill D.O., Barker D.M., Wang W., Powers, J.G. 2005. A Description of the Advanced Research WRF Version 2. NCAR Technical Note. http:/www.wrf-model.org.

Soares, P.M.M., Cardoso, R.M., Miranda, P.M.A., de Medeiros, J., Belo-Pereira, M. and Espirito-Santo, F. 2012. WRF high resolution dynamical downscaling of ERA Interim for Portugal. Climate Dynamics, DOI 10.1007/s00382-012-1315-2.

Soehodho, S. 2011. C40 Cities Climate Leadership Group, http://planetforward.org/idea/jakarta%E2%80%99s-deputy-governor-poverty and-climate-change-are-linked/

Solaiman, T.A. and Simonovic, S.P. 2011. Development of probability based intensity-duration-frequency curves under climate change. Water Resources Research Report, No. 072, Facility for Intelligent Decision Support, Department of Civil and Environmental Engineering, London, Ontario, Canada.

State of the Climate: Global Analysis for Annual 2009. 2010. http://www.ncdc.noaa.gov/sotc/global/2009/13

Stedinger, J.R. and Tasker, G.D. 1985. Regional hydrologic analysis, 1, ordinary, weighted and generalized least squares compared. Water Resources Research, 21(9), pp. 1421-1432.

Stedinger, J.R., Vogel, R.M. and Foufoula-Georgiou, E. 1993. Frequency analysis of extreme events. Handbook of Hydrology, Maidment, D.R. (ed.). McGraw-Hill, New York, 18.1–18.66.

Stokstad, E. 1999. Scarcity of rain, stream gages threatens forecasts. Science, 285, pp. 1199.

Sun, L. and Ward, M. N. 2006. Climate Downscaling: Assessment of the Added Values Using Regional Climate Models. Earth and Environmental Science, pp. 15-29.

Sun, L, Semazzi, F.H.M., Giorgi, F. and Ogallo, L. 1999a. Application of the NCAR regional climate model to eastern Africa. Part I: Simulation of the short rains of 1998. Journal of Geophysical Research ,104, pp. 6529–6548.

Sun, L, Semazzi, F.H.M., Giorgi, F. and Ogallo, L. 1999b. Application of the NCAR regional climate model to eastern Africa. Part II: Simulation of interannual variability of short rains. Journal of Geophysical Research, 104, pp. 6549–6562.

Takle, E.S., Gutowski Jr., W.J., Arritt, R.W., Pan, Z., Anderson, C.J., Silva, R., Caya, D., Chen, S.C., Christensen, J.H., Hong, S.Y., Juang, H.M.H., Katzfey, J., Lapenta, W.M., Laprise, R., Lopez, P., McGregor, J. and Roads, J.O. 1999. Project to intercompare regional climate simulations (PIRCS). Journal of Geophysical Research, 104, pp. 19443–19449.

Tambunan, M.P. 2007. Flooding area in the Jakarta province on February 2 to 4 2007, 28th Asian Conference on Remote Sensing, Putra World Trade Centre (PWTC), Kuala Lumpur Malaysia.

Texier, P. 2008. Floods in Jakarta: when the extreme reveals daily structural constraints and mismanagement. Disaster Prevention and Management, Vol. 17, No.3, pp. 358-372.

Thodsen, H. 2007. The influence of climate change on stream flow in Danish rivers. Journal of Hydrology, 333, pp. 226–238.

Tukey, J.W. 1958. Bias and confidence in not quite large samples (Abstract). Annals of Mathematical Statistics, 29, pp. 614.

United Nations Framework Convention on Climate Change (UNFCCC). 2007. Climate Change: Impacts, vulnerabilities and adaptation in developing countries, Climate Change Secretariat (UNFCCC), Bonn, Germany.

Uppala, S.M., Kallberg, P.W., Simmons, A.J., Andrae, U., da Costa Bechtold, V., Fiorino, M., Gibson, J.K., Haseler, J., Hernandez, A., Kelly, G.A., Li, X., Onogi, K., Saarinen, S., Sokka, N., Allan, R.P., Andersson, E., Arpe, K., Balmaseda, M.A., Beljaars, A.C.M., van de Berg, L., Bidlot, J., Bormann, N., Caires, S., Chevallier, F., Dethof, A., Dragosavac, M., Fisher, M., Fuentes, M., Hagemann, S., Hólm, E., Hoskins, B.J., Isaksen, L., Janssen, P.A.E.M., Jenne, R., McNally, A.P., Mahfouf, J-F., Morcrette, J-J., Rayner, N.A., Saunders, R.W., Simon, P., Sterl, A, Trenberth, K.E., Untch, A., Vasiljevic, D., Viterbo, P. and Woollen, J. 2005. The ERA-40 reanalysis. Quarterly Journal of the Royal Meteorological Society, 131, pp. 2961-3012. http://www.ecmwf.int/research/era/.

Varis, O., Kajander, T. and Lemmela, R. 2004. Climate and water: From climate models to water resources management and vice versa. Climatic Change, 66, pp. 321–344.

Veneziano, D., Lepore, Ch., Langousis, A. and Furcolo, P. 2007. Marginal methods of intensity-duration-frequency estimation in scaling and nonscaling rainfall. Water Resources Research, 43, W10418. DOI:10.1029/2007WR006040.

Vincent, L.A. and Mekis, E. 2006. Changes in daily and extreme temperature and precipitation indices for Canada over the twentieth century. Atmosphere Ocean, 44, pp. 177–193.

von Storch, H. 1995. Spatial patterns: EOFs and CCA, in Analysis of Climate Variability: Applications of Statistical Techniques. Chapter 13, pp. 227 – 258, Springer, New York.

von Storch, H., Zorita, E. and Cubasch, U. 1993. Downscaling of global climate change estimates to regional scales: An application to Iberian rainfall in wintertime. Journal of Climate, 6, pp. 1161–1171.

von Storch, H., Langenberg, H. and Feser, F. 2000. A spectral nudging technique for dynamical downscaling purposes. Monthly Weather Review, 128, pp. 3664–3673.

Walsh, K.J. 2004. Tropical cyclones and climate change: unresolved issues. Climate Research, 27, pp. 77–84.

Wang, Y.Q., Leung, L.R., McGregor J.L., Lee, D.K., Wang, W.C., Ding, Y.H. and Kimura, F. 2004. Regional climate modeling: Progress, challenges, and prospects. – Journal of the Meteorological Society of Japan, 82, pp. 1599–1628.

Whetton, P.H. 2001. Use of GCMs in Regional Climate Studies CSIRO. The Environmental and Societal Impacts Group//The National Center for Atmospheric Research

Wigley, T.M.L. 2005. The climate change commitment. Science, 307, pp. 1766–1769.

Wilby, R.L. and Wigley, T.M.L. 1997. Downscaling generalcirculation model output: a review of methodsand limitations. Progress in Physical Geography, 21, pp. 530–548.

Wilby, R.L., Hay, L.E. and Leavesley, G.H. 1999. A comparison of downscaled and raw GCM output: implications for climate change scenarios in the San Juan River basin, Colorado. Journal of Hydrology, 225, pp. 67-91.

Wilby, R.L., Wigley, T.M.L, Conway, D., Jones, P.D., Hewitson, B.C., Main, J. and Wilks, D.S. 1998. Statistical downscaling of general circulation model output: a comparison of methods. Water Resources Research, 34, pp. 2995–3008.

Wilby, R.L., Troni, J., Biot, Y., Tedd, L., Hewitson, B.C., Smith, D.M. and Sutton, R.T. 2009. A review of climate risk information for adaptation and development planning. International Journal of Climatology, 29, pp. 1196 1215.

Wilk, J., Kniveton, D., Andersson, L., Layberry, R., Todd, M.C., Hughes, D., Ringrose, S. and Vanderpost, C. 2006. Estimating rainfall and water balance over the Okavango River Basin for hydrological applications. Journal of Hydrology, 331, pp. 18-29.

World Wildlife Fund (WWF). 2009. Mega-Stress for Mega-Cities: A Climate Vulnerability Ranking of Major Coastal Cities in Asia

Wratt, D. and Mullan, B. 2008. Climate Change Scenarios for New Zealand, NIWA National Climate Centre, in collaboration with the Royal Society of New Zealand

Xu, C.Y. 1999. From GCMs to river flow: a review of downscaling methods and hydrologic modelling approaches. Progress in Physical Geography, 23, pp. 229–249.

Xu, C.Y., Widen, E. and Halldin, S. 2005. Modelling hydrological consequences of climate change – progress and challenges. Advances in Atmospheric Sciences, Vol. 22, No. 6, pp. 789-797.

Xu, C.Y., Gong, L., Jiang, T., Chen, D. and Singh V.P. 2006. Analysis of spatial distribution and temporal trend of reference evapotranspiration in Changjiang (Yangtze River) catchment. Journal of Hydrology, 327, pp. 81–93.

Yagouti, A., Boulet, G., Vincent, L.A., Vescovi, L and Mekis, E. 2008. Observed changes in daily temperature and precipitation indices for Southern Quebec, 1960 2005. Atmosphere Ocean, 46(2), pp. 243-256.

Yusuf, A. A. and Francisco, H. 2009. Climate Change Vulnerability Mapping for Southeast Asia. Economy and Environment Program for Southeast Asia (EEPSEA).

Zhang, Q., Xu, C.Y, Gemmer, M. and Chen, Y.Q. 2008a. Changing properties of precipitation concentration in the Pearl River basin, China. Stochastic Environmental Research & Risk Assessment, DOI 10.1007/s00477-008-0225-7.

Zhang, Q., Xu, C.Y. and Yang, T. 2008b. Variability of water resource of the Yellow River basin. Water Resources Management, DOI 10.1007/s11269-008-9320-2.

Zhang, Q., Xu, C.Y., Tao, H. Jiang, T. and Chen, Y.Q. 2010. Climate changes and their impacts on water resources in the arid regions: a case study of the Tarim River basin, China. Stochastic Environmental Research and Risk Assessment, 24, pp. 349-358.

Zorita, E. and von Storch, H.. 1997. A survey of statistical downscaling techniques. GKSS report 97/E/20.

APPENDIX A

IPCC GHG emissions scenarios:
[Source: IPCC, 2007a]

The IPCC has developed multiple scenario families to explore the uncertainties behind potential trends in global developments and GHG emissions. The IPCC decided that narrative storylines, based on the futures and scenario literature would be the most coherent way to describe their scenarios, for the following reasons:

· To help the team to think more coherently about the complex interplay between scenario driving forces within and across alternative scenarios and to enhance the consistency in assumptions for different parameters.

· To make it easier to explain the scenarios to the various user communities by providing a narrative description of alternative futures that goes beyond quantitative scenario features.

· To make the scenarios more useful, in particular, to analysts contributing to IPCC Working Groups II (Climate Impacts, Adaptation and Vulnerability) and III (Mitigation of Climate Change). The demographic, social, political and technological contexts described in the scenario storylines are all important in the analysis of the effects of policies to either adapt to climate change or to reduce GHG emissions.

· To provide a guide for additional assumptions to be made in detailed climate impact and mitigation analyses because at present no model or scenario can possibly respond to the wide variety of informational and data needs of the different user communities of long-term emissions scenarios.

The different story lines developed by the IPCC are described in brief below.

A1 - The A1 storyline and scenario family describes a future world of very rapid economic growth, global population that peaks in mid-century and declines thereafter and the rapid introduction of new and more efficient technologies. Major underlying themes are convergence among regions, capacity building and increased cultural and social interactions with a substantial reduction in regional differences in per capita income. This family develops into three groups that describe alternative directions of technological change in the energy system. The three A1 groups are distinguished by their technological emphasis: fossil-intensive (A1FI), non-fossil energy sources (A1T) or a balance across all sources (A1B) (where balanced is defined as not relying too heavily on one particular energy source, on the assumption that similar improvement rates apply to all energy supply and end use technologies).

A2 - The A2 storyline and scenario family describes a very heterogeneous world. The underlying theme is self- reliance and preservation of local identities. Fertility patterns across regions converge very slowly, which results

in continuously increasing population. Economic development is primarily regionally oriented and per capita economic growth and technological change more fragmented and slower than other storylines.

B1 - The B1 storyline and scenario family describes a convergent world with the same global population that peaks in mid-century and declines thereafter, as in the A1 storyline, but with rapid change in economic structures toward a service and information economy, with reductions in material intensity and the introduction of clean and resource-efficient technologies. The emphasis is on global solutions to economic, social and environmental sustainability, including improved equity, but without additional climate initiatives.

B2 - The B2 storyline and scenario family describes a world in which the emphasis is on local solutions to economic, social and environmental sustainability. It is a world with continuously increasing global population, at a rate lower than A2, intermediate levels of economic development and less rapid and more diverse technological change than in the B1 and A1 storylines. While the scenario is also oriented towards environmental protection and social equity, it focuses on local and regional levels

APPENDIX B

APPENDIX B1

Validation sites for (3-step) DCD approach – Ipoh, Seremban, Melaka and Johor Bahru Meteorological stations in Peninsula Malaysia

Kuala Lumpur to	Distance (Km)
Ipoh	175
Seremban	55
Melaka	120
Johor Bahru	295

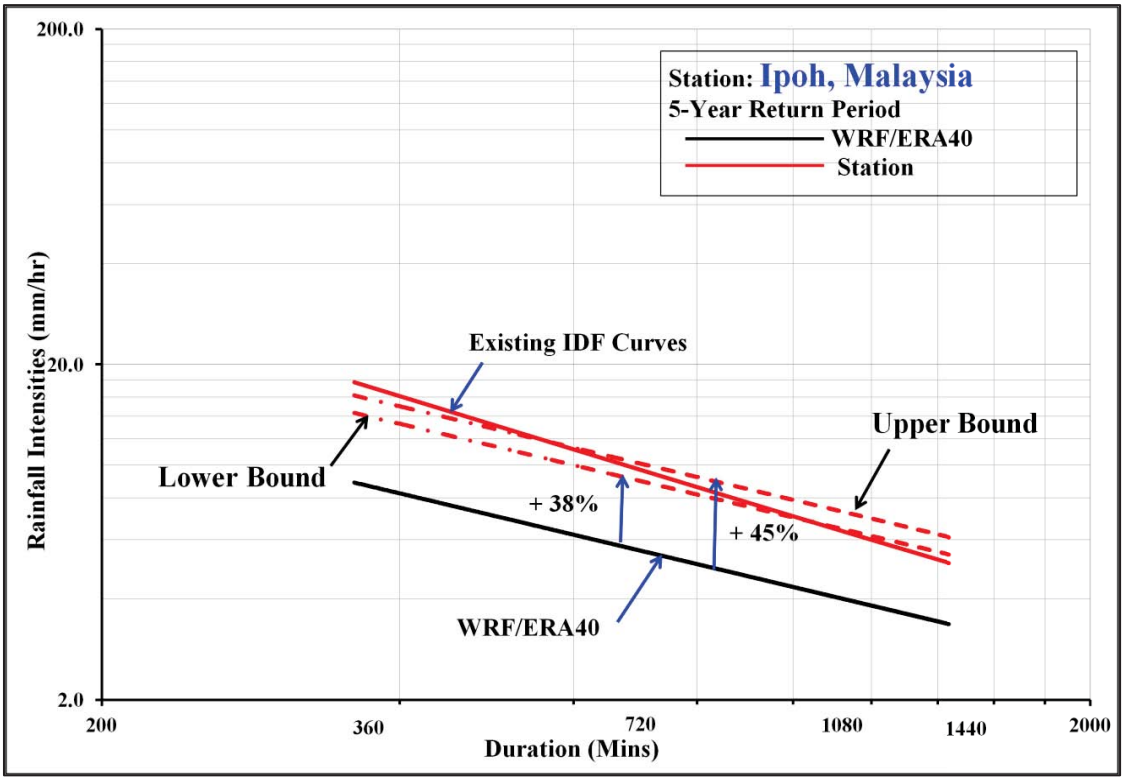

Figure B1-1a: WRF/ERA40 projected present day rainfall intensities anomalies from the existing IDF curve (5-year return period): Ipoh Meteorological Station

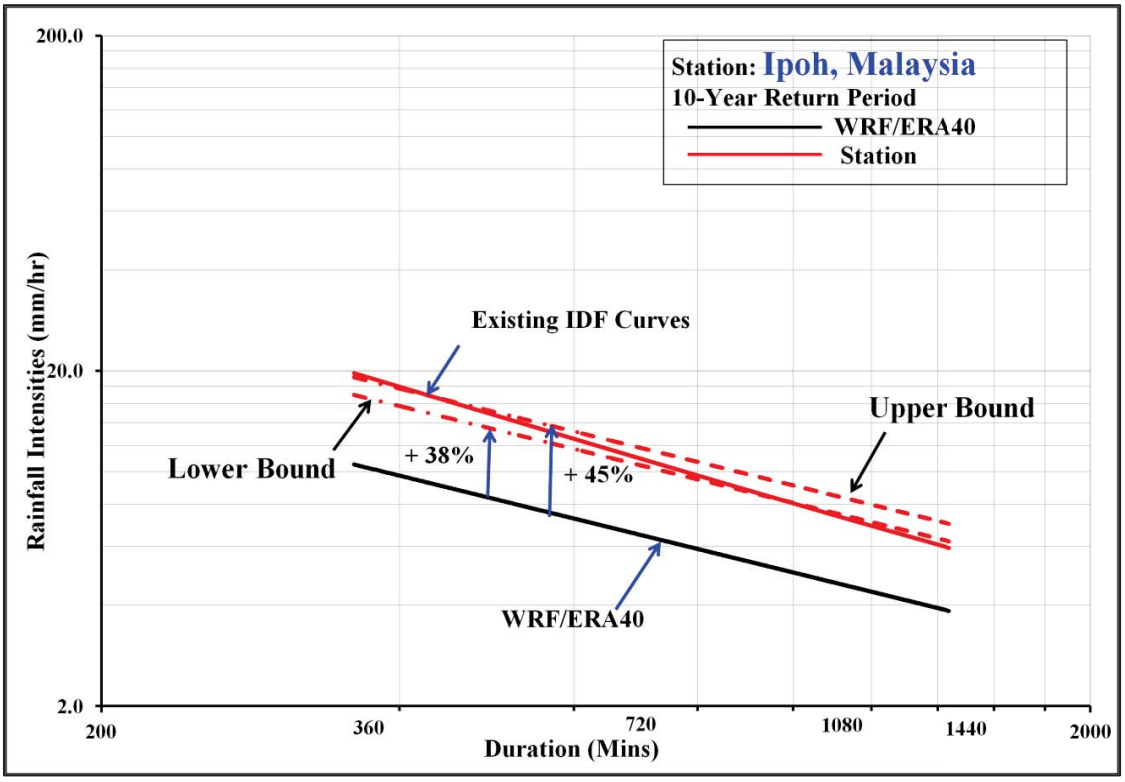

Figure B1-1b: WRF/ERA40 projected present day rainfall intensities anomalies from the existing IDF curve (10-year return period): Ipoh Meteorological Station

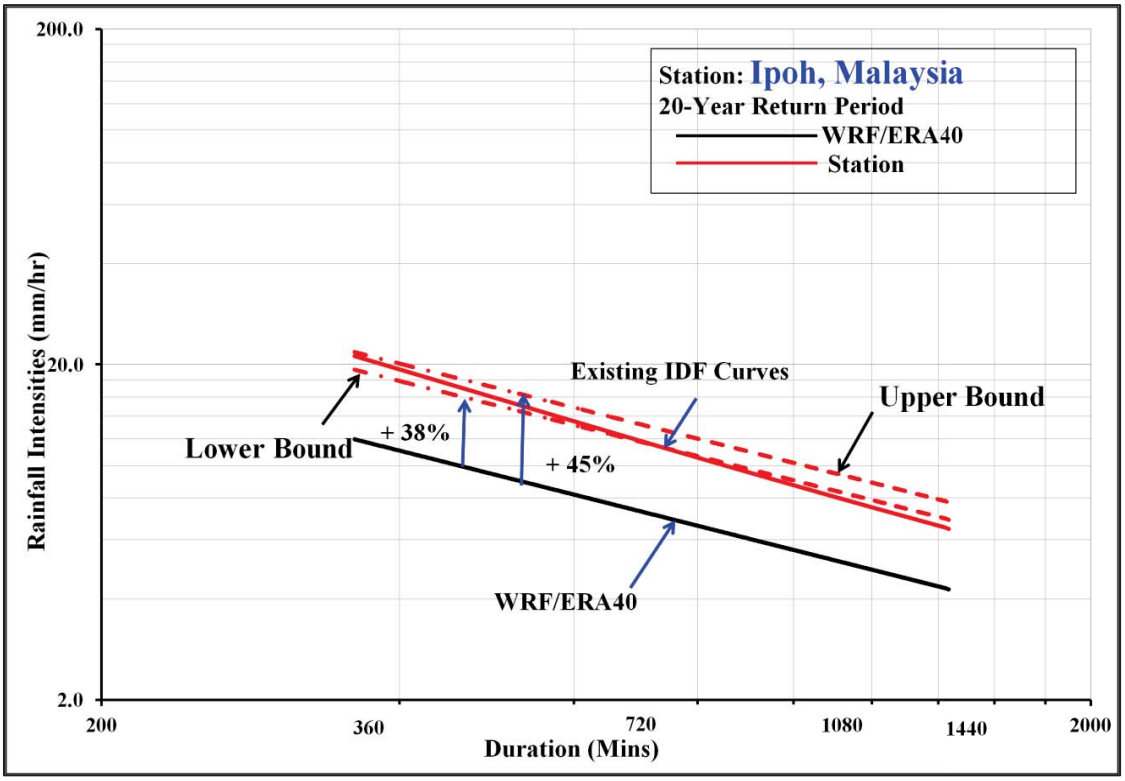

Figure B1-1c: WRF/ERA40 projected present day rainfall intensities anomalies from the existing IDF curve (20-year return period): Ipoh Meteorological Station

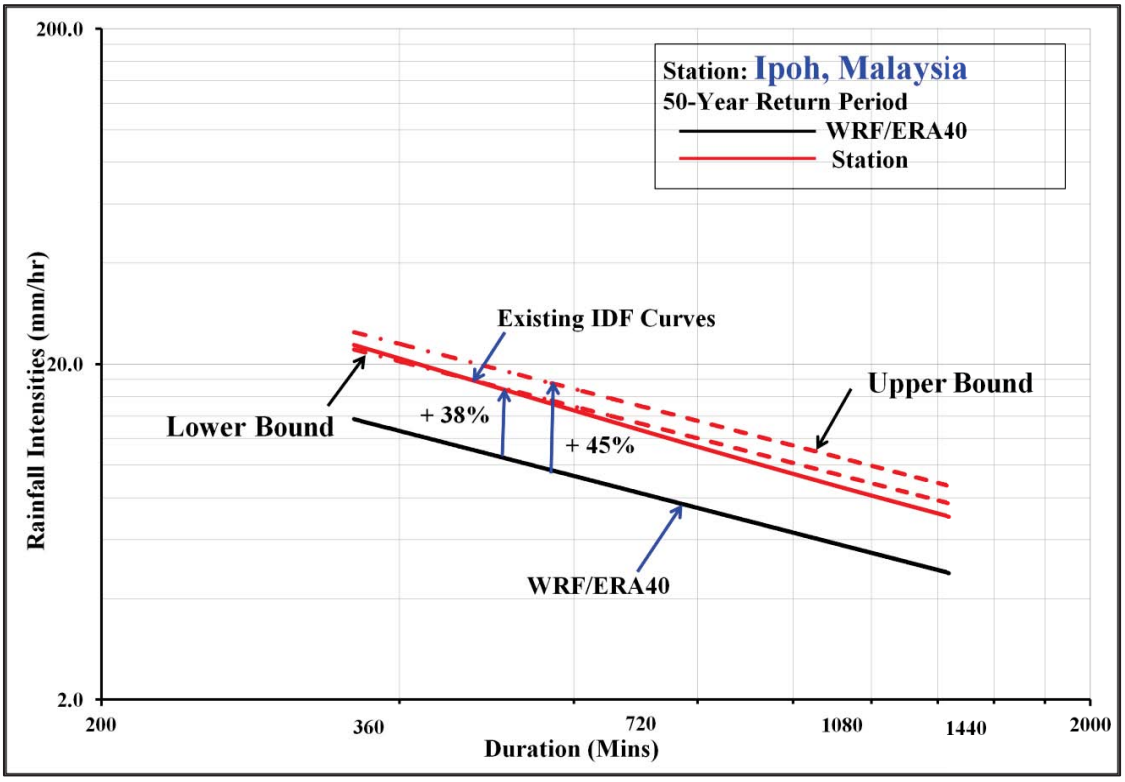

Figure B1-1d: WRF/ERA40 projected present day rainfall intensities anomalies from the existing IDF curve (50-year return period): Ipoh Meteorological Station

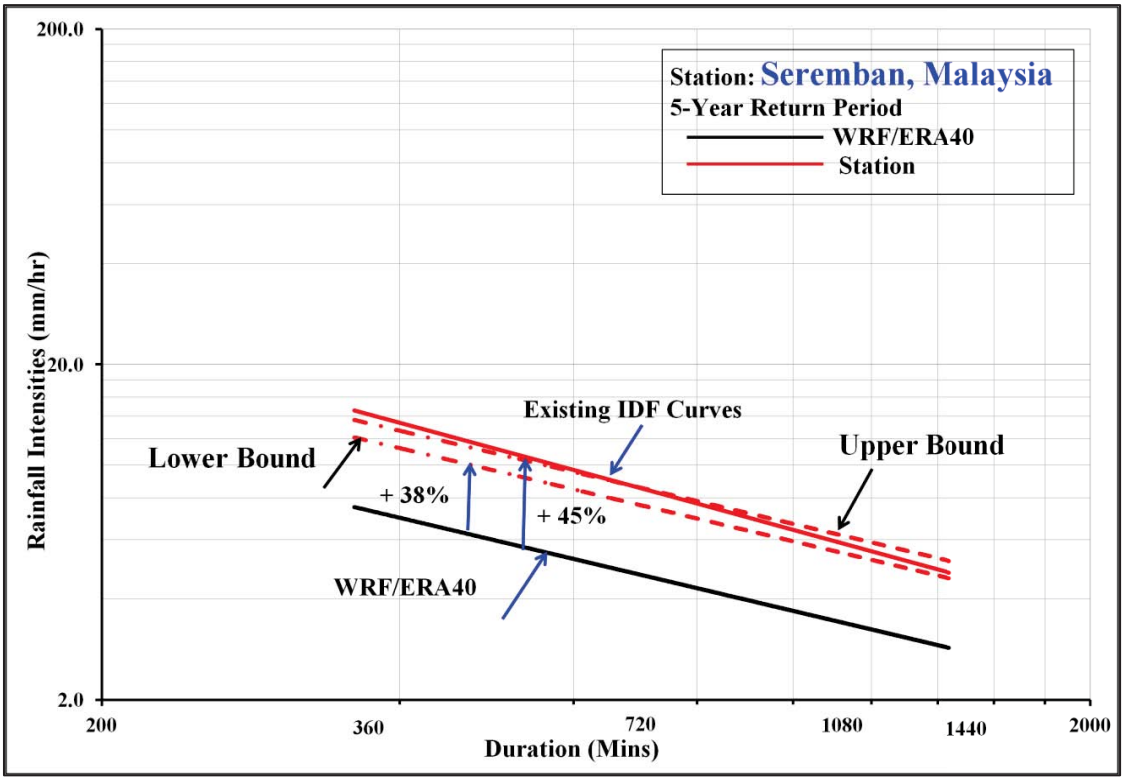

Figure B1-2a: WRF/ERA40 projected present day rainfall intensities anomalies from the existing IDF curve (5-year return period): Seremban Meteorological Station

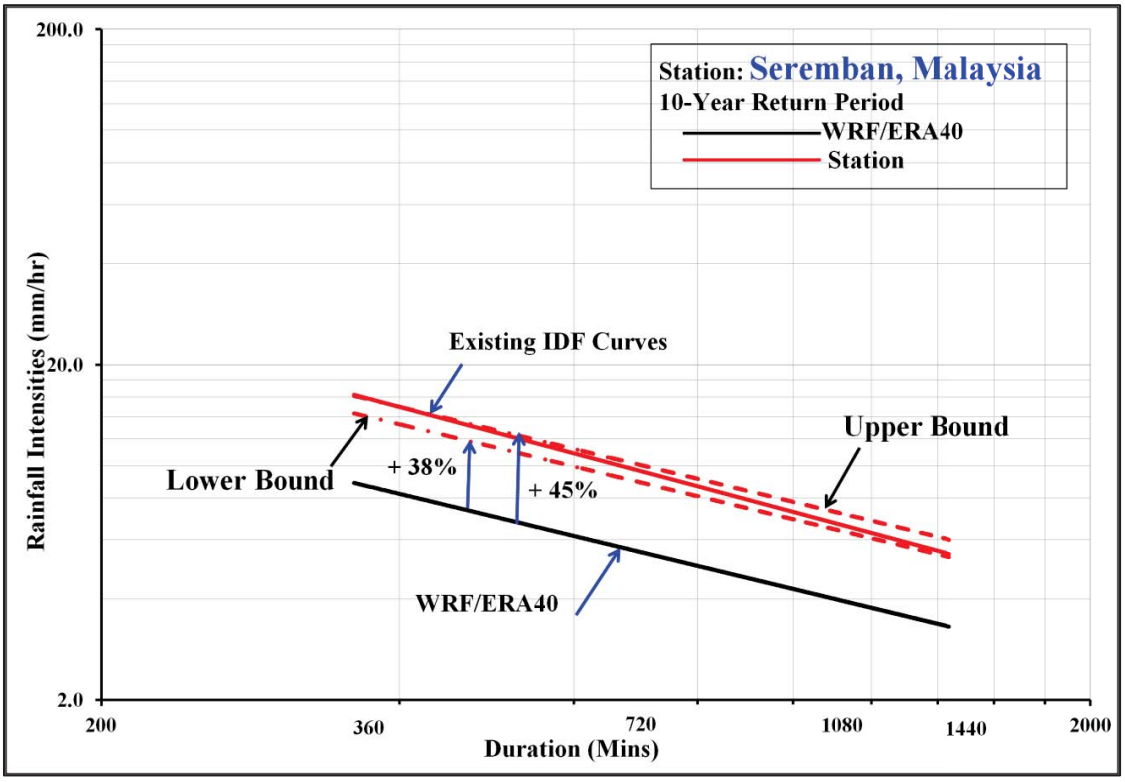

Figure B1-2b: WRF/ERA40 projected present day rainfall intensities anomalies from the existing IDF curve (10-year return period): Seremban Meteorological Station

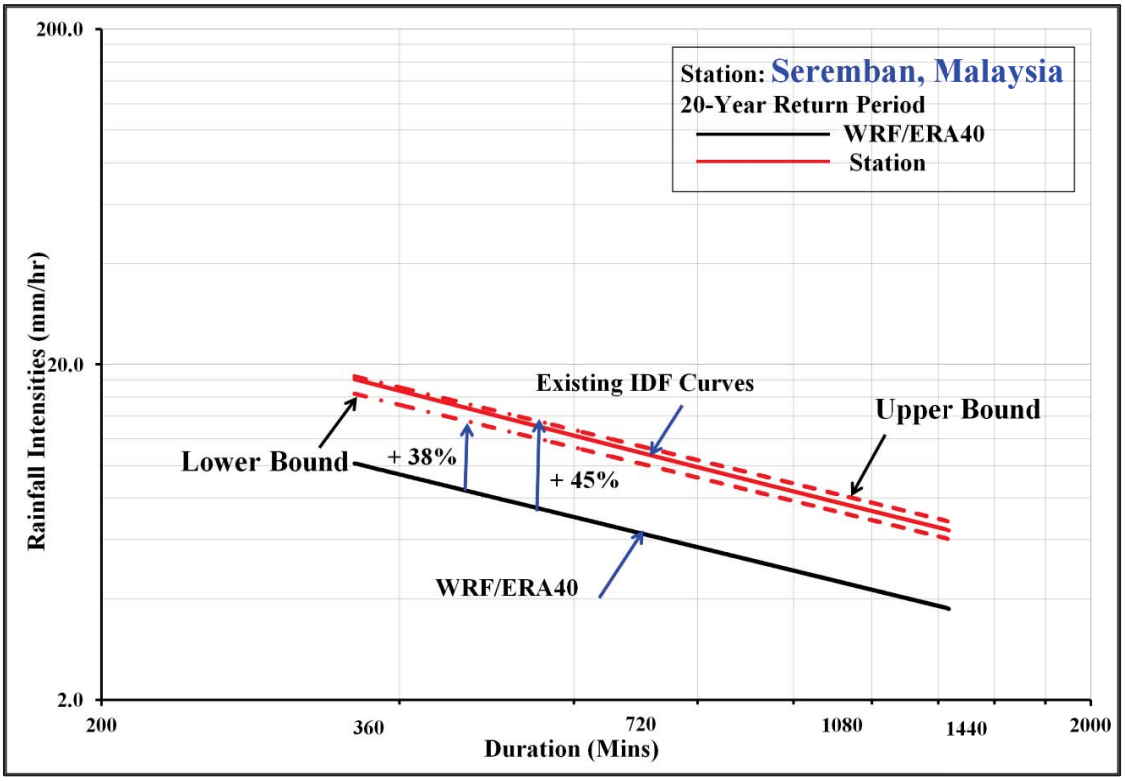

Figure B1-2c: WRF/ERA40 projected present day rainfall intensities anomalies from the existing IDF curve (20-year return period): Seremban Meteorological Station

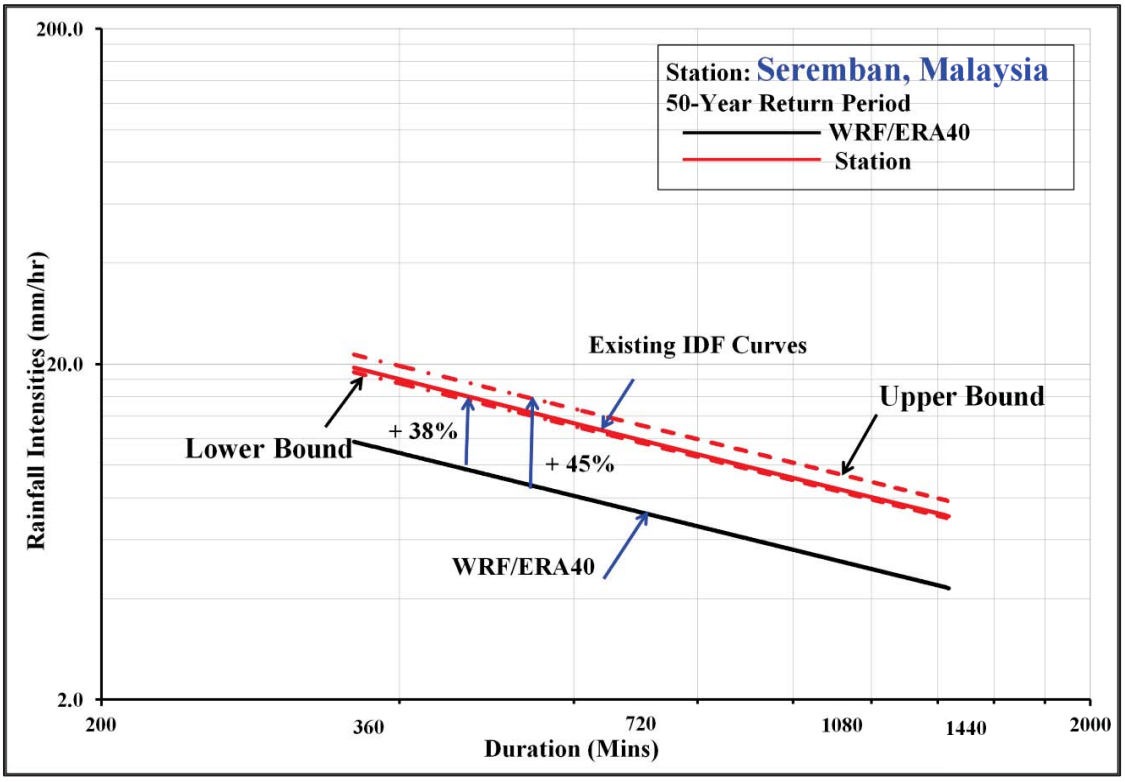

Figure B1-2d: WRF/ERA40 projected present day rainfall intensities anomalies from the existing IDF curve (50-year return period): Seremban Meteorological Station

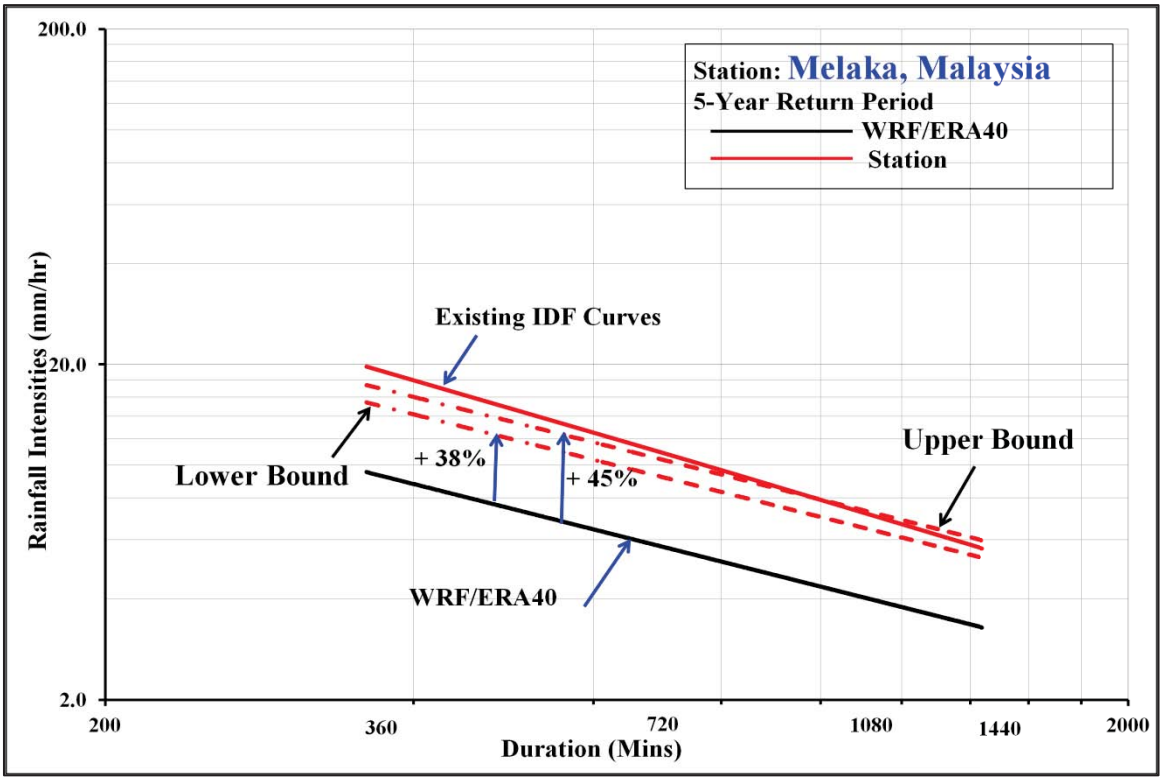

Figure B1-3a: WRF/ERA40 projected present day rainfall intensities anomalies from the existing IDF curve (5-year return period): Melaka Meteorological Station

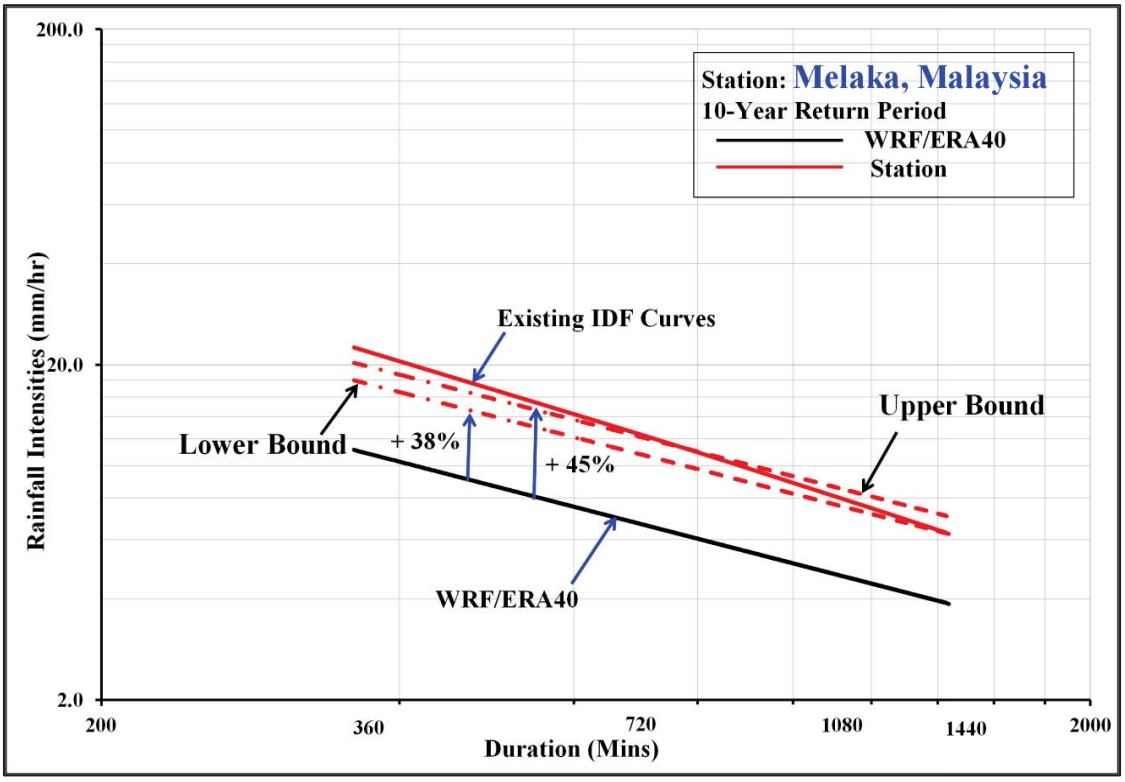

Figure B1-3b: WRF/ERA40 projected present day rainfall intensities anomalies from the existing IDF curve (10-year return period): Melaka Meteorological Station

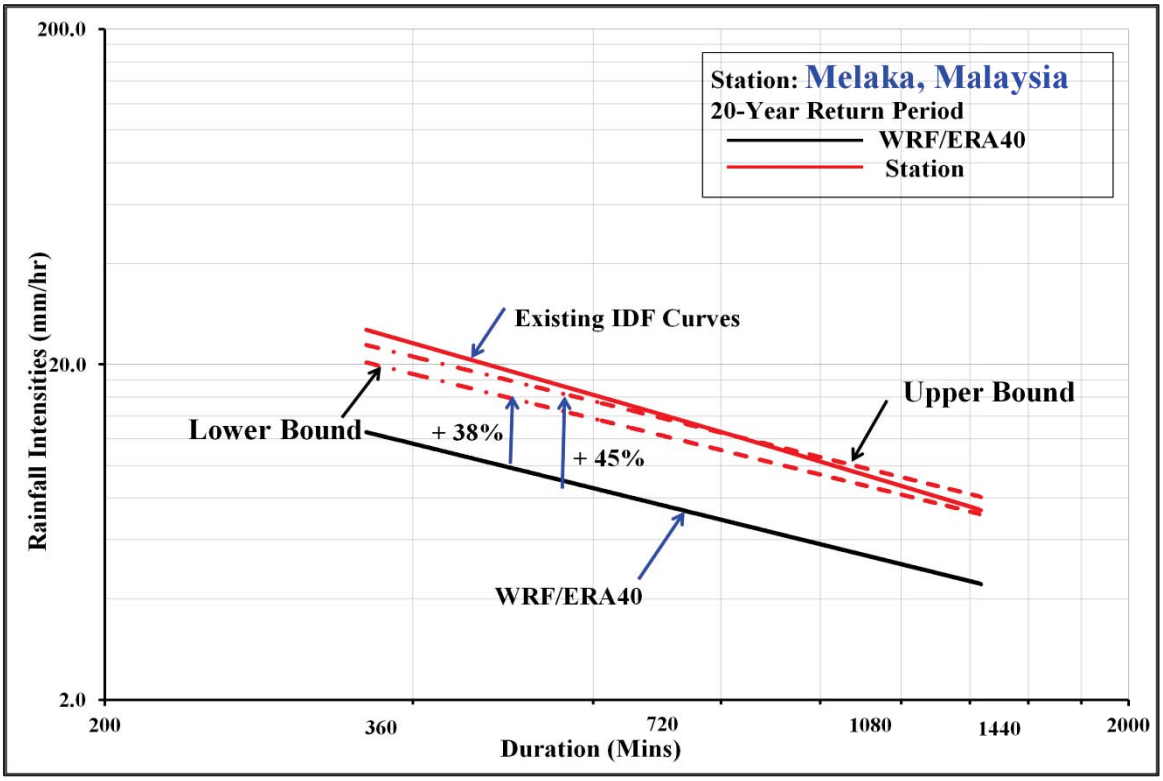

Figure B1-3c: WRF/ERA40 projected present day rainfall intensities anomalies from the existing IDF curve (20-year return period): Melaka Meteorological Station

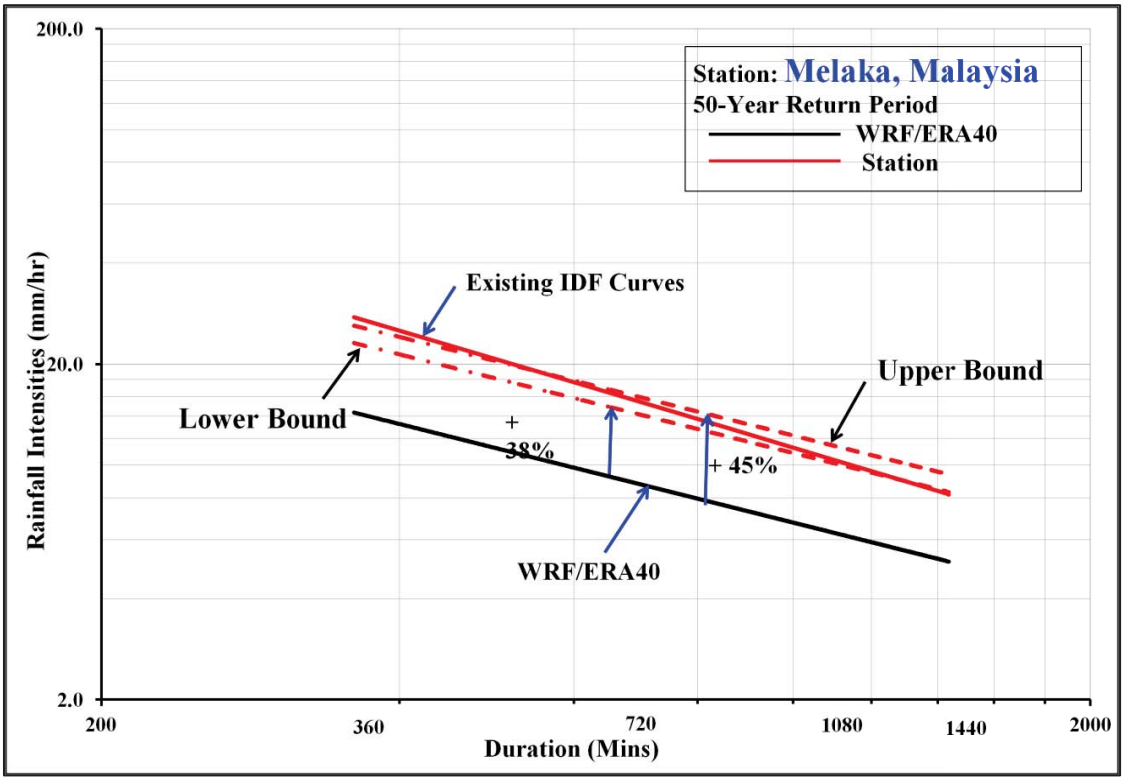

Figure B1-3d: WRF/ERA40 projected present day rainfall intensities anomalies from the existing IDF curve (50-year return period): Melaka Meteorological Station

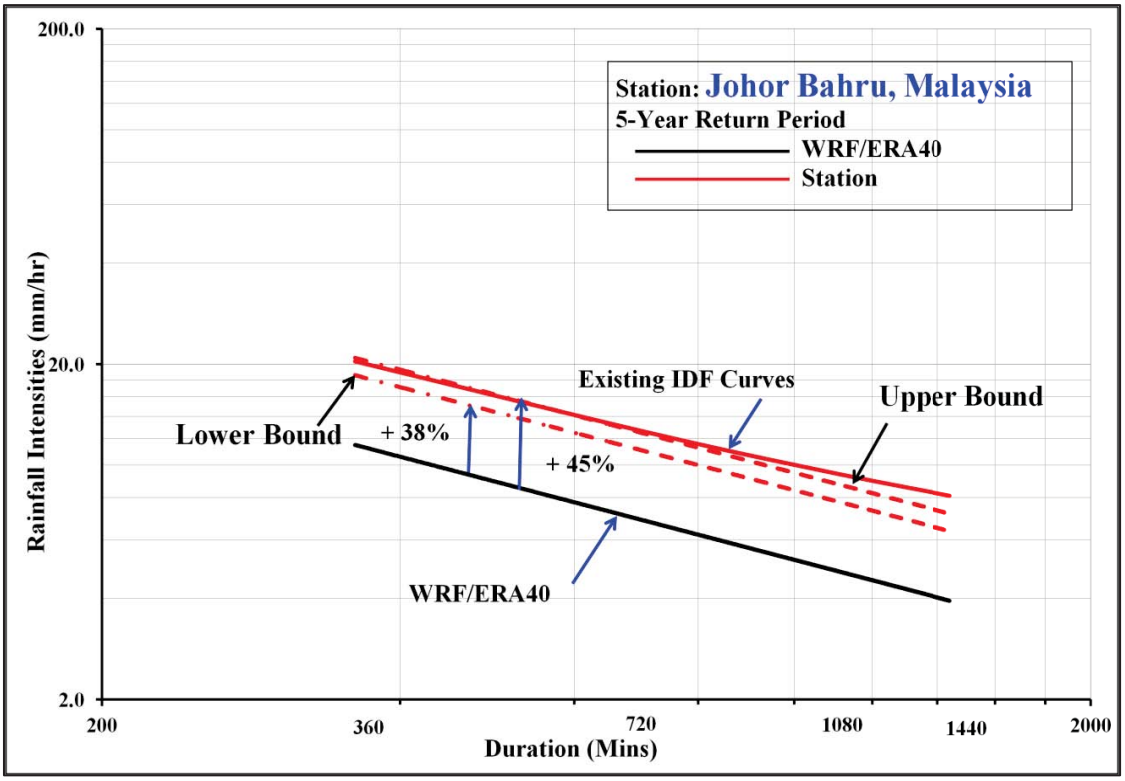

Figure B1-4a: WRF/ERA40 projected present day rainfall intensities anomalies from the existing IDF curve (5-year return period): Johor Bahru Meteorological Station

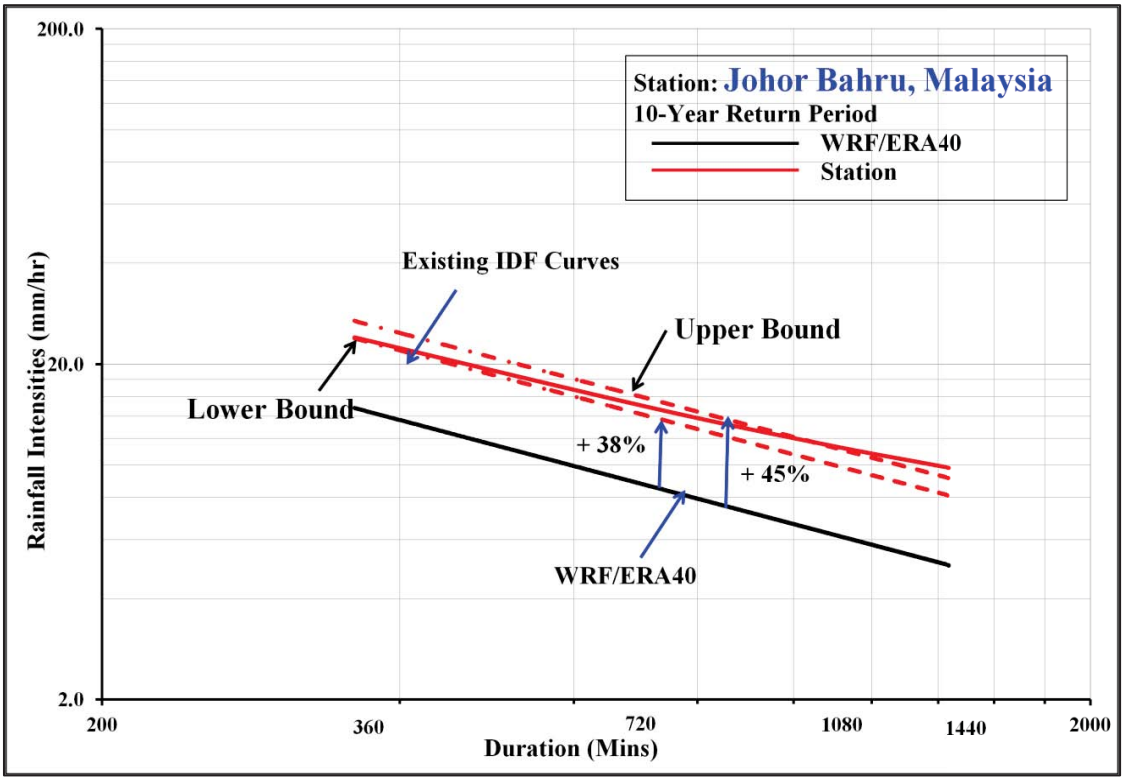

Figure B1-4b: WRF/ERA40 projected present day rainfall intensities anomalies from the existing IDF curve (10-year return period): Johor Bahru Meteorological Station

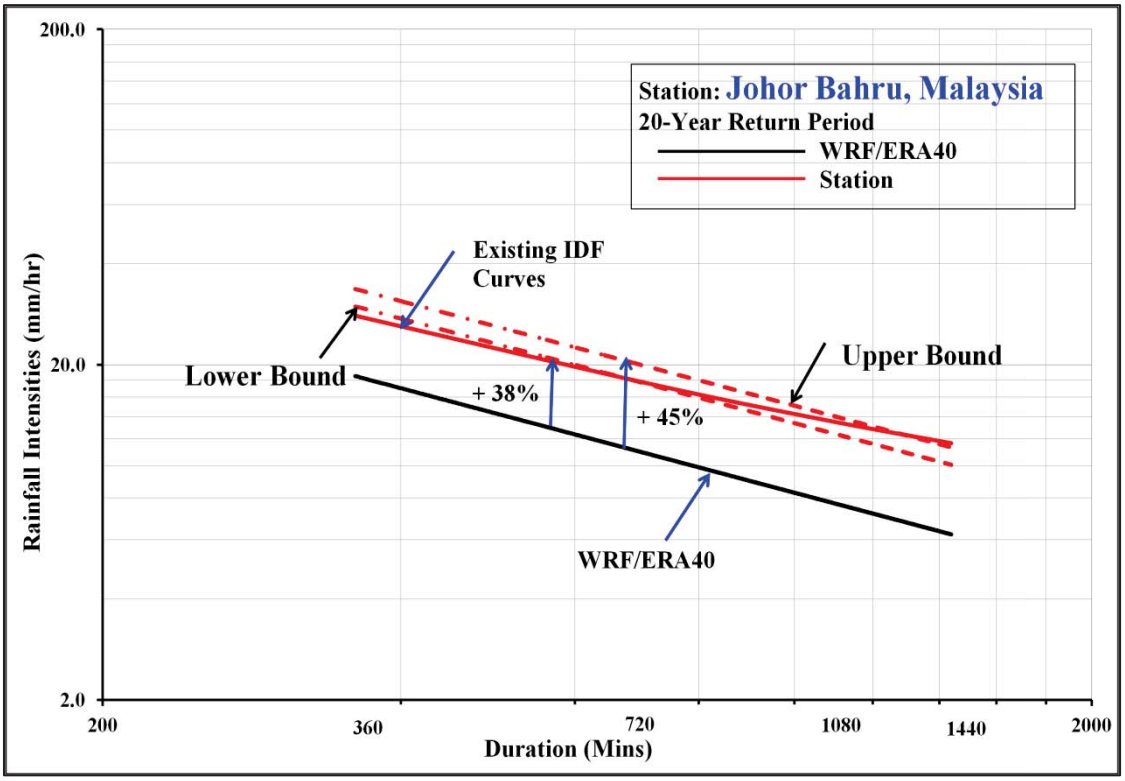

Figure B1-4c: WRF/ERA40 projected present day rainfall intensities anomalies from the existing IDF curve (20-year return period): Johor Bahru Meteorological Station

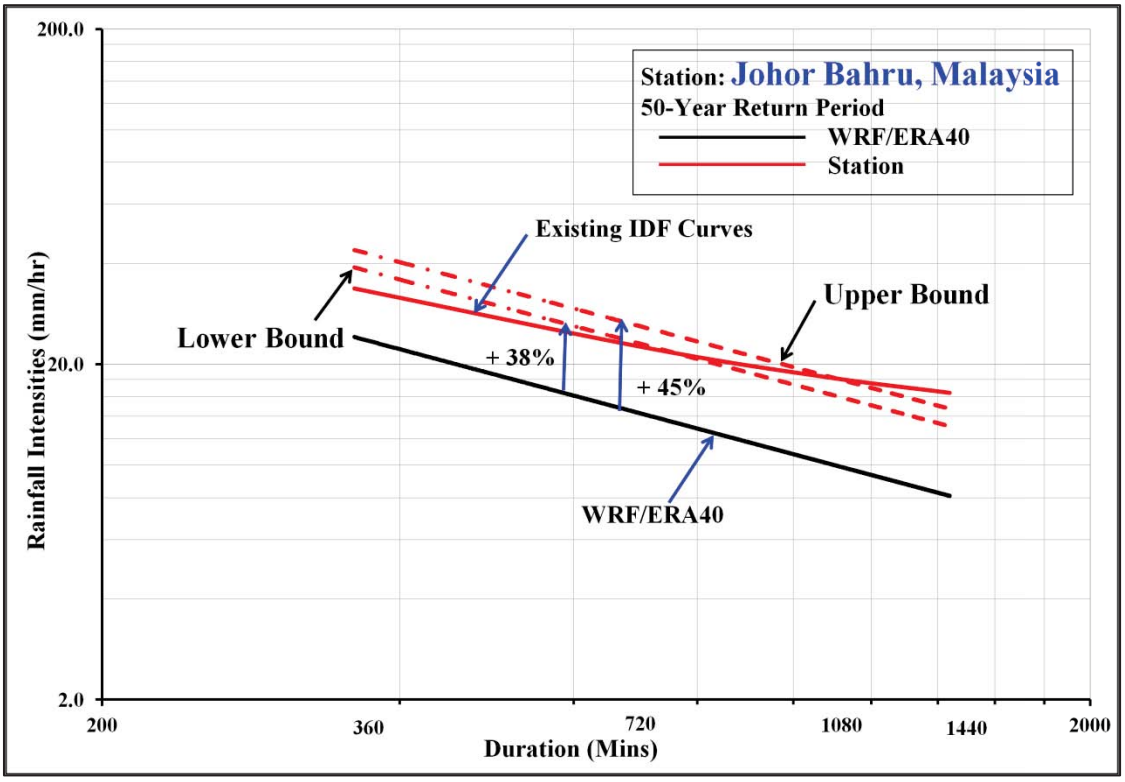

Figure B1-4d: WRF/ERA40 projected present day rainfall intensities anomalies from the existing IDF curve (50-year return period): Johor Bahru Meteorological Station

APPENDIX B2

Projected future climate IDF curves for Darmaga Station

Return Period	**:**	**5, 10, 25 and 50-year**
Period	**:**	**2011-2040, 2041-2070 and 2071-2100**
GCM/Scenario	**:**	**WRF/ECHAM A2, WRF/CCSM A2, WRF/CCSM A1FI and WRF/CCSM A1B**

Station	**:**	**Darmaga Station**
Period	**:**	**2011-2040**
GCM/Scenario	**:**	**WRF/ECHAM A2**

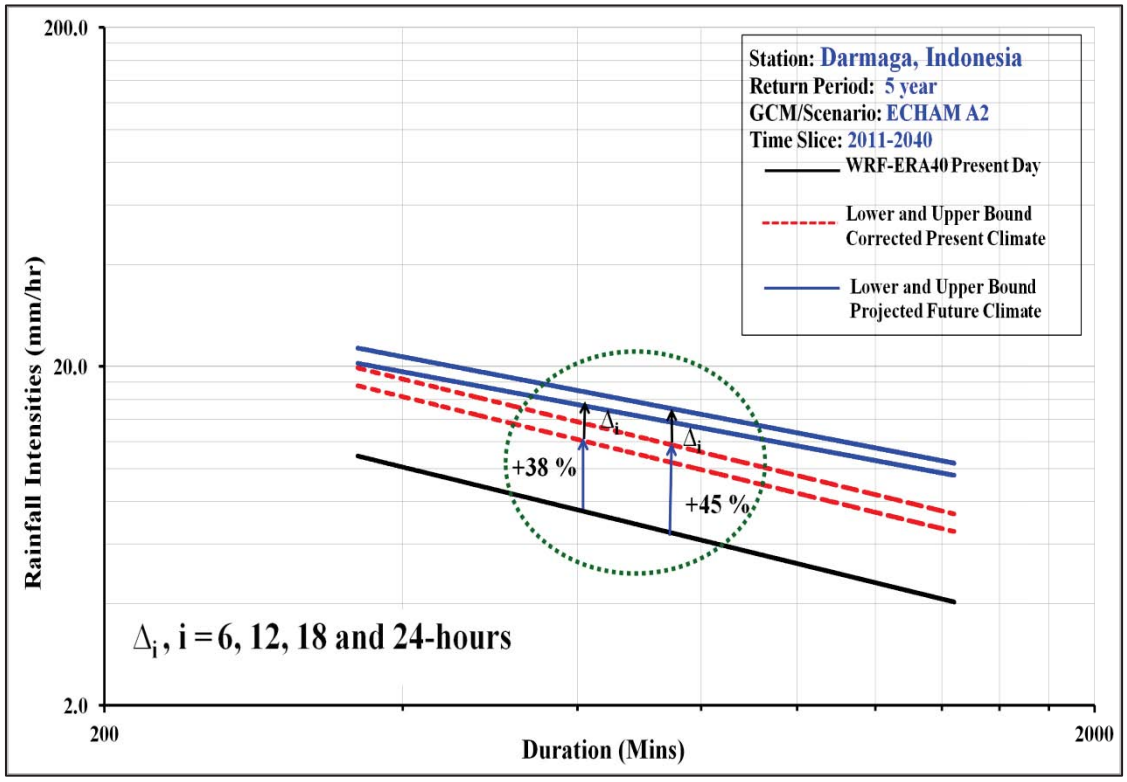

Figure B2-1a: Projected future climate IDF curves (5-year return period, 2011-2040, WRF/ECHAM A2): Darmaga Station

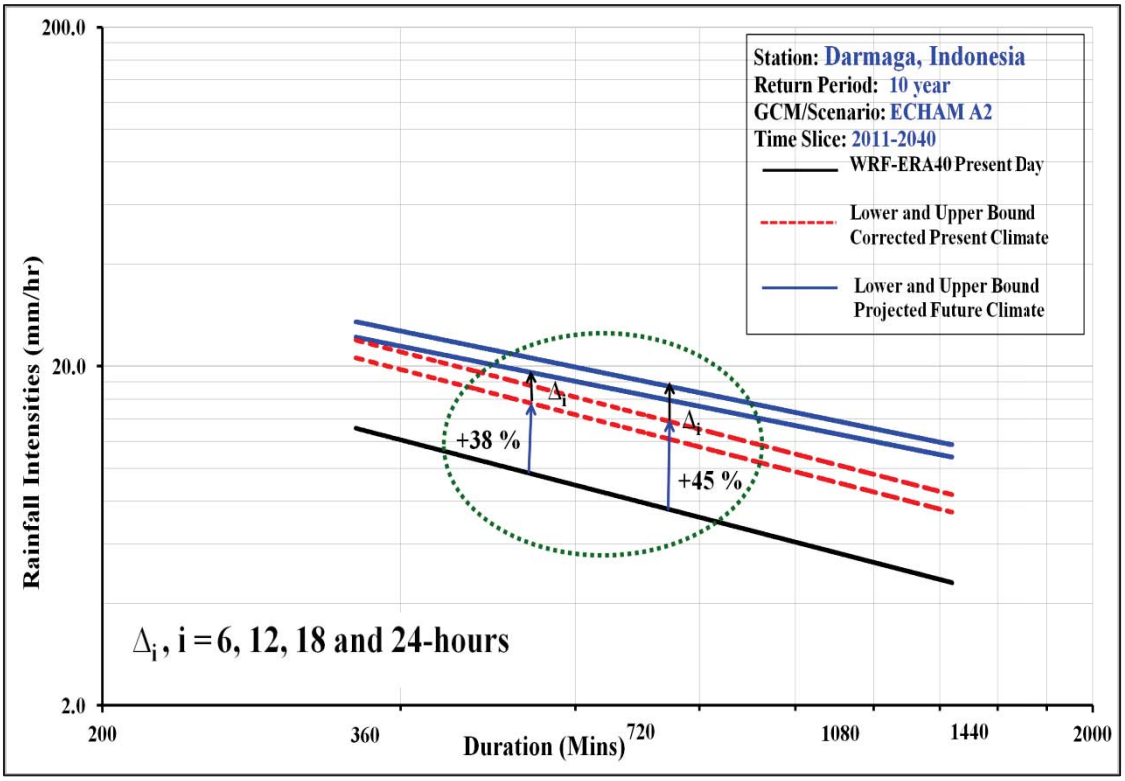

Figure B2-1b: Projected future climate IDF curves (10-year return period, 2011-2040, WRF/ECHAM A2): Darmaga Station

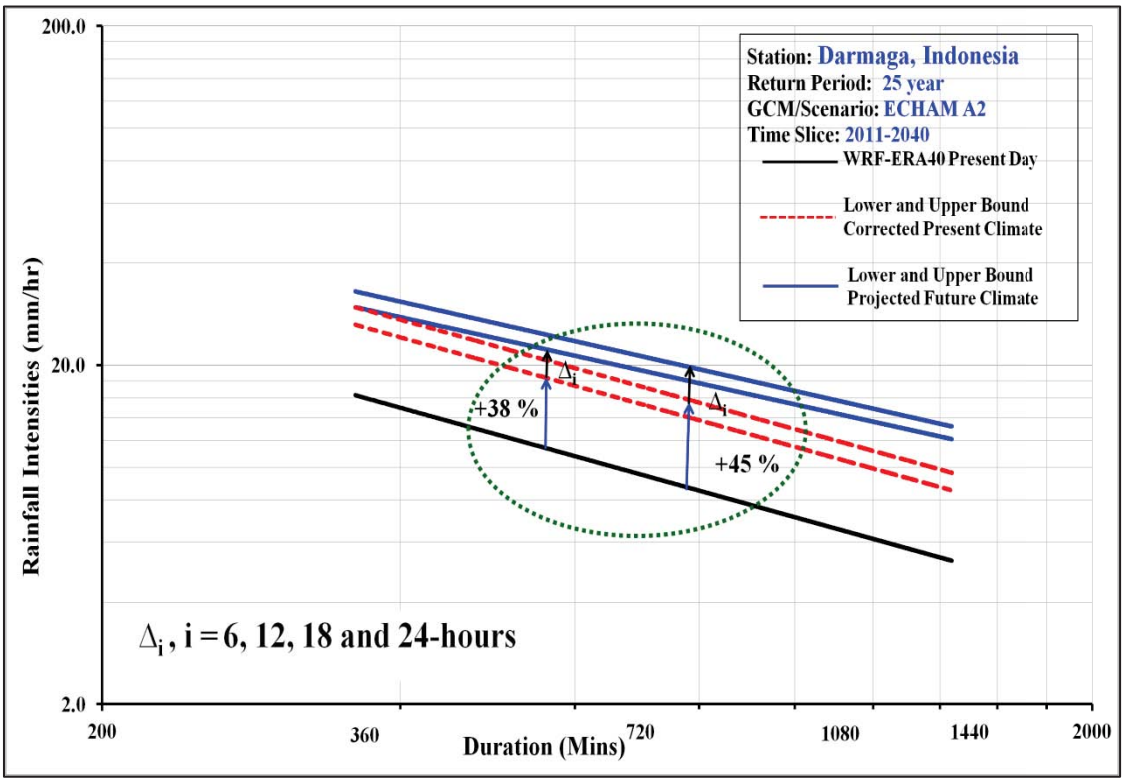

Figure B2-1c: Projected future climate IDF curves (25-year return period, 2011-2040, WRF/ECHAM A2): Darmaga Station

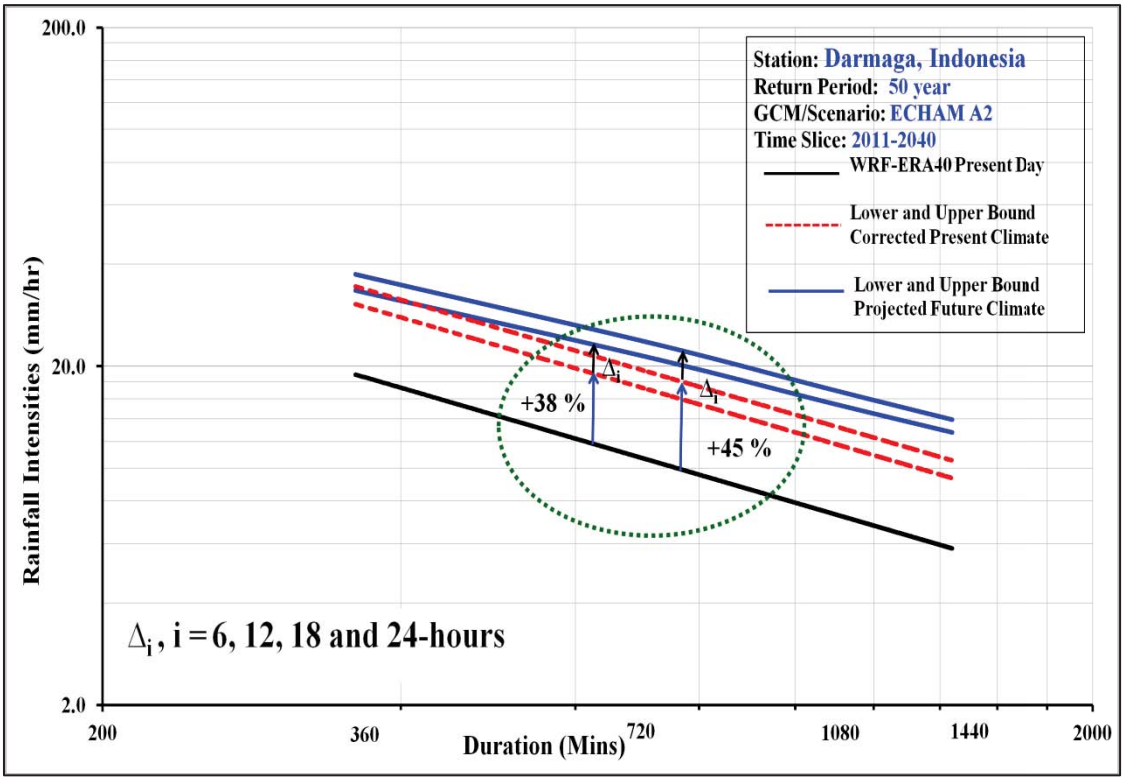

Figure B2-1d: Projected future climate IDF curves (50-year return period, 2011-2040, WRF/ECHAM A2): Darmaga Station

Station : Darmaga Station
Period : 2041-2070
GCM/Scenario : WRF/ECHAM A2

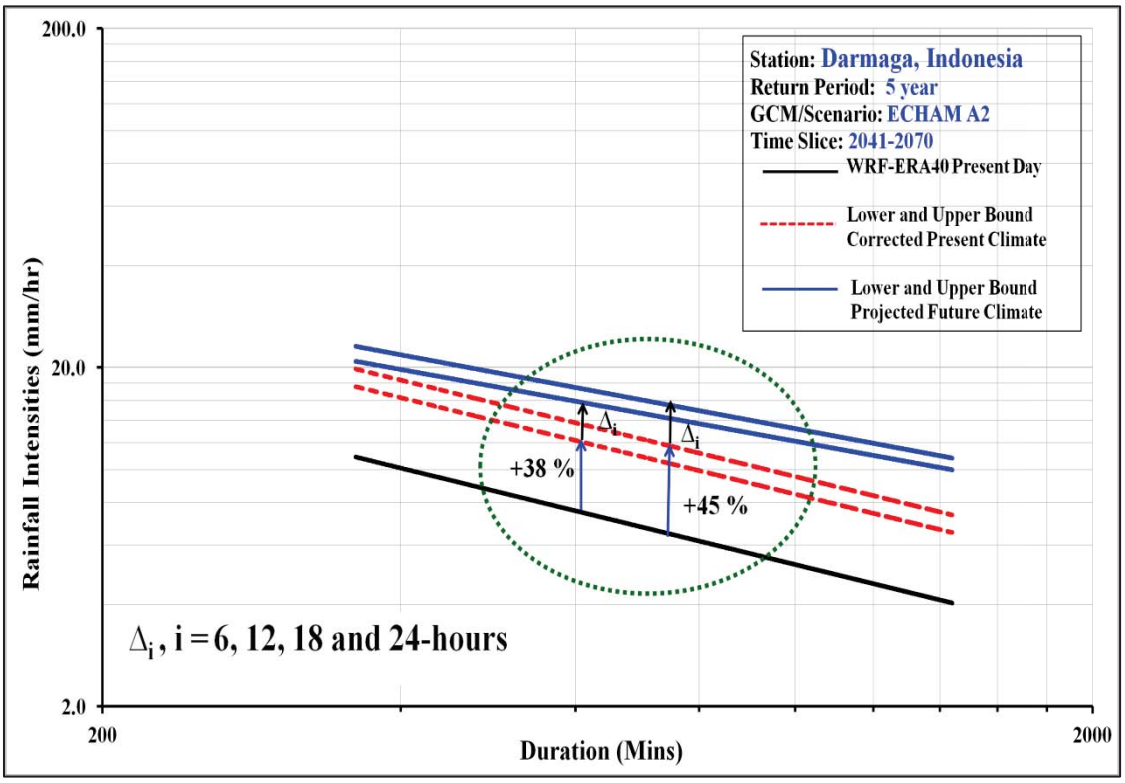

Figure B2-2a: Projected future climate IDF curves (5-year return period, 2041-2070, WRF/ECHAM A2): Darmaga Station

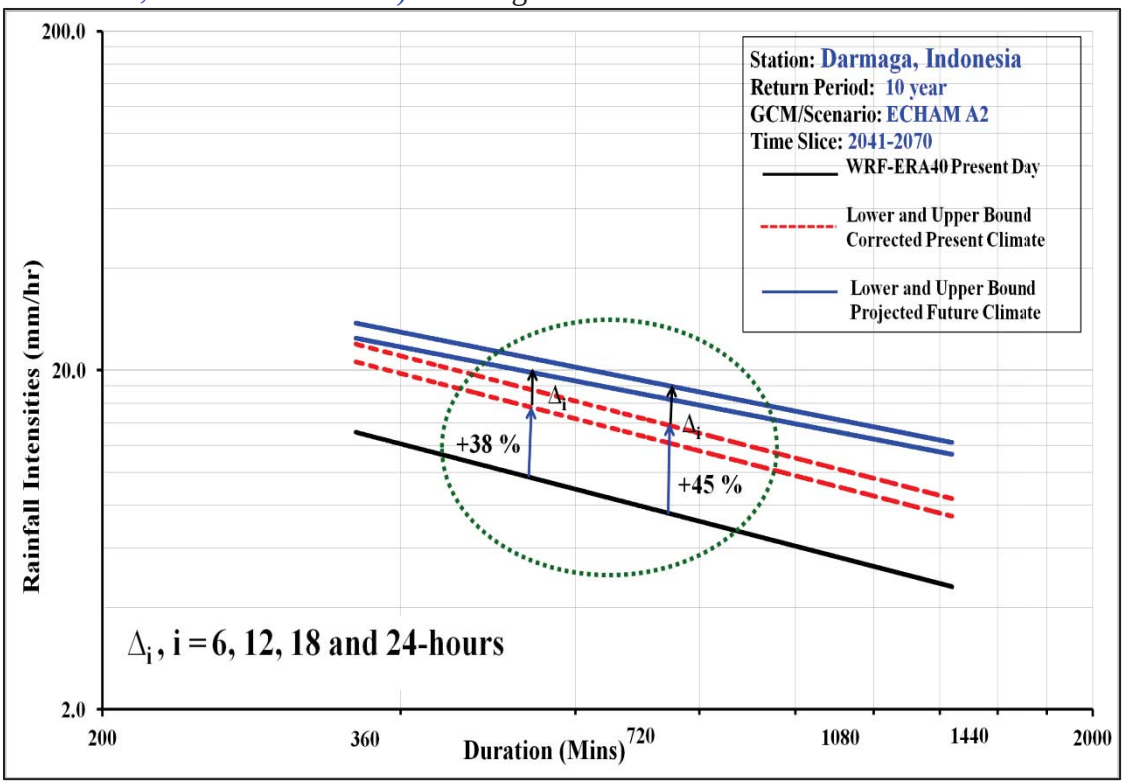

Figure B2-2b: Projected future climate IDF curves (10-year return period, 2041-2070, WRF/ECHAM A2): Darmaga Station

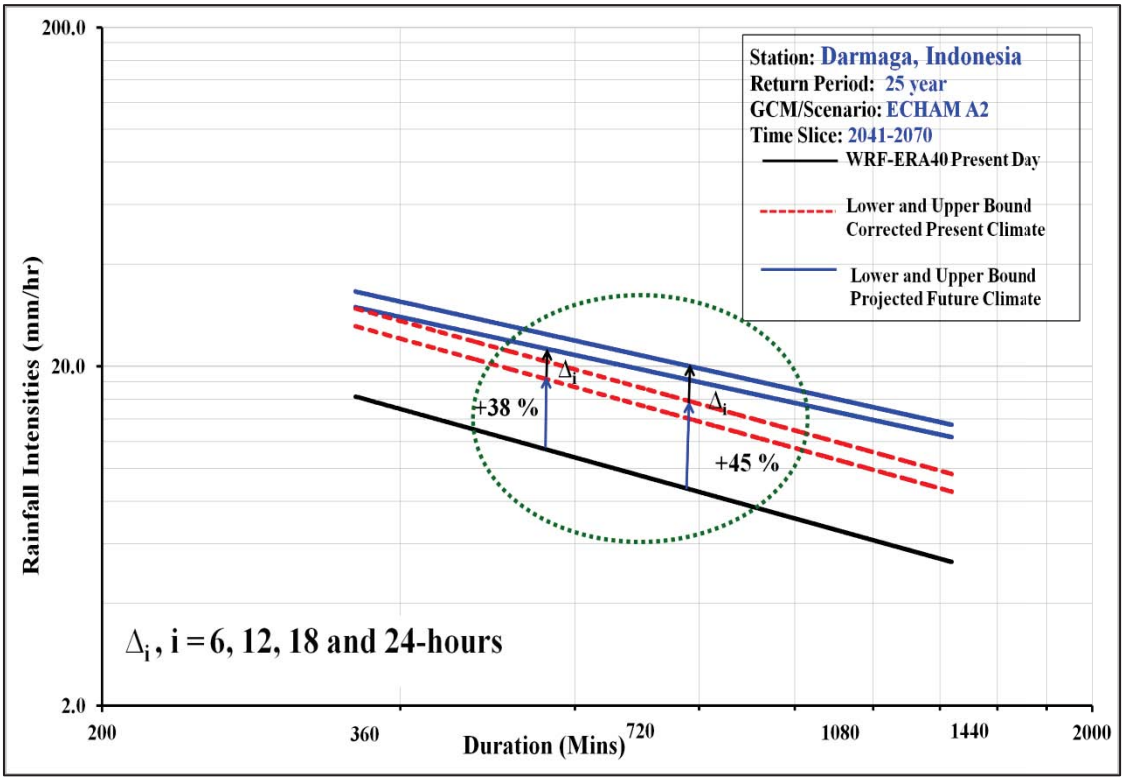

Figure B2-2c: Projected future climate IDF curves (25-year return period, 2041-2070, WRF/ECHAM A2): Darmaga Station

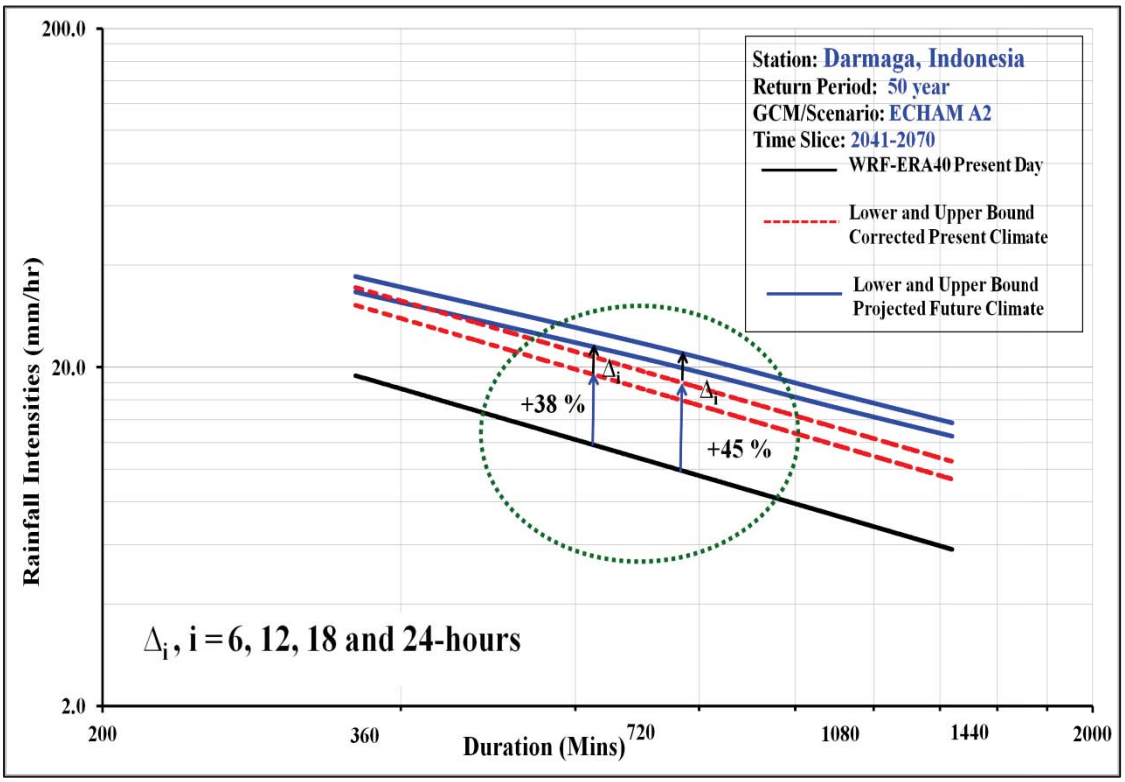

Figure B2-2d: Projected future climate IDF curves (50-year return period, 2041-2070, WRF/ECHAM A2): Darmaga Station

Station : Darmaga Station
Period : 2011-2040
GCM/Scenario : WRF/CCSM A2

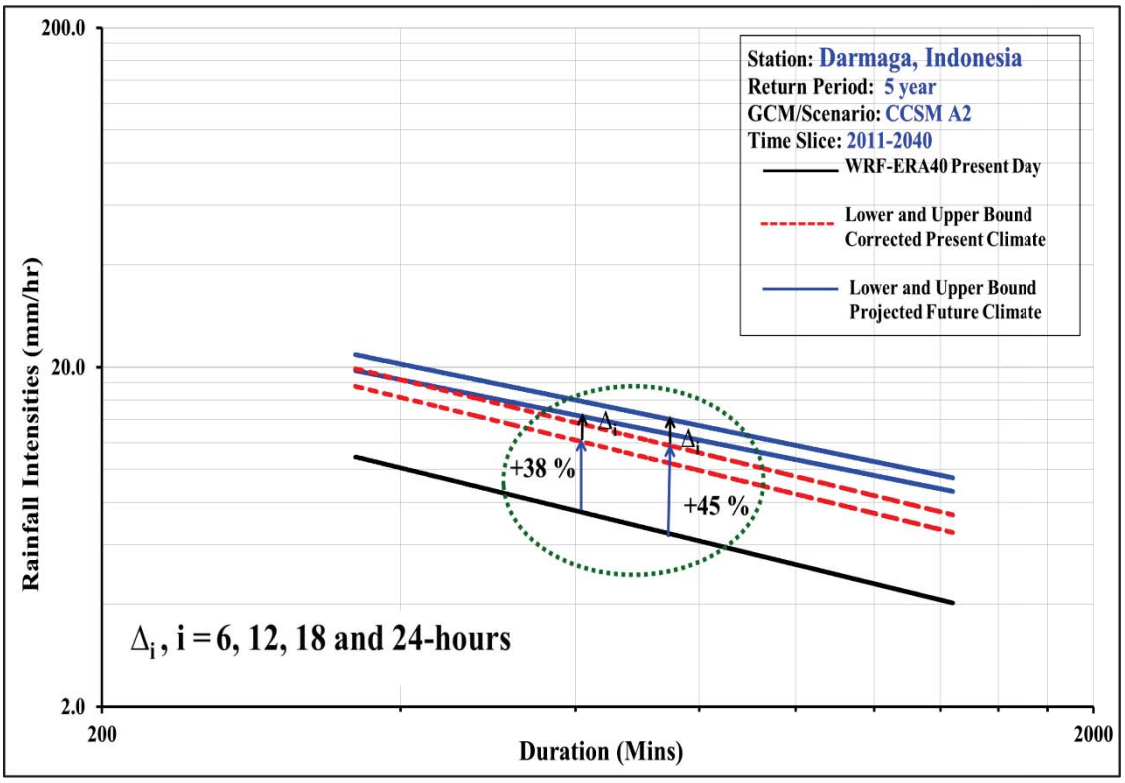

Figure B2-3a: Projected future climate IDF curves (5-year return period, 2011-2040, WRF/CCSM A2): Darmaga Station

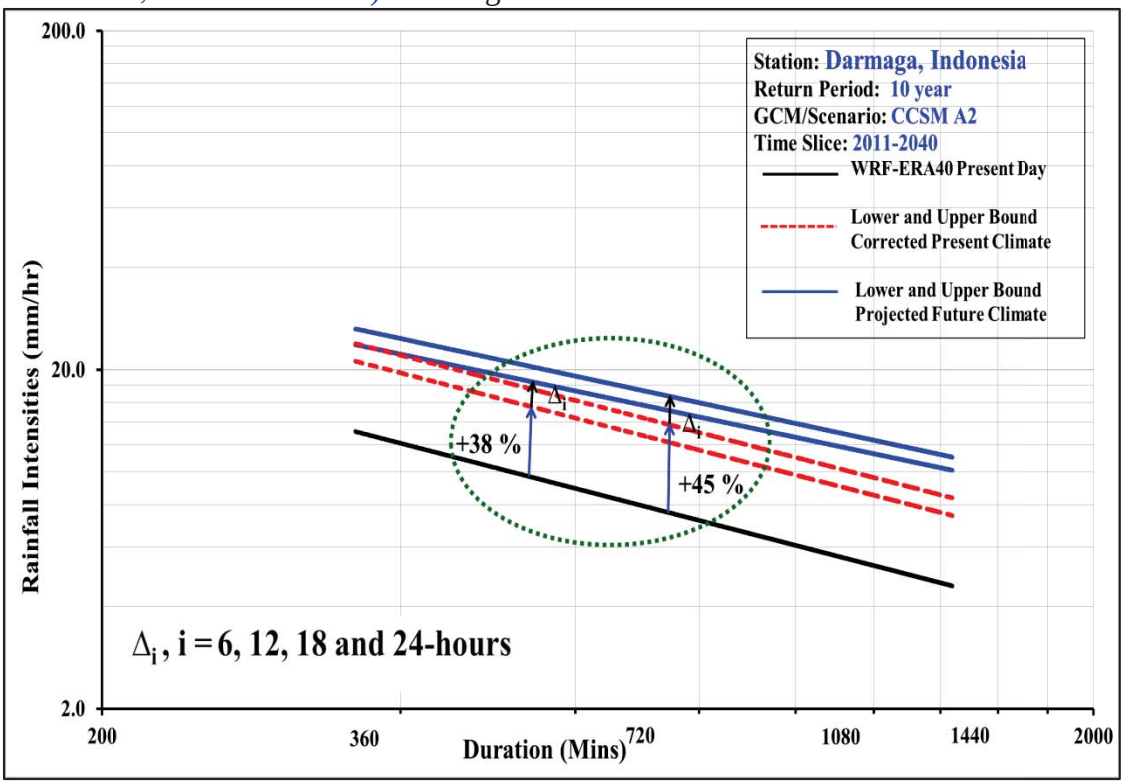

Figure B2-3b: Projected future climate IDF curves (10-year return period, 2011-2040, WRF/CCSM A2): Darmaga Station

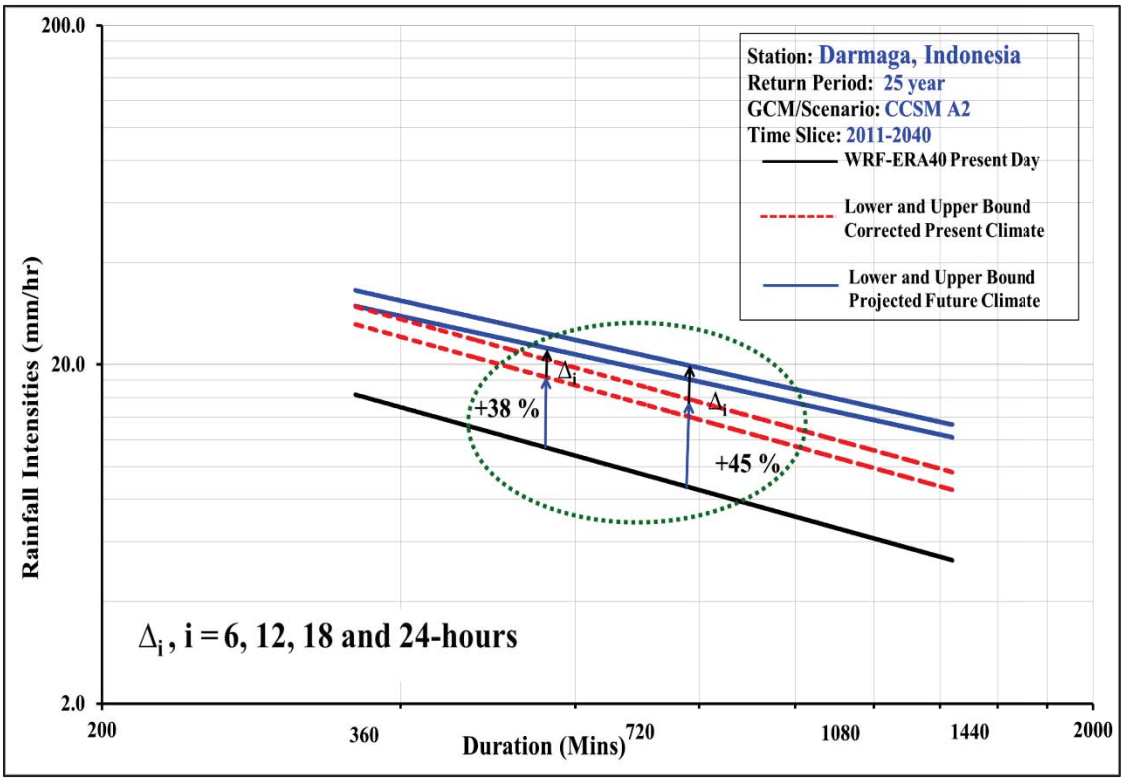

Figure B2-3c: Projected future climate IDF curves (25-year return period, 2011-2040, WRF/CCSM A2): Darmaga Station

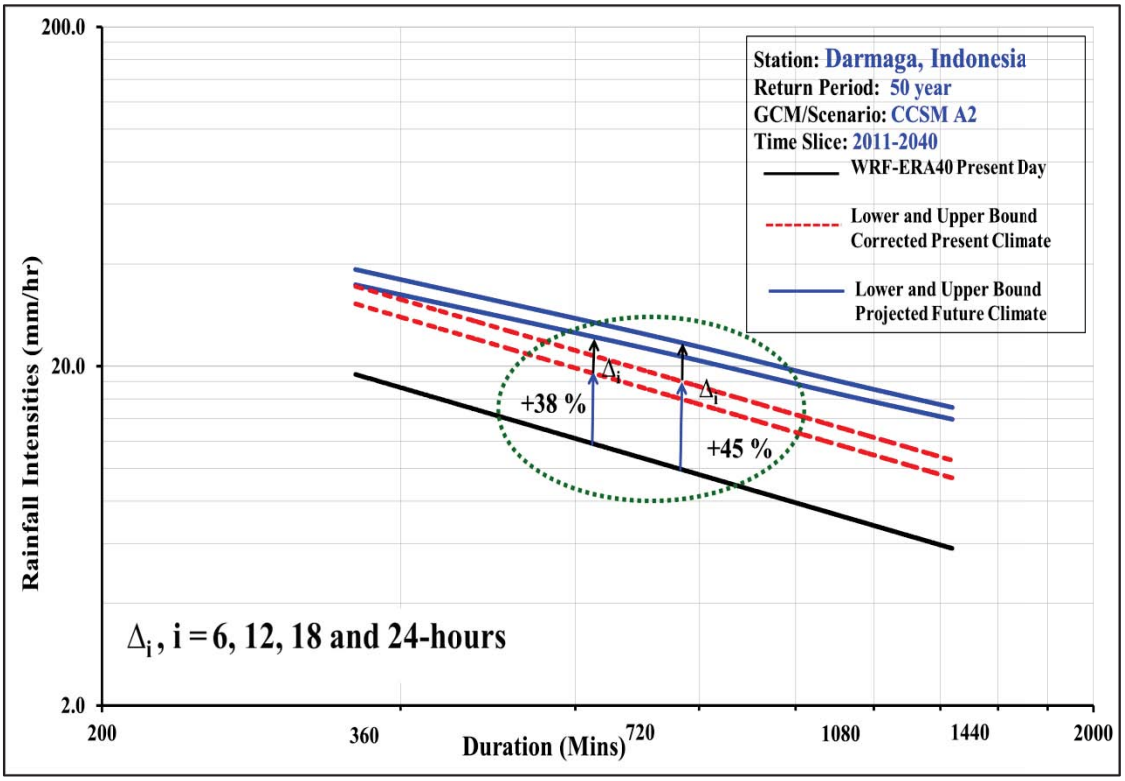

Figure B2-3d: Projected future climate IDF curves (50-year return period, 2011-2040, WRF/CCSM A2): Darmaga Station

Station : Darmaga Station
Period : 2041-2070
GCM/Scenario : WRF/CCSM A2

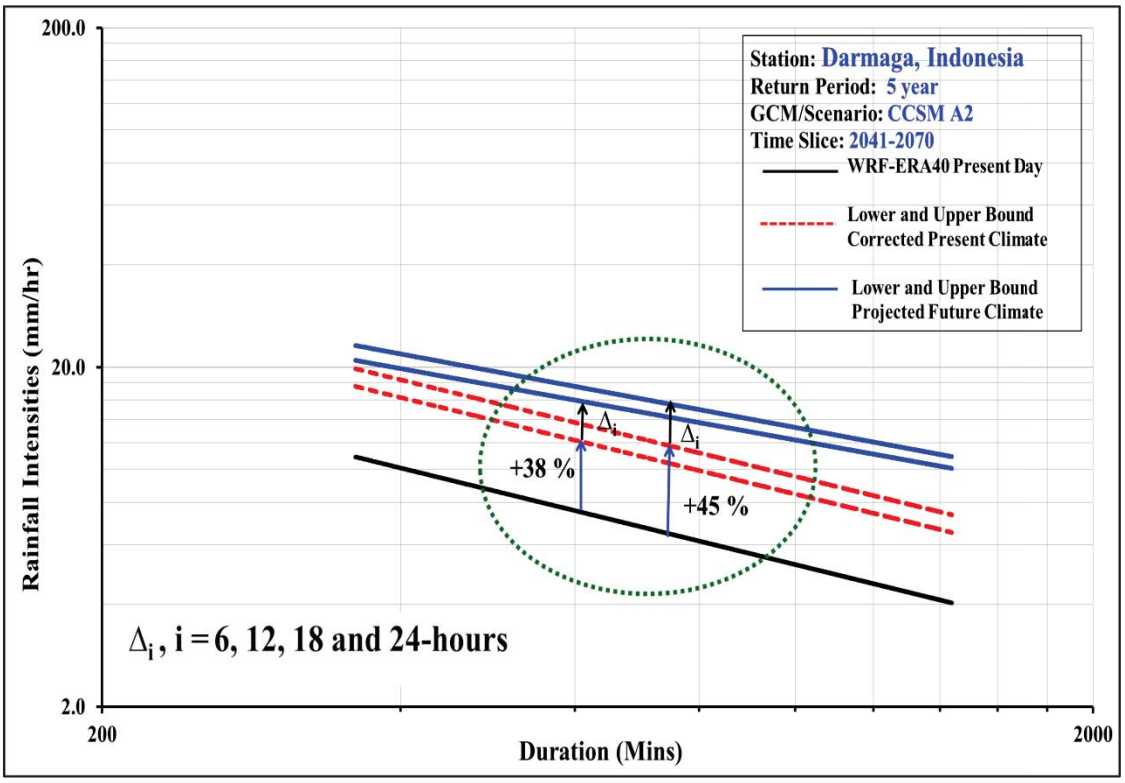

Figure B2-4a: Projected future climate IDF curves (5-year return period, 2041-2070, WRF/CCSM A2): Darmaga Station

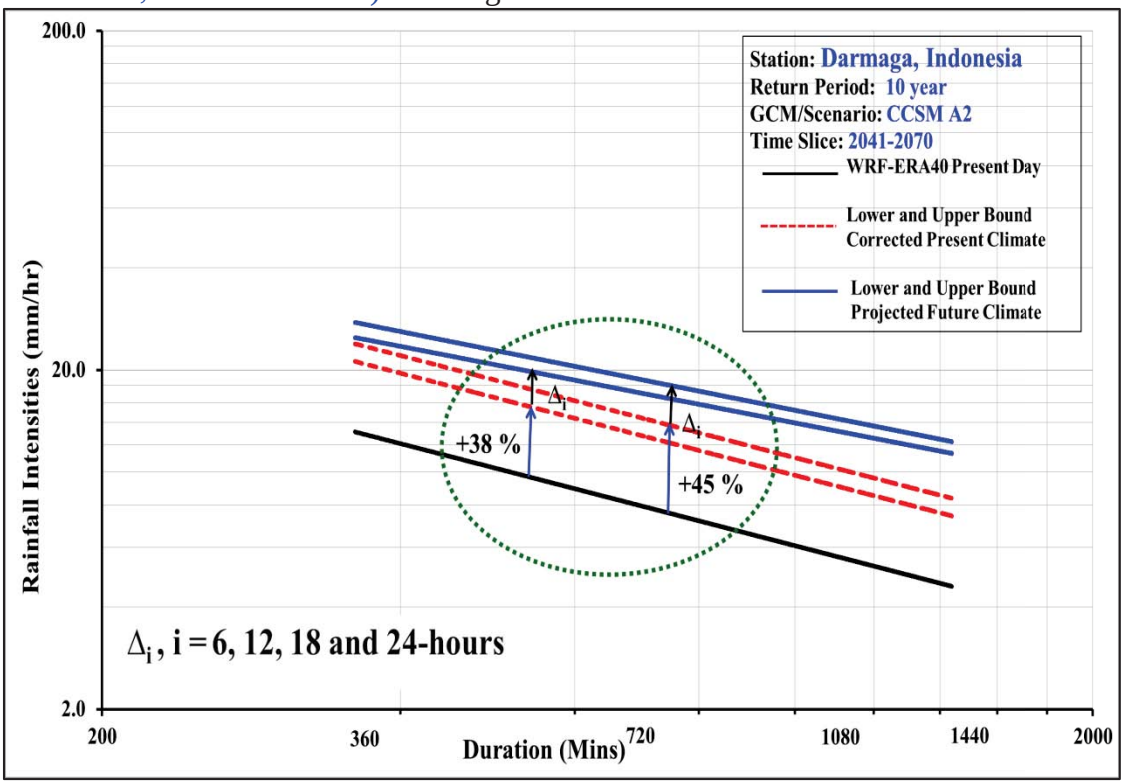

Figure B2-4b: Projected future climate IDF curves (10-year return period, 2041-2070, WRF/CCSM A2): Darmaga Station

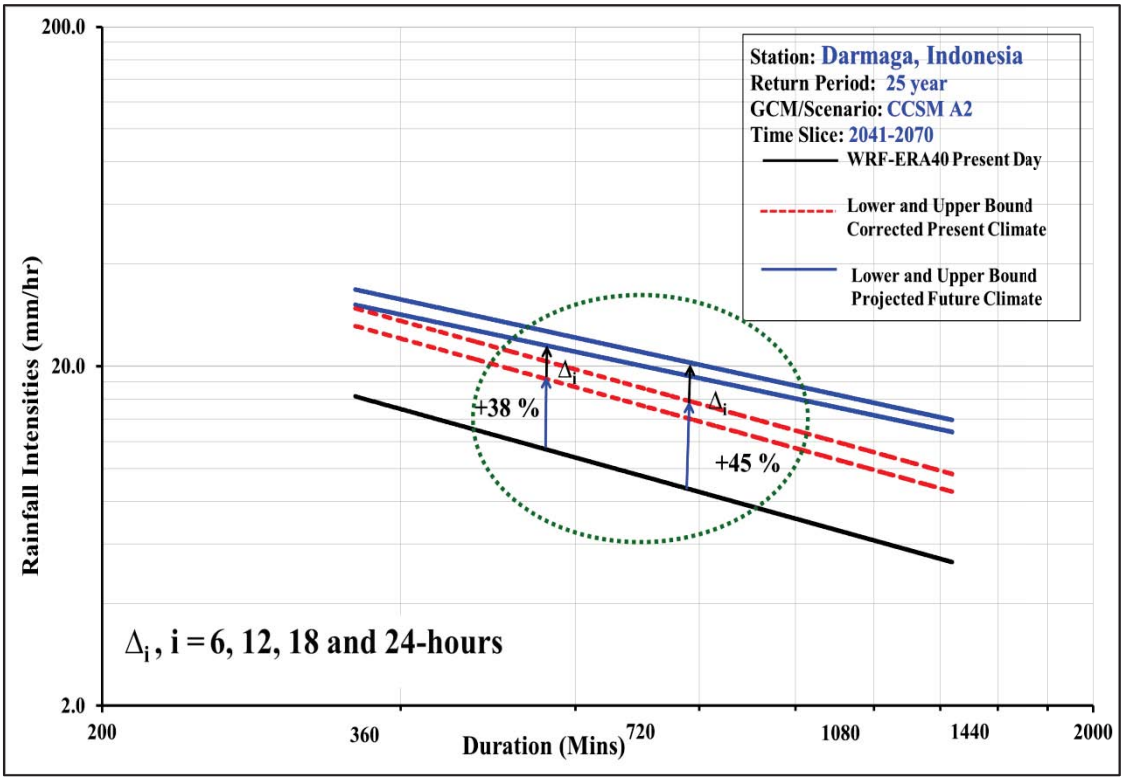

Figure B2-4c: Projected future climate IDF curves (25-year return period, 2041-2070, WRF/CCSM A2): Darmaga Station

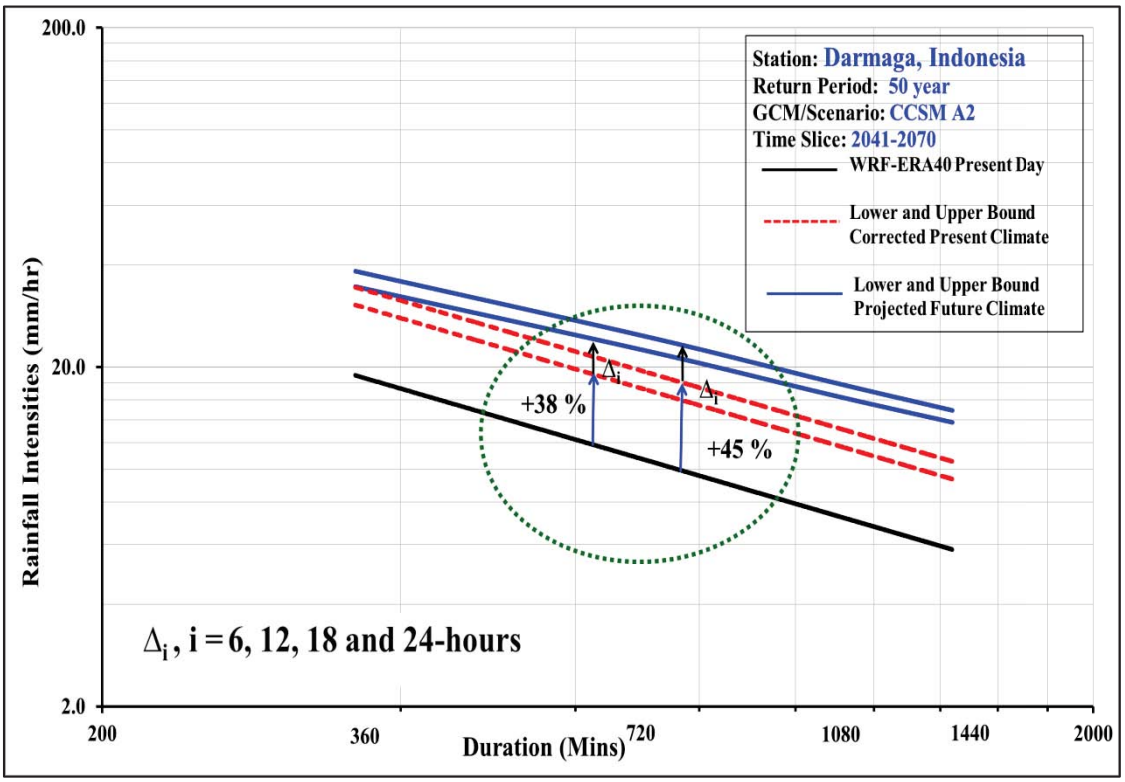

Figure B2-4d: Projected future climate IDF curves (50-year return period, 2041-2070, WRF/CCSM A2): Darmaga Station

Station : Darmaga Station
Period : 2071-2100
GCM/Scenario : WRF/CCSM A2

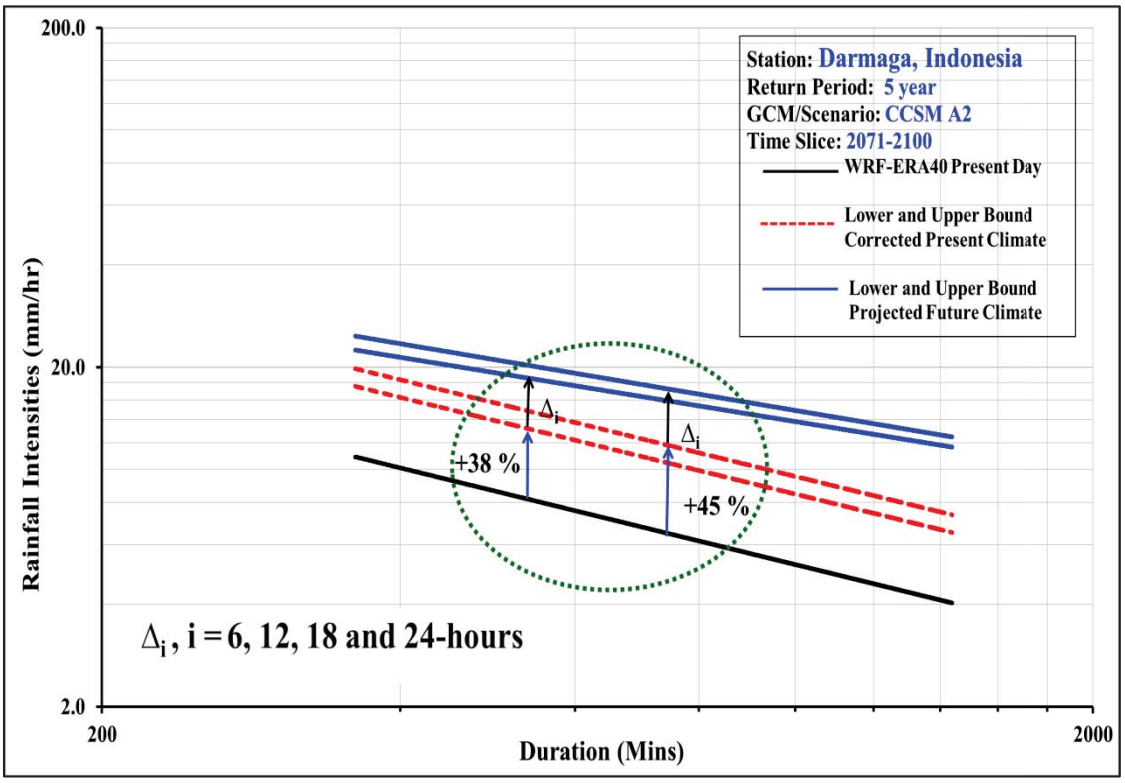

Figure B2-5a: Projected future climate IDF curves (5-year return period, 2071-2100, WRF/CCSM A2): Darmaga Station

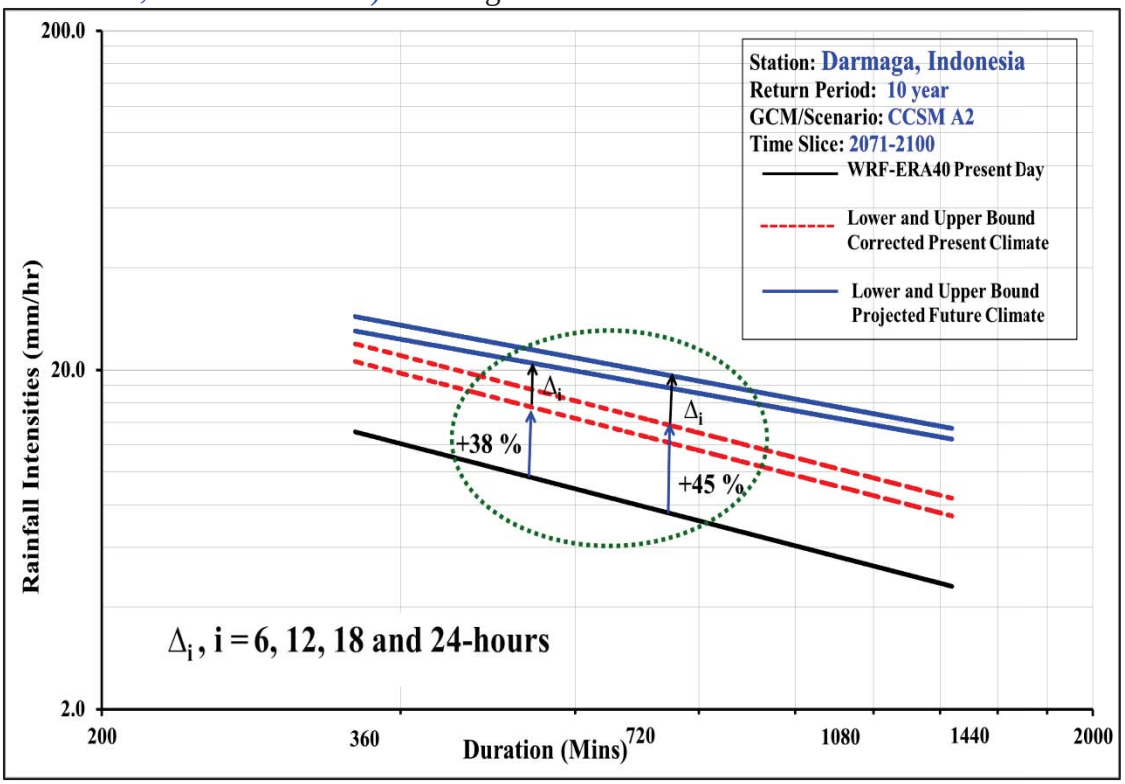

Figure B2-5b: Projected future climate IDF curves (10-year return period, 2071-2100, WRF/CCSM A2): Darmaga Station

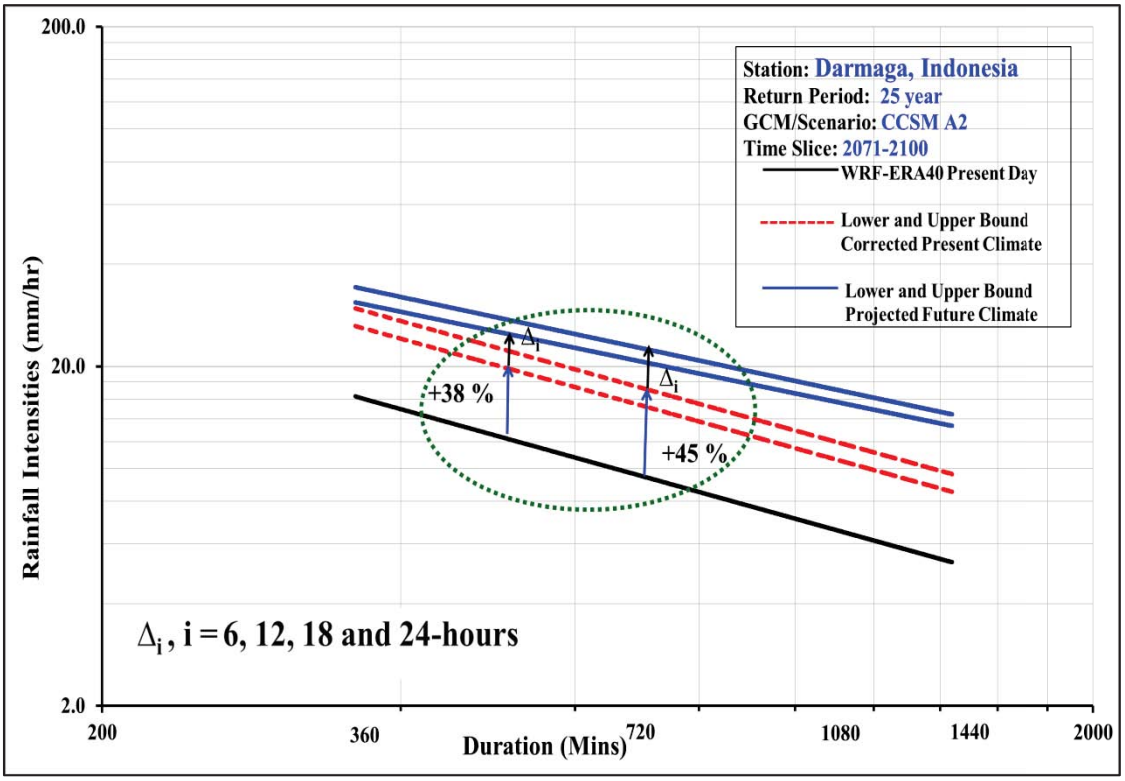

Figure B2-5c: Projected future climate IDF curves (25-year return period, 2071-2100, WRF/CCSM A2): Darmaga Station

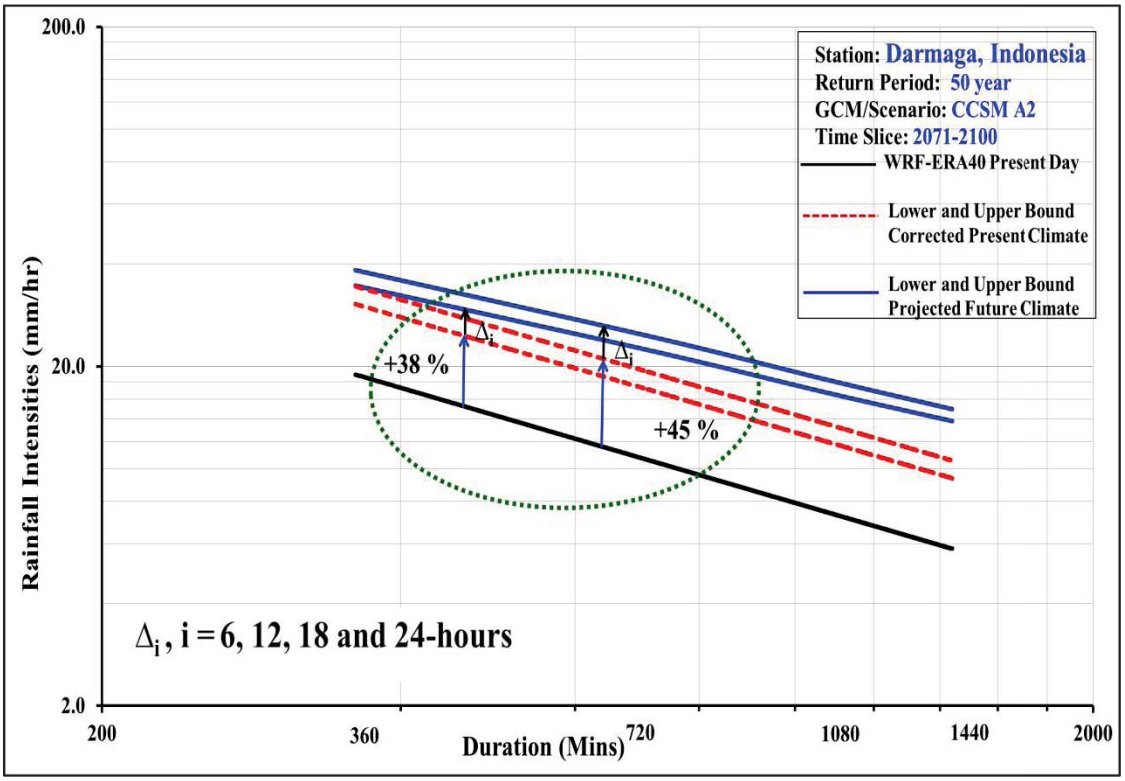

Figure B2-5d: Projected future climate IDF curves (50-year return period, 2071-2100, WRF/CCSM A2): Darmaga Station

Station : Darmaga Station
Period : 2011-2040
GCM/Scenario : WRF/CCSM A1FI

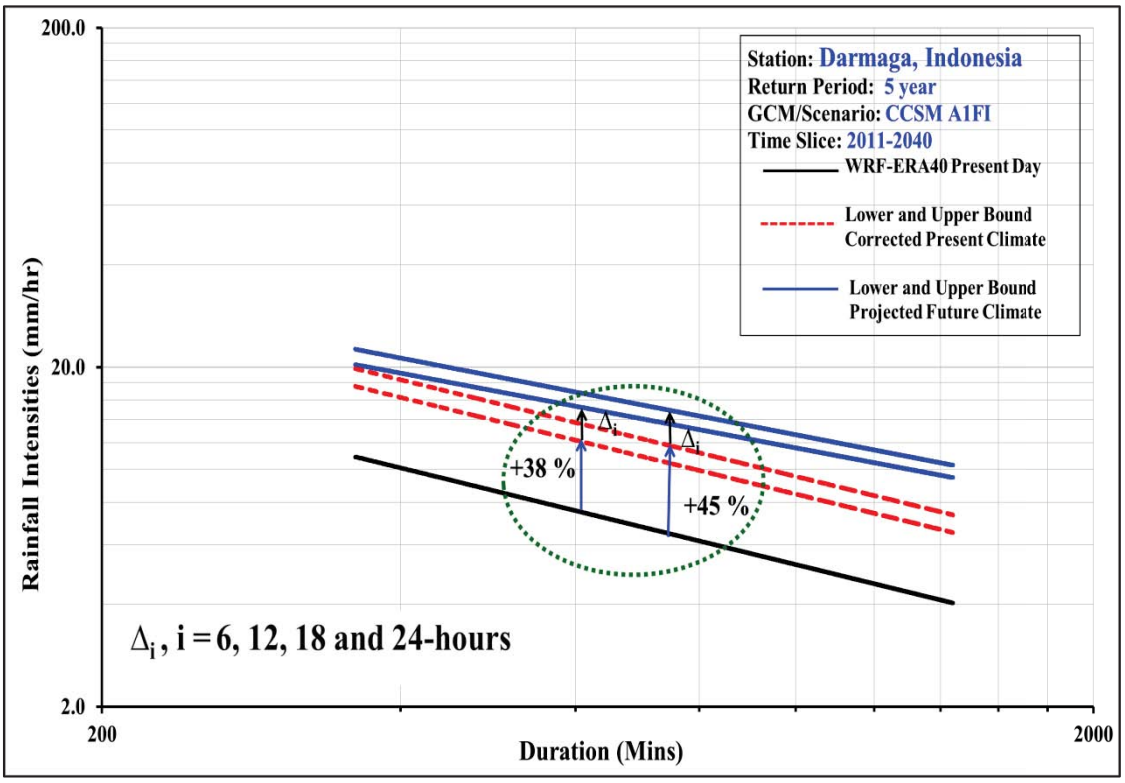

Figure B2-6a: Projected future climate IDF curves (5-year return period, 2011-2040, WRF/CCSM A2): Darmaga Station

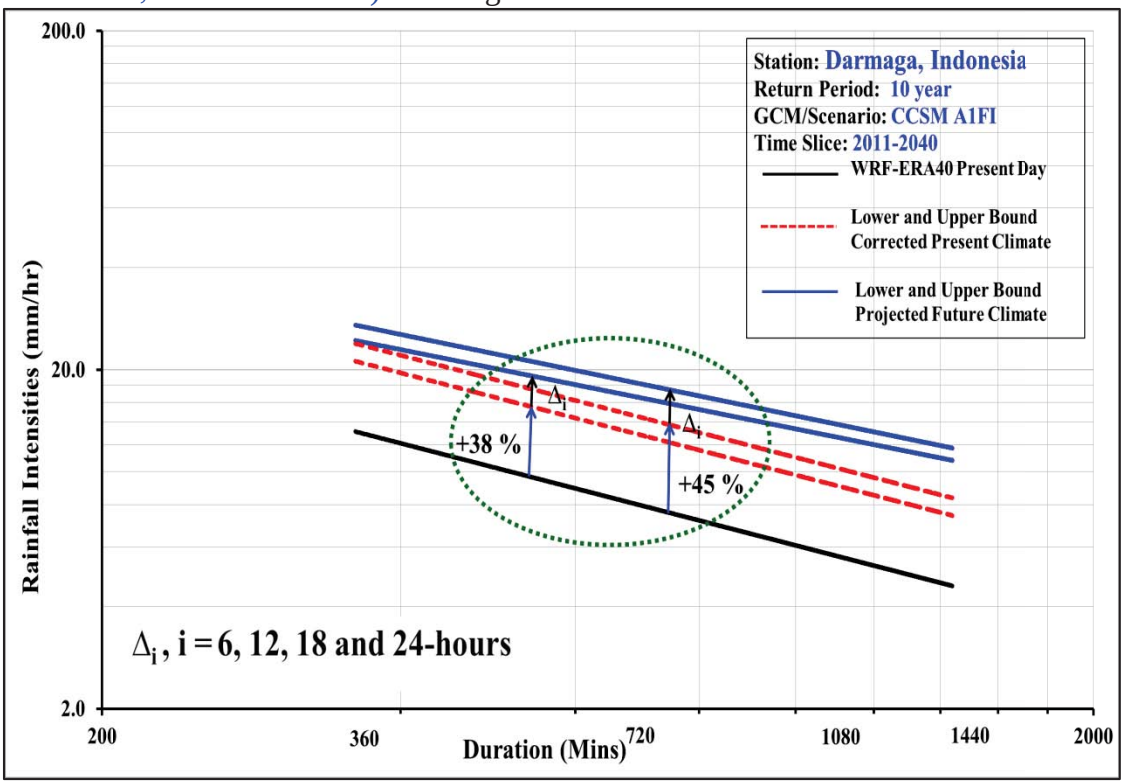

Figure B2-6b: Projected future climate IDF curves (10-year return period, 2011-2040, WRF/CCSM A2): Darmaga Station

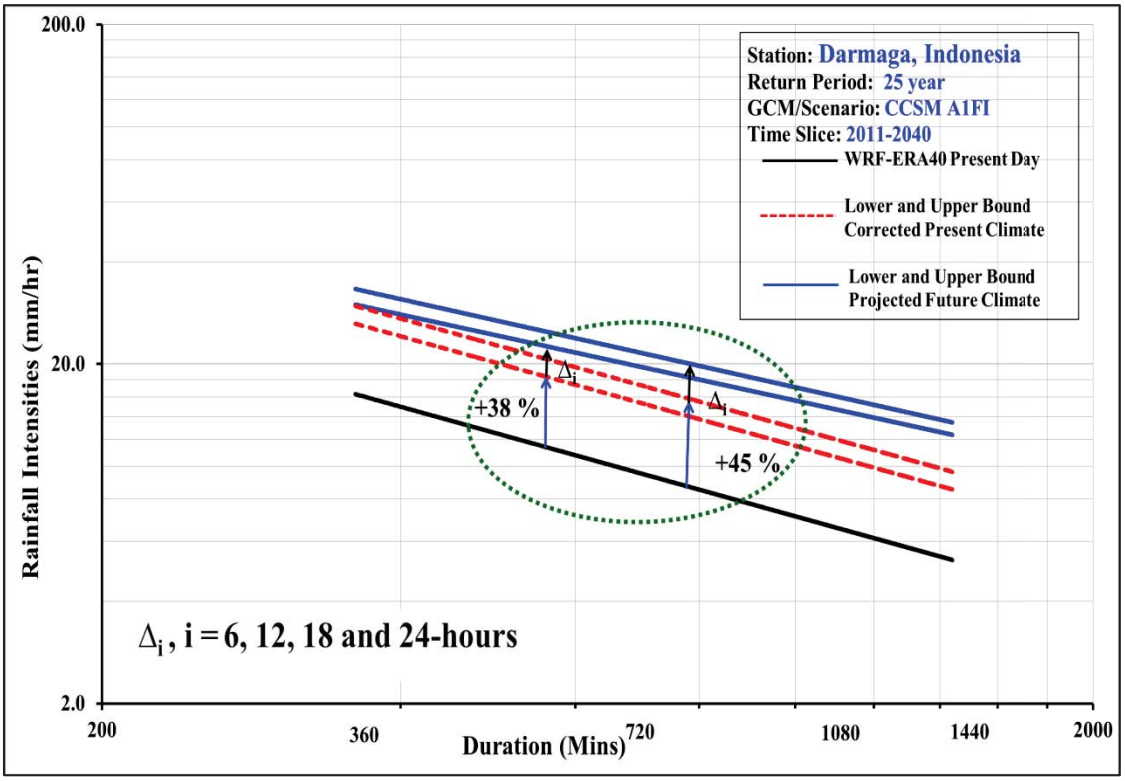

Figure B2-6c: Projected future climate IDF curves (25-year return period, 2011-2040, WRF/CCSM A2): Darmaga Station

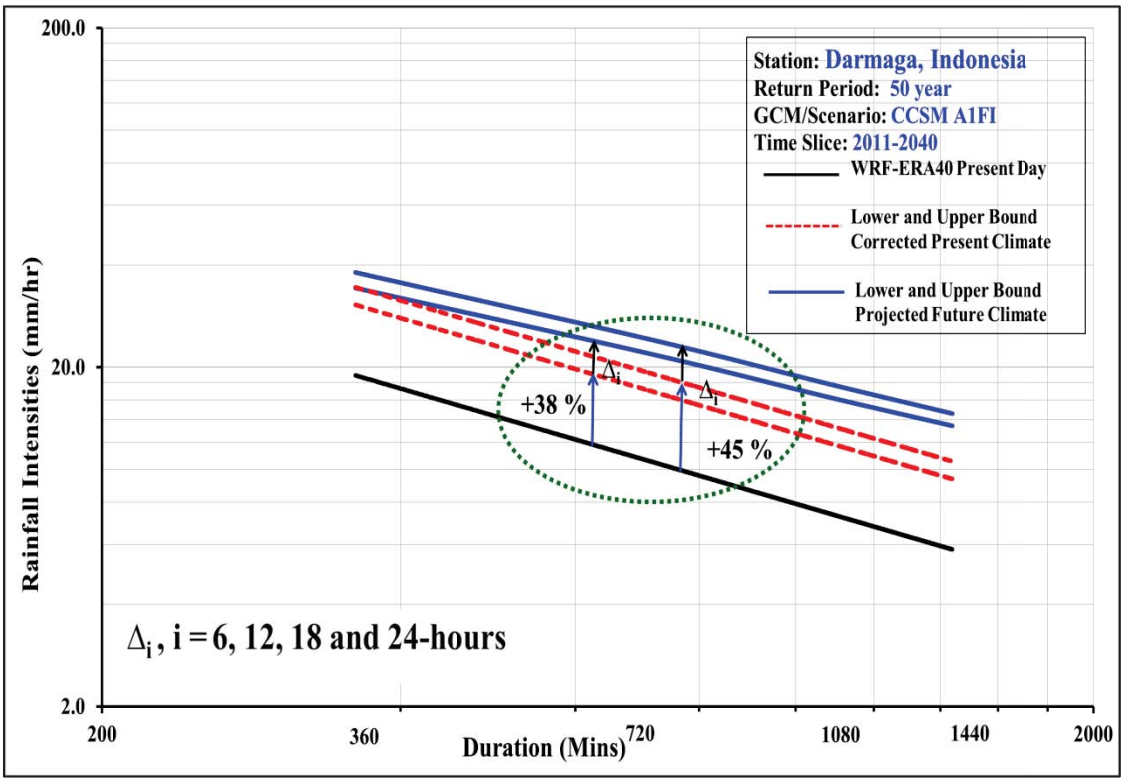

Figure B2-6d: Projected future climate IDF curves (50-year return period, 2011-2040, WRF/CCSM A2): Darmaga Station

Station : Darmaga Station
Period : 2041-2070
GCM/Scenario : WRF/CCSM A1FI

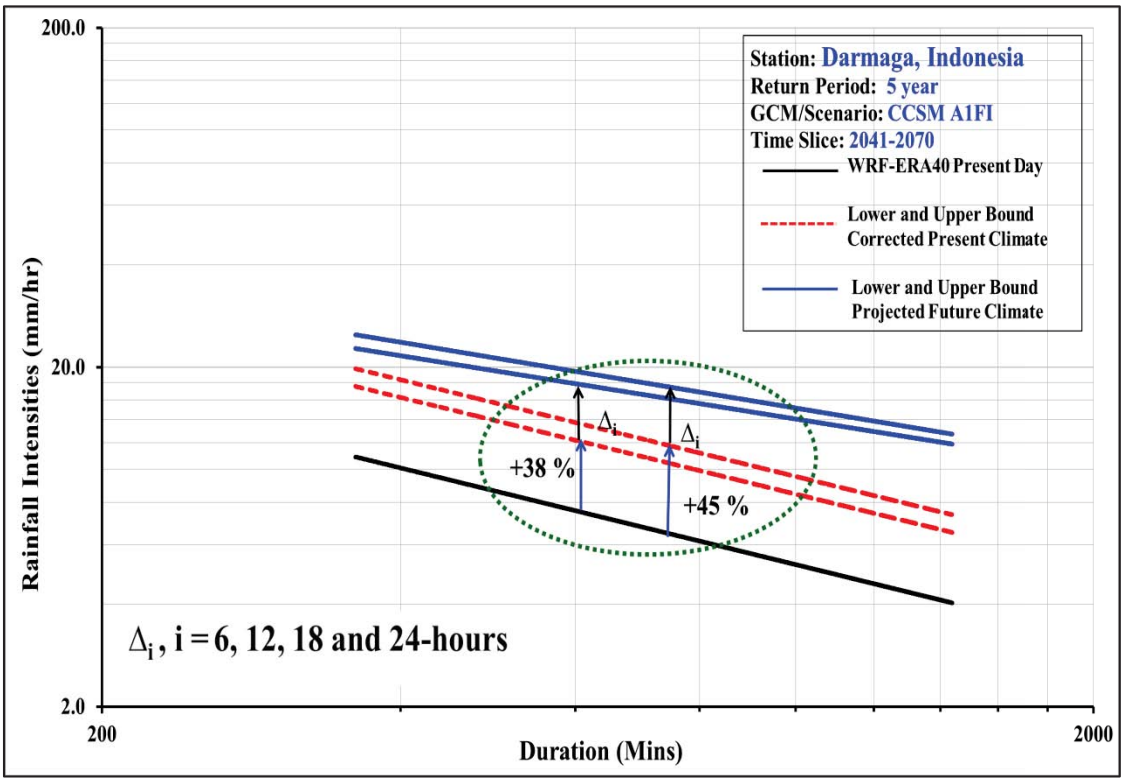

Figure B2-7a: Projected future climate IDF curves (5-year return period, 2041-2070, WRF/CCSM A2): Darmaga Station

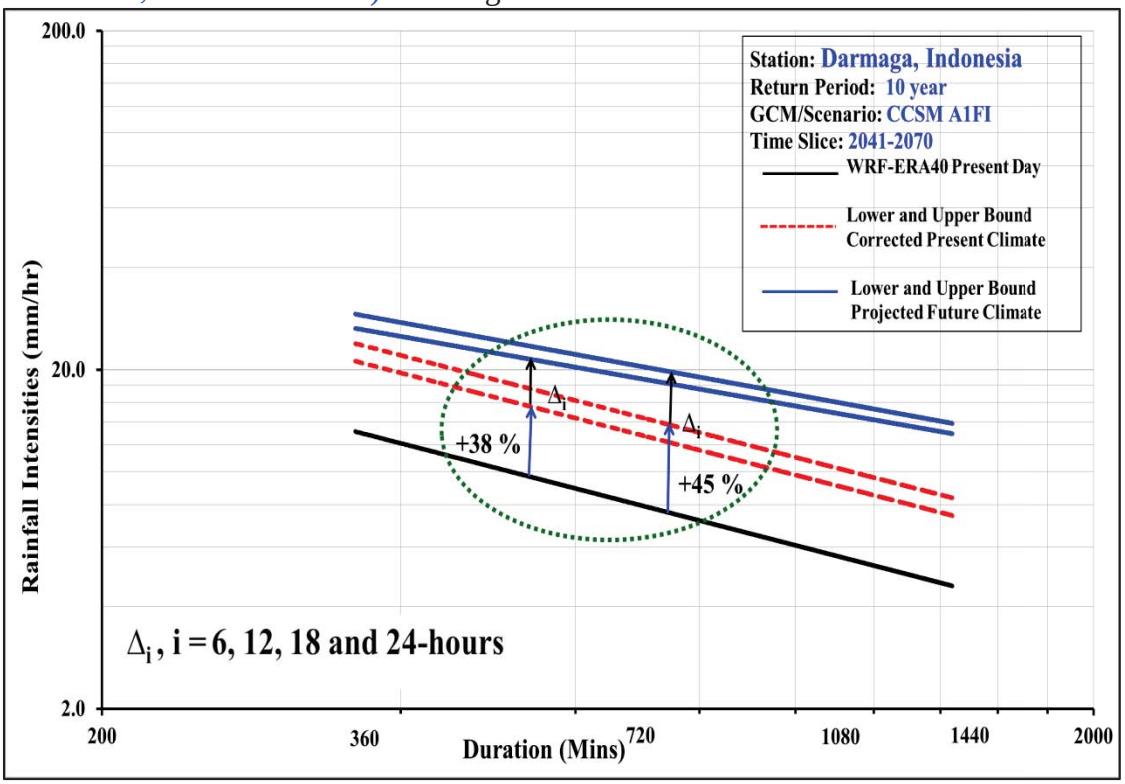

Figure B2-7b: Projected future climate IDF curves (10-year return period, 2041-2070, WRF/CCSM A2): Darmaga Station

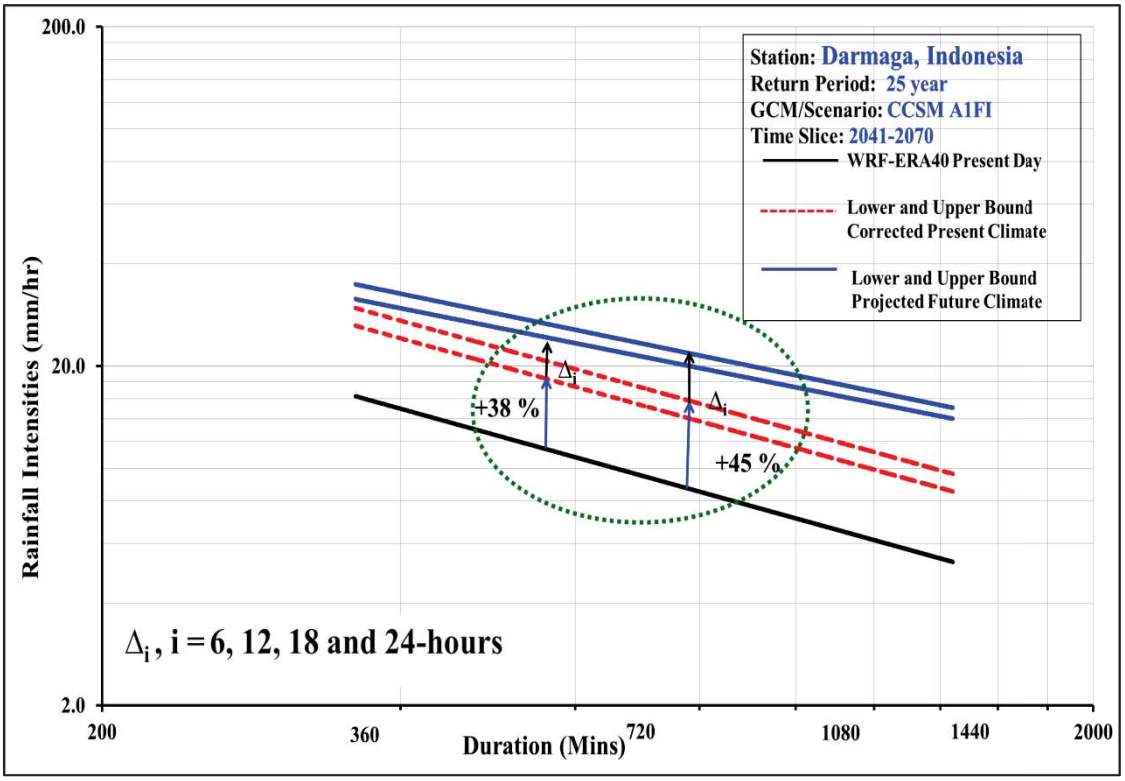

Figure B2-7c: Projected future climate IDF curves (25-year return period, 2041-2070, WRF/CCSM A2): Darmaga Station

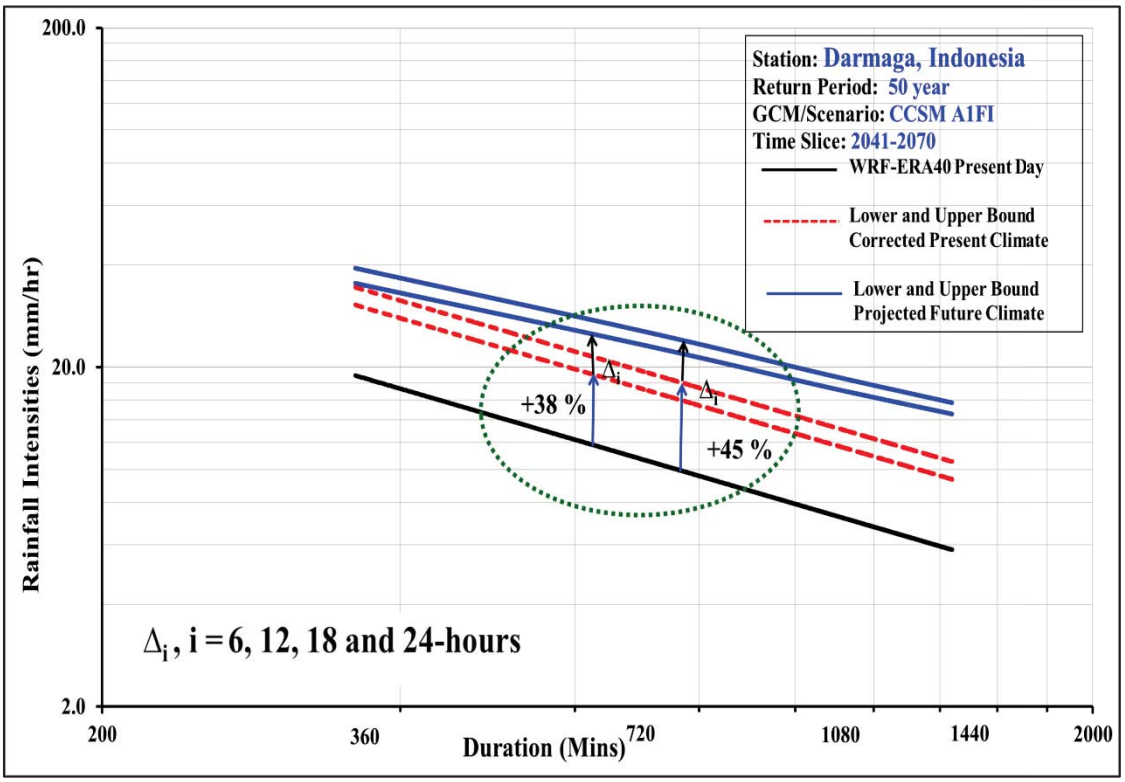

Figure B2-7d: Projected future climate IDF curves (50-year return period, 2041-2070, WRF/CCSM A2): Darmaga Station

Station : Darmaga Station
Period : 2071-2100
GCM/Scenario : WRF/CCSM A1FI

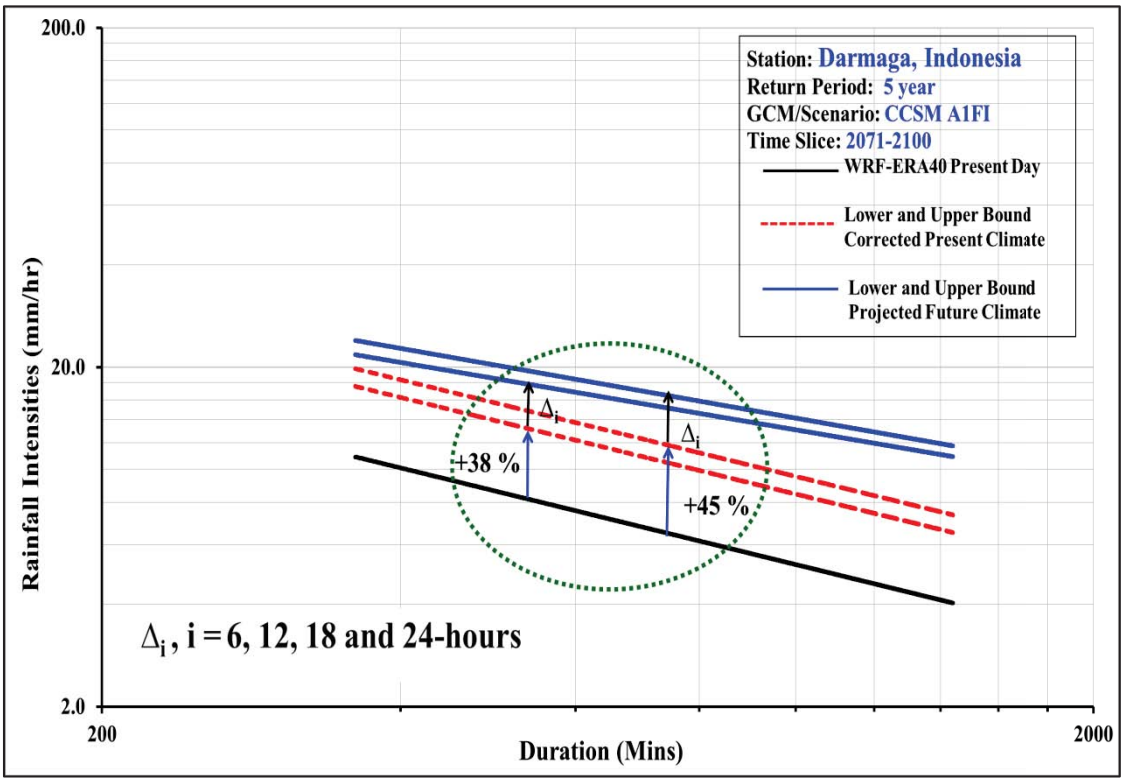

Figure B2-8a: Projected future climate IDF curves (5-year return period, 2071-2100, WRF/CCSM A2): Darmaga Station

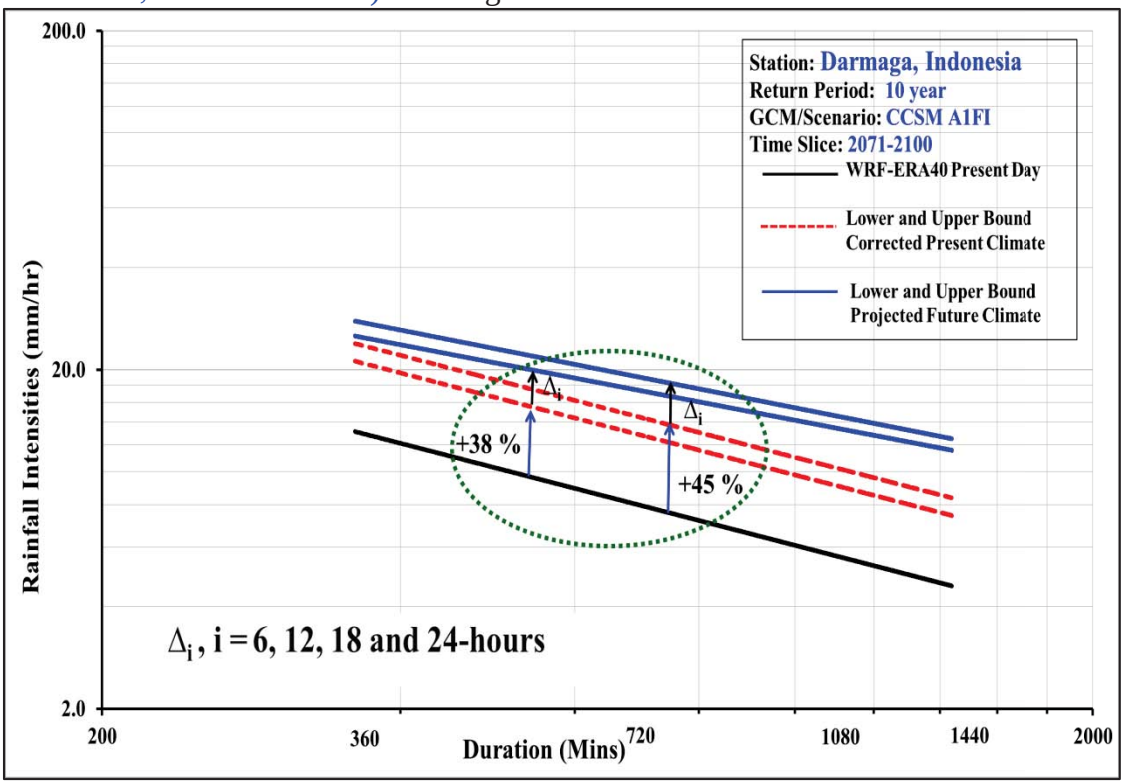

Figure B2-8b: Projected future climate IDF curves (10-year return period, 2071-2100, WRF/CCSM A2): Darmaga Station

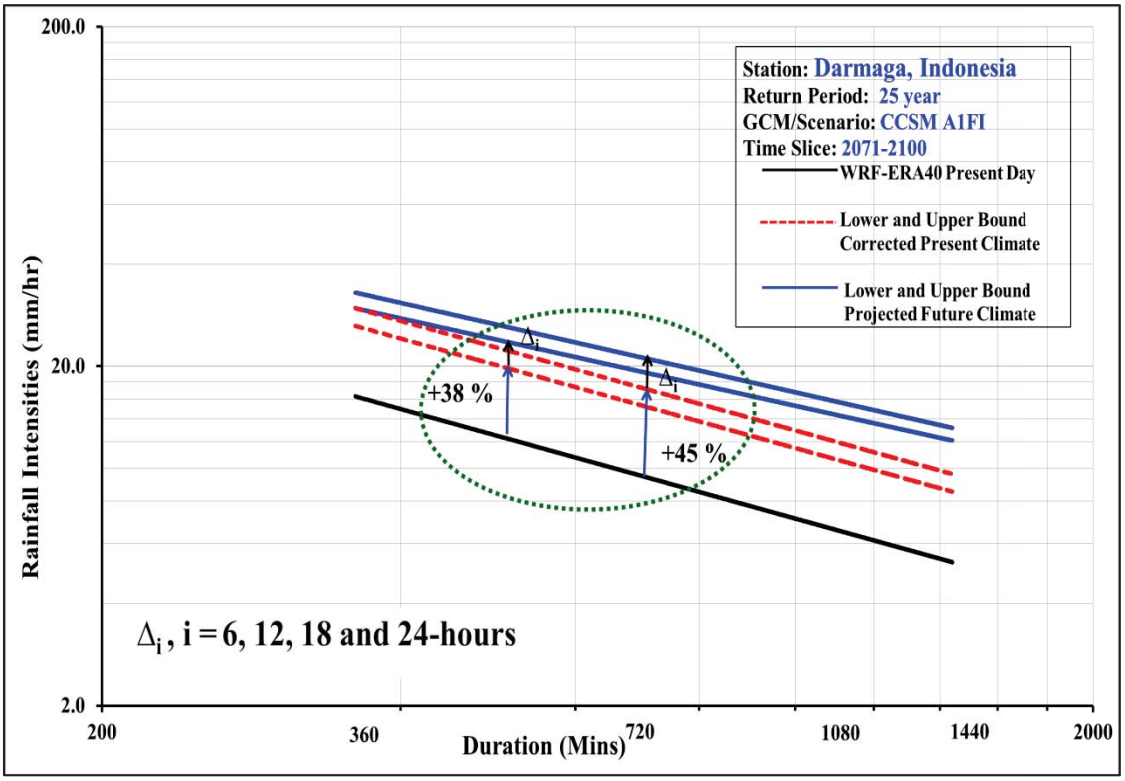

Figure B2-8c: Projected future climate IDF curves (25-year return period, 2071-2100, WRF/CCSM A2): Darmaga Station

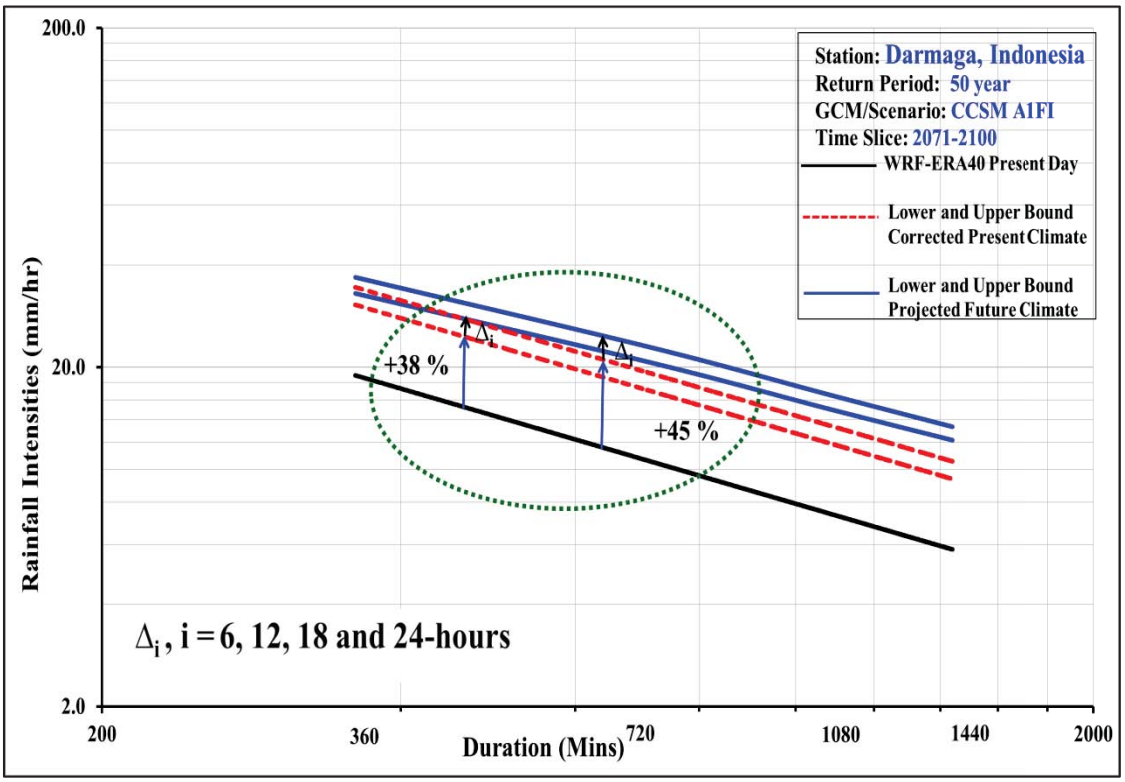

Figure B2-8d: Projected future climate IDF curves (50-year return period, 2071-2100, WRF/CCSM A2): Darmaga Station

Station : Darmaga Station
Period : 2011-2040
GCM/Scenario : WRF/CCSM A1B

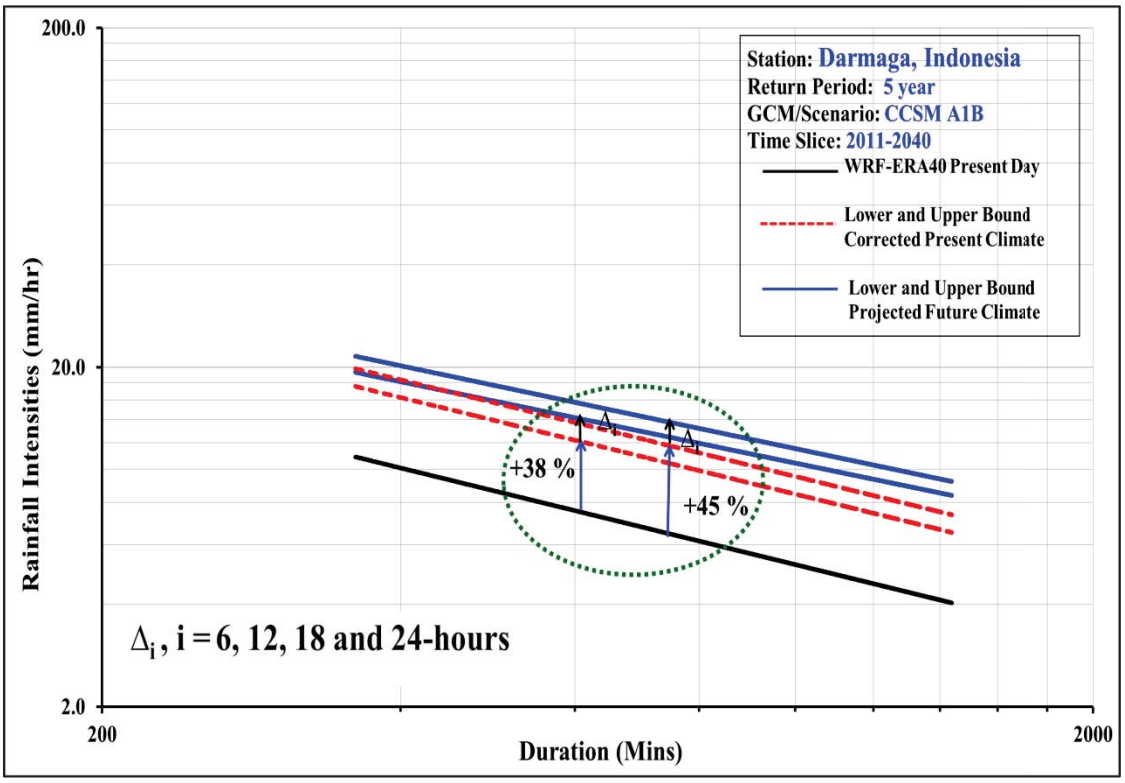

Figure B2-9a: Projected future climate IDF curves (5-year return period, 2011-2040, WRF/CCSM A1B): Darmaga Station

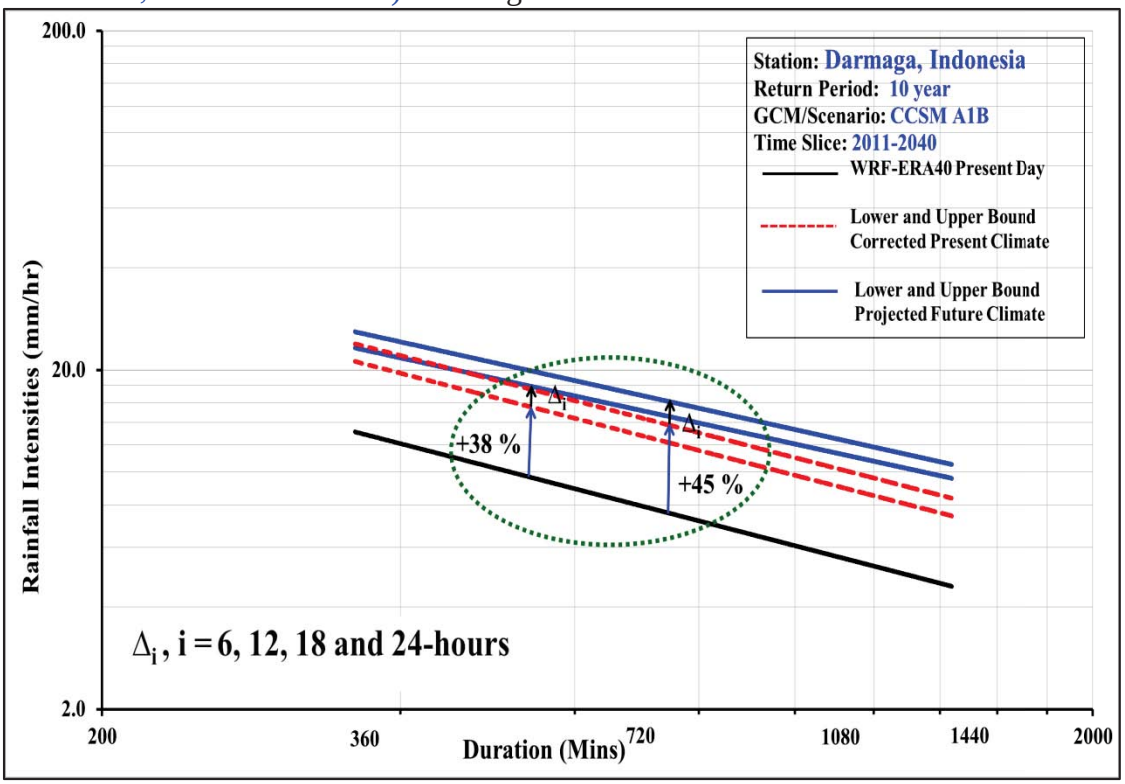

Figure B2-9b: Projected future climate IDF curves (10-year return period, 2011-2040, WRF/CCSM A1B): Darmaga Station

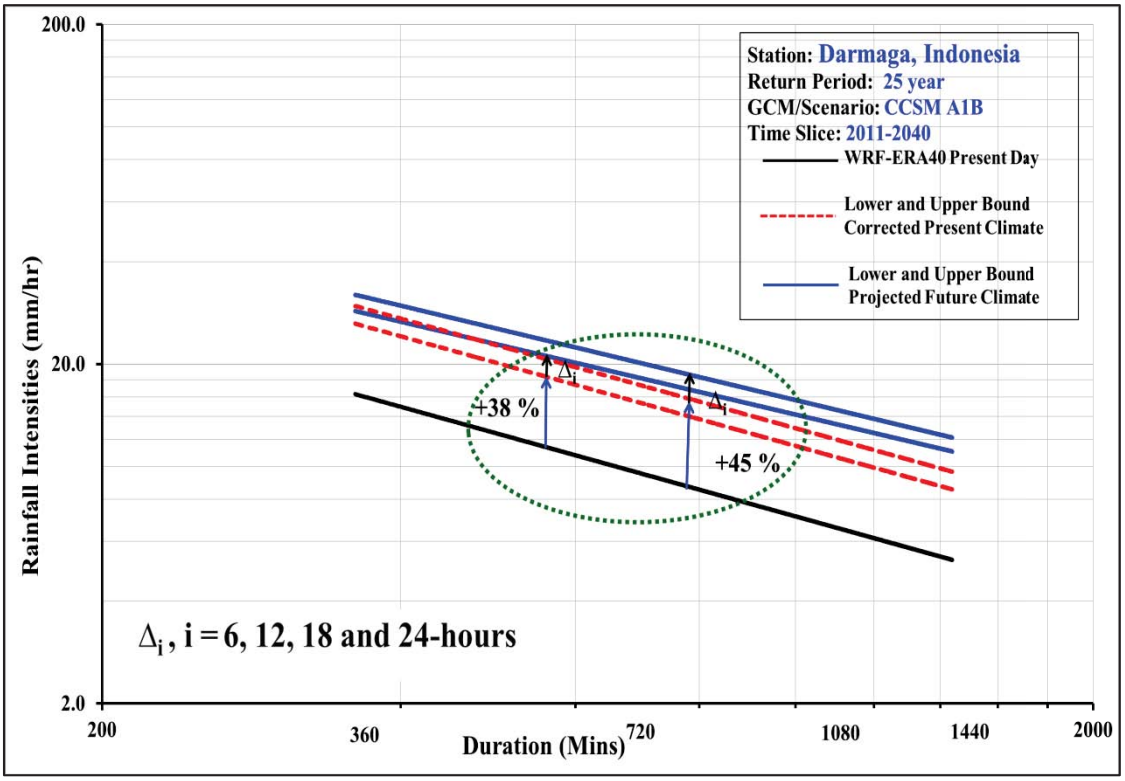

Figure B2-9c: Projected future climate IDF curves (25-year return period, 2011-2040, WRF/CCSM A1B): Darmaga Station

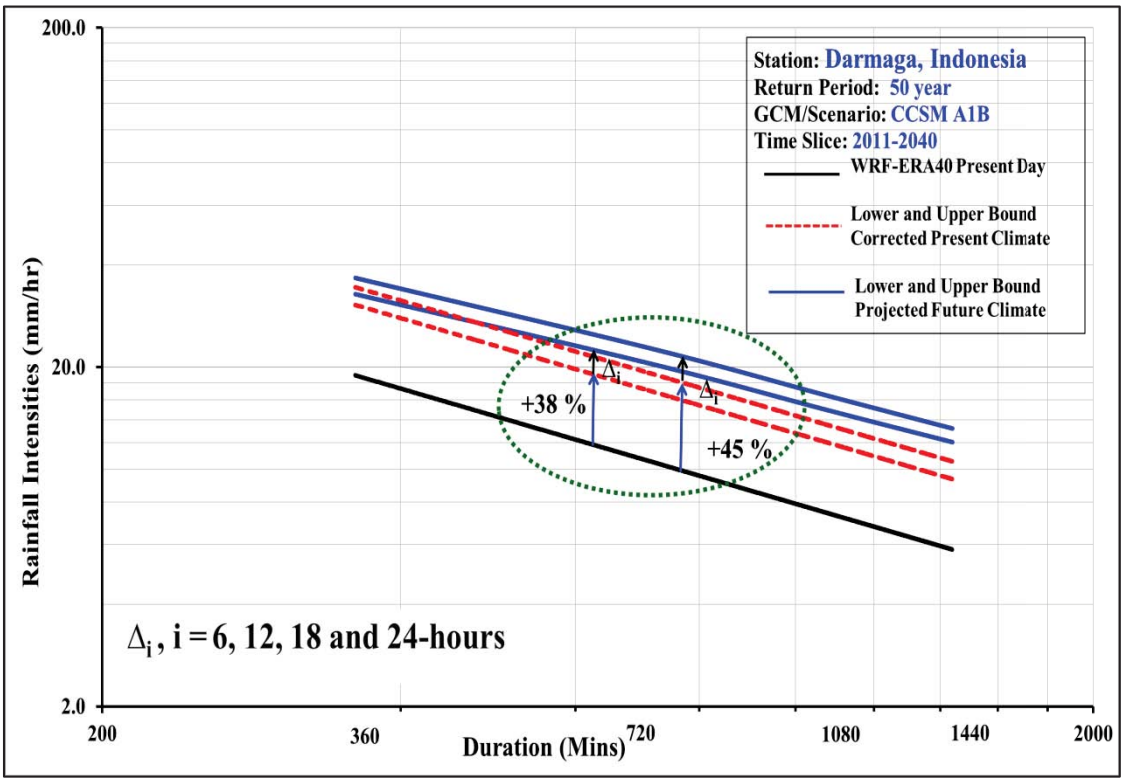

Figure B2-9d: Projected future climate IDF curves (50-year return period, 2011-2040, WRF/CCSM A1B): Darmaga Station

Station : Darmaga Station
Period : 2041-2070
GCM/Scenario : WRF/CCSM A1B

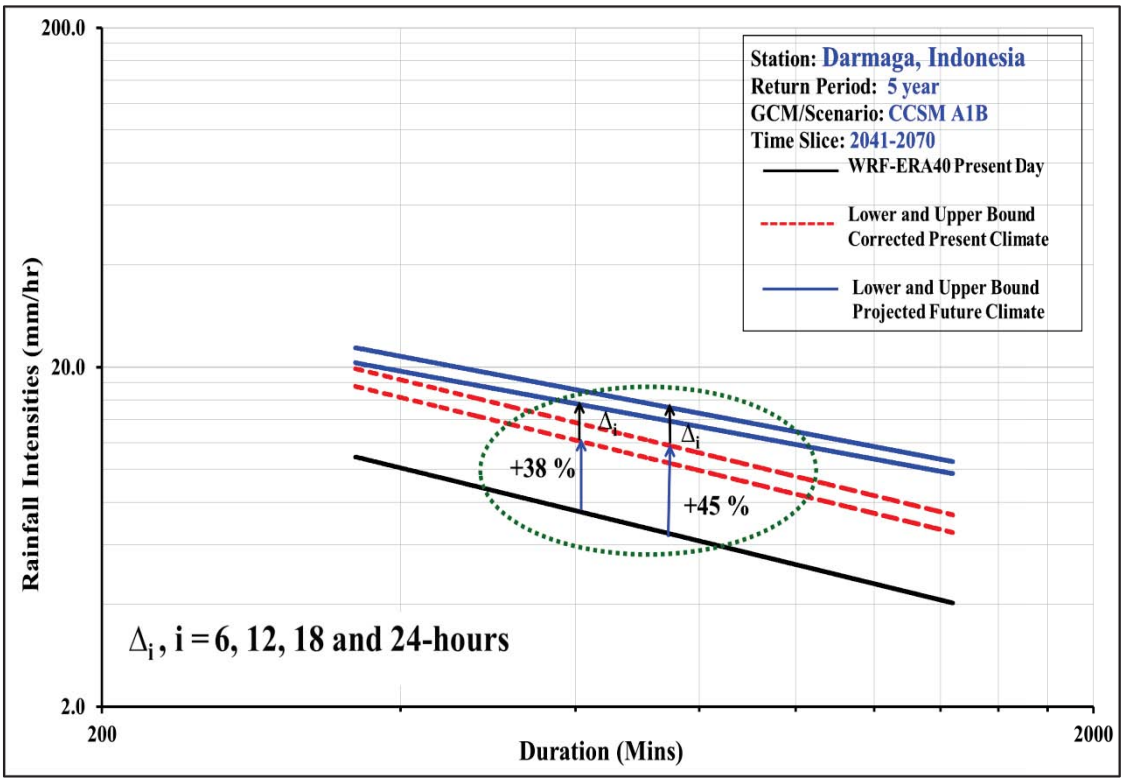

Figure B2-10a: Projected future climate IDF curves (5-year return period, 2041-2070, WRF/CCSM A1B): Darmaga Station

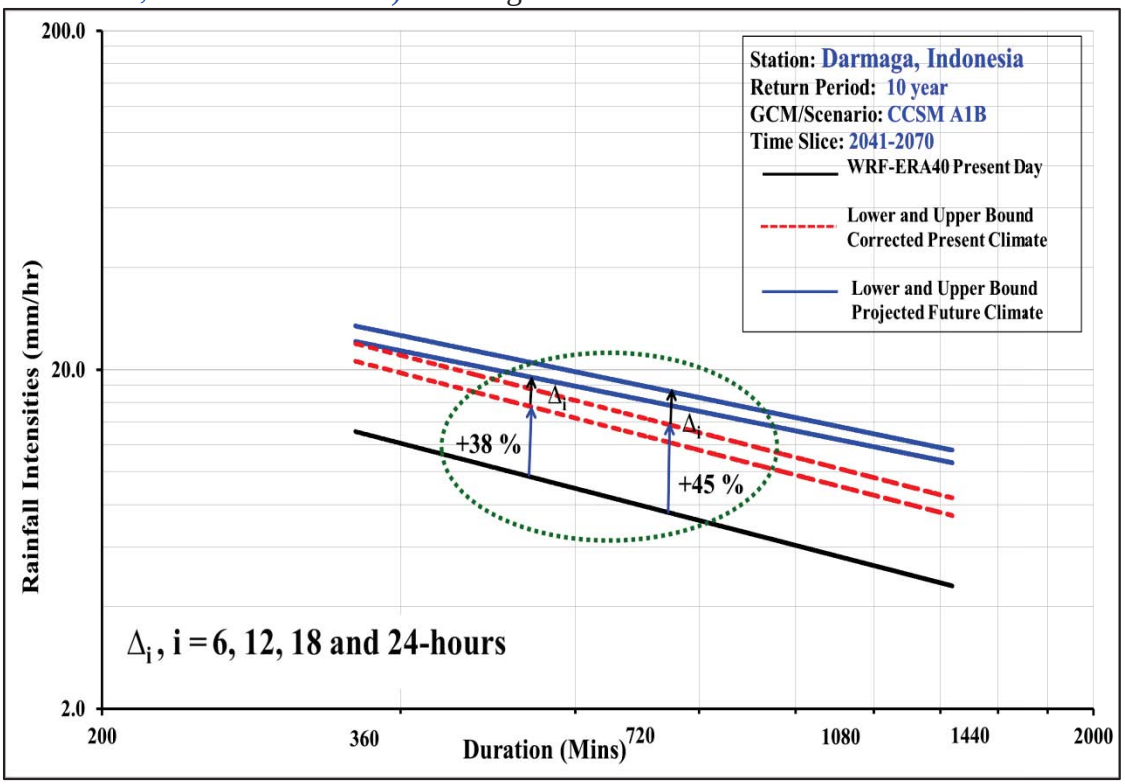

Figure B2-10b: Projected future climate IDF curves (10-year return period, 2041-2070, WRF/CCSM A1B): Darmaga Station

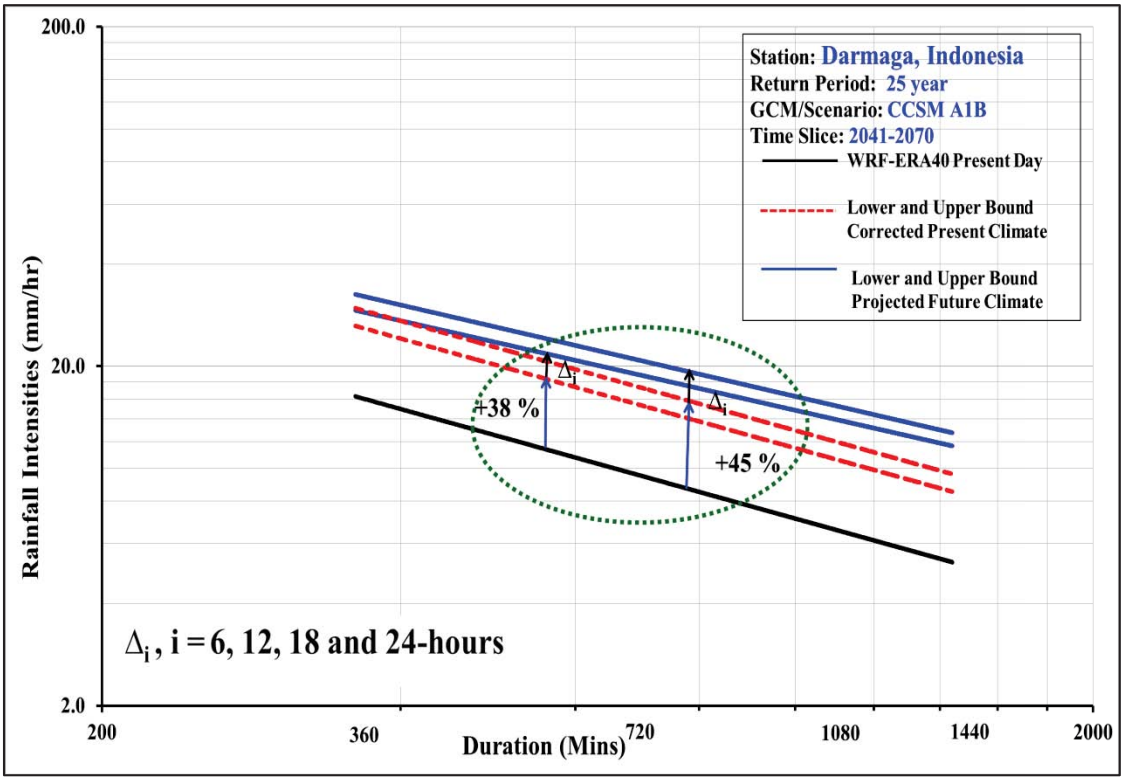

Figure B2-10c: Projected future climate IDF curves (25-year return period, 2041-2070, WRF/CCSM A1B): Darmaga Station

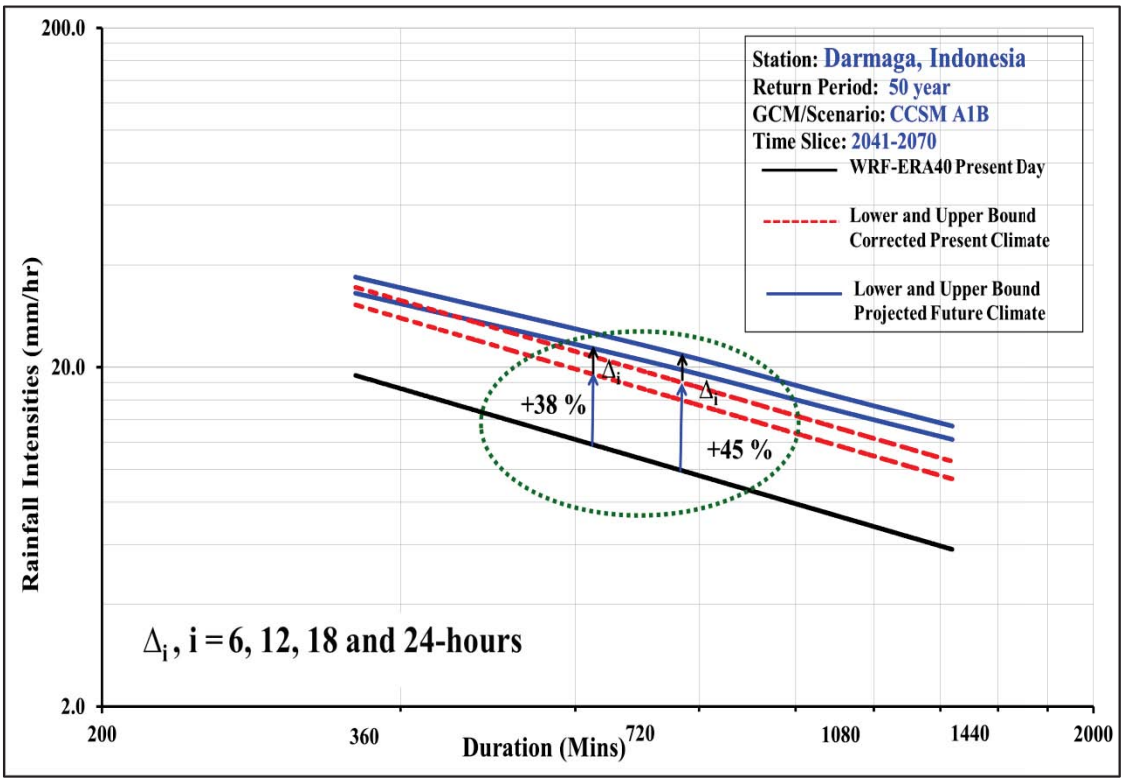

Figure B2-10d: Projected future climate IDF curves (50-year return period, 2041-2070, WRF/CCSM A1B): Darmaga Station

Station : Darmaga Station
Period : 2071-2100
GCM/Scenario : WRF/CCSM A1B

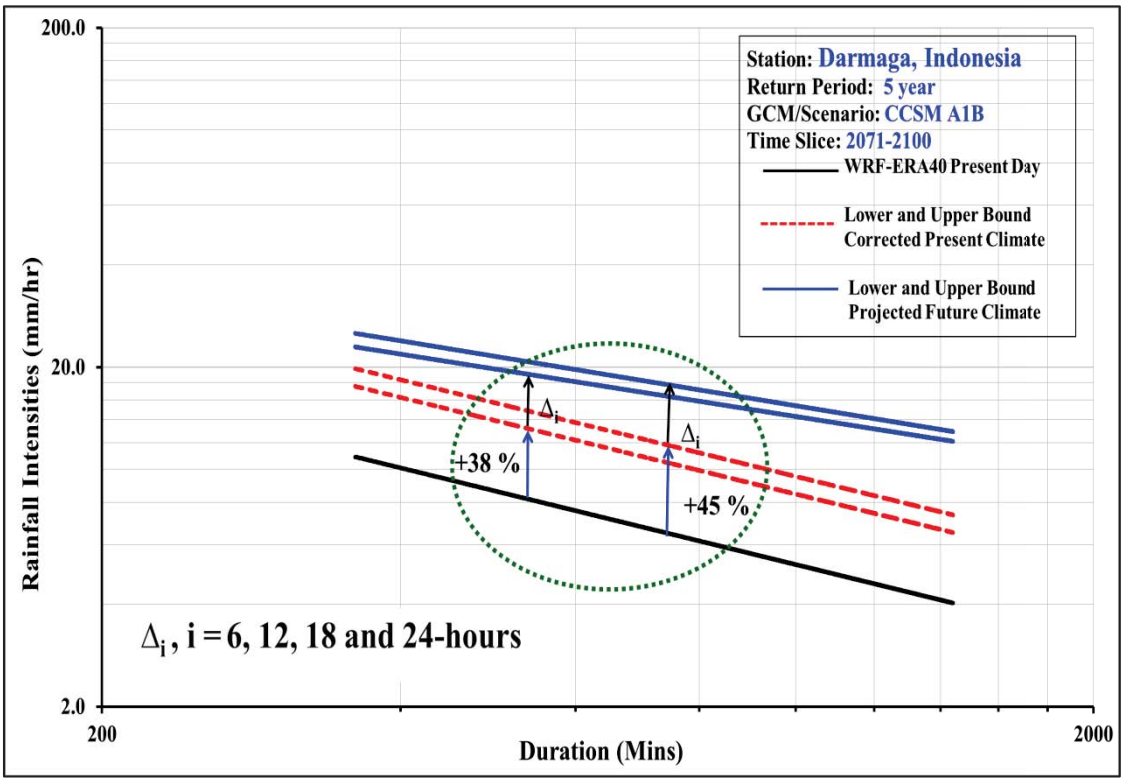

Figure B2-11a: Projected future climate IDF curves (5-year return period, 2071-2100, WRF/CCSM A1B): Darmaga Station

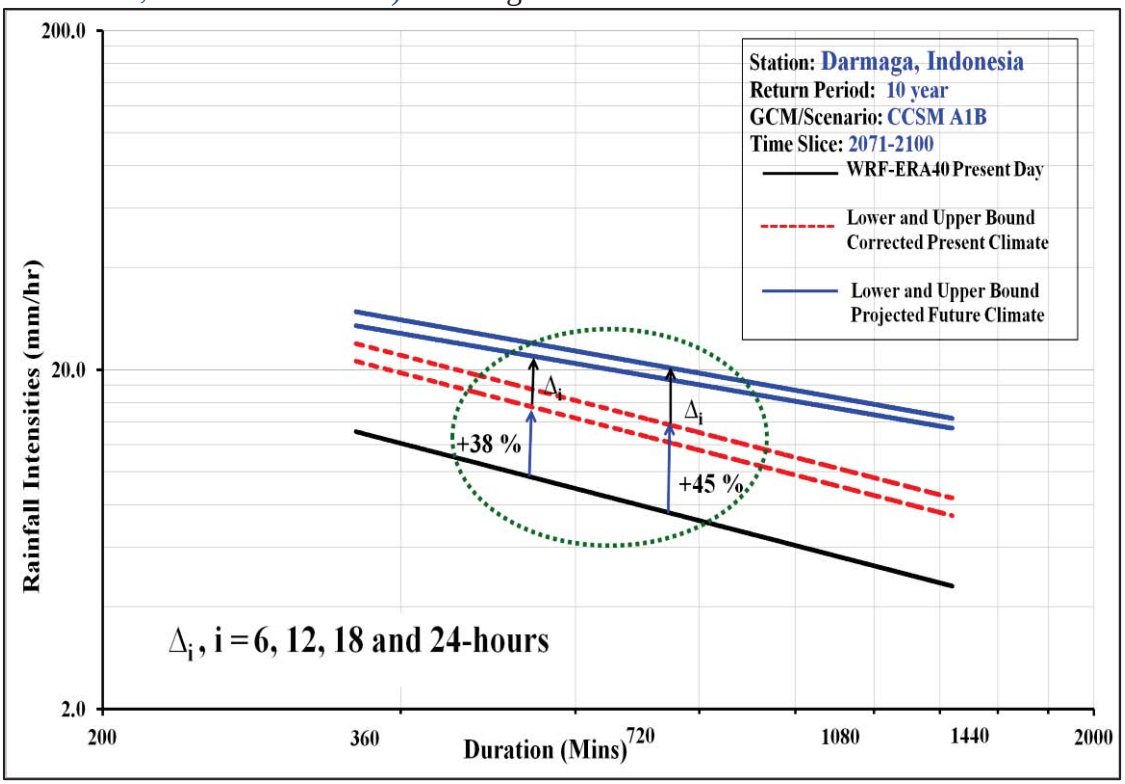

Figure B2-11b: Projected future climate IDF curves (10-year return period, 2071-2100, WRF/CCSM A1B): Darmaga Station

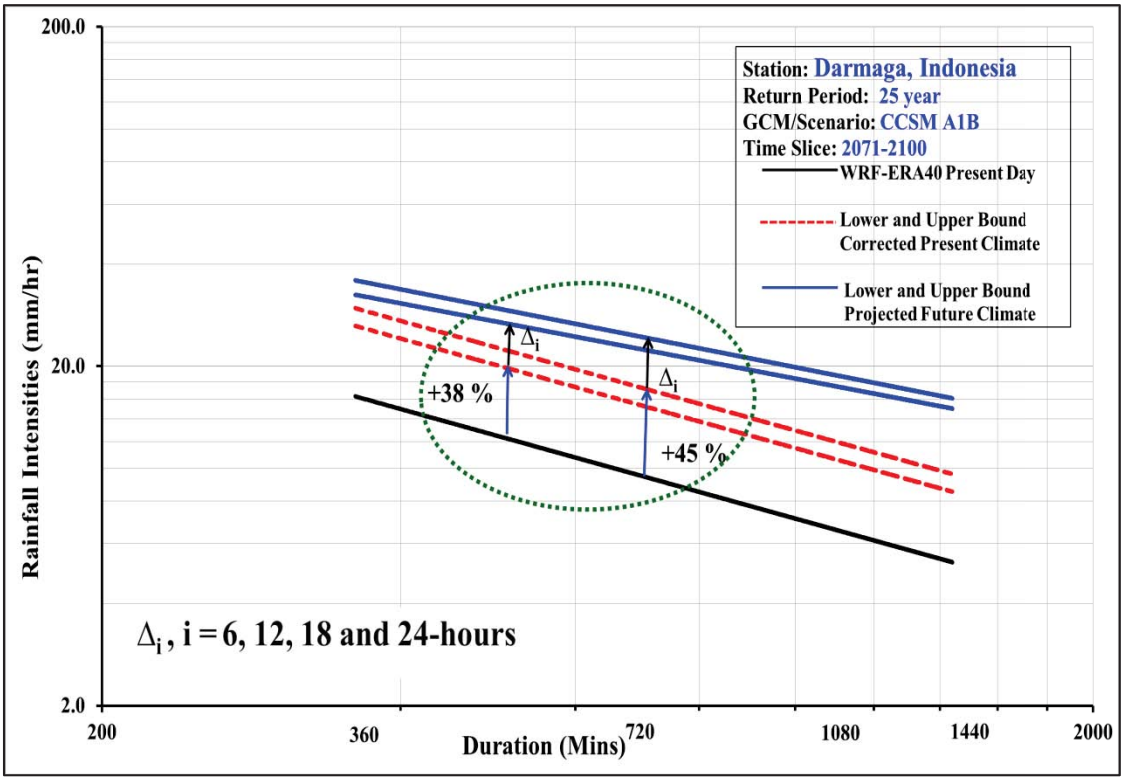

Figure B2-11c: Projected future climate IDF curves (25-year return period, 2071-2100, WRF/CCSM A1B): Darmaga Station

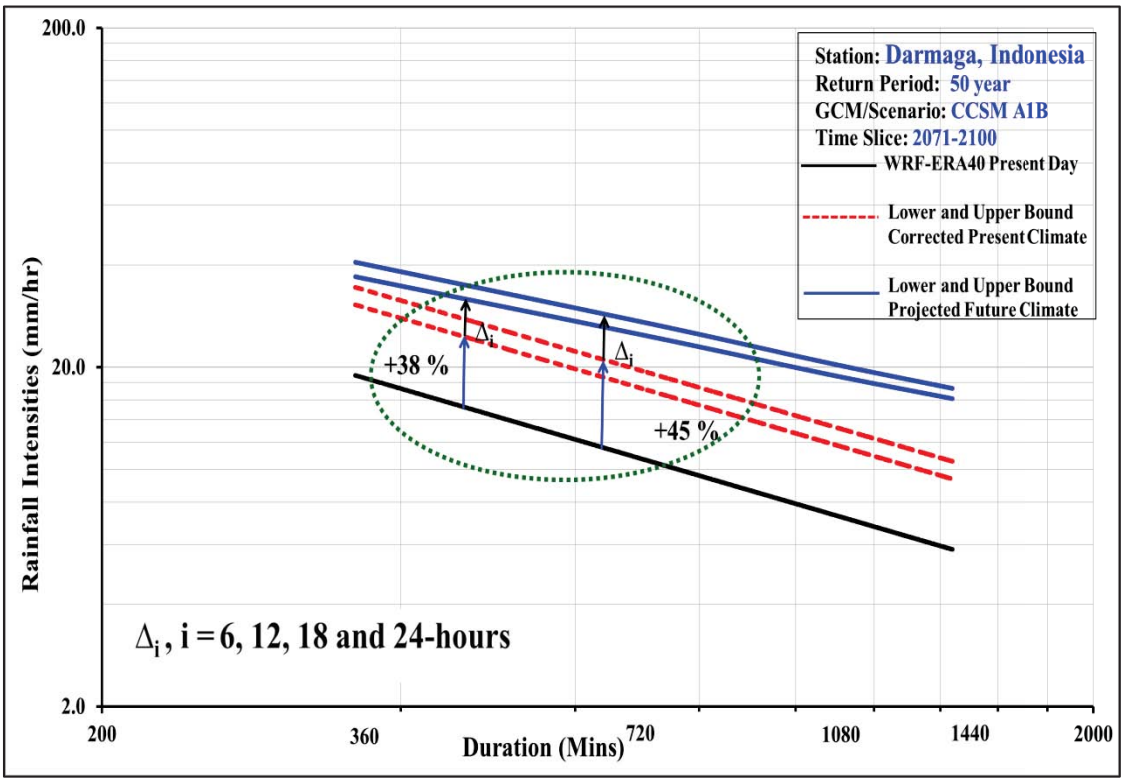

Figure B2-11d: Projected future climate IDF curves (50-year return period, 2071-2100, WRF/CCSM A1B): Darmaga Station

APPENDIX B3

Projected future climate IDF curves for Jakarta Meteorological Station

Return Period	**:**	**5 and 10-year; 25 and 50-year**
Period	**:**	**2011-2040, 2041-2070 and 2071-2100**
GCM/Scenario	**:**	**WRF/ECHAM A2, WRF/CCSM A2, WRF/CCSM A1FI and WRF/CCSM A1B**

Station	**:**	**Jakarta Meteorological Station**
Period	**:**	**2011-2040**
GCM/Scenario	**:**	**WRF/ECHAM A2**

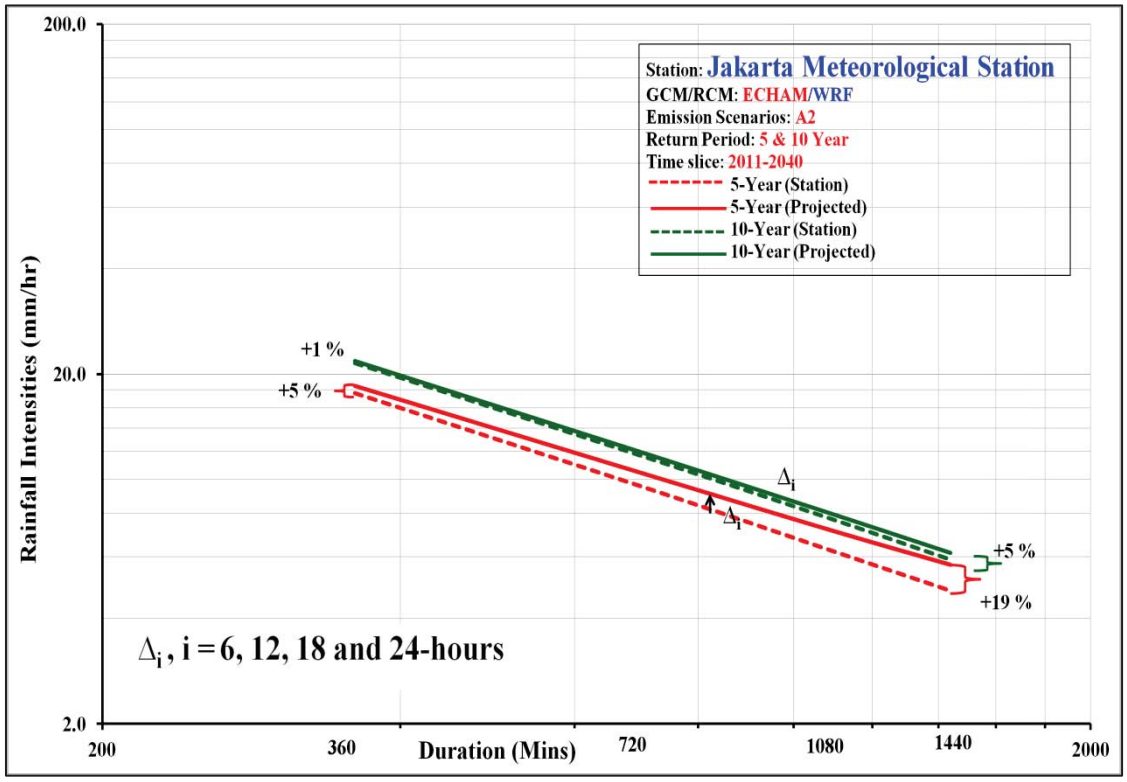

Figure B3-1a: Projected future climate IDF curves **(5 and 10 year return periods, 2011-2040, WRF/ECHAM A2)**: **Jakarta Meteorological Station**

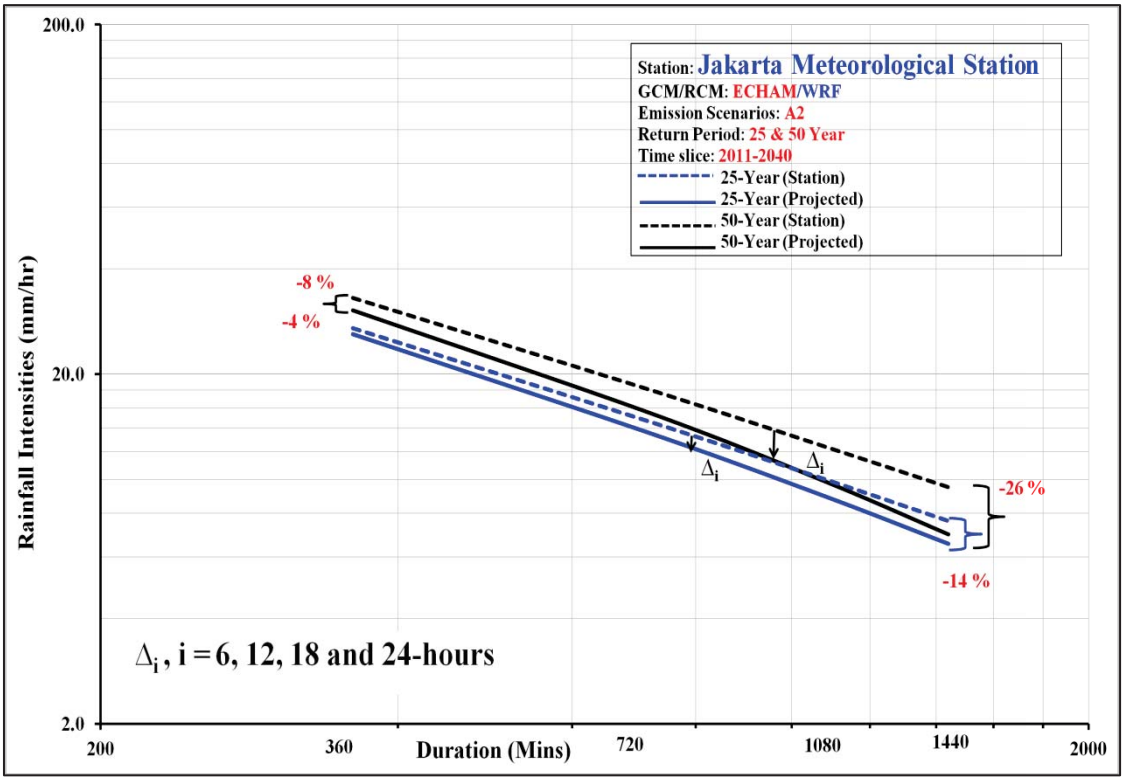

Figure B3-1b: Projected future climate IDF curves **(25 and 50 year return periods, 2011-2040, WRF/ECHAM A2)**: **Jakarta Meteorological Station**

Station : Jakarta Meteorological Station
Period : 2041-2070
GCM/Scenario : WRF/ECHAM A2

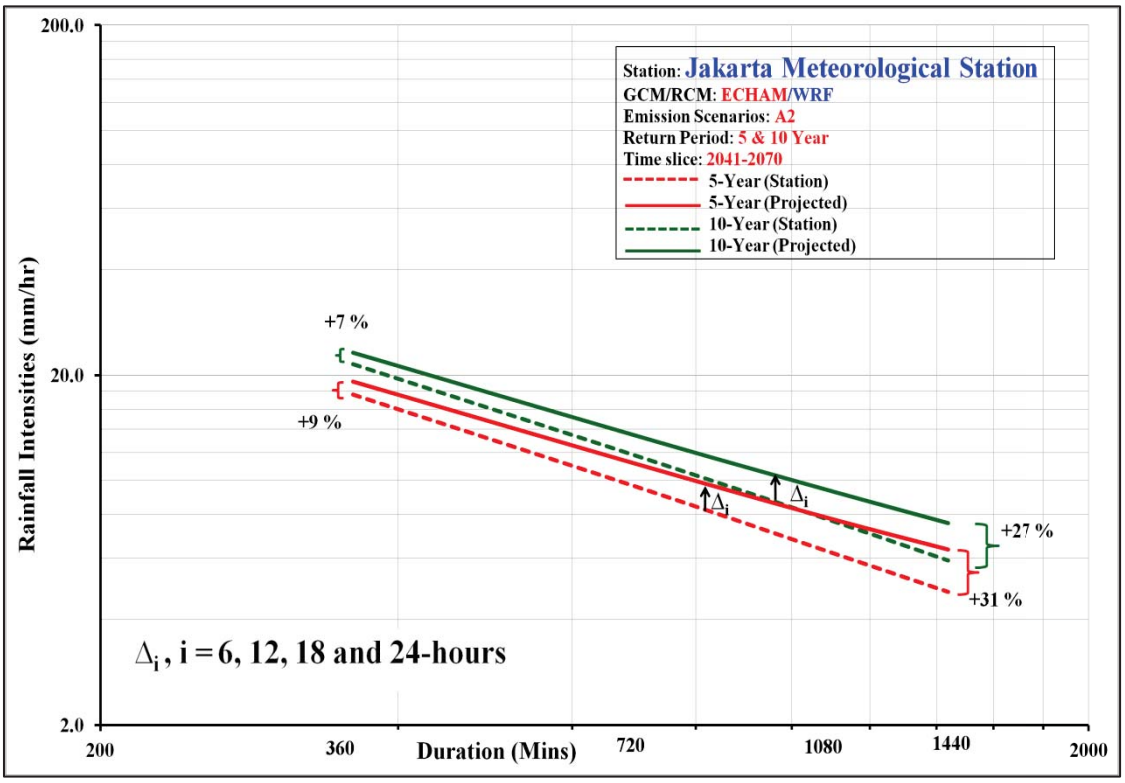

Figure B3-2a: Projected future climate IDF curves **(5 and 10 year return periods, 2041-2070, WRF/ECHAM A2)**: **Jakarta Meteorological Station**

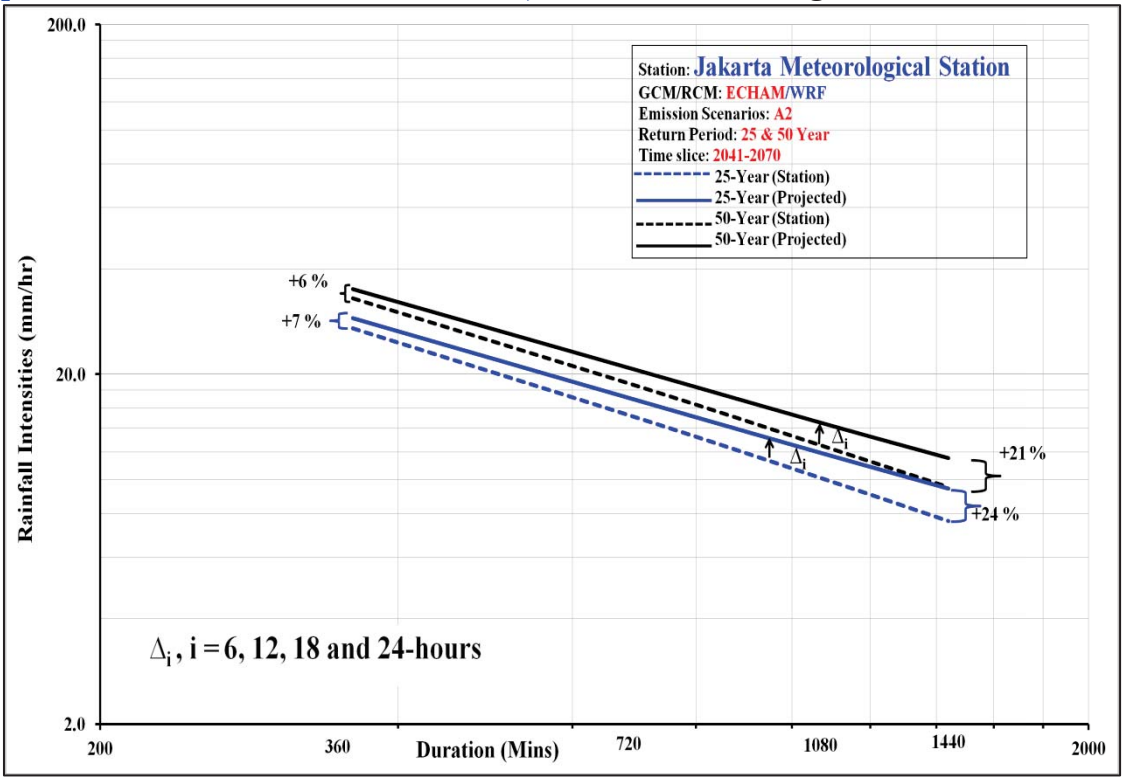

Figure B3-2b: Projected future climate IDF curves **(25 and 50 year return periods, 2041-2070, WRF/ECHAM A2)**: **Jakarta Meteorological Station**

Station : Jakarta Meteorological Station
Period : 2011-2040
GCM/Scenario : WRF/CCSM A2

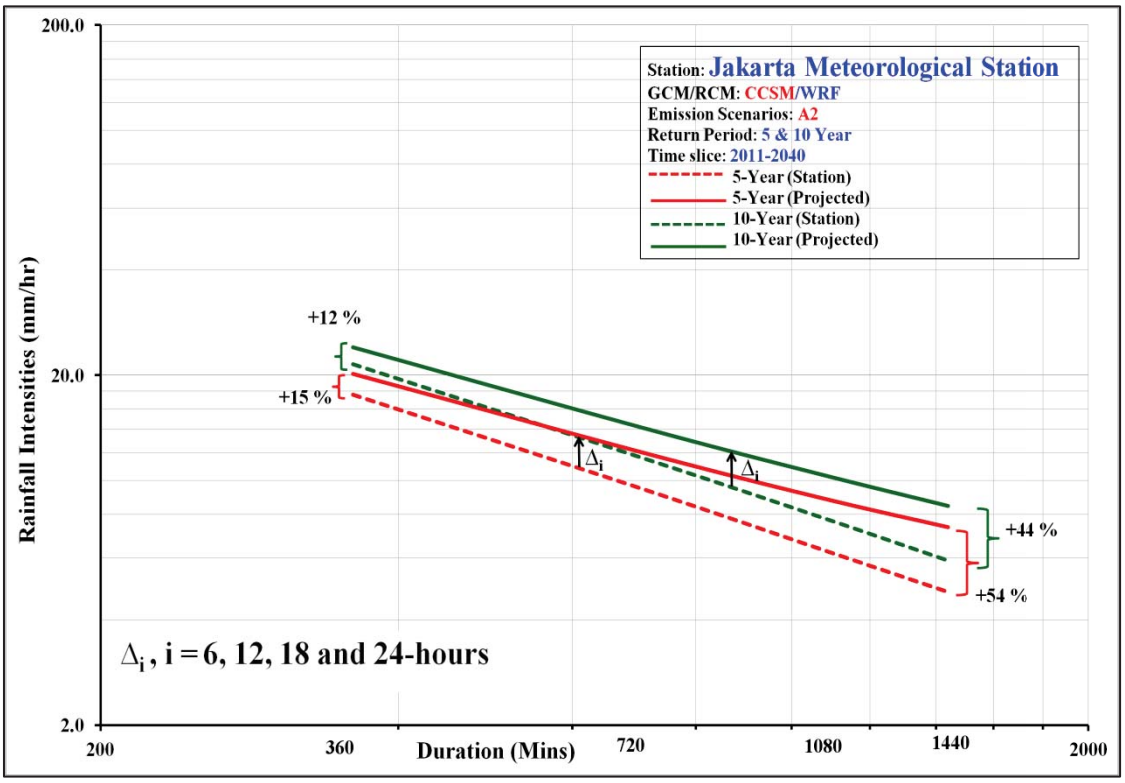

Figure B3-3a: Projected future climate IDF curves **(5 and 10 year return periods, 2011-2040, WRF/CCSM A2)**: **Jakarta Meteorological Station**

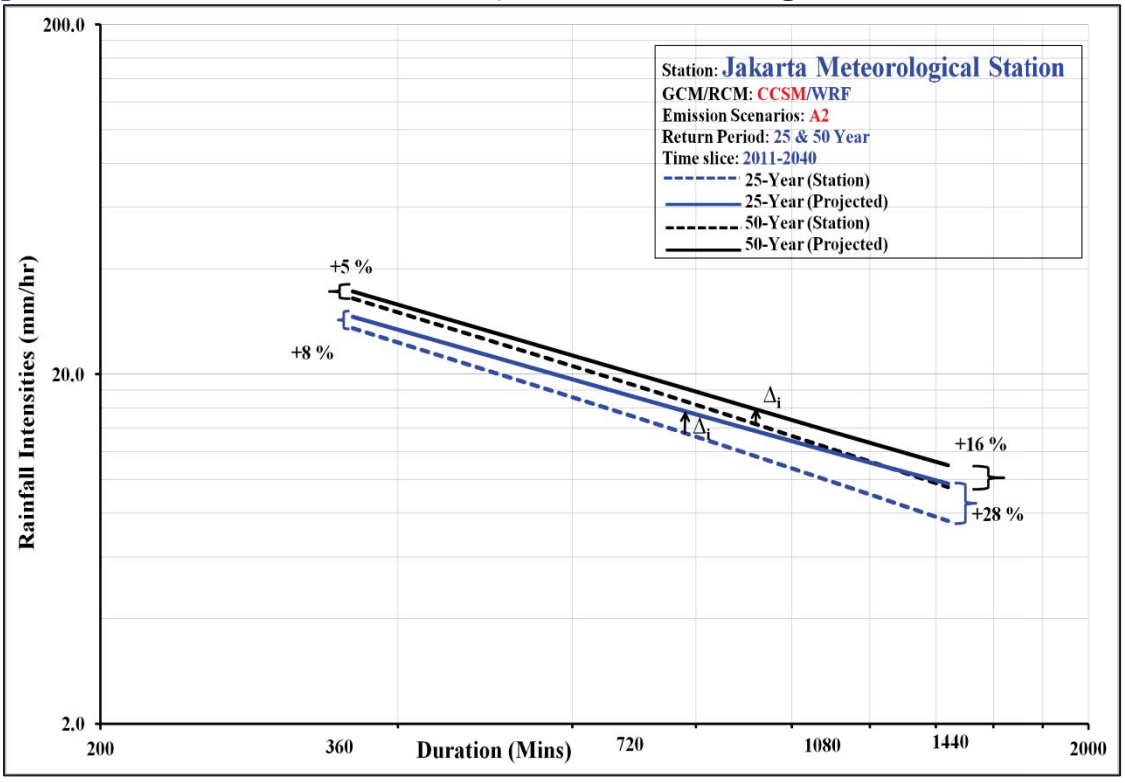

Figure B3-3b: Projected future climate IDF curves **(25 and 50 year return periods, 2011-2040, WRF/CCSM A2)**: **Jakarta Meteorological Station**

Station : Jakarta Meteorological Station
Period : 2041-2070
GCM/Scenario : WRF/CCSM A2

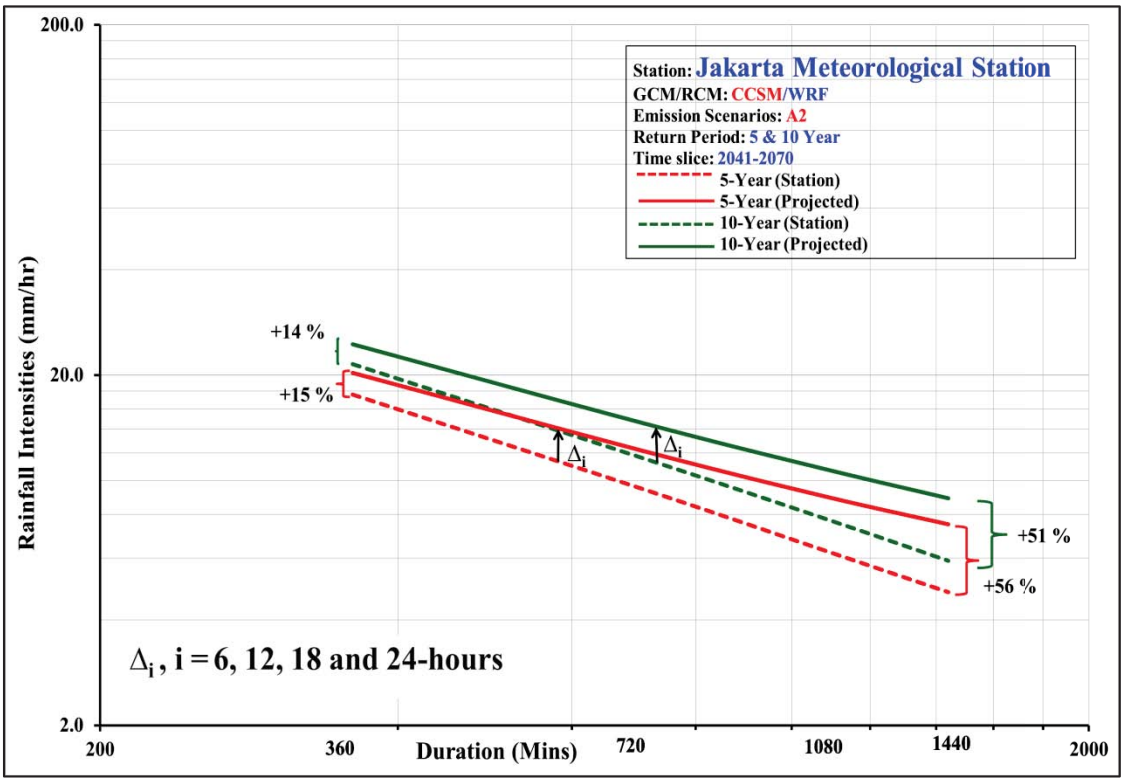

Figure B3-4a: Projected future climate IDF curves **(5 and 10 year return periods, 2041-2070, WRF/CCSM A2)**: **Jakarta Meteorological Station**

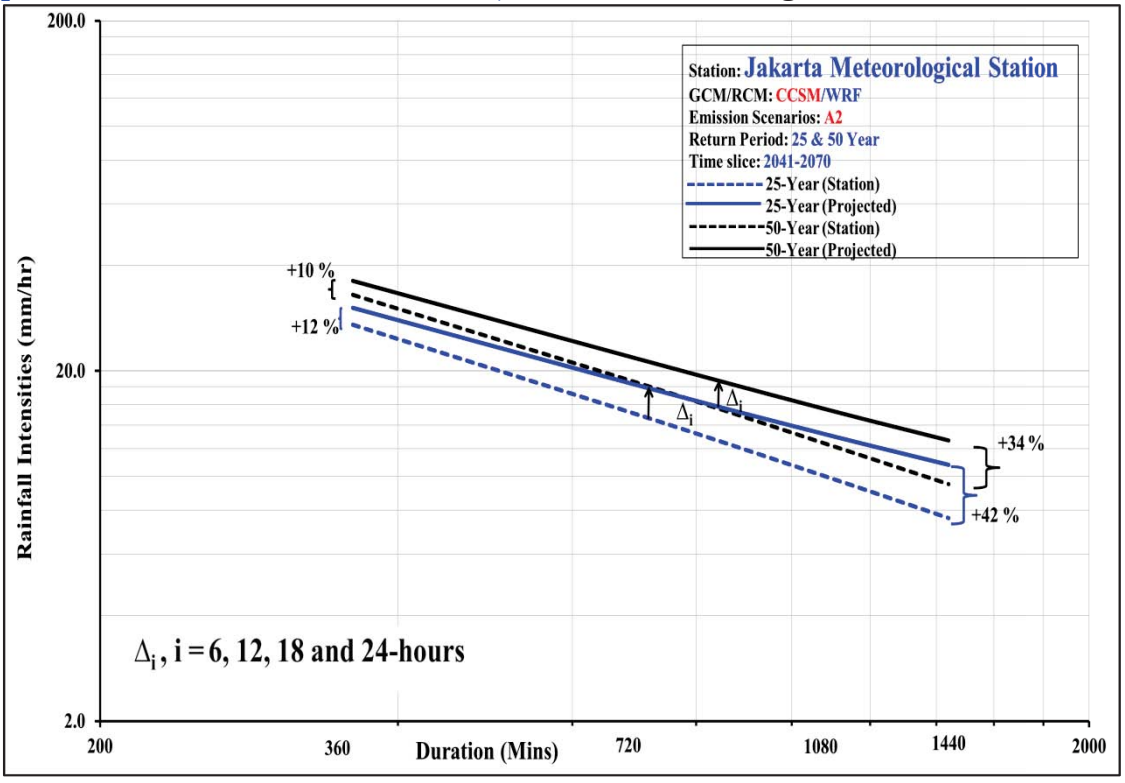

Figure B3-4b: Projected future climate IDF curves **(25 and 50 year return periods, 2041-2070, WRF/CCSM A2)**: **Jakarta Meteorological Station**

Station : Jakarta Meteorological Station
Period : 2011-2040
GCM/Scenario : WRF/CCSM A1FI

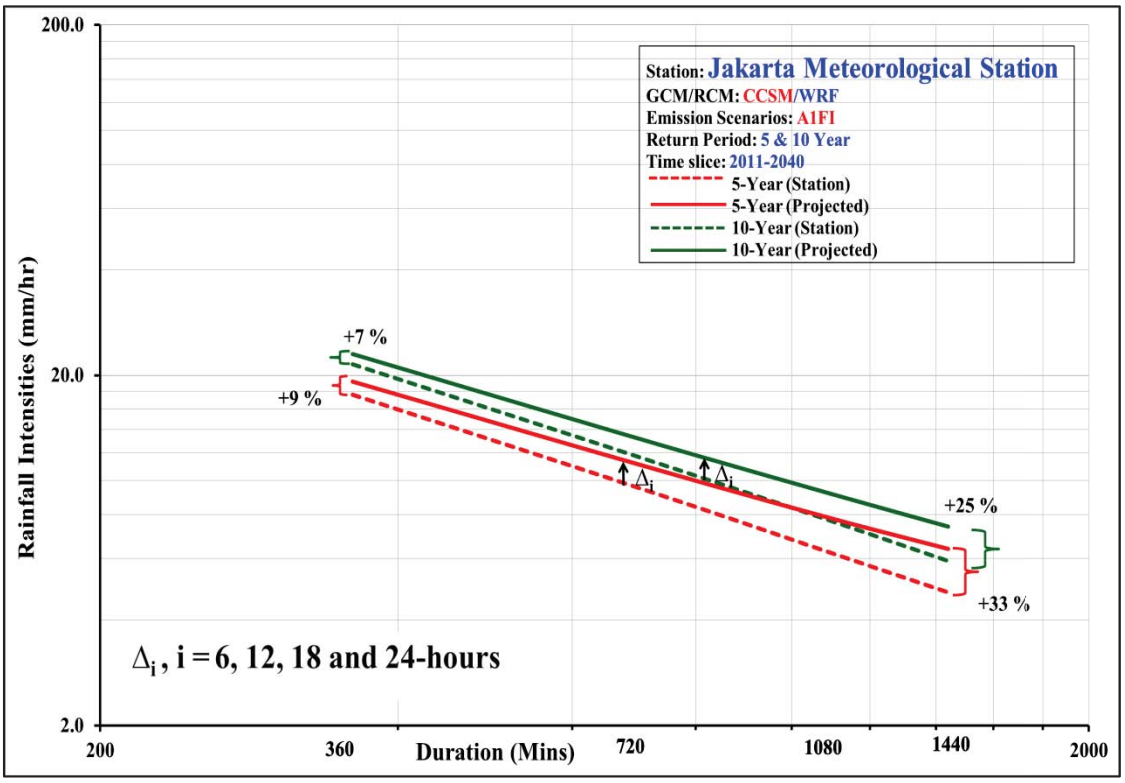

Figure B3-5a: Projected future climate IDF curves **(5 and 10 year return periods, 2011-2040, WRF/CCSM A1FI)**: **Jakarta Meteorological Station**

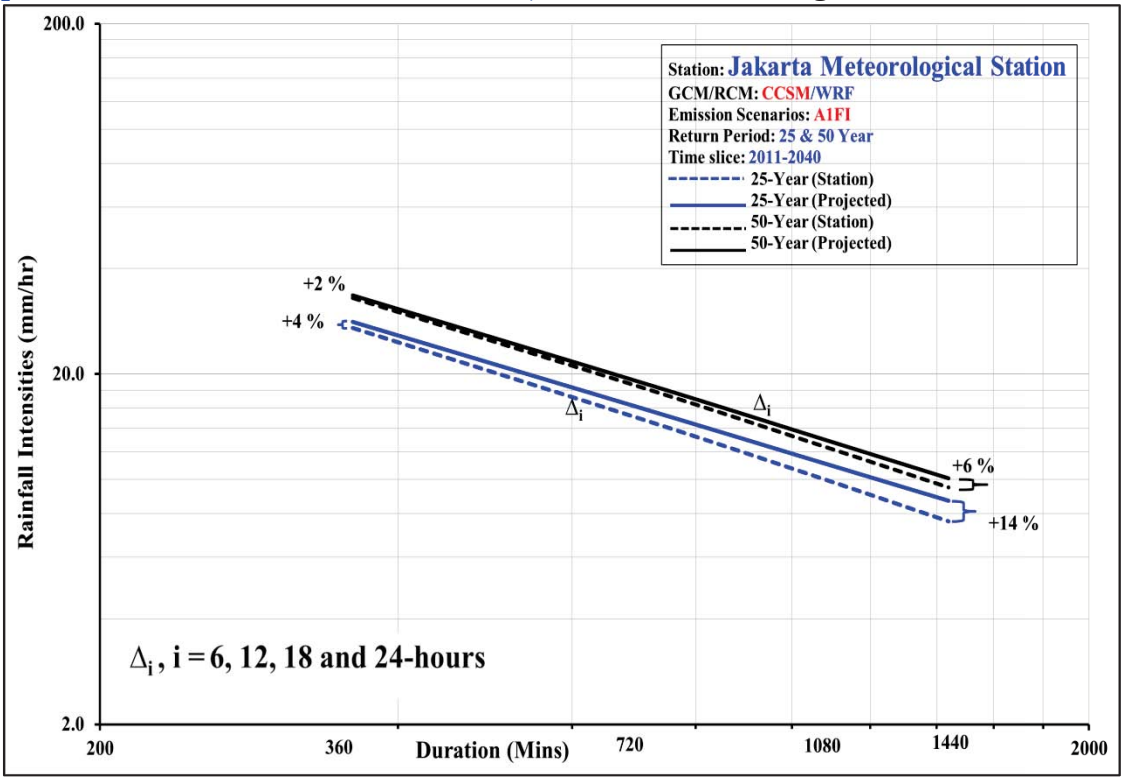

Figure B3-5b: Projected future climate IDF curves **(25 and 50 year return periods, 2011-2040, WRF/CCSM A1FI)**: **Jakarta Meteorological Station**

Station : Jakarta Meteorological Station
Period : 2041-2070
GCM/Scenario : WRF/CCSM A1FI

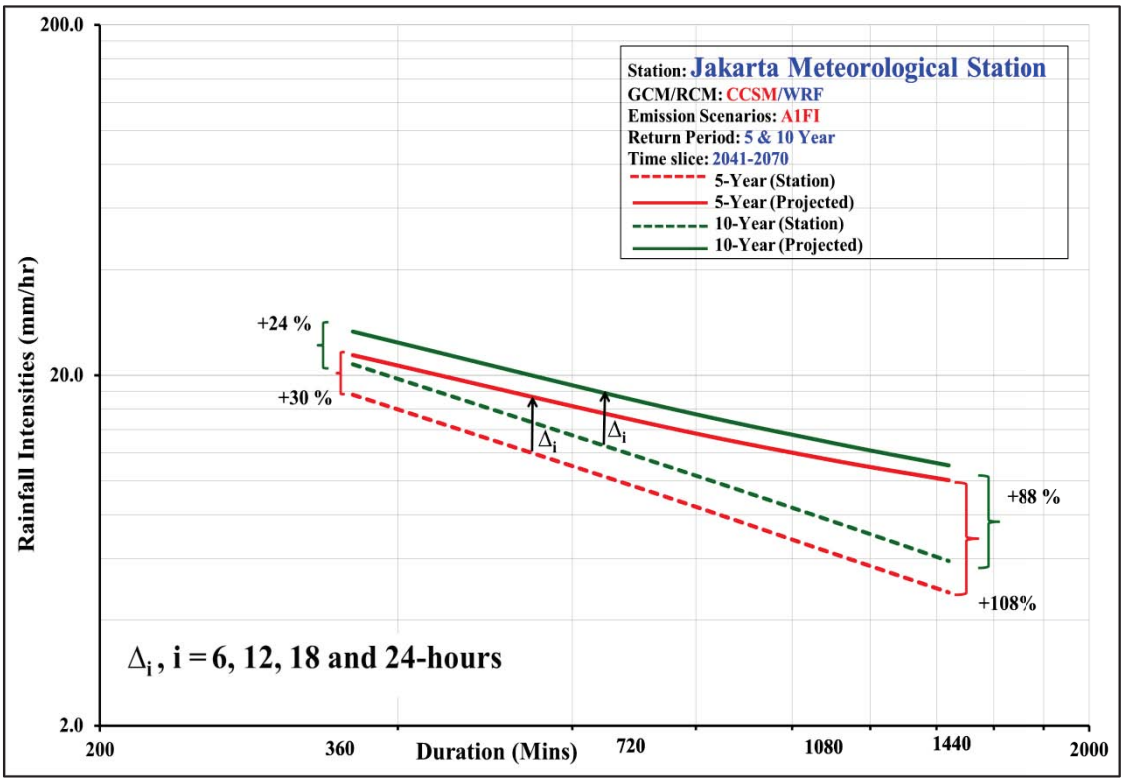

Figure B3-6a: Projected future climate IDF curves **(5 and 10 year return periods, 2041-2070, WRF/CCSM A1FI)**: **Jakarta Meteorological Station**

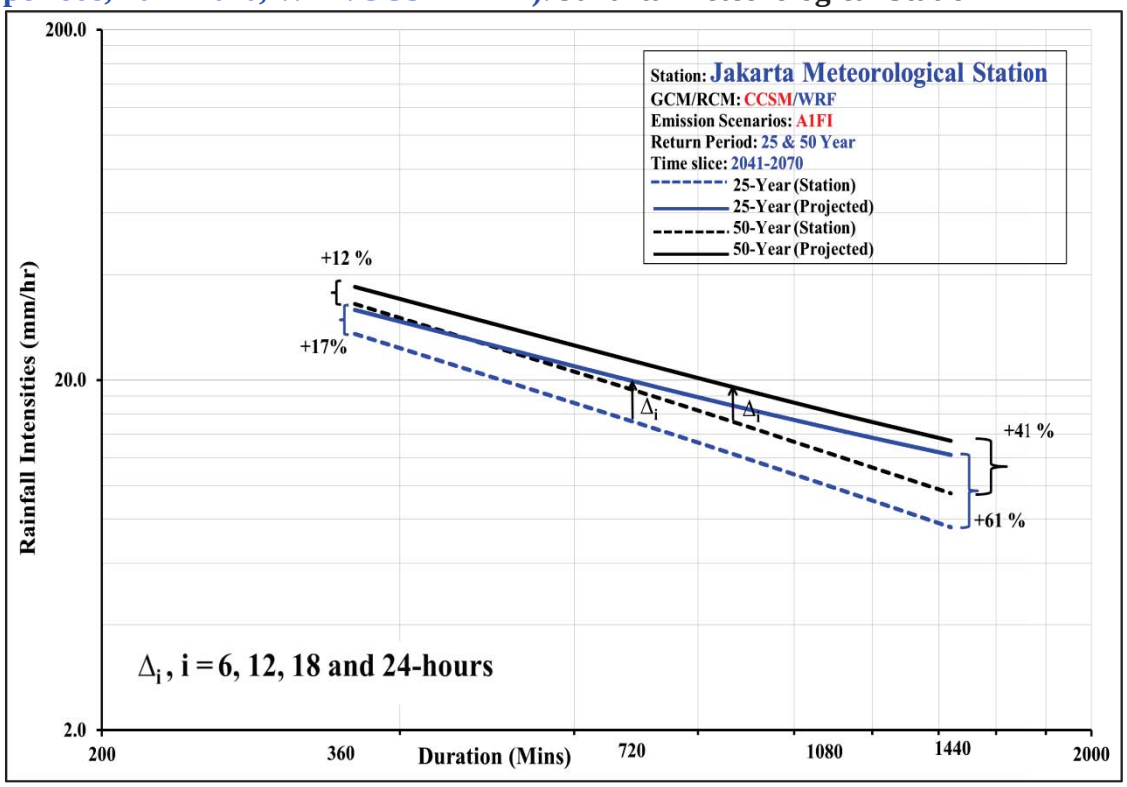

Figure B3-6b: Projected future climate IDF curves **(25 and 50 year return periods, 2041-2070, WRF/CCSM A1FI)**: **Jakarta Meteorological Station**

Station : Jakarta Meteorological Station
Period : 2011-2040
GCM/Scenario : WRF/CCSM A1B

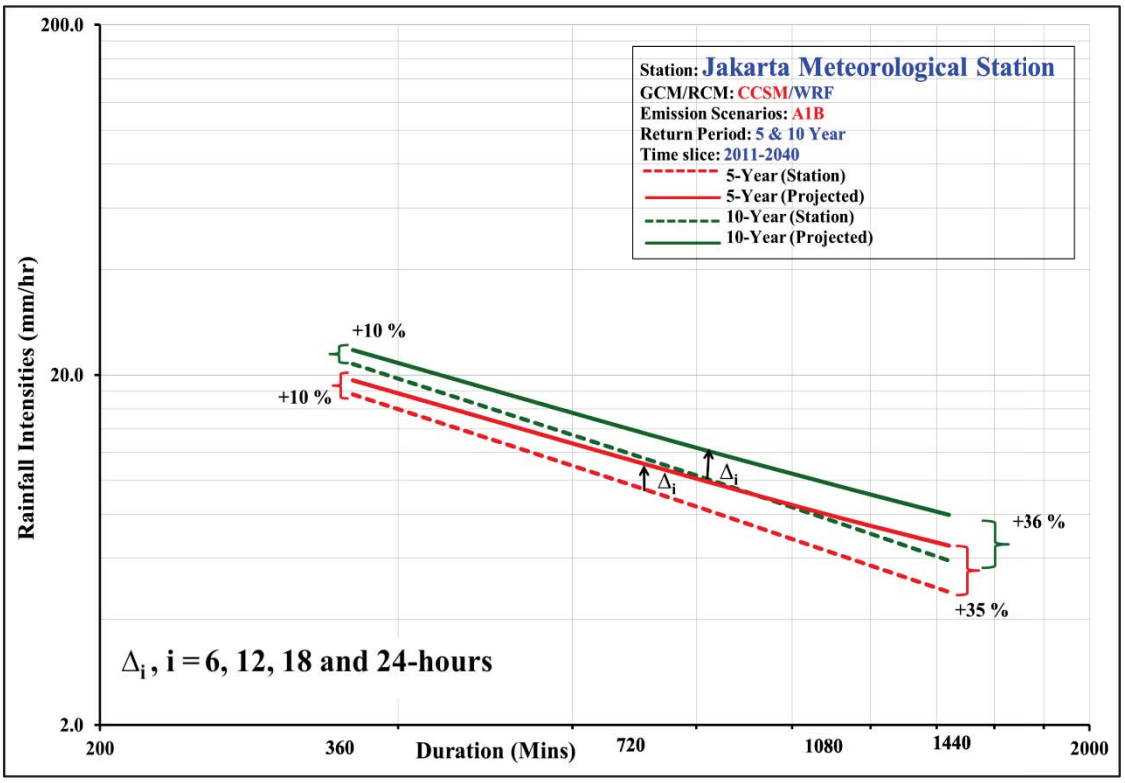

Figure B3-7a: Projected future climate IDF curves **(5 and 10 year return periods, 2011-2040, WRF/CCSM A1B)**: **Jakarta Meteorological Station**

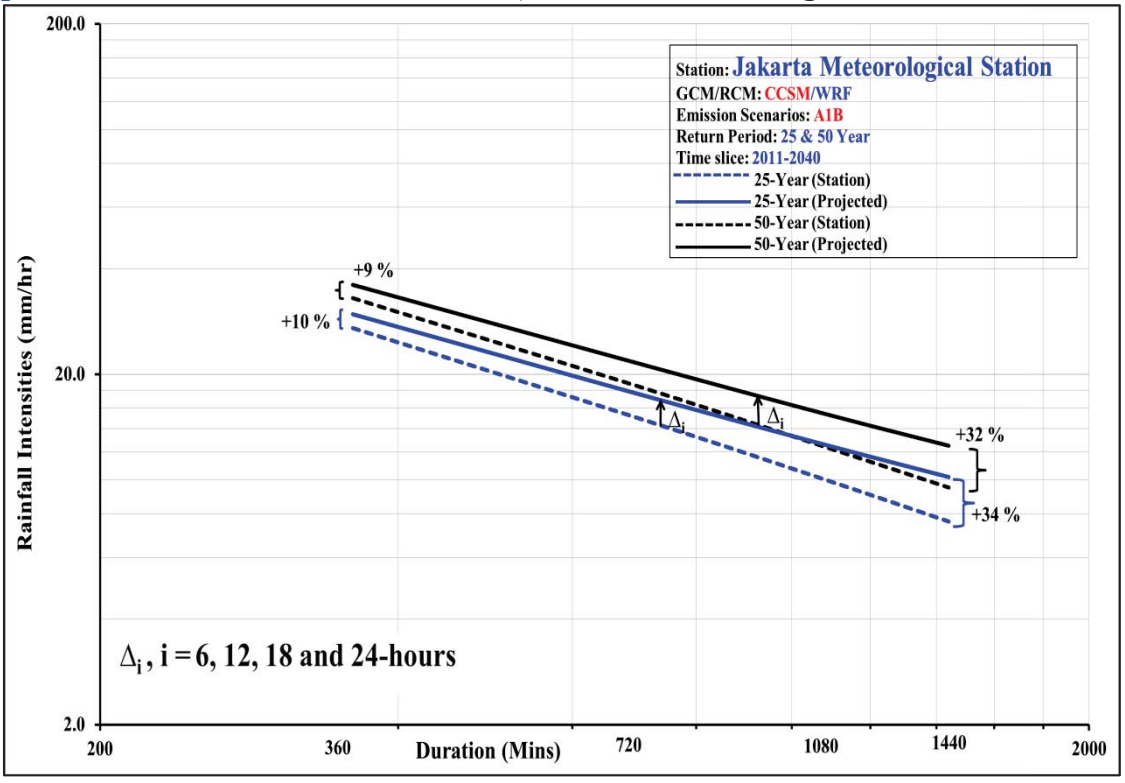

Figure B3-7b: Projected future climate IDF curves **(25 and 50 year return periods, 2011-2040, WRF/CCSM A1B)**: **Jakarta Meteorological Station**

Station : Jakarta Meteorological Station
Period : 2041-2070
GCM/Scenario : WRF/CCSM A1B

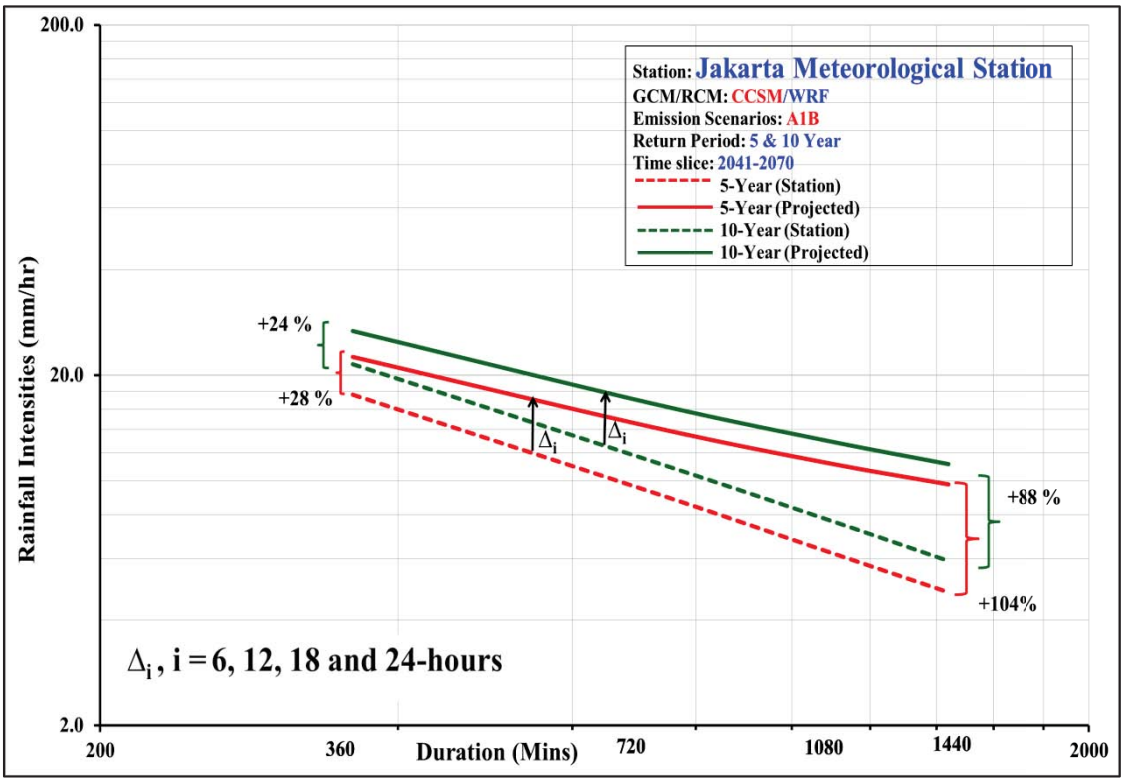

Figure B3-8a: Projected future climate IDF curves **(5 and 10 year return periods, 2041-2070, WRF/CCSM A1B)**: **Jakarta Meteorological Station**

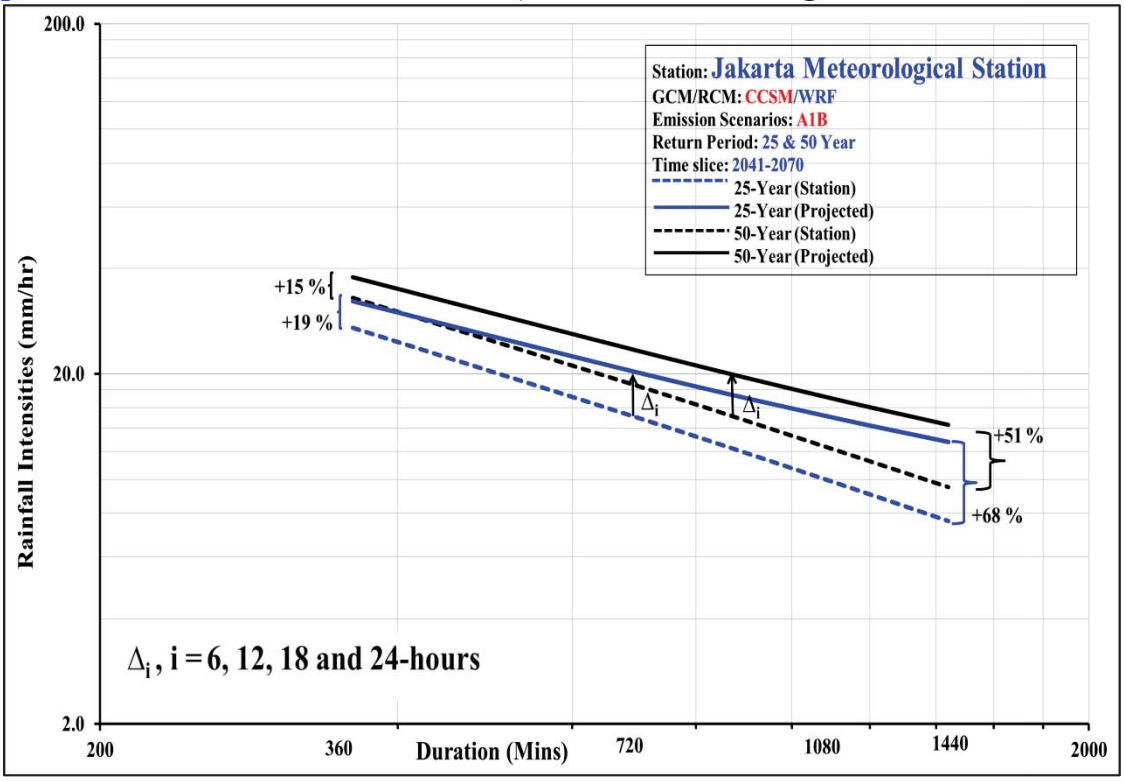

Figure B3-8b: Projected future climate IDF curves **(25 and 50 year return periods, 2041-2070, WRF/CCSM A1B)**: **Jakarta Meteorological Station**

APPENDIX B4

Comparison between IDF Curves of 3 cities for 5 and 10-year Return Period; WRF/ECHAM and A2 emission scenario, for all the three time slice (2011-2040, 2041-2070 and 2071-2100)

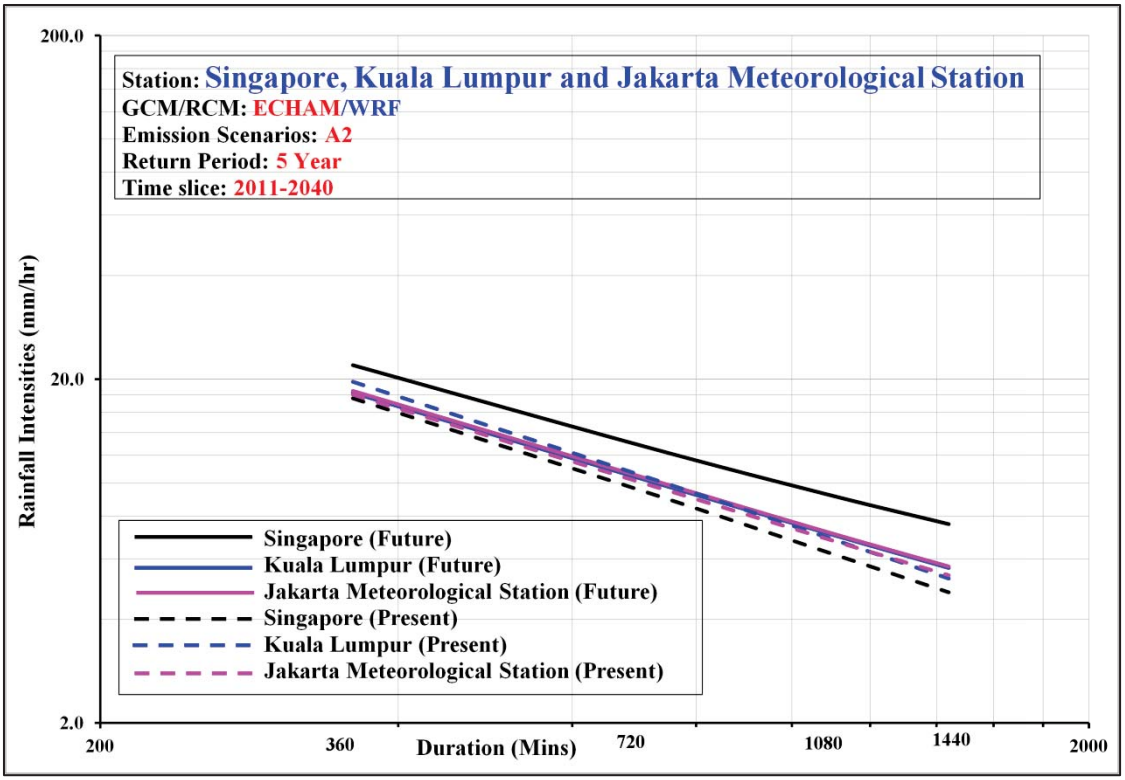

Figure B4-1a: Comparison between projected IDF curves for different cities (5 year return period, WRF/ECHAM A2) in time slice 2011-2040: Singapore, Kuala Lumpur and Jakarta Meteorological Station

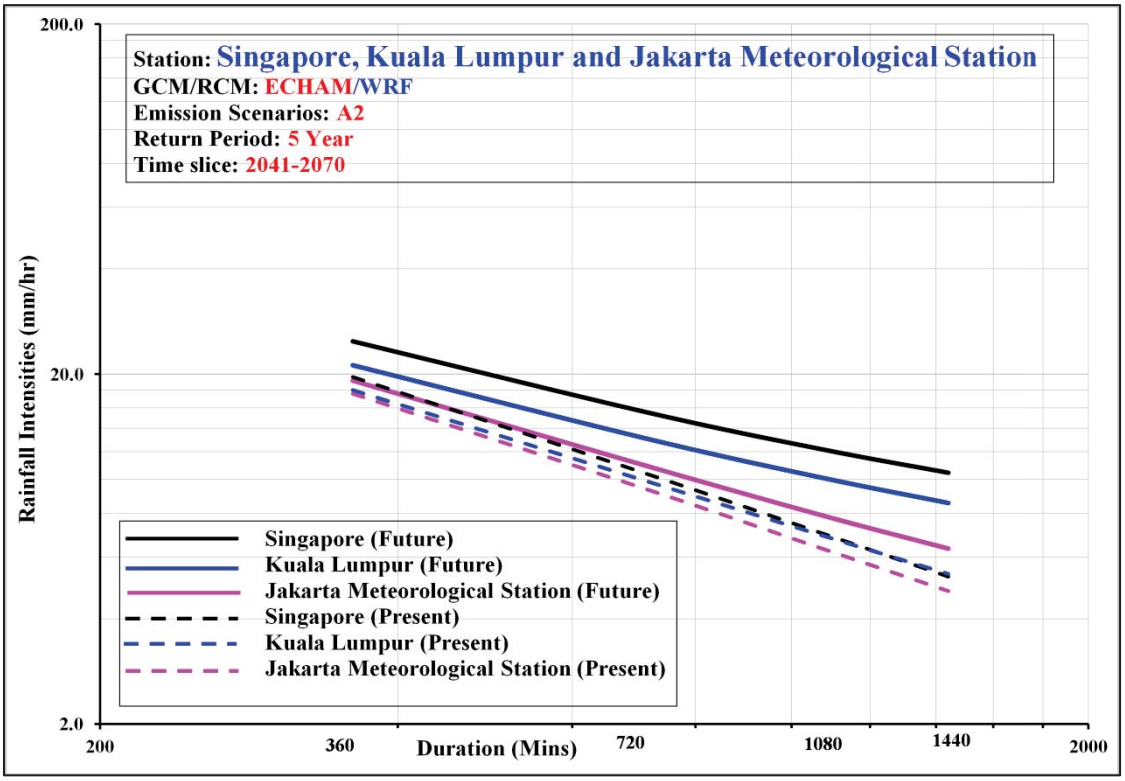

Figure B4-1b: Comparison between projected IDF curves for different cities (5 year return period, WRF/ECHAM A2) in time slice 2041-2070: Singapore, Kuala Lumpur and Jakarta Meteorological Station

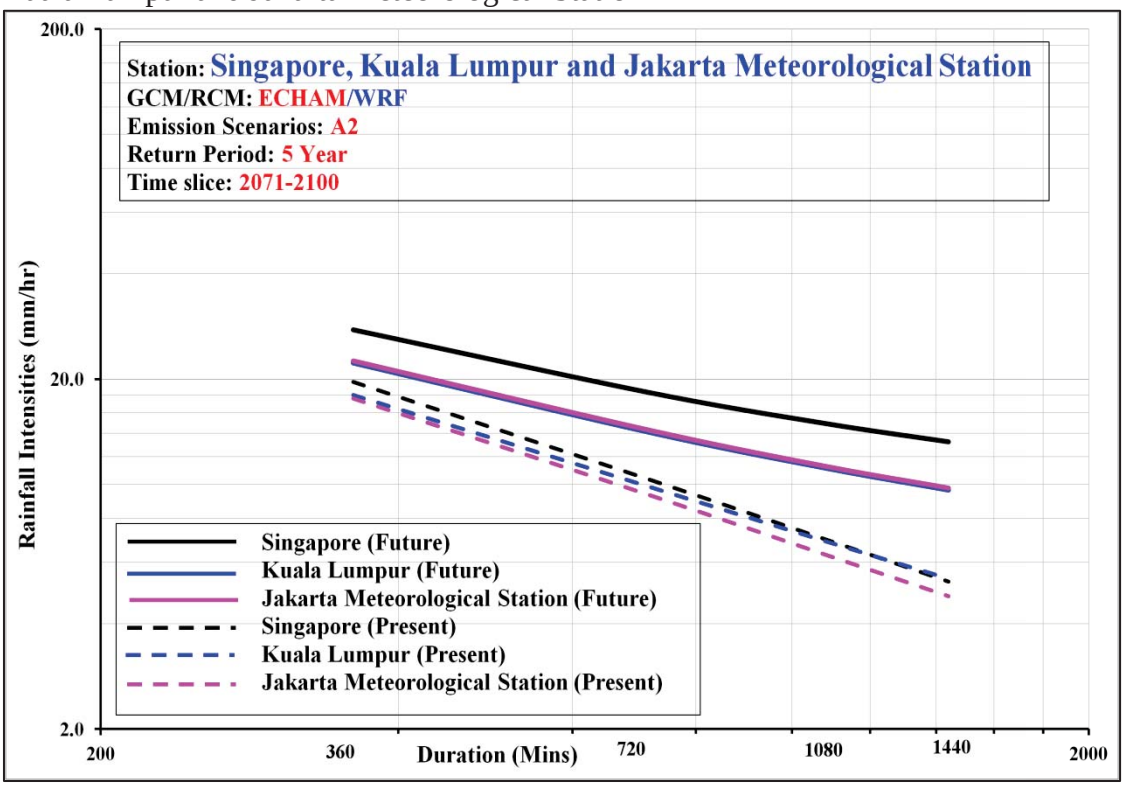

Figure B4-1c: Comparison between projected IDF curves for different cities (5 year return period, WRF/ECHAM A2) in time slice 2071-2100: Singapore, Kuala Lumpur and Jakarta Meteorological Station

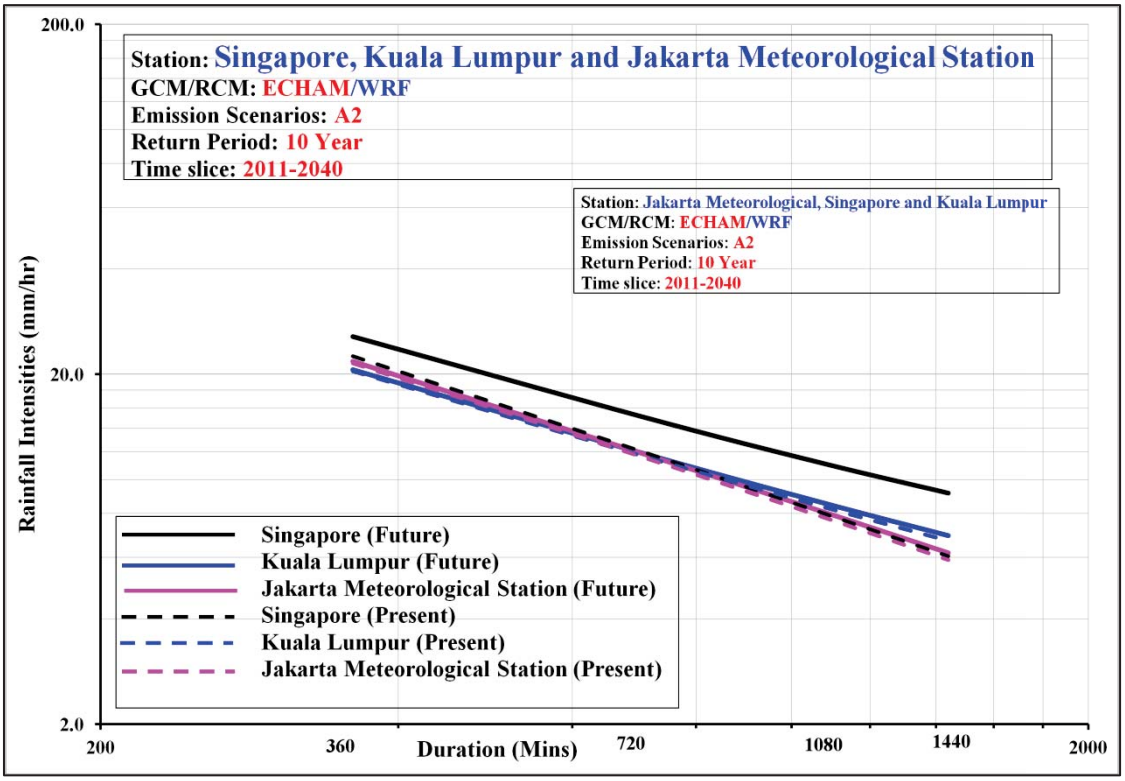

Figure B4-2a: Comparison between projected IDF curves for different cities (10 year return period, WRF/ECHAM A2) in time slice 2011-2040: Singapore, Kuala Lumpur and Jakarta Meteorological Station

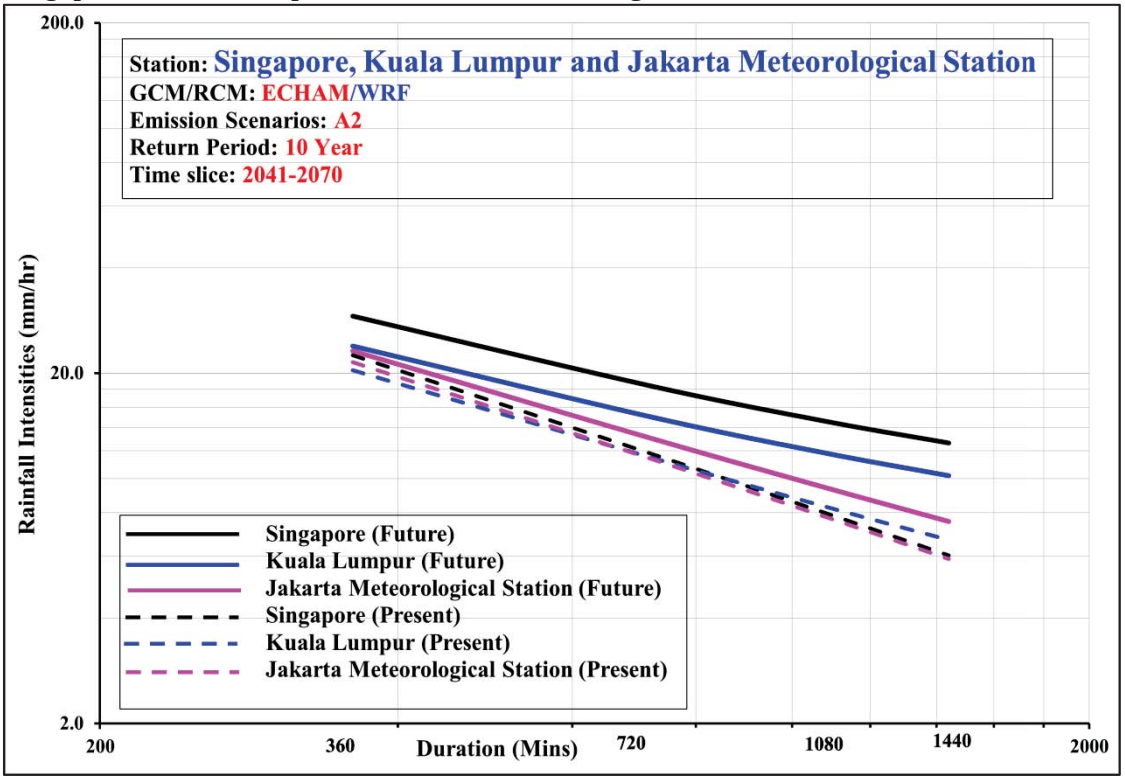

Figure B4-2b: Comparison between projected IDF curves for different cities (10 year return period, WRF/ECHAM A2) in time slice 2041-2070: Singapore, Kuala Lumpur and Jakarta Meteorological Station

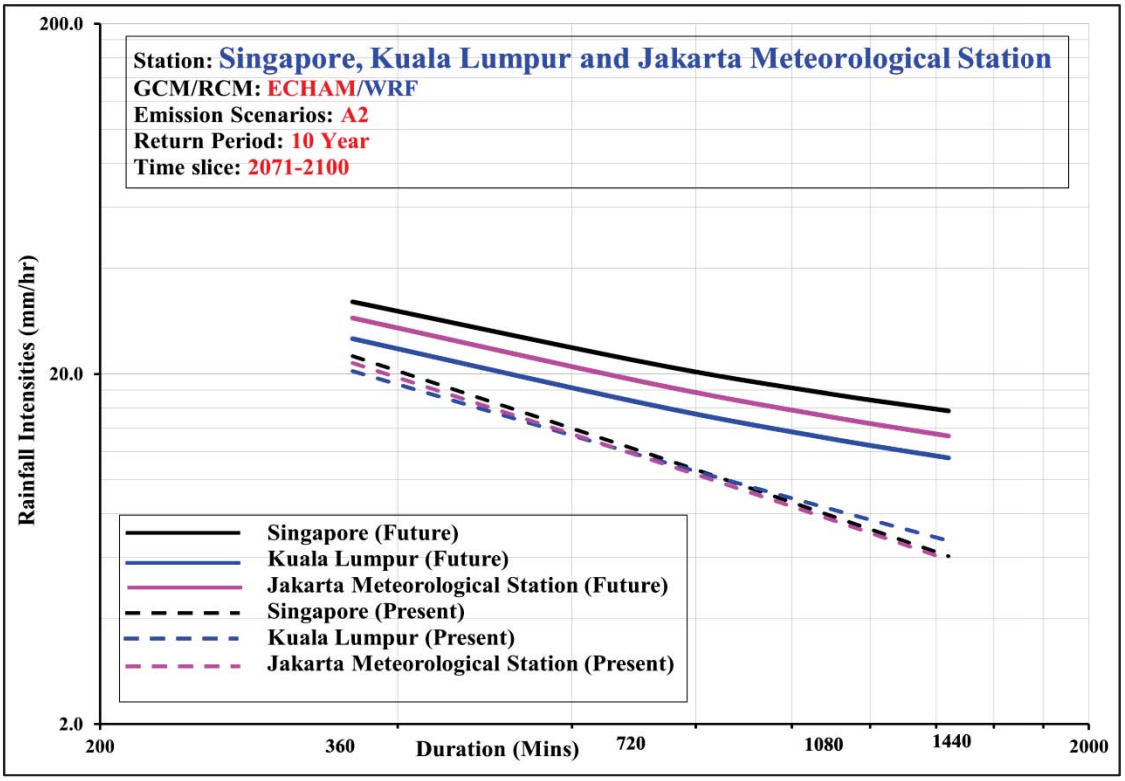

Figure B4-2c: Comparison between projected IDF curves for different cities (10 year return period, WRF/ECHAM A2) in time slice 2011-2100: Singapore, Kuala Lumpur and Jakarta Meteorological Station

APPENDIX B5

Comparison between IDF Curves of 3 cities under WRF/ECHAM and A2 emission scenario (2011-2040 and 2041-2070)

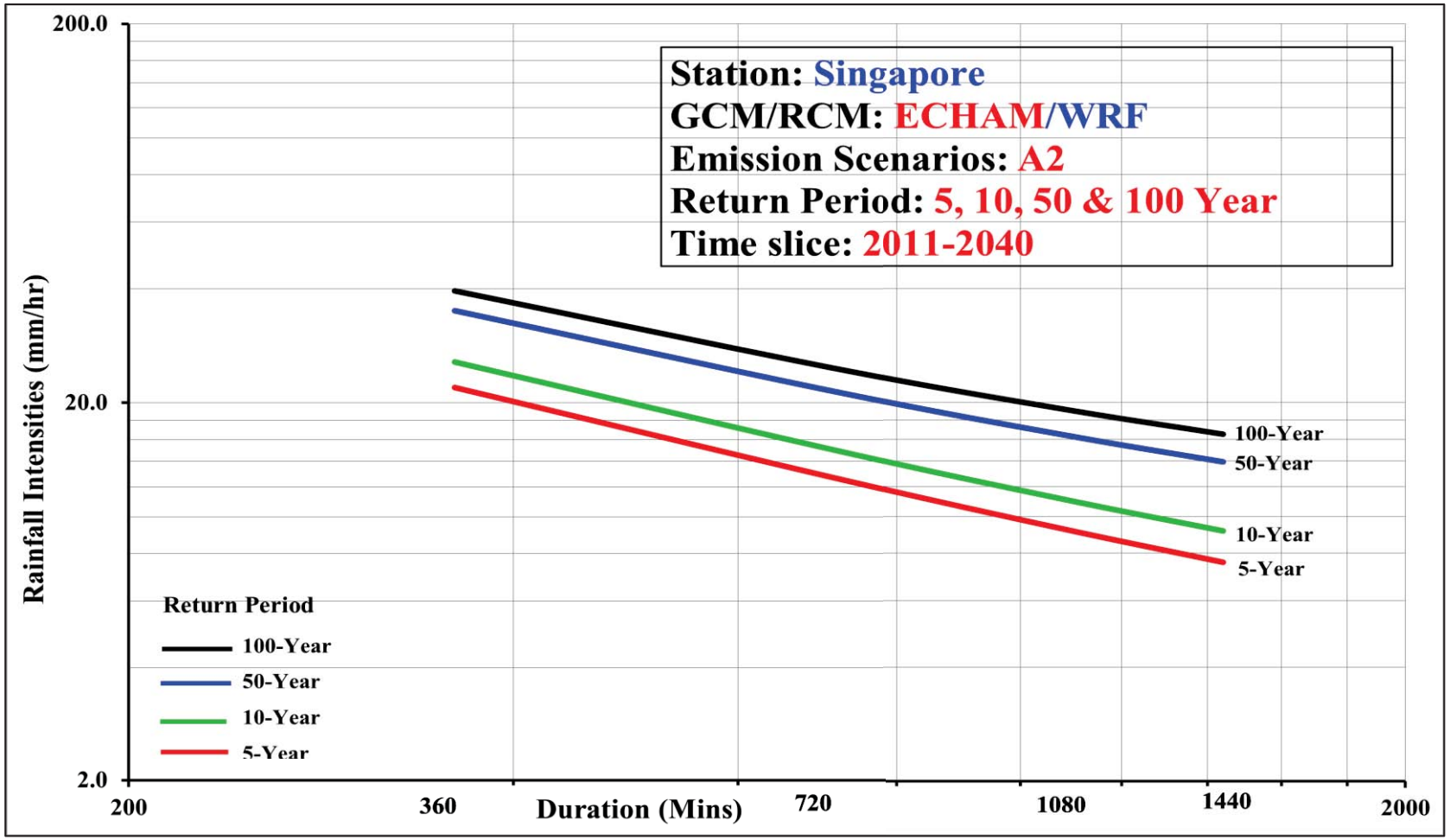

Figure B5-1a: Future climate IDF Curves (2011-2040) derived from **WRF/ECHAM A2**: **Singapore**

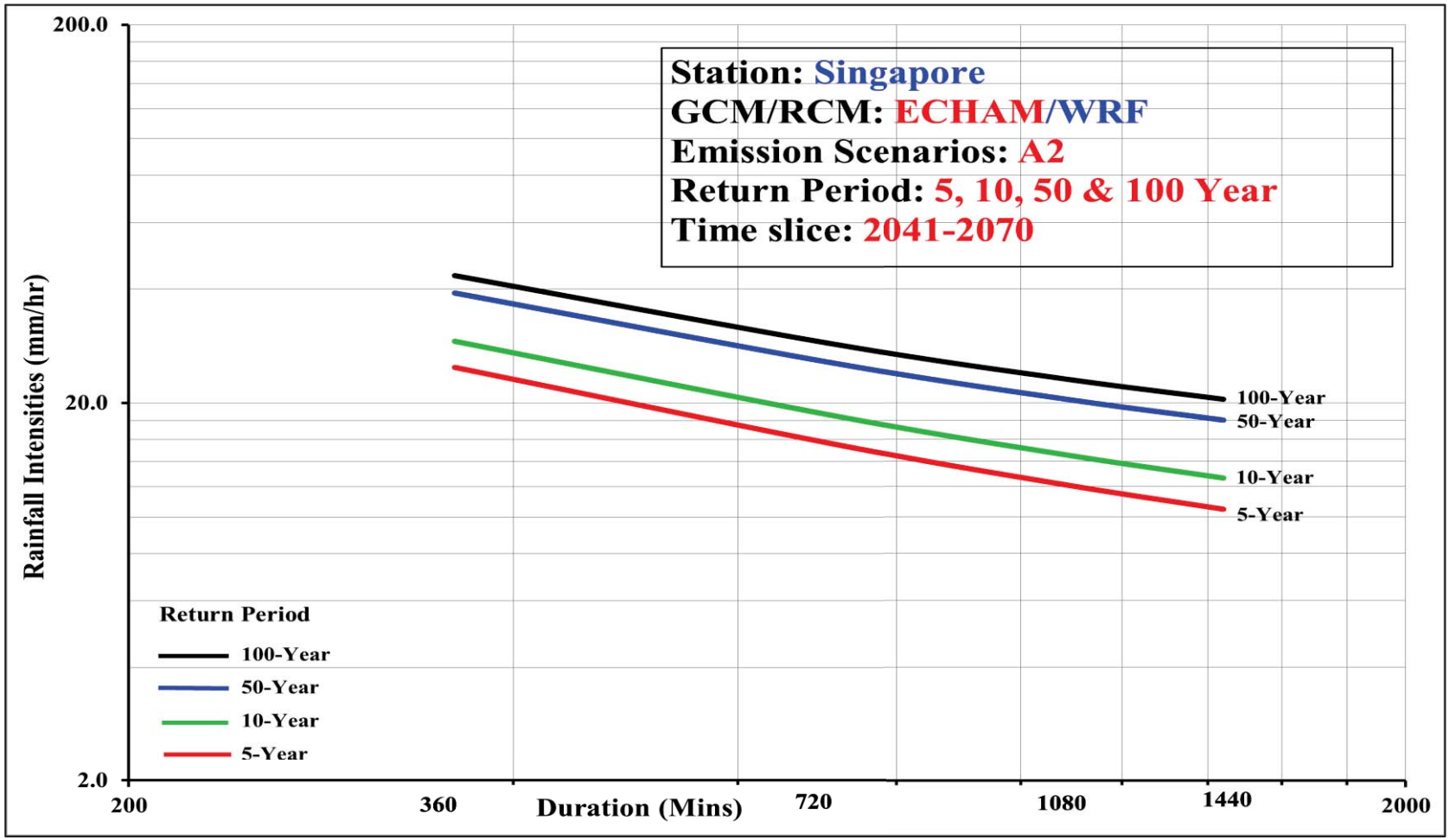

Figure B5-1b: Future climate IDF Curves (2041-2070) derived from **WRF/ECHAM A2**: **Singapore**

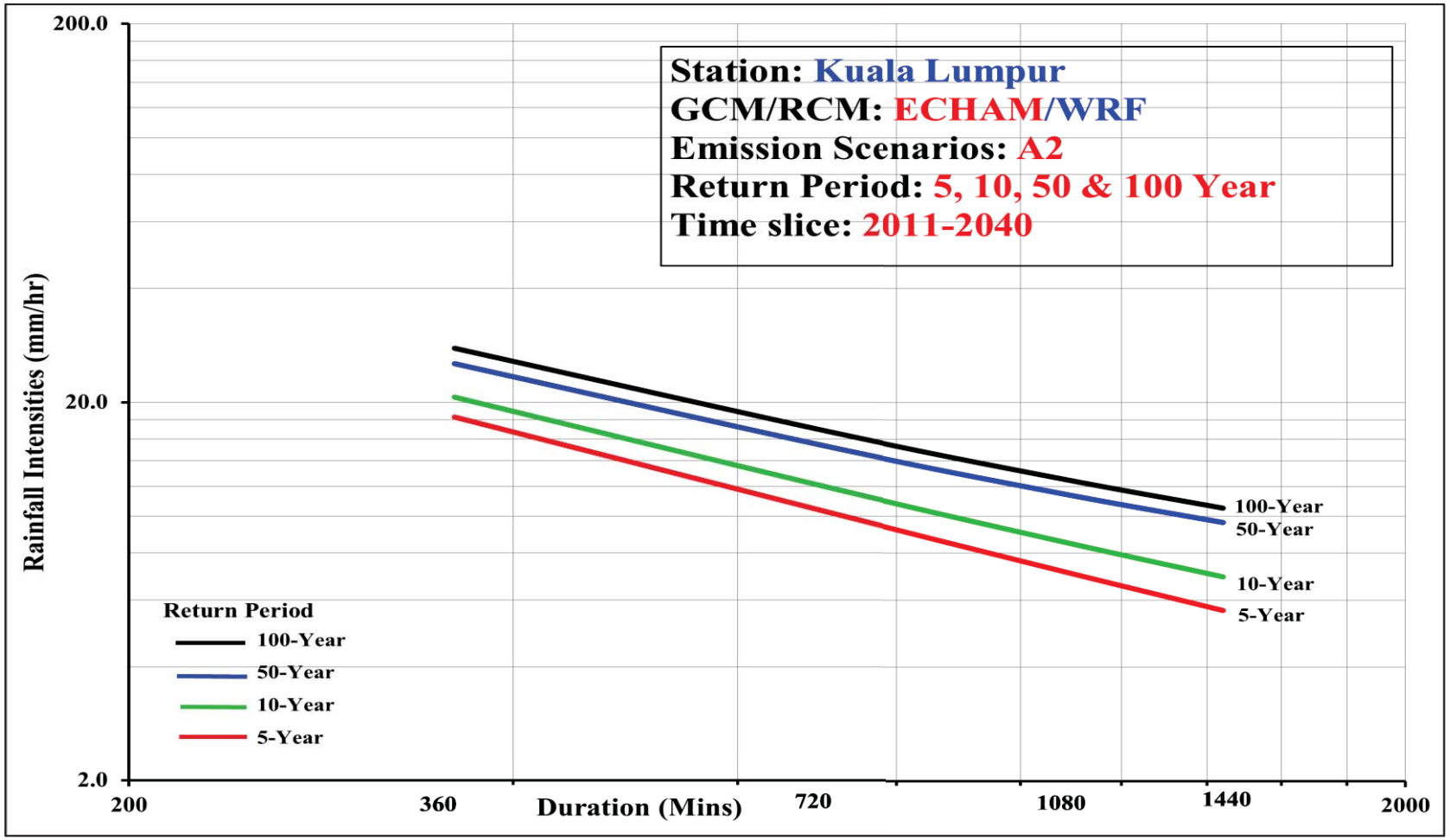

Figure B5-2a: Future climate IDF Curves (2011-2040) derived from **WRF/ECHAM A2**: **Kuala Lumpur**

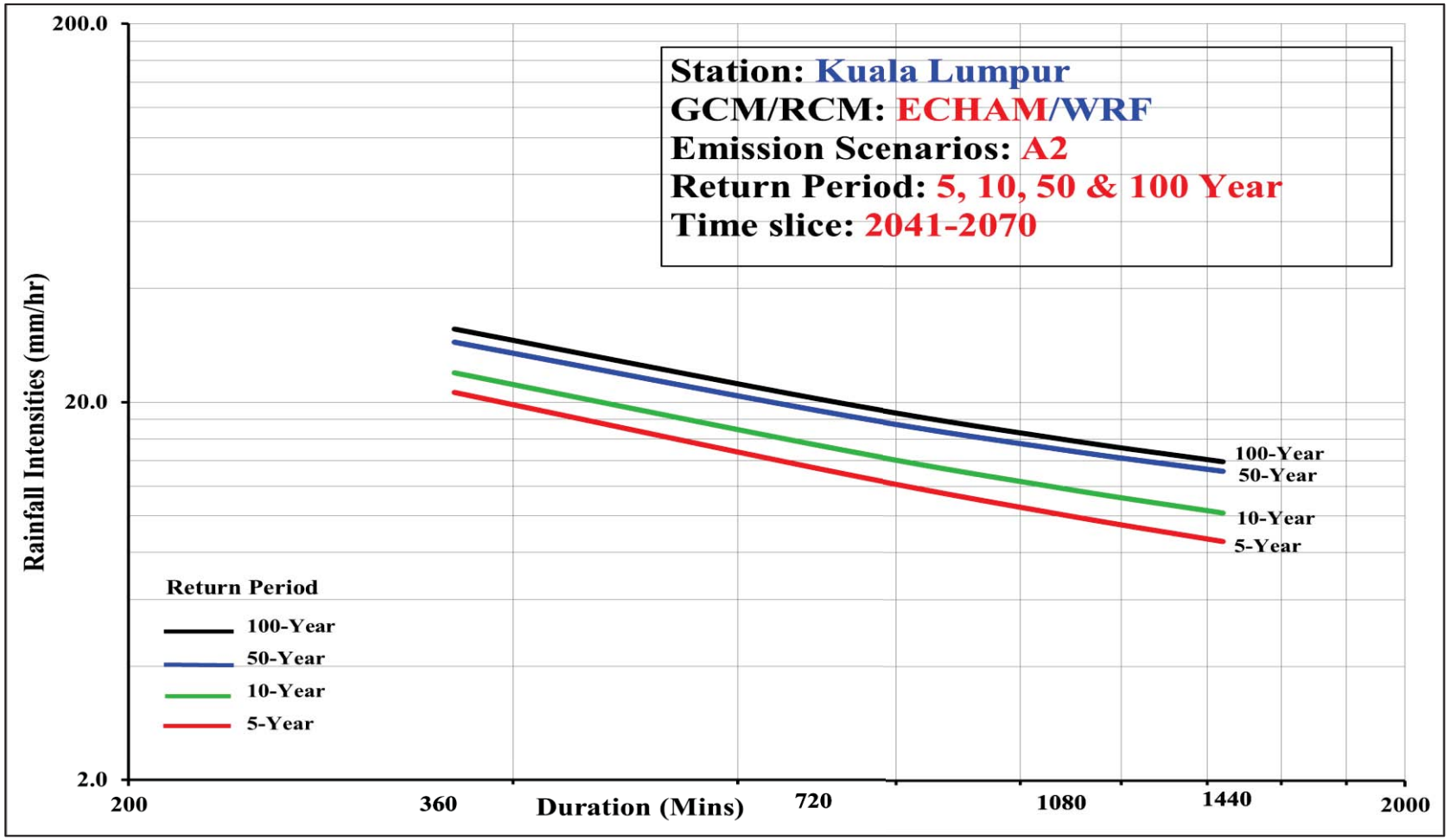

Figure B5-2b: Future climate IDF Curves (2041-2070) derived from **WRF/ECHAM A2**: **Kuala Lumpur**

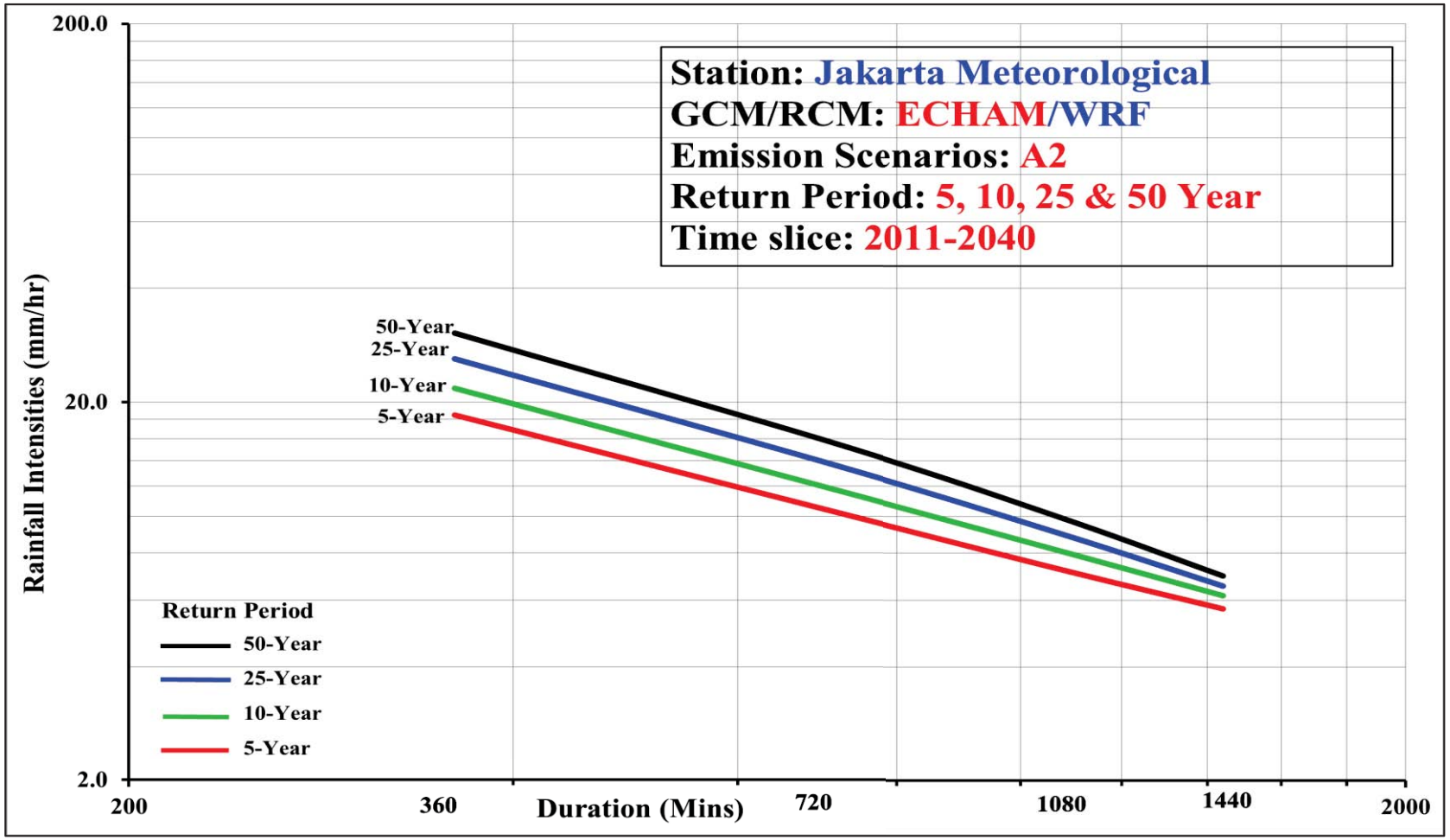

Figure B5-3a: Future climate IDF Curves (2011-2040) derived from **WRF/ECHAM A2**: **Jakarta**

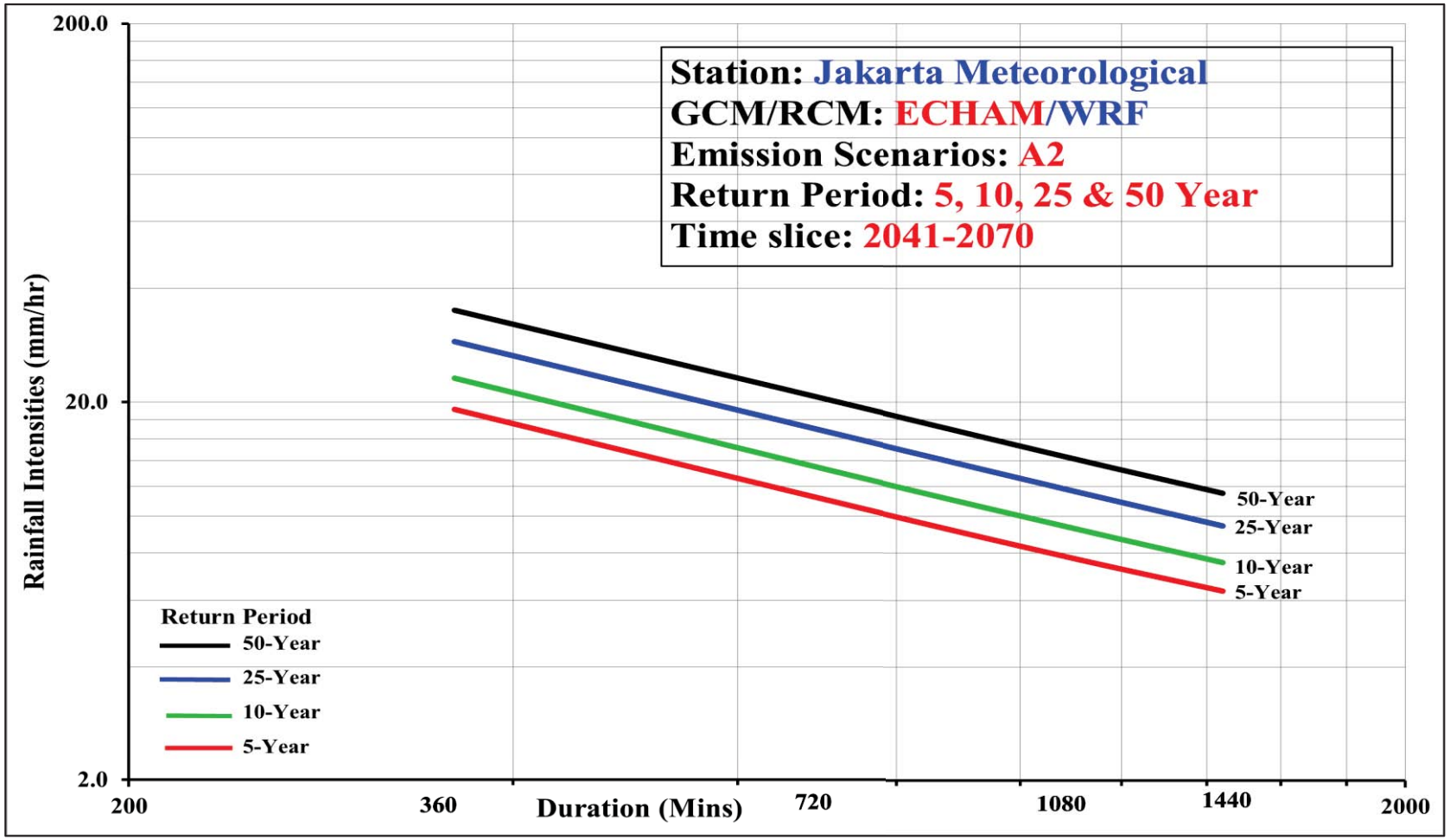

Figure B5-3b: Future climate IDF Curves (2041-2070) derived from **WRF/ECHAM A2**: **Jakarta**

Table B1-1. Coordinates of meteorological stations used to validate proposed approach

STATION	LONGITUDE	LATITUDE	COUNTRY
Ipoh	**101° 7’ E**	**4° 39’ S**	**Malaysia**
Seremban	**101° 56’E**	**2° 43’ S**	**Malaysia**
Melaka	**102° 15’ E**	**2° 17’ N**	**Malaysia**
Johor Bahru	**103° 38’ E**	**1° 40’ N**	**Malaysia**